DEEP-WATER SANDSTONES OF THE TOURELLE FORMATION

SEDIMENTOLOGY AND REGIONAL IMPLICATIONS OF DEEP-WATER SANDSTONES OF THE TOURELLE FORMATION, ORDOVICIAN, QUEBEC

by

RICHARD NICHOLAS HISCOTT, B.Sc.

A Thesis

Submitted to the School of Graduate Studies

in Partial Fulfilment of the Requirements

for the Degree

Doctor of Philosophy

McMaster University

September, 1977

DOCTOR OF PHILOSOPHY (1977) McMASTER UNIVERSITY

(Geology) Hamilton, Ontario

TITLE: Sedimentology and Regional Implications of Deep-water Sandstones of the Tourelle Formation, Ordovician, Quebec.

AUTHOR: Richard Nicholas Hiscott, Hon. B.Sc. (Brock University)

SUPERVISOR: Professor G. V. Middleton

NUMBER OF PAGES: xxv, 542

ABSTRACT

Coarse sandstones of the allochthonous Lower Ordovician Tourelle Formation occur in spectacular exposures along the south shore of the St. Lawrence River. The formation is characterized by thick-bedded, coarse, massive sandstones. Individual graded beds may be tens of metres thick, and may contain slabs of shale, siltstone, or bedded chert up to 16 m in length. Cross-stratification and unusual near-horizontal stratification are the only internal depositional structures. Fluid-escape pillars indicate post-depositional liquefaction. Associated facies are thick shale units, rippled siltstones, slurry sandstones, classical turbidites, slump sheets, and clastic injections.

The Tourelle Formation was deposited on the channelized mid-fan of a submarine-fan complex. Several major channels (to 13 m deep) contain sandstone fills which thin upward. Most asymmetric megasequences thin upward, and are also interpreted as channel fills. These cycles average 20 m thick. A model for the filling of submarine fan channels is presented. Well-defined thinning or thickening upward trends are not common, although thinning upward cycles dominate sequence (Markov) analysis.

At some outcrop localities, packets of coarse sandstone alternate with thick shale horizons, interpreted as mud blankets over abandoned mid-fan lobes. Rippled siltstones are interpreted

as overbank deposits adjacent to distributary channels.

Thick sandstones can be divided into stratified or massive layers, which may be capped by normal tractional structures. Inverse-graded stratification bands (to 10 cm thick) are based by a near-horizontal scour surface. Several such "bands" form a division of stratification. Stratified layers are well graded (distribution grading), and have a strong and consistent a-axis fabric, with long axis parallel to flow. Upcurrent imbrication exceeds 20°. These layers were deposited beneath supercritical turbidity currents. Stratification bands formed by progressive "freezing" of a flowing grain layer at the base of the current.

Massive layers may be well graded, poorly graded, inverse-to-normally graded, or ungraded. a-axis grain orientation is most strongly developed at the base and top of layers. The middle parts of individual units may have bimodal or isotropic fabrics, with both upcurrent and downcurrent imbrications. Most massive layers, or divisions, were deposited rapidly from dense, supercritical turbulent suspensions as a result of decreasing current capacity at velocities on the order of 10 m s^{-1}. Unusually thick layers containing enormous blocks were probably transported by laminar debris flows on slopes of 0.02 to 0.05.

The average composition of Tourelle sandstones is 45.6% quartz, 8.2% feldspar, 13.4% rock fragments, 16.1% chloritic matrix, and 15.3% calcite "cement". These sands contained 10 to

15% primary detrital matrix. The most distinctive rock fragments are radiolarian chert, and mafic to felsic volcanic detritus. The heavy mineral suite contains rounded ultrastable zircon and tourmaline, abundant epidote group minerals and garnet, unstable prismatic hornblende and pyroxene, and 18% transluscent cherry-red chromite.

Tourelle detritus was derived by erosion of rising cordillera and obducted ophiolites in the interior of the nascent Taconic orogenic belt, and represents the first influx of detritus from a southeastern source. Previous sediments were eroded directly from the Grenville shield and its fringing carbonate bank. These sediments were recycled to form Tourelle sands.

A plate tectonic model is proposed which involves closing of a marginal ocean basin along a southeastward-dipping subduction zone, collision of the ancient continental margin of North America with a volcanic arc situated on a micro-continent of crystalline Grenville basement, and obduction of a large sheet of ophiolite. Previously published models do not provide a source area for the Tourelle Formation, and must be considered inadequate.

The Tourelle dispersal system consisted of a series of small, closely-spaced and coalescing submarine fans which were consistently deflected to the west along a sloping, elongate depositional trough.

ACKNOWLEDGEMENTS

The author wishes to express his sincere gratitude to Professor G. V. Middleton, his research supervisor, for guidance and encouragement during the progress of research and for many valuable suggestions for improving the manuscript.

Many of the ideas presented in this thesis were developed during discussions with Serge Biron of the Ministère des Richesses Naturelles of Quebec, Dr. Wayne T. Jolly of the Geology Department, Brock University, Dr. Peter J. McCabe during his tenure of a postdoctoral fellowship in the Geology Department, McMaster University, Dr. Robert K. Stevens of the Geology Department, Memorial University of Newfoundland, and Dr. Roger G. Walker of the Geology Department, McMaster University. All of these individuals are sincerely thanked for their assistance.

This thesis has been greatly improved by comments from the author's supervisory committee: Dr. Middleton, Dr. Walker, and Dr. Alan A. Smith of the Civil Engineering Department, McMaster University.

The following are also thanked for their assistance: Maureen Dickson for assistance in fabric studies and printing of photographs, Daria Love for assistance in the field, Jack Whorwood for photographic work and technical advice, Don Falkiner and Len Zwicker for preparation of thin sections and fabric samples, John Muysson for assistance in conducting

chromium analysis, Mrs. Doris Hiscott for aid in preparing coloured maps, and Ms. Helen Elliot for typing the final manuscript.

Financial assistance, through National Research Council of Canada operating grants to Dr. Middleton, and through a National Research Council 1967 Science Scholarship awarded to the author, is gratefully acknowledged.

TABLE OF CONTENTS

TABLE OF CONTENTS (cont'd)

TABLE OF CONTENTS (cont'd)

TABLE OF CONTENTS (cont'd)

TABLE OF CONTENTS (cont'd)

TABLE OF CONTENTS (cont'd)

TABLE OF CONTENTS (cont'd)

ILLUSTRATIONS

ILLUSTRATIONS (cont'd)

ILLUSTRATIONS (cont'd)

ILLUSTRATIONS (cont'd)

ILLUSTRATIONS (cont'd)

ILLUSTRATIONS (cont'd)

ILLUSTRATIONS (cont'd)

ILLUSTRATIONS (cont'd)

ILLUSTRATIONS (cont'd)

LIST OF TABLES

LIST OF TABLES (cont'd)

CHAPTER I

INTRODUCTION

Rationale

Coarse granular sandstones of the Lower Ordovician Tourelle Formation occur in spectacular exposures on a broad wave-cut terrace along the south shore of the St. Lawrence River (Figure 1.1). These coarse sandy facies are associated with finer sandstones, siltstones, and shale (see Chapter II). At two localities, thick beds of sandstone have been carved into large pillars (Figure 1.2), or "tourelles" (French equivalent), by wave erosion. The presence of these conspicuous pillars induced Logan (1846) to refer to the coarse sandstone beds as "Pillar sandstones". Logan initially assigned these deposits to the Sillery Formation (Logan, 1863), a name which has since fallen into disuse because of its application at one time or another to sedimentary rocks of widely differing ages (Rasetti, 1946).

The Tourelle Formation is characterized by a high proportion of thick-bedded, coarse, graded, massive sandstones. Individual sandstone beds may be tens of metres thick with channelled bases, and may contain large slabs of shale,

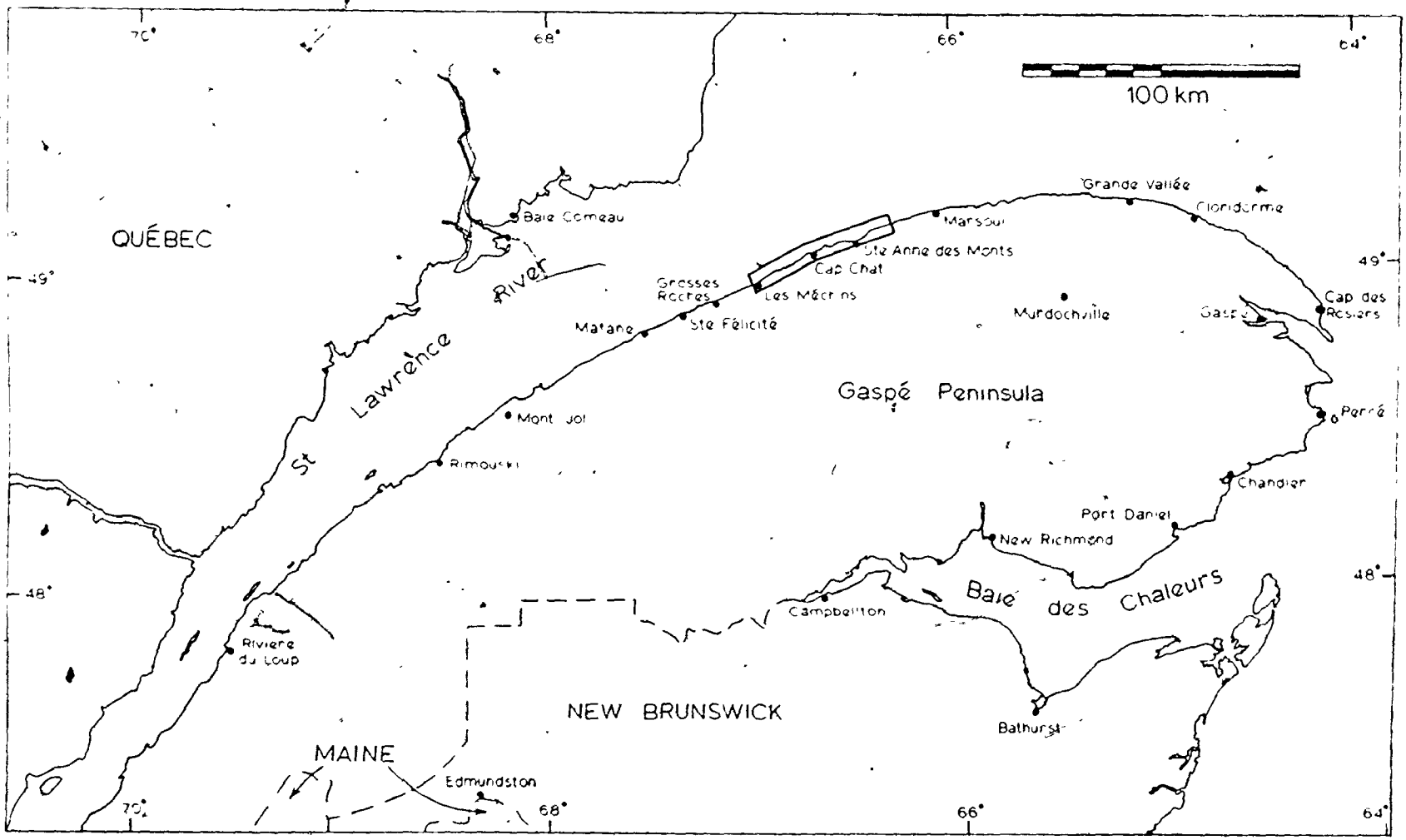

Fig. 1.1. Geographical location map. The outlined area is enlarged in figure 1.5 a and b, and contains all exposures of the Tourelle Formation which are considered in this thesis.

Fig. 1.2. Sandstone pillar (tourelle) on the wave-cut platform at Cap Ste-Anne. This pillar is about 9 m (30 feet) high, and is situated at the base of a sandstone channel-fill.

siltstone or bedded chert suspended in sandstone. Rare cross-stratification and unusual horizontal stratification are the only internal depositional structures in these thick sandstones. Post-depositional liquefaction is indicated by the presence of coarse fluid-escape pillars recording elutriation of fine matrix material.

These unusual, coarse sandstone deposits are associated with slumped units and with graded sandstones possessing all attributes of classical turbidites (Walker and Mutti, 1973; Walker, 1976). In thick massive sandstones, inorganic sole markings (scour and tool marks) and grading are common. Abundant cross-stratification and shallow-water fauna are absent, indicating deposition in deep water, below storm wave-base. These features are consistent with deposition on a submarine fan (Normark, 1970; Nelson and Kulm, 1973; Walker and Mutti, 1973), but are not included in facies models for other sedimentary environments.

The present submarine-fan model has been derived both from observations in the modern environment (Normark, 1970; Haner, 1971) and from synthesis of stratigraphic data from ancient flysch successions (Mutti and Guibaudo, 1972; Mutti and Ricci Lucchi, 1972). Modern studies have yielded information on topography and surface sediments, but fail to allow assessment of subsurface stratigraphy or detailed facies characteristics. Close similarities between the modern and

ancient models, however, have allowed them to be combined, as illustrated in Figures 1.3 and 1.4 (for further discussion see Nelson and Kulm, 1973; Walker and Mutti, 1973; Mutti, 1974; Walker, 1976 and in press).

This thesis is concerned primarily with deposits referred to as massive sandstones by Walker (1976), or as massive sandstones without dish structure (facies B2 of Walker and Mutti, 1973). Whereas detailed facies models complete with hydrodynamic interpretations have been published for both classical turbidites (Bouma, 1962; Harms and Fahnstock, 1965; Walker, 1965; Allen, 1970) and resedimented conglomerates (Davies and Walker, 1974; Walker, 1975a, 1976), massive sandstones remain poorly understood. These deposits have been interpreted as residing in mid-fan channels (Figure 1.3), but depending on availability of coarser source material, they may also be the dominant facies in inner fan channels (see, for example, Stanley, 1967, 1975).

The Tourelle Formation has been chosen for study because it contains a high proportion of massive sandstone layers. Analysis of stratigraphic relationships and facies organization should permit these massive sandstones to be assigned to a particular depositional site in the submarine fan model. Detailed facies analysis of these sandstone layers should then allow conclusions to be drawn concerning depositional mechanics and paleohydraulics.

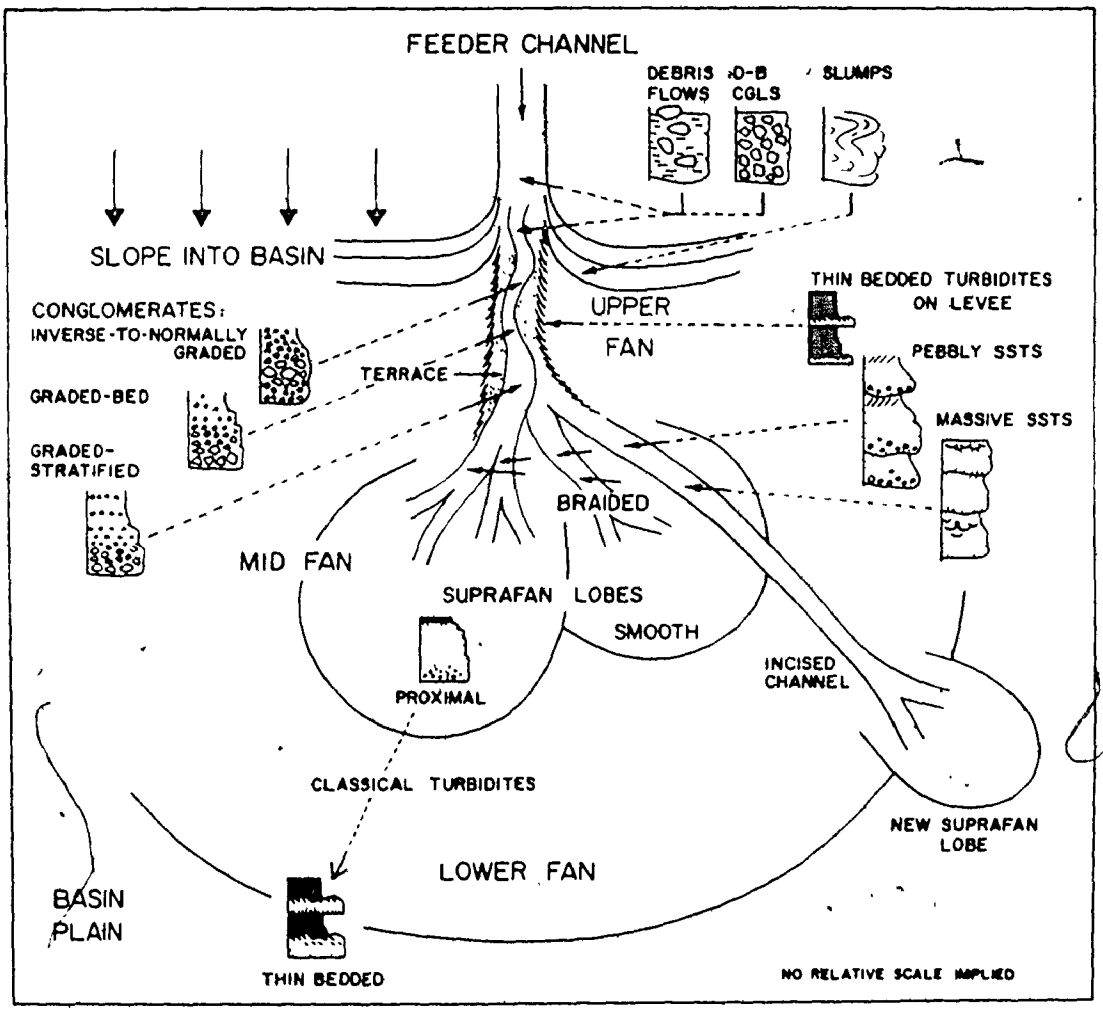

Fig. 1.3. Schematic representation of the submarine fan environmental model. The inferred depositional setting of various conglomerates, pebbly sandstones, massive sandstones, and classical turbidites are indicated. D-B is disorganized bed conglomerate model. Submarine fan geometry and channel patterns are derived from studies of modern fans. Figure courtesy of R.G. Walker.

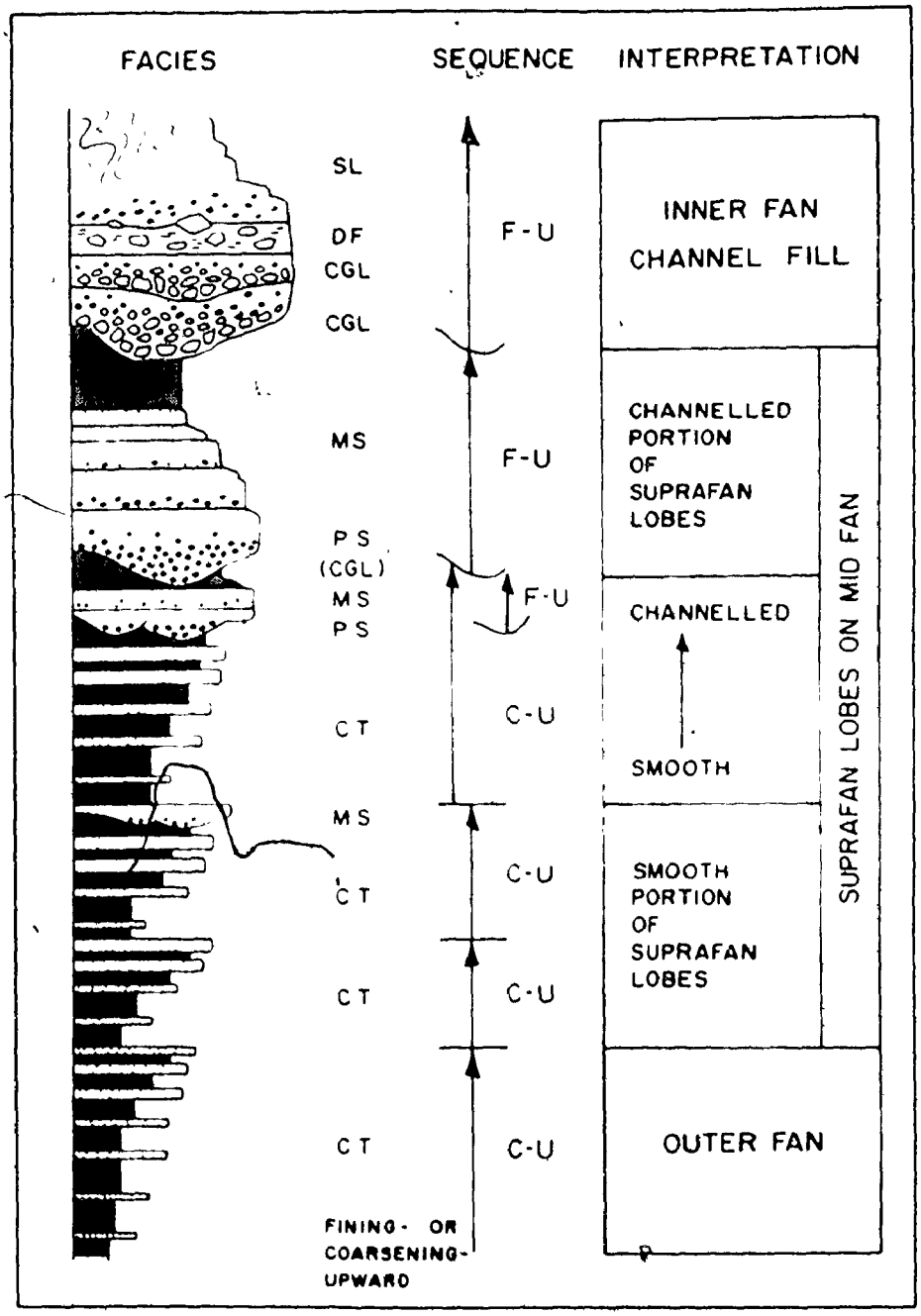

Fig. 1.4. Hypothetical submarine fan stratigraphic sequence produced by fan progradation. C.T., classical turbidite; M.S., massive sandstone, P.S., pebbly sandstone; D.F., debris flow. Arrows show thickening- and coarsening-upward sequences (C-U) and thinning- and fining-upward sequences (F-U). The progradational sequence is based on ancient submarine fan deposits. Figure is taken from Walker (1976).

The Tourelle Formation also provides crucial information concerning initiation of the Ordovician Taconic orogeny (Rodgers, 1970). Prior to Tourelle deposition, the stratigraphic record in the Canadian Appalachians indicates derivation of clastic detritus from the Grenville Province of the Canadian shield (Lajoie and others, 1974; St. Julien and Hubert, 1975), or from a carbonate platform fringing the craton (Rodgers, 1968). These deposits are consistent with what one would expect to find within a continental rise prism deposited on an Atlantic-type, passive, continental margin (Heezen, 1974; Sheridan, 1974). In contrast, the Arenigian Tourelle Formation, along with lithologically similar sandy deposits in western Newfoundland (Stevens, 1970), contains fragments of radiolarian chert, andesitic to rhyolitic volcanic detritus, chromite grains, and rare detrital serpentine (R.K. Stevens, unpubl. manuscript). Because these sediments were deposited shortly before emplacement of allochthonous sedimentary masses and ophiolites on the continental margin (Rodgers, 1965; Williams and Stevens, 1974), it is probable that the Tourelle source terrain was intimately involved in continental margin developments which culminated in orogeny. For this reason, provenance of the coarse sandstone detritus will be studied in an effort to reconstruct tectonic development at this critical time in Appalachian evolution.

Area of Study

The Tourelle Formation is exposed in the area outlined in Figure 1.1. Inland exposures are poor, so that study was confined to the wave-cut platform which is accessible at low tide along the entire coast. Tidal range varies from 3.0 to 4.5 m. Steep to vertical dips allow examination of large cross-sections through the sedimentary section.

Twelve separate outcrop areas (Figure 1.5 a and b; areas A to M, excluding I) were selected for concentrated investigation on the basis of extent and continuity of exposure. These areas are tabulated in relation to standard Military Grid References, aerial photograph numbers (Ministère des Terres et Forêts du Québec), and locality names in Table 1.1. Individual area maps and composite stratigraphic sections are presented in Appendix I.

Regional Setting

Cambrian and Ordovician flysch is preserved in an almost continuous belt along the western side of the Appalachian orogen from Newfoundland to southeastern Tennessee (Enos, 1969a). Much of this belt is allochthonous (Rodgers and Neale, 1963; Zen, 1968; Williams and Stevens, 1974; St. Julien and Hubert, 1975; Williams, 1975). The most recent compilation of Quebec

Fig. 1.5 a and b. Geological map of the study area (a - west, b - east), modified from Biron (1972, 1974). The legend appears on map b. Cap des Rosiers "Formation" should be replaced by Cap des Rosiers Group. Study areas A through M are indicated, and are accompanied by equal-area paleocurrent rose diagrams. These rose diagrams are discussed in Chapter VII.

1 of

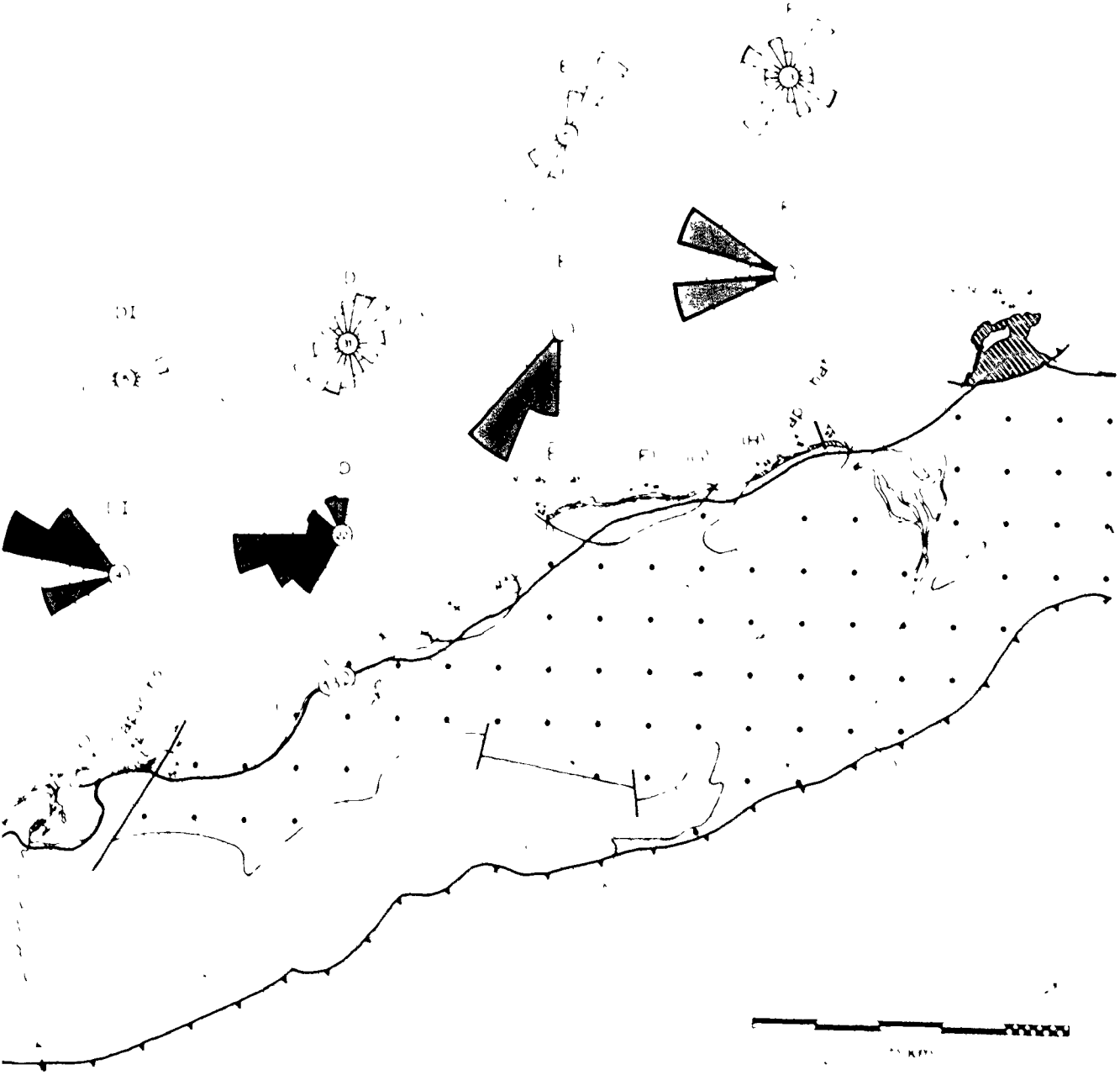

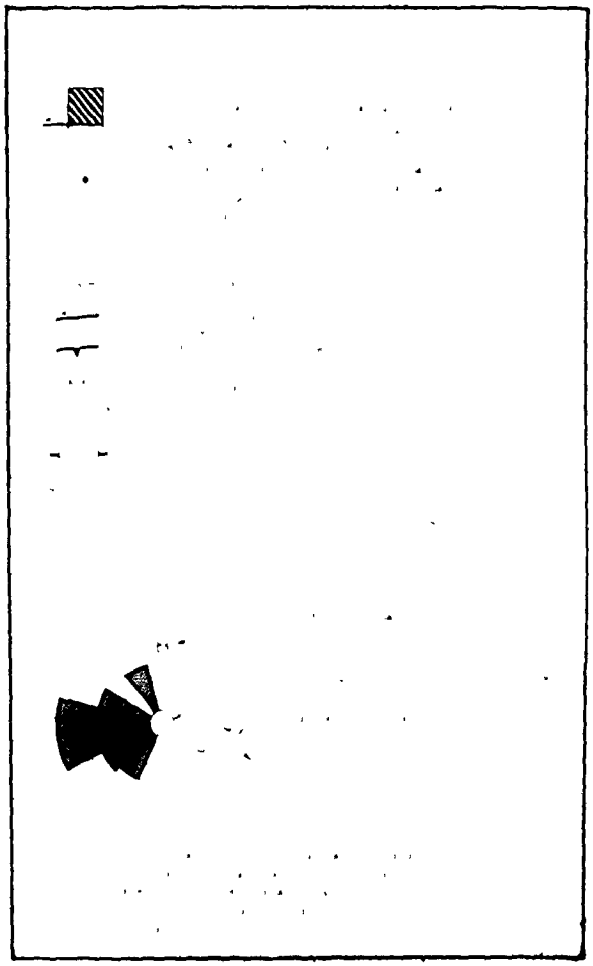

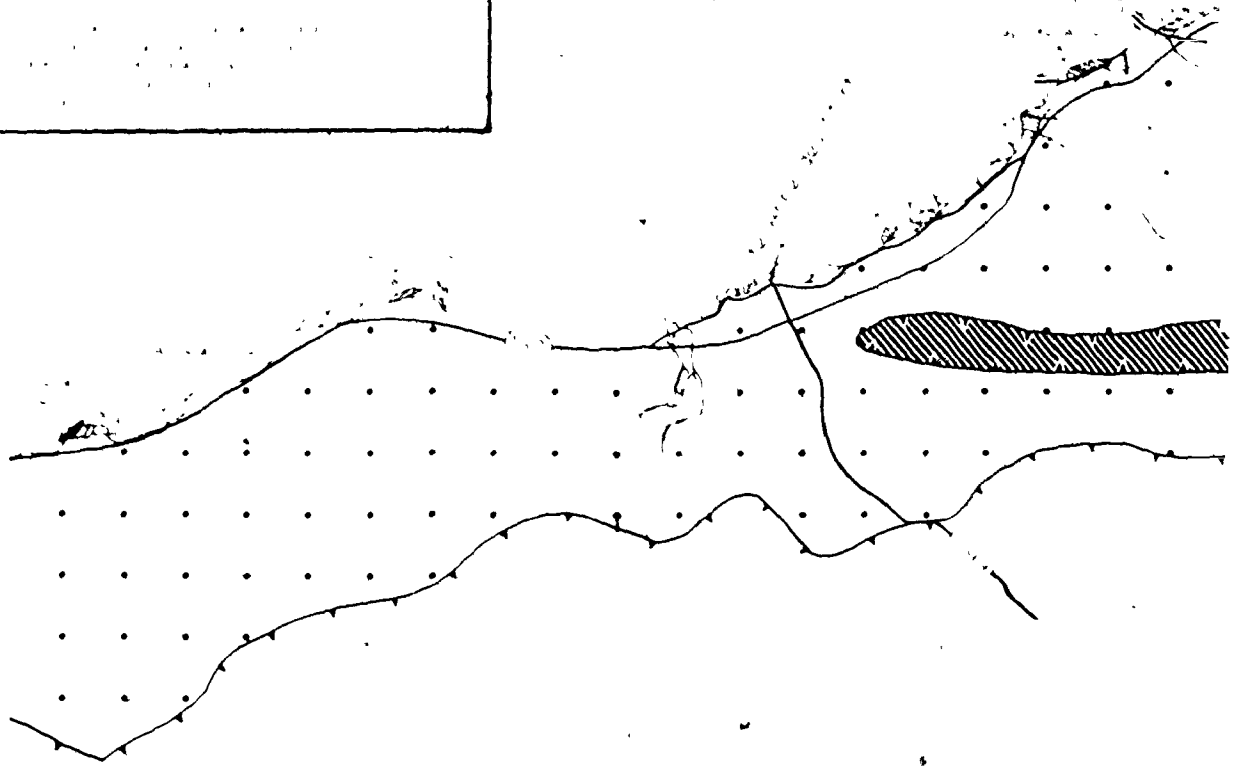

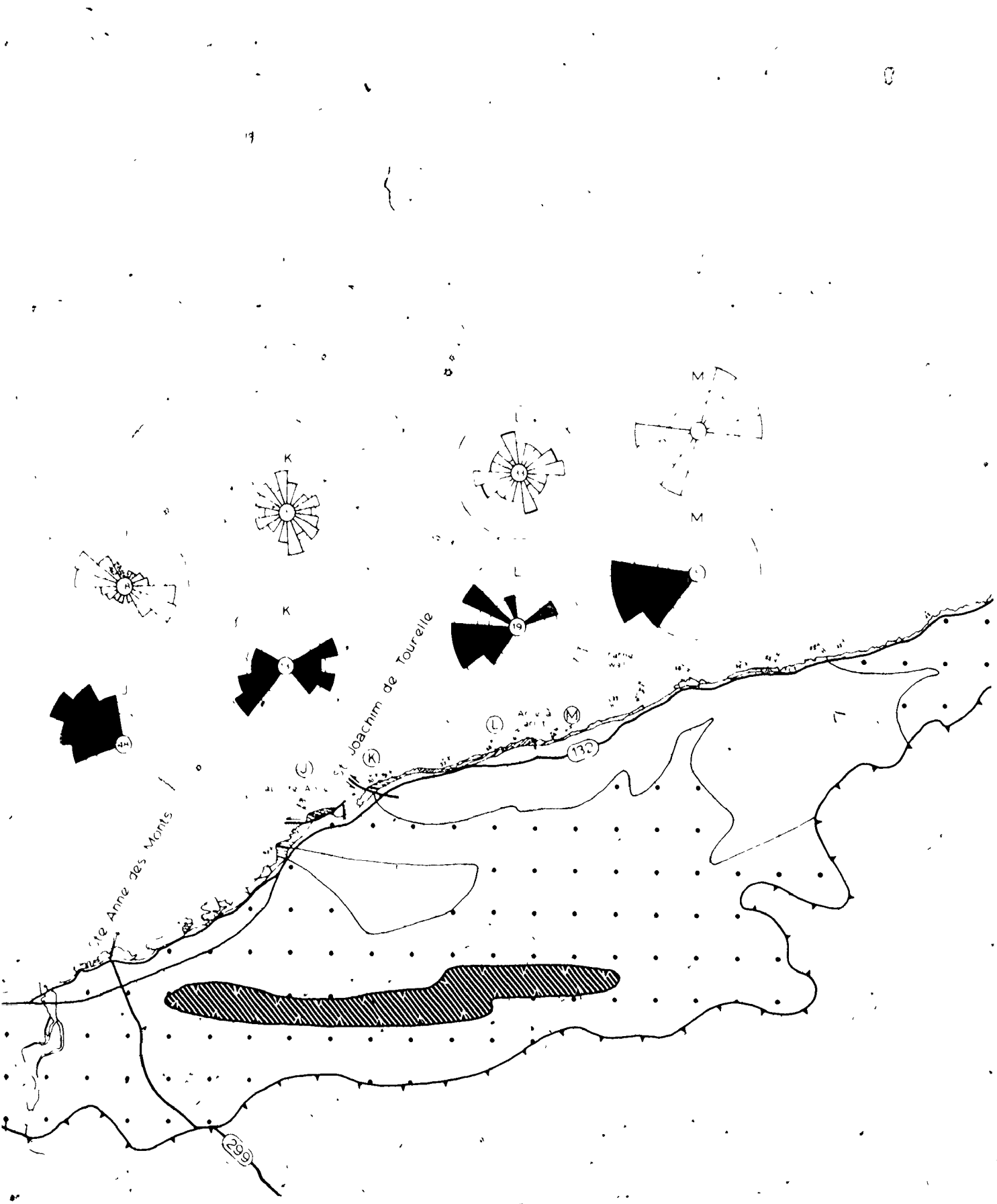
K
L
M
K
L
M
19
Joachim de Tourelle
Ste Anne des Monts
132
299

Table 1.1

Location references and geographic names

Area	Grid reference	Airphoto	Geographic name (if available)
A	502317	Q64105.238-L.4E	Cap des Méchins
B	516323	Q64105.240-L.4E	Petits Méchins
C	530332	Q64105.240-L.4E	Romieu-Dalibaire Tp. line
		Q64105.242-L.4E	
DI	567350	Q64105.246-L.4E	Baie des Capucins (west)
D	584355	Q64105.248-L.4E	Capucins
E	646395	Q64106.96-L.5AW	le Cap-Chat
F	659398	Q64106.94-L.5AW	Ruisseau à Fournier
G	668400	Q64106.94-L.5AW	
H	682405	Q64106.92-L.5AW	ville de Cap Chat
J	875478	Q64106.103-L.6E	Cap Ste-Anne
K	883483	Q64106.105-L.6E	Pointe de la Tourelle
L	909491	Q64106.107-L.6E	Anse à Carlot (west)
M	922495	Q64106.109-L.6E	Anse à Carlot (east)

Appalachian geology is presented by St. Julien and Hubert (1975), from which a simplified regional geological map has been drawn (Figure 1.6). The essential elements to be considered in a regional summary are arranged stratigraphically and in structural stacking order in Figure 1.7.

Shickshock Group

The Shickshock Group can be correlated on lithologic grounds with several other representatives of a metamorphosed shale-feldspathic sandstone assemblage, containing varying proportions of basic volcanic rocks, that occurs throughout the Northern Appalachian and Caledonian belt (Quebec - Masonville Fm, Brompton Fm, Caldwell Group, Armagh Fm, Shickshock Group, Maquereau Fm; Newfoundland - Fleur de Lys Supergroup, Kennedy, 1975a; British Isles - Dalradian Supergroup, Kennedy, 1975b). Cambrian strata of known age found within the allochthonous external domain (St. Julien and Hubert, 1975) are also considered to be lithologically correlative units (Quebec - Charny Group, Anse Maranda Fm, Granby sandstone, Mawcook slate, St. Roch Fm, St. Damase Fm, Orignal Fm, Cap Enragé Fm; Newfoundland - Maiden Point Fm, Summerside Fm).

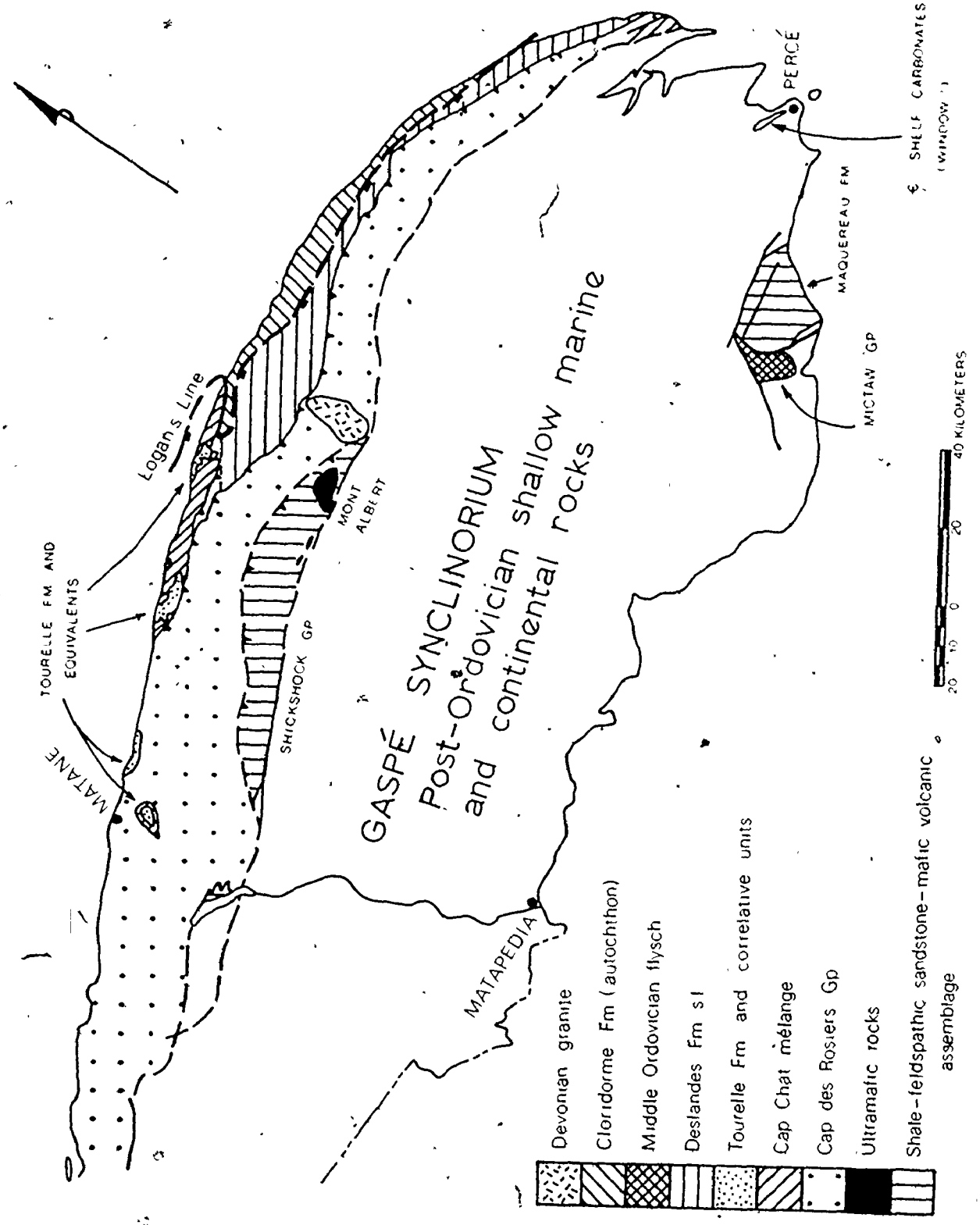

Fig. 1.6. Regional geological map of the Gaspé Peninsula modified from St. Julien and Hubert (1975).

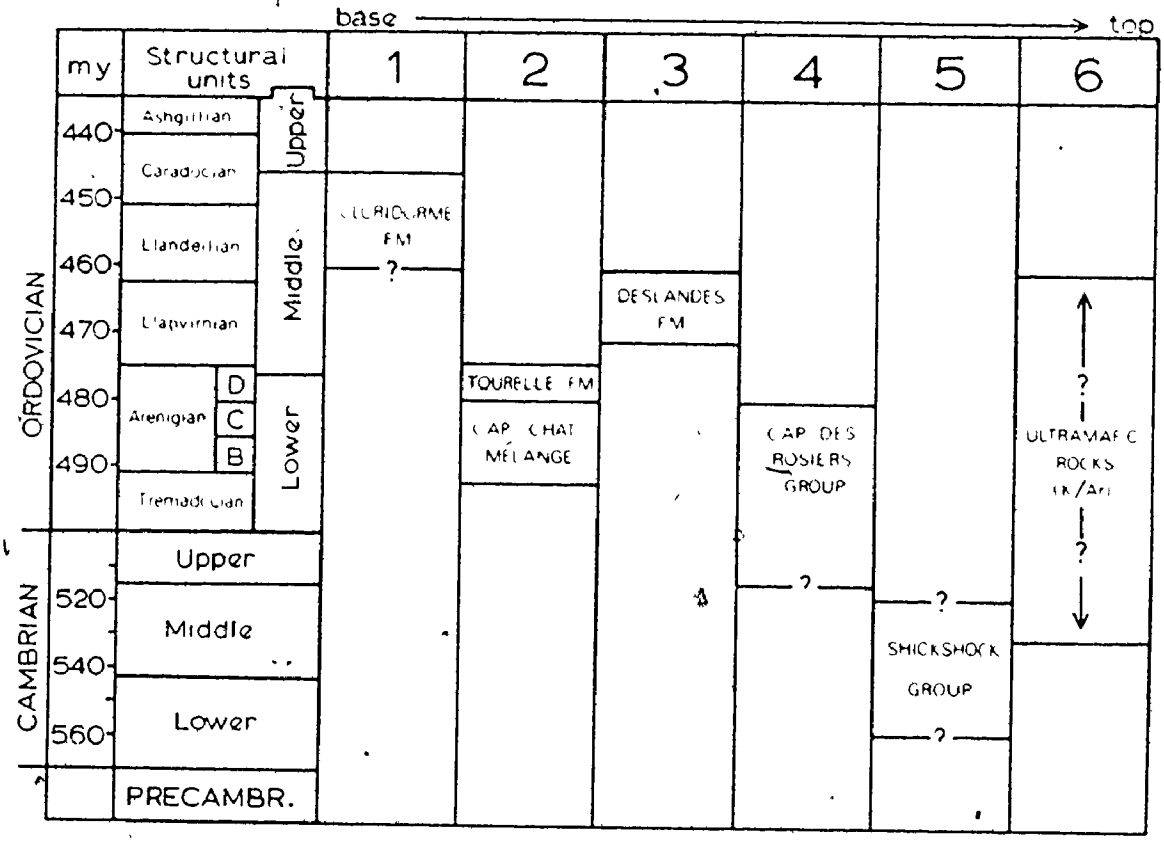

Fig. 1.7. Stratigraphic table of various Cambrian and Ordovician stratigraphic units in, or adjacent to, the study area. 1, autochthon; 2 to 6, separate thrust sheets. Structural unit 3 is generally absent in this area. The lowest allochthonous structural unit contains the Tourelle Formation. Structural unit 4 is the Rivière Ste-Anne nappe. The Cap Chat mélange is lithologically identical to the upper part of the Cap des Rosiers Group. This figure is modified from Biron (1974).

Arkose containing 20-45% feldspar and 28-60% quartz (Ollerenshaw, 1967), and slate are volumetrically more important than volcanic rocks in the area of Lake Matapedia, but the bulk of the Shickshock Group elsewhere is dominated by meta-volcanic rocks (commonly pillowed where least metamorphosed) which reach the albite-epidote-amphibolite facies of regional metamorphism. The exact age of these lavas and associated sediments is uncertain, as is their structural relationship with the Cap des Rosiers Group (Mattinson, 1964; Ollerenshaw, 1967; Poole and Rodgers, 1972, p. 167; Biron, 1974). K-Ar hornblende dates from unaltered amphibolite (440 ± 20 m.y.) and a K-Ar muscovite age (413 ± 16 m.y.) from Shickshock Group samples (Wanless and others, 1973) indicate metamorphic ages or perhaps partial argon loss during the later Acadian orogeny, and not the age of sedimentation or of extrusion of the lava flows.

Ultramafic Rocks

The main outcrops of ultramafic rocks occur on Mont Albert and Mount Serpentine. The former occurrence is best described and will be discussed below. These ultramafic rocks form part of a much more extensive but discontinuous trend of ultramafic bodies from Hare Bay in northwestern Newfoundland to the Canada - U.S.A. border south of Quebec City.

These masses have been interpreted as obducted slices of oceanic crust (Church and Stevens, 1971; Laurent, 1975; Williams, 1975).

Mont Albert consists of serpentinized peridotite with lenses of dunite, pyroxenite, and chromite (MacGregor and Smith, 1963; St. Julien and others, 1972), all dipping at approximately 60° to the south or south-west. The ultramafic body rests on top of a thermal metamorphic aureole approximately 450 metres thick which, along with similar aureoles beneath ophiolite complexes in western Newfoundland (Williams and Smyth, 1973), can probably be interpreted as the result of obduction of hot oceanic crust onto the continental margin. Biotite and muscovite from the Mont Albert aureole (Poole and others, 1964) yield an emplacement age of 495 ± 35 m.y. (K-Ar). This compares well with a hornblende $^{40}Ar/^{39}Ar$ release spectra age for obduction of the Bay of Islands ophiolite in western Newfoundland of 460 ± 5 m.y. (Dallmeyer and Williams, 1975).

Upper Cambrian and Lower Ordovician Strata

Both the Tourelle Formation and lithologies of the Cap Chat Mélange will be discussed in later chapters. Lithologically, the mélange unit is identical to the upper part of the Cap des Rosiers Group in the Rivière Ste-Anne Nappe (Biron, 1974).

The dominant lithologies found in this group are red, green, or banded green and black shales and mudstones, siltstones (siliciclastic, calcareous, and dolomitic), sandstones of sub-arkose to sub-greywacke composition, marly mudstones, ribbon limestones, and continuous resistant bands of quartz arenite and limestone conglomerate. This slope and base-of-slope assemblage, which is characterized by coarse lenses or channels of quartz arenite and limestone conglomerate, occurs throughout the Quebec Appalachians (Lévis Fm, Pointe-de-la-Martinière Fm, St. Hénédine Fm, Stanbridge Fm, Kamouraska Fm, Ladrière Fm) as documented by St. Julien and Hubert (1975). Similar bank-foot limestone breccias occur throughout most of the Appalachian belt, and give a rough estimate of the location of the continental margin in Late Cambrian-Early Ordovician time (Rodgers, 1968).

Middle Ordovician Strata

The Deslandes Formation (Biron, 1974) crops out in a small structural sliver at Cap des Méchins, and comprises siltstone layers with occasional fine sand bases, and thin calcisiltites. Its origin is not known. In contrast, the autochthonous Middle Ordovician Cloridorme Formation, which is best described as classical distal flysch, has been studied in great detail by Enos (1969a,b). Paleoflow in the Cloridorme

was almost exclusively from east to west, and is interpreted to represent axial transport of turbidity currents in an elongate foredeep trough. Petrographic characteristics of the Cloridorme Formation will be examined in Chapter VII.

Previous Work

Logan (1863, p. 262-3) discussed "four synclinal areas occupied by green sandstones of the Sillery series", which are located, from west to east, (1) between Ste-Félicité and Grosses Roches (Béland, 1957), (2) between Les Méchins and Capucins, (3) in the vicinity of Cap Chat, and (4) both west and east of St-Joachim de Tourelle. Logan's hand-sample descriptions and field observations of coarse Tourelle sandstones are outstanding in their detail.

McGerrigle (1954) conducted a regional stratigraphic investigation which included "Deepkill" strata (Tourelle Formation and Cap des Rosiers Group of this thesis) in area (4). He mentioned the presence of several sandstone beds greater than 10 m thick, briefly discussed sedimentary structures, and concluded that the "Pillar sandstones" were shallow-water deposits. He also observed the segregation of facies into packets of coarse sandstone beds, and thick shaly horizons. Perhaps the most important conclusion of McGerrigle's study, however, is that graptolite fauna collected

from shales in the Tourelle Formation correspond to the uppermost zone D (Raymond, 1914) of the Lévis Formation at Quebec City. Zone D correlates with the Glyptograptus dentatus zone of late Arenig time.

Biron (1972, 1973, 1974, Ph.D. thesis Laval University) has remapped Cambrian and Ordovician rocks north of the Gaspé Synclinorium from Mont St-Pierre (east of Marsoui) to Les Méchins. His maps and stratigraphic compilations were invaluable in the early stages of research for this thesis, and show all outcroppings of the Tourelle Formation, which comprises Logan's "Pillar sandstones", interbedded siltstones and shales, thick shale horizons, and dolomitic siltstones. As a result of Biron's work, the Tourelle Formation has been formally recognized in Logan's areas (2), (3), and (4).

Age and Correlative Units

Riva (personal communication, 1975) has confirmed McGerrigle's correlation of the Tourelle Formation with zone D of the Levis Formation. Corresponding graptolite zones in Britain are the Didymograptus hirundo (7) and the lower D. bifidus (8) zones. Dewey (1974) lists the Isograptus caduceus (8) zone as a standard North American equivalent, whereas the corresponding zone proposed by Berry (1960) from studies in Texas is the Pseudoclimacograptus tentaculatus zone.

All of the above are indicative of late Arenig to very earliest Llanvirn time.

Tourelle-like lithologies are not restricted to that area outlined in Figure 1.1. Units of the same or similar age are the Blow-Me-Down Brook Formation in the Humber Arm allochthon of western Newfoundland (Stevens, 1970), and parts of the Métis Formation of Liard (1973) between Matane and Mont Joli. In addition, impure sandstones of Logan's area (1) between Ste-Félicité and Grosses Roches (Béland, 1957), although undated, are assumed to be a continuation of the same lithologic unit. If it is indeed true that these mineralogically distinctive and lithologically similar units are time correlative, and that they were all the result of the same tectonic event in the orogenic belt, then the total length of continental margin involved in this late Arenigian diastrophism and clastic sedimentation would be approximately 1000 km.

Structure

The large scale structural pattern is that of a stack of imbricated nappes with the nappes containing the oldest rocks generally resting upon those containing the youngest rocks (St. Julien and Hubert, 1975). The line of intersection between the frontal thrust of the nappe zone and the present

land surface is called Logan's Line.

The Tourelle Formation, and underlying Cap Chat "mélange", occupy the lowest structural unit of the allochthon (Figure 1.7). This lowest slice is overlain by the Rivière Ste-Anne Nappe, and is characterized by shallow plunging folds trending ENE and overturned to the northwest. These first folds show no cleavage development. Later modifications include brittle faulting, gentle folding about north-south axes, and local cleavage development. A more detailed evaluation of the style of deformation in the chaotic portion of the Cap des Rosiers Group immediately below the Tourelle Formation will be given in Chapter VIII.

Aims and Outline of the Thesis

The thesis can be divided into three parts.

(i) Chapters II and III describe the various sedimentary facies found in the Tourelle Formation, and the spatial inter-relationship of these facies. The purpose of these chapters is to discover the specific depositional environments of thick, coarse, massive sandstones in the Tourelle submarine-fan system, and to provide additional information on facies organization in deep-sea fan deposits.

(ii) Chapters IV and V are concerned with fabric and depositional mechanisms of thick massive sandstones in the

submarine environment.

(iii) The remaining chapters of the thesis (VI to IX) consider composition and provenance of sandstone detritus (Chapters VI and VII), basin analysis and paleogeography (Chapters VIII and IX), and reconstruction of tectonic events which led to initiation of Tourelle deposition and which culminated in emplacement of sedimentary nappes and ophiolites on the continental margin of North America (Chapter IX).

CHAPTER II

FIELD DESCRIPTION: TOURELLE FORMATION

Field Methods

Seven months were spent in the field during the summers of 1974, 1975, and 1976. All except one month was spent working within the boundaries of the Tourelle Formation.

Low tide aerial photographs at a scale of 1:9600 (flown 1964) allowed the available coastal outcrop of the formation to be scrutinized for structurally unbroken and stratigraphically continuous localities amenable to detailed sedimentological studies. Twelve such localities are labelled alphabetically in Figure 1.5. Within each of these "areas", one or more stratigraphic section was measured. Except in the case of multiply interbedded thin siltstones and shales, each sedimentary layer was measured and described in relation to thickness, basal and upper grain sizes, grading, contacts, sedimentary structures, composition, colour, and any outstanding features such as the inclusion of large allochthonous blocks or the presence of fluid-escape structures. Grain size was estimated by comparison with

prepared discs of sieved sand encompassing one phi (ϕ) intervals from -1 ϕ to 5 ϕ. (Dimensionless grain size in phi units is defined as negative logarithm to the base 2 of grain size in mm.) Comparison of visual estimates with grain size distribution curves (Chapter V) indicates that this method yields an estimate of the coarsest quartile of the size distribution. A similar method of grain size determination in the field was employed by Ricci Lucchi (1969b), although he described the measure as an estimate of modal size.

In general, more than one section was measured at each locality, allowing lateral correlation and tracing of individual beds. These within-area correlations were only rarely hampered by apparent strike-slip faults with stratigraphic displacements of up to 100 m (see area L outcrop map, Appendix I). In many of these cases, correlations were nevertheless possible as a consequence of the appearance of persistent sandstone beds in thick shale horizons on either side of the fault. Complete stratigraphic sections with inter-section correlations are available for each area in the rear pocket of the thesis.

Paleocurrent measurements were recorded using a protractor and spirit level mounted on a plexiglass sheet. Because fold plunges are generally less than 10° to 15°, current measurements were simply rotated about the strike

direction (Ramsay, 1961), except at areas A and M where further plunge corrections were necessary.

Nomenclature

Several features of the Tourelle Formation, such as the presence of thick amalgamated sandstones with unusual sedimentary structures, require the presentation of a consistent and simple descriptive nomenclature (Figure 2.1).

A bed is a lithologically homogeneous sedimentary unit, or a unit showing only minor internal lithological variation, which was originally deposited on a more or less horizontal surface. A bed need not be structurally homogeneous, and may contain erosion surfaces suggesting depositional breaks. A bed composed of more than one layer is termed an amalgamated bed (Walker, 1966).

A layer is a sedimentary unit not broken by recognizable internal erosion surfaces or other discontinuities indicating a break in sedimentation (Wood and Smith, 1959; Stanley and Bouma, 1964; Ricci Lucchi, 1969a). A layer need not be structurally homogeneous provided that the boundaries between different structural divisions are gradational. A layer represents the sediment deposited by one sedimentation event.

A division is a structurally homogeneous part of a

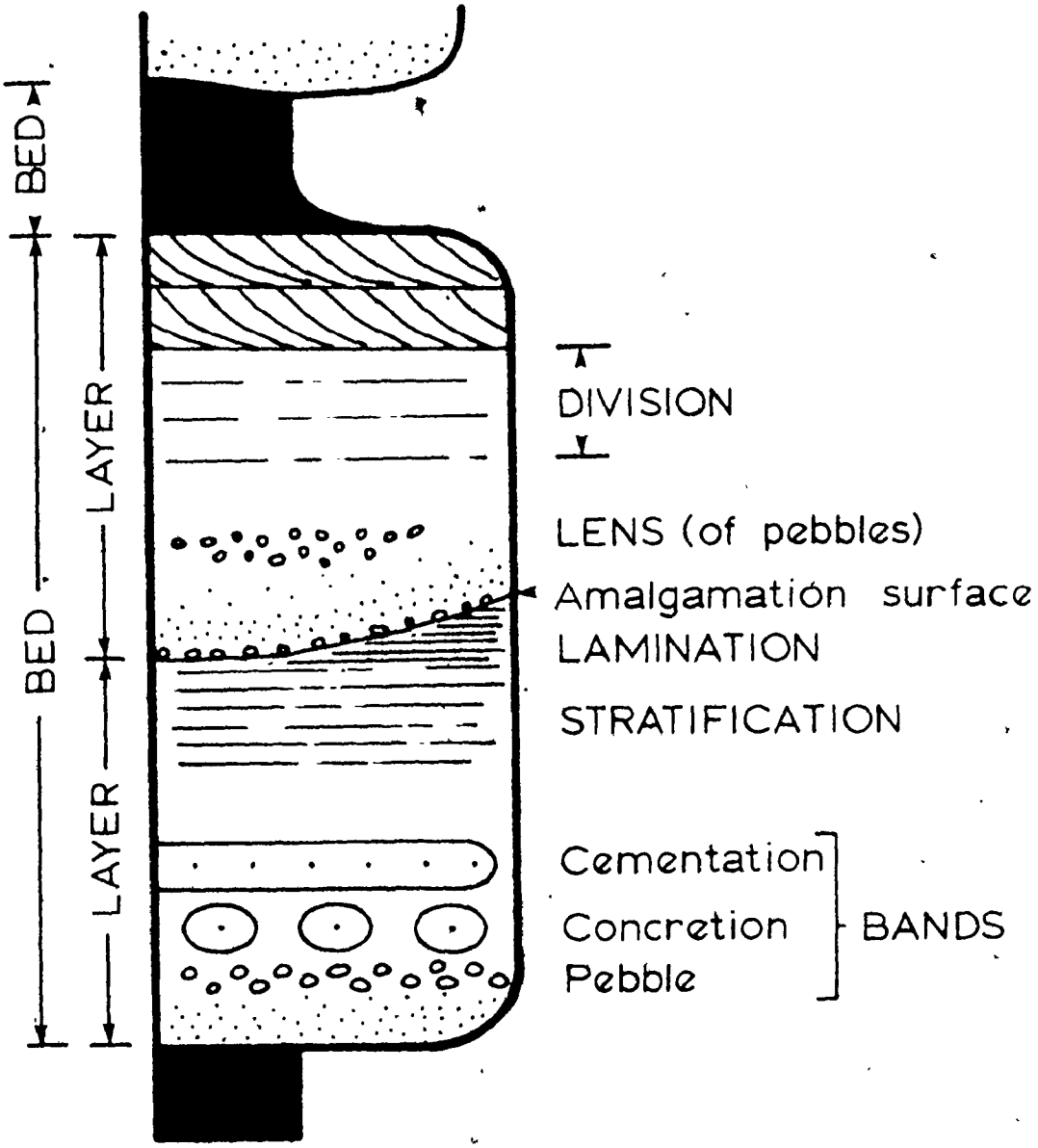

Fig. 2.1. Graphic summary of terminology used for outcrop subdivision. See text for definitions.

layer. In turbidite classification, the five divisions of Bouma (1962) are frequently employed. Bouma's original term "interval" is replaced by division as suggested by Walker (1965).

A band is a part of a layer which differs from the remainder in terms of colour, presence of pebbles or concretions, cementation, etc., and is horizontally continuous. This allows the following variations: pebble band, concretion band, cementation band.

A lamination is a more or less distinct alternation of materials which differ one from the other in grain size or composition. The spacing of this alternation must not exceed one centimetre. Lamination at an angle distinctly different from the horizontal is called cross-lamination.

Stratification is identical to lamination but with no restriction on thickness. In this thesis it is used as a general term if spacing of the alternations is greater than one centimetre. The individual components of a division of stratification are called stratification bands.

General Facies Classification

During field study, 4323 m of stratigraphic section were measured within the Tourelle Formation. Because several overlapping sections were measured at most localities, only

2364 m of this total can be viewed as unique stratigraphy. Correlations were not possible between separate outcrop areas, so that time correlative strata may have been measured more than once. For this reason, it is suspected that the entire formation may only be 500 to 1000 m thick, although its top is never exposed.

Sedimentary facies are classified below on the basis of field experience gained during study of the Tourelle Formation. These facies are considered to be the most useful for descriptive purposes. Throughout the thesis, underlined short forms, presented below, will be used as facies descriptors.

Facies 1: thick shale horizons - thick shale (1).

Facies 2a: interbedded grey shale and siliciclastic siltstones, with rare calcisiltites - siltstones (2).

Facies 2b: interbedded red or green shale and yellow-weathering dolomitic siltstones - dolomitic siltstones.

Facies 3: slurry sandstones (3).

Facies 4: sandstones less than 2 m thick, graded, and with the top preserved - thin sandstones (4).

Facies 5: sandstones less than 2 m thick, graded, and with a truncated top - truncated sandstones (5).

Facies 6: thick sandstones (6):

subfacies 6a: layers less than 2 m thick, composed of pebbly granular material;

subfacies 6b: all graded sandstone layers greater than 2 m thick;

subfacies 6c: all coarse sandstone layers with no grading or only very slight grading near the top of the layer.

Facies 7: conglomerate.

Facies 8: slumps and olistoliths.

Facies 9: clastic injections (dikes and sills).

Table 2.1 indicates the abundance of each facies within the Tourelle Formation. In this table, and in all ensuing discussion, "Tourelle Formation" will refer only to the 2364 m of unique section previously mentioned. Shale constitutes only 19% of this thickness. Figure 2.2 presents histograms of layer thickness for each of the above facies except dolomitic siltstones and conglomerate, both of which are uncommon. These histograms are plotted using a geometric scale of layer thickness, because it is generally observed that the frequency distribution of this variable is approximately log-normal (Ricci Lucchi, 1969a). Means are arithmetic means.

Table 2.1

Facies proportions and mean characteristics for the Tourelle Formation

Facies	No. of layers or horizons (facies 1, 2)	Percent of section	Thickness (cm)		Succeeding shale	
			$\bar{x}$	s	$\bar{x}$	s
1	52	6.2	274	221		
2a	203	12.9	147	281		
2b	3	0.1	46	23		
3	233	4.3	43	33	5	9
4	576	16.0	64	46	8	11
5	556	17.1	71	48		
6a	32	1.3	94	51	2	7
6b	198	32.5	379	225	4	12
6c	17	3.3	443	537	6	22
7	2	0.1	106	43		
8	11	0.4	91	64		
9	13	0.1	20	14		

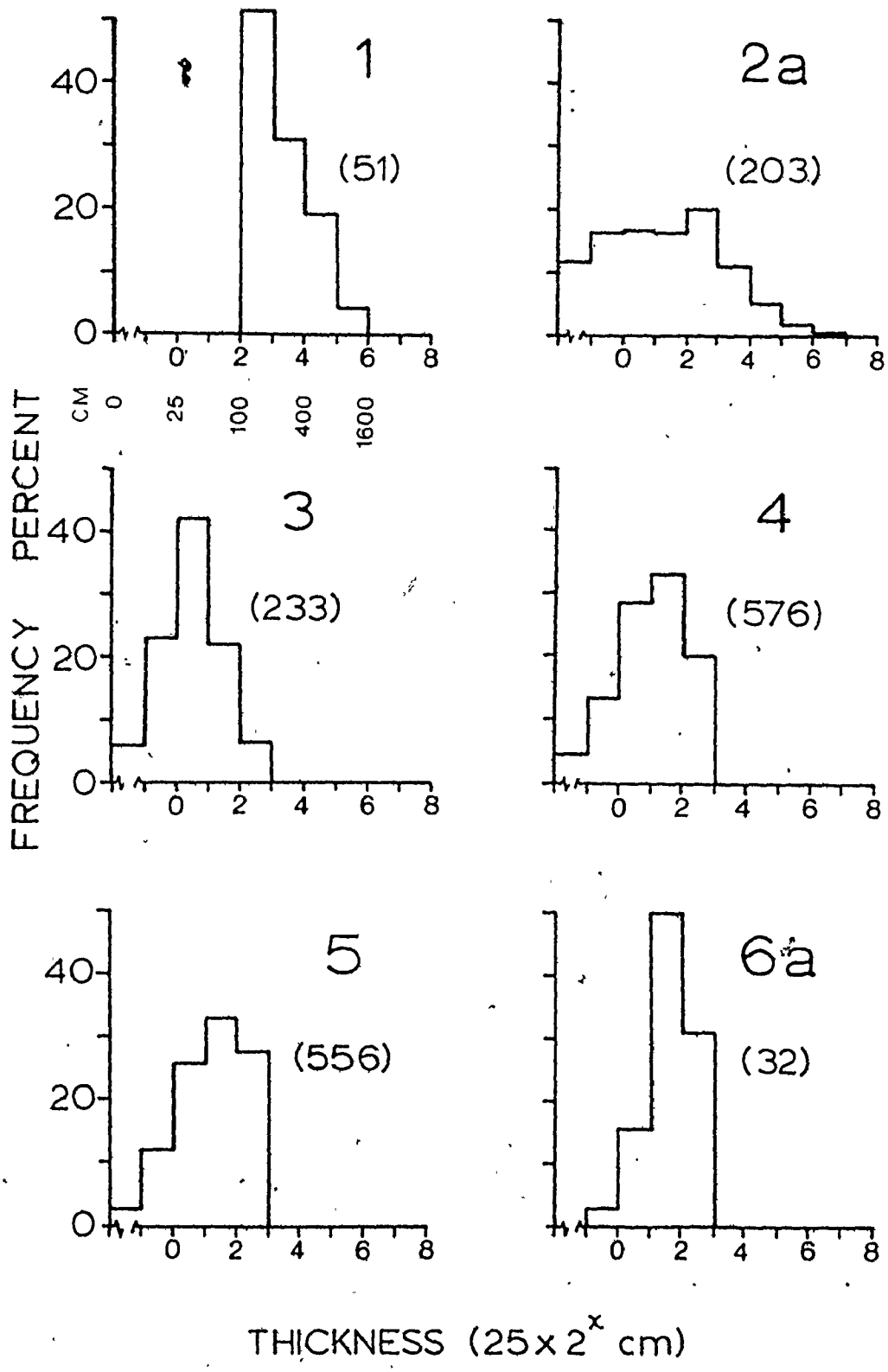

Fig. 2.2. Caption on next page.

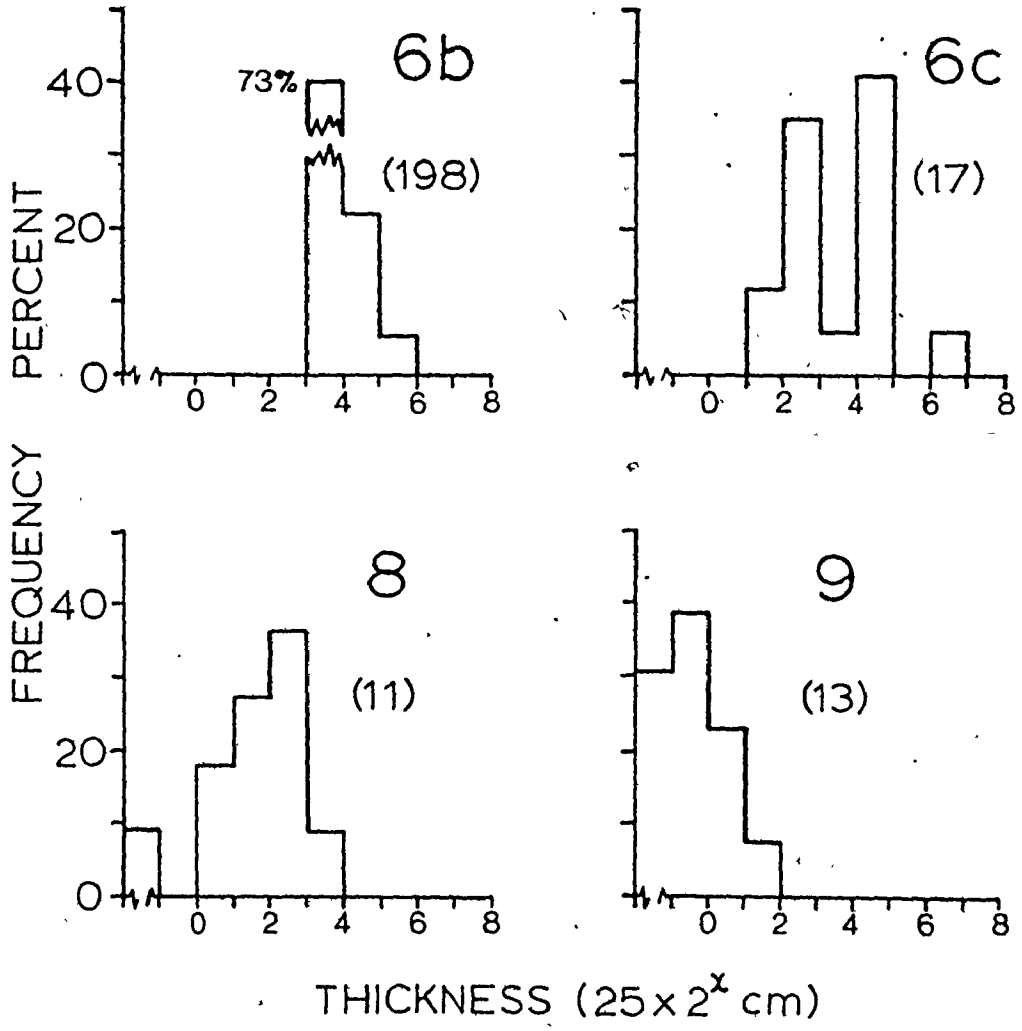

Fig. 2.2 continued. Histograms of (i) facies thickness for facies 1 and 2a, and (ii) layer thickness for facies 4, 5, 6 (a, b and c), 8, and 9. Numbers along the thickness scale are exponents which must be applied to base 2. The resultant is then multiplied by 25 to give thickness in centimetres. Thickness in centimetres is provided for facies 1 as an example. The number of separate units or layers is presented in brackets below the facies number. Facies 9 (clastic injections) does not include sills at the base of area J.

The major clastic facies are subdivided in Table 2.2 on the basis of occurrence and sequence of internal depositional structures. Siltstones (2) and thin sandstones (4) contain a significant number of layers which can be described by the Bouma (1962) scheme of turbidite classification. These are designated as classical turbidites (Walker, 1976). Truncated (5) and thick sandstones (6) contain important proportions of both massive sandstones and sand layers with sedimentary structures that are uncommon in most turbidite formations.

Facies 1: thick shale horizons

This facies is restricted to shale beds greater than 100 cm thick above siltstones (2), or shale beds greater than 100 cm thick above sandstones after subtracting a "turbidite shale" allowance of 50% of the sandstone layer thickness (up to a maximum of 50 cm).

Shales are commonly massive, and break into disc-shaped fragments having conchoidal boundaries. Colour is 5G 3/1 (Goddard and others, 1970). Beds may also be cm-laminated with alternating grey and green-grey bands.

Table 2.2

Facies breakdown according to sedimentary structures and sequences

	Structure or sequence	Percent abundance for each facies						
		2a	3	4	5	6a	6b	6c
CLASSICAL TURBIDITES	$T_{a(d)}$	1.6	80.7	50.2	68.7	90.6	42.4	76.5
	$T_{ab(d)}$	0.5	-	4.0	5.0	3.1	2.0	-
	$T_{abc(d)}$	0.7	-	9.2	1.8	-	0.5	-
	$T_{ac(d)}$	1.4	13.3	20.5	3.8	-	9.1	-
	$T_{b(d)}$	4.8	0.4	1.6	1.6	-	0.5	-
	$T_{bc(d)}$	14.7	0.4	2.8	0.2	-	-	-
	$T_{c(d)}$	69.4	4.3	0.5	0.2	-	-	-
	T_d	4.6	-	-	-	-	-	-
	reversals	2.3	0.4	0.5	0.4	-	0.5	-
EXOTIC	≺	-	0.4	3.0	3.4	-	3.5	-
	≺ & —··—·—	-	-	0.5	-	-	2.5	-
	—···—	-	-	6.6	10.8	3.1	26.8	11.8
	scour lam.	-	-	1.0	5.2	3.1	14.1	11.8

≺ - Cross-stratification; —··— - coarse near-horizontal stratification

Facies 2a: interbedded shale and siltstones

The general aspect of this facies is shown in Figure 2.3. The siltstones are generally siliciclastic, with less than 2% calcisiltites. Shale averages 57%, with a range between 10% and 90%. Individual siltstone layers are 1 to 50 cm thick, with rare thicker exceptions. Colour both fresh and weathered is 5G 3/1. Ripples and ripple-drift cross-lamination are by far the most common depositional structures, with various degrees of convolution superimposed (Figure 2.4). The climbing ripples most closely resemble types A or C of Jopling and Walker (1968). These ripples are generally not straight-crested, but rather have a sinuous form, which appears to be the prime cause of stoss side erosion (type A). This erosion results in the exposure of ripple-troughs on the upper obliquely beveled surfaces of some siltstone (2) layers. Current directions inferred from this rib-and-furrow structure agree with directional sole mark orientations. Sole marks are restricted to rare deposit-feeder trails, narrow grooves (striations), and microflutes, which are scour marks propagated from vertical worm-tube defects originally present in the underlying shale.

Because the material comprising the siltstone layers is of very fine sand to coarse silt size (3 ϕ to 5 ϕ), grading is not an obvious feature. Bases are sharp, however, and tops grade into overlying shale. In 2.6% of these layers,

Fig. 2.3. Facies 2a: siltstones (2)

(A) Interbedded siltstones and shale below Cap Ste-Anne channel. Note thickening upward trend in siltstones. Top is to the left.

(B) Thick horizon of siltstones at area FIV. Top is to the right. Scale 1 m.

(C) Abundant centimetre-thick siltstones separated by silty shale partings, area FIV. Scale in centimetres.

(D) Abundant siltstones above Cap Ste-Anne channel fill. Top is to the right. Thickest beds are about 20 cm thick. This horizon is compared with area K in Figure 2.37.

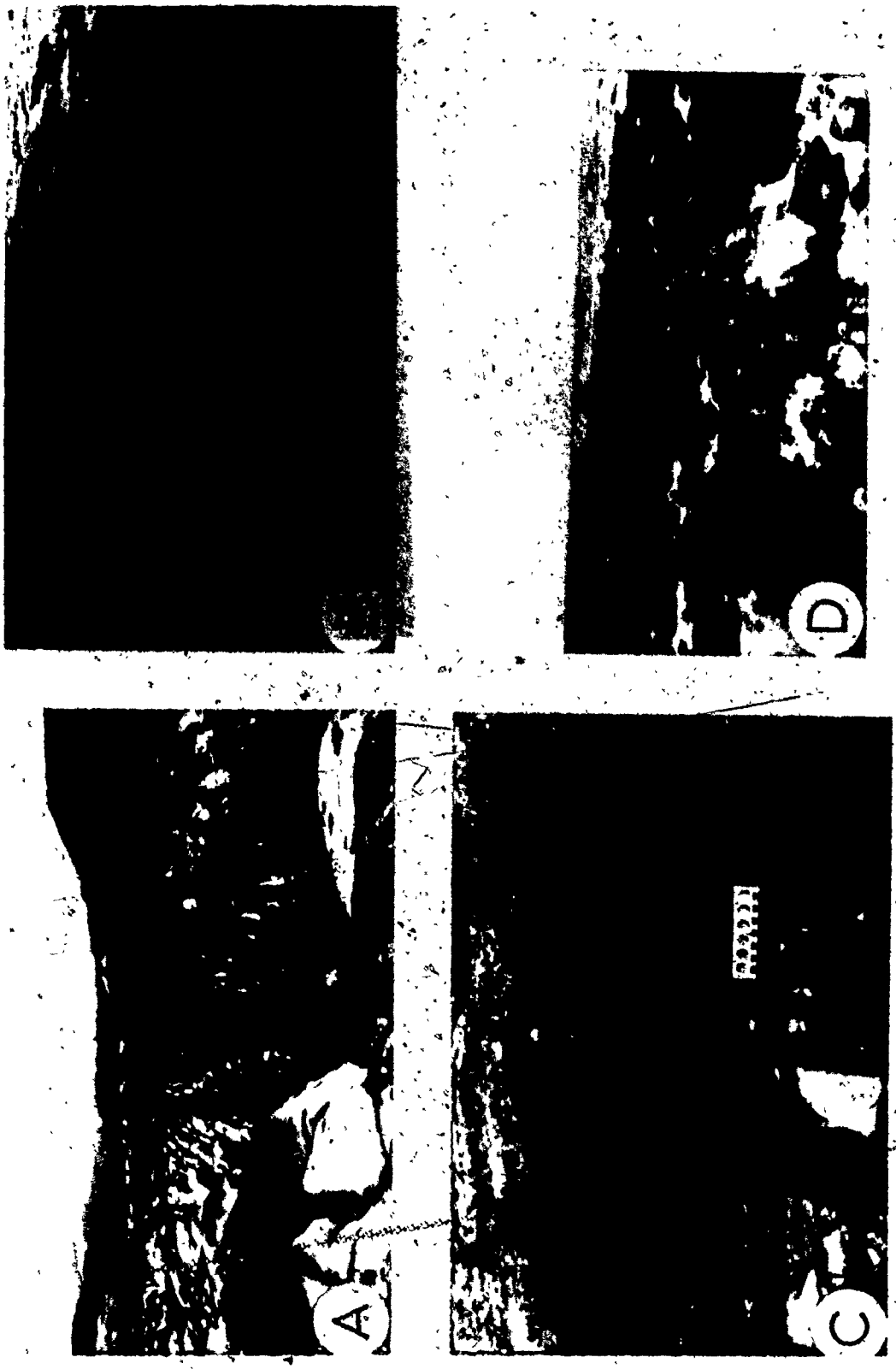

FIG. 2.3

Fig. 2.4. Facies 2a: siltstone sedimentary structures.

(A) Ripple-drift cross-lamination in a siltstone layer above the Cap Ste-Anne channel, area J. Scale in centimetres.

(B) Amalgamated siltstone bed above the Cap Ste-Anne channel, area J. Both layers are rippled. Note deformed ripples in upper layer.

(C) Strongly convoluted siltstone, area J. Scale bars are 10 cm.

(D) Upper surface of siltstone layer in lowest shaly horizon, area L. Ripples have unusually straight crests (picked out by white chalk). Scale in centimetres.

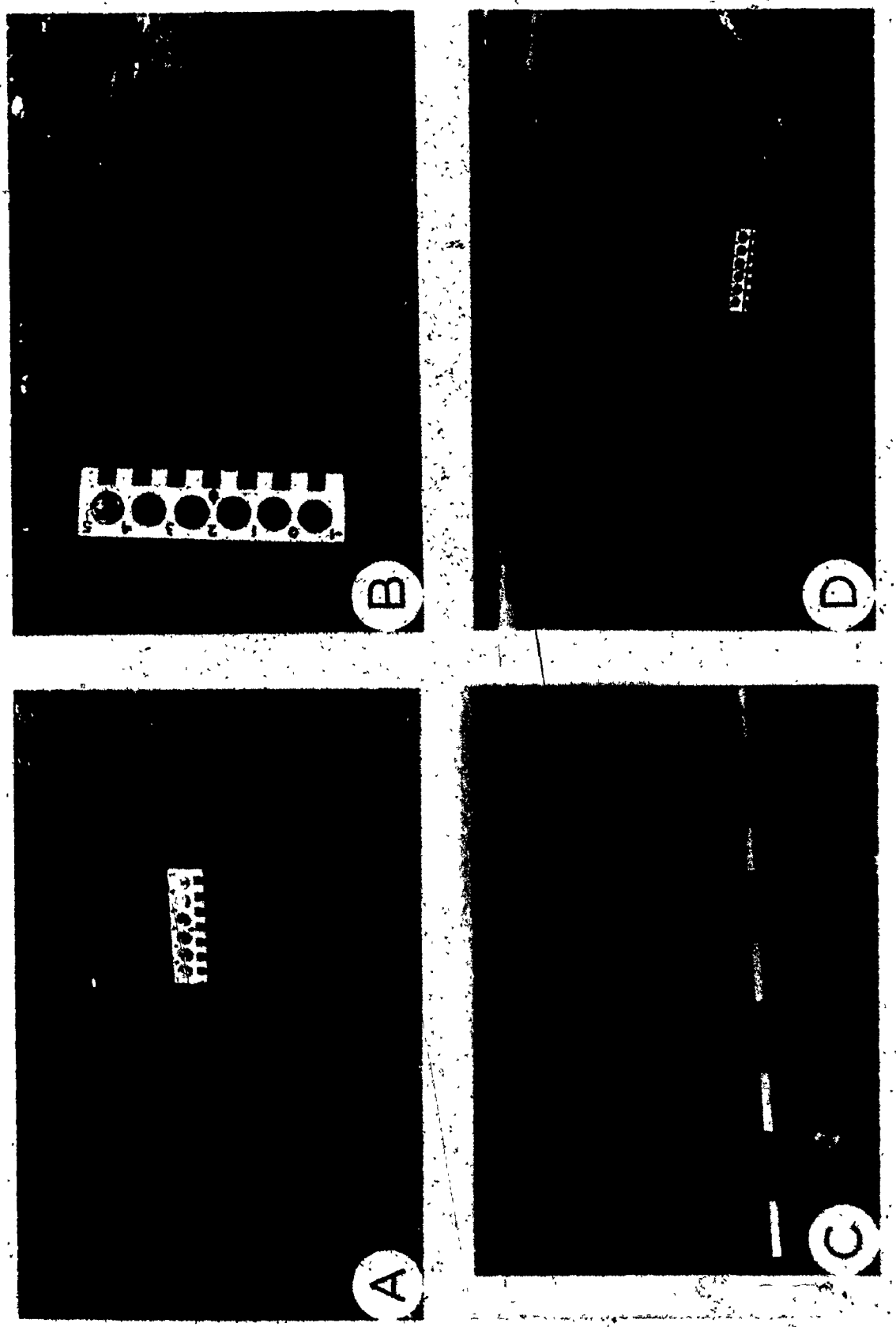

FIG. 2.4

basal grain size rises to 2 ϕ, and grading is easily visible.

Table 2.2 (p. 35) shows the proportion of layers in this facies which can be assigned to variations of the Bouma turbidite model. Note that for this facies, as distinct from all others listed, 74% of all individual siltstone layers are not represented due to either poor exposure, thinness, or grouping of many thin layers during section measurement. Hence Table 2.2 summarizes data only for thicker, better exposed layers.

Facies 2b: interbedded shale and dolomitic siltstones (Figure 2.5)

Shale in this facies has a "primary" red colouration (10R 3/4) with reduction to green (5G 2/1) in bands parallel to bedding or in envelopes around clastic injections. Individual dolomitic siltstone layers range from 1 to 10 cm in thickness and show various combinations of ripples, convoluted ripples, convolute lamination, and parallel lamination. Ripples may have thin red or green mud drapes (Figure 2.5), suggesting either alternating periods of ripple migration and fall-out of clay-sized particles from the overlying water column, or deposition of silt and clay together with the latter consisting of flocculated mud pellets.

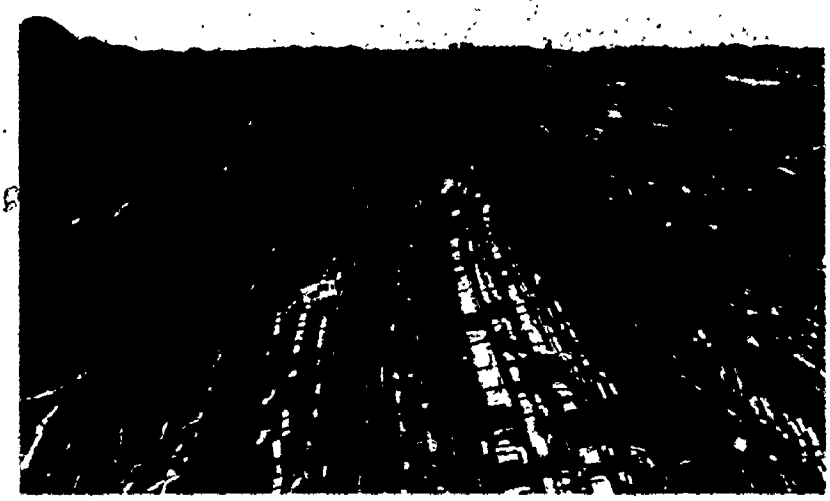

Fig. 2.5. Dolomitic siltstone facies at the base of area J. Resistant beds are siltstone. Shale is red and green. Large bars on notebook are each 5 cm. Top is to the right.

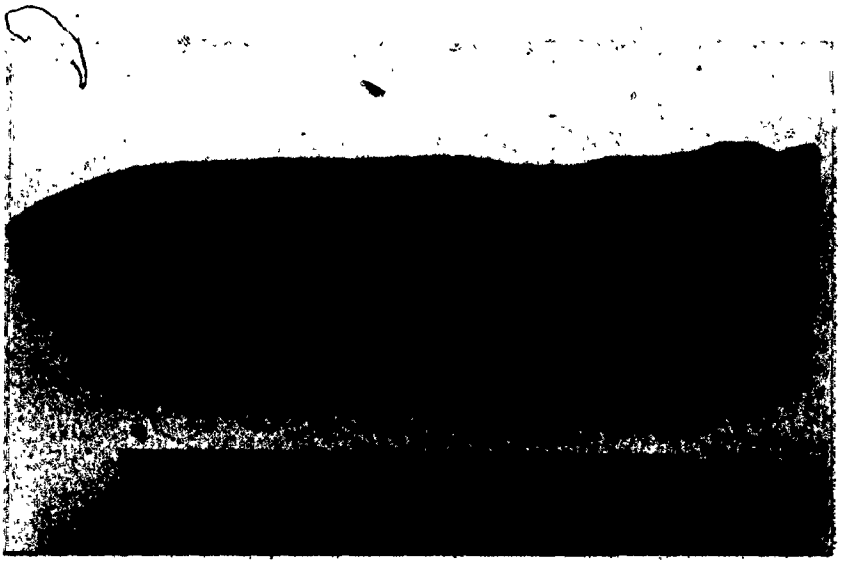

Rippled dolomitic siltstone layer with red (dark) mud drapes. Some ripples are deformed. Scale is in centimetres and inches.

Both horizontal trails and vertical worm tubes are common sole markings, but the siltstones themselves are not bioturbate. No inorganic sole markings have been found in this facies of the Tourelle Formation, although a few identical dolomitic siltstones in the underlying Cap des Rosiers Group display flutes or grooves (Chapter VIII). These yellowish-weathering siltstones occur only at the base of the formation, and in fact serve to mark the lower formational boundary both by their abundance (siltstone: shale = 7:3) and by their association with red shale and clastic injections. At area A, rare thin chert bands are also present.

A partial cation analysis of a dolomitic siltstone layer west of Marsoui (Jones, 1934) can be interpreted in terms of carbonate minerals as follows:

$(CaMg_{0.97}Fe_{0.03})(CO_3)_2$	71.5%
FeO	1.6%
Al_2O_3	3.5%
insolubles (quartz?)	23.4%

Facies 3: slurry sandstones

This facies is characterized by fine to coarse sand dispersed in abundant muddy matrix. One to two cm shale chips with random orientations are ubiquitous (Figure 2.6). Larger shale and chert clasts, and slabs of shale and calcisiltite up to several metres long, are not uncommon. Massive layers account for approximately 80% of this facies. Of these, 20% contain rip-up clasts between 10 and 100 cm in apparent length, and 6% contain slabs from 1 to several metres in length, in spite of the fact that the mean layer thickness is only 43 cm. These layers are easily weathered, and in areas of poor exposure can be mistaken for shale. Fortunately, light green and blue-green (5BG 6/2) shale rip-up clasts help circumvent this problem. Bases are with few exceptions flat and sharp, while tops grade into shale. A swirled appearance, convolute bedding, and pseudonodule formation are locally developed. This facies is in some cases laterally associated with slumps and olistoliths, suggesting a genetic link.

Morris (1971) suggests that "slurried bedding" (Wood and Smith, 1959, p. 173) is emplaced by slumping of loose sand and varying amounts of mud. This explanation appears justified for Tourelle slurry sandstones (3).

Fig. 2.6. Facies 3: Slurry sandstones (3).

(A) Vertically oriented limestone clast at area L. Scale in centimetres.

(B) General appearance of a slurry sandstone layer (area D) with abundant black and pale green shale rip-ups. Note dispersed coarse sand grains.

(C) Slurry sandstone layer at area L containing large block of green shale.

(D) Amalgamation surface between two facies 3 layers at area B. Note abundant disoriented shale chips and dispersed coarse sand grains.

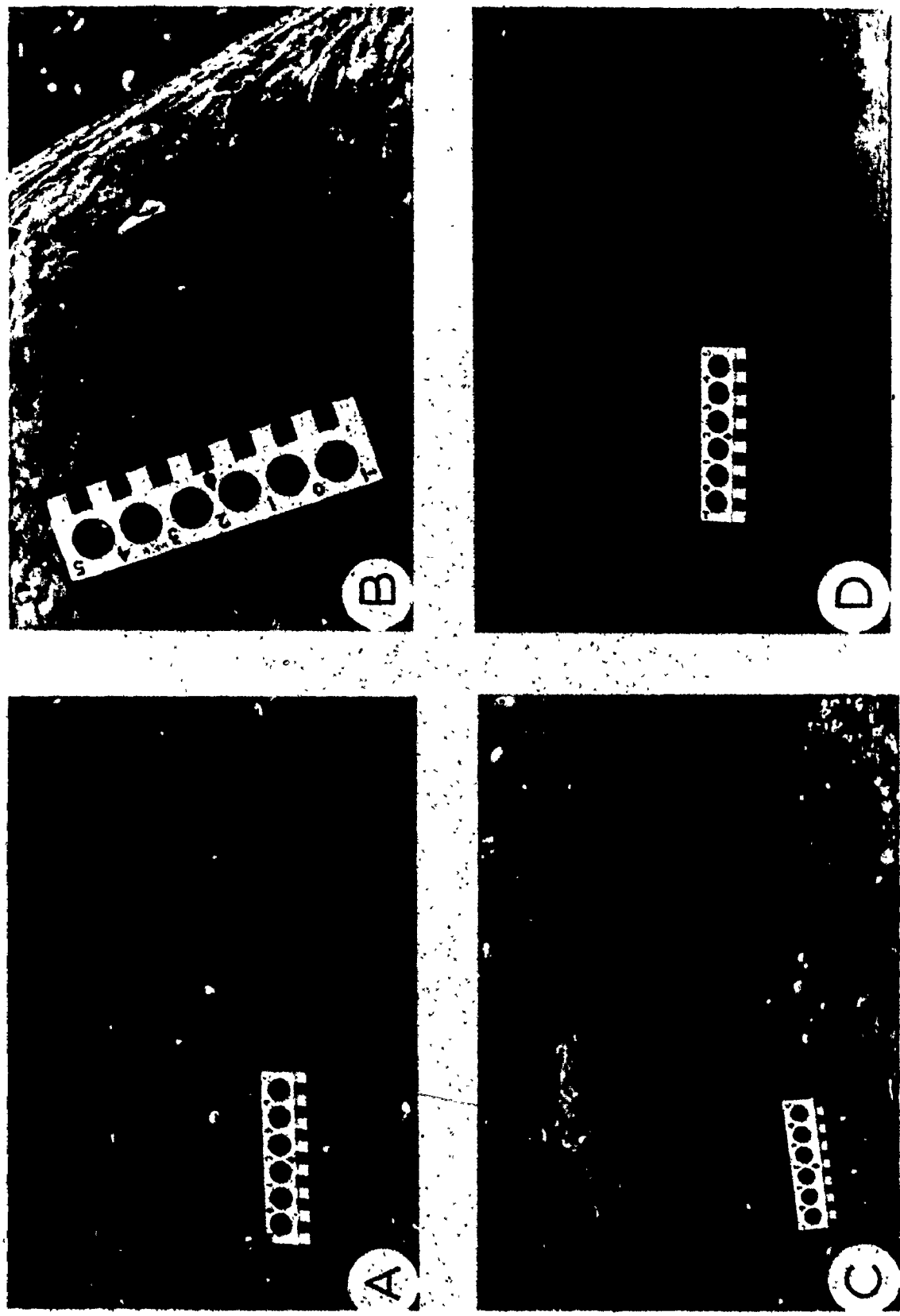

FIG. 2.6

Facies 4, 5 and 6: coarse sandy layers

These facies contain all coarse sandstone layers in the Tourelle Formation.

Photographs showing the field occurrence of thin sandstones (4) (Figure 2.7), truncated sandstones (5) (Figure 2.8), and the three subfacies of thick sandstones (6) (6a - Figure 2.9, 6b - Figure 2.10, 6c - Figure 2.11) are presented on the following pages.

In addition to sedimentary structures commonly encountered in classical turbidites (Walker, 1976) coarse sandstones (particularly thick sandstones (6)) contain three additional structures more common in exotic mass flows: cross-stratification, coarse near-horizontal stratification, and fluid-escape structures. More detailed analysis of certain aspects of these structures is presented in Chapters IV and V.

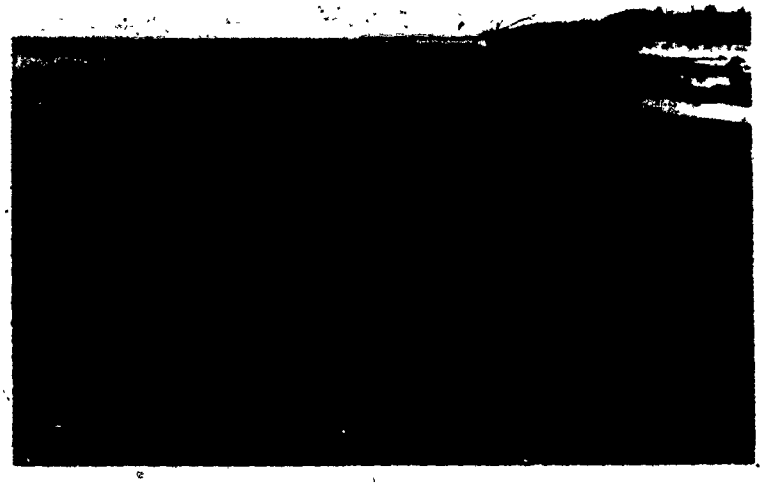

Fig. 2.7. Thin sandstones (4) passing up into a fine horizon at area FIV. Scale 1 m. Top is to the right.

Thin sandstones (4) separated by thin shale beds at area J. Scale 1 m. Top is to the left.

Fig. 2.8. Facies 5: Truncated sandstones (5).

(A) General view of this facies at area L. Scale 1 m. Top is to the right.

(B) Truncated sandstones (5) near the base of a thickening upward sequence, area L. Scale 1 m. Top is to the right.

(C) Stratified and graded truncated sandstone layer within an amalgamated bed at area L. Scale bars are 10 cm. Note loaded base and irregular eroded top.

(D) Amalgamated truncated sandstones (5) at the top of the Cap Ste-Anne channel fill (area J). Scale 1 m. Top is to the left.

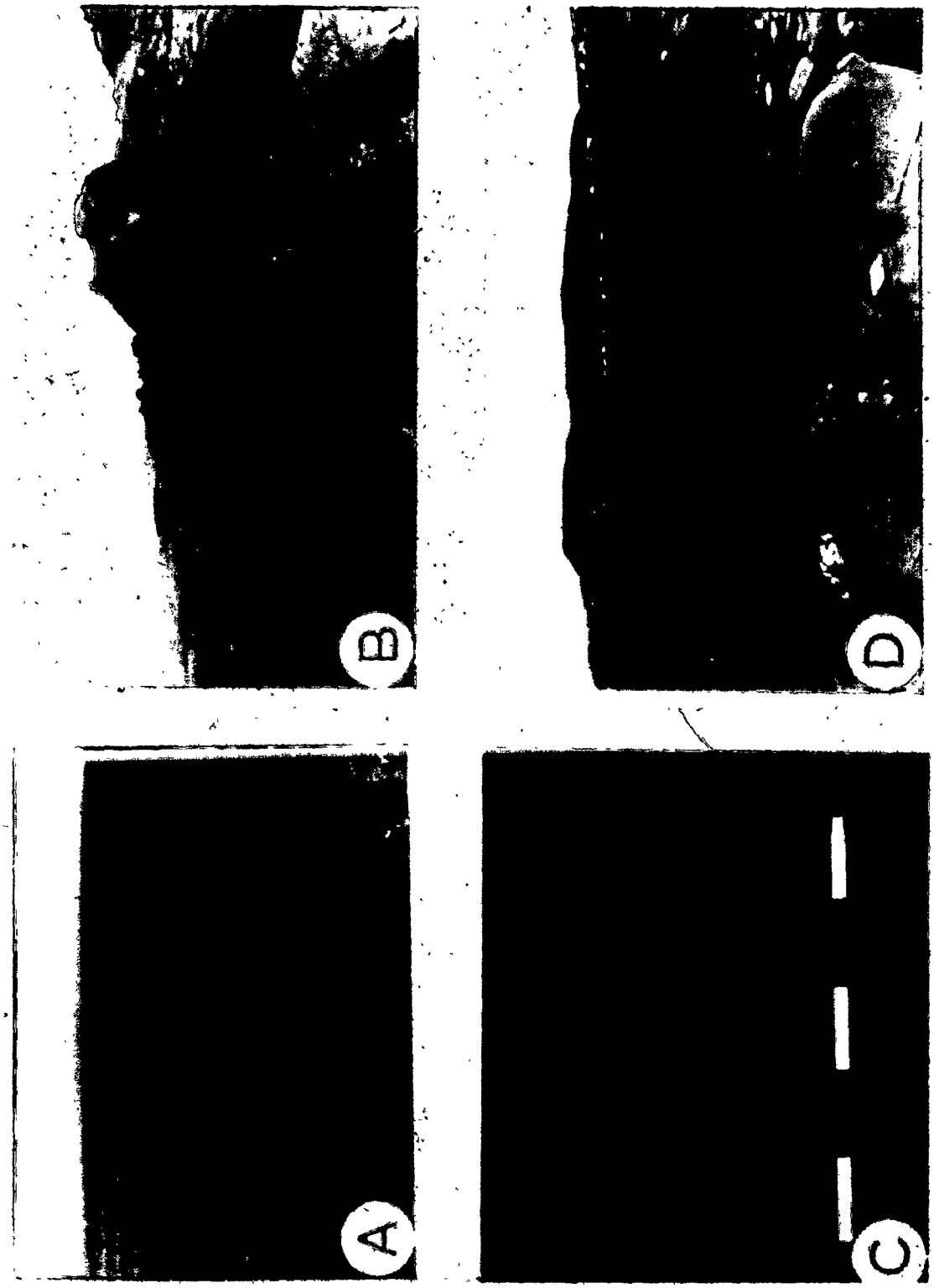

FIG. 2.8

Fig. 2.9. Thick sandstone subfacies 6a, area L.

(A) Loaded base of a layer containing a lens of shale rip-up clasts. Scale 15 cm.

(B) Irregular amalgamation surface in graded, granular to coarse sandstones of this subfacies.

(C) Deeply erosive base of a granular sandstone of this subfacies, cut into the finer top of a similar graded layer. These asymmetric features may be transverse scours.

(D) Close-up of granular sandstone. Scale contains discs of sand in 1 ϕ intervals from -1 ϕ to 5 ϕ. Most of the larger clasts are black shale or chert.

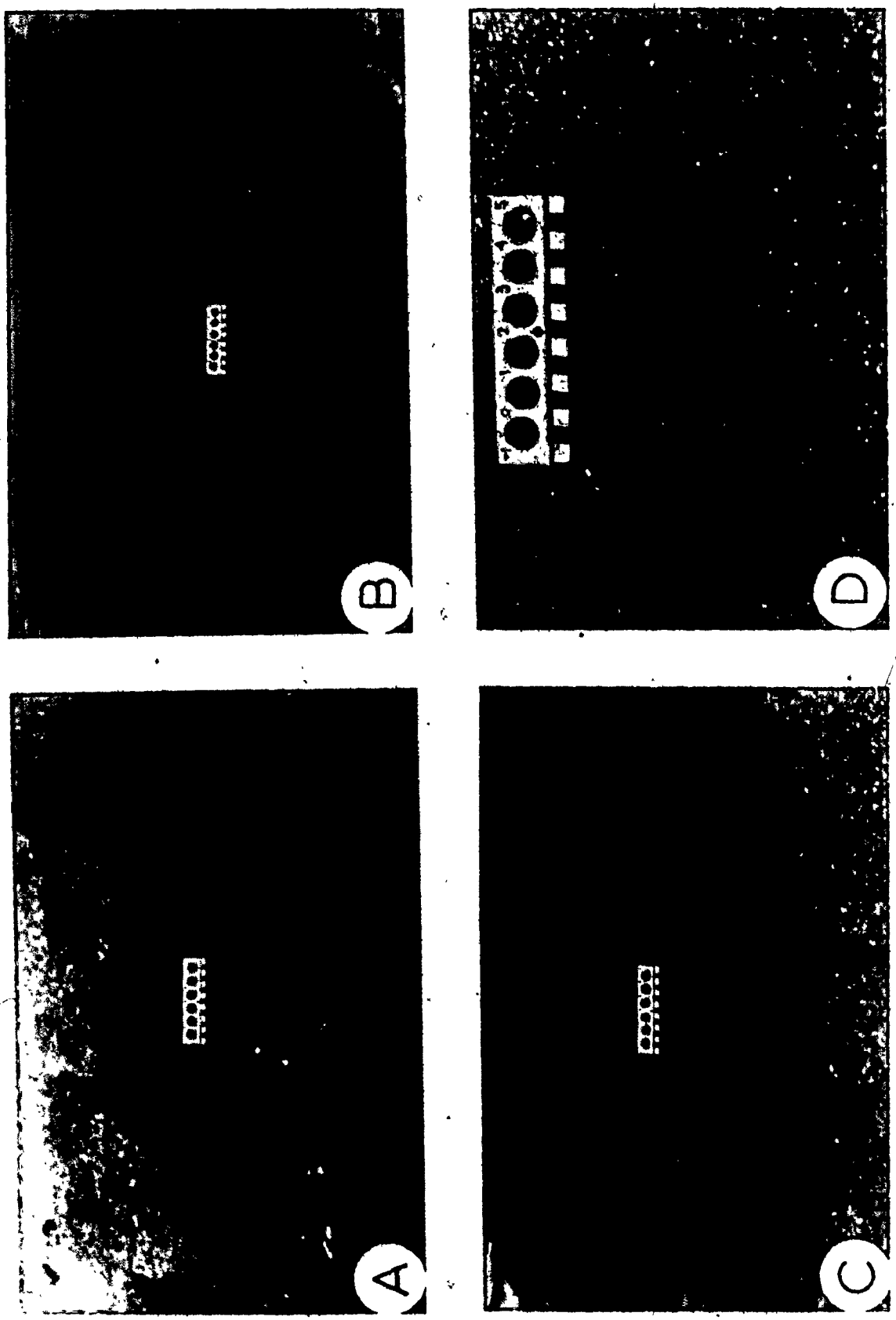

FIG. 2.9

Fig. 2.10. Thick sandstone subfacies 6b.

(A) General view of thick beds of this facies at the base of area F. Scale 1 m. Top is to the right.

(B) Thick amalgamated beds below the Cap Chat lighthouse, area E. The boundaries of individual layers are marked. Two thinning upward sequencies are visible in the cliff exposure. Note figure for scale.

(C) Single thick graded layer of massive sand at area A. Scale 1 m. Top is to the left. Note scattered concretions.

(D) Thick sandstone (6) layer at area A, with faint internal stratification in lower part. Scale 1 m. Top is to the right. This layer overlies a slurry sandstone (3) containing a 270 x 30 cm slab of calcisiltite.

FIG. 2.10.

Fig. 2.11. Thick sandstone subfacies 6c.

(A) Massive ungraded channel-fill sandstone, area J. This layer is about 22 m thick and contains scattered concretions and sheet structure. The upper 1 m fines to rippled fine sand. Scale 1 m. Top is to the left.

(B) & (C) Additional views of the layer appearing in (A). In (C), top is to the right. All scales are 1 m.

(D) Internal scour surface in a 14 m thick layer at area E. Grain size remains essentially constant across the discontinuous erosion surface. Scale is in centimetres.

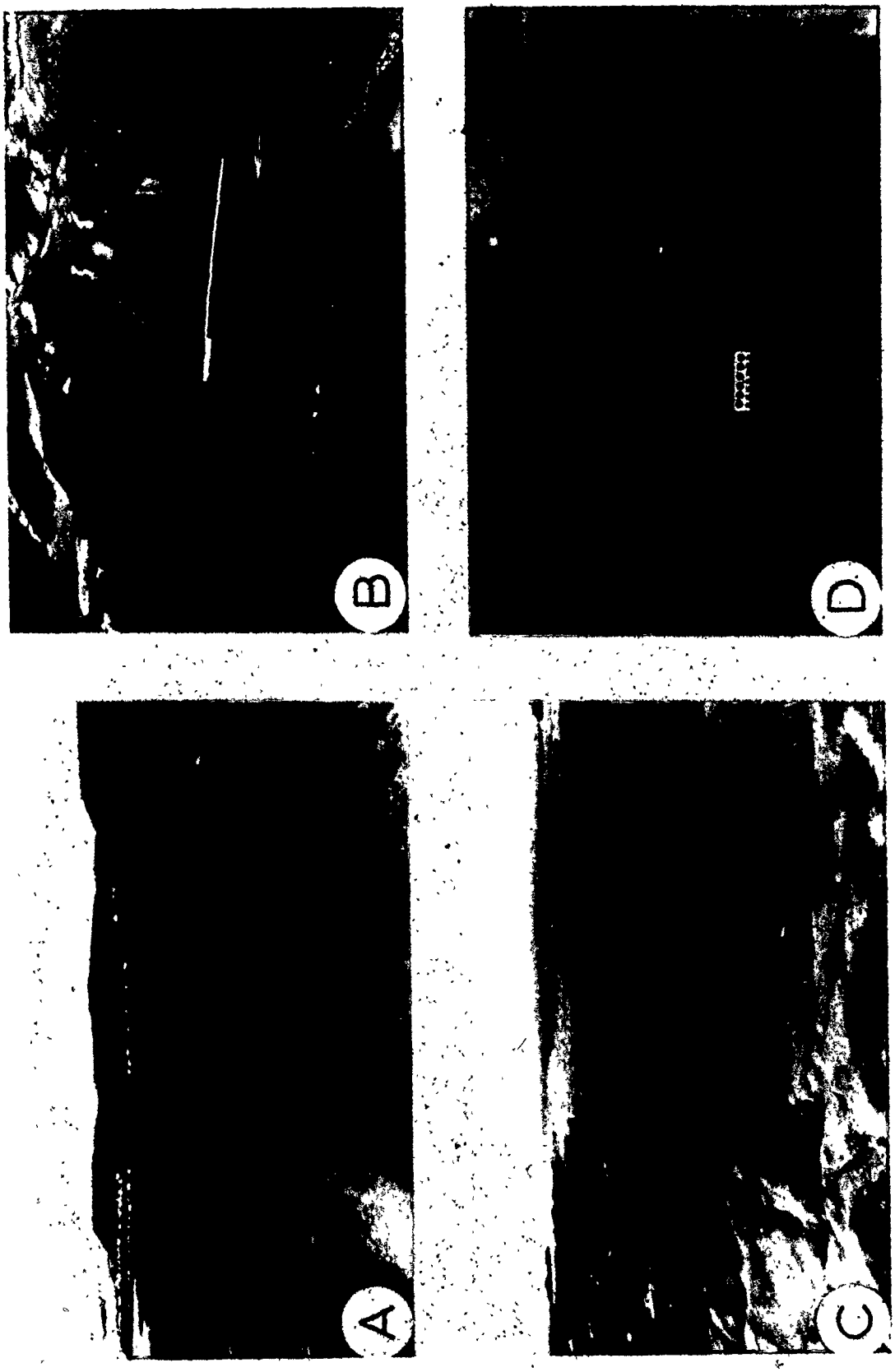

FIG. 2.11

Cross-stratification (Figure 2.12)

In 66% of all occurrences, cross-stratification comprises a division of winnowed medium to coarse sand at the top of thick sandstone (6) layers. 6% of recorded cross-stratification forms a discrete sedimentary layer. Preserved set height ranges from 15 to greater than 100 cm. The 15 to 25 cm sets commonly occur as a coset of 2 to 4 sets and sometimes show positive construction analogous to ripple-drift cross-lamination. The larger sets are solitary scour fills.

Coarse near-horizontal stratification (Figure 2.13)

This stratification is the dominant sedimentary structure of most truncated (5) and thick sandstones (6). Individual stratification bands are from several cm to greater than 10 cm in thickness, with the following idealized upward progression:

(i) basal horizontal to near-horizontal erosion surface;

(ii) subdivision of inverse-graded sand. Grading is from 2 ϕ or 3 ϕ to approximately 1 ϕ. This subdivision may constitute the entire stratification band;

(iii) subdivision of massive, -1 ϕ to 1 ϕ sand which commonly shows good grain imbrication.

Fig. 2.12. Cross-stratification in thick sandstones (6).

(A) Coset of cross-stratification in medium sand at area K. Scale is 15 cm. The bed forms which produced this cross-stratification climbed (toward the right) up the stoss sides of downstream bed forms.

(B) Close-up of (A). Note asymptotic bases of cross-stratification sets. This coset is overlain by an amalgamation surface.

(C) Thick scour-fill cross-stratification set in granular to coarse sandstone at area C. Scale 15 cm. Top is to the right.

(D) 50 cm set of cross-stratification in coarse sand at area E. Scale 15 cm.

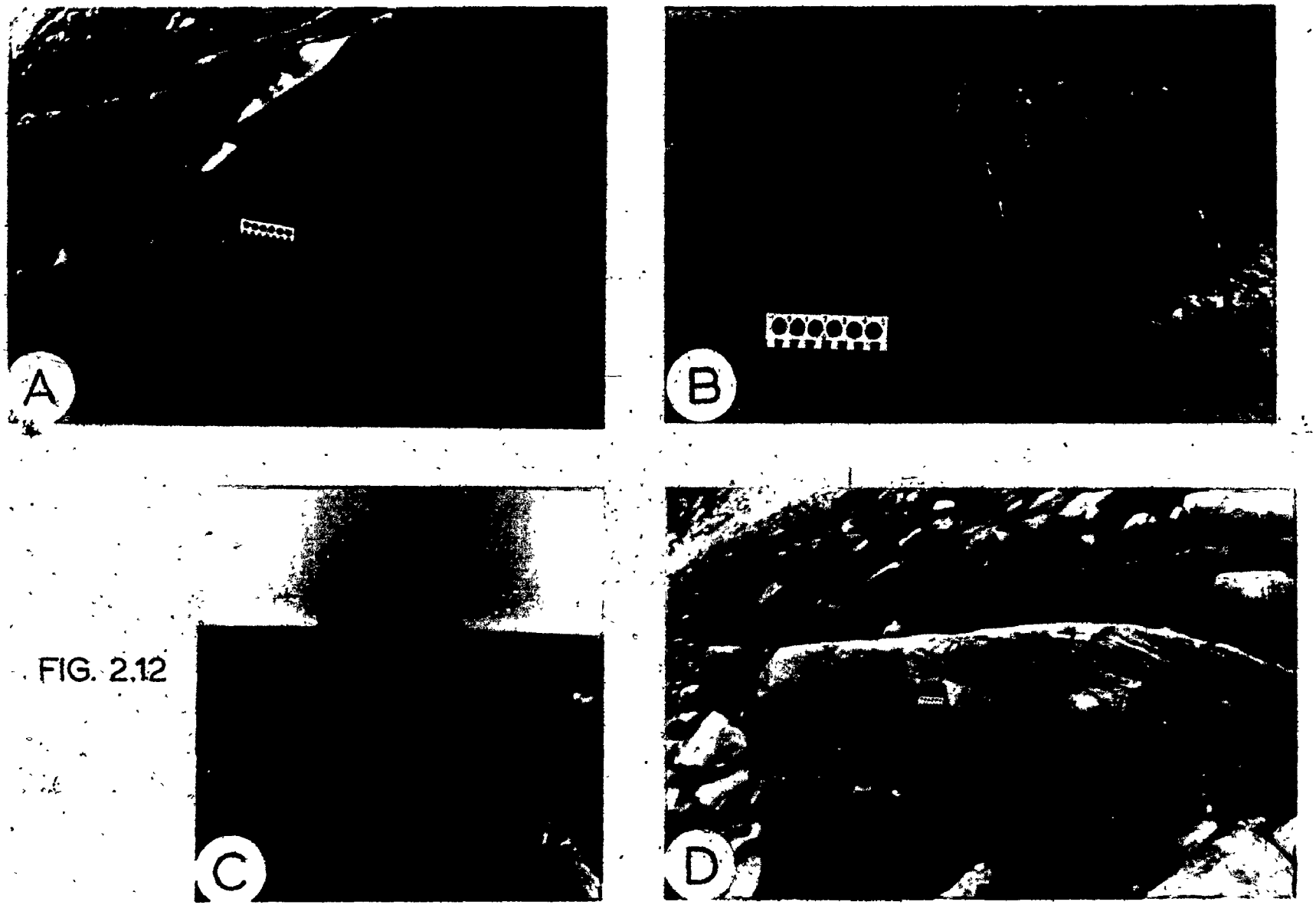

FIG. 2.12

Fig. 2:13. Coarse, near-horizontal stratification.

(A) Thick graded layer formed almost entirely of unusual coarse stratification, and found at the top of the Cap Ste-Anne channel fill, area J. Stratification bands become thinner with increasing height in the layer. Scale 15 cm. Top is to the right.

(B) Coarse stratification at area C, with spacing of about 5 cm. This division is underlain by massive sandstone.

(C) Close-up of coarse stratification at area C, showing basal erosion surfaces (arrows) and inversely graded stratification bands. Top is to the right. Scale in centimetres.

(D) Close-up of stratification bands at area DI, showing inverse grading from basal erosion surfaces (arrows). Individual stratification bands are about 5 cm thick. Scale in centimetres.

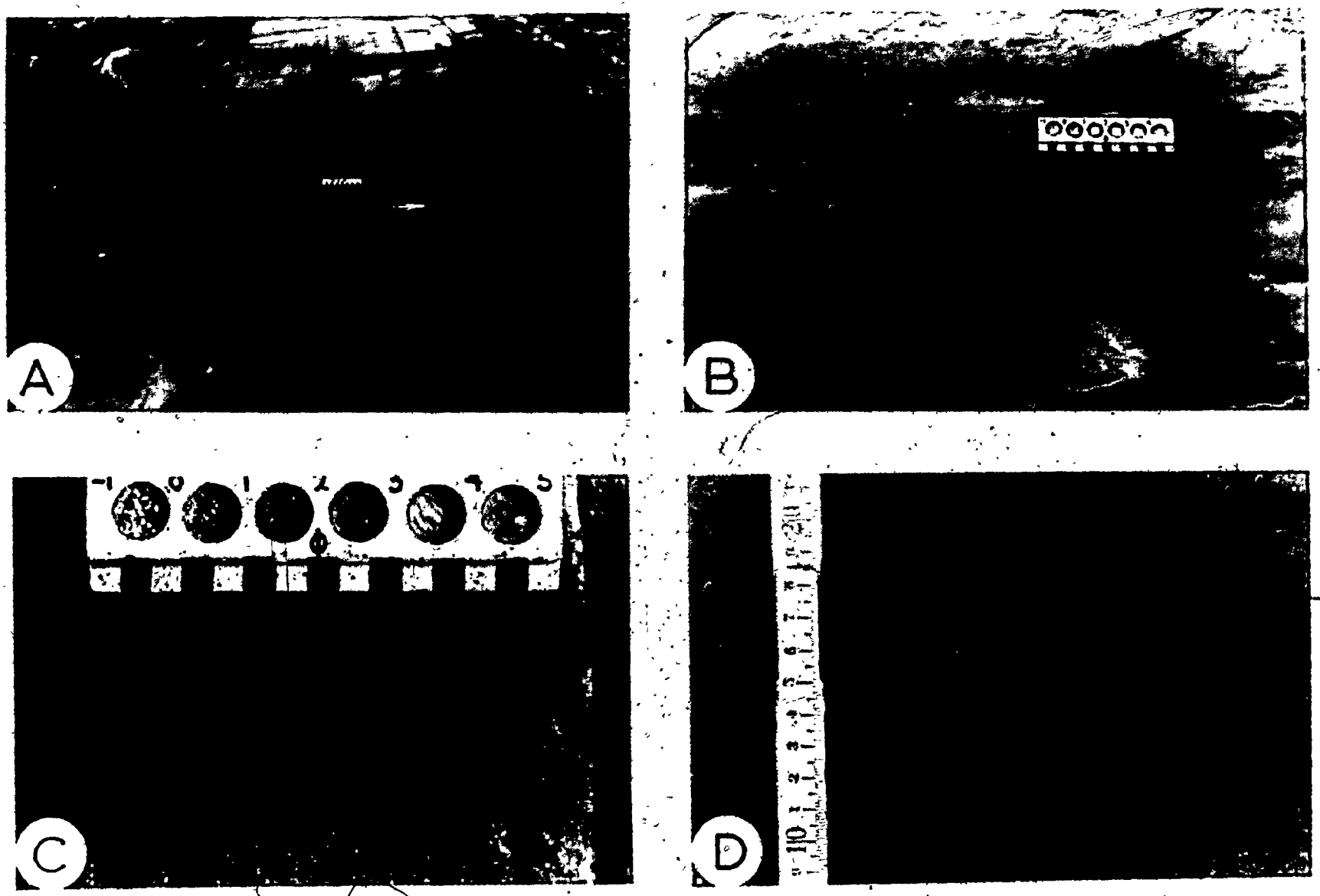

FIG. 2:13

The above progression is repeated several times to produce a division of coarse stratification. Basal scour surfaces in each stratification band may converge laterally due to differential erosion. In most cases, this structure appears on the outcrop scale as well-behaved, plane, horizontal stratification. Careful tracing of individual stratification band boundaries in a layer at area C, however, shows the degree to which individual bands can deviate from original horizontality (Figure 2.14). At only one locality was this variety of stratification observed to pass laterally into a solitary large set of cross-stratification.

Fluid-escape structures

The three varieties of fluid-escape features found in coarse sandstones of the Tourelle Formation are all vertical to near-vertical dewatering conduits. Dish structure (Wentworth, 1967), which is frequently found in sandstones of comparable type in other formations, is absent, perhaps due to poor sorting and lack of early consolidation laminations (Lowe, 1975). The observed varieties of fluid-escape structures are described below.

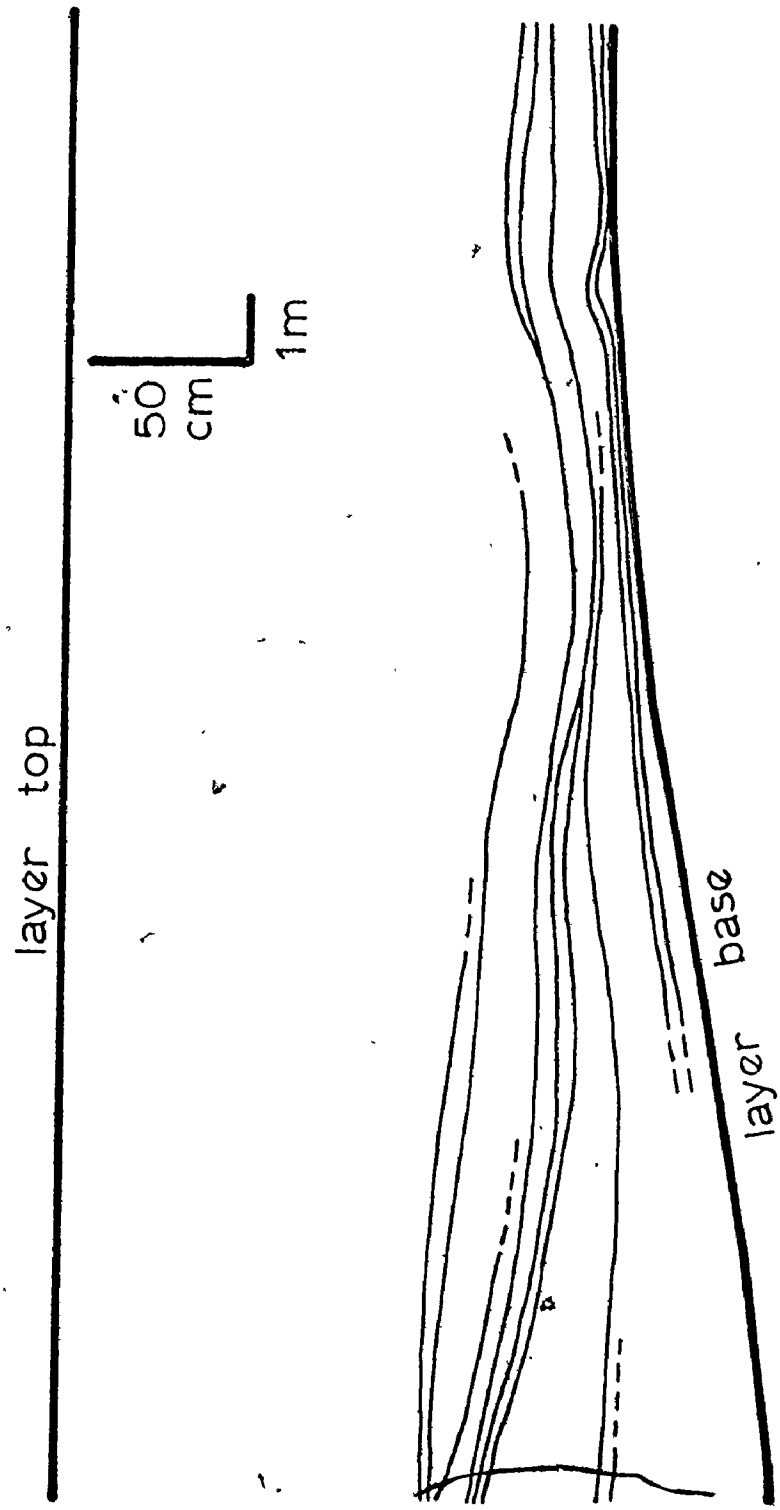

Fig. 2.14. Example of behavior of coarse stratification over a horizontal distance of 19 m at area C. This irregular internal erosion is unusual. Most coarse stratification is parallel and continuous on outcrop scale. This figure is drawn with a 5x vertical exaggeration.

(i) Coarse pillars (Figure 2.15) are columnar zones depleted in matrix, and may have complex three-dimensional geometry. In some cases, even the coarsest grains were fluidized and washed upward, as shown by the presence in the pillar of coarser grains than in the surrounding sandstone. These pillars are not truncated by internal laminations, and in some cases may even cross layer boundaries. The pillars generally have a diameter of 1 to 3 cm, and correspond to type B pillars of Lowe (1975).

(ii) Sheet structure (Laird, 1970) consists of parallel, vertical planes of fluid escape, several grain diameters thick, with 1 to 2 cm spacing between planes. Laird (1970) reported these planes to be parallel to a-axis grain orientation. This structure is relatively rare in the Tourelle Formation, and most examples are indistinct. At one locality, sheet structure is segmented into parallel "books" perpendicular to the planes (Figure 2.16). The reason for such an arrangement is unclear.

(iii) Wispy channels are only a few grain diameters across, are columnar in form, and are only a few centimetres in length. They are particularly associated with slurry sandstones (3).

Fluid-escape structures are present in 12% of all thin sandstones (4) and truncated sandstones (5), and in 0%, 41% and 46% of subfacies 6a, 6b and 6c layers, respectively.

Figure 2.15. Coarse fluid-escape pillars.

(A) Closely spaced, long, straight pillars in a thick sandstone (6) layer between areas F and G.

(B) Sinuous pillars in massive sand at area L. Scale bars are 10 cm.

(C) Three-dimensional fluid-escape structure (pillar?) at area G, which resembles a loosely-gathered curtain. Scale bars are 10 cm.

(D) Broad complex pillar at area G which cuts across an amalgamation surface. Scale bars are 10 cm.

(E) Close-up of (D) showing deformation of lamination (arrow) and transportation of coarse grains up the pillar through a fine horizon.

(F) Thick pillar at area G which transported coarse granular sand upward from the base of the layer. Scale in centimetres.

(G) Irregular sinuous pillar in the same layer shown in (B).

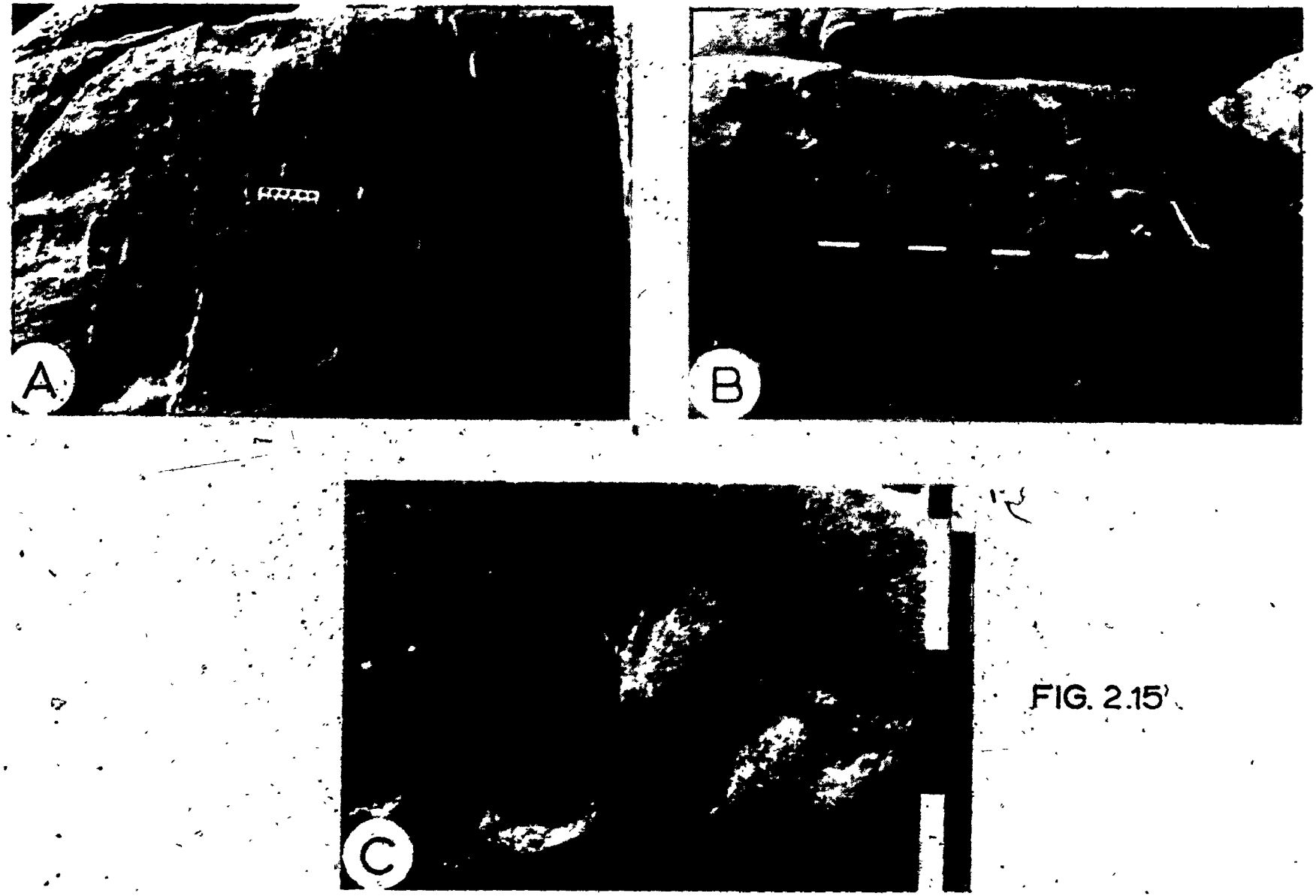

FIG. 2.15

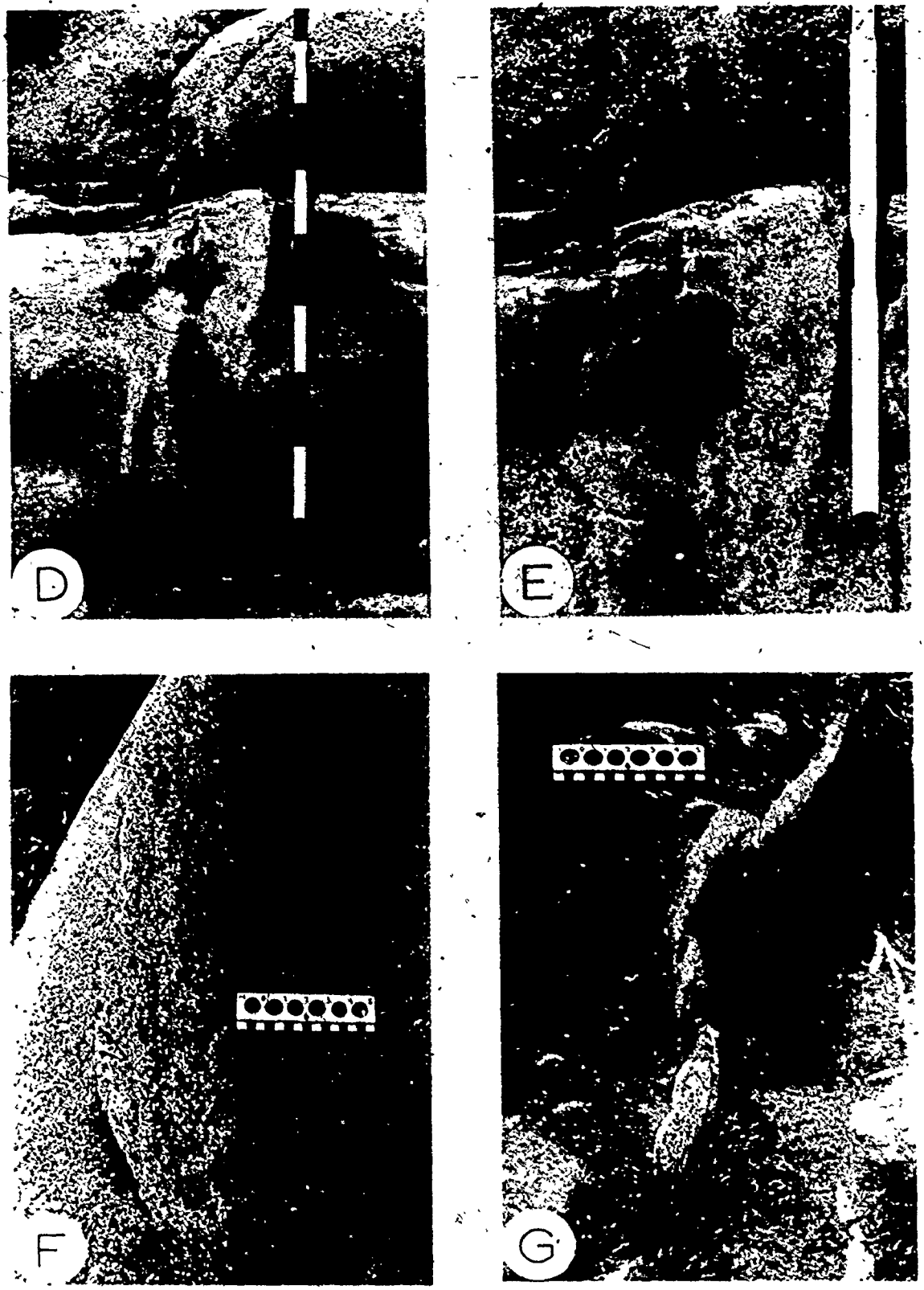

FIG 2.15
cont'd

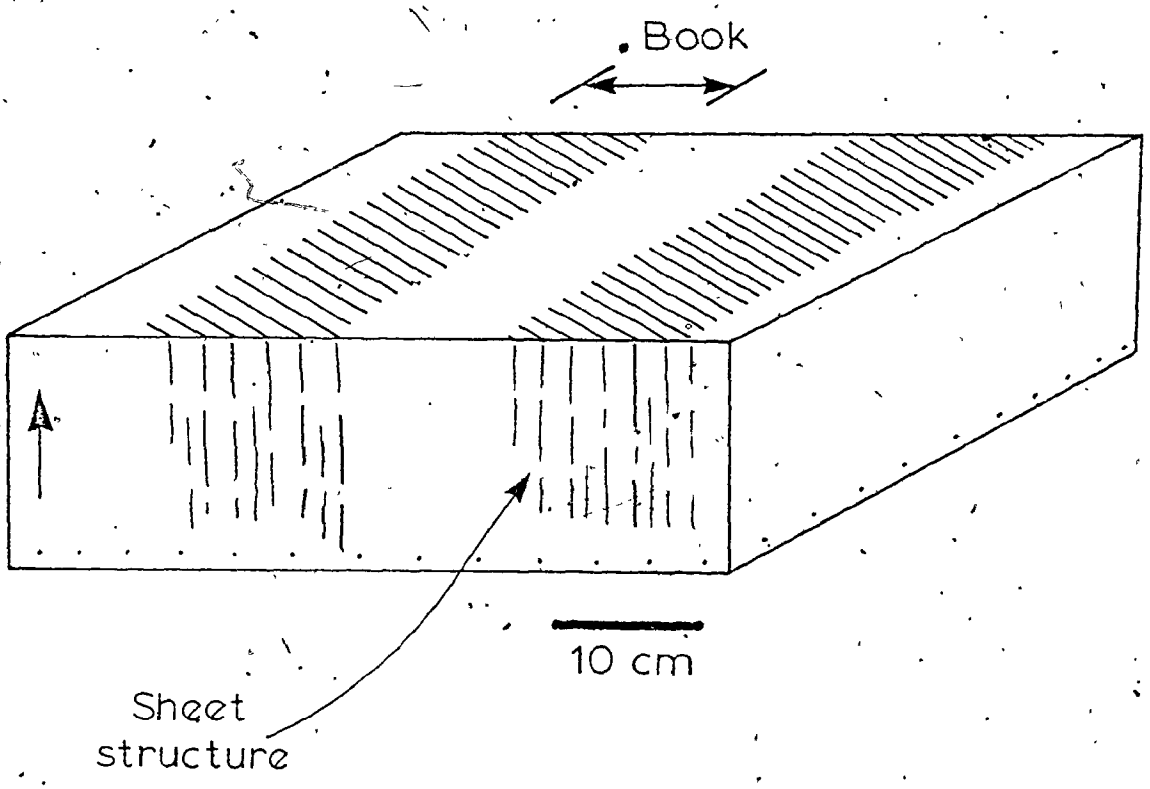

Fig. 2.16. Block diagram of graded bed at area L showing an unusual occurrence of sheet structure. Sheets are separated into individual elongate "books".

General facies characteristics

Figures 2.18 through 2.22 present diagramatic representations of the most commonly occurring sedimentary structure sequences for thin, truncated, and thick sandstones, along with summaries of the frequency of occurrence of various layer properties. A key to the summary charts is presented in Figure 2.17.

The sedimentary structure sequences presented in the following diagrams account for 77% of thin sandstones (4) (Figure 2.18), 83% of truncated sandstones (5) (Figure 2.19), 91% of subfacies 6a (Figure 2.20), 70% of subfacies 6b (Figure 2.21) and 77% of subfacies 6c (Figure 2.22).

Thin sandstone (4) characteristics

This facies is characterized by normal grading which generally conforms to one of two styles. These are (1) continuous decrease in grain size from base to top, or (2) grading producing a convex-upward profile with most size decrease taking place in the upper part of the layer. Although 60% of bases are flat, irregular erosive bases are also common.

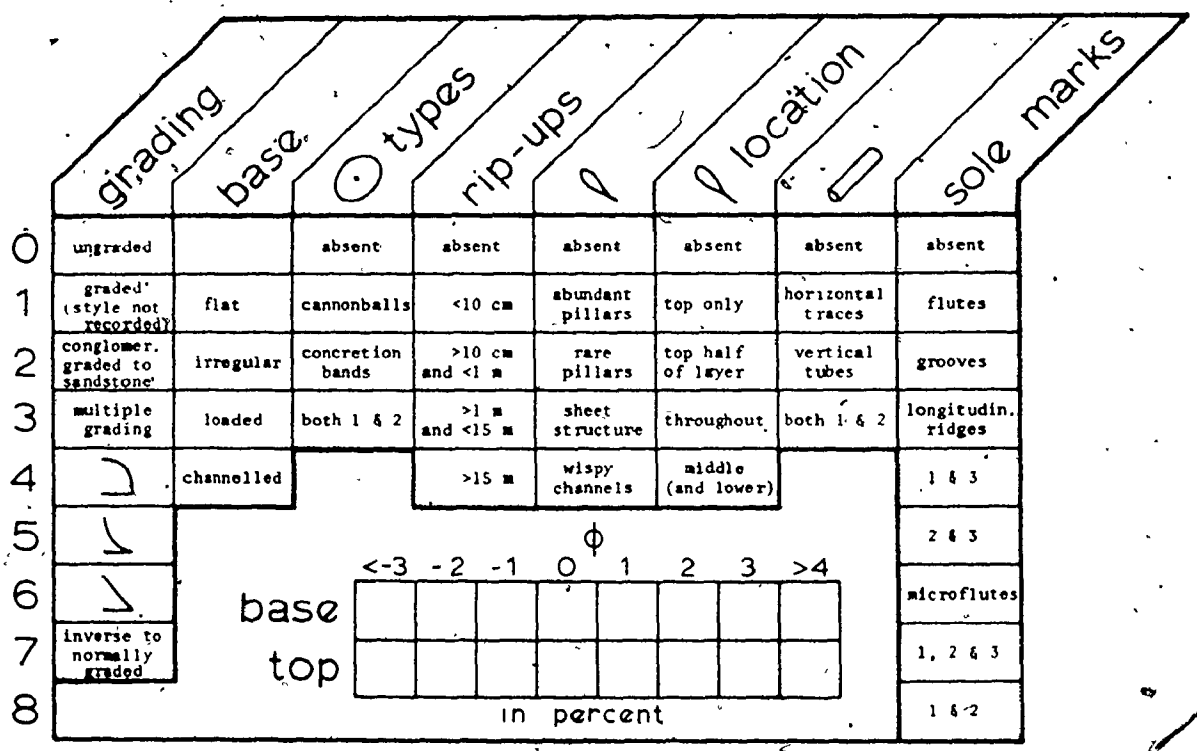

Fig. 2.17. Key to charts of layer properties.

⊙ - concretions, ρ - fluid-escape structures, ✎ - fossil traces. The relative abundances of different types of grading, for example, are indicated by a cumulative bar scale in the grading column (Figures 2.18 to 2.22). If the upper left-hand box is half filled, then 50% of all layers with the structure sequence shown in the accompanying diagram are ungraded. The percentages of layers with various basal and upper grain sizes are also tabulated.

Figs 2.18 through 2.22. These figures summarize the most common sedimentary structure sequences for thin sandstones (4) (Fig. 2.18), truncated sandstones (5) (Fig. 2.19), subfacies 6a (Fig. 2.20), subfacies 6b (Fig. 2.21) and subfacies 6c (Fig. 2.22). Five digit numbers indicate the sequence of internal divisions according to the following classification:

1 - massive or graded division,
2 - internal scour surfaces,
3 - upper flow regime plane lamination,
4 - ripples and climbing ripples;
5 - convolution,
6 - low angle cross-stratification (only 1 occurrence),
7 - cross-stratification,
8 - muddy lamination (Bouma division d),
9 - coarse near-horizontal stratification,
0 - top of the layer.

For example, a layer with number 14500 has, from the base upward, divisions of (i) massive sand, (ii) ripples, and (iii) convolution. These are shown with their relative thicknesses in the accompanying diagram. Zeros indicate the end of the structure sequence. The percentage underneath the five digit number indicates the proportion of the facies or subfacies accounted for by the particular sedimentary structure sequence.

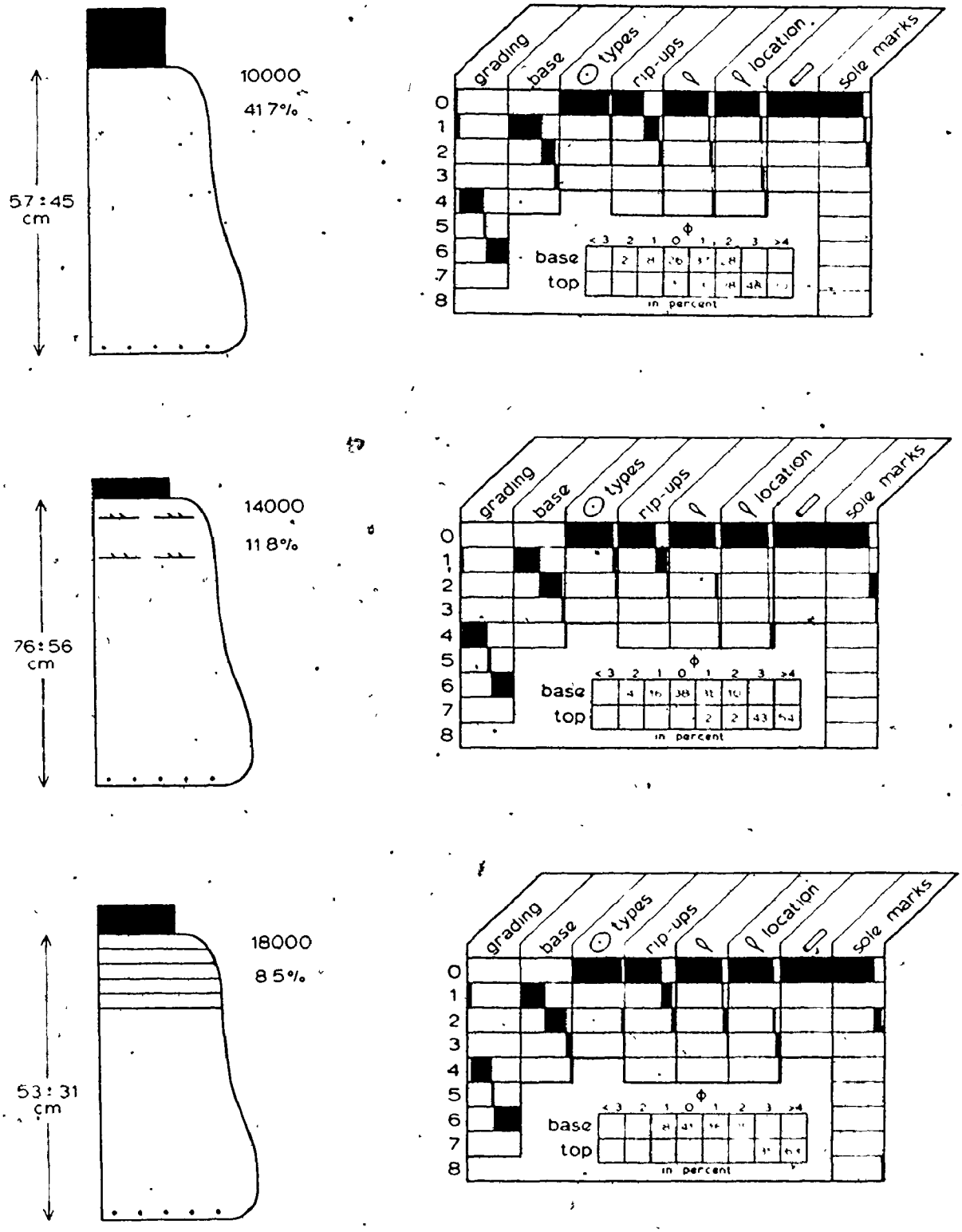
10000
41 7%
57 : 45
cm
grading
base
types
rip-ups
location
sole marks
0
1
2
3
4
5
6
7
8
base
top
in percent
14000
11 8%
76 : 56
cm
18000
8 5%
53 : 31
cm

FIG. 2.18

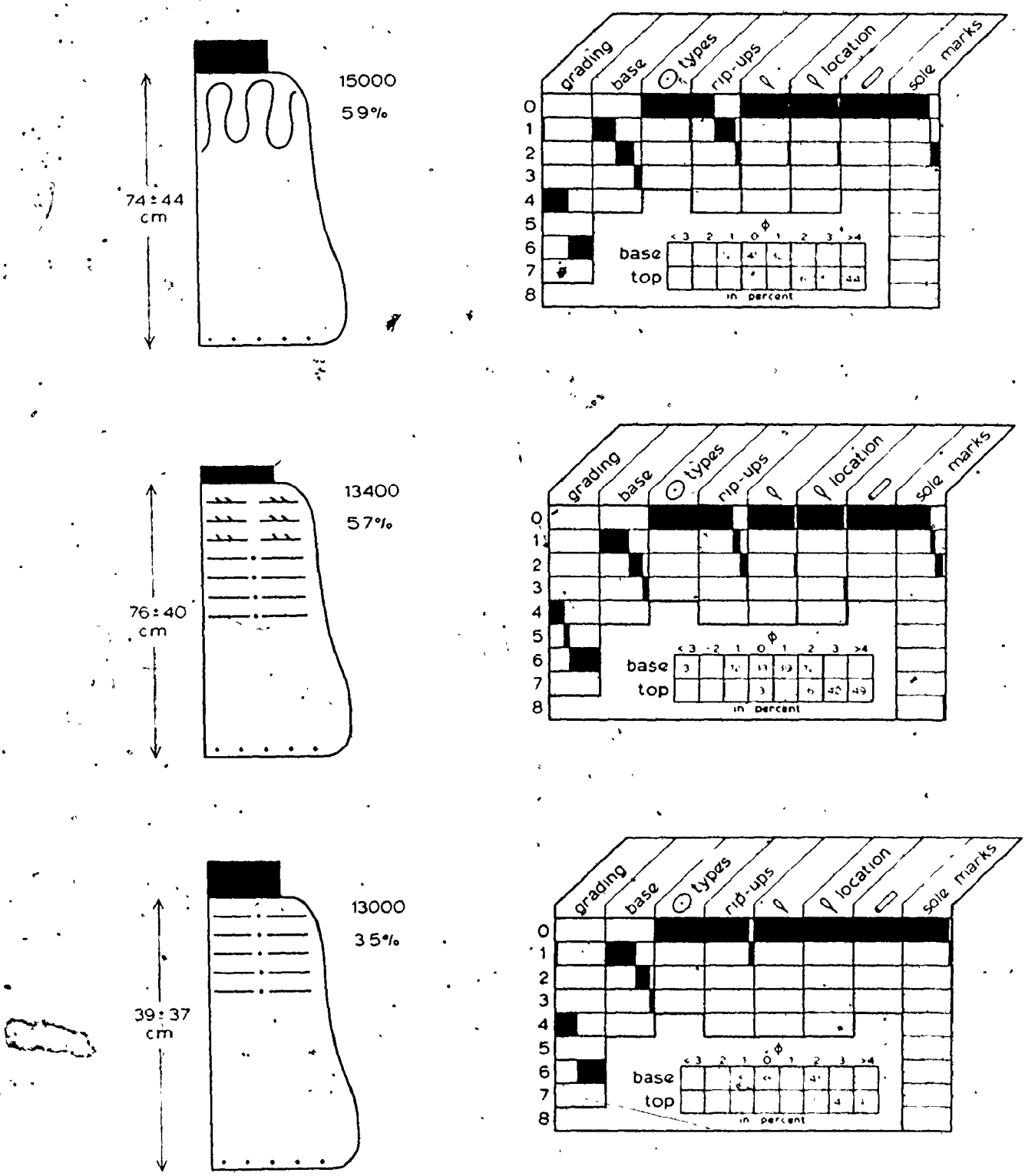

FIG. 2.18 cont'd

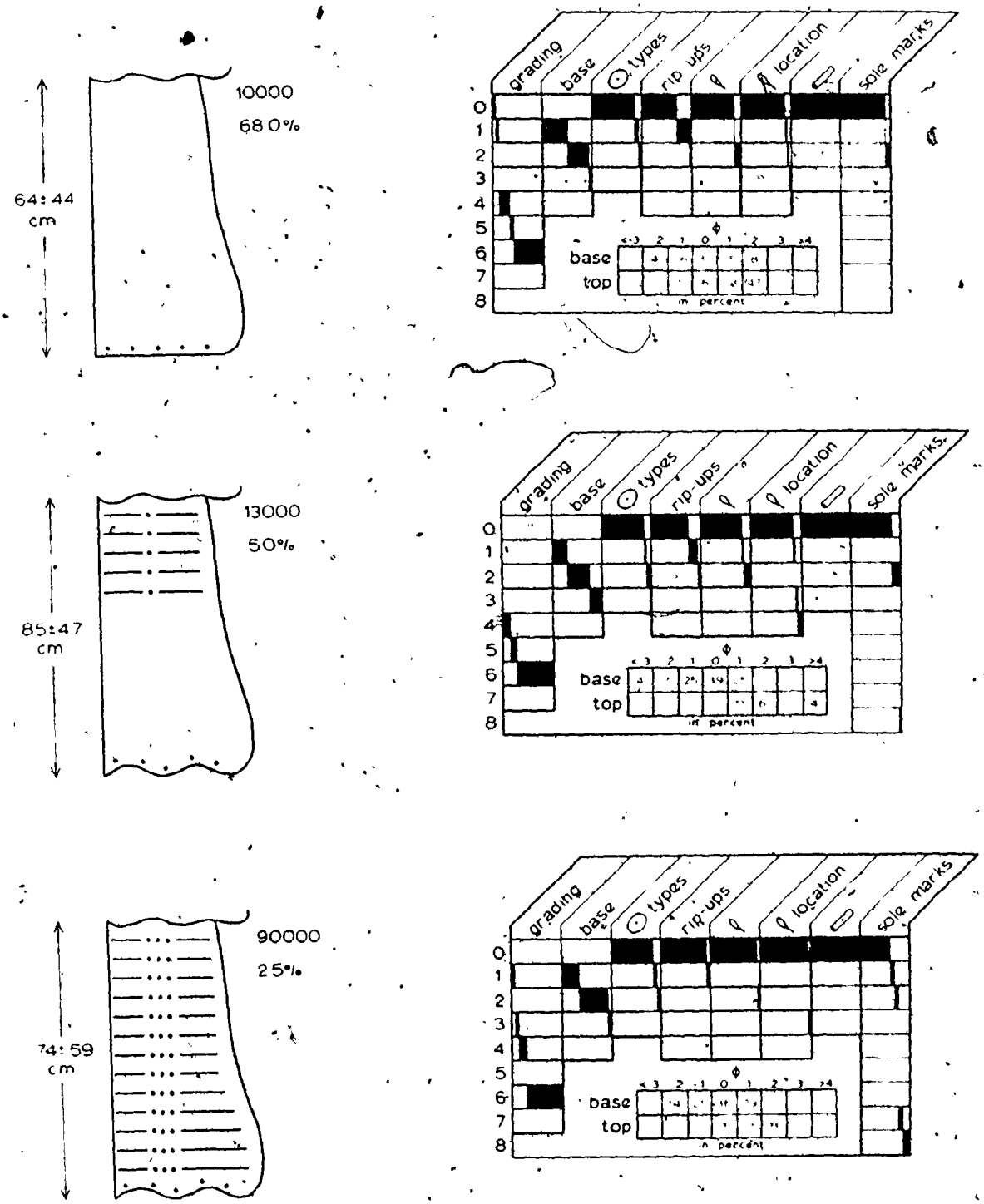
10000
68.0%
64±44
cm
grading
base
types
rip-ups
location
sole marks
0
1
2
3
4
5
6
7
8
base
top
in percent
13000
5.0%
85±47
cm
90000
2.5%
74±59
cm

FIG. 2.19

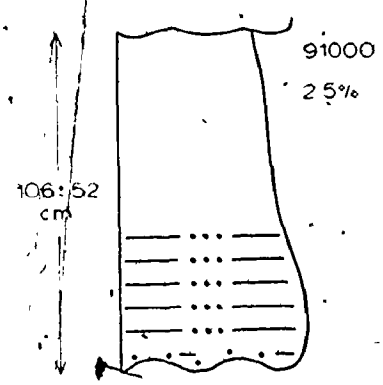

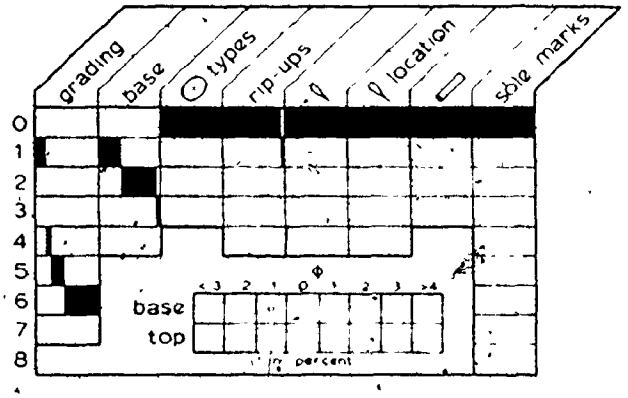

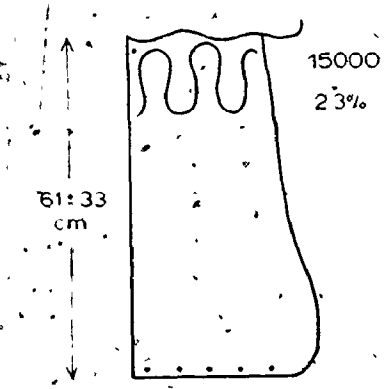

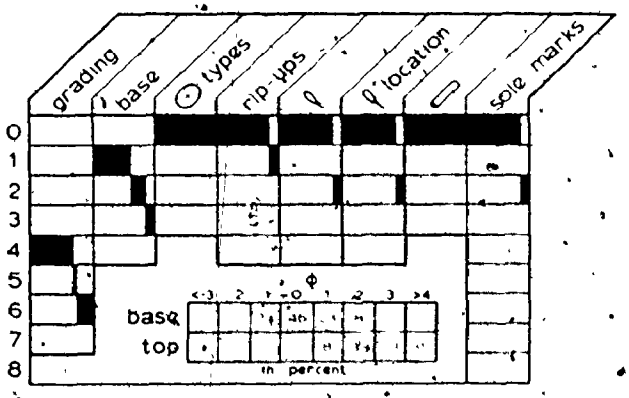

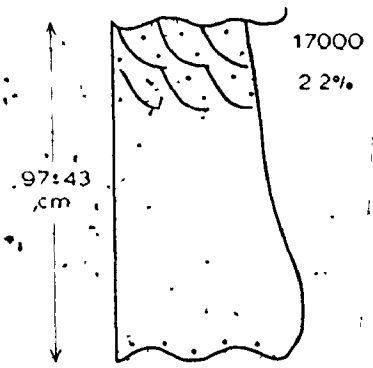

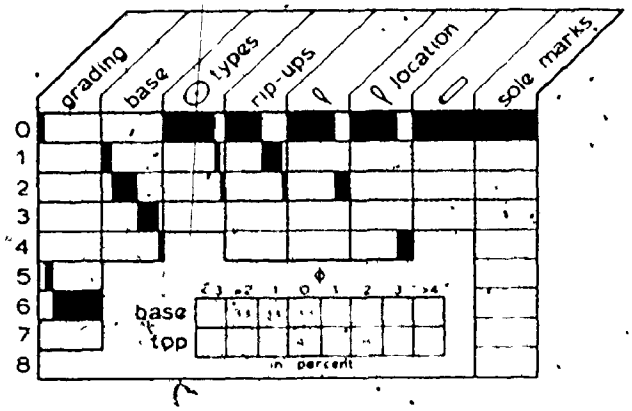

FIG. 2.19 cont'd

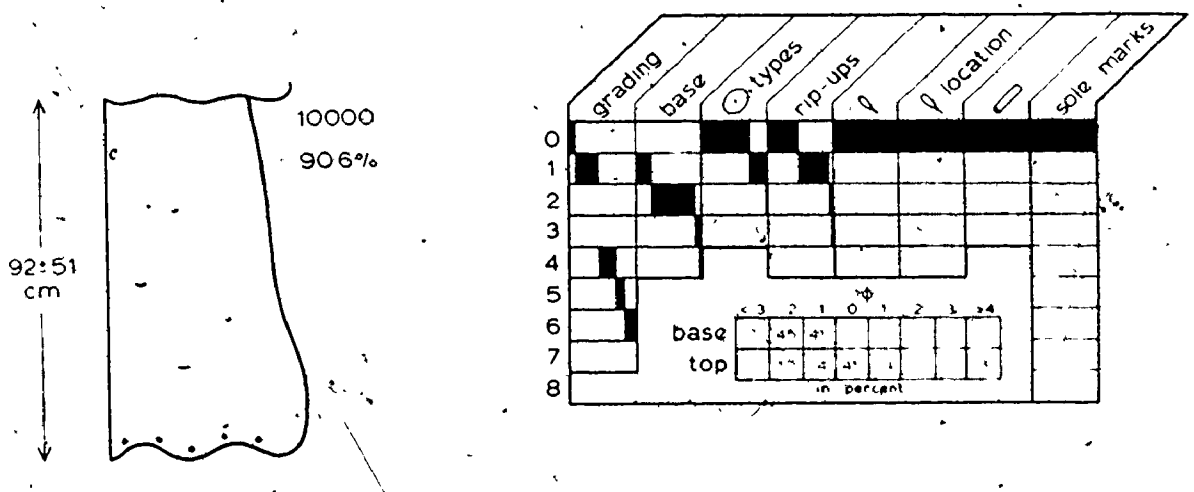

FIG. 2.20

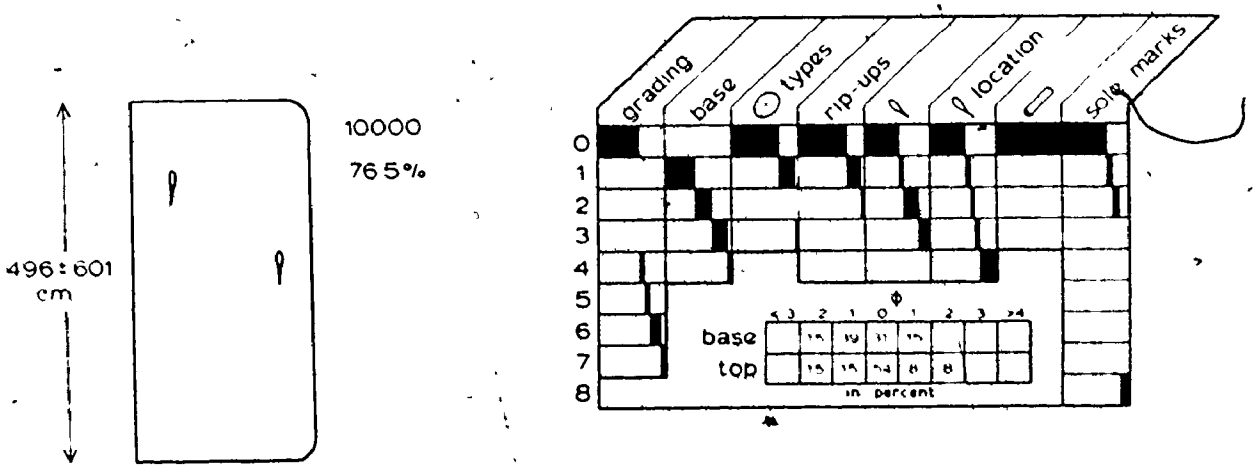

FIG. 2.22

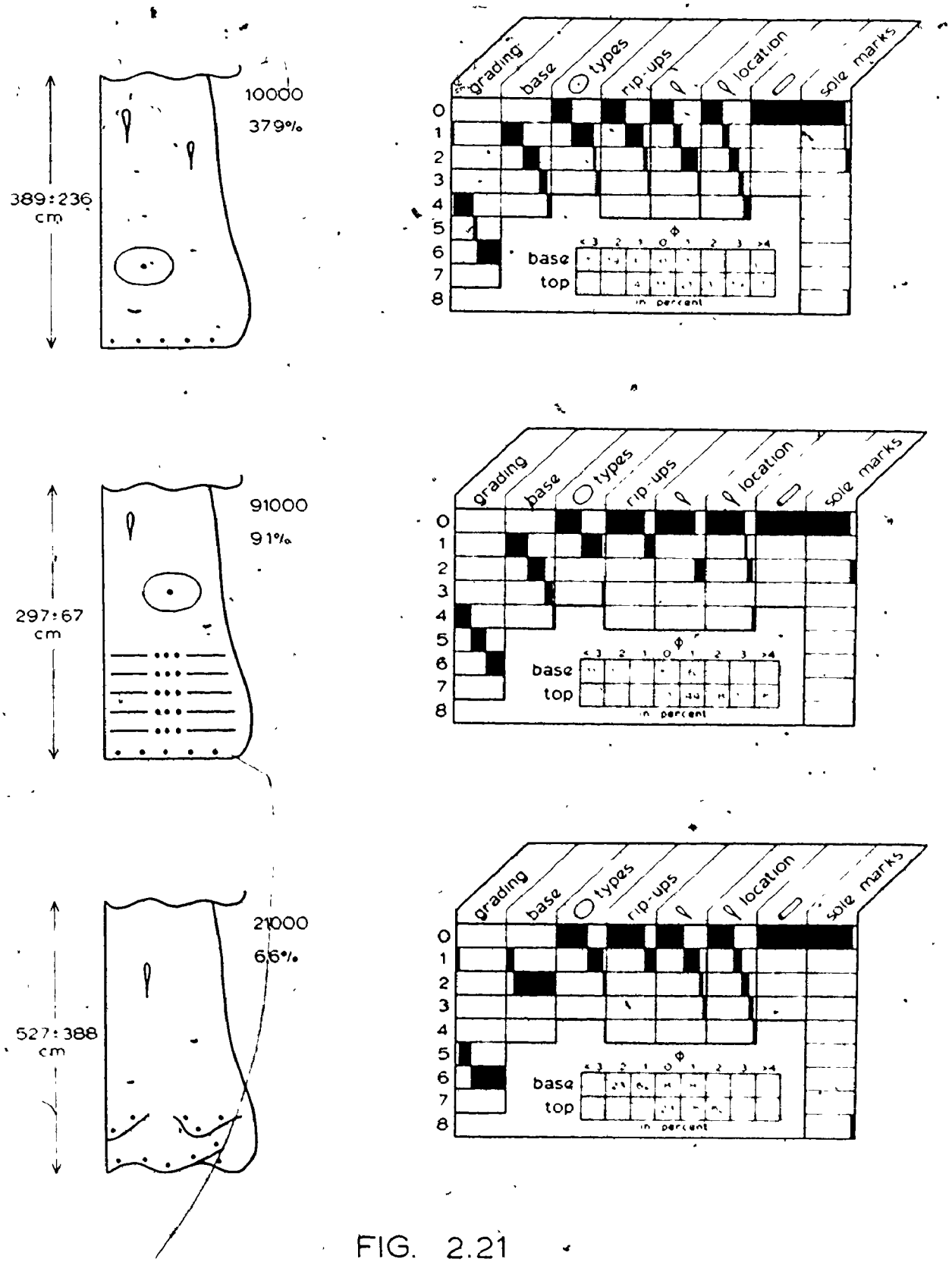
10000
379%
389:236
cm
grading
base
types
rip-ups
location
sole marks
0
1
2
3
4
5
6
7
8
base
top
in percent
91000
91%
297:67
cm
21000
66%
527:388
cm

FIG. 2.21

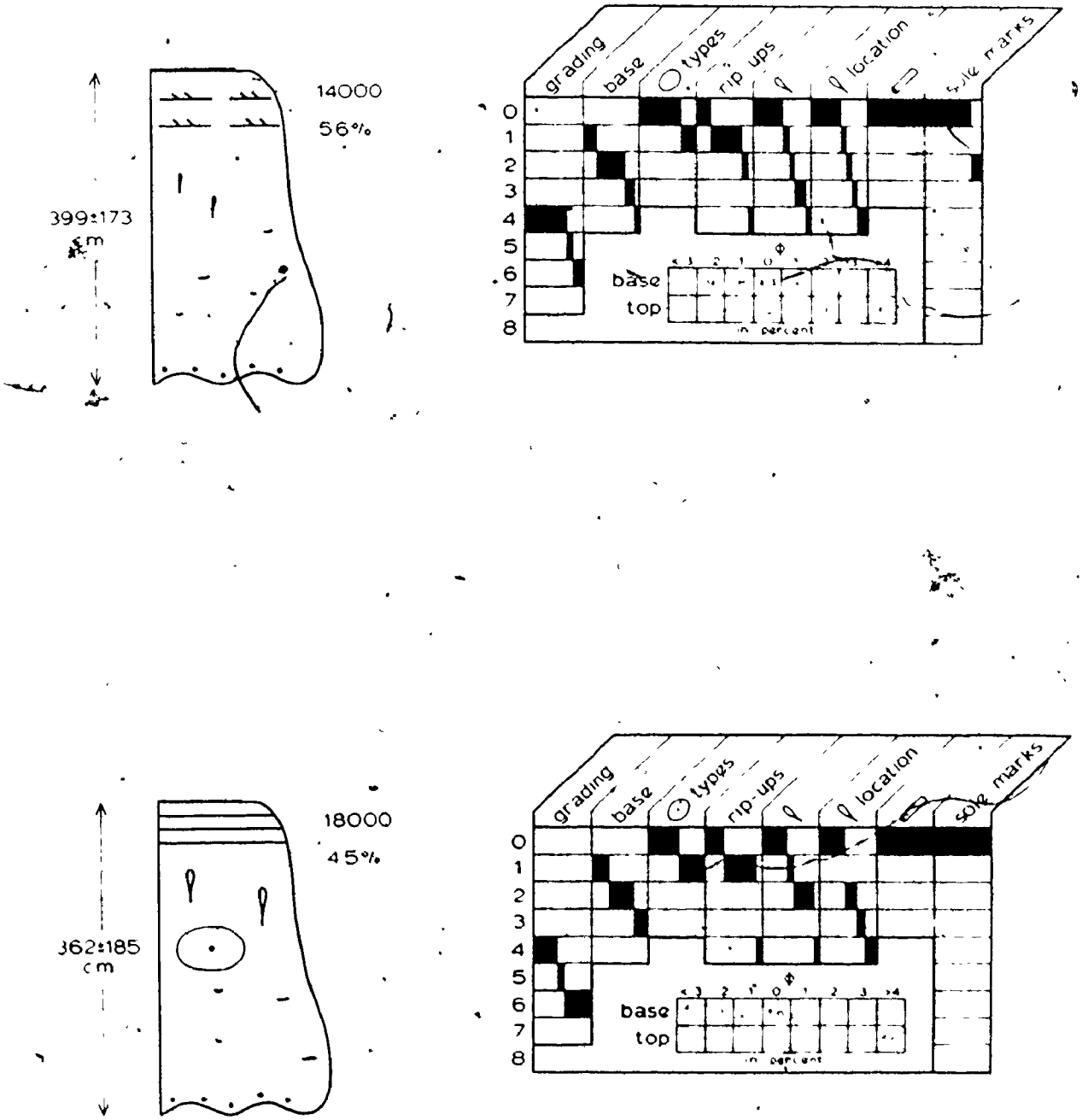

FIG. 2.21 cont'd

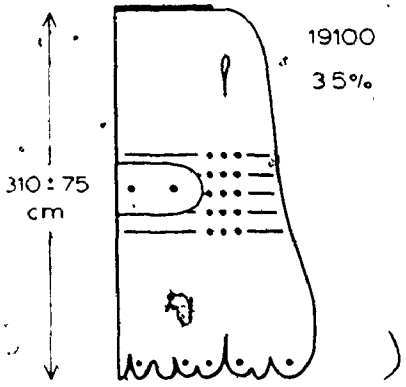

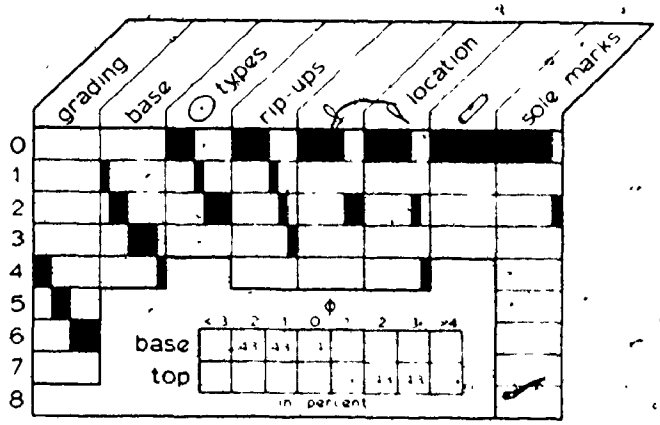

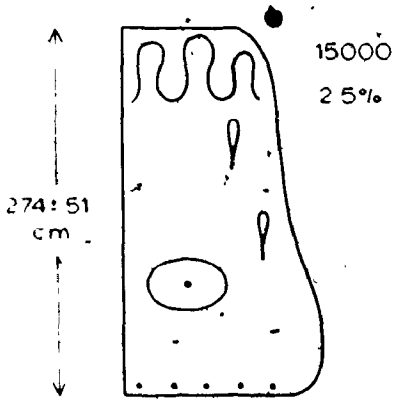

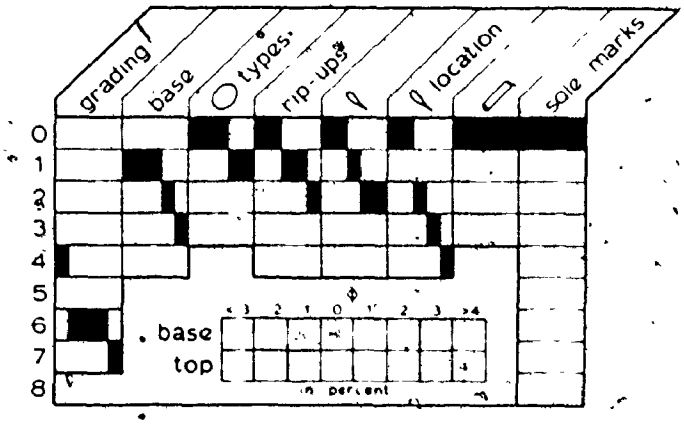

FIG. 2.21 cont'd

Loaded bases are uncommon, and channelling is rare and unimportant. Also quantitatively unimportant are concretions, fluid-escape structures, and fossil traces, which are so minor as to remain unrecorded in the most frequently occurring structure sequences. Rip-up clasts occur in about 20 to 40% of all layers, and are generally shale, but may include siltstone or chert. These rip-ups are generally less than 10 cm across. Less than 10% of all layers contain rip-ups from 10 to 100 cm in apparent length. Inorganic sole markings, observed on approximately 20% of all layers, are predominantly grooves, with flutes being less common (Figure 2.23). Modal basal grain size is 0 ϕ to 1 ϕ, with modal upper size being 3 ϕ to 4 ϕ.

Truncated sandstone (5) characteristics

Again normal grading is characteristic. Continuous size decline is most common, because fine layer tops have been truncated. Bases are approximately equally divided between flat and irregular. Massive layers capped by cross-stratification commonly have loaded bases. Concretions are generally absent. Fossil traces were not recorded. Fluid-escape structures, if present, are confined to rare, coarse pillars at various levels in the layers. Rip-up clasts are again almost entirely confined to dimensions less than 10 cm.

Fig. 2.23. Sole markings on thin and truncated sandstones.

(A) Large, bulbous, and loaded flutes on a 1 m thick detached block at area J. Flow was from left to right, as shown by the arrow. Scale 1 m.

(B) Microflutes on the base of a thin sandstone (4) layer at area J. These features are scour marks propagated from worm-tube defects in underlying shale. Flow was toward the bottom of the photograph. Scale in centimetres.

(C) Long thin flutes covering the sole of a truncated sandstone (5) at area L. Flow was from left to right. Barnacle is about 1 cm across.

(D) Fluted grooves or longitudinal ridges on a truncated sandstone (5) at area L. Flow was from upper right to lower left. Scale 15 cm.

(E) Large striated groove on thin sandstone layer at area J. Scale 15 cm.

(F) Grooves on two separate layers (area D) which are at right angles to one another. Scale 1 m.

(G) Grooves and longitudinal ridges on the base of a sandstone layer west of Ste-Félicité. The sandstones are probably Tourelle equivalents. Scale 1 m.

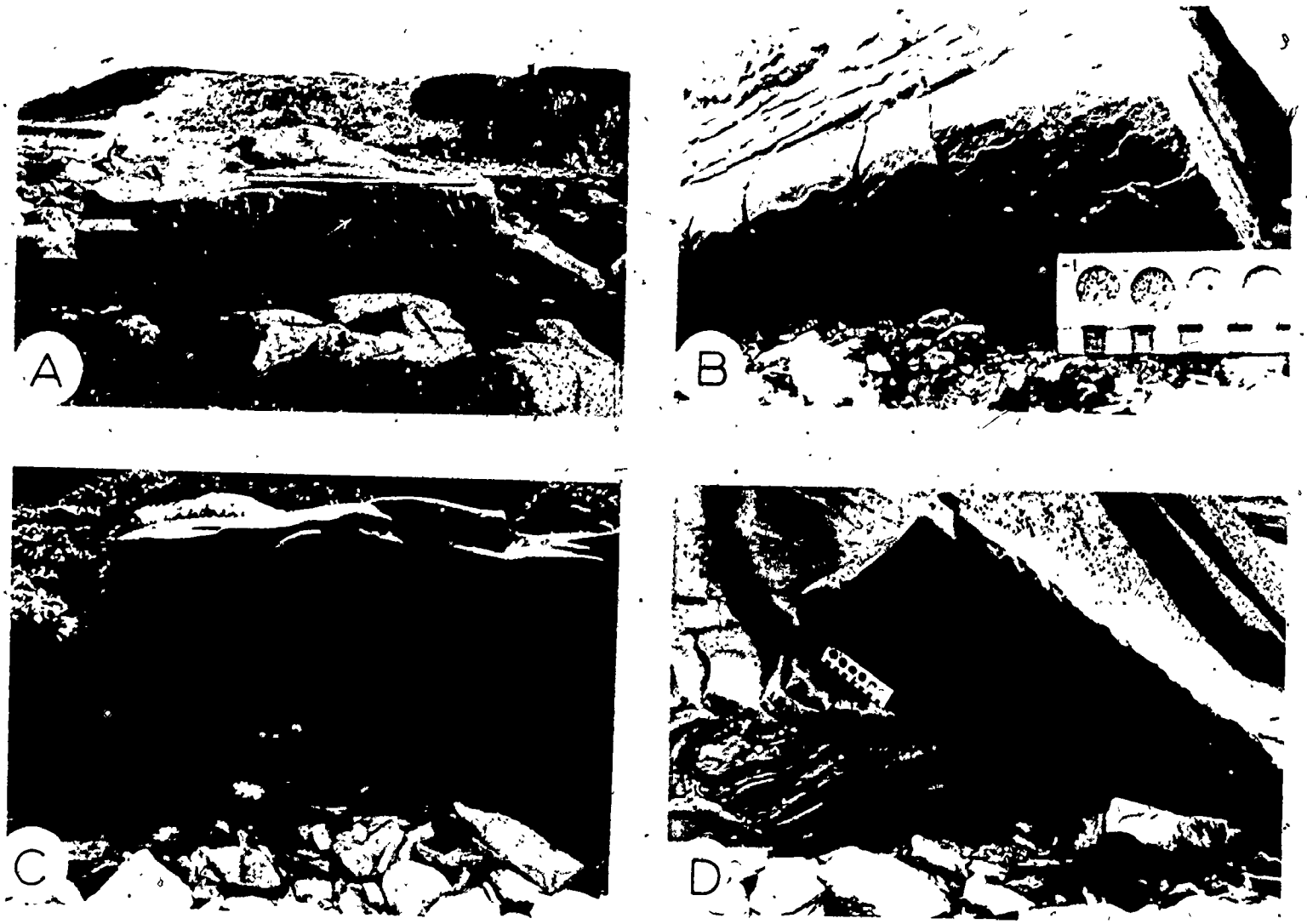

FIG. 2.23

FIG. 2.23
cont'd

Inorganic sole markings were recorded less frequently than for thin sandstones (4), as a result of infrequent exposure of soles within amalgamated beds. Again, grooves were most often recorded, with flutes and longitudinal ridges being less common (Figure 2.23). Modal basal and upper grain sizes are -1 ϕ to 0 ϕ and 1 ϕ to 2 ϕ, respectively.

Subfacies 6a characteristics

This subfacies is characterized by strongly imbricate, massive, granular sand. Modal basal grain size is -2 ϕ to -1 ϕ (upper mode 0 ϕ). Graded layers dominate, with several styles of grading being represented. Less than 10% of all layers are ungraded. Bases are generally irregular, and may possess asymmetric scours which are believed to represent transverse scour marks (see Figure 2.9). Approximately 50% of all layers contain rip-up clasts less than 10 cm in diameter. Because of amalgamation, no sole markings were seen. Fluid-escape structures were also not observed, probably because (i) the coarseness of the sediment allowed unimpeded intergranular fluid-escape, or (ii) slow deposition produced a stable grain packing. This stable packing would preclude both post-depositional liquefaction and resultant localized fluid-escape. It should be noted that this subfacies occurs only at areas K, L and M (Figure 1.5), although equally coarse

subfacies 6b layers can be found throughout the formation.

Subfacies 6b characteristics

This subfacies contains 80% of all thick sandstone (6) layers, and hence has a greater diversity of sedimentary structure sequences than other subfacies. Because the seven sequences displayed in Figure 2.21 account for only 70% of all layers, reference should be made to Table 2.2 (p. 35) for further information concerning depositional structures. Several generalizations can be made on the basis of data presented in Figure 2.21.

(i) Normal grading is consistently developed, with only a few layers having basal inverse grading before reverting to normal grading. Modal basal grain size is -1 ϕ to 0 ϕ. The upper mode lies between 1 ϕ and 2 ϕ for layers with truncated tops, and between 3 ϕ and 4 ϕ for layers with top preserved.

(ii) Less than 50% of all bases are flat, with most others being irregular or loaded. Approximately 10% of all bases show channelling.

(iii) Concretions (Figure 2.24) are predominantly elliptical to spherical "cannonballs", and are much more common than in other sandstone facies. Concretion formation will be discussed in Chapter VI.

Fig. 2.24. Concretions in subfacies 6b massive sandstones.

(A) Spherical "cannonball" concretions associated with fluid-escape pillars at area L. Note the shale rip-up clasts within "cannonballs".

(B) Concretion bands in a thick sandstone (6) at area M-west. Scale 1 m. Top is to the left.

(C) Thick cementation band in coarse sandstone at area L. Many of these bands reveal faint stratification. Scale 1 m.

(D) Upper surface of sandstone layer at area L, showing calcareous concretions. Scale 1 m.

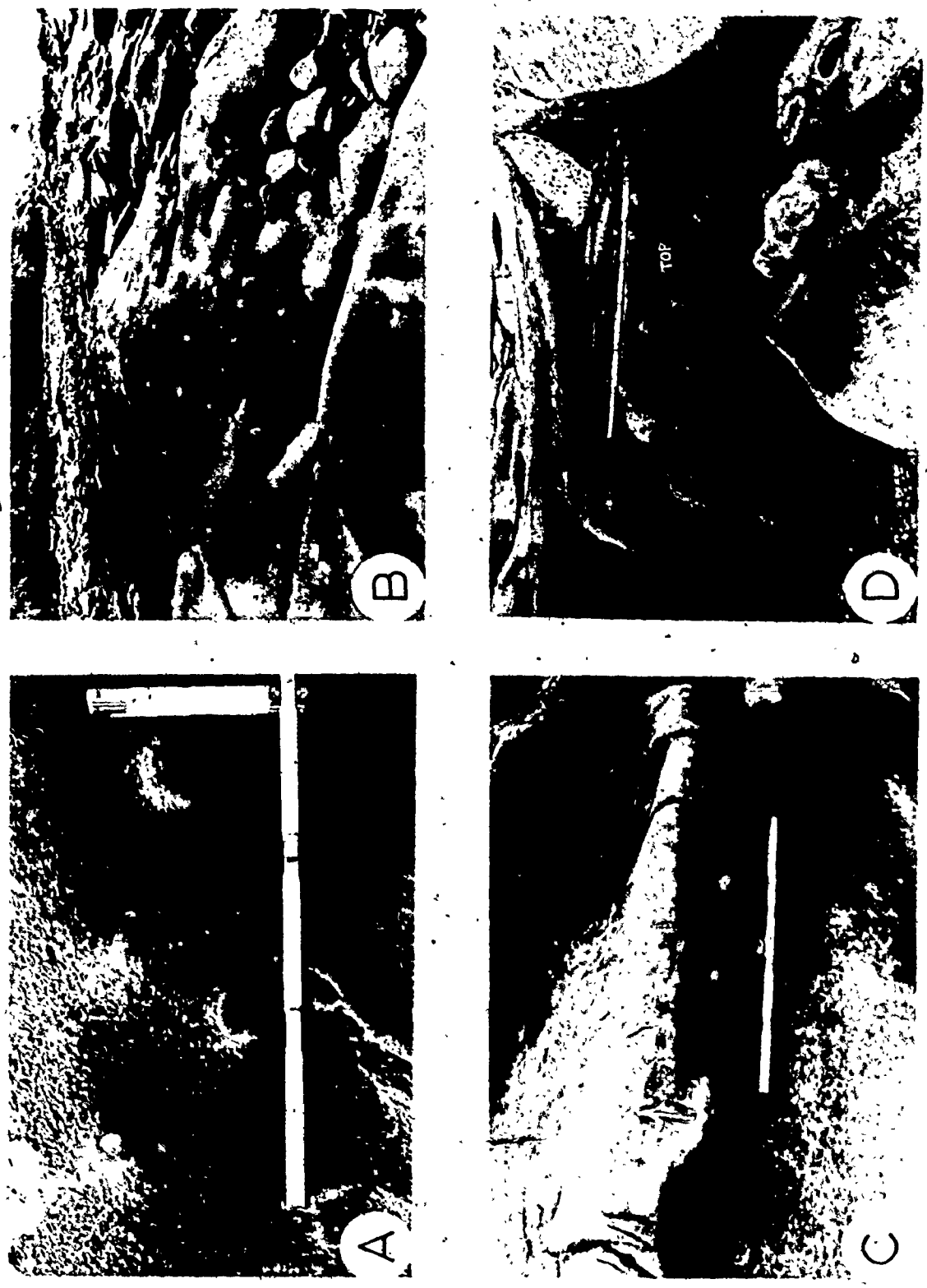

FIG. 2.24

(iv) Fluid-escape structures are also more abundant than in other sandstones, and occur at various levels in subfacies 6b layers, although there is a slight preference for the upper parts of layers. These structures, which are usually type B pillars of Lowe (1975), are quite abundant in some layers (see Figure 2.15).

(v) The abundance of rip-up clasts less than 10 cm in diameter is similar to that in previous facies. Of great importance, however, is the presence in sandstone layers of larger blocks of shale, dolomitic siltstone, or bedded chert, which range in maximum size from 1 to greater than 15 m. The largest slabs are found at area K (Figure 2.23). Several of these large blocks are shown in Figure 2.26. Their significance will be discussed in Chapter V.

(vi) Sole markings, which were observed on approximately 10% of all layers, are dominantly groove casts. Flutes are less common, but may be quite large (Figure 2.27). In many cases, large basal irregularities on thick layers of this subfacies were only partially exposed on the rather flat wave-cut terrace, making it impossible to ascertain their geometry.

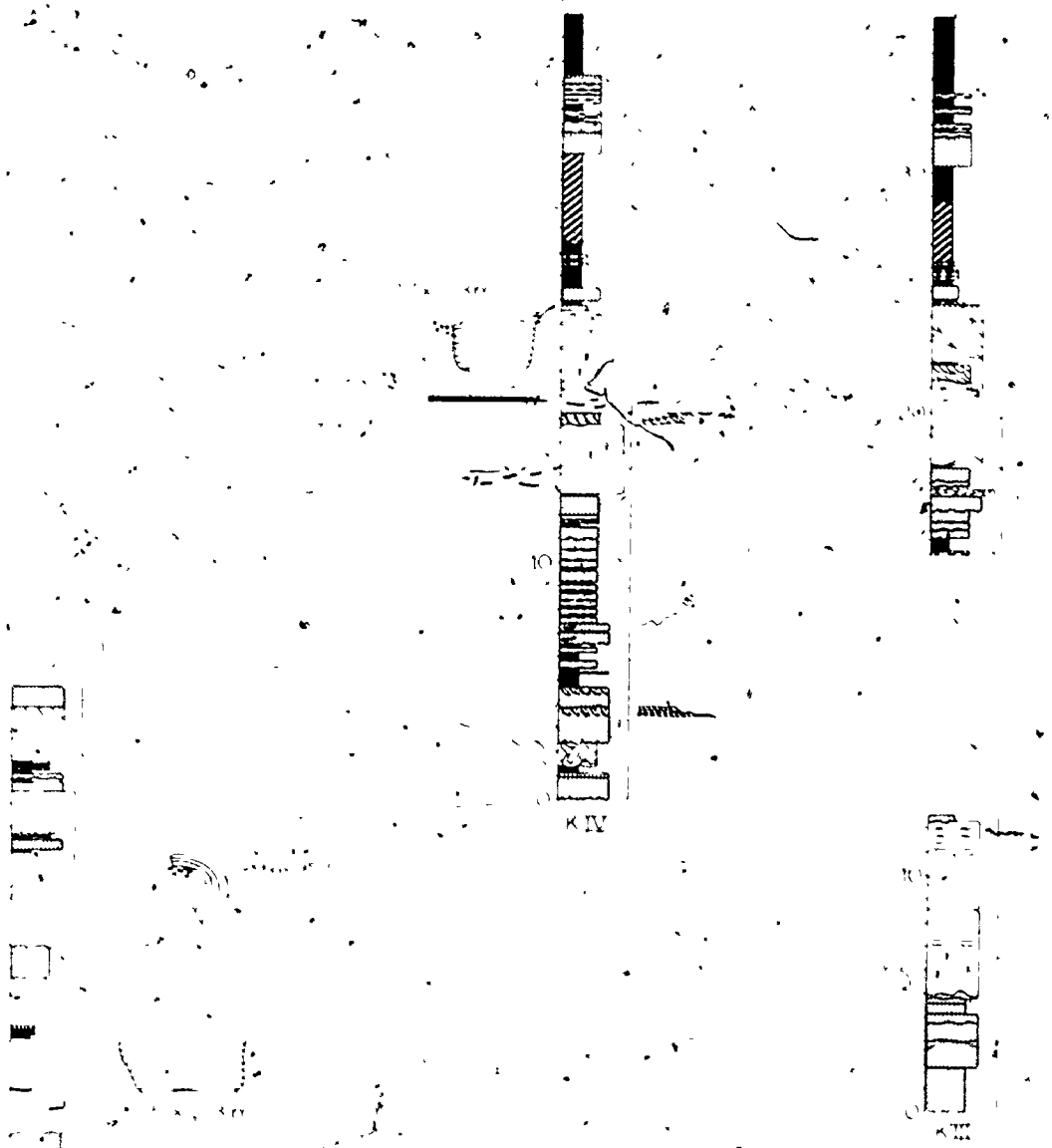

Slide block environment
Area K

Fig. 2.25

Fig. 2.26. Large blocks and slabs within thick sandstone (6) layers.

(A) Large 30 x 300 cm shale raft in a 5.2 m thick layer, area D. Scale 1 m. Top is to the left.

(B) 25 x 2.3 m dolomitic siltstone block in the top of a 4 m thick sandstone layer, area K. Scale 1 m. Top is to the left.

(C) 17 x 2.3 m bedded chert block which originally projected from the top of a 4.3 m thick sandstone layer, area K. The block settled into the top of the layer some time after deposition of an overlying thin sandstone (4). Top is to the right.

(D) Bent end of bedded chert block shown in (C). Scale 1 m. Top is up.

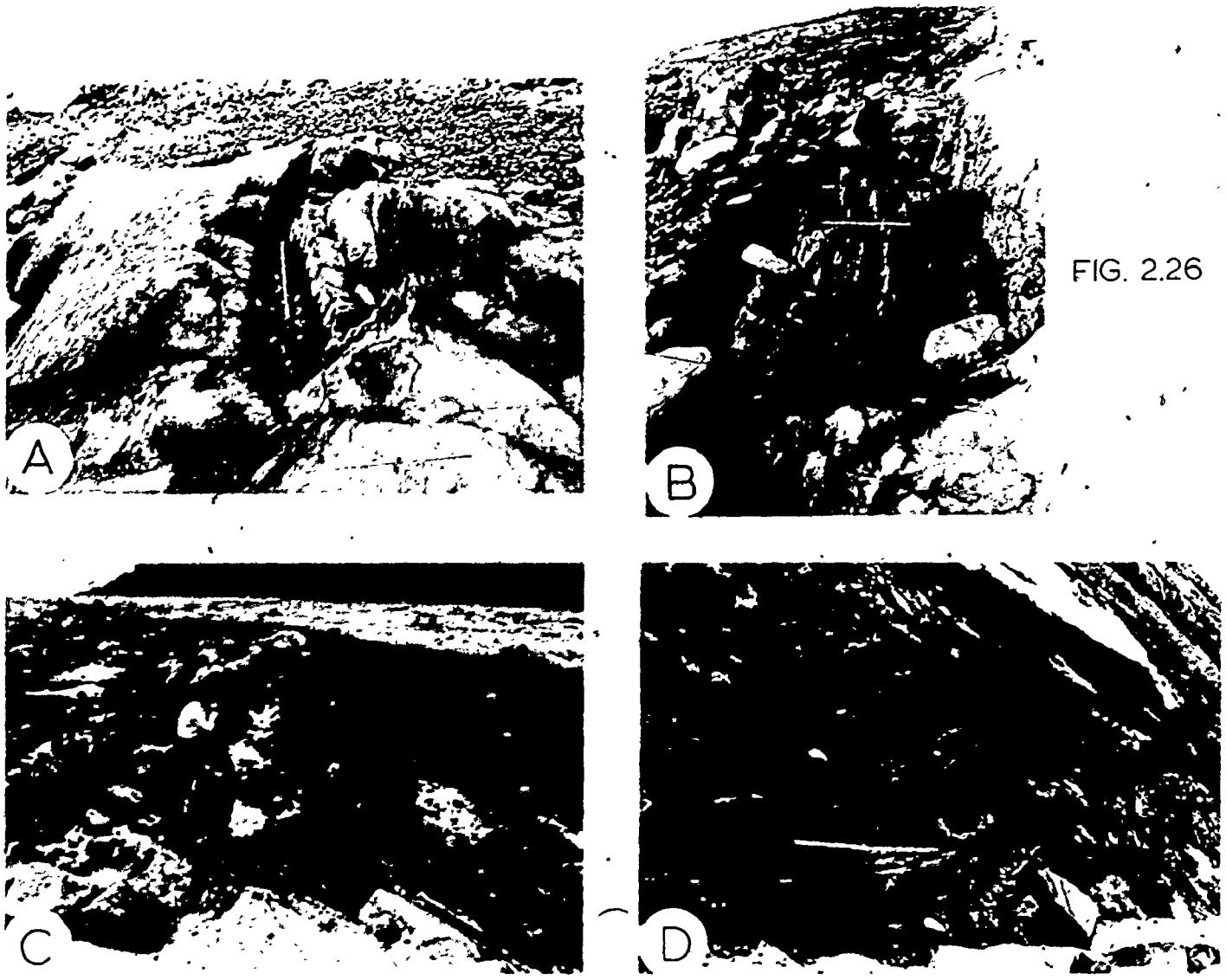

FIG. 2.26

Fig. 2.27. Sole markings on thick sandstones (6).

(A) Large bulbous flutes on a 435 cm thick, stratified sandstone east of area C. Flow was from right to left. This layer corresponds to fabric station 1 in Chapter IV.

(B) Striated grooves on a 2.2 m thick stratified layer at area J. Scale 1 m.

(C) Small flutes on a 10.5 m thick graded layer at area N-east. The flutes are filled with coarse sandstone containing limestone pebbles. Current flowed in the direction indicated by the arrow. This layer corresponds to fabric station 3 in Chapter IV.

(D) Large striated groove on 2 m thick, inverse-to-normally graded sandstone layer at area E. Scale 15 cm.

FIG. 2.27

Subfacies 6c characteristics

This subfacies contains only massive sandstone layers. Approximately 60% of these layers are ungraded, with the remainder showing slight upward fining or basal inverse grading. Surprisingly, almost half of all layers have flat bases, with irregular and loaded bases almost equally divided among the remainder. Cannonball concretions and fluid-escape structures are common, with the latter showing a preference for the middle and lower parts of layers. Sole marks are equally divided between flutes and grooves (Figure 2.27). The modal basal and upper grain sizes are -1 ϕ to 0 ϕ, and 0 ϕ, respectively. The layer thickness distribution for this subfacies is bimodal (Figure 2.2?, p. 32). Those layers comprising the mode less than 2 m in thickness would probably have been recorded as subfacies 6b layers had they not been truncated in their ungraded lower portion. For this reason, all future discussion of subfacies 6c will be restricted to ungraded or very slightly graded layers which are greater than 4 m in thickness. Grooves are more common than flutes for these thick layers.

Facies 7: conglomerate and conglomerate-based sandstones

Only two layers belonging to facies 7 are tabulated in Table 2.1. There are only a few conglomerate layers in all stratigraphic sections, and these are restricted to area M (Appendix I), and to the eastern end of area L.

This facies includes any layer possessing more than a basal veneer of clasts greater than 4 mm in size, and therefore does not include layers with a basal transported band of exhumed concretions (areas E and G). The implication of these concretion clasts will be discussed in Chapters V and VI.

Conglomerate is generally associated with deep scours or channel fills. The three principal varieties are listed below.

(i) Shale rip-up breccia with interstitial coarse sand matrix.

(ii) Chert-pebble conglomerate with dispersed cobbles and a granular sand matrix (Figure 2.28). This variety occurs in only one layer at area M-east, although isolated chert pebbles and rare cobbles are not uncommon in thick sandstones (6). The layer of chert conglomerate contains lenses of granular sand, is apparently composite in nature, and grades eastward into granular sand before being truncated by an irregular channel wall. Some chert clasts show lamination and truncated lamination. Others contain dispersed,

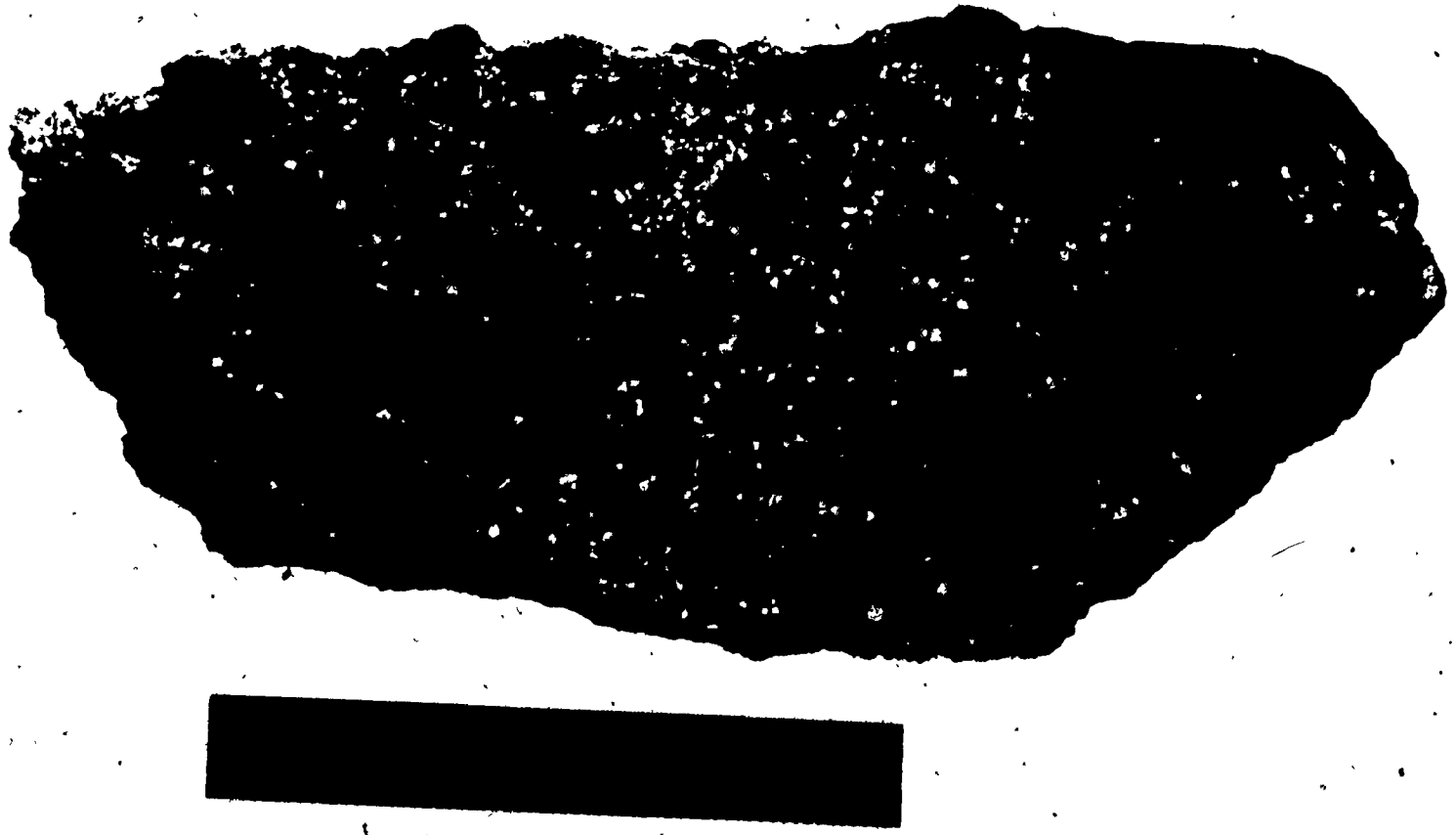

Fig. 2.28. Chert conglomerate with granular sand matrix, area M-east. Scale is in centimetres and inches.

infilled, radiolarian tests. All chert is either brown or green.

(iii) Clast-supported, limestone-pebble breccia with a coarse sand matrix (Figure 2.29). This is the most densely packed of the three types, and contains angular, equant clasts of micrite, pelmicrite, and pelbiomicrite (Folk, 1968). Preserved body fossils include disarticulated brachiopods, crinoid segments and column sections, echinoderm spines, calcareous algae, bryozoan fragments, ostracods, Girvanella sp. (alga), and Maclurites sp. (gastropoda). Conodonts separated from the limestone clasts indicate an Arenigian to Llanvirnian age and derivation from the North Atlantic (open marine) conodont province (identification by C.R. Barnes, University of Waterloo, Canada. For a discussion of provincialism in Ordovician conodonts, the reader is referred to Barnes and Fåhraeus, 1975). Similar open-marine fauna have been found by L.E. Fåhraeus (personal communication to Williams and Stevens, 1974) in the bank-margin facies of the Ordovician Table Head Formation in western Newfoundland.

The most easterly limestone-breccia channel fill at area M-east consists of about 40% massive conglomerate (Figure 2.29) which passes upward into coarse sandstone through a narrow transition of interstratified coarse sand, and pebble conglomerate. Similar limestone breccias higher in this section also display stratification and grading. For

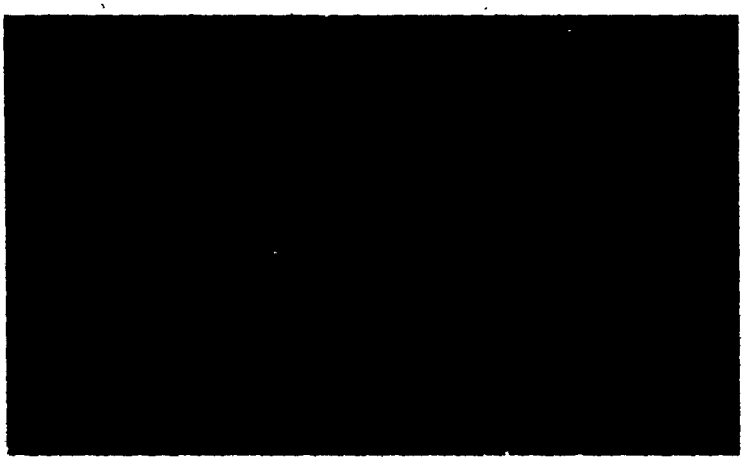

Fig. 2.29. Limestone breccia, area M-east. Scale 15 cm.

Transition from limestone breccia (right) to stratified coarse sand and pebbly sand (middle) to coarse sandstone (left) in a channel fill at area M-east. Scale 1 m. Top is to the left.

this reason, these layers are assigned to the graded-stratified, resedimented conglomerate model of Walker (1975a).

Facies 8: slumps and olistoliths

Included in this facies are (i) clastic layers that show evidence of downslope movement in a coherent state with overturned to recumbent intraformational folding, (ii) shale horizons with broken siltstone and chert layers, and (iii) rare slabs of chert, siliceous shale, or dolomitic siltstone up to greater than 30 m in length. A systematic description of representatives of this facies will be undertaken from west to east. A single asterix (*) is used to recommend examination of the relevant area map and composite section in Appendix I. When reference to more complete stratigraphic columns in the pocket of the thesis is necessary, a double asterix (**) will be used.

The lowest 35 m of section at area A* comprises the upper part of the deformed Cap des Rosiers Group, overlain by four or five structurally distinct slices of dolomitic siltstone that are assumed to have slid into place prior to deposition of Tourelle sands. These show different degrees of internal soft-sediment deformation which do not pass into adjacent slices. Internal slump folds are truncated by the next slide block (Figure 2.30), and at least two of

Fig. 2.30. Slumped dolomitic siltstones (right) truncated and overlain by another undeformed slide block (left) at area A, Cap des Méchins.

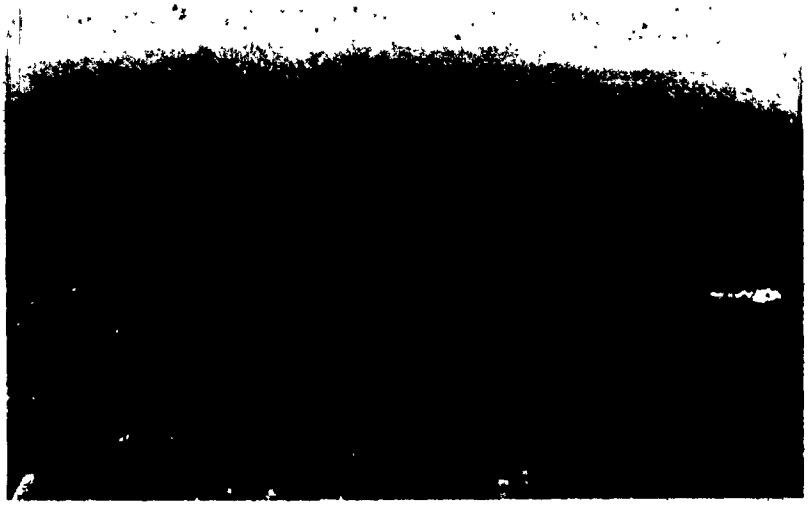

Slip plane (arrows) between two slide blocks of dolomitic siltstone at area A. There is an angular divergence between bedding in the two blocks. Scale 1 m. Top is to the right.

these slide blocks are based by a band of broken strata less than 25 cm thick. Where internal deformation is not present, slide surfaces are indicated by small angular divergences between bedding planes, producing low angle, oblique truncation of stratigraphy in the lowermost slide block (Figure 2.30).

On the east side of Cap des Mechins (area A**) a spectacular slumped horizon is intimately associated with a large allochthonous slab (olistolith) of dolomitic siltstone (Figure 2.31). Smaller blocks of dolomitic siltstone are found in overlying sandstone layers. It is possible that as the large slide block was emplaced, it bulldozed previous deposits in front of it, resulting in the associated contorted slump horizon. Slump folds measured at this locality define a paleoslope dip which is rotated 50° clockwise from the mean of sole marks.

Area D* (Capucins) contains many scattered slide blocks and associated slump horizons. These slumped units are associated with slurry sandstones (3). The largest slumped horizon can be traced across the entire outcrop area **. There actually appear to be two separate sedimentary slides represented here. The lowermost consists of deformed grey shale and thin chert bands separating large olistoliths of red shale. The upper slumped layer comprises a layer of slurry sandstone containing at least one large olistolith of

Fig. 2.31. Slumped horizon of sandstone beds on the east side of Cap des Méchins (area A). See text for discussion. This slump is truncated abone by an erosive coarse sandstone. Scale 1 m. Top is to the left.

dolomitic siltstone.

As was the case at area A, the base of the Tourelle Formation at area J is characterized by major slumping involving two dolomitic siltstone beds in a much thicker shale horizon (Figure 2.32). The direction of overturning adjacent to slip planes suggests a strong component of movement from west to east.

At area L* there is a slumped sandstone layer, similar to that found at area A, at a height of 61 m in the composite section. This layer is 250 cm thick and consists of long recumbent flow-folds of coarse sand. At a height of 44 m in section LXIV** is one of the largest slide blocks yet observed in the Tourelle Formation. It is partially submerged in a tidal pool, but is easily identified by the yellowish colour of its siltstone beds. Also present within the block are bands of brown chert and thin clastic dikes. The block measures 31 by 6 m, and is in line, along strike, with smaller blocks of the same composition between sections LXII and LXIII.

Facies 9: injection structures (Morris, 1971)

With rare exception, these injections are restricted to the basal transition zone of the Tourelle Formation, and are associated with red and green shales, or dolomitic

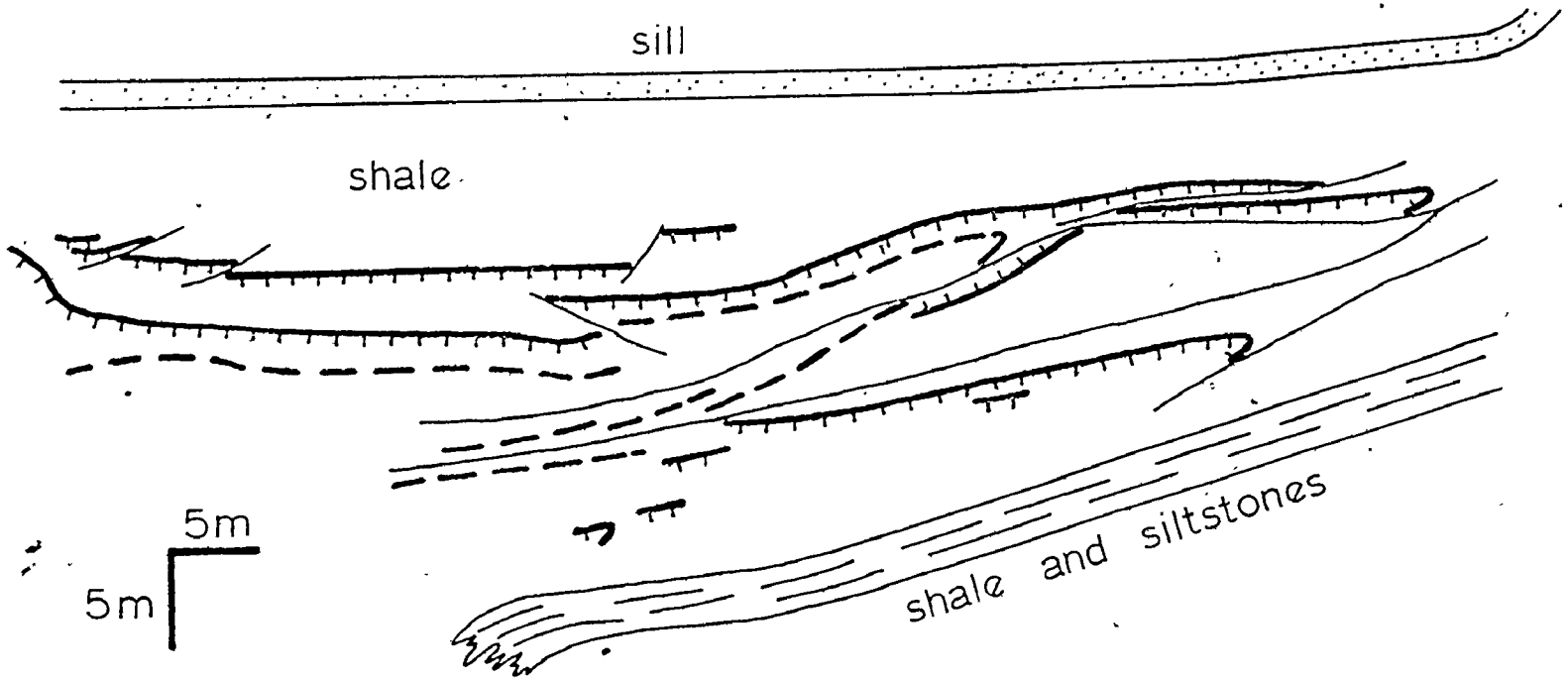

Fig. 2.32. Slumped horizon below sandstone injections at area J. The slump involves shale, a distinctive amalgamated dolomitic siltstone bed (▬▬, barbs on base), and a single dolomitic siltstone layer (▬ ▬). The siltstone beds are repeated several times as a result of telescoping along slide surfaces (———). Sandstones at area J were deposited parallel with the sill at the top of the sketch.

siltstones (areas G, H, J). The most common variety consists of sills which may exceed 1 m in thickness. These sills are internally structureless, except for one or two occurrences of fluid-escape structures. They are generally ungraded (8% show normal grading), and have both sharp flat bases and tops. Grain size varies from coarse to fine sand.

The best exposure of injection structures is found at area J. A detailed outcrop map is presented in Figure 2.33. In addition to features mentioned above, sills exhibit both pinch and swell thickness variation and local cross-cutting relationships, and may disrupt adjacent siltstone layers. Large cross-cutting dikes feed several of these sills (Figure 2.34). Figure 2.35 is an equal-area stereographic plot of poles to oblique dikes in shale, following rotation of bedding to a horizontal position about the strike line. Lithologic control of dike orientation in muds was probably at a minimum. Instead, the liquified sand escaped upward along the most favourable pressure gradient. The stereographic plot shows a strong concentration of poles at right angles to the mean current direction for the area. If the flows moved down, rather than across the slope, then the dike orientation could be explained as intrusion along a pressure gradient from a laterally adjacent channel. The data cluster only to one side of the mean current direction, which would be consistent with location of a major channel

1 of.

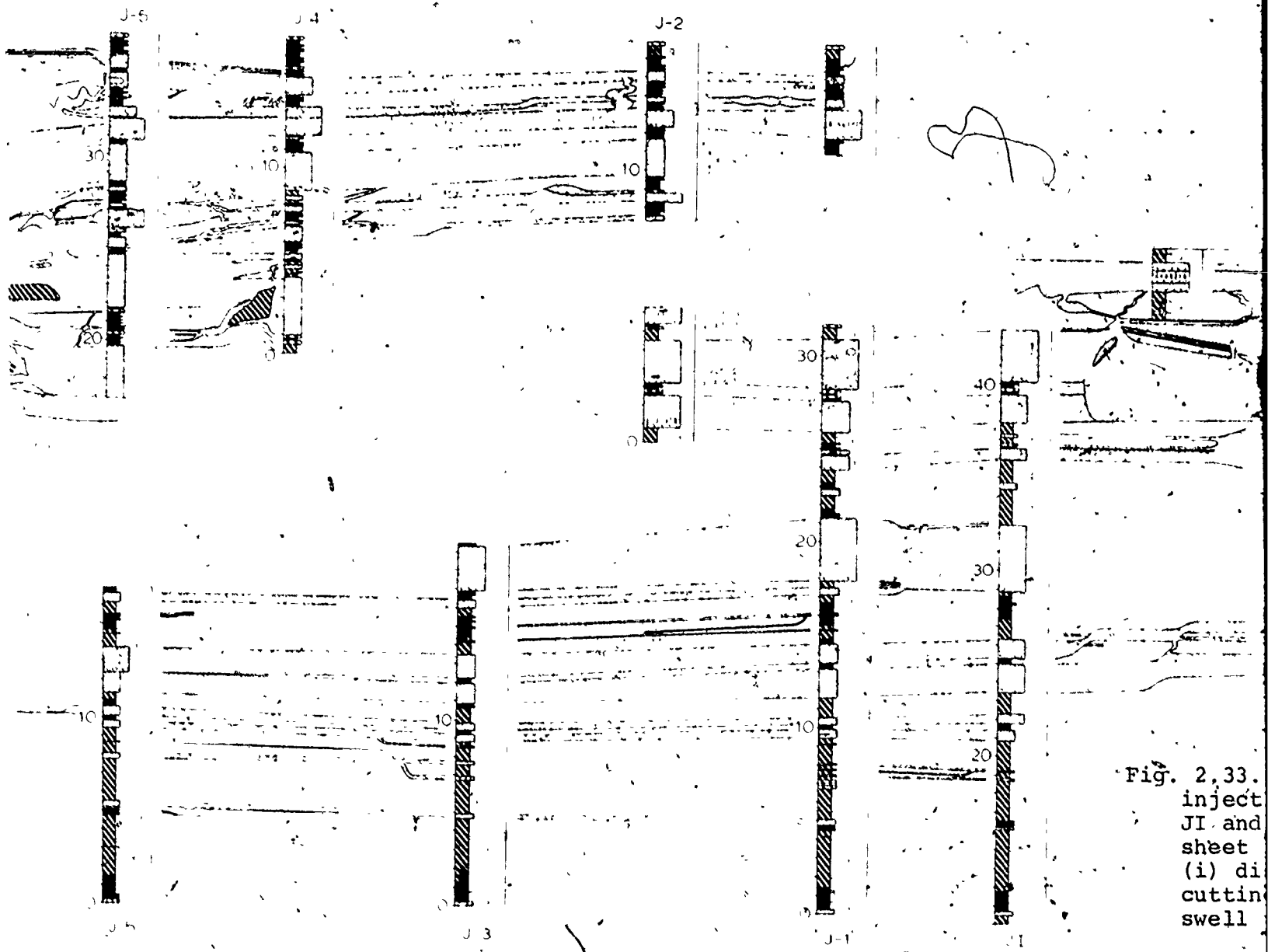

Fig. 2,33.
inject
JI and
sheet
(i) di
cuttin
swell

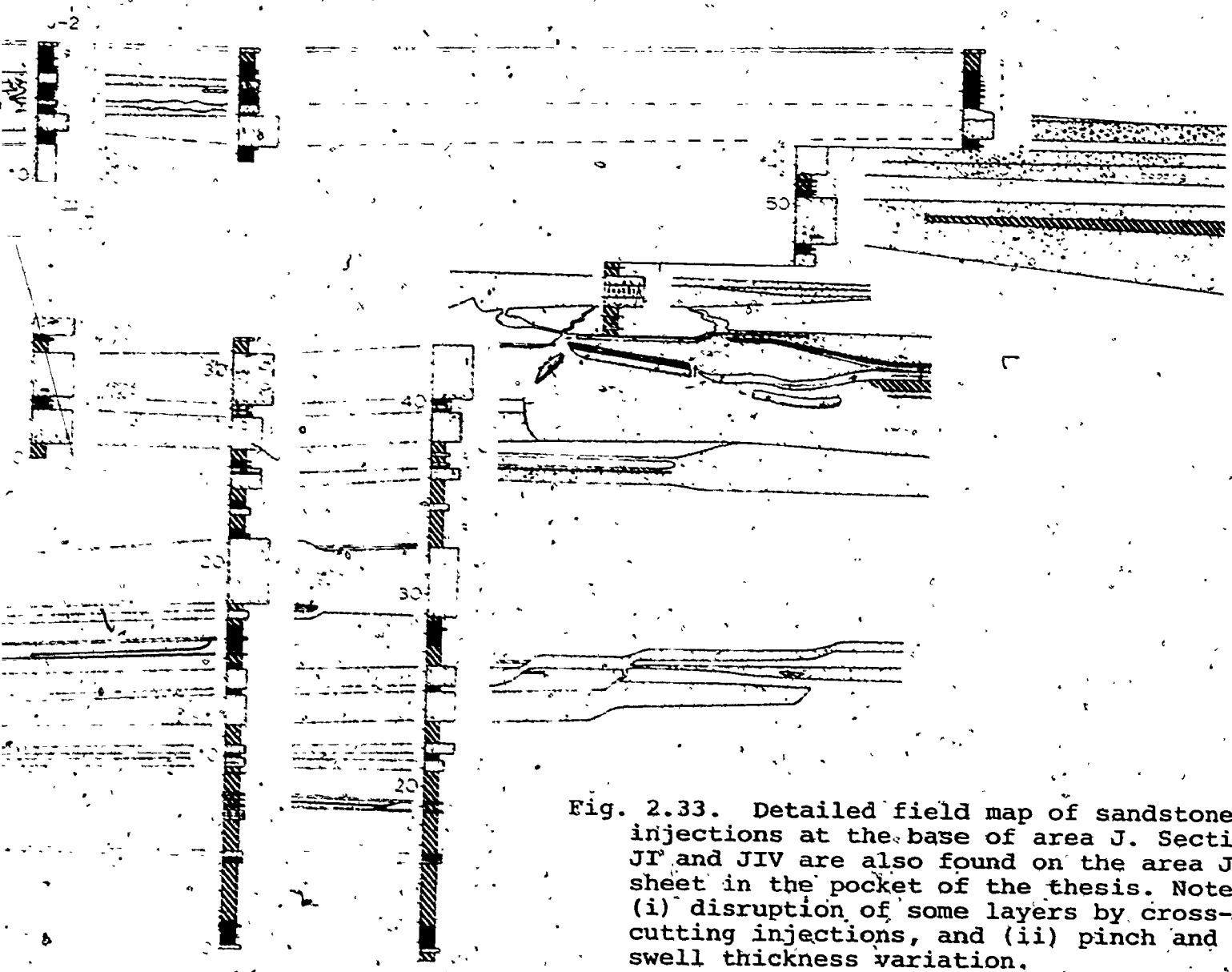

Fig. 2.33. Detailed field map of sandstone injections at the base of area J. Sections JI and JIV are also found on the area J sheet in the pocket of the thesis. Note (i) disruption of some layers by cross-cutting injections, and (ii) pinch and swell thickness variation.

Fig. 2.34. Sandstone injections, area J.

(A) Large sinuous clastic dike connecting three sharp-topped sills. Scale 1 m. Top is to the left.

(B) Sandstone dike penetrating dolomitic siltstone layers. The siltstones are bent upward in the direction of sand injection. This may, however, be a result of compaction.

(C) Two thin sandstone sills (grey) in a dolomitic siltstone unit. These are connected by a straight dike of equal thickness. Scale 15 cm.

(D) Irregular clastic dike showing pinch and swell thickness variation as it cuts through a unit of dolomitic siltstone. Scale 1 m. Top is to the right.

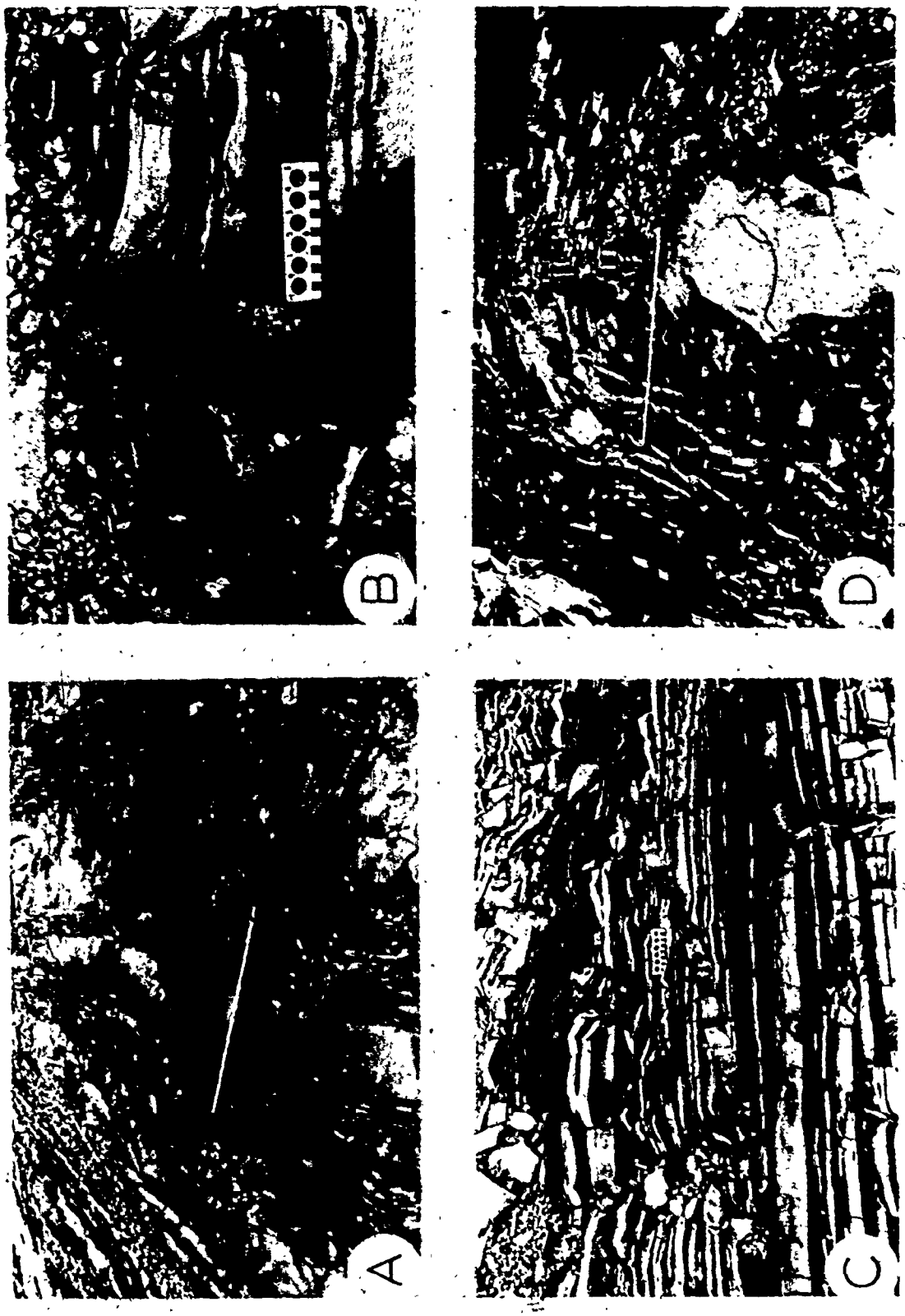

FIG. 2.34

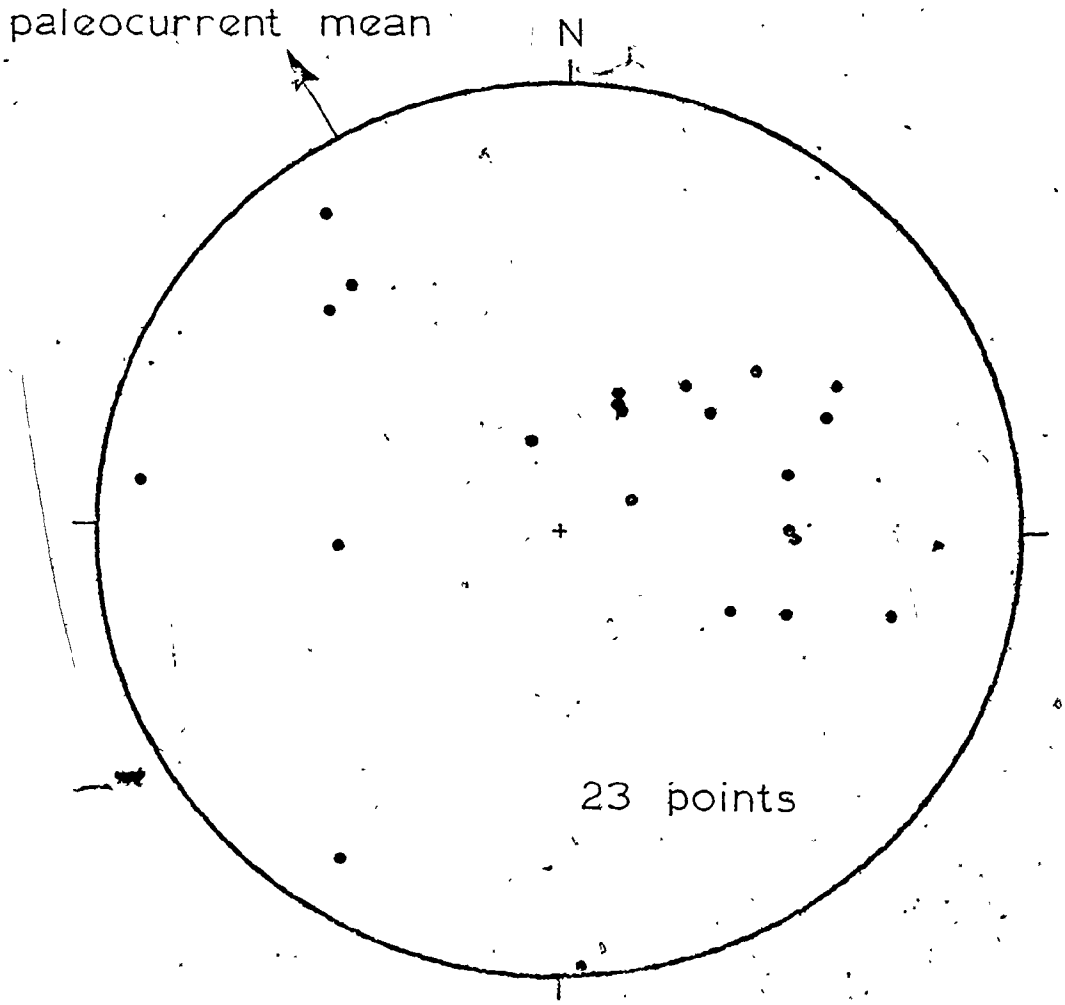

Fig. 2.35. Plot of rotated poles to crosscutting sandstone dikes. N-S-E-W plane is parallel to layering. Note the strong clustering of poles plunging NE and at right angles to the mean current direction.

somewhere to the southeast of area J at the time of clastic injection. The fact that channelling is observed at area J (Chapter III) lends some support to this hypothesis.

The localization of clastic injection within dolomitic siltstone and red shale horizons may result from a lower permeability perpendicular to bedding than is found in coarse sandstones and silty shales at higher levels in the formation. Hence liquified sand would remain in a fluid state without losing its pore water and could be squeezed laterally along planes of weakness. Initial introduction of the liquified sand into these horizons is less easily explained. Lateral introduction from the margin of a thick channel-fill sequence has already been suggested. Perhaps, as an alternative, coarse sandstones were actually deposited alternately with dolomitic siltstones, followed by in situ liquefaction, flowage under overburden pressures, and injection. The interbedding of sandstone layers of Tourelle lithology with the upper part of the Cap des Rosier Group is indeed found west of Marsoui (see Chapter VIII). This latter hypothesis encounters difficulties, however, in explaining the sharp tops of all injected layers and the complete absence of silty grey shale.

Fossil Traces

The trace fossil assemblage of the Tourelle Formation is preserved in positive hyporelief (Seilacher, 1964) on bases of thin sandstones (4) and dolomitic siltstones. These fossil traces are extremely rare, with all well exposed specimens displayed in Figure 2.36. Vertical tubes are almost exclusively confined to the dolomitic siltstone facies, indicating that erosion of the substrate by the depositing current was slight. The casts of these tube apertures may show evidence of down-current scouring.

Thin sandstones (4) display three varieties of horizontal crawling (repichnia) and feeding (pascichnia) traces. These forms resemble Phycodes, Planolites and Helminthopsis. Individual traces are approximately 0.5 cm across and of varying length. This assemblage probably reflects activity along the interface between sand and mud layers after deposition, because substrate scouring would remove or modify surface horizontal traces in this environment.

Dörjes and Hertwick (1975) indicate that modern crawling traces of intrasedimentary feeders can be found from near-shore environments to beyond the edge of the continental shelves. Vertical and U-shaped tubes, however, are restricted to shelf depths due to a decreasing availability of suspended food with depth. Active submarine canyon and fan systems, however, probably funnel particulate

Fig. 2.36. Fossil traces on the soles of thin sandstones (4). Traces on dolomitic siltstones are illustrated in Chapter VIII (Figure 8.22). Trace fossils are named on the basis of similarity with published illustrations.

(A) Phycodes, area A. Scale in centimetres.

(B) Phycodes (?), area A. Scale 15 cm.

(C) Planolites, area A. Scale 15 cm.

(D) Phycodes, Ste-Anne des Monts. Scale 15 cm.

(E) Helminthopsis, area J. Scale in centimetres.

(F) Vertical tubes, at area A, some of which appear to be paired. Scale in centimetres. Most infillings have been replaced by pyrite.

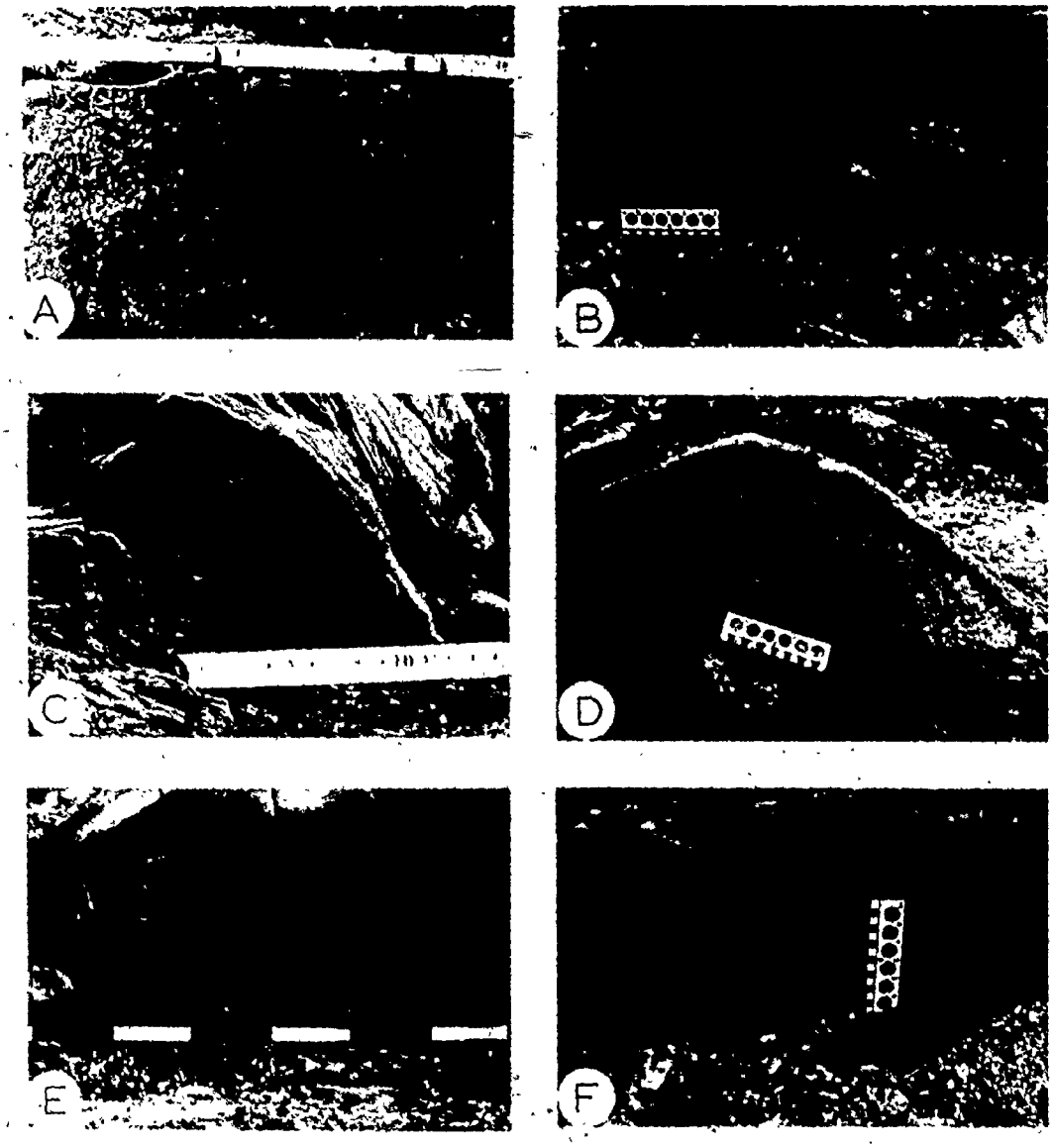

FIG. 2.36

organic detritus into slope and base-of-slope environments, allowing suspension feeders to be substrate rather than depth controlled. Submarine levees would be particularly well suited to population by suspension-feeding organisms (vertical and U-shaped tubes) because of abundant fine suspended detritus and a firm silty substrate.

The trace fossil assemblage associated with dolomitic siltstones will be discussed in Chapter VIII as this facies is more common in the Cap des Rosiers Group.

General Facies and Environmental Interpretation

Several features of the Tourelle Formation are predicted by the submarine-fan facies model (Walker and Mutti, 1973; Walker, 1976 and in press), but are not characteristic of other depositional environments. Most notable of these are (i) the association of thick, coarse, graded sandstones with layers possessing all attributes of classical turbidites, (ii) influx of coarse clastic detritus into a depositional environment otherwise characterized by deposition of mud, (iii) lack of evidence for reworking of sands by wave action, and (iv) the presence of deep channels associated with thinning upward sequences (Chapter III). In the present submarine-fan model (Walker, 1976), coarse sandstones and conglomerates are allocated to the leveed inner-fan channel

(see Figure 1.3), or to channels or suprafan lobes of the mid-fan. Classical proximal turbidites (thin sandstones (4)) may be found on the outer mid-fan, or as lateral equivalents to amalgamated sandstone packets. A more precise evaluation of the depositional environment of coarse sandstones, within the framework of the submarine-fan model, will be the subject matter of the next chapter.

The Tourelle Formation was deposited either on, or at the base of, a submarine slope. Evidence for this slope comes from several extensive slump sheets found interlayered with Tourelle sandstones. In addition, large allochthonous blocks of lithified strata which are incorporated in thick sandstones (6) can be ascribed to undercutting and plucking from the walls of upslope canyons (for modern examples, see Shepard and Dill, 1966, p. 106-7, and Palmer, 1976). Slurry sandstones (3) contain abundant muddy matrix, large rafts of shale or siltstone, and are frequently lateral associates of slumped horizons. It has been suggested that slurry sandstones result from slumping of muds and unconsolidated sand (Morris, 1971), with transportation by grain flow in the viscous regime (Carter, 1975) or by debris flow (Carter, 1975; Hampton, 1975). Hence this facies also provides evidence for a submarine slope.

On the basis of criteria outlined by Nelson and others (1975) and Mutti (1977), units containing abundant ripple-

drifted siltstones (2) can be interpreted as overbank deposits along the margins of submarine-fan channels. This interpretation is reinforced by comparison of a shale and siltstone horizon which occurs at both areas J and K. Correlation is based on the presence at both localities of a distinctive coarse calcarenite layer. Although these outcrops are now less than one kilometre apart, the thickness of the horizon and the percentage of siltstone layers decreases markedly from J to K (Figure 2.37). Rapid decrease in competence during overbank spill would explain this change. Some siltstones at area J also thicken upward (Figure 2.3), which may result from channel aggradation and increased overbank spill.

Thin siltstone layers and extensive thick shales (1) which occur at areas K and L (Appendix I) may represent interchannel muds, or thick mud blankets deposited on top of abandoned mid-fan distributary-channel and lobe systems (Walker, in press). These shaly horizons will be discussed in Chapter III.

Dolomitic siltstones will be interpreted with other Cap des Rosiers Group lithologies in Chapter VIII.

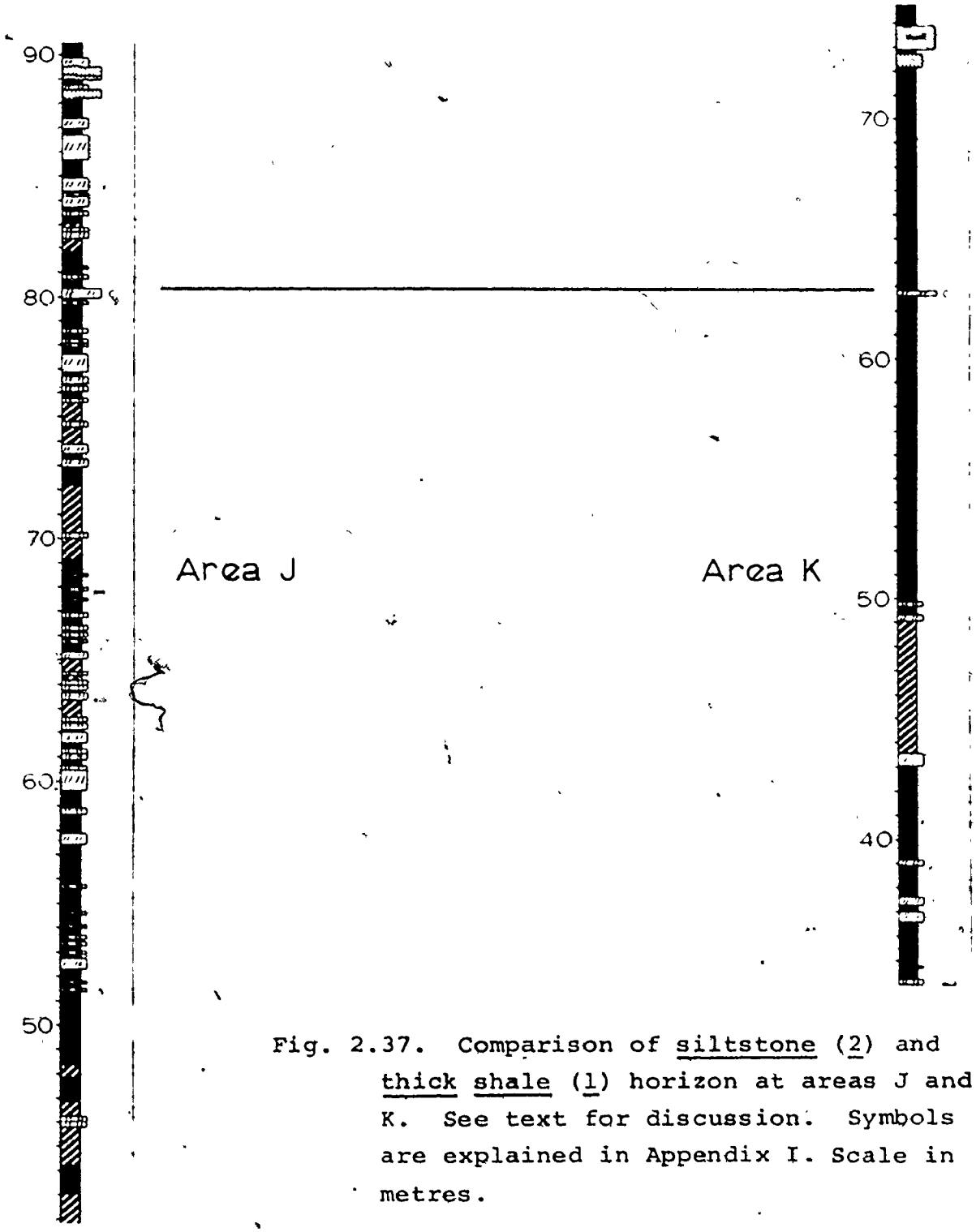

Fig. 2.37. Comparison of siltstone (2) and thick shale (1) horizon at areas J and K. See text for discussion. Symbols are explained in Appendix I. Scale in metres.

Summary

The Tourelle Formation was studied at twelve separate localities. Composite sections from these outcrop areas total 2364 m in thickness, which is interpreted to be at least twice the thickness of the entire formation.

All strata within the Tourelle Formation can be assigned to one of 9 facies. These are (1) thick shales, (2a) siltstones, (2b) dolomitic siltstones, (3) slurry sandstones, (4) thin sandstones, (5) truncated sandstones, (6) thick sandstones, (7) conglomerate, (8) slumps and olistoliths, and (9) clastic injections. Sandstone facies (4) to (6) comprise 70% of the total stratigraphy, and are dominated by thick sandstones (6) containing unusual sedimentary structures. Whereas thin sandstones (4) and many truncated sandstones (5) can be described using the Bouma turbidite classification, thick sandstones (6) may contain cross-stratification, internal scour surfaces, or unusual near-horizontal coarse stratification. Most layers, however, are massive and may be poorly graded, ungraded, or inverse-to-normally graded. Post-depositional pore-fluid escape is indicated by locally abundant fluid-escape structures. These thick sandstones (6) may also contain enormous blocks of shale, dolomitic siltstone, or bedded chert up to 16 m in length which appear to be suspended within the sandstone layers.

Conglomerate is surprisingly uncommon in a formation containing such thick mass flows, and is generally restricted to the fill of large channels. Limestone-pebble breccia is formed of fragments of shallow-water carbonate containing a diverse fauna and pelletal grains.

At a few localities, extensive slump sheets or isolated olistoliths are found interlayered with Tourelle sandstones. These slumps are associated with matrix-rich slurry sandstones (3) containing large slabs of siltstone beds and abundant smaller rip-up clasts of shale. Slumps and slides are particularly abundant at the base of the formation. Dolomitic siltstones and clastic injections are also essentially confined to the lower formational boundary.

Trace fossils are confined to siltstones (2), dolomitic siltstones, and thin sandstones (4). Both horizontal trails and paired and unpaired vertical tubes are present. Analogy with the behavior of modern trace-forming organisms suggests that this assemblage was formed at depths similar to those found on the upper parts of modern continental slopes.

Characteristics of facies found within the Tourelle Formation conform with predictions of the submarine-fan facies model. Coarse, thick sandstones are generally assigned to submarine-fan channels or suprafan depositional lobes (Figure 1.3). The presence of large sand-filled channels in the Tourelle Formation lends support to this hypothesis.

Rippled siltstones (2) are believed to represent overbank spill from these channels. Thick shales (1), however, may have been deposited as mud blankets over abandoned mid-fan lobes and channel complexes. A more comprehensive environmental interpretation will be the subject matter of the next chapter.

CHAPTER III

FACIES ORGANIZATION

General Description

Internal facies organization is not constant throughout the Tourelle Formation, but conforms to one of four "schemes".

(I) Coarse sandstone beds interbedded with thin shale or siltstone (2) units (areas B, C, DI, D and E). There is no tendency for sands to be segregated into packets.

(II) Alternating thick horizons of shale (1) or siltstones (2), and packets of medium to coarse sandstone (areas A, CVIII, FIV, J, K and L). Packets exposed at area J are shown in Figure 3.1. At area L, one sandstone packet can be traced along strike for 916 m (Figure 3.2). Paleoflow is generally to the west and parallels strike direction. Thin sandstones (4) and most truncated sandstones (5) (stippled pattern) are parallel sided, and can be successfully traced across the outcrop area. Some truncated sandstones (5) and most thick sandstones (6) have irregular thickness due to local scouring and shallow channelling. This presents difficulty in correlation of individual layers between sections.

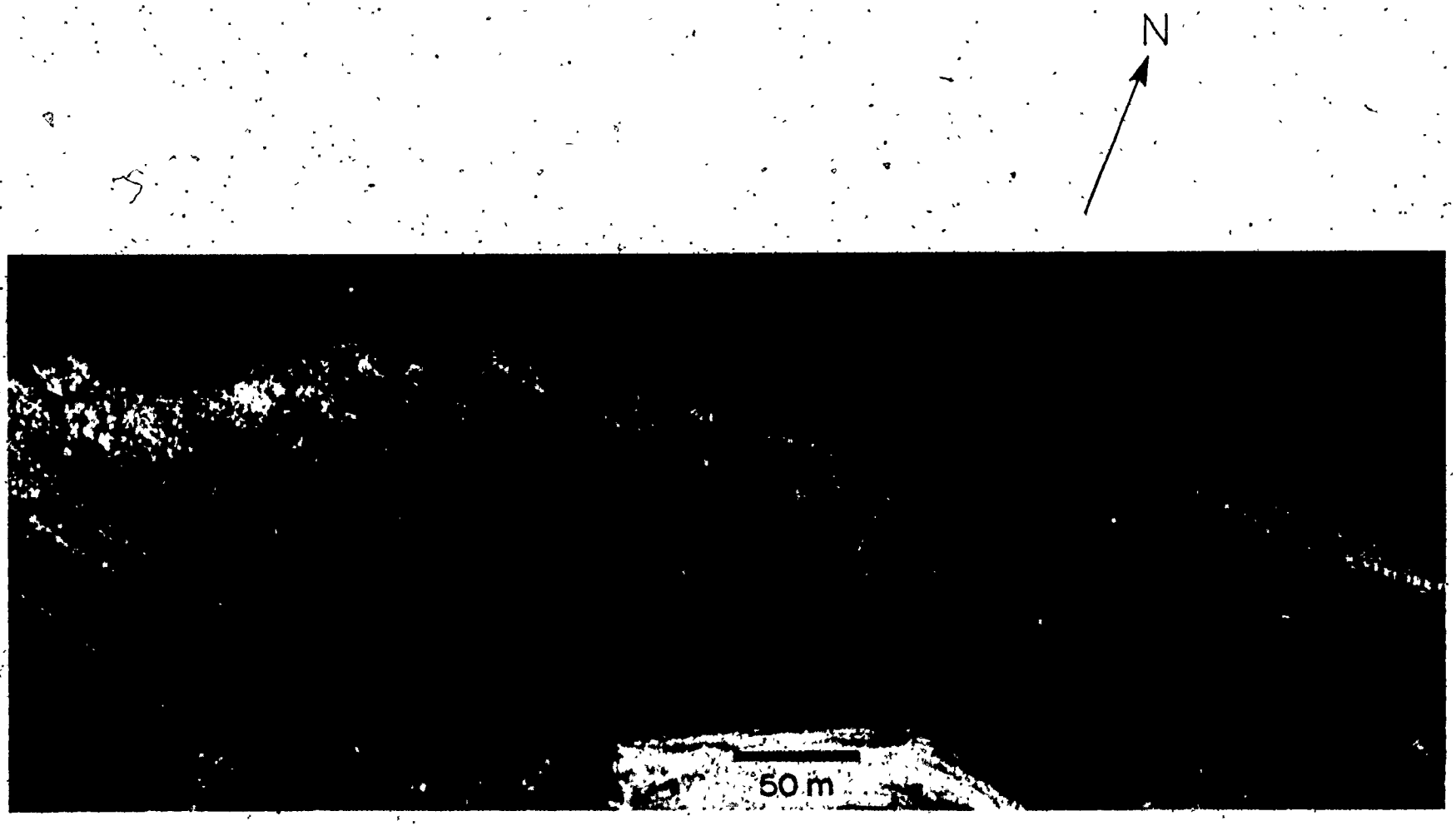

Fig. 3.1. Facies organization at area J, showing segregation of sandstones into thick amalgamated packets (labelled 1 to 6). Note the channelized base of packet J5. Area J conforms to facies scheme II.

Fig. 3.2. Western part of laterally extensive sandstone packet at area L. This overlies thick shales (1) and siltstones (2). The entire packet appears on full section drawings in the pocket of the thesis. Symbols are explained in Appendix I. Vertical exaggeration is 5 x.

coarse sandstone
Area L

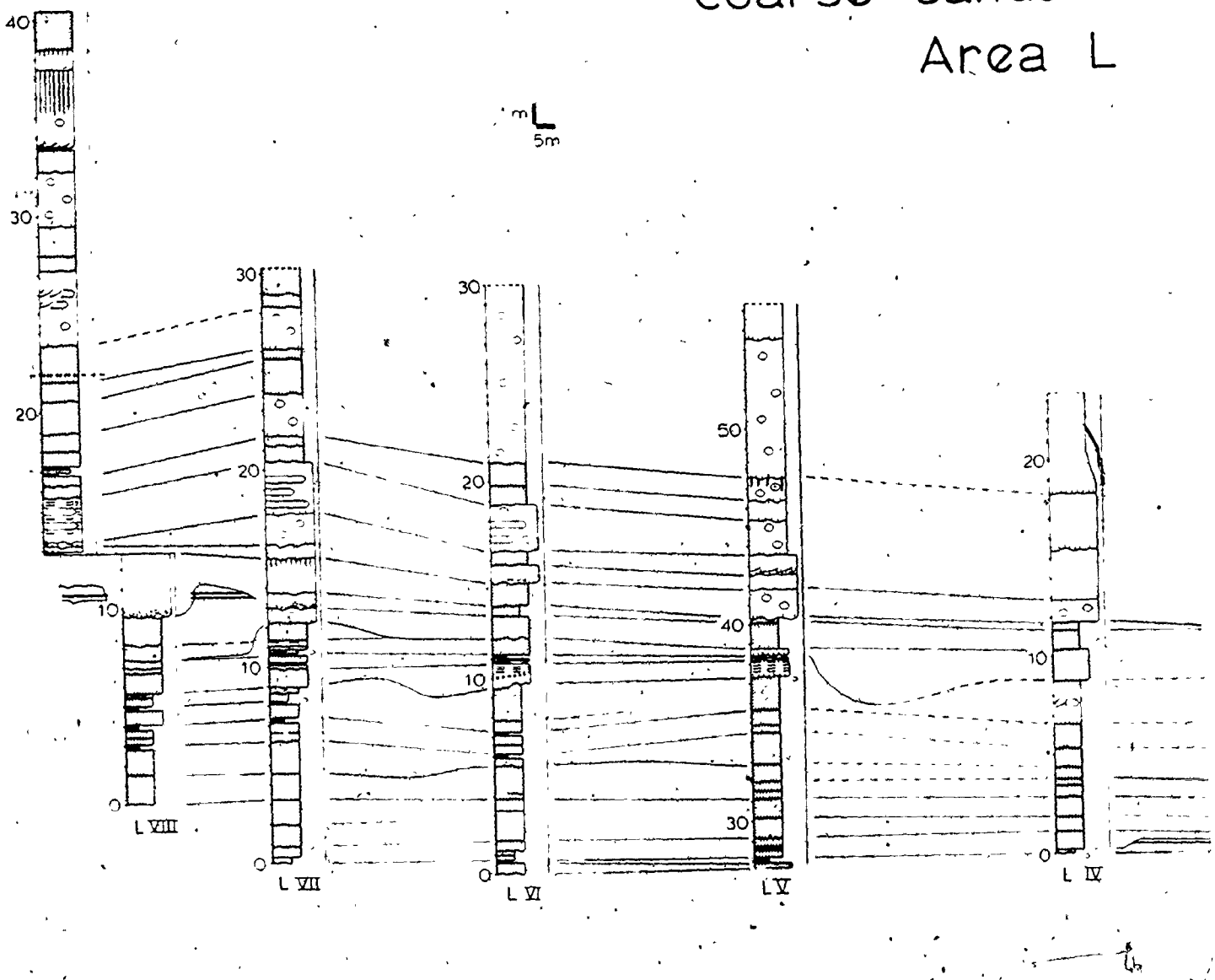

1 of.

coarse sandstone facies
Area L

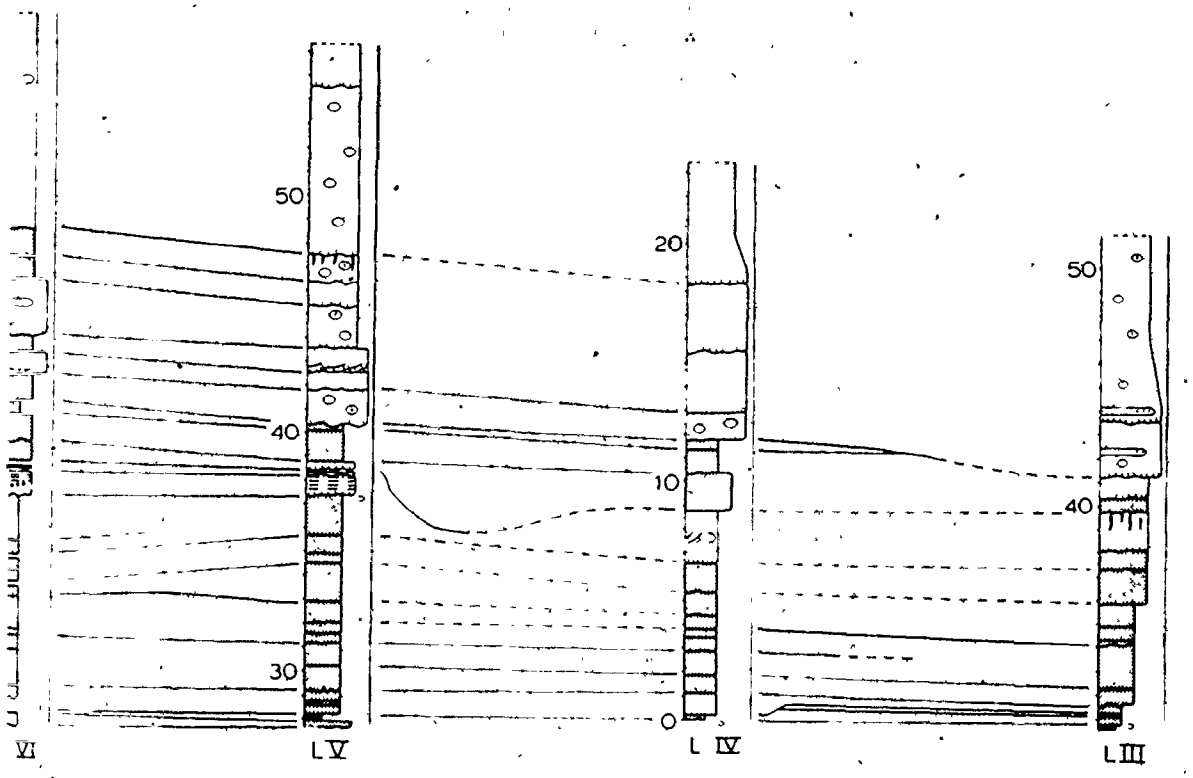

(III) Sequences of amalgamated coarse sandstones and fine-pebble conglomerates with little or no fine material (areas G, M-west and M-east).

(IV) Coarse sandstone packets overlain by very thick siltstone (2) units (area F).

In the discussions which follow, conglomerate will be grouped with thick sandstones (6). Figure 3.3 indicates facies proportions for the schemes defined above. Scheme IV consists of only one representative and will not be analysed in subsequent sections. Scheme III is composed of stratigraphic sections which essentially contain only two facies. These areas are best appreciated through study of their composite sections (Appendix I). Schemes I and II account for 87% of all measured stratigraphic intervals. Figure 3.4 shows facies abundances for these schemes. The following distinguishing characteristics should be noted.

(i) Thick shales (1) and siltstones (2) comprise less than 10% of scheme I, with these facies having below average thickness. Scheme II, in contrast, has about 35% of these fine-grained facies, with thicknesses above average.

(ii) Scheme I contains a greater thickness proportion of slurry sandstones (3) and thick sandstones (6).

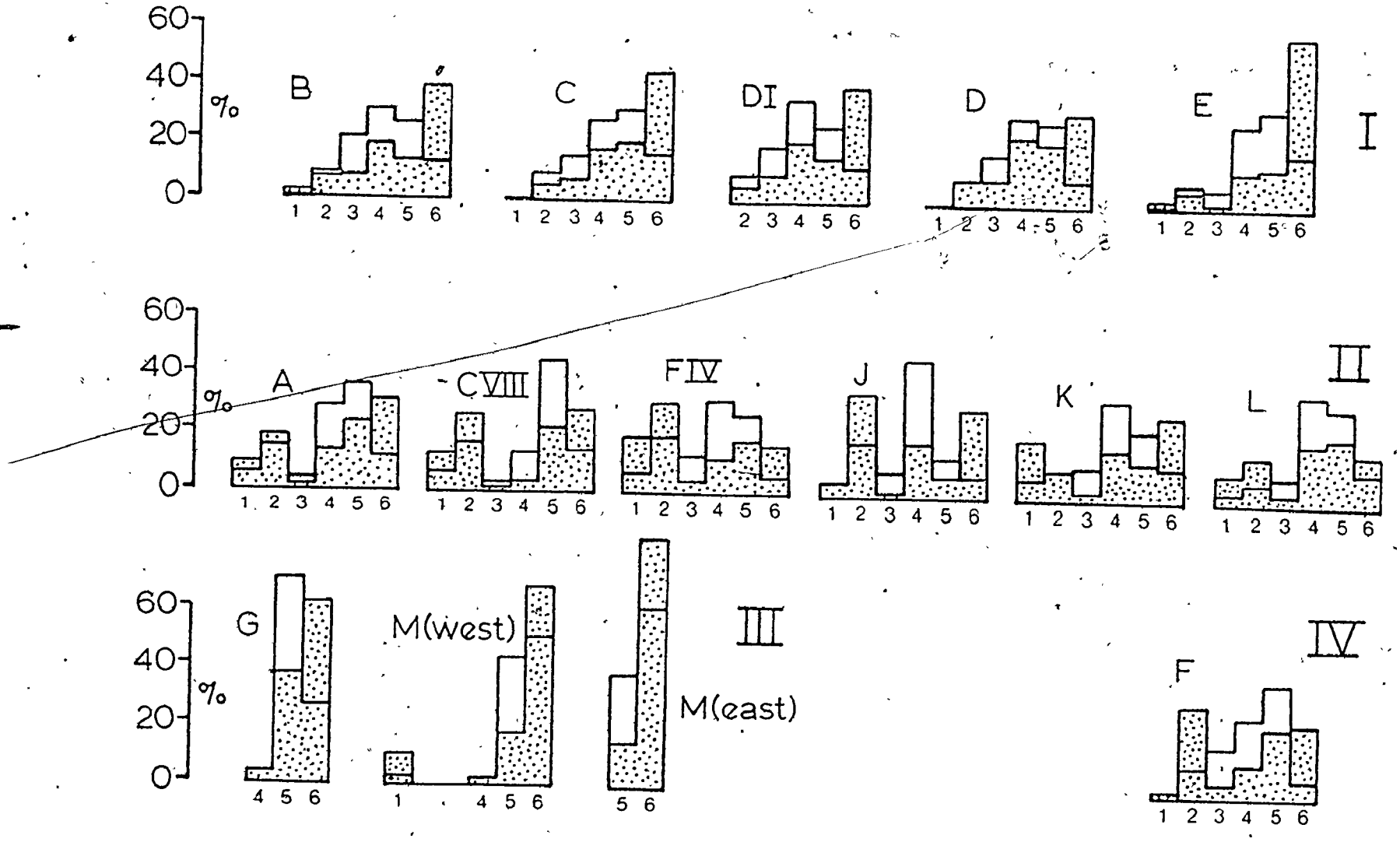

Fig. 3.3. Proportions of facies 1 to 6 (in %) for schemes I to IV. Proportions are both for number of layers (unpatterned) and total thickness (stippled). When the stippled histogram exceeds the layer-% histogram for a particular facies, it has above average thickness. For a review of facies descriptors, see the summary for Chapter II.

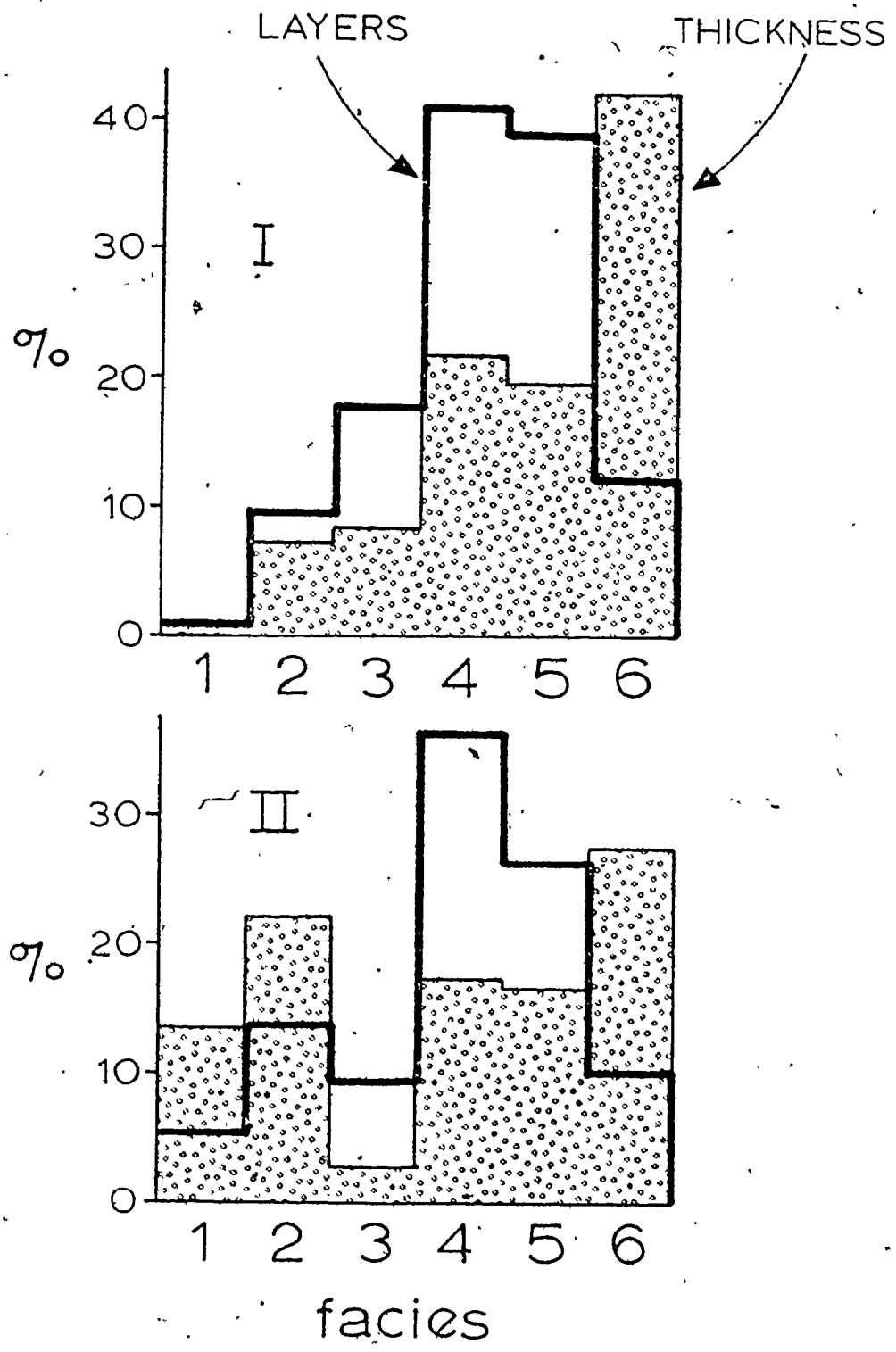

Fig. 3.4. Relative facies abundances for schemes I and II. Format is identical to figure 3.3.

Further similarities and dissimilarities between these two schemes will be documented in subsequent sections, followed by a comparison of characteristics of each scheme with those of submarine fan subenvironments. On the basis of these comparisons, it will be argued that the Tourelle Formation was deposited in the mid-fan region, with coarsest sandstones representing the fill of mid-fan channels.

Markov Chain Analysis

A valuable technique for the study of facies organization consists of a statistical analysis of patterns in the upward transitions between the various facies (states). A Markov process is one in which the probability of occurrence of a particular state in a time or space sequence (chain) depends upon the preceding state or states. In terms of conditional probability,

$$P(A|B) = \frac{P(A \cap B)}{P(B)} \neq P(A)$$

for a first order Markov process.

In the treatment which follows, only the presence of first order memory will be sought. Transition count matrices will be constructed for an embedded Markov chain model (Krumbein and Dacey, 1969), which does not allow transitions

between layers of the same state.

Let F(I,J) denote the number of upward transitions from state I to state J, where elements in brackets are variable subscripts. Row totals (SR) and column totals (SC) are defined as follows.

$$SR(I) = \sum_{J=1}^{N} F(I,J) \quad \ldots\ldots \text{ row total}$$

$$SC(J) = \sum_{I=1}^{N} F(I,J) \quad \ldots\ldots \text{ column total}$$

$$\text{also,} \quad T = \sum_{I=1}^{N} \sum_{J}^{N} F(I,J) \quad \ldots\ldots \text{ grand total}$$

The upward transition probability associated with element F(I,J) is given by

$$P(I,J) = \frac{F(I,J)}{SR(I)}$$

We can then define an independent trials probability matrix, R, which divides the number of upward transitions observed for any state among the potential receptor states, according to their relative observed abundances. This is the matrix that we would expect to observe if no Markov process was governing sedimentation. Mathematically,

$$R(I,J) = \frac{SC(J)}{T-SC(I)}$$

The matrix of differences, D, between P and R, has elements

$$D(I,J) = P(I,J)-R(I,J)$$

It is possible to test an observed transition count matrix for presence of first order Markov memory by employing a standard chi-squared test, as outlined by Billingsley (1961, p. 17) or Gingerich (1969, p. 331). The test statistic, with (N^2-2N) degrees of freedom, is

$$\chi^2_{obs} = \sum_{I=1}^{N} \sum_{J=1}^{N} \left[\frac{[F(I,J)-SR(I)\cdot R(I,J)]^2}{SR(I)\cdot R(I,J)} \right]$$

The null hypothesis for this test is that no difference exists between the independent trials probability matrix and the observed transition probability matrix. If this null hypothesis is rejected, then a first order Markov process can be assumed. It then becomes possible to test individual matrix elements, for which D(I,J) exceeds zero, to determine at what level of significance individual transition counts differ from independent trial counts (Hobday and Mathew, 1975). This test statistic, with 1 degree of freedom, is

$$\chi^2_{I,J} = \frac{[F(I,J)-SR(I)\cdot R(I,J)]^2}{SR(I)\cdot R(I,J)}$$

Arrow weights on transition diagrams can then be designed to indicate significance level.

Before carrying out separate Markov chain analyses for schemes I and II, the transition count matrices for the two schemes were tested for stationarity using a chi-squared test outlined by Harbaugh and Bonham-Carter (1970). The null hypothesis of stationarity was rejected (99% level), substantiating the claim of a real difference between facies schemes I and II.

Tables 3.1 and 3.2 present matrices F, P, R and D for schemes I and II, respectively, as well as indicating the result of the chi-squared test for a first order Markov property. Figures 3.5 and 3.6 indicate transitions which occur with a higher frequency than would be produced by a random interplay of states present in the observed proportions.

In spite of the previously documented differences in facies organization and abundances between facies schemes I and II, comparison of the two diagrams indicates a strong resemblance, which probably corresponds to a gross similarity in depositional environment and processes. The following features of these diagrams are especially noteworthy.

(i) Truncated sandstones (5) and thick sandstones (6) form an intimate couplet which is entered randomly (these facies may lie on top of all other facies without preference). This behavior is expected for the fill of channels, with channel bases having cut down to varying levels in underlying deposits.

Table 3.1

Markov chain analysis : Scheme I

F

	(1)	(2)	(3)	(4)	(5)	(6)
Thick shales(1).....	0	2	0	2	2	0
Siltstones (2).....	9	0	23	31	17	8
Slurry sandstones (3).....	0	21	0	45	27	8
Thin sandstones (4).....	1	54	44	0	66	25
Truncated sandstones (5)..	0	6	24	81	0	38
Thick sandstones (6).....	0	5	8	31	32	0

(T = 606)

P

0.000	.333	0.000	.333	.333	0.000
.060	0.000	.274	.369	.202	.095
0.000	.208	0.000	.446	.267	.079
.005	.284	.232	0.000	.347	.132
0.000	.040	.161	.544	0.000	.255
0.000	.066	.105	.408	.421	0.000

R

0.000	.147	.165	.317	.240	.132
.012	0.000	.191	.369	.278	.153
.012	.174	0.000	.375	.244	.196
.014	.212	.239	0.000	.346	.190
.013	.190	.214	.411	0.000	.171
.011	.167	.188	.361	.273	0.000

D

0.000	.187	-.165	.017	.093	-.132
.048	0.000	.083	.002	-.076	-.057
-.012	.834	0.000	.071	-.017	-.077
-.005	.073	-.006	0.000	.001	-.058
-.013	-.150	-.053	.132	0.000	.064
-.011	-.105	-.083	.047	.148	0.000

$$\chi^2_{obs,24} = 91.9$$

$$P(\chi^2_{24} > \chi^2_{obs}) = 7.03 \times 10^{-10}$$

Table 3.2

Markov chain analysis: Scheme II

	(1)	(2)	(3)	(4)	(5)	(6)
Thick shales (1)	0	32	2	5	2	1
Siltstones (2)	37	0	8	38	13	6
Slurry sandstones (3)	6	7	0	23	13	2
Thin sandstones (4)	4	54	16	0	49	19
Truncated sandstones (5)	0	2	14	67	0	25
Thick sandstones (6)	1	6	4	16	26	0

F

(T = 492)

0.000	.762	.048	.119	.048	.024
.361	0.000	.078	.373	.127	.059
0.000	.136	0.000	.511	.269	.084
.020	.390	.113	0.000	.345	.134
0.000	.019	.128	.628	0.000	.231
.019	.113	.075	.382	.491	0.000

P

0.000	.224	.093	.331	.229	.118
.167	0.000	.113	.301	.263	.136
.094	.225	0.000	.333	.238	.110
.122	.294	.129	0.000	.308	.155
.100	.258	.113	.393	0.000	.136
.096	.238	.100	.339	.235	0.000

R

0.000	.537	-.058	-.212	-.101	-.094
.253	0.000	-.034	-.069	-.136	-.077
-.094	-.078	0.000	.179	.099	-.074
-.094	.006	-.016	0.000	.045	-.021
-.100	-.241	.017	.237	0.000	.095
-.077	-.117	-.025	-.038	.256	0.000

D

$$\chi^2_{obs,24} = 253.3$$

$$P(\chi^2_{24} > \chi^2_{obs}) = 5.61 \times 10^{-12}$$

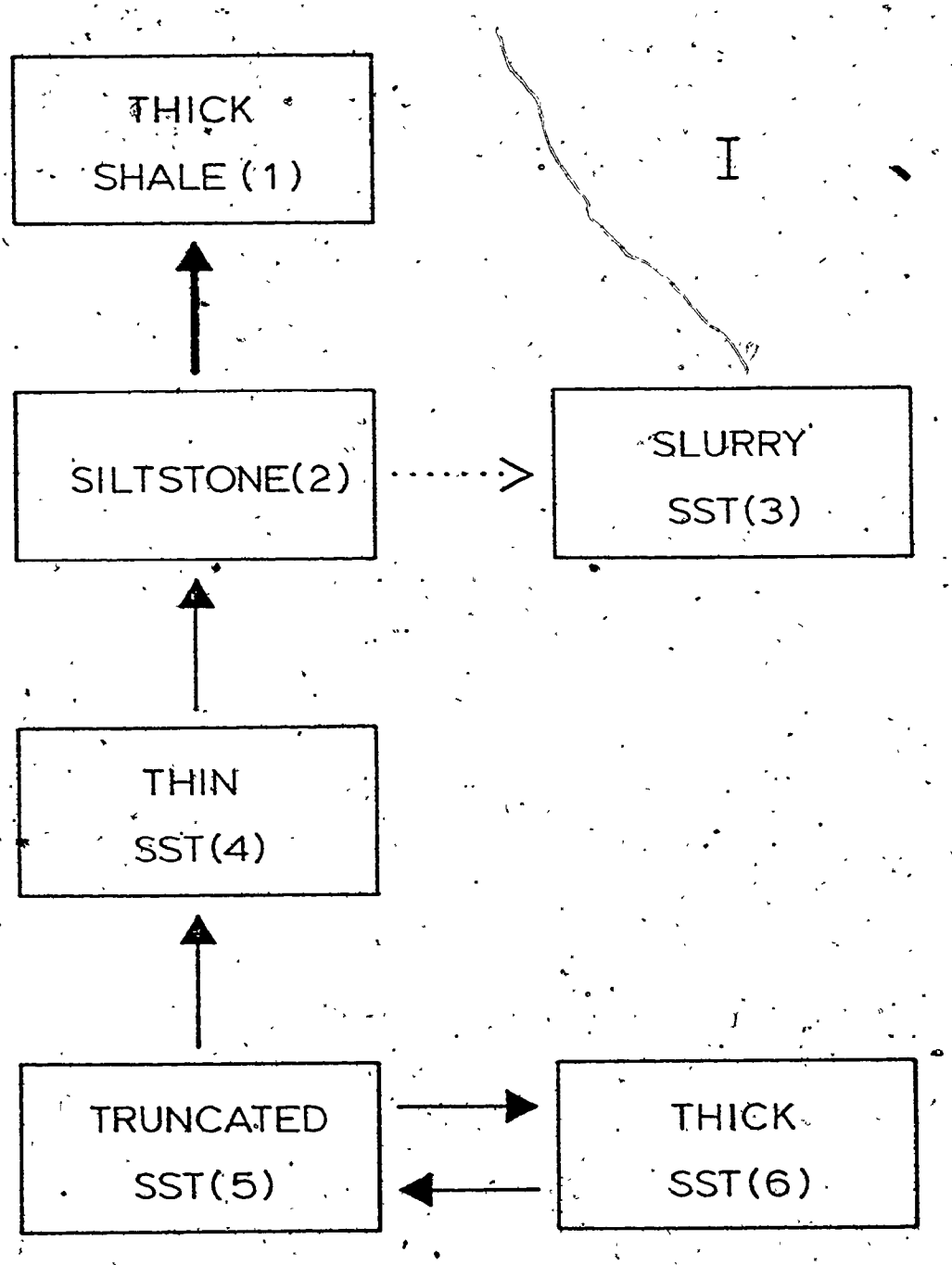

Fig. 3.5. Transition diagram for facies scheme I. Arrow weights signify significance of individual transitions at greater than (i) 99% (——), (ii) 95% (——), (iii) 90% (– – –), or (iv) 80% (·····).

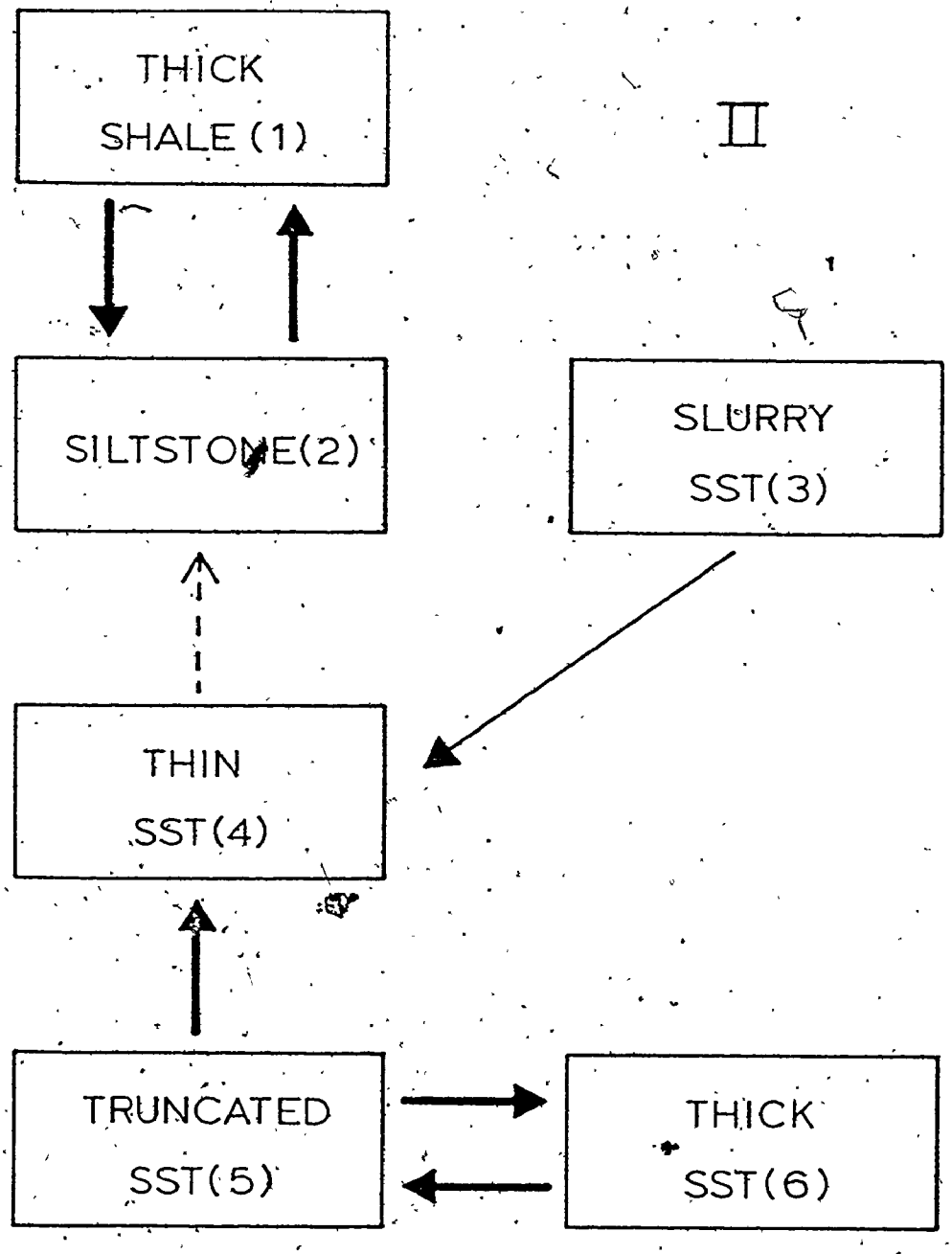

Fig. 3.6. Transition diagram for scheme II. Arrow weights signify significance of individual transitions at greater than (i) 99% (———), (ii) 95% (——), (iii) 90% (- - -), or (iv) 80% (·····).

(ii) There is a distinct progression upward from coarse to fine deposits, which can be described as both a thinning- and fining upward sequence.

(iii) Slurry sandstones (3) occur in near-random fashion. Only under scheme II do these layers preferentially underlie thin sandstones (4). This random entry agrees well with the earlier interpretation of these layers as the products of slumping of mud and unconsolidated sand. The occurrence of these slumps would likely have been controlled by factors independent of normal fan processes.

Entropy Analysis

Hattori (1976) has introduced the concept of entropy for evaluation of transition count matrices. This analysis requires one more matrix, Q, which contains as elements probabilities related to downward transitions.

$$Q(I,J) = \frac{F(I,J)}{SC(J)}$$

Entropy after deposition for facies I is defined as

$$E_I^{post} = -\sum_{J=1}^{n} P(I,J) \cdot \log_2 P(I,J)$$

If $E_I^{post} = 0$, one of the P(I,J)'s is 1, and the others are zero, resulting in an entropy minimum for upward transition.

As more transitions to other states are allowed, entropy increases.

In a similar fashion, entropy before deposition is defined as

$$E_I^{pre} = - \sum_{J=1}^{N} Q(I,J) \cdot \log_2 Q(I,J)$$

Because entropy increases with the number of states, entropies are normalized by dividing by E(max), where

$$E(max) = -\log_2 \left[\frac{1}{N-1}\right]$$

This manipulation yields new variables R^{post} and R^{pre} which can then be plotted against one another (Figure 3.7). Facies which plot above the line $R^{post} = R^{pre}$ are more affected by previous states and have less influence on succeeding deposits than do facies which plot on the line. Similarly, facies which plot below the line are less influenced by preceding events and dictate more strongly subsequent deposition.

The following features exhibited by the Tourelle data deserve comment.

(i) Of the three major sandstone facies (excluding slurry sandstones (3)) truncated sandstones (5) most strongly predict subsequent deposition. It will be shown in a later section that this facies may occupy the base of channel fills beneath major thick sandstones (6), as well as serving as

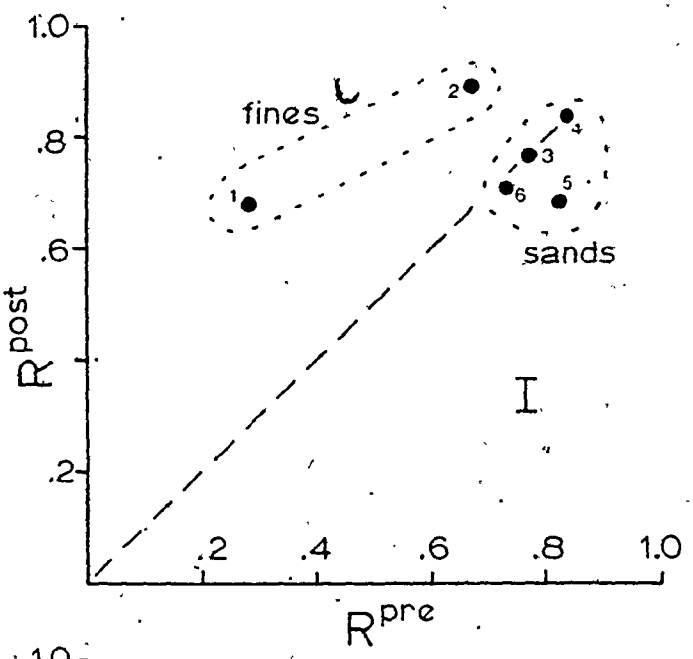

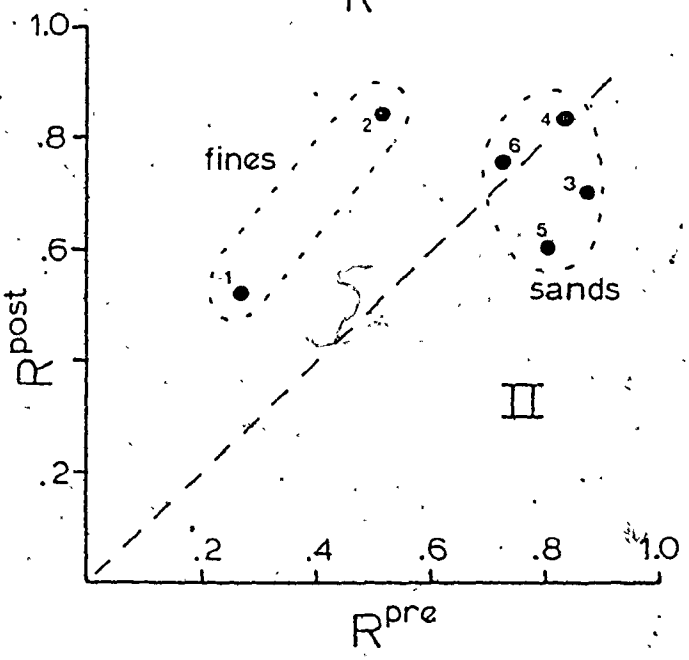

Fig. 3.7. Entropy diagrams for schemes I and II. Numbered points represent different facies.

a link between thick channel layers and succeeding fine deposits.

(ii) All sandstone facies are associated with high entropies for both upward and downward transitions. This strong random element in sedimentation is screened out by Markov analysis, leaving the impression of consistent thinning upward. This, however, is not the case.

(iii) Sandstone facies form a cluster of points distinct from thick shales (1) and siltstones (2). These latter facies are strongly influenced by preceding states, but exert little control on subsequent deposition. This characteristic would be expected for facies at the top of fining upward cycles deposited in channels, because scouring by the next channel would be an independent event, as would be the accumulation of its fill.

Channels

Several major channels with relief of greater than 5 m are present in the Tourelle Formation.

Cap des Méchins channel

This poorly exposed feature (area A) is approximately

7 m deep and is cut into laminated shale. The channel wall is inclined at 35° to primary layering. Fill consists of a graded sand layer (0 to 2 ϕ).

Cap Chat channel (Figure 3.8)

This channel is exposed at area E, and cuts down at least 13 m into coarse sandstones. Neither the base nor the top of the channel wall are seen. The channel fill consists of coarse to granular thick sandstones (6) with the lower part of the channel containing a chaotic mixture of coarse sandstone and large shale blocks.

Area F channel

The erosional wall of this channel is not exposed, but is inferred on the basis of downward thickening of coarse sandstones between section FI and FIII (see sections in pocket). A minimum estimate of channel depth is 8 m, with downcutting into siltstones (2).

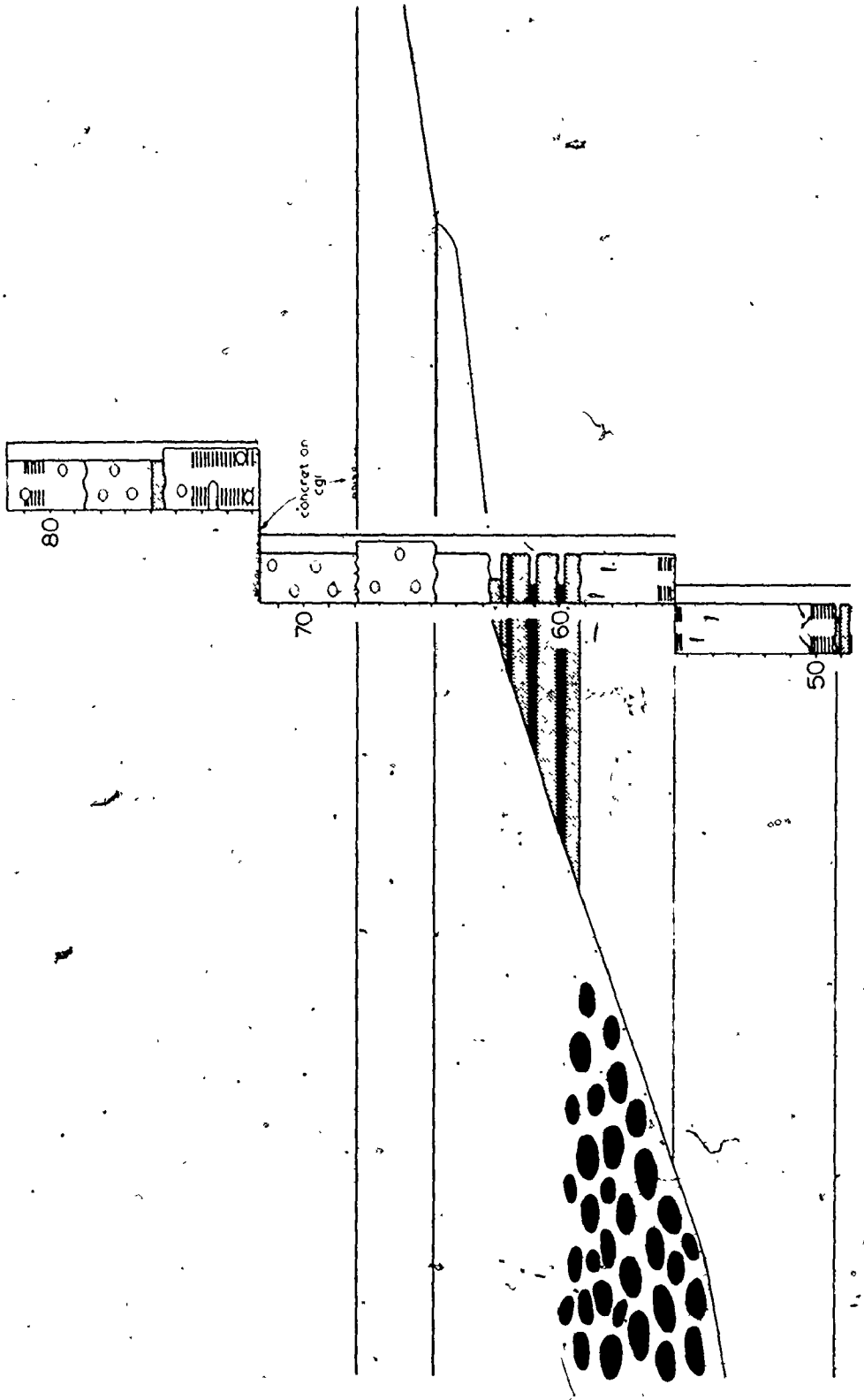

Fig. 3.8. Cap Chat channel, area E. Scale is in metres.

Cap Ste-Anne channel (Figure 3.1 and Figure 3.9)

This large broad channel is found near the village of St-Joachim de Tourelle (area J). Channel relief is 9 m. over a horizontal distance of 50 m. Paleocurrent data suggest that the outcrop view is only about 20° away from a true cross-sectional view of the feature. The channel cuts into thin sandstones (4) and siltstones (2). The fill shows a thinning and generally fining upward configuration and is overlain by ripple-drifted siltstones (2) and shale. This thinning upward fill conforms with the observation of Ricci Lucchi (1975a) that 77% of all channelized cycles show a thinning-upward trend.

Anse à Carlot channel

This feature appears on the area M composite section (Appendix I). The channel is cut to a depth of about 10 m in coarse thick sandstones (6). The fill again appears to thin upward, with a 16 m thick, graded sand unit at the base of the channel. This unit contains bands (trains) of limestone pebbles which extend from the channel wall for some distance into the fill. These pebble bands diverge toward the base of the channel (Figure 3.10), and may be the product of pulses during one depositional event, as the

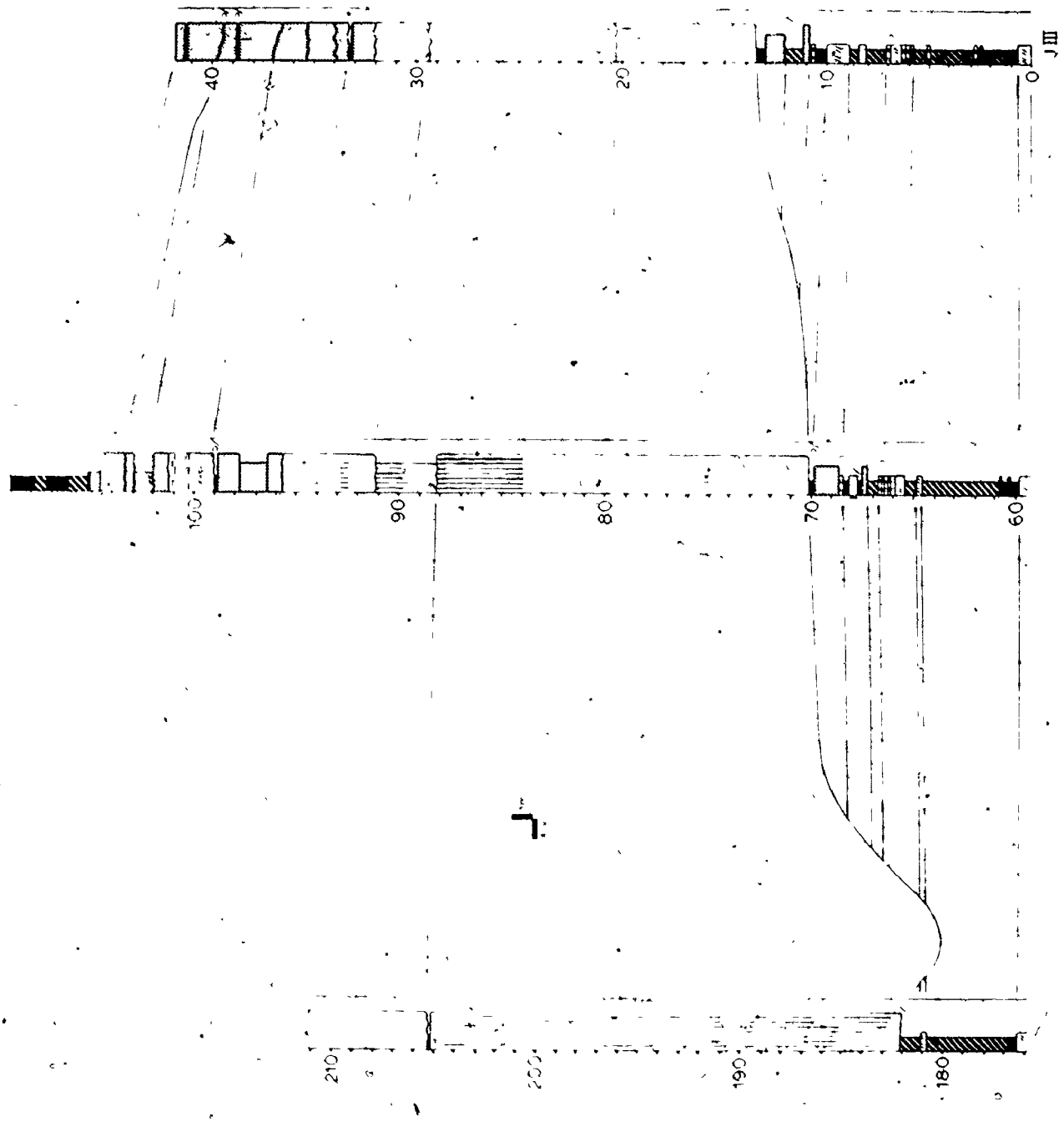

Fig. 3.9. Cap Ste-Anne channel. Symbols in Appendix I.

entire channel fill appears to consist of one graded unit. These pebble bands may only be preserved along the channel margins because of more intense re-suspension of clasts in the middle of the channel. A large sandstone pillar is located at the base of this channel fill.

Channelling on a smaller scale is present at sections MV and MVI, suggesting that the larger channel is not an atypical feature of this environment.

Ste-Marthe channel

This channel is included here for completeness, although it is found well to the east of all outcrop areas. It lies above the deformed Cap des Rosiers Group west of Ste-Marthe. The channel is cut into shale and thin calcisiltites of the Cap des Rosiers Group, which are here strongly deformed and broken (see Chapter VIII). The coarse to pebbly granular sandstone fill of the channel has resisted deformation, and exhibits a stepped margin (Figure 3.11). The extent of downcutting perpendicular to layering is in excess of 50 m. Shale which is absent in the channel fill occurs with bedded chert above the channel.

The extent of downcutting into the top of the Cap des Rosiers Group, and the thinness of the Tourelle sandstone unit at this locality, suggest that this channel may be the

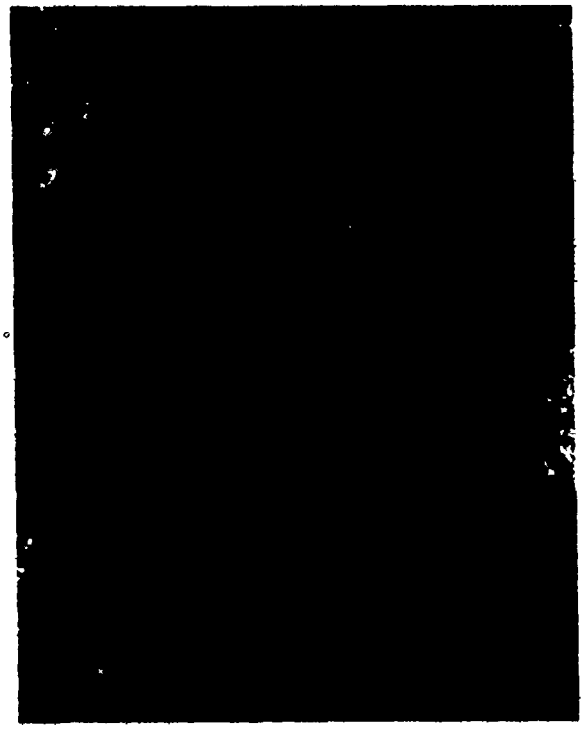

Fig. 3.10. Diverging pebble bands at base of Anse à Carlot channel. Scale 1 m. Top direction is indicated.

Fig. 3.11. Ste-Marthe channel as seen from cliffs above. Bar scale is approximately 50 m. Note stepped margin.

wall of a submarine canyon cutting across the Ordovician slope and funnelling sand to a submarine fan below.

Layer Thickness Trends

Examination of stratigraphic trends in layer thickness and grain size in ancient submarine-fan deposits has revealed the presence of both thinning and fining upward, and thickening and coarsening upward cycles (Mutti and Ricci Lucchi, 1972; Mutti and Guibaudo, 1972; Mutti, 1974; Ricci Lucchi, 1975a, 1975b). These have collectively been called megasequences. Ricci Lucchi (1975a) observed that 77% of channelized cycles display a thinning upward trend, whereas 63% of non-channelized cycles thicken upward. The remaining cycles have a complex or symmetric form.

When viewed in the field without the aid of stratigraphic section drawings, asymmetric cycles in the Tourelle Formation are seldom obvious. Only at areas E, F, J, L and N were megasequences easily recognized during general outcrop examination. Re-examination of composite sections allowed several additional cycles to be distinguished. All thinning upward (positive) and thickening upward (negative) cycles are indicated alongside composite sections in Appendix I. Definition of some of these megasequences is more subjective than others, particularly if the base or top is not bounded

by a unit of thick shale (1) or siltstone (2). The best thinning upward sequences are found at areas DI (115 to 141 m), E (84 to 143 m, 145 to 184 m), F (39 to 57 m, 58 to 70 m), FIV (0 to 19 m) and J (182 to 222 m), while the best thickening upward cycles are at areas A (50 to 71 m), C (31 to 51 m), J (65 to 95 m), K (45 to 62 m) and L (30 to 55 m).

Table 3.3 summarizes thickness statistics for positive and negative cycles within facies schemes I to IV. Examination of these statistics and composite sections leads to the following observations and generalizations.

(i) Much of the Tourelle Formation is not characterized by obvious cycles. Instead, bundles of layers with similar thickness alternate with bundles containing thicker or thinner layers. Isolated thick layers may give the impression of thickening or thinning upward when no trend actually exists. False cycles of this type have nevertheless been classified as asymmetric cycles by Ricci Lucchi (1975a; see in particular his figures 23 and 25), casting doubt on his claim that asymmetric cycles are commonplace in submarine-fan deposits. For example, much of areas C, DI, D and L defy classification into thinning or thickening upward sequences.

(ii) The base of the formation (areas A and J) begins with a thickening upward cycle. With only one exception (area B), negative cycles always underlie positive cycles.

Table 3.3

Thickness statistics for asymmetric megasequences

Facies scheme	thinning upward (+)				thickening upward (-)			
	no.	%	$\bar{x}$ (m)	s (m)	no.	%	$\bar{x}$ (m)	s (m)
I	14	82	21	14	3	18	14	4
II	9	60	17	9	6	40	19	7
III	2	100	25		0	0		
IV	2	100	15		0	0		

no. - total number of cycles observed

% - percent of all asymmetric cycles

$\bar{x}$ - mean thickness of cycles in metres

s - one standard deviation about $\bar{x}$

(iii) 82% of asymmetric cycles in areas conforming to scheme I thin upward. For scheme II, this proportion decreases to 60%. Areas J, K and L (scheme II) not only contain the majority of thickening upward sequences, but also are characterized by segregation of sandstones into thick, often amalgamated, packets which are separated by equally thick horizons of thick shale (1) and siltstones (2).

(iv) Asymmetric cycles within major channels thin upward without exception (areas E, F, J, M-east).

(v) The mean thickness of thinning upward sequences is about 20 m. The thickest positive cycles are found at area E, associated with the Cap Chat channel. On the basis of point (iv) above, and observations of Ricci Lucchi (1975a), it is reasonable to assume that these sequences are channel fills. 20 m will be used as a rough estimate of channel depth (see Chapter V).

(vi) Several thinning upward cycles begin with truncated sandstone(s) (5) before giving way to thick sandstones (6) (areas DI, E - 145 to 184 m; F - 39 to 57 m; FIV - 0 to 19 m; K - 110 to 124 m). This means that some thinning upward sequences possess a minor basal thickening upward trend superimposed on the major positive cycle.

(vii) Slurry sandstones (3) tend to occur most frequently at the top of thinning upward cycles in association with shale, thin sandstones (4) and siltstones (2). If we accept

the hypothesis that slurry sandstones (3) are the product of slumping of unconsolidated sand and mud, then it is not surprising that they are most common during channel abandonment, when mud deposition increases in importance. It is possible, nevertheless, that emplacement of these layers was unrelated to channel processes. They may only appear to be more frequent at the top of positive cycles because coarse sandstone deposition was less frequent.

The formation of negative (thickening upward) cycles is attributed to progradation of suprafan depositional lobes (Mutti and Guibaudo, 1972; Walker and Mutti, 1973; Mutti, 1974; Ricci Lucchi, 1975a; Walker, 1976). Attempts to draw analogy between thinning and fining upward cycles in submarine fan channels, and similar cycles in meandering rivers, have met with skepticism because of the lack of concrete evidence for lateral accretion deposits in modern or ancient examples (Mutti, 1974). Meandering submarine valleys and thalweg channels have certainly been reported on modern fans (Shepard, 1966; Nelson and others, 1970; Normark, 1970) and on the ocean floor (Chough and Hesse, 1976), but the meander loops have not been shown to migrate, probably because of confinement by cohesive submarine levees. Small-scale lateral accretion in ancient fan channels has been tentatively suggested by Kruit and others (1975) and Walker (1975b, his Figures 13 and 14; personal communication, 1977).

Meckel (1972) has described the formation of fining upward sequences in delta distributaries, where vertical rather than lateral accretion dominates, but the processes involved do not entail channel plugging (see below), and are not comparable to processes which operated in the Tourelle depositional environment.

Ricci Lucchi (1975a) suggests that changes in longitudinal gradient, and the shallowing and widening of channel cross-sections (causing decreasing volume of flows) may lead to channel abandonment and preservation of a positive cycle. Bypassing of currents over or around topographically high sand deposits may also result in emplacement of thinner layers (Enos, 1969b; I.P. Martini, personal communication, 1976).

Figure 3.12 outlines the essential features of thinning upward cycles in the Tourelle Formation. This diagram is based on (i) examination of thinning upward cycles in Appendix I, and (ii) transition diagrams derived from Markov analysis (Figures 3.5 and 3.6). Markov diagrams are unfortunately least useful for this purpose because of the large element of randomness introduced by those parts of the formation which cannot be subdivided into megasequences. The overall thinning upward trend in Figure 3.12 is interpreted to result from progressive abandonment of a channel after plugging by a large flow (Walker, 1977). Because

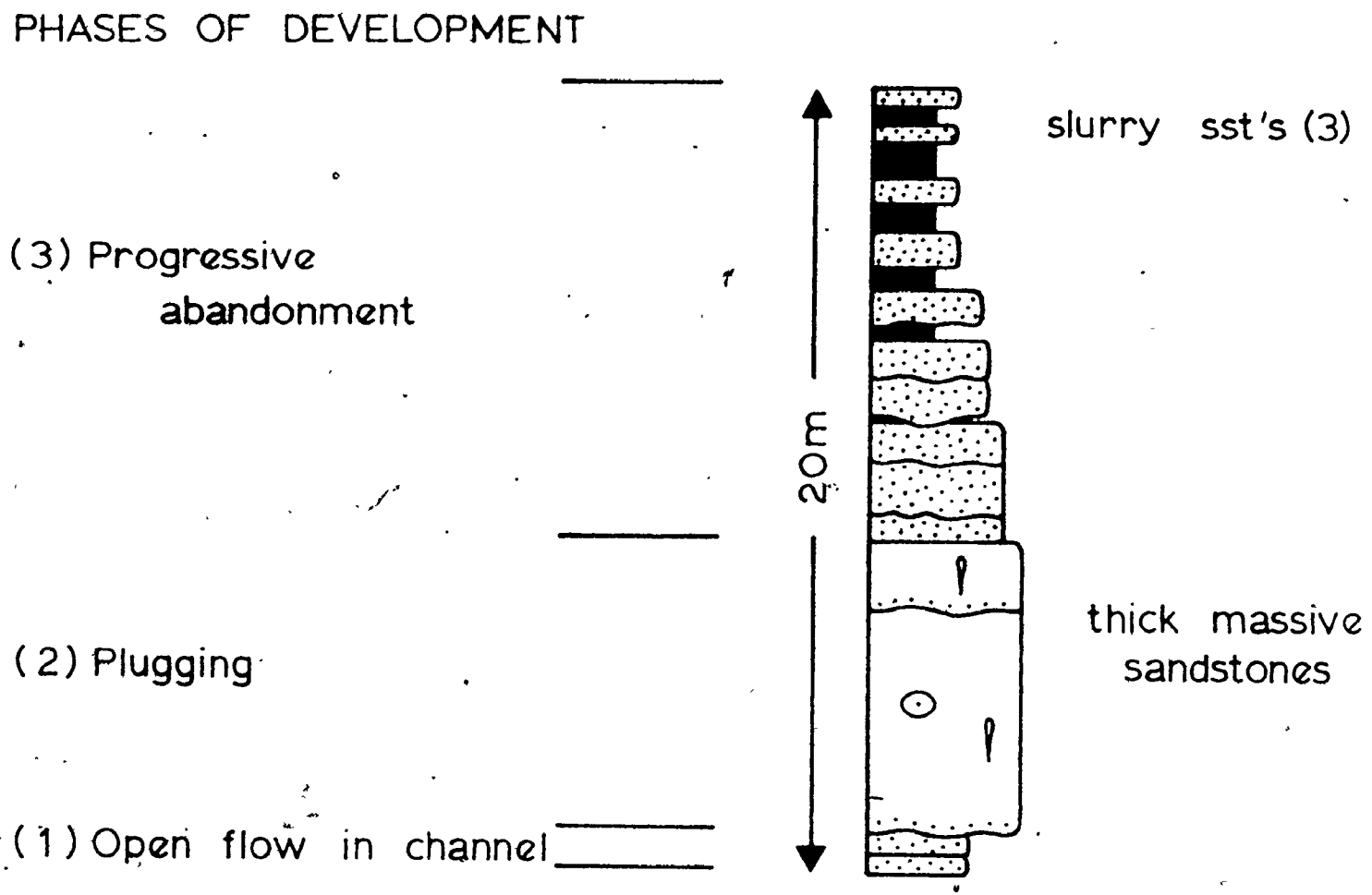

Fig. 3.12. Schematic representation, and interpretation, of thinning upward sequences in the Tourelle Formation. Shale breccia, if present, would be in the bottom of the channel. Channels may be cut into any facies.

submarine-fan channels serve as conduits which funnel density currents onto the suprafan lobes, it is likely that they remain open over a considerable period of time (phase 1), with little or no net deposition of coarse detritus. Any record of this period should consist of thin truncated sandstones (5), perhaps deposited from the tails of large currents which travelled through the channel. Why, then, do these channels become plugged (phase 2)? The thick basal sandstones in most inferred Tourelle channels are massive thick sandstones (6). Evidence presented in Chapter V suggests that these massive sands were transported as very high concentration turbidity currents, or as viscous, sandy debris flows. Both varieties of sediment gravity flow would be susceptible to rapid deposition or "freezing" on slopes which would present no obstacle to normal turbidity currents. It is therefore believed that channel plugging (phase 2) can be attributed to rapid deposition from large flows which were moving as dense turbulent suspensions or debris flows (with or without additional support from dispersive pressure and excess pore-fluid pressure). In support of this interpretation, channel plugging on a subaerial alluvial fan has been observed to result from accumulation of debris during the flood stage of flow (Eckis, 1928). Truncated sandstones (5) at the base of some channels cannot be interpreted as partially eroded thick sandstones (6), which would

call into question the hypothesis of channel plugging by an "unusual" flow. These thinner layers are characteristically well graded (Figure 2.19). The lower metre or so of most thick sandstones (6), however, is essentially ungraded, and may contain internal scour surfaces. There is therefore a real difference in sedimentation between phase (1) and phase (2).

After plugging, the submarine-fan channels were progressively abandoned (phase 3) due to shallowing and widening of channel cross-section and an associated increase in overbank spill. Gradual filling of the depression would decrease the gradient of the dispersal system and eventually lead to avulsion up-fan and occupation of a new channel with steeper gradient. Even after avulsion, spill-over from the new channel might still follow the shallow abandoned depression, and contribute thin, fine layers to the top of the thinning upward cycle.

Paleocurrent Trends

Before proceeding with an analysis of stratigraphic variation of paleocurrent data, the relative precisions and directional homogeneity of different current indicators, measured on layers of different facies, will be reviewed. Many areas do not possess a wide enough variety of structures

and occurrences for such an assessment. In particular, thick sandstones (6) are never abundant enough to indicate significant differences from other sandstone facies. For these reasons, this analysis of structures and facies will centre on areas J and L. Figures 3.13 and 3.14 present equal-area rose diagrams for these two areas. In particular, note the following features.

(i) Flute casts exhibit a narrower range of azimuths than do groove casts. This fact is well documented by other studies (for a review see Dzulynski and Walton, 1965). Groove casts on sandstone layers may either cross or show systematic variations in orientation (Figure 3.15).

(ii) Mean current directions inferred from flutes, grooves, or longitudinal ridges in the same facies are not significantly different.

(iii) All coarse sandstone facies yield the same current direction.

(iv) Ripple marks at the top of layers at area J give current directions which are rotated consistently clockwise in relation to other indicators.

(v) Siltstones (2) indicate flow parallel with that of other facies at area J, but perpendicular to sandstone paleocurrent data at area L. This degree of divergence may be the result of spilling of currents over channel margins.

Fig. 3.13. Equal area rose diagrams of orientation data, area J. Flutes (⊃), grooves (/), longitudinal ridges (/) and ripple "troughs" (⟶) are treated separately. For grooves, readings are symmetrically distributed about the origin, because these tool marks yield no information on the sense of current movement. The number of layer means which contribute to each rose diagram are indicated.

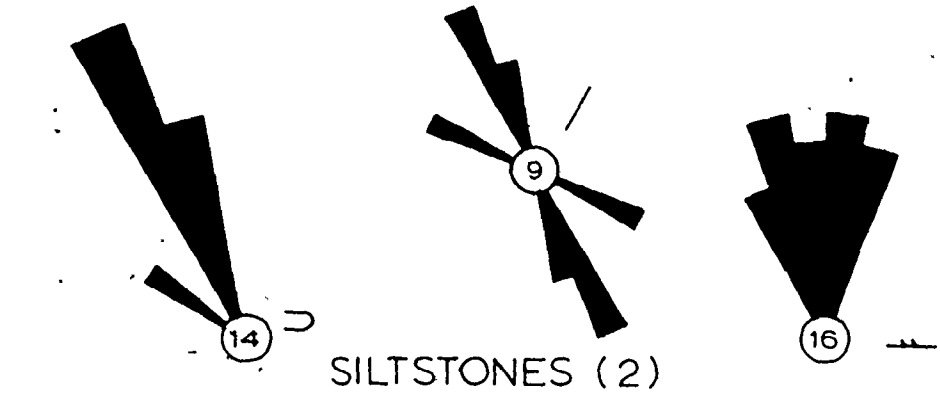

SILTSTONES (2)

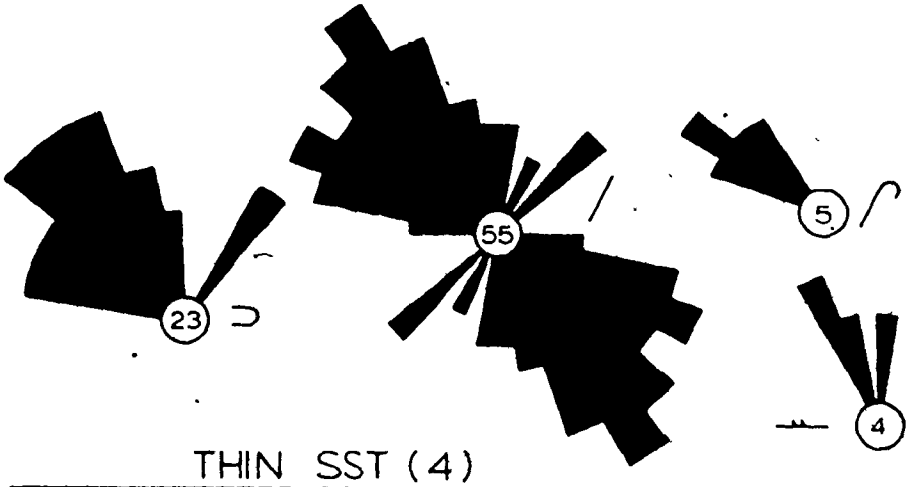

THIN SST (4)

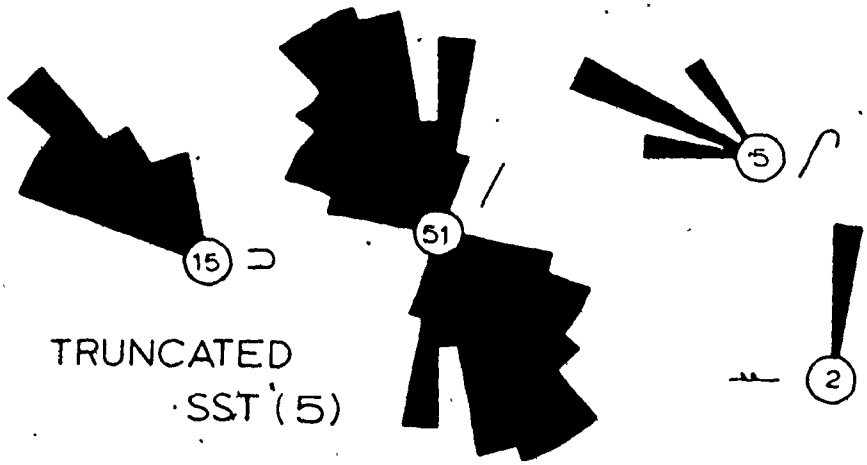

TRUNCATED SST (5)

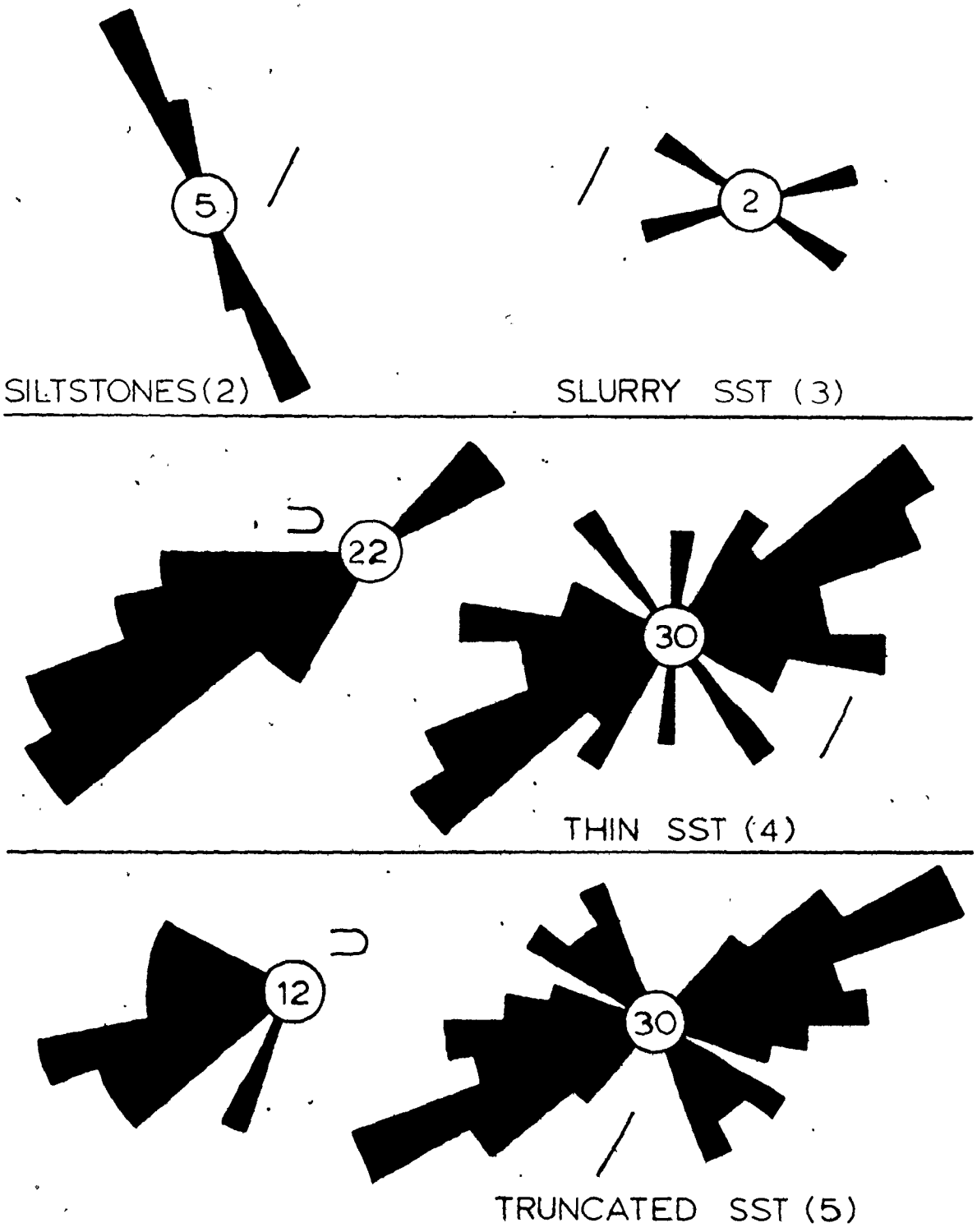

Fig. 3.14. Equal area rose diagrams, area L. For further explanation, see figure 3.13.

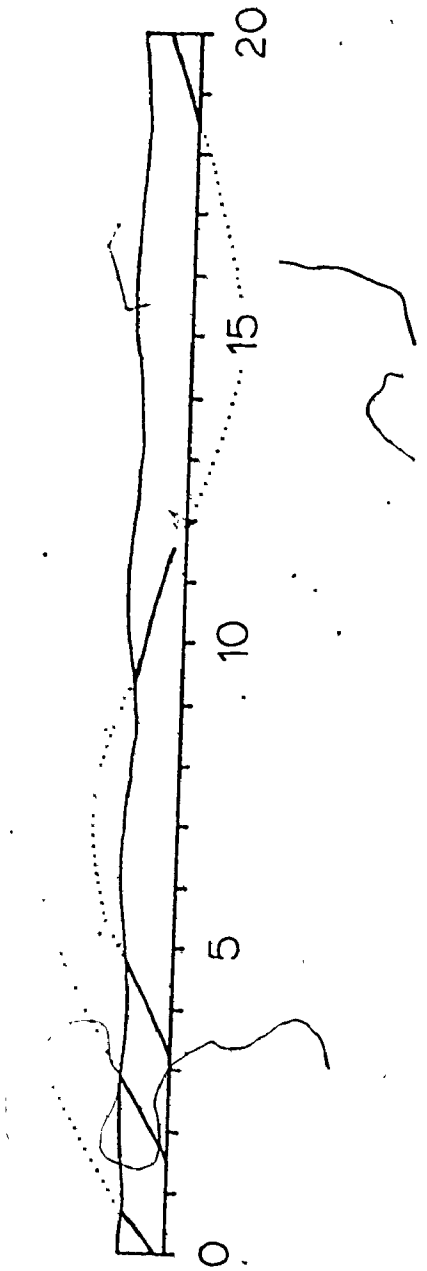

Fig. 3.15. Systematic swinging, or meandering, of groove casts on the base of a truncated sandstone (5) layer at area L. Scale is in metres.

Trough cross-bedding, where observed, yields current directions which agree closely with sole markings on stratigraphically adjacent layers.

Stratigraphic trends

Only areas D, J, K and L are suitable for evaluation of stratigraphic variations in paleoflow (Figures 3.16, 3.17, 3.18 and 3.19, respectively). Area D conforms to scheme I; J, K and L belong to scheme II with separate sandstone packets (numbered consecutively from base to top of each section).

Examination of these figures leads to the following observations.

(i) Paleocurrents are consistent within individual thinning upward sequences, and are generally consistent within sandstone packets (areas J, K and L). Any variability appears to result from progressive swings in the current direction through time (packets J1, J5, J6, L3), except at the base or top of packets, where paleocurrent variability is greatest (packets K4, L2). This general consistency within positive megasequences is strong evidence that they were not formed by contributions from two different sources, one more proximal and one more distal.

Figs 3.16 to 3.19. Stratigraphic plots of paleocurrent data for areas D, J, K and L. The columns have been designed to allow easy comparison with composite sections (Appendix I). Vertical scale is in metres. Each plotted orientation represents the mean of all sole markings on one layer. An arrow-head is present if the sense of current flow is known. Unless otherwise specified, all data represents measurements from flutes, grooves, or longitudinal ridges. Bold dots to the left of arrows indicate that the measurement was made on a siltstone (2) layer, with readings either being from sole markings or ripple troughs. Thinning upward (black) or thickening upward (stippled) cycles are indicated in the columns. For areas J,K and L (scheme II), the locations of numbered sandstone packets (such as those shown in figure 3.1) are shown to the right of the column.

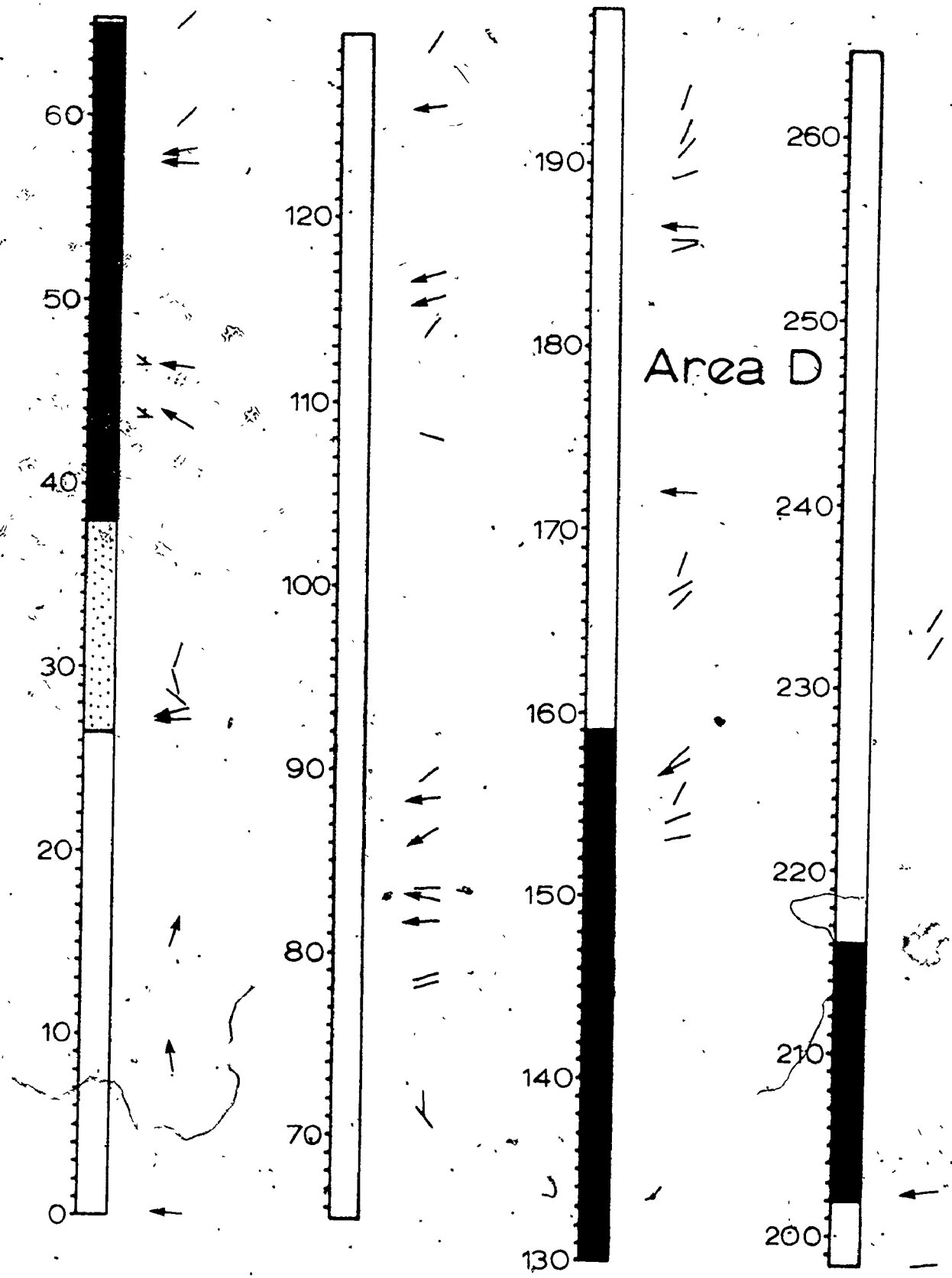
60
50
40
30
20
10
0
120
110
100
90
80
70
190
180
170
160
150
140
130
260
250
240
230
220
210
200
Area D

Fig. 3.16.

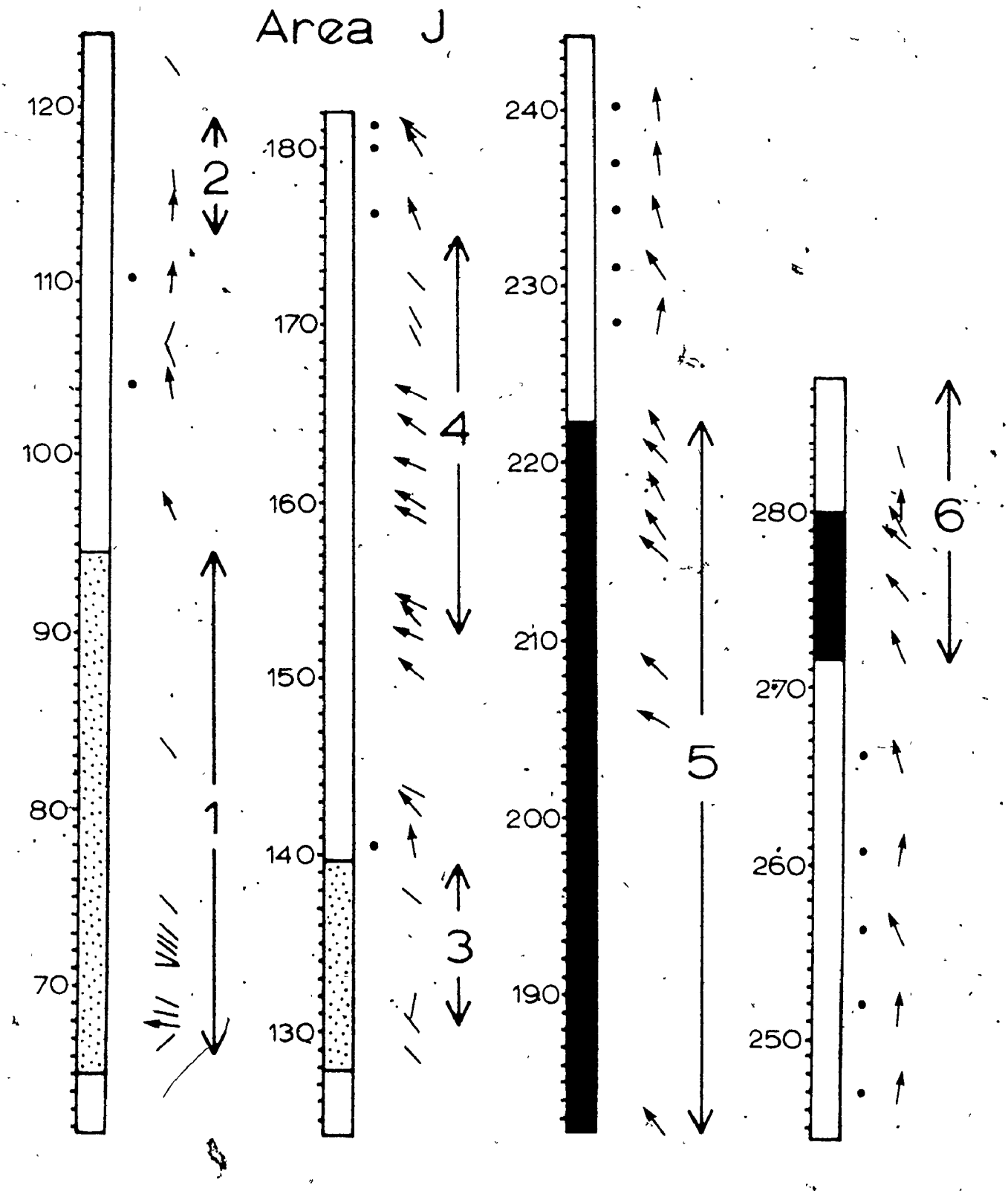
Area J
120
110
100
90
80
70
180
170
160
150
140
130
240
230
220
210
200
190
280
270
260
250
1
2
3
4
5
6

Fig. 3.17.

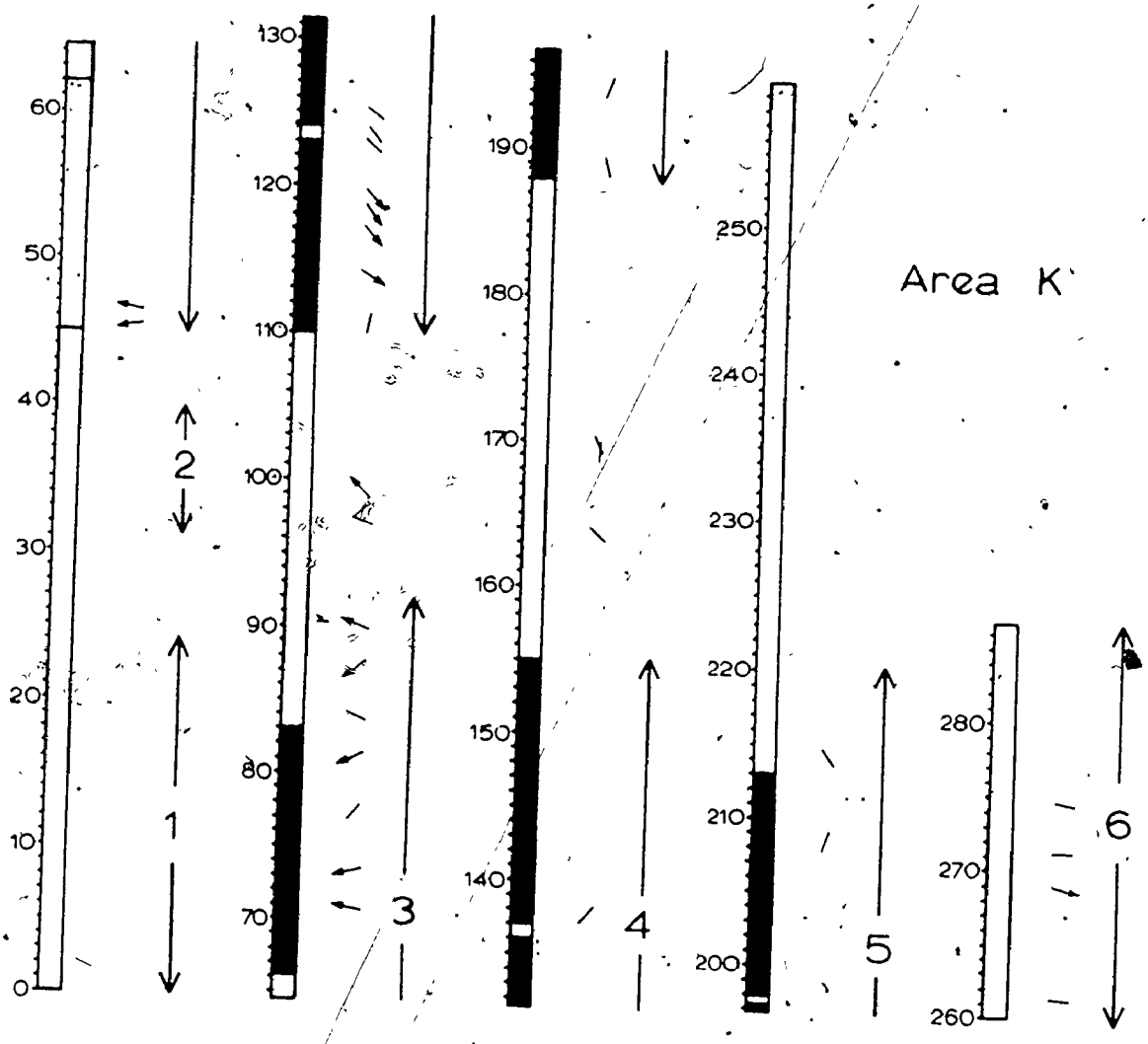
Area K
0
10
20
30
40
50
60
70
80
90
100
110
120
130
140
150
160
170
180
190
200
210
220
230
240
250
260
270
280
1
2
3
4
5
6

Fig. 3.18.

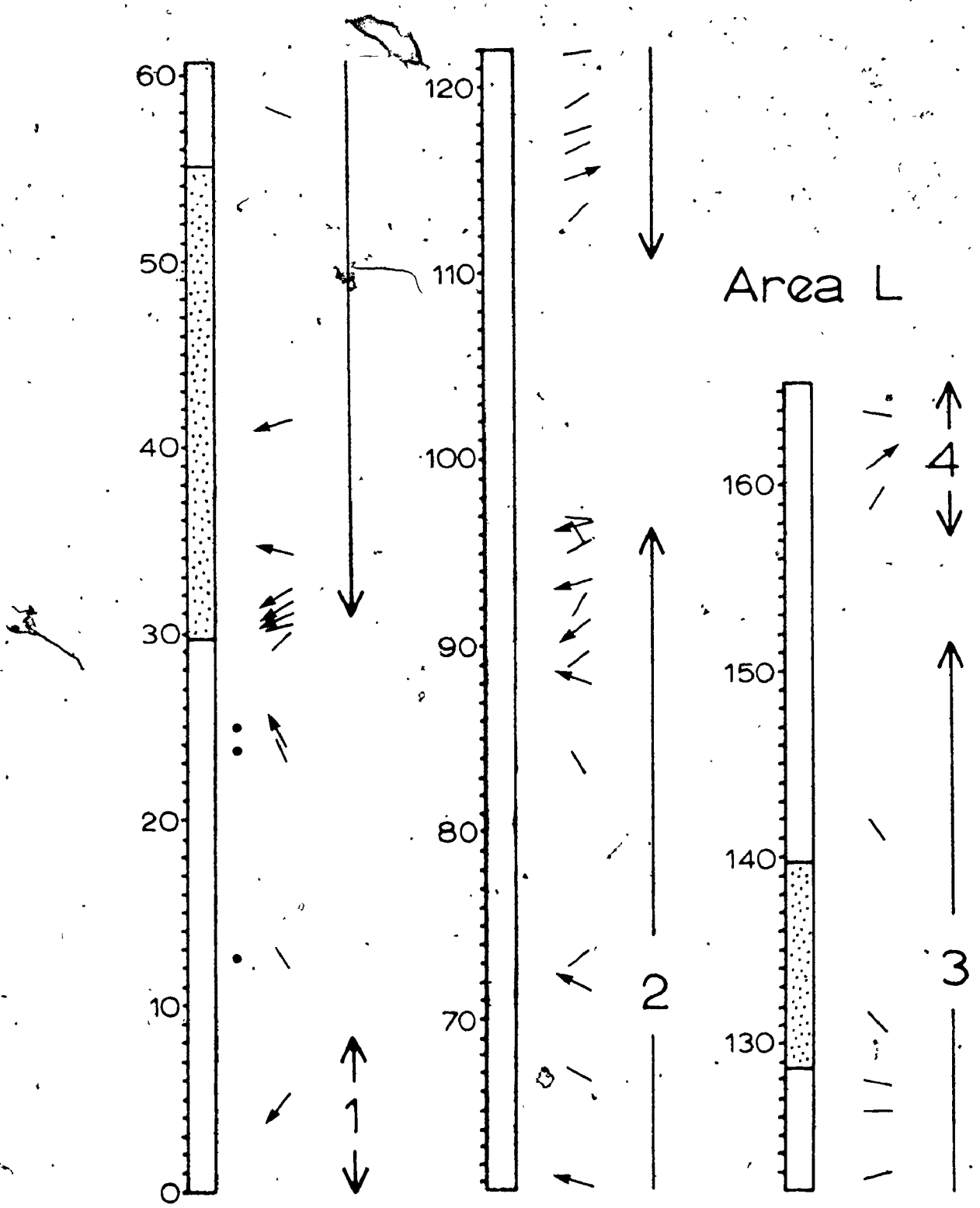

Fig. 3.19.

(ii) Current direction is less consistent in thickening upward cycles (areas D, J), suggesting less effective confinement of flow.

(iii) Interpacket siltstones (2) diverge from current directions in bounding sandstone packets. At area J, the angle of divergence is 20 to 30°; siltstones (2) between packets L1 and L2 are at right angles to packet paleoflow.

(iv) Packets K4, K6, L3 and L4 show almost complete reversals in current direction when compared to subjacent packets. These reversals occur above thick units of thick shales (1) and siltstones (2), and indicate development of entirely new flow patterns through time. These paleoflow reversals will be discussed in the next section and in Chapter VII.

Depositional Environment

Requirements

Several observations have been made in preceding sections and in Chapter II which must be accommodated in any interpretation of depositional environment.

(i) Areas conforming to facies scheme II are characterized by an alternation of coarse sandstone packets with thick

units (up to 40 m thick) of thick shales (1) and siltstones (2) containing rare interbedded thin sandstones (4) or slurry sandstones (3). In contrast, areas within facies scheme I do not contain thick units of fine sediment (muds). Table 3.4 compares several features associated with these two facies schemes. These all suggest that facies scheme I was deposited further up-fan than scheme II.

(ii) The majority of asymmetric megasequences thin upward (Table 3.4), although 40% of scheme II asymmetric cycles thicken upward. More importantly, all deep channels have sandstone fills which thin upward. This observation supports the conclusion of Mutti (1974) and Ricci Lucchi (1975a) that thinning upward sequences generally imply channels. Because thinning upward cycles are dominant, they dictate the results of sequence analysis (Markov analysis). It must be stressed, however, that much of the Tourelle stratigraphy cannot be divided into positive or negative cycles, which is not predicted by the present submarine fan model (Walker and Mutti, 1973; Walker, 1976). This large degree of randomness contributes to high entropies for all sandstone facies.

(iii) Thick sandstones (6) may contain large slabs of bedded chert or dolomitic siltstone with dimensions exceeding 1 x 15 m. These allochthonous slabs could not have travelled very far from their source, which was probably the oversteepened walls of a submarine canyon. Mechanisms for transporting

Table 3.4

Comparison of facies schemes I and II

	Characteristic	I	II
(1)	Layer-percent thick sandstones (6)	12	10
(2)	Thickness-percent thick sandstones (6)	42	27
(3)	Mean[1] thickness of thick sandstones (6)	339 cm	313 cm
(4)	Layer-percent slurry sandstones (3)	17	9
(5)	Thickness-percent slurry sandstones (3)	8	3
(6)	Number of channels	1	2
(7)	Maximum channel depth (m)	13+	9
(8)	Percent thinning upward cycles	82	60
(9)	Percent thickening upward cycles	18	40
(10)	Mean[1] positive cycle thickness (m)	21	17

[1]All means are arithmetic

these slabs are discussed in Chapter V.

(iv) Large slumps have been recognized, particularly at area D (Capucins), where they are associated with thick slurry sandstones (3). These features suggest proximity to steep slopes and submarine canyon walls as sources for slumped material and slide blocks.

(v) Paleocurrent measurements within thinning upward cycles and sandstone packets are internally consistent. Thickening upward cycles show more internal dispersion. Separate sandstone packets (scheme II), however, may have mean flow directions radically different from adjacent packets. In extreme cases (areas K and L), packets display a mean current direction nearly 180° opposed to those of subjacent packets. Paleocurrent measurements on interpacket siltstones (2) also diverge from trends in bounding packets, with maximum divergences of 90°.

Interpretation

To facilitate interpretation of depositional environment, a few areas will be selected and, on the basis of descriptions and requirements mentioned above, will be arranged in relative order according to proximity to the upstream feeder channel. The reader is encouraged to become familiar with the spectrum of facies organizations present

in the formation by successively viewing the following composite sections in Appendix I (arranged in order from most proximal to most distal): areas M-east, E, D, J and K.

The most obvious changes moving from area M-east to area K are listed below.

(i) Visible channelling decreases in importance, and thinning upward cycles become thinner. Sequences which thicken upward also begin to appear.

(ii) Grain size generally decreases.

(iii) The proportion of thick sandstones (6) decreases.

(iv) Thick shales (1) and siltstones (2) gradually increase in abundance, and finally form thick horizons between packets of coarse sandstone. These thick fine units are extremely important in environmental interpretation and will be discussed below.

The present submarine-fan model (Walker, 1976, and in press) predicts deposition of thick muds (comprising clays and silts) on the outer-fan fringe, on levees adjacent to deep inner-fan channels, and as mud blankets over abandoned mid-fan distributary channel and lobe complexes (see Figure 1.3).

There is no evidence in the Tourelle Formation for deposition in an inner-fan channel. Only at the Ste-Marthe channel do Tourelle sandstones cut into muds of the Cap des Rosiers Group. Elsewhere (areas A and J), the formational

base begins with a thickening upward sequence typical of the mid-fan (Mutti, 1974; Ricci Lucchi, 1975a; Walker, 1976). The presence of both thinning and thickening upward cycles, and large sand-filled channels is also consistent with deposition on a mid-fan. Walker (in press) interprets subsurface section BB' in Hsu (1977, his Figure 4) as superposition of a thinning upward channel sequence on top of a thickening upward lobe sequence at the boundary between the channelized and non-channelized mid-fan. These sequences are separated by a mud blanket, which was deposited on top of the lower abandoned mid-fan system. A similar interpretation is proposed for areas J and K, with sandstone packets being the deposits of separate mid-fan channel and lobe complexes. As suggested in Chapter II (Figure 2.37), however, it is probable that abundant siltstones (2) are the result of overbank spill from channels of a subsequent mid-fan dispersal system, particularly as ripple-drift cross-lamination is common in these siltstones, suggesting rapid fall-out from suspension.

Mid-fan complexes might be expected to shingle either upcurrent, or downcurrent, or laterally, so that successive packets could show thinning upward (channels?) or thickening upward (prograding lobe?) trends. More complex cycles, or lack of cycles, may result from (i) progressive abandonment of a depositional lobe, (ii) aggradation of a lobe without progradation, or (iii) continuous aggradation of a channel.

with deposition from flows of variable volume.

Because areas M-east, E and D were logically deposited in more proximal environments than areas J and K (but not necessarily at the same place or time), they are assigned to the upper mid-fan distributary system. Mud blankets are not characteristic of these areas because channels closer to the fan apex would be active more frequently. They would not be unoccupied long enough to receive a thick mud blanket.

A comparison of Tourelle channel depths (inferred from the thickness of thinning upward cycles), with channels of modern fan systems may suggest approximate dimensions for the Tourelle submarine fan(s). On the Astoria Fan (Nelson and Nilsen, 1974), the inner fan channel is 200 m deep. Mid-fan distributary channels range in depth from 50 to 80 m. On the Bengal Fan (Curray and Moore, 1974) mid-fan channels range up to 100 m in depth. Thinning upward cycles average 20 m thick in the study area, with the thickest cycles at area E (average of 43 m). These are all less thick than the depths of modern channels mentioned above, and suggest that the Tourelle fan(s) was smaller and steeper than either the Astoria or Bengal Fans. If this is true, then the smaller La Jolla Fan (30 x 22 km) may be a more reasonable modern analogue.

Areal relationships

Is there any temporal or spatial arrangement of mid-fan deposits in the study area (Figure 1.5)? All areas which expose the base of the formation (areas A and J) consist of mid-fan deposits with mud blankets. There is reason to believe that areas J, K and L are roughly correlative (see Figure 2.37), and therefore are all near the base of the formation. Area M, interpreted to have been close to a feeder channel, lies stratigraphically above area L and indicates westward progradation of fan facies. As expected, therefore, sediment coarseness increases from area J to area L. The extremely thick sandstone layers associated with the Cap Chat channel at area E indicate proximity to another feeder channel or canyon (see Chapter VII). Less proximal facies scheme I deposits are located immediately downcurrent from the Cap Chat channel (areas B, C, DI, and D). It therefore appears that proximal and distal mid-fan deposits can be roughly correlated between outcrop areas. Tourelle sedimentation began with non-channelized deposition on mid-fan lobes, followed by westward progradation of the channel facies. These observations will be critical to paleogeographic reconstruction of the Tourelle depositional environment in Chapter IX.

Paleocurrent reversals

How can paleocurrent reversals at areas K and L best be explained? All other localities indicate current flow roughly from east to west. Evidence presented in Chapter VII indicates derivation of Tourelle detritus from the southeast, and suggests a paleoslope to the NW. Sandstone paleocurrents generally indicate flow directed to the west of this paleoslope dip. If currents were indeed consistently deflected to the left, looking down-fan, an asymmetric fan would have resulted. On rare occasions, avulsion may have occurred to form a channel cutting obliquely across the fan to the right of the paleoslope dip (Figure 3.20). Paleocurrents associated with such a channel could be almost 180° different from flow directions in previous deposits.

An alternative explanation involves overlap of adjacent, small, submarine-fan systems. Channel depths inferred from positive cycle thicknesses, and depositional slopes estimated in Chapter V, both suggest small, steep fans. The Cap Chat channel and the Anse à Carlot channel are interpreted to be associated with separate feeder channels, or submarine canyons (Chapter VII), and are only 28 km apart. Eastward flow from the Cap Chat feeder channel, or from another source between Cap Chat and Ste-Anne des Monts, could account for the paleoflow reversal (Figure 3.21).

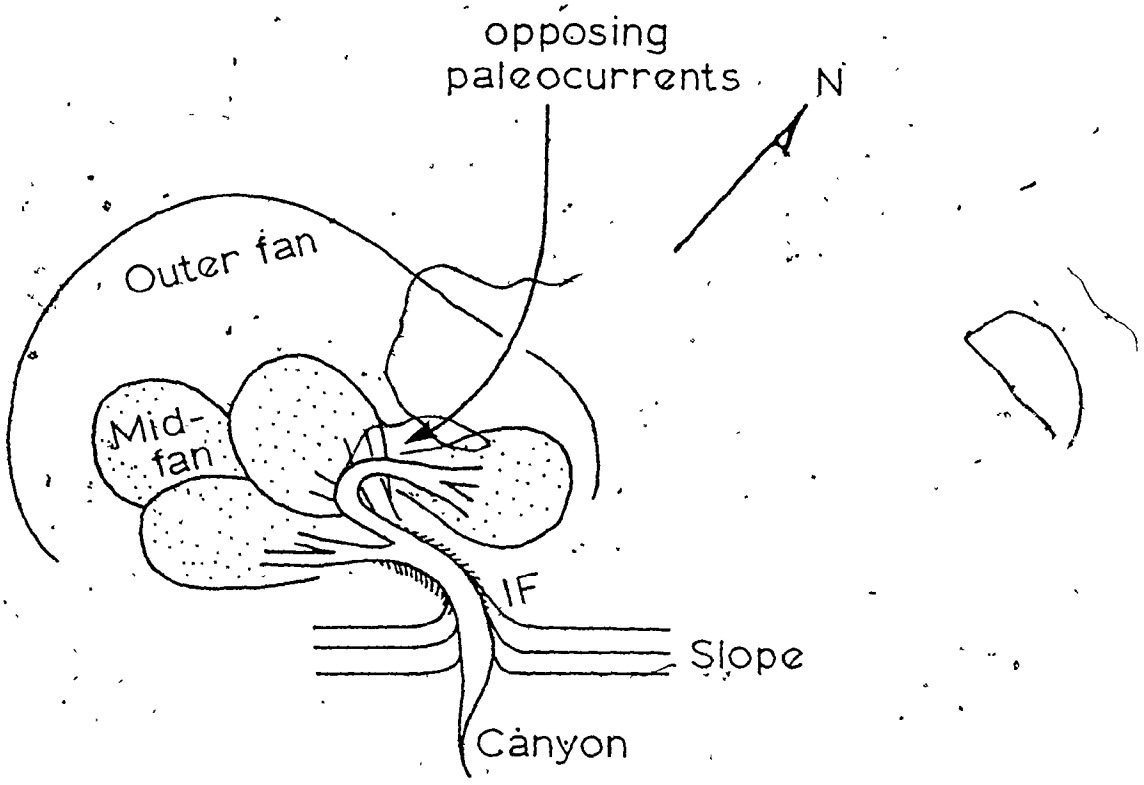

Fig. 3.20. Schematic model for production of opposing paleocurrents on an asymmetric submarine fan by avulsion. No relative scale is implied. IF = inner fan.

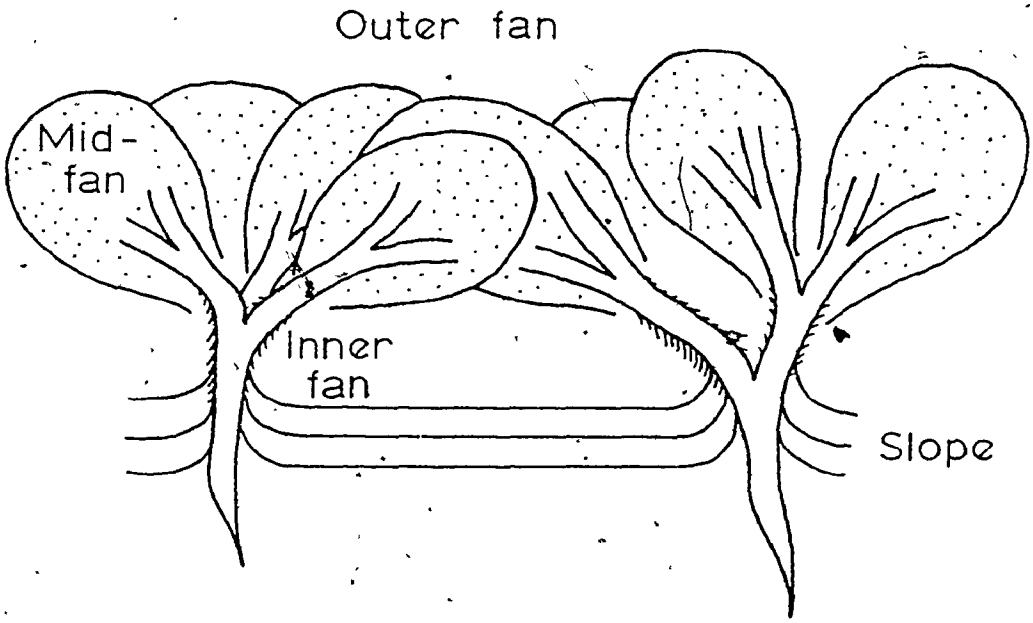

Fig. 3.21. Schematic model for production of opposing paleocurrents by overlap of adjacent fans. No relative scale is implied. Note that these fans share the same outer fan region.

Unfortunately, paleoflow at areas F and G is also from east to west; suggesting that the Cap Chat channel was not a source for eastward-flowing currents. It is still possible, however, that a submarine canyon in the vicinity of Ste-Anne des Monts has since been eroded.

The problem of paleocurrent reversals will be considered again in Chapter VII.

Summary

Areas A to M can be assigned to one of four depositional schemes on the basis of facies proportions. Schemes I and II account for 87% of all Tourelle stratigraphy considered in this study. Scheme I contains more slurry sandstones (3) and thick sandstones (6) than scheme II, and fewer thick shales (1) and siltstones (2). Most areas which conform to scheme II are characterized by segregation of coarse and fine sediments. Coarse, commonly amalgamated, sandstones occur in thick packets which are bounded by equally thick horizons of thick shale (1) and/or siltstones (2).

Markov analysis suggests common controls behind the deposition of both facies schemes. Transition diagrams indicate an overall pattern of thinning and fining upward, beginning with thick and truncated sandstones. This pattern

reflects the presence of numerous thinning upward cycles within the formation. Thickening upward sequences are far less common, and are confined to the lower parts of those stratigraphic sections which conform to depositional scheme II. Markov analysis also discloses the weak association of slurry sandstones (3) with other facies. This observation is consistent with the hypothesis that these layers were formed by slumping of mud and unconsolidated sands independent of normal fan processes.

In spite of an underlying tendency toward thinning upward, the bulk of the Tourelle Formation cannot be divided into asymmetric megasequences. This lack of apparent pattern may be the result of random truncation of asymmetric sequences by fan channels. Several major channels, with maximum depth in excess of 13 m, have been observed. They are generally based by truncated or thick sandstones, and invariably contain a thinning-upward fill. For this reason, thinning upward cycles are identified with fan channels, in accordance with observations of other workers. If it is assumed that the thickness of a thinning upward cycle approximates the depth of the channel in which it was deposited, then channels on the Tourelle fan(s) were about 20 m deep.

The internal characteristics of thinning upward sequences can be used to construct a model for filling of submarine-fan channels. This model involves three phases of development:

(1) a period of open flow through the channel, during which a few truncated sandstones (5) are deposited; (2) plugging of the channel by one or more thick sandstone (6) layers, deposited by rapid fall-out from suspension or by "freezing" of a dense dispersion or debris flow; and (3) progressive abandonment of the channel as a result of increased overbank spill, decreased longitudinal gradient, and eventual avulsion up-fan. Slurry sandstones (3) are concentrated at the top of channel fills because of (i) increased accumulation of muds during the phase of progressive abandonment, or (ii) a decrease in sedimentation rate of other facies.

Individual sandstone packets at areas J, K, and L are interpreted as separate mid-fan distributary systems. Although paleoflow within individual packets is very consistent, adjacent packets can have radically different current directions. At areas K and L, some packets were deposited by currents flowing almost opposite to those which deposited most other packets.

The fine horizons between sandstone packets may be up to 40 m thick, and consist of thick shales (1), or siltstones (2). The thick shales (1) at areas K and L are interpreted as mud blankets deposited on top of abandoned parts of mid-fan lobes and distributary channels. Fine horizons dominated by siltstones (2) (area J), may represent overbank spill from newly established distributary channels, particularly as

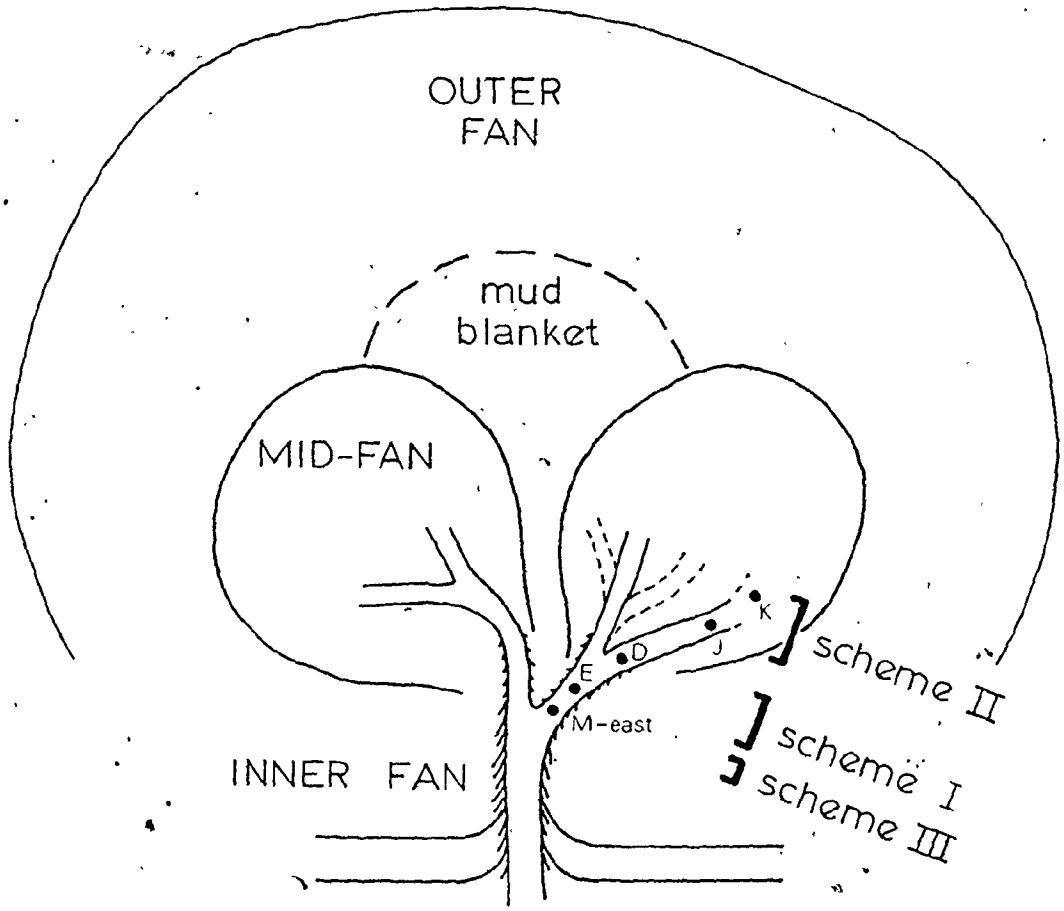

Fig. 3.22. Diagramatic representation of relative positions of areas M-east, E, D, J, and K in an idealized submarine fan system. No relative scale is implied. All strata in these areas were not deposited at the same time or on the same fan lobes.

flow directions obtained from siltstones may diverge from paleocurrents within subjacent sandstone packets.

On the basis of facies abundances, layer thicknesses, and the relative proportions of thickening and thinning upward cycles, depositional schemes and field localities can be assigned to various sub-environments of a submarine fan (Figure 3.22). It is believed that all Tourelle facies schemes were deposited on the mid-fan. Most areas can be assigned to various locations within a mid-fan distributary channel complex.

Paleocurrent reversals between sandstone packets at areas K and L may have resulted from (i) channel switching on an asymmetric fan, or (ii) overlap of small, coalescing fan systems. A comparison of inferred channel depths with channels on modern mid-fans suggests that the Tourelle fans were small and probably steep. This hypothesis is consistent with the observed spacing of feeder channels (Chapter VII), and with an interpretation involving coalescing submarine fans.

CHAPTER IV

FABRIC OF FACIES 6 THICK SANDSTONES

Previous Results

Appositional anisotropic fabric (Pettijohn, 1957) in sand-sized materials has been investigated experimentally and theoretically by Dapples and Rominger (1945), Schwarzacher (1951), Rusnak (1957), Rukavina (1965), Rees (1968), and Johansson (1976). Sand-sized grains, which can be viewed as triaxial prolate ellipsoids, are found to lie with their long axis (a-axis) parallel to the flow direction of the depositing current. The a-axis is also inclined (or plunges) upstream, resulting in an imbricate fabric. Rukavina (1965) suggested that high density turbidity currents deposit sand grains with a current-parallel fabric, whereas low density currents produce current-normal or random orientations. Current-normal pebble fabrics in fluvial gravels are attributed to rolling of the clasts along the stream bed (Rust, 1972; Füchtbauer, 1974). At higher transport velocities, current-parallel fabrics become dominant (Johansson, 1976). Rukavina's experimental data suggest that individual turbidite layers should show an increase in current-normal and random fabrics

from base to top, and in a downcurrent direction. Detailed field studies of thin turbidites by Parkash and Middleton (1970), however, do not support these predictions. Instead, deviation of a-axis fabric increases upward in layers due to current meandering.

Fabric studies of density current deposits in the ancient record reveal a-axis anisotropic fabrics with varying relationships to sole markings (for a comprehensive review see Parkash and Middleton, 1970). Most investigations have been concerned with fabric of classical turbidite layers less than 1 m thick (Smoor, 1960; McBride and Kimberly, 1963; Stanley, 1963; Spotts, 1964; Scott, 1966; Colburn, 1968; Parkash and Middleton, 1970).

One to 2 m thick layers

Onions and Middleton (1968) reported irregular deviation of grain orientation from sole markings, coupled with good upcurrent imbrication. Basal samples possessed more non-significant orientations and greater deviations from sole markings than did samples from higher levels. Bouma (1962) observed a-axis orientation normal to sole marks with upcurrent imbrication in the lower half of layers giving way to down-current imbrication at higher levels. These results are corroborated by the observation of similar sole-normal

orientations in coarse poorly sorted sands by Hand (1961). Laird (1970) discovered that strong anisotropic fabrics in massive sandstones agree remarkably well with the orientation of sheet structure, suggesting that appositional fabric can control post-depositional fluid escape. Robertson (1976) reported unimodal, bimodal, and isotropic fabrics from massive sandstones of the Chetco Formation, Oregon. a-axis orientation was observed to swing clockwise from the base, and then counter-clockwise at higher levels in the bed. Imbrication angle ranged upward to a maximum of 50°.

Layers greater than 2 m thick

It is this range of layer thickness which corresponds most closely to thick sandstones (6) of the Tourelle Formation. However, fabric studies of thick, massive or crudely stratified sandstones are virtually non-existent. Sestini and Pranzini (1965) investigated the fabric of medium sandstone samples from the bases of 1 to 4 m thick massive layers of the Macigno Sandstone, Italy. They found statistically significant grain orientations in excellent agreement with sole markings. Some samples displayed weak secondary modes (bimodal and polymodal). Two of three thick layers possessed significant upcurrent imbrication. The third imbrication was not significant. Imbrication measurements revealed the

existence of clusters of grains encompassing areas from 80 to 150 mm^2 which were variously imbricate up or downcurrent.

Experimental Details

Ten thick sandstone (6) layers were selected for fabric studies (Table 4.1). These can be roughly divided into two groups: massive sandstones with or without internal scour surfaces or fluid-escape structures; and coarsely stratified layers. Eight- to 12-cm long, 2.5 cm diameter cores were taken using a portable GSC rock sampling drill (obtained from J.K. Smit and Sons Diamond Products Limited, Toronto, Canada). The cores were drilled along the dip of the layers after orienting the core barrel with the dipmeter of a Brunton compass. Cores were taken at pre-selected intervals throughout sandstone layers. The rock surface was marked prior to drilling to ensure proper orientation (Figure 4.1). The estimated maximum error associated with this sampling process is ± 5° for both orientation and imbrication measurements.

Most previous studies have employed thin sections and a standard petrographic microscope with point-counting stage in order to measure fabric elements. It was discovered, however, that acetate peels taken from stained specimens prepared as outlined in Appendix II yielded excellent surface replicas which could be used to study preferred grain orientation.

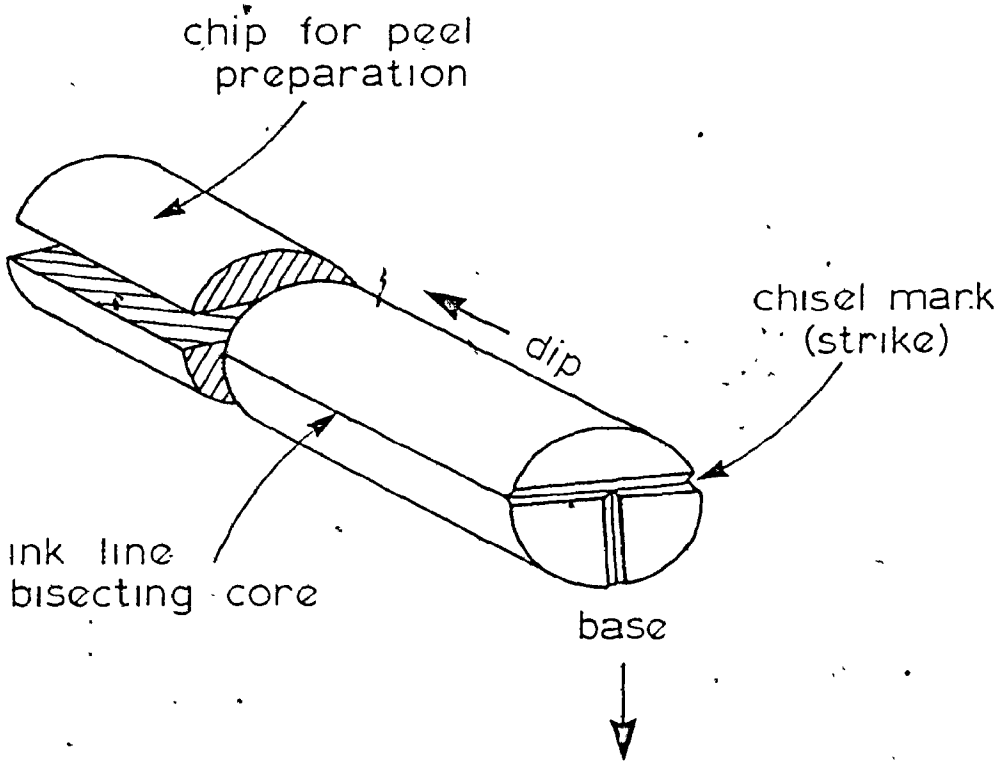

FIG. 4.1. Orientation of rock cores taken for fabric study. Saw cuts necessary for acetate peel preparation are indicated.

Table 4.1

Location of fabric sampling stations

Station number	Area and section	Composite section location (metres)
1	C	sampled east of CVIII
2	AII	116.5 - 119.3
3	MIII	13.0 - 23.5
4	MIa	16.0 - 24.2
5	LX	4.0 - 6.2
6	AII	69.9 - 84.7
7	BI	101.1 - 106.4
8	EI	92.5 - 106.8
9	JI	82.2 - 205.2
10	JIII	39.8 - 41.2

These acetate peels were oriented on the stage of a Shadow-master microprojector and projected onto a sheet of tracing paper with a magnification of 50 or 100 times depending on grain size. Only quartz and feldspar grains (appearing white in the red stained matrix) with a maximum dimension of greater than 0.1 mm (100x) or 0.2 mm (50x) and b/a ratio (Figure 4.2) of less than 0.7 were measured, and then only if the grain involved fell on an intersection point of a square grid of

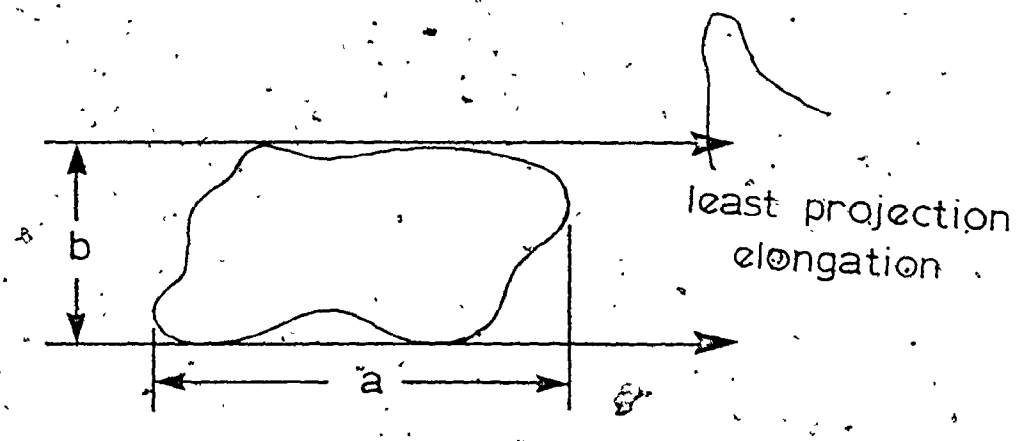

Fig. 4.2. Definition of grain dimensions and "least projection elongation" (Dapples and Rominger, 1945). "b" is defined as the perpendicular distance between the most closely spaced parallel lines tangent to the grain. "a" is perpendicular to "b", as shown. "Least projection elongation" is in the direction of "a".

one inch (2.5 cm) spacing superimposed on the microprojector glass. Grains which satisfied these criteria were outlined on the tracing paper and numbered. The acetate peel was translated as necessary on the Shadowmaster stage until 100 grains had been circled. At a later time, lines were drawn through each grain according to the "least projection elongation" criterion (Figure 4.2), unless the grain displayed bilateral symmetry in its longest dimension, in which case the trace of the symmetry plane was chosen. These lines were then measured against true north, grouped into 10 degree classes from 0° to 180°, and subjected to a chi-squared test proposed by Tukey to search for departures in one direction from a circular distribution (Harrison, 1957; Middleton, 1965). This test is equivalent to the Rayleigh test as outlined by Curray (1956). Vector magnitudes were also calculated for each sample.

To ensure that the chi-squared test was actually being applied to unimodal fabric distributions, equal-area rose diagrams were plotted for each sample. In the case of apparent bimodality, the Tukey chi-squared test was repeated following a 4 θ transformation. The data was also re-run using only readings from the coarsest (greater than 0.35 mm) and most elongate grains (b/a less than 0.5) in order to determine whether the modes corresponded to contrasting behavior of different grain sizes.

All samples which yielded a chi-squared significance level of less than 0.20 were selected for imbrication measurements. The remaining section of core was cut perpendicular to layering, in the direction of preferred orientation and processed as before.

Field sample locations 1 and 7 were each drilled at several sub-stations along strike, with sub-stations being labelled alphabetically. At each station, specimens taken at successively greater heights above the sole were numbered from zero upward.

Accuracy and Consistency of Measurements

An experiment was carried out in order to ascertain the degree of operator variation in fabric measurement, and to allow confidence limits to be assigned to individual orientation determinations. Four operators each measured 100 fabric elements in two specimens, and then repeated the process several weeks later. Because many grains can be outlined on the Shadowmaster screen without moving the peel, each operator was able to work with exactly the same image area. Hence, for each measurement, variation between the results of different operators contains no contribution from within-specimen variation.

Tables 4.2 and 4.3 tabulate experimental results for

Table 4.2

Data for operator experiment on vector means

Specimens	operators			
	RH	MD	ST	RT
1aO	186	178	190	185
	151	164	152	144
1eO	149	150	150	147
	137	144	134	147

Table 4.3

Data for operator experiment on vector magnitudes

Specimens	operators			
	RH	MD	ST	RT
1aO	27.14	31.24	30.42	37.42
	23.50	23.54	23.75	22.22
1eO	35.34	29.99	31.64	33.35
	27.98	26.54	25.00	35.58

vector mean and vector magnitude, respectively. An analysis of variance (ANOVA) for two variables with replication (Dixon and Massey, 1957) was performed on both sets of data. Interaction between operators and specimens was found to be insignificant in both cases, allowing the ANOVA to be carried out using a two-variable single-observation format (Tables 4.4 and 4.5). The residual error term includes sampling error in grain selection, operator inconsistency, and interaction between operators and specimens.

For both vector mean and vector magnitude (L), operator variation is not significant. Because "residual error" mean squares exceed "among operators" mean squares, it is not possible to estimate operator variances from this analysis. It is important, however, to be able to attach error limits to fabric measurements in order to have some idea of the significance of differences between vector means and sole markings, or imbrication means and primary layering. This error term is composed of three parts: (1) specimen collection error, (2) operator inaccuracy, and (3) sampling error resulting from the choice of fabric elements to be measured. An additional error results from within-specimen variation. As this is different for each specimen, a general estimate is not possible.

Because the hypothesis of differences between operators was rejected, we can pool "deviations about the mean" for all

Table 4.4

ANOVA for vector means

Source of variation	SS	df	MS	F_{obs}	$F_{.95}$	
between specimens	2304	1	2304	9.90	4.84	**
among operators	28.50	3	9.50	0.04	3.59	N.S.
residual error	2560.5	11	232.8			
total	4893	15				

Table 4.5

ANOVA for vector magnitudes

Source of variation	SS	df	MS	F_{obs}	$F_{.95}$	
between specimens	42.90	1	42.90	1.87	4.84	N.S.
among operators	52.77	3	17.59	0.77	3.59	N.S.
residual error	252.73	11	22.98			
total	348.40	15				

measurements and estimate the accuracy of grain orientation determinations in this study. This accuracy can be expressed as a standard deviation, and is found to be 5.3°.

Curray (1956) presents a graph showing the relationship between vector magnitude (in percent) and the standard deviation of a "wrapped" linear normal distribution. These standard deviations can be used to calculate confidence limits in the normal manner. The confidence limits are in effect an estimate of sampling error. Figure 4.3 is a plot of 90% confidence limit magnitudes against vector magnitude, with histograms of the frequency of occurrence (in percent) of various L values for both orientation and imbrication measurements. Samples with a chi-squared significance level (S.L.) greater than 0.20 are considered to have a random fabric. It would appear that in general, 90% confidence limits are ± 10° for orientation measurements, and ± 7 or 8° for imbrication measurements.

In summary, we can assume the following maximum error estimates for vector means based on a sample size of 100 grains.

(1)	orientations:	field sampling error	± 5°
		operator inaccuracy	± 5°
		sampling error (C.L.'s)	± 10°
(2)	imbrications:	field sampling error	± 5°
		operator inaccuracy	± 5°
		sampling error (C.L.'s)	± 7°

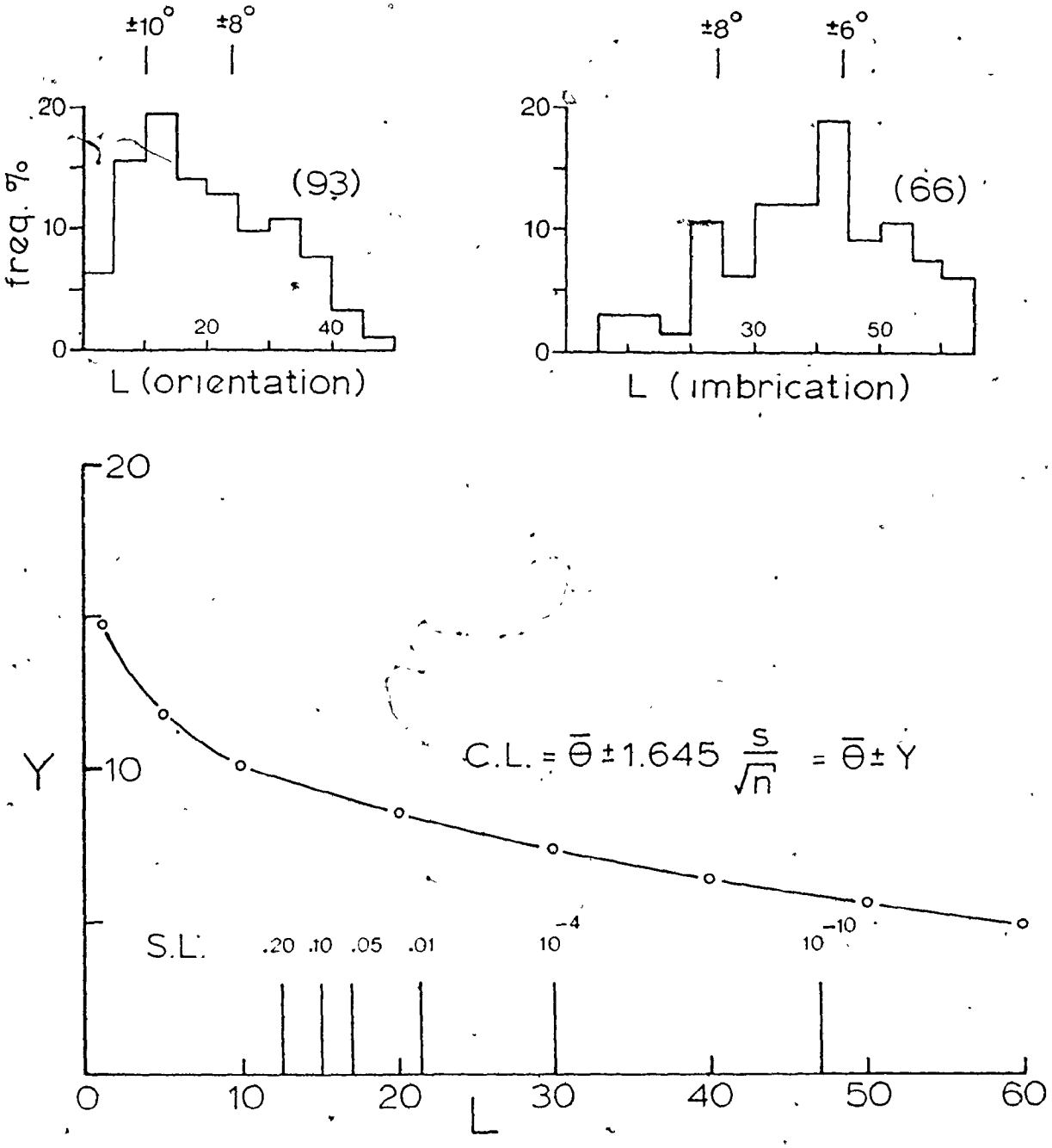

Fig. 4.3. Upper: histograms of vector magnitude (L) for orientations and imbrications. Lower: graph to determine 90% C.L.'s for "wrapped" linear normal distribution (0 to 180°) with n=100. "s" values are from Curray (1956, p.123). Values of ±Y from this graph are plotted above the upper histograms.

Maximum error for orientations is ± 20°. The error estimate for imbrication measurement will be rounded off to ± 15°.

In order to accurately estimate the vector mean of a sandstone fabric, it is necessary to measure sufficient fabric elements to ensure that no sharp fluctuations of the vector mean will occur for larger sample sizes. When this situation is achieved, we say that the flatness point has been reached. Raup and Miesch (1957) describe a technique which allows the position of the flatness point to be calculated after 50 measurements. Samples 2a1 and 6a2, which both have a Tukey chi-squared S.L. of approximately 0.05, indicate that 100 points are sufficient to reach this plateau. Because we desire comparisons in S.L. between samples of different vector magnitude, 100 points are deemed to be a suitable sample size for all orientation measurements.

Sample Homogeneity

Internal variability within single acetate peels (2.5 x 4.0 cm) was first suspected when carrying out the operator error experiment. Replicate measurements were carried out on different areas of each acetate peel. Table 4.6 presents the means and standard deviations for each measurement and the result of a t-test with the null hypothesis of equal means for each case.

Table 4.6

t-test for within-specimen homogeneity

Specimen	Measure	Measurements 1	Measurements 2	t_{obs}	S.L.=$2P(t_6>t_{obs})$	
1a0	$\bar{x}$	184.8	152.8			
	s^2	24.92	68.92	6.61	0.0006	**
1e0	$\bar{x}$	149.0	140.5			
	s^2	2.00	36.33[1]	2.75	0.033	*

[1] An F-test for equality of variances gives fairly strong evidence against H_o. However, this is not too serious for inferences about the mean.

** Strong evidence against H_o.

* Fairly strong evidence against H_o.

Sample 1a0 exhibits internal heterogeneity to the extent that measurements 1 and 2 yield statistically different means. Sample 1e0 shows the same property to a lesser degree. This explains the large residual-error mean square in Table 4.4. This micro-scale heterogeneity, also reported by Griffiths and Rosenfeld (1954) and Smoor (1960), appears to result from the presence of clusters of grains sharing a parallel fabric due to mutual interaction during deposition. This fabric does not coincide with the vector mean. These clusters are called micro-domains, and may be up to 15 mm^2 in cross-sectional area (Figure 4.4). As a result, the effective size of individual fabric elements is increased in some samples to the level of micro-domains and the flatness point is not attained due to lack of sufficient sample size. In some cases, entire fields of view possessed orientations different from the mean. If these are also separate orientation domains, then maximum size would increase to at least 40 mm^2.

An examination of Shadowmaster tracings of elongate grains allowed micro-domains to be identified in samples 1a3, 1b0, 1c1, 1e0, 1e2, 1g2, 2a3, 2a7, 3a0, 3a4, 4a1, 4a5, 6a3, 7a0, 7a1, 7b2, 7b4, 7c1, and 9a4. Of these samples, 37% possess random fabric, and an additional 16% are bimodal. Figure 4.4e in particular suggests that bimodality is the aggregate expression of a mosaic of mutually perpendicular micro-domains. An interpretation of this phenomenon will be deferred until Chapter V.

Fig. 4.4. Examples of orientation micro-domains taken from Shadowmaster tracings. Sample vector means are indicated as outlined in the caption for figure 4.5, with the top of the page being designated as north. All scale bars are 1 mm. Micro-domains are separated by light dashed lines. In the case of (e) and (f), the micro-domains which appear have been drawn from different fields of view in the same peel.

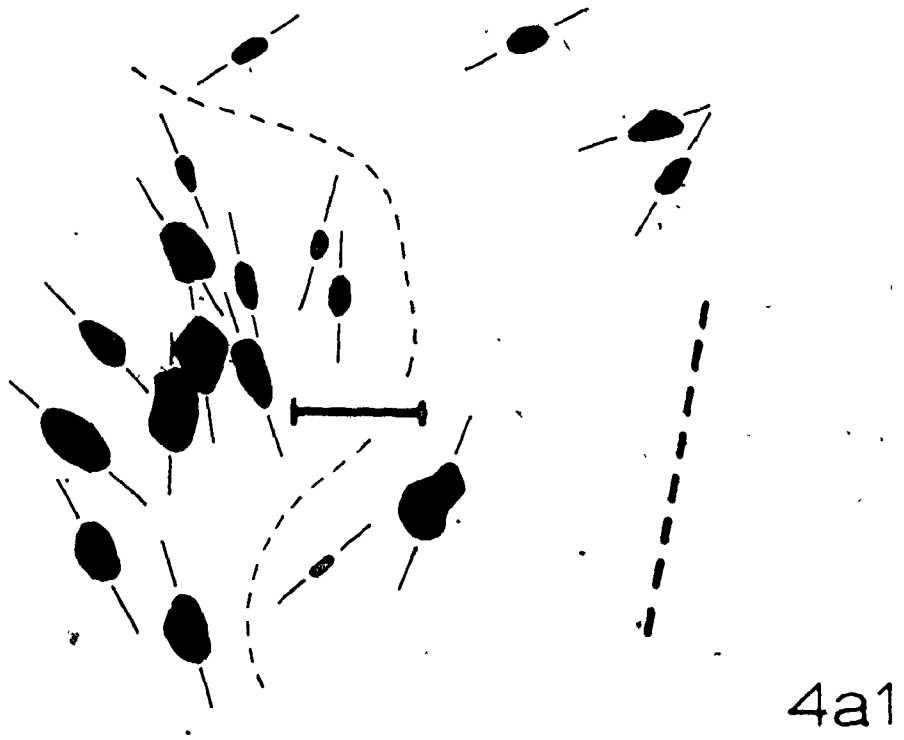

FIG 4.4a

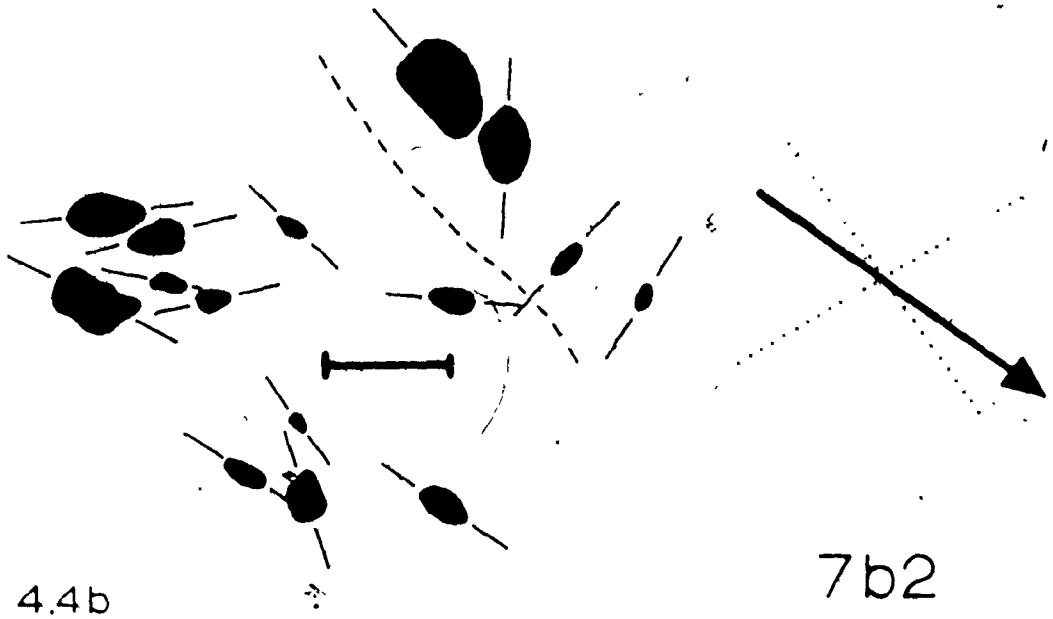

FIG. 4.4b

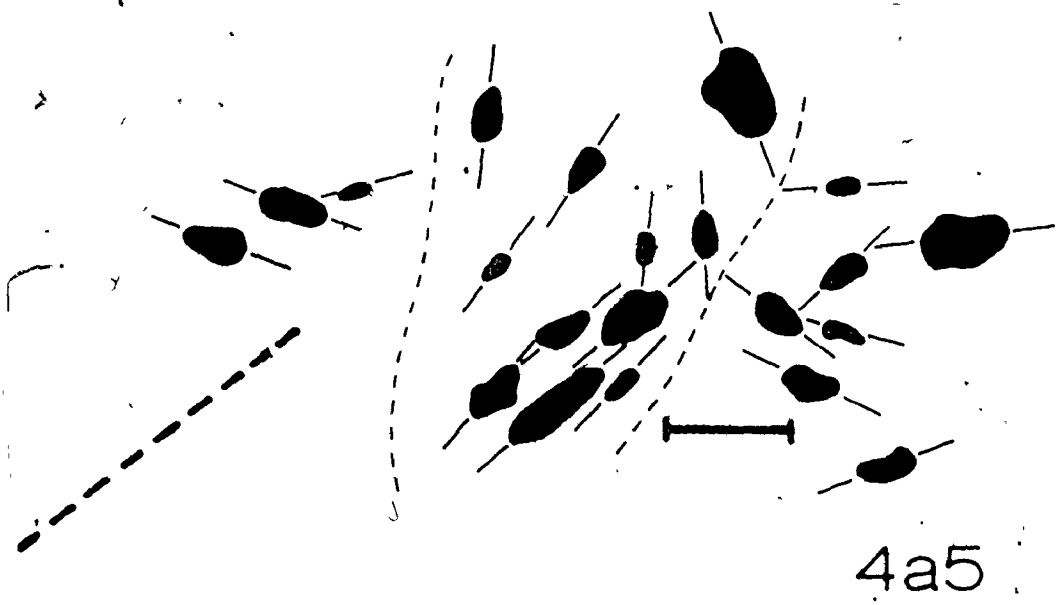

FIG. 4.4c

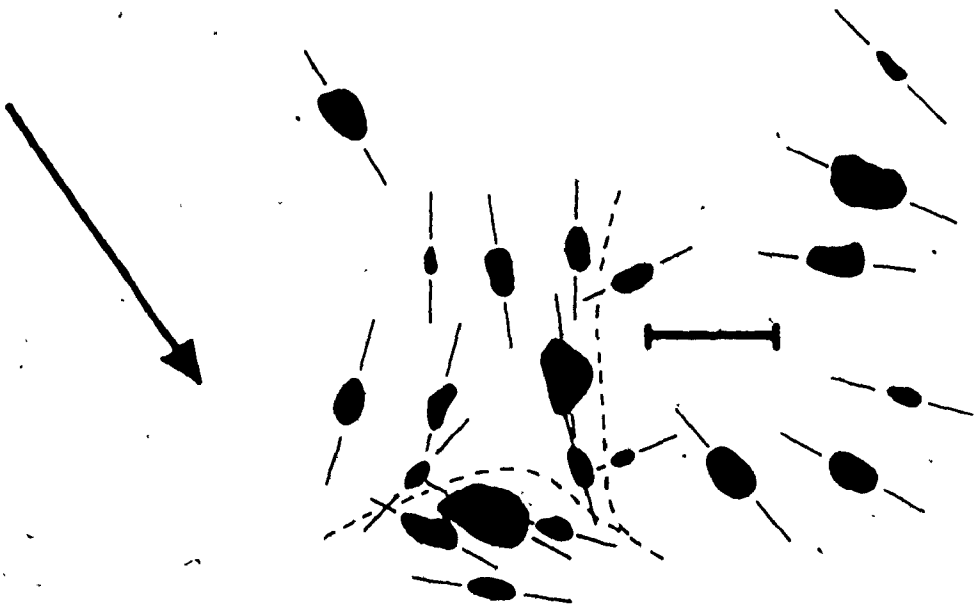

FIG 4.4d

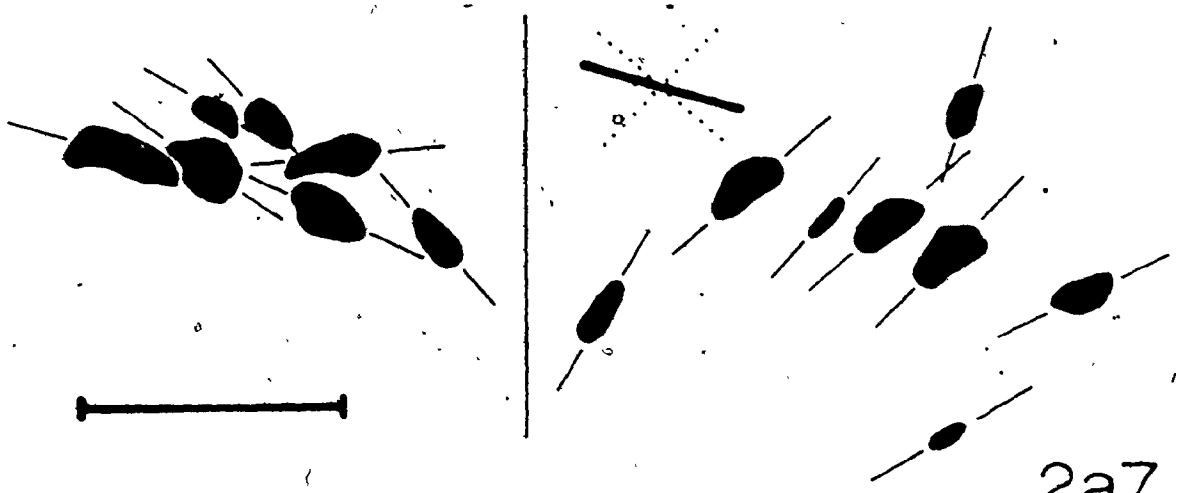

FIG. 4.4e

FIG. 4.4f

FIG. 4.4g

Fabric Data

One fabric diagram for each sampling station is presented in Figures 4.5 (stratified layers) and 4.6 (massive layers). More than one set of samples were taken at stations 1 and 7 to investigate large-scale variations in orientation (see next section). These additional fabric diagrams appear in Appendix III, along with grain-size variation diagrams for all sample locations. These grain sizes are averages of the 10 largest quartz grains visible on the Shadowmaster screen at 25x or 100x magnification, depending on specimen coarseness. Imbrication and orientation statistics appear in Appendix IV.

Stratified Layers

Recall that coarse stratification in thick sandstones (6) consists of a "horizontal" erosion surface overlain by fine sand, with inverse grading upward into medium to coarse sand. This sequence, called a stratification band, is repeated many times to produce a division of coarse stratification. Samples of both fine and coarse components were taken at stations 1, 2 and 10 (Figure 4.5).

Fig. 4.5. Fabric diagrams for stratified thick sandstone (6) layers. Specimens are designated as massive (m), or as coarse (c) or fine (f) parts of stratification bands. Vector means are plotted assuming north to lie at the top of each diagram. Orientations with a significance level (S.L.) of less than 0.20 are plotted with a solid line. Vector means of "random" samples (S.L. greater than 0.20) are shown with a dashed line. If bimodality exists, the positions of the modes are indicated with dotted lines. The sense of current flow derived from imbrication measurements (assuming upcurrent imbrication) is indicated by a full arrow head for significant imbrications (greater than 15°), or by an open arrow head for non-significant imbrications.

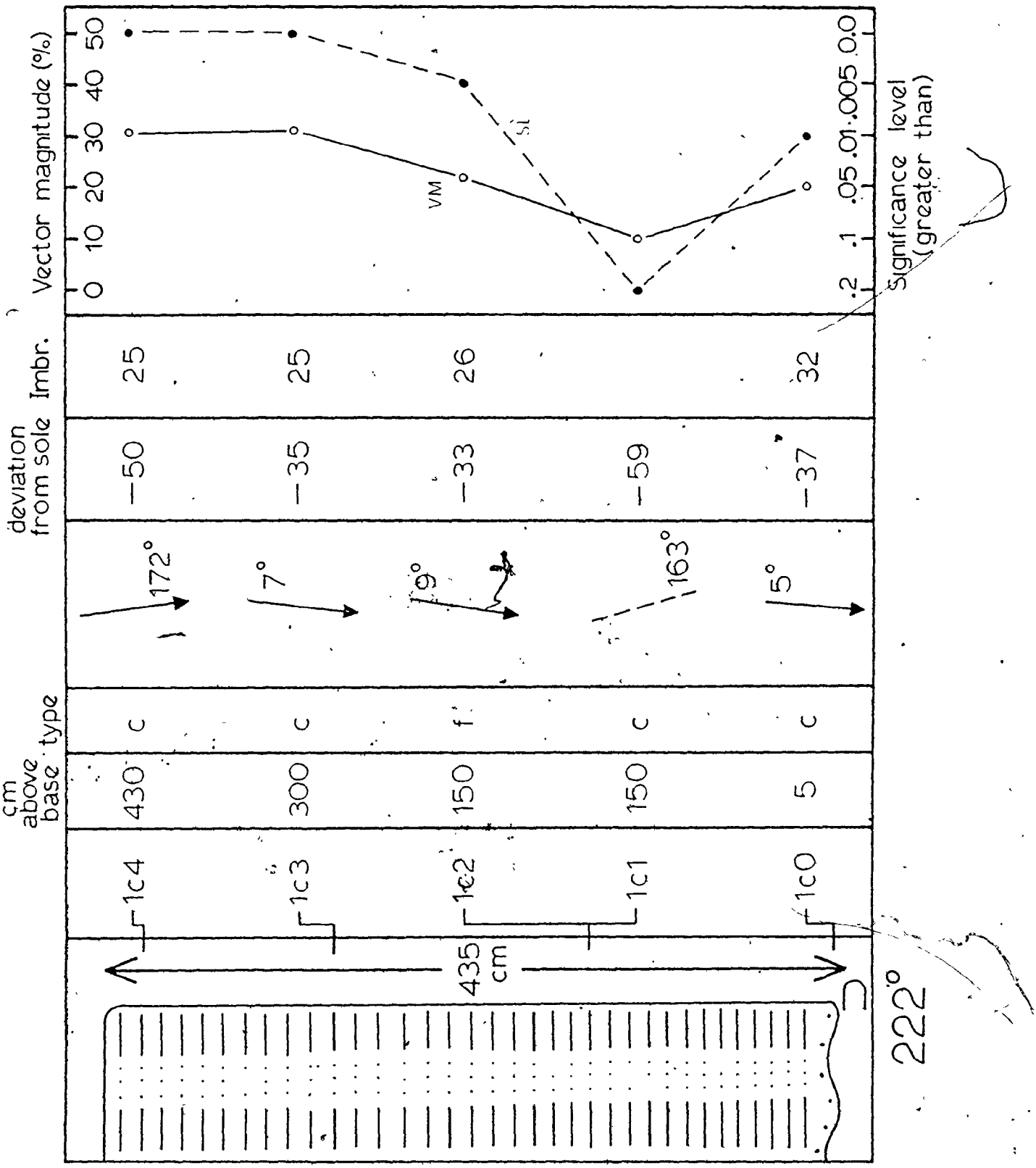
Vector magnitude (%)
0 10 20 30 40 50
VM
SL
Significance level (greater than)
.2 .1 .05 .01 .005 0.0
Imbr.
25 25 26 32
deviation from sole
−50 −35 −33 −59 −37
172°
7°
9°
163°
5°
cm above base
430 300 150 150 5
type
c c f c c
1c4 1c3 1c2 1c1 1c0
435 cm
222°

Fig. 4.5a.

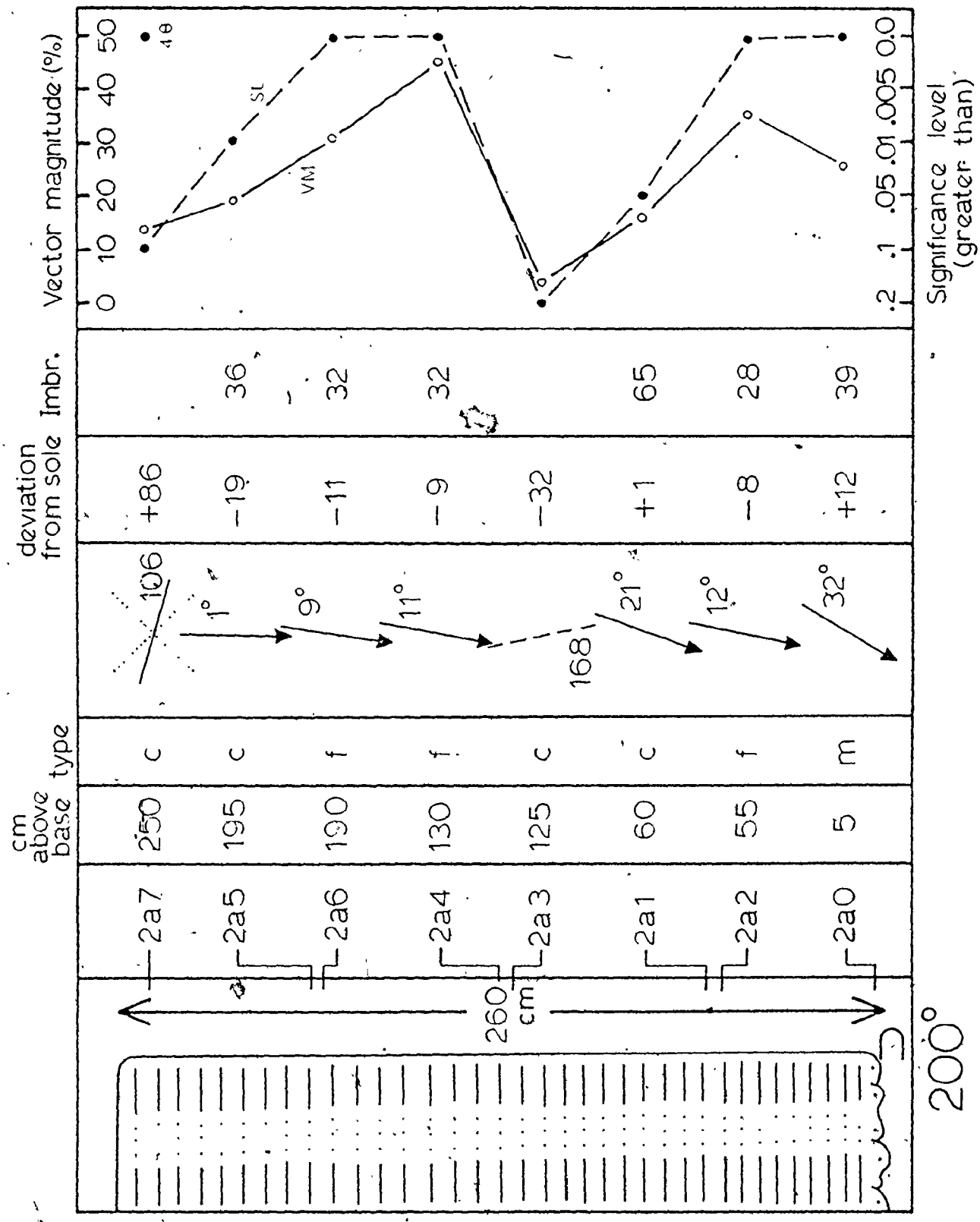
Vector magnitude (%)
0 10 20 30 40 50
SL
VM
Significance level (greater than)
.2 .1 .05 .01 .005 0.0
Imbr.
36
32
32
65
28
39
deviation from sole
+86
-19
-11
-9
-32
+1
-8
+12
cm above base
250
195
190
130
125
60
55
5
type
c
c
f
f
c
c
f
m
106
1°
9°
11°
168
21°
12°
32°
2a7
2a5
2a6
2a4
2a3
2a1
2a2
2a0
260 cm
200°

Fig. 4,5b.

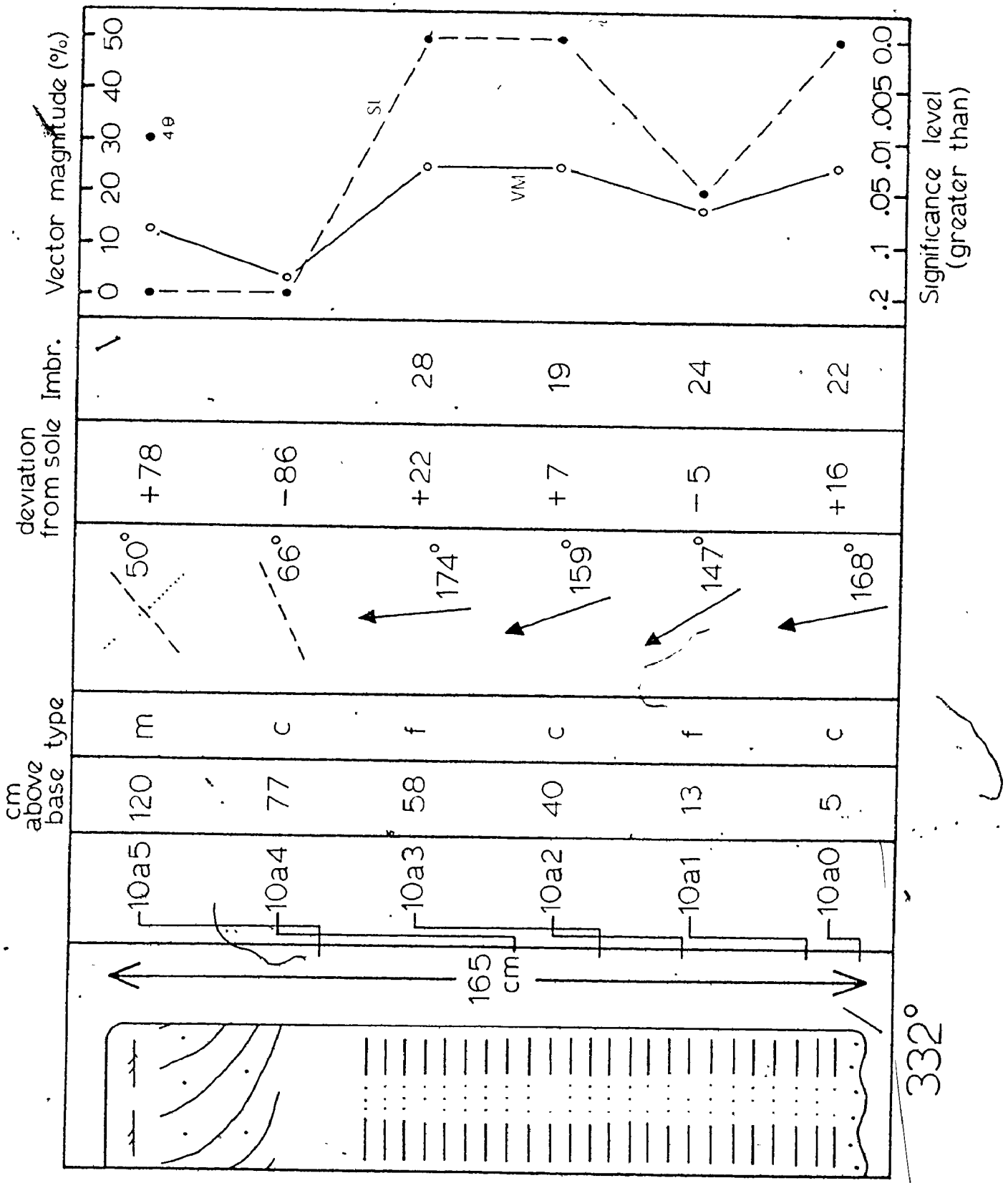
Vector magnitude (%)
0 10 20 30 40 50
SI
VM
Significance level (greater than)
.2 .1 .05 .01 .005 0.0
deviation from sole
Imbr.
+78
-86
+22
+7
-5
+16
28
19
24
22
50°
66°
174°
159°
147°
168°
cm above base
type
m
c
f
c
f
c
120
77
58
40
13
5
10a5
10a4
10a3
10a2
10a1
10a0
165 cm
332°

Fig. 4.5c.

Grain orientations at stations 2 and 10 agree remarkably well with sole markings. Station 1 exhibits a consistent anticlockwise (negative) deviation from flute casts. The following general observations can be made.

(i) Anisotropic appositional fabrics are remarkably consistent, with little upward variation through several metres of sediment.

(ii) There is a tendency for strong basal orientations to be overlain by poorly aligned material followed by an upward improvement in preferred orientation. The minimum in vector magnitude at lcl persists at this height in the layer through almost all station 1 sample locations.

(iii) Fabric deteriorates in the upper part of layers. This trend is not seen at station 1 because erosion has removed the top of the layer.

(iv) Fine samples from the base of individual stratification bands frequently have higher vector magnitudes than coarse samples, particularly at station 2, where grain-size contrast is greatest (see Appendix III).

(v) Imbrication is consistently upcurrent with imbrication angles in excess of 20°. Sample 2a1 has an extremely high angle of 65°.

Massive layers

Visual inspection of Figure 4.6 shows strong similarities between the fabric of all massive layers except station 9 (Figure 4.6g), which displays a consistent vector mean orientation throughout the lower 9 m of a channel fill sandstone. Imbrication is either upcurrent or not significant at station 9. Note also the presence of sheet structure, which Laird (1970) reports to be parallel to strong a-axis grain orientation. Deviation from sole markings is consistently in a clockwise direction (positive).

Layers at stations 3, 4, 5 and 7 (Figure 4.6a, b, c and e) have good basal preferred orientation followed by a general upward deterioration of fabric. This trend may be reversed at the top of the layer (5 and 7, as well as 8). In contrast, layers at stations 6 and 8 (Figure 4.6d and f) begin with bimodal fabrics followed by a short-lived upward improvement in unimodal preferred orientation.

The following generalizations can be made concerning fabric of the massive interiors of all layers except that at station 9.

Fig. 4.6. Fabric diagrams for massive thick sandstone (6) layers. For further explanation, see the caption for figure 4.5.

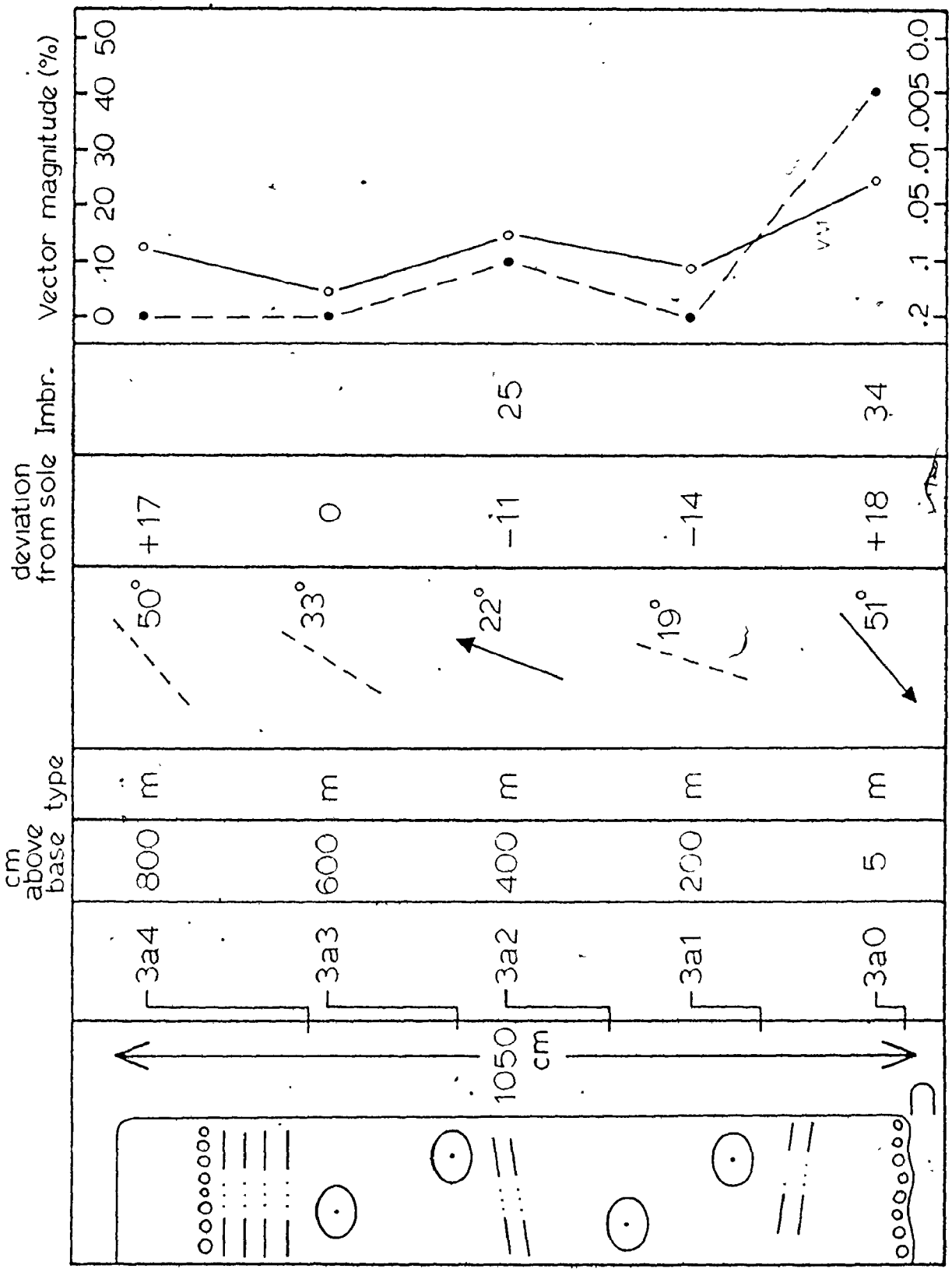
Vector magnitude (%)
0 10 20 30 40 50
Significance level (greater than)
.2 .1 .05 .01 .005 0.0
Imbr.
25
34
deviation from sole
+17
0
-11
-14
+18
50°
33°
22°
19°
51°
cm above base
800
600
400
200
5
type
m
m
m
m
m
3a4
3a3
3a2
3a1
3a0
1050 cm
213°

Fig. 4.6a.

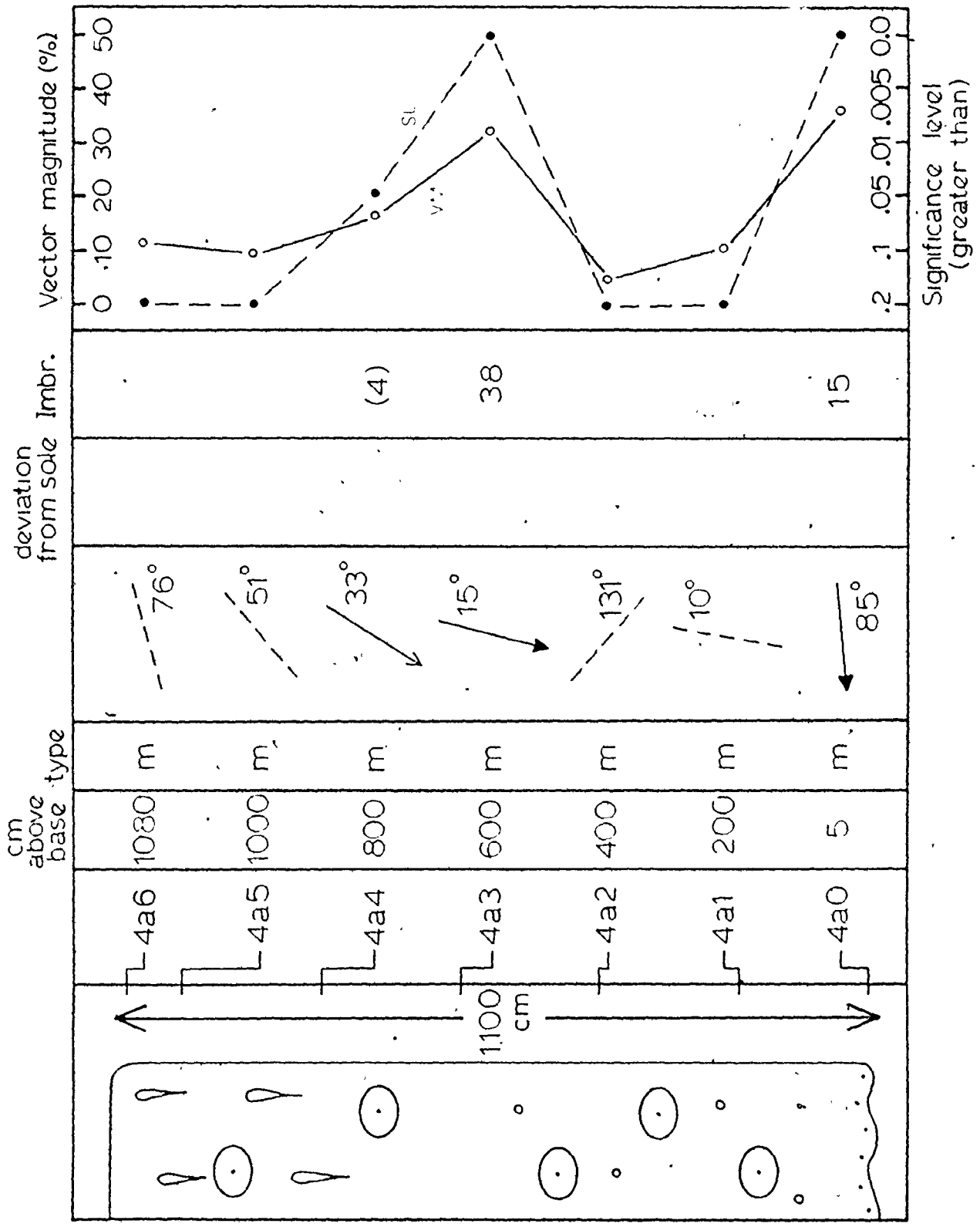
Vector magnitude (%)
0 10 20 30 40 50
St.
V.
Significance level (greater than)
.2 .1 .05 .01 .005 0.0
deviation from sole
Imbr.
(4)
38
15
76°
51°
33°
15°
131°
10°
85°
cm above base
type
1080 m
1000 m
800 m
600 m
400 m
200 m
5 m
4a6
4a5
4a4
4a3
4a2
4a1
4a0
1100 cm

Fig. 4.6b.

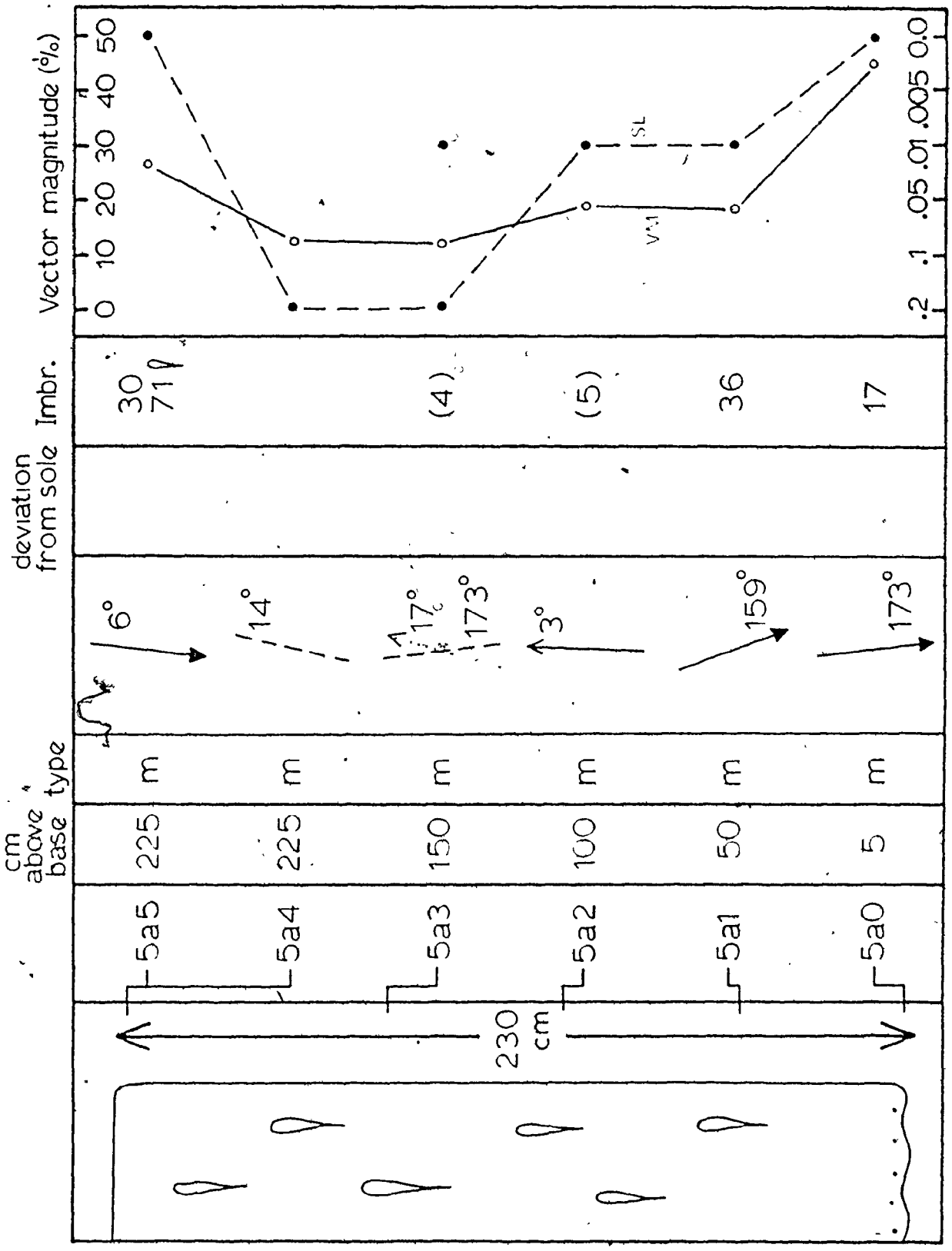
Vector magnitude (%)
0 10 20 30 40 50
Significance level (greater than)
.2 .1 .05 .01 .005 0.0
SL
V1
deviation from sole
Imbr.
30
71
(4)
(5)
36
17
6°
14°
17°
173°
3°
159°
173°
cm above base
type
m
225
225
150
100
50
5
5a5
5a4
5a3
5a2
5a1
5a0
230 cm

Fig. 4.6c.

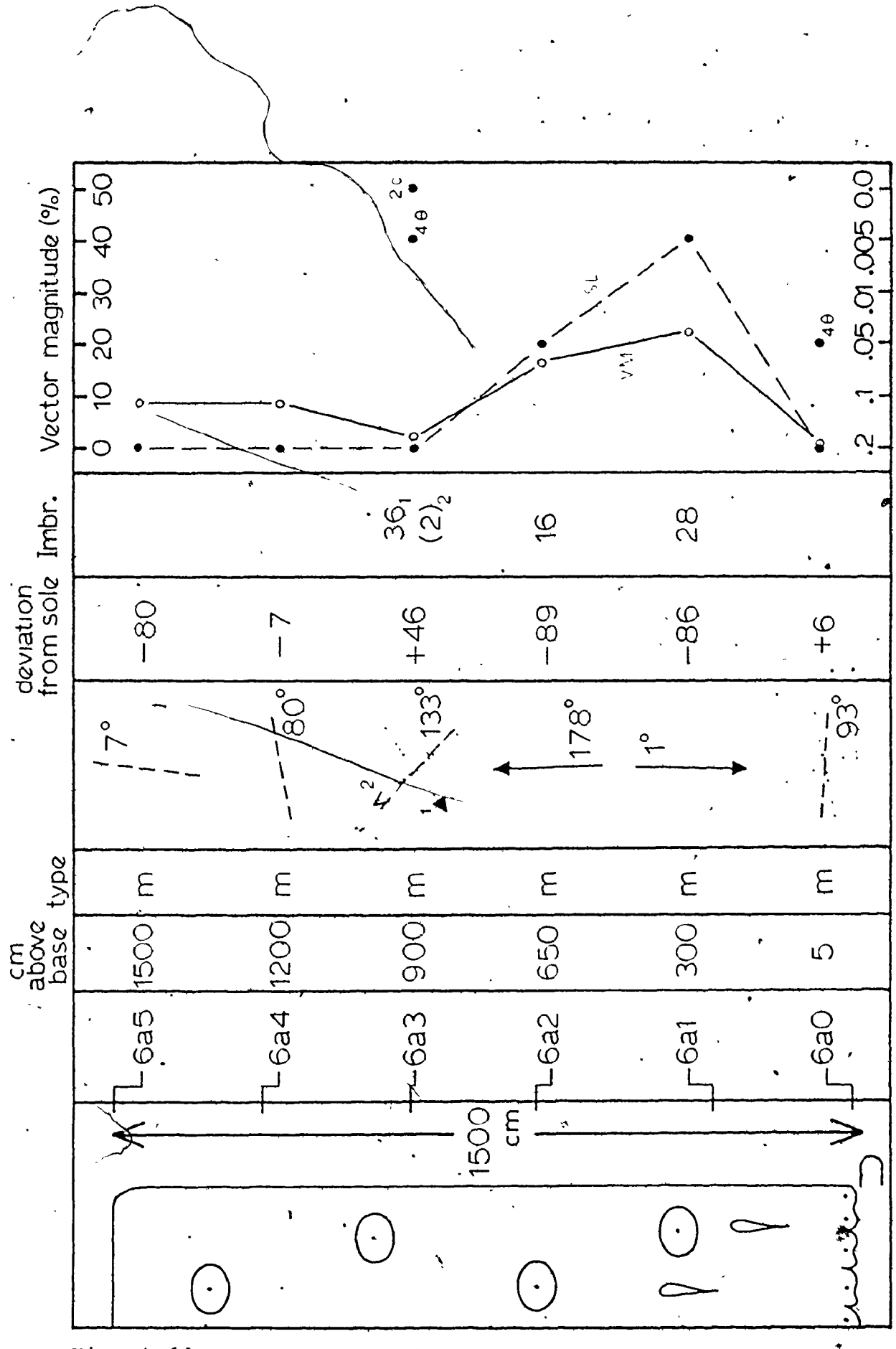
Vector magnitude (%)
0 10 20 30 40 50
Significance level (greater than)
.2 .1 .05 .01 .005 0.0
Imbr.
deviation from sole
cm above base
type
6a5 1500 m
6a4 1200 m
6a3 900 m
6a2 650 m
6a1 300 m
6a0 5 m
−80
−7
+46
−89
−86
+6
36
(2)
16
28
7°
80°
133°
178°
1°
93°
1500 cm
267°

Fig. 4.6d.

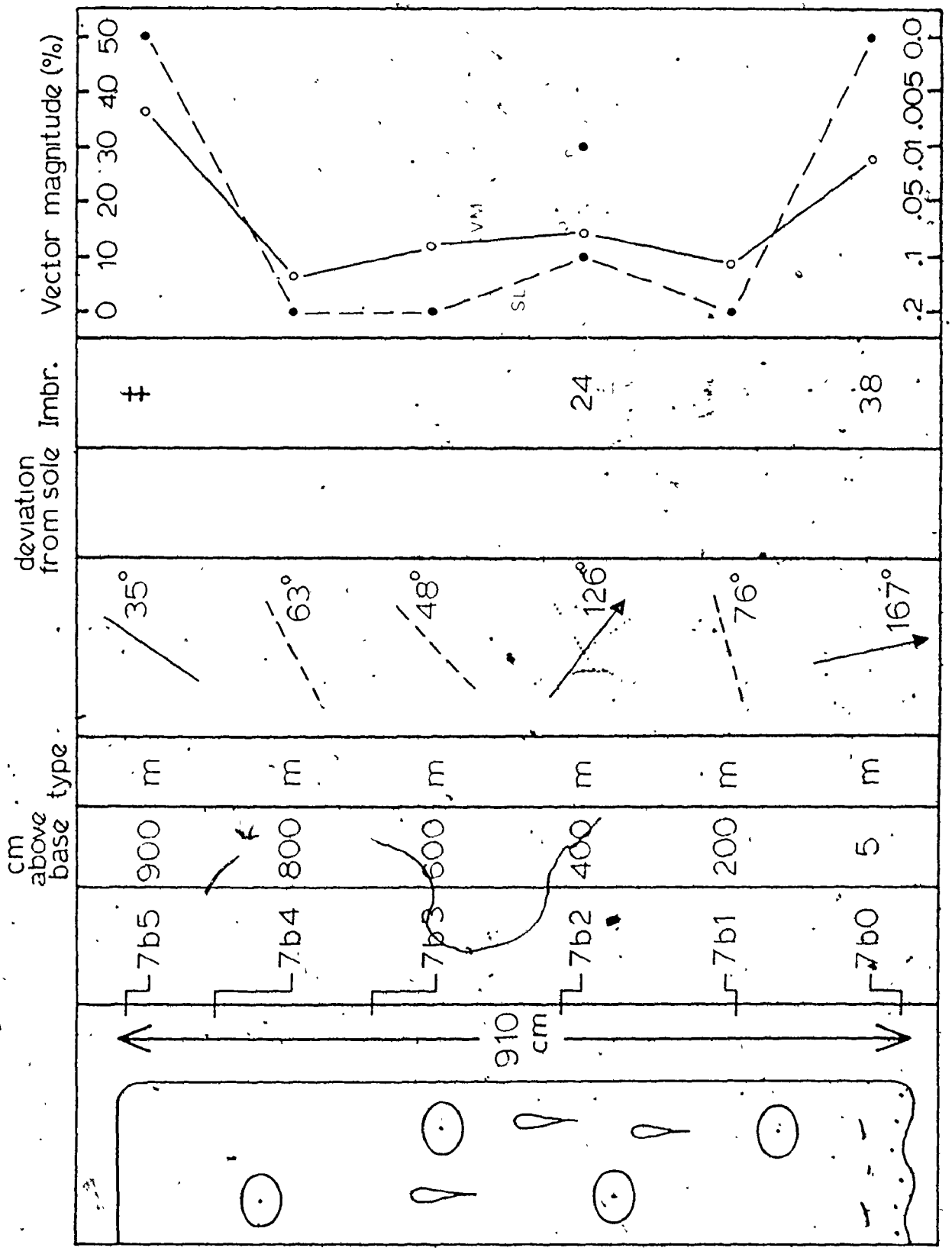
Vector magnitude (%)
0 10 20 30 40 50
Significance level (greater than)
.2 .1 .05 .01 .005 0.0
VM
SL
Imbr.
24
38
deviation from sole
35°
63°
48°
126°
76°
167°
type
m
cm above base
900
800
600
400
200
5
7b5
7b4
7b3
7b2
7b1
7b0
910 cm

Fig. 4.6a.

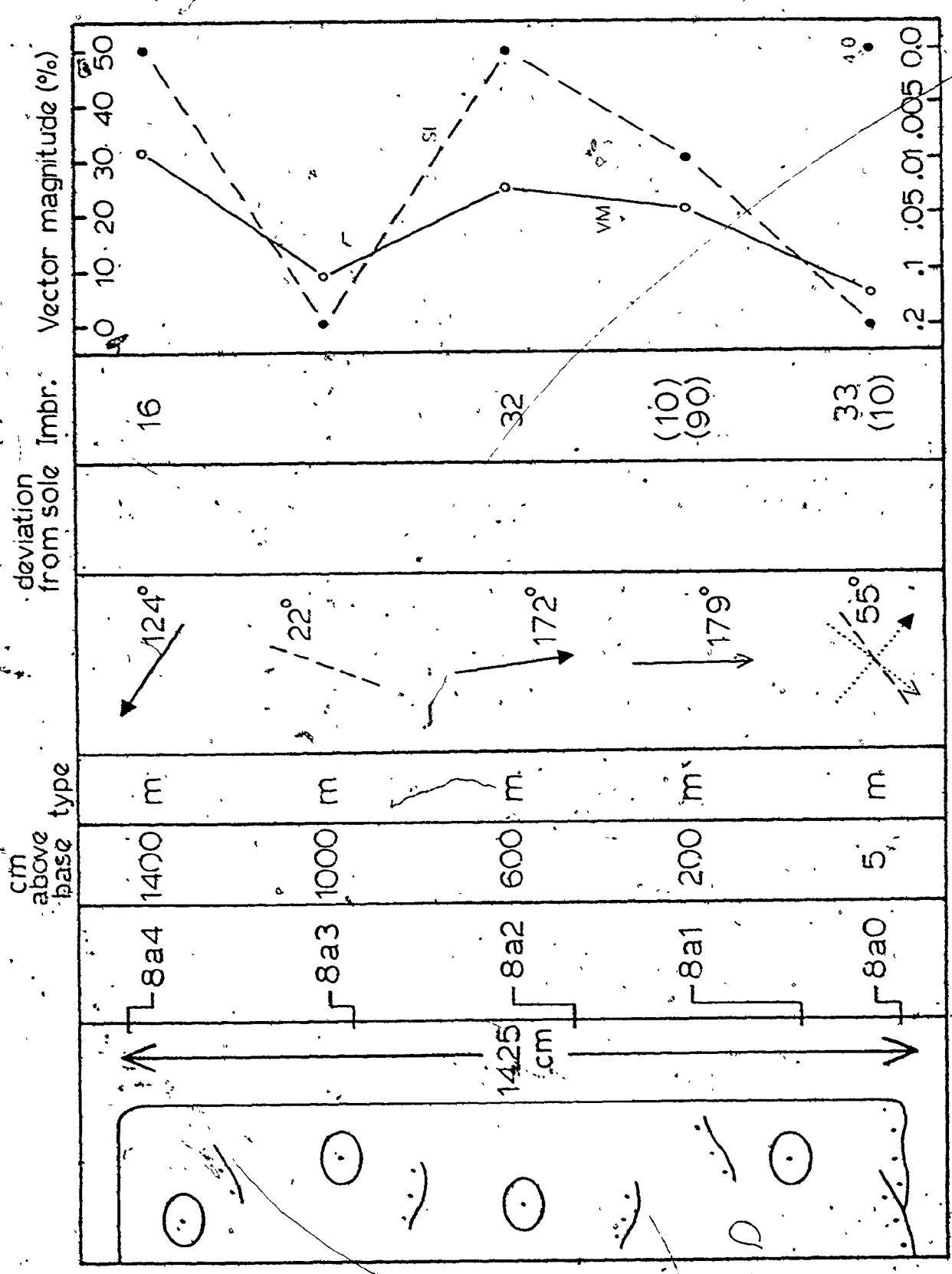
Vector magnitude (%)
0 10 20 30 40 50
SI
VM
.2 .1 .05 .01 .005 0.0
Significance level (greater than)
deviation from sole
Imbr.
16
32
(10) (90)
33 (10)
124°
22°
172°
179°
55°
cm above base
type
1400 m
1000 m
600 m
200 m
5 m
8a4
8a3
8a2
8a1
8a0
1425 cm

Fig. 4.6f.

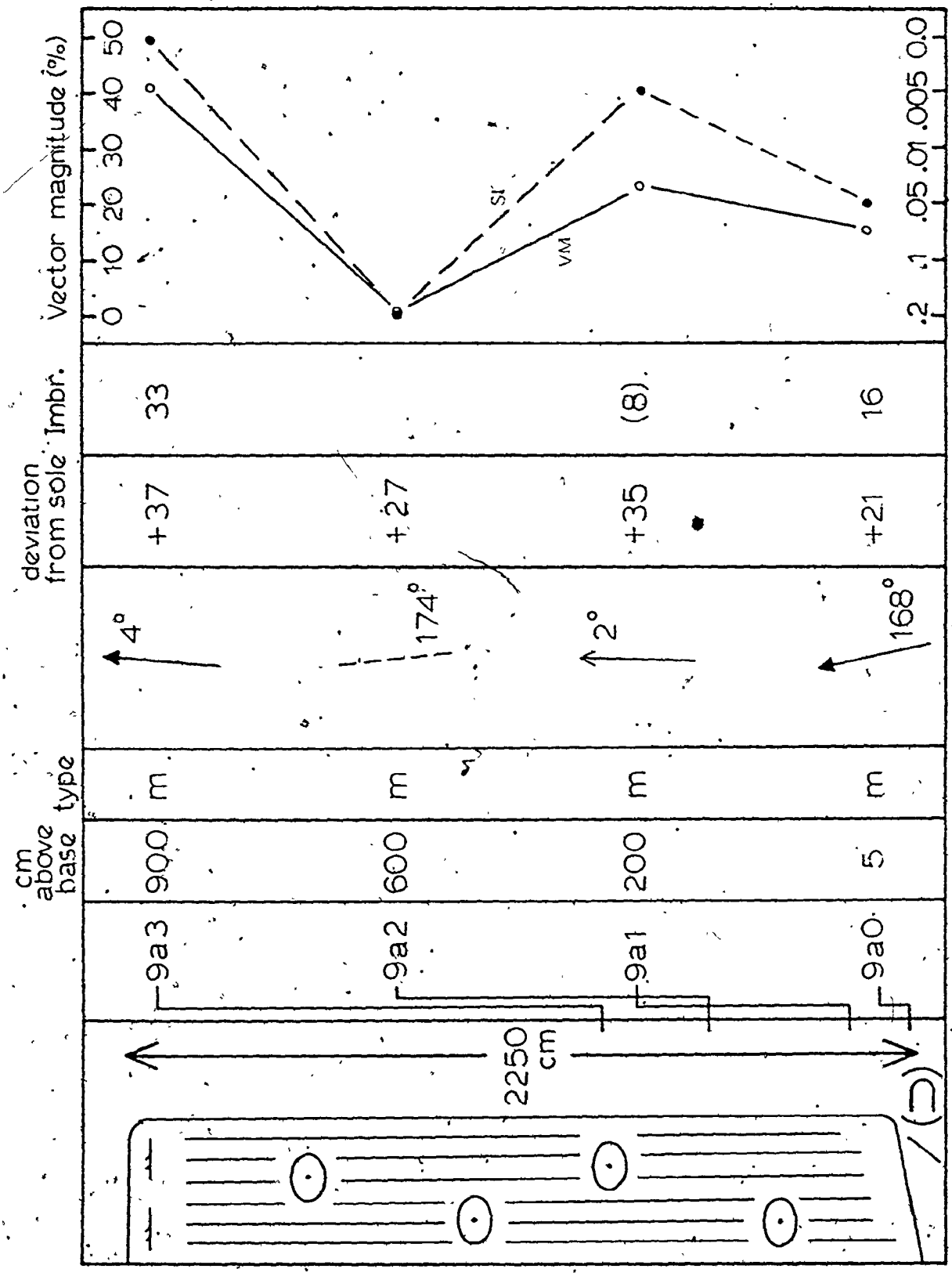
Vector magnitude (%)
0 10 20 30 40 50
SI
VM
.2 .1 .05 .01 .005 0.0
Significance level (greater than)
deviation from sole
Imbr.
33
(8)
16
+37
+27
+35
+21
4°
174°
2°
168°
cm above base
type
m
900
600
200
5
9a3
9a2
9a1
9a0
2250 cm
327°

Fig. 4.6g.

(i) Isotropic (random) or bimodal fabrics are common. Random fabrics may still possess preferred orientation of the coarse size fraction (5a3, 6a3). In bimodal samples, only one mode shows significant imbrication. In samples 8a0 and 6a3 this is the weakest of the two modes, and in the latter case, also the finest of the two modes. The presence of a fine imbricate mode and a non-imbricate coarse mode at right angles to the first would normally suggest that the coarse mode preserves a current-normal fabric due to rolling of clasts on the bed.

(ii) Whereas some layers show internal consistency of vector means (Figure 4.6a and c), there is a tendency for considerable vertical variation in a-axis preferred orientation and pronounced deviation from sole markings.

(iii) Imbrication may be non-significant (less than 15°), bimodal (8a1), or may reverse polarity (6a1 to 6a2).

(iv) The expulsion of pore water through fluid-escape pillars caused strong local disruption of appositional fabric as indicated by an imbrication angle of 71° obtained from a fluid-escape pillar at 5a5. This is not surprising, as evidence exists that escaping pore water was able to transport even the coarsest components of the size distribution (Chapter II).

Large-scale Variations

Several sub-stations were sampled at stations 1 and 7 to study variations in preferred orientation (Figures 4.7 and 4.8). If we can assume these larger-scale variations to be typical of stratified and massive layers, then the following generalizations can be made.

(i) Stratified layers show remarkable consistency of vector means both vertically and laterally (Figure 4.7 shows more lateral than downcurrent variation). Preferred orientations are most divergent from one another and from sole markings at the base of the layer, with an upward improvement in parallelism. This observation is exactly opposite to that which Parkash and Middleton (1970) demonstrated from the study of thin massive turbidites (less than 20 cm thick) over greater horizontal distances. Onions and Middleton (1968) reported greatest deviations from sole markings in basal samples.

(ii) Without exception, imbricate samples from stratified divisions show an upcurrent polarity.

(iii) Massive layers show as much lateral variability in preferred orientation as is observed vertically (Figure 4.8). The only exception to this may be found in basal samples, which show more lateral consistency both in vector mean and in imbrication at station 7. Whether this imbrication is upcurrent or downcurrent is unclear because of

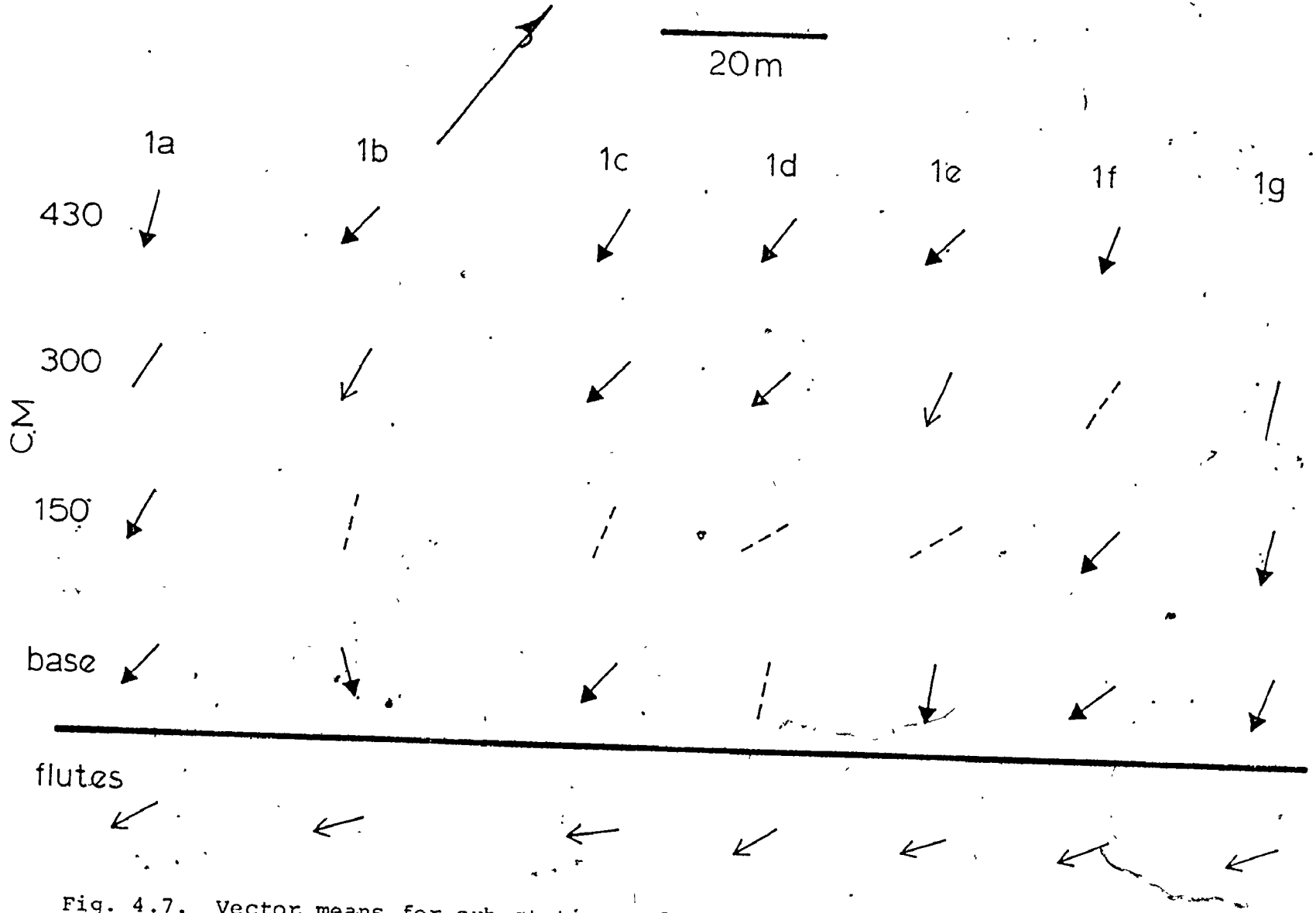

Fig. 4.7. Vector means for sub-stations of a stratified layer at station 1. Horizontal scale is distance between sub-stations. Vertical scale is height in the layer (cm). See figure 4.5 for explanation of symbols. Distance between sub-stations a and g is 135 m.

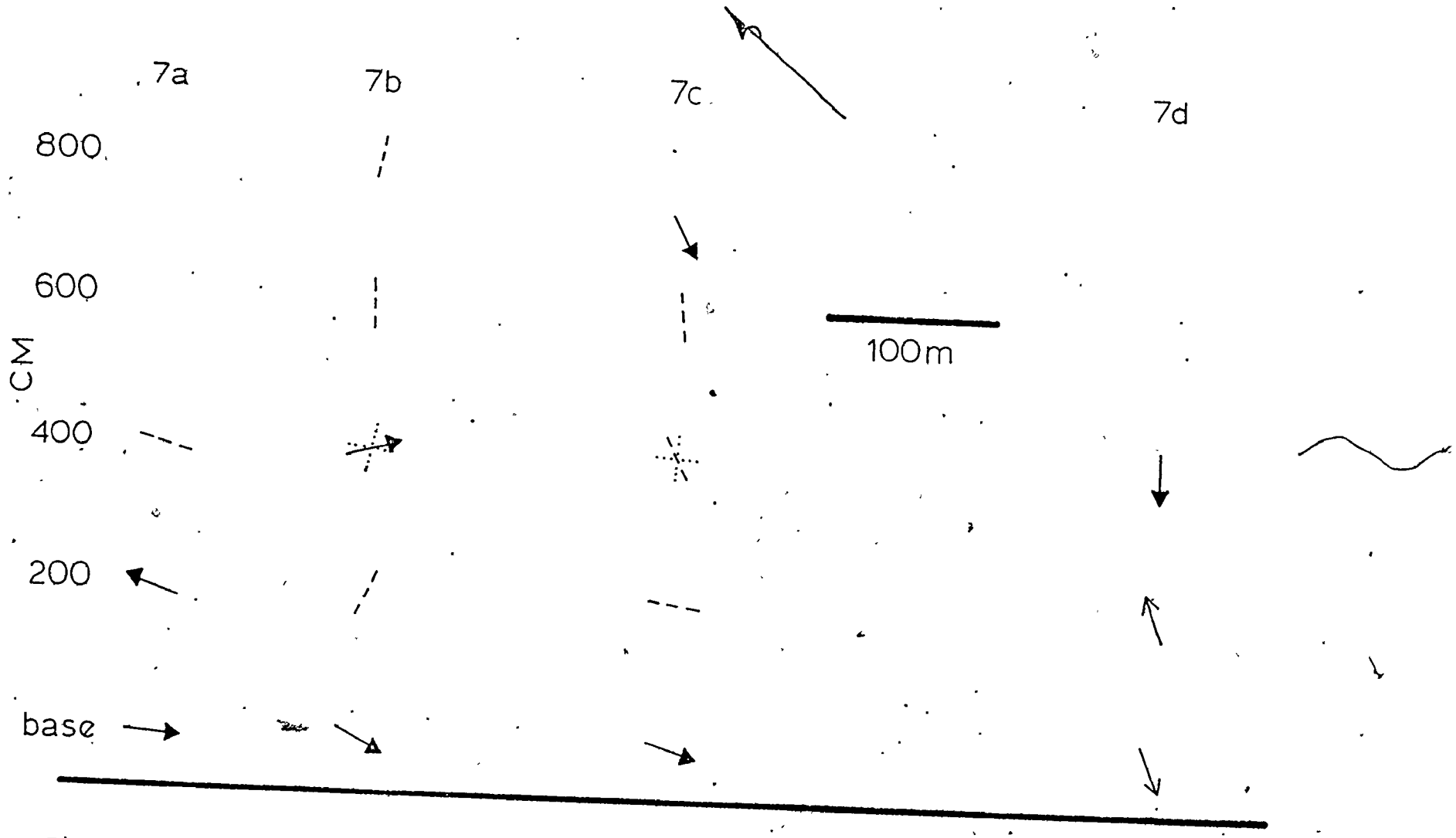

Fig. 4.8. Vector means for sub-stations of a massive layer at station 7. Horizontal scale is distance between sub-stations. Vertical scale is height in the layer (cm). See figure 4.5 for explanation of symbols. Distance between sub-stations a and d is 570 m.

imbrication reversals at higher levels in the layer. If paleocurrents for the rest of area B can be applied to this layer as well (Figure 1.4a), then these would appear to be downcurrent imbrications. Similar variability in imbrication from thick massive sandstones has been reported by Bouma (1962) and Sestini and Pranzini (1965).

Summary

Thick sandstones (6) analysed in this chapter can be divided on the basis of internal structures into (i) stratified, well graded layers, and (ii) massive, graded to ungraded layers. This division is also valid for evaluation of appositional fabric. Stratified layers show consistent a-axis fabric with upcurrent imbrication. Massive layers, particularly in their middle portions, are characterized by disorganized, bimodal, or variable fabrics with both up- and down-current imbrications. Additional fabric characteristics are summarized below. Interpretation of these characteristics in the next chapter will contribute to an evaluation of depositional mechanics of thick sandstones (6).

Stratified layers

(i) a-axis grain orientation shows little variation through several metres of sediment.

(ii) Except for a minimum in vector magnitude near the base of layers, preferred grain orientation is strong. Vector magnitude may again decrease at the top of layers.

(iii) The fine sub-divisions of stratification bands show stronger a-axis alignment than the coarse sub-divisions.

(iv) Imbrication is consistently upcurrent, with 77% of imbrication angles being greater than 20°. All imbrications are steeper than 10°. Because the maximum error for imbrication determinations is ± 15°, however, several of these small imbrication angles are not statistically significant. The contributing error terms likely confound one another in the majority of cases, however, so that many of these low imbrications may be geologically significant. Imbrication angle shows no obvious correlation with vector magnitude of the a-axis orientation (Figure 4.9), except that the lowest imbrication angles are associated with the poorest preferred orientations. This result is opposite to observations of Walker (1977) on fabric of resedimented conglomerates in Oregon. Walker concluded that (i) steep imbrications allow pebbles to pivot against their neighbours, resulting in greater dispersion of long axes, and (ii) gently dipping pebbles (at the top of layers) have a strong a-axis

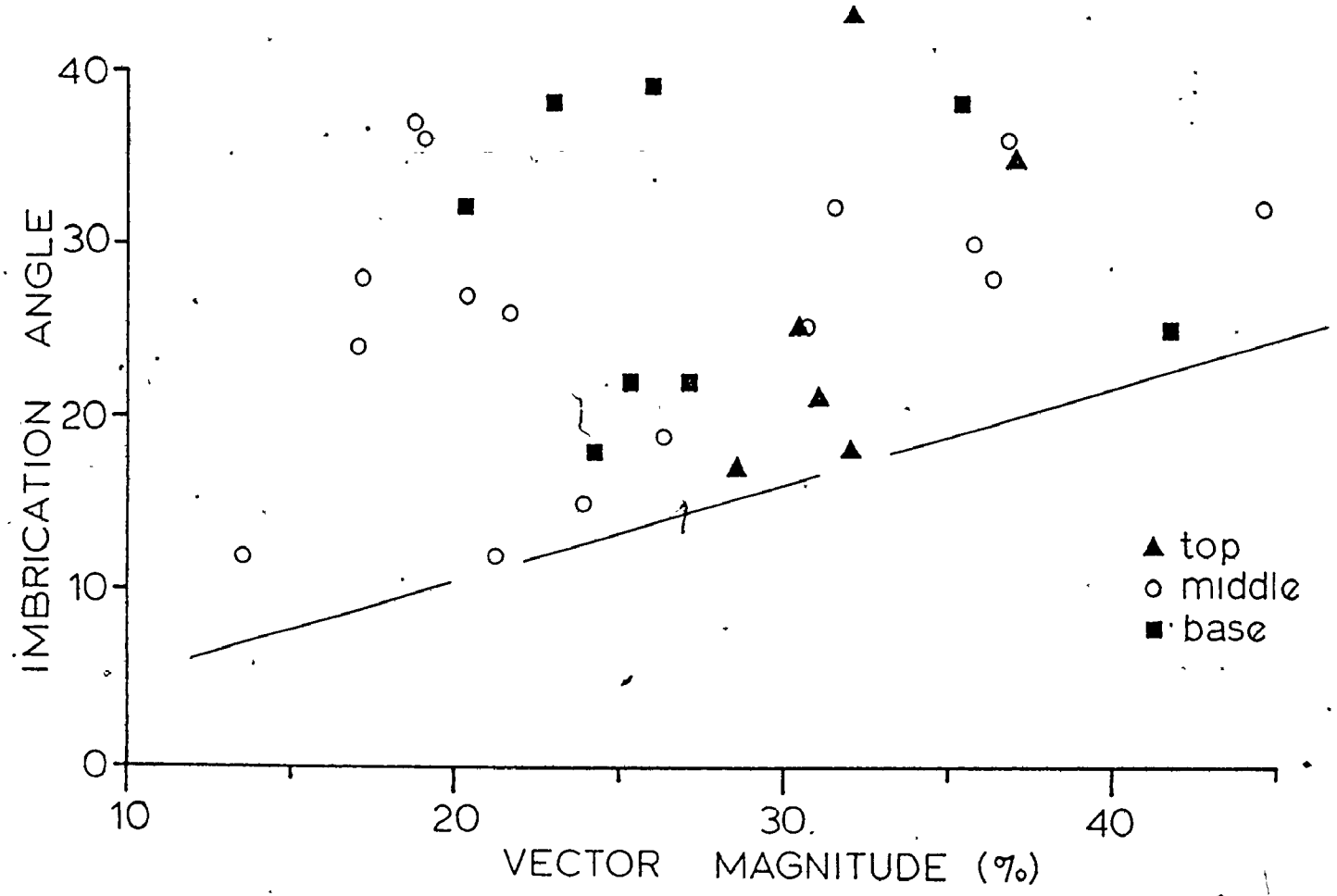

Fig. 4.9. Plot of imbrication angle against vector magnitude of a-axis orientation for stratified layers (stations 1, 2, 10). Because station 1 has 7 sub-stations, data from this locality dominate the plot. Height in the layer is indicated by the use of different symbols.

alignment. Imbrication in stratified thick sandstones (6) also shows no correlation with height in the layer.

(v) Grain orientation is consistent for 140 m along strike at station 1. Lateral parallelism of fabric is best displayed at the top of the layer.

Massive layers

(i) Grain orientation is generally strongest at the base and top of layers. Basal samples may be bimodal. The middle portions of massive layers are characterized by isotropic (random) or bimodal fabrics.

(ii) Bimodal samples generally show little tendency for modes to be grain size dependent. In sample 6a3, however, the non-imbricate mode corresponds to the largest fabric elements, suggesting orientation of the a-axes of coarse grains perpendicular to flow. In most samples, bimodality is interpreted to be the aggregate expression of a mosaic of mutually perpendicular micro-domains.

(iii) Considerable stratigraphic variation of grain orientation, and large deviations from sole markings, are common in the middle of layers.

(iv) For layers in which upcurrent and downcurrent directions could be distinguished, 45% of imbrications are upcurrent and steeper than 20°, 31% are upcurrent and less

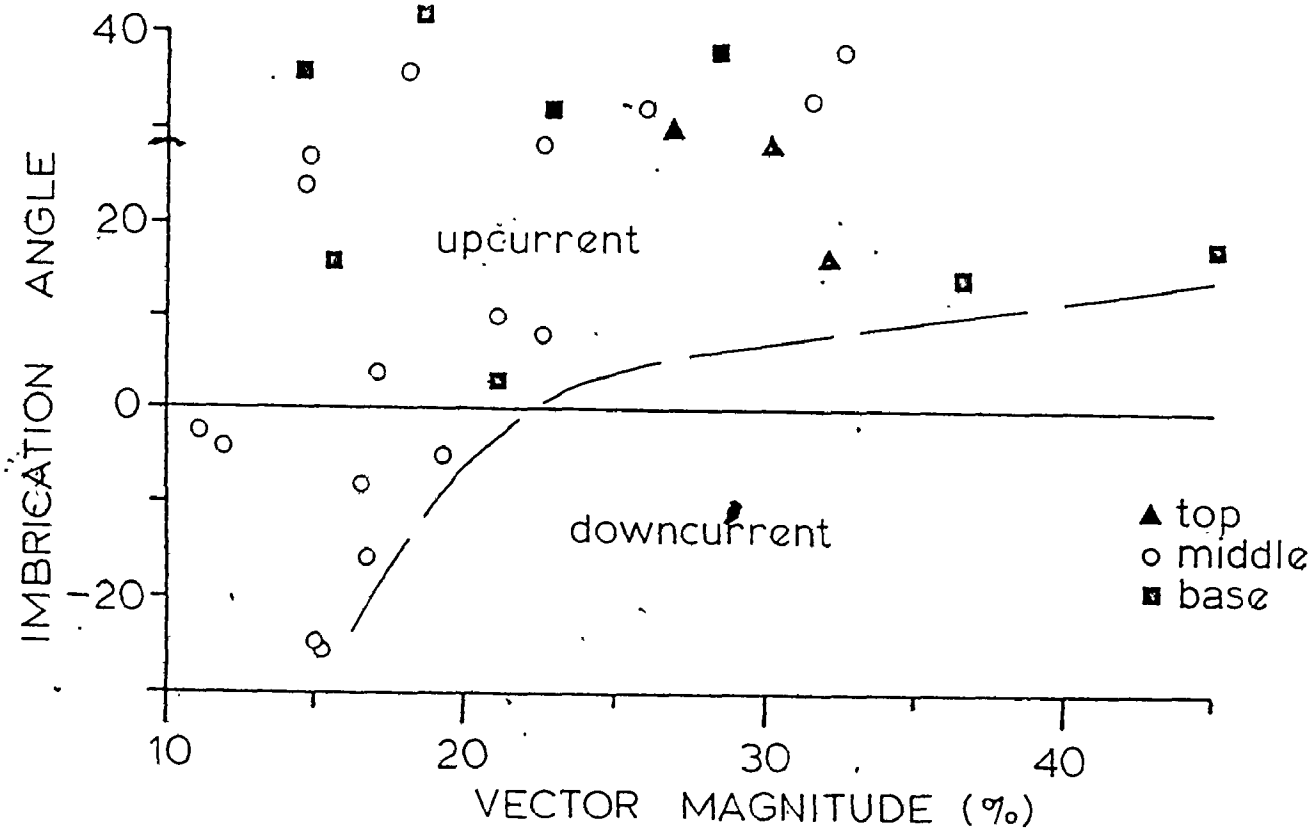

Fig. 4.10. Plot of imbrication angle against vector magnitude of a-axis orientation for massive layers (stations 3, 4, 5, 6, 7, 8, 9). Upcurrent imbrication is positive; downcurrent imbrication is negative. Height in the layer is indicated by the use of different symbols.

steep than 20°, and 24% are downcurrent. All downcurrent imbrications, and 9 of 10 imbrications which are either less than 10° (upcurrent) or downcurrent, come from specimens taken in the middle portions of massive layers (Figure 4.10). For positive (upcurrent) imbrications, there is little correlation between a-axis orientation and imbrication, or between imbrication angle and height in the layer. Negative imbrications are characterized by poor preferred orientations.

(v) Except for basal samples, a-axis fabric at station 7 shows great variability throughout the layer and between sub-stations.

(vi) Station 9 is atypical because a strong, and stratigraphically consistent, a-axis fabric is developed. This fabric is assumed to be parallel to sheet structure. Imbrication is upcurrent.

CHAPTER V

DEPOSITION OF THICK SANDSTONES (6)

"My opinion is, that the various structures which I have described are so intimately connected with the circumstances under which they were formed, that nothing but perseverance is required to enable us to determine the depth and velocity of the current, and the rate of deposition, with more or less accuracy, from the existing peculiarities of ancient stratified rocks. If there be only an apparent probability of doing this, it is surely better to make the attempt and fail than to be content with our present ignorance and to make no effort at all"

- Henry Clifton Sorby (1859)

Transport Mechanisms

Although there is some disagreement on the nomenclature for different submarine, gravity-induced, sedimentation mechanisms (for example, see Sanders, 1965; Carter, 1975), the general nature of these mechanisms is now widely accepted.

This discussion is restricted to those processes which involve grain-by-grain transport of sediment into deep water, and therefore excludes gravity-induced slumps and slides (Dott, 1963).

Sediment gravity flow (Middleton and Hampton, 1976) is applied to sediment transport in which movement parallel to the bed is induced directly by the pull of gravity on the constituent particles in the flow. In fluid gravity flow, it is the fluid which is driven by gravity (for example, in rivers); particles are carried along as passive passengers by the flow. In order for sediment gravity flow to operate, however, particles must be suspended (dispersed) above the bed by one of four mechanisms: (1) turbidity current flow, in which the sediment is supported by the upward component of fluid turbulence, (2) grain flow, in which the sediment is supported by direct grain-to-grain interactions (collisions or close approaches), (3) liquefied flow, in which the sediment is dilated and supported by interstitial pore fluid, and (4) debris flow, in which the larger grains are supported by a "matrix" of interstitial fluid and fine sediment, which has a finite yield strength (modified from Middleton and Hampton, 1976).

Turbidity currents

The mechanics of turbidity current flow and deposition as deduced from flume experiments are treated in detail by Middleton (1966a,b, 1967). These experiments, coupled with field observations from the ancient record, indicate the following characteristics of turbidity current deposits (turbidites).

(i) Size grading is almost universally present, being the result of (a) decay of initial turbulence and therefore decreasing competency and capacity through time, (b) decreasing competency and capacity in the tail of the current, and (c) concentration of coarse grains in the head of the current and longitudinal size grading from head to tail during flow (Middleton and Hampton, 1976). The base of each turbidite is sharp and may be erosive. Deposits of dilute turbidity currents display distribution grading, in which the entire size distribution shifts to finer sizes from the bottom to the top of the layer, whereas deposits of high-concentration flows only show vertical grading of the coarsest percentiles of the size distribution (coarse-tail grading of Middleton, 1967). The tops of layers commonly grade progressively into overlying mud.

(ii) Sole markings on the bases of layers are in many cases the result of fluid scour (flutes), indicating the presence of turbulent eddies at the base of the flow (Allen, 1971).

(iii) Internal sedimentary structures appear in a definite sequence as deposition proceeds (Bouma, 1962). This sequence of sedimentary structures has been interpreted hydrodynamically in terms of deposition from a waning turbulent flow (Walker, 1965; Harms and Fahnestock, 1965) through analogy with bed forms produced in flumes under conditions of controlled flow (Simons and others, 1965). The complete "Bouma sequence" consists of a lower massive or graded division (T_a), a division of upper flow regime plane lamination (T_b), a division of ripples, climbing ripples, or convoluted ripples (T_c), an upper division of muddy lamination (T_d), and an overlying interturbidite mud (division e).

Turbidity current deposits have been described from abyssal plains in ocean basins, for which bottom slopes of 0.001 to 0.0001 are common (Horn and others, 1971).

Grain flow

Grain flow is made possible by "dispersive pressure", which opposes gravity when a cohesionless layer of grains is sheared (Bagnold, 1956). Dispersive pressure is produced by momentum change associated with grain interaction during shearing. Grain flow can operate in two regimes. In the viscous regime, momentum change results from interaction of grains and interstitial fluid as grains come into close

proximity. As elastic grain-to-grain collisions increase in importance, grain flow moves into the inertial regime.

For grain flows in which the interstitial fluid is water, slopes of about 30° are necessary to maintain flow (Lowe, 1976a; Middleton and Southard, 1977, p. 8.14). Slopes of this magnitude are rare on the ocean floor, and are certainly not found on submarine fans. Grain flow is therefore inadequate to explain long-distance transport of marine sands. Dispersive pressure may nevertheless be important in providing additional grain support during flow of high-concentration turbidity currents or viscous debris flows, or during final stages of deposition from sediment gravity flows.

One of the consequences of grain interaction during shearing of a concentrated dispersion is inverse grading. Jostling of grains allows the finest particles to work their way toward the base of the flow ("kinetic sieve" of Middleton, 1970). This mechanism would probably not be as effective in sandy flows containing an interstitial fluid denser than water, due to viscous force on fine grains.

Liquefied flow

Liquefaction (Terzaghi, 1956; Andresen and Bjerrum, 1967) involves the transfer of support from grain contacts to the interstitial fluid following disturbance of an unstable packing structure. Pore-fluid pressure rises sharply. As long as grains are supported by the pore fluid, the sediment has little strength and behaves like a fluid with viscosity on the order of ~~1000~~ times that of water (Middleton and Hampton, 1976).

Andresen and Bjerrum (1967) described flow of liquefied sand on slopes of 2° to 3°, and demonstrated that sand porosities of 46 to 50% were necessary for spontaneous liquefaction. Once liquefaction occurs, however, excess pore pressures begin to dissipate by intergranular flow and settling of grains, or by local fluid expulsion within fluid-escape pillars. Intergranular flow is believed to be responsible for formation of dish structure (Lowe and LoPiccolo, 1974). Unless the liquefied flow accelerates down a slope, becomes turbulent, and passes into the realm of turbidity current flow, dissipation of pore fluid pressure results in freezing of the layer from the base upward (Lowe, 1976b). An entire layer of fine sand 10 m thick will consolidate in a few hours (Van der Knaap and Eijpe, 1969; Middleton, 1969; Lowe, 1976b) although poorly sorted sediment would probably lose pore fluid only at a rate characteristic

of its finest component grains. It is these grains which would determine the permeability of the sediment. Using data tabulated by Lowe (1976b), a 10 m thick layer of poorly sorted coarse sand with a lower grain size limit of 4 ϕ would consolidate in 3.3 hours. Coarse Tourelle sandstones also contain silt-sized quartz grains, so that liquefied flows may have been able to maintain their identity for well over 3 hours. It is more likely, however, that liquefied sands quickly become turbulent and evolve into turbidity currents (Middleton and Hampton, 1973; Lowe, 1976b). Rapid deposition of sediment from the turbidity current at a later time could re-institute high pore-fluid pressures and provide additional grain support similar to that present in liquefied flows.

Final consolidation and expulsion of pore fluid would result in the formation of dish structure and fluid-escape pillars. Grading would be poorly developed.

Debris flow

In debris flow, grains are maintained above the bed by a cohesive matrix of mud and finer particles. The matrix possesses a yield strength which is the sum of cohesion and internal frictional resistance. Johnson (1970) proposed a Coulomb-viscous model for debris flow which states that flow will only occur if the component of weight (per unit area)

parallel with the bed exceeds the yield strength. Even when this requirement is realised, flow will occur only where shear stress exceeds yield strength. For this reason, debris flow is characterized by a "rigid plug", which moves above the shearing flow. In subaqueous debris flow, reverse shearing at the upper interface may cause the plug to move below the surface (Einstein, 1941; Hampton, 1972; Middleton and Hampton, 1976).

Particles in a debris flow are maintained above the bed by three forces: (i) strength of the matrix, (ii) bouyancy in the dense matrix, and (iii) dispersive pressure. Dispersive pressure is the least important force. Hampton (1975) conducted a series of experiments on debris flow which led to the following important conclusions.

(i) Competence (the size of the largest transported grain) is not a function of flow velocity.

(ii) Competence of unsheared debris is higher than competence of sheared debris by approximately 1 mm in coarse sand sizes. Because shearing occurs below the rigid plug at the base of the flow, debris flow deposits may show slight inverse grading.

(iii) The clay content of a deposit from a flow just strong enough to carry coarsest sand (2 mm) would be about 19%. This is certainly an overestimate, however, because these experiments were carried out using a kaolin and water

slurry as matrix. Other clay slurries, particularly those containing montmorillonite, are much stronger than kaolinite slurries. For example, a montmorillonite-seawater slurry with 68% water has the same strength as a kaolinite-seawater slurry with 50% water content.

Rodine and Johnson (1976) analysed debris flow in terms of the concentration of clastic debris which can be carried without causing particle interlocking. They concluded that interlocking in poorly sorted debris flows does not occur until matrix (= clay plus water) falls below 5 to 11 volume percent. This allows debris flows to be almost as dense as their constituent grains and accounts for the ability of these flows to carry enormous solid blocks while flowing on slopes of 1° to 5° (Sharp and Nobles, 1953).

Debris-flow deposits should be characterized by sediment with positive-skewed size distributions (fine tail). Whereas this transport process has no means of sorting different sizes, competence requirements (Hampton, 1975) result in truncation of the size distribution at some maximum size. Sole markings should be restricted to grooves and slide marks. Grading may be inverse at the base of the layer and poor (possible coarse-tail grading) in the middle of the deposit (Middleton and Hampton, 1976). Normal grading might be expected in large flows which become turbulent (Enos, 1977; Middleton and Southard, 1977, p.8.16). Large

blocks (if present) can occur in the middle of the flow or projecting from the top.

Because debris flows possess a yield strength, their boundaries should be steep, somewhat like the meniscus of a water drop on a flat surface (Johnson, 1970). Rodine and Johnson (1976), however, suggest that poorly sorted debris may require only a very low yield strength, so that wedge-shaped boundaries might be more common.

Grading and Grain-Size Distributions

In order to allow comparison between fabric and grain size data, the same samples used for fabric analysis were used in this study (see Chapter IV).

Acetate peels used for grain-orientation determinations were examined on the Shadowmaster microprojector at 25x or 100x, depending on grain size. The ten largest quartz grains visible on the screen were measured and averaged to yield an estimate of maximum size for each sample. Middleton (1962) found that maximum size is a much more sensitive indicator of grading in massive "turbidite" sandstones than mean size. The results of these measurements are plotted in Figure 5.1. Stratified layers (stations 1, 2a and 10a) show consistent and well defined normal grading of coarse sub-divisions, through a maximum of 435 cm of sediment (station 1). Massive

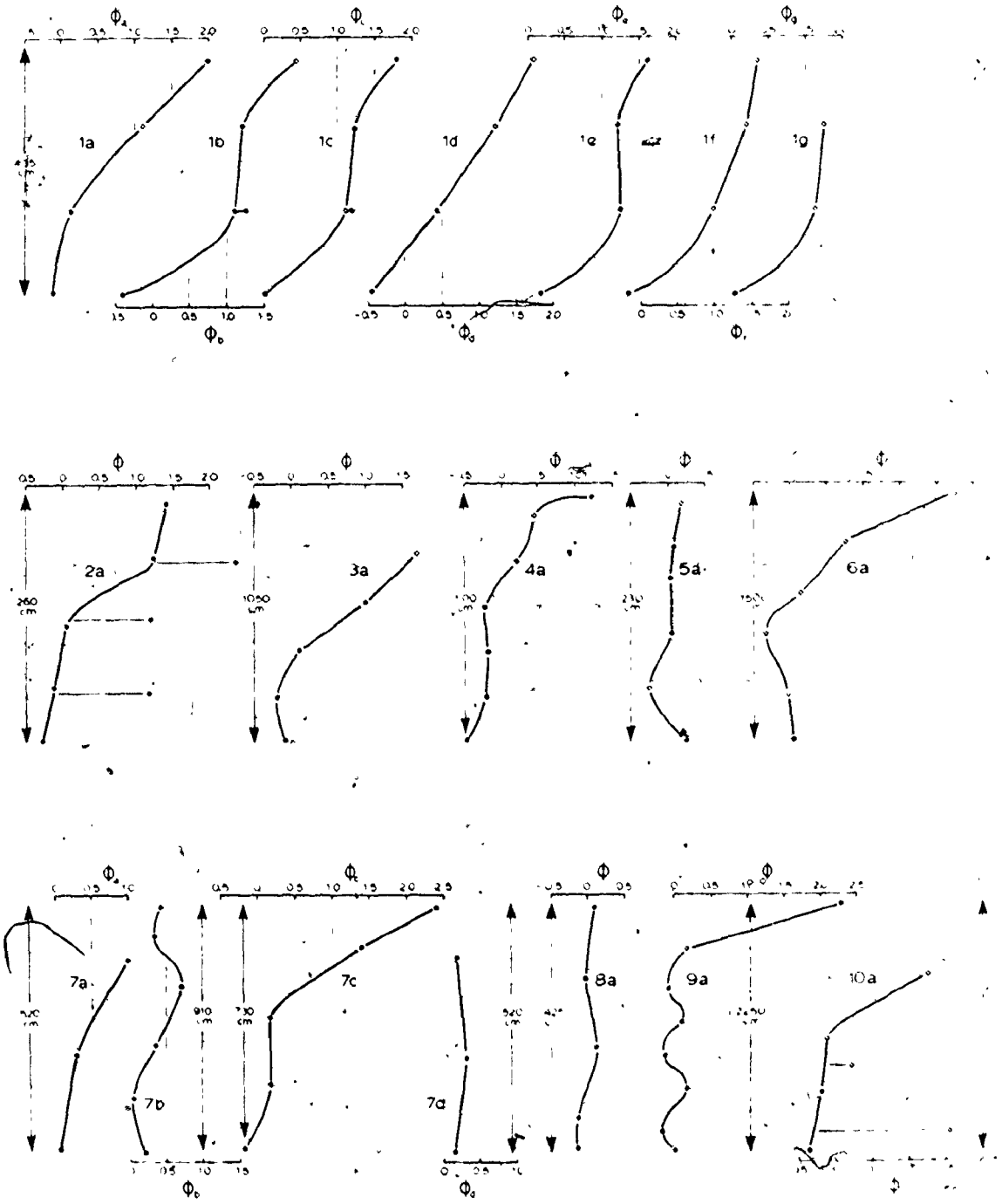

Fig. 5.1. Variation of maximum grain size with height in the layer for all fabric sub-stations. See text for discussion.

layers (sub-stations 3a through 9a) may display normal grading (sub-stations 4a, 7a and 7c), inverse-to-normal grading (sub-stations 3a, 5a, 6a and 7b), irregular grading (sub-station 9a), or may be essentially ungraded (sub-stations 7d and 8a). Inverse grading at the base of layers is often quite subtle, so that only a few examples were recognized in the field on the basis of visual grain-size estimation (see sections in the pocket of the thesis).

In order to further evaluate grading, and to characterize grain-size distributions of thick sandstones (6), all specimens from sub-stations 1d, 6a and 8a were thin-sectioned and point-counted (Glagolev procedure) for grain size. This method yields a volume frequency distribution. 250 points were counted in each sample. If the same grain fell under the cross-hairs twice, it was counted as two measurements. Only quartz and feldspar grains larger than 0.03 mm (5 ϕ) were measured. Middleton (1962) found that truncation of equally coarse sandstones from the Charny Formation at 4 ϕ did not introduce significant error into the estimation of population parameters such as mean and sorting. For this reason, no attempt was made to determine the degree of truncation in this study. Grain-size statistics, including Fisher's k and g statistics (Fisher, 1948, p. 70-76), standard skewness (x_3) and kurtosis (x_4) measures (Blatt and others, 1972), and percent matrix and calcite "cement" are tabulated

in Table 5.1. For large samples, the variances of g_1^2 (skewness measure) and g_2 (kurtosis measure) are known, so that it is possible to determine whether or not observed departures of g_1^2 and g_2 from zero are significant at (say) the 95% probability level (Middleton, 1962).

Examination of these data and cumulative probability curves (Figure 5.2) stimulates the following observations.

(i) The coarse sub-divisions of stratified layers (sub-station 1d) show consistent distribution grading from the base to the top of layers. Size distributions are either normal, or positively skewed (basal samples), as a result of truncation of the coarse tail. Middleton (1962) reported a similar decrease in positive skewness from the base to the top of turbidites. Sorting (m_2) is moderate to poor (verbal classification of Folk, 1968). Although sorting appears to improve consistently from the base of the layer upward, this may simply be the result of truncation of all samples at 5 ϕ. There is no statistical evidence to suggest leptokurtic or platykurtic distributions.

(ii) Samples from sub-station 6a (massive layer) are generally positively skewed (truncation of the coarse tail) and may be leptokurtic (6a1, 6a4) or platykurtic (6a0, 6a2). Both Figures 5.1 and 5.2 show inverse-to-normal grading for this layer. Sorting is poorest in the middle of the layer (6a2, 6a3), and best at the top (moderately sorted, Folk, 1968).

Table 5.1

Grain size statistics for thick sandstone (6) layers (250 points per T.S.)

Substation	sample	mean(ϕ)	m_2	m_3	m_4	k_3	k_4	g_1^2	g_2	x_3	x_4	% matrix (100 pts)	% calcite (100 pts)
1d	0	1.12	1.44	0.98	6.15	0.99	-0.02	0.323*	-0.011	0.282	-0.035	12	10
	1	1.98	1.16	1.03	4.67	1.05	0.69	0.694*	0.511	0.414	0.477	21	12
	2	2.33	0.95	0.25	2.28	0.25	-0.40	0.072	-0.442	0.134	-0.457	9	8
	3	2.92	0.71	0.10	1.42	0.10	-0.09	0.027	-0.170	0.081	-0.190	21	16
6a	0	1.54	1.86	1.33	8.15	1.34	-2.21	0.276*	-0.634*	0.261	-0.645	14	2
	1	0.89	1.09	1.09	4.50	1.10	1.02	0.935*	0.858*	0.481	0.817	3	4
	2	1.27	2.97	1.44	19.43	1.45	-6.99	0.080	-0.787*	0.140	-0.796	7	1
	3	1.65	1.92	0.90	9.01	0.91	-1.97	0.116*	-0.533	0.169	-0.546	16	1
	4	1.87	0.98	0.95	3.58	0.96	0.75	0.968*	0.775*	0.489	0.736	20	6
	5	2.73	0.73	0.36	1.49	0.37	-0.09	0.342*	-0.170	0.291	-0.191	18	11
8a	0	1.66	1.81	-0.07	7.69	-0.07	-2.14	0.001	-0.647*	-0.014	-0.658	14	--
	1	1.92	1.59	0.22	7.47	0.22	-0.09	0.012	-0.034	0.055	-0.057	13	1
	2	2.13	1.50	0.17	5.31	0.17	-1.41	0.009	-0.623*	0.046	-0.634	16	3
	3	2.12	1.59	0.30	6.20	0.31	-1.38	0.023	-0.541	0.075	-0.555	24	3
	4	2.25	1.55	0.15	6.36	0.15	-0.78	0.006	-0.322	0.038	-0.339	24	3

If the population distribution is normal, 95% confidence limits for g_1^2 and g_2 are 0±0.0911 and 0±0.601.

(*) indicates values of g_1^2 and g_2 that fall outside these limits.

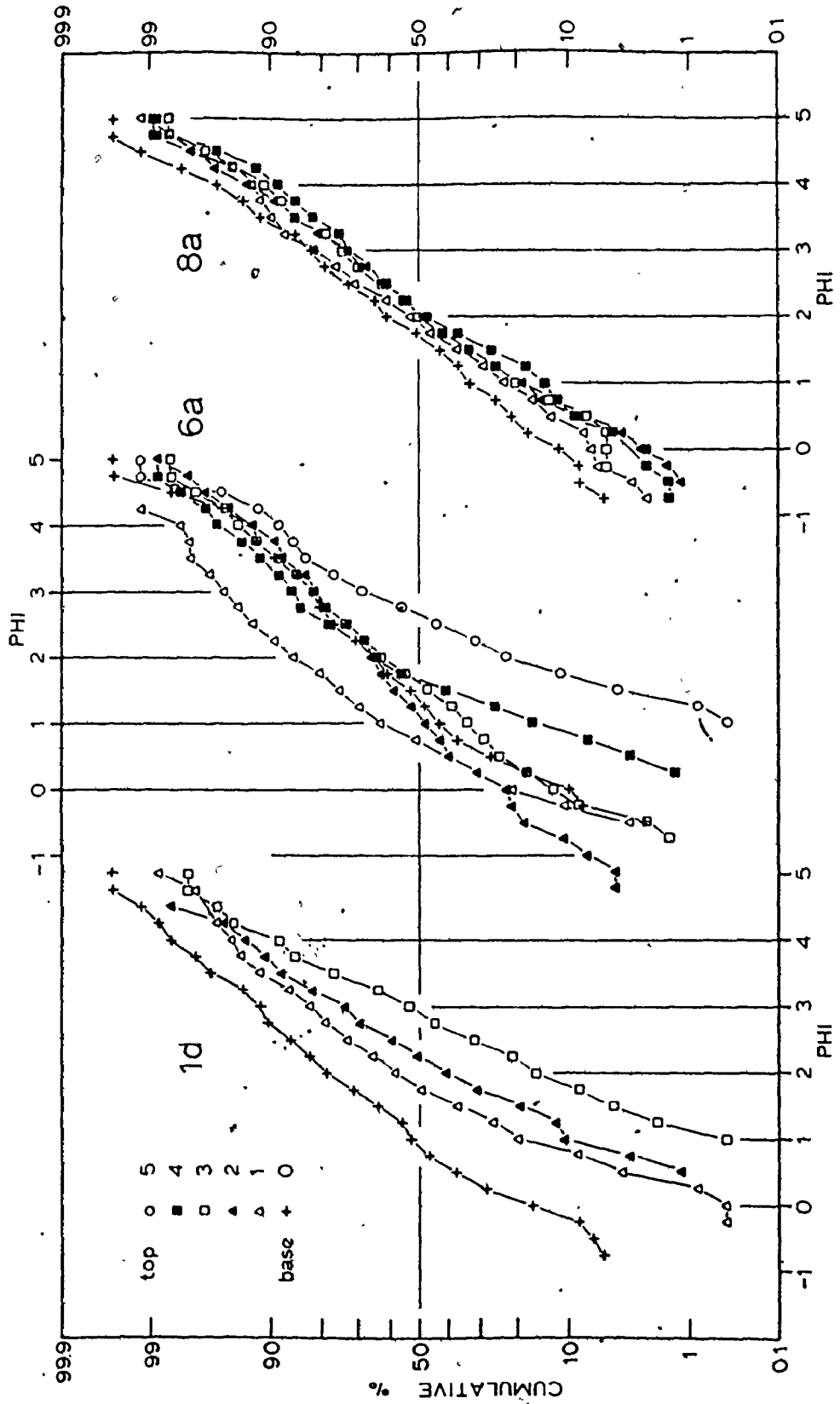

Fig. 5.2. Cumulative grain-size distribution curves for substations 1d (stratified), 6a (massive) and 8a (massive). The relative position in the layer of each sample is indicated. See text for discussion. Statistics for these curves are presented in Table 5.1.

(iii) The layer at sub-station 8a shows total variation from base to top (1425 cm) of only 0.6 ϕ in mean size. Although mean grain size varies so little, there is a consistent decrease from base to top. This suggests that the grading is real and therefore geologically significant. Maximum size also shows this very slight overall grading (Figure 5.1). Not only are all 8a samples similar in mean and maximum size, but grain size distributions are remarkably alike, suggesting that the transporting flow was unable to produce more than the slightest grain-size segregation.

(iv) Chloritic matrix content is quite variable at sub-station 1d, but increases from the base to the top of the layer at sub-stations 6a and 8a. This is particularly true if percent calcite "replacement" is added to percent chloritic matrix to yield an estimate of original detrital matrix (see Chapter VI). All but 5 to 10% of this total is believed to represent primary matrix. Most of this matrix, however, was composed of clay minerals; not quartz and feldspar grains.

Layer Thickness Distribution

Examination of Figure 2.2 (p. 32) shows that facies 4, 5 and 6a layer thickness distributions are truncated at the arbitrary upper thickness limit of 2 m. Similarly,

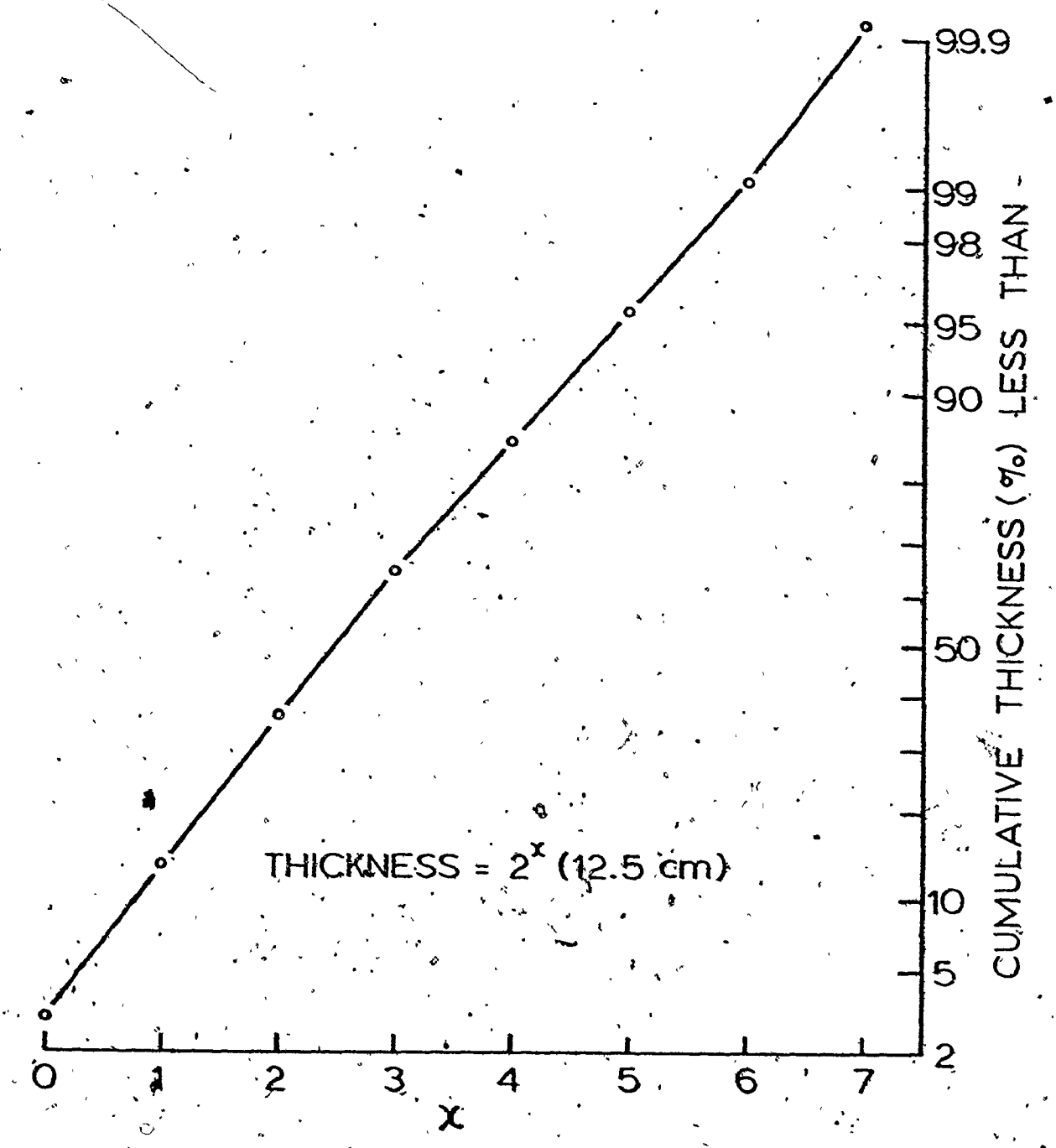

Fig. 5.3. Cumulative thickness distribution of facies 4, 5, and 6 sandstones plotted on log-probability paper. These data define an unskewed normal distribution. Thickness is given as an exponent which must be applied to base 2. The result is multiplied by 12.5 cm to give the thickness.

subfacies 6b appears artificially truncated at its lower limit of 2 m. When thickness data from all sandstone facies (4, 5 and 6) are combined, however, they produce an unskewed, log-normal distribution (Figure 5.3). There is a very slight break in slope at layer thickness equal to 100 cm.

It is not unreasonable to conclude that all sandstone layers in the Tourelle Formation belong to the same layer thickness population. Thin sandstones (4) have been classified using the turbidite model (Bouma, 1962; Blatt and others, 1972), and are best explained as having been deposited from turbulent suspension (see Chapter II). If thick sandstones (6) are characterized by a different depositional mechanism, then there must be a continuum between this mechanism and turbidity-current deposition to account for layers of intermediate thickness. Corbett (1972) and Moore (1973) have used similar reasoning to suggest a common depositional process for both thin and thick deep-water sandstones.

Depositional Structures

Observations of sedimentary structure sequences in classical turbidites have proven to be a powerful tool for the understanding of hydrodynamics of deposition (Walker, 1965; Harms and Fahnestock, 1965). Transitions between depositional structures in subfacies 6b and 6c thick sandstones

were studied using a first order Markov chain model as outlined in Chapter III. The following states were recognized:

scour surface

1 - massive or graded division

2 - internal scour surfaces

3 - upper flow regime plane lamination

4 - ripples or climbing ripples

5 - convolution

7 - medium to large scale cross-stratification

8 - muddy lamination

9 - coarse near-horizontal stratification.

Table 5.2 presents matrices F, P, R and D for this analysis, and the results of a chi-squared test for first order Markov behavior. Figure 5.4 is a transition diagram with arrows weighted according to the significance of transitions between individual states.

Examination of Figure 5.4 and matrix F (transition count matrix) indicates that depositional structures can be divided into two groups.

Traction plus fall-out structures

Except for cross-stratification (7), these depositional structures correspond to turbidite divisions b (3), c (4, 5) and d (8). Convolution, however, almost invariably occurs

Table 5.2

Markov chain analysis: Depositional structures

	Scour	(1)	(2)	(3)	(4)	(5)	(7)	(8)	(9)
Scour surface../.....	0	155	20	2	8	8	0	8	37
Massive or graded(1).....	135	0	10	13	21	10	9	12	23
Internal scour (2).....	6	27	0	0	0	0	0	3	1
Plane lamination(3).....	7	1	0	0	5	1	2	0	0
Ripples(4).	25	0	0	0	0	0	0	3	0
Convolution(5).....	12	0	3	0	0	0	1	0	0
Cross-stratification(7)...	9	0	0	2	1	0	0	0	0
Muddy lamination(8).....	16	0	0	0	0	0	0	0	0
Coarse stratification(9)..	0	50	2	0	1	2	0	1	0

P

0.000	.724	.093	.009	0.000	3.000	0.000	0.000	.173
.579	0.000	.043	.056	.090	.043	.039	.052	.099
.125	.044	0.000	0.000	0.000	0.000	0.000	0.000	.031
.438	.063	0.000	0.000	.313	.063	.125	0.000	0.000
.893	0.000	0.000	0.000	0.000	0.000	0.000	.107	0.000
.923	0.000	0.000	0.000	0.000	0.000	.077	0.000	0.000
.750	0.000	0.000	.167	.083	0.000	0.000	0.000	0.000
1.000	0.000	0.000	0.000	0.000	0.000	0.000	0.000	0.000
.897	.006	.032	0.000	.016	.032	0.000	.016	0.000

R

0.000	.566	.070	.041	.060	.032	.029	.039	.140
.545	0.000	.081	.043	.071	.033	.031	.041	.155
.360	.392	0.000	.029	.047	.022	.020	.027	.103
.351	.383	.053	0.000	.046	.021	.020	.026	.100
.358	.390	.054	.028	0.000	.022	.020	.027	.102
.349	.380	.052	.028	.046	0.000	.020	.026	.100
.349	.379	.052	.029	.046	.021	0.000	.026	.099
.351	.382	.052	.028	.046	.021	.020	0.000	.100
.379	.412	.057	.030	.050	.023	.021	.028	0.000

D

0.000	.159	.016	-.032	-.060	-.032	-.029	-.039	.025
.035	0.000	-.039	.013	.019	.010	.006	.011	-.057
-.235	.451	0.000	-.029	-.047	-.022	-.020	-.027	-.071
.086	-.320	-.053	0.000	.267	.041	.105	-.026	-.100
.535	-.390	-.054	-.028	0.000	-.022	-.020	.080	-.102
.574	-.380	-.052	-.028	-.046	0.000	.057	-.026	-.100
.401	-.379	-.052	.189	.038	-.021	0.000	-.026	-.099
.649	-.382	-.052	-.028	-.046	-.021	-.020	0.000	-.100
-.282	.394	-.074	-.038	-.053	.089	-.021	-.012	0.000

$$\chi^2_{obs,63} = 297.9$$

$$P(\chi^2_{63} > \chi^2_{obs}) = 1.73 \times 10^{-11}$$

Fig. 5.4. Transition diagram for thick sandstone (6) sedimentary structures, with interpretation. All arrows indicate individual transitions which are significant at greater than the 99% level (see Chapter III). There are no transitions which are significant between the 80% and 99% levels. The structures are numbered as outlined on the previous page. Black dots indicate that transitions to the next scour surface are significant at greater than the 95% level. There are no preferred transitions from structures 1, 2, or 9 to tractional structures.

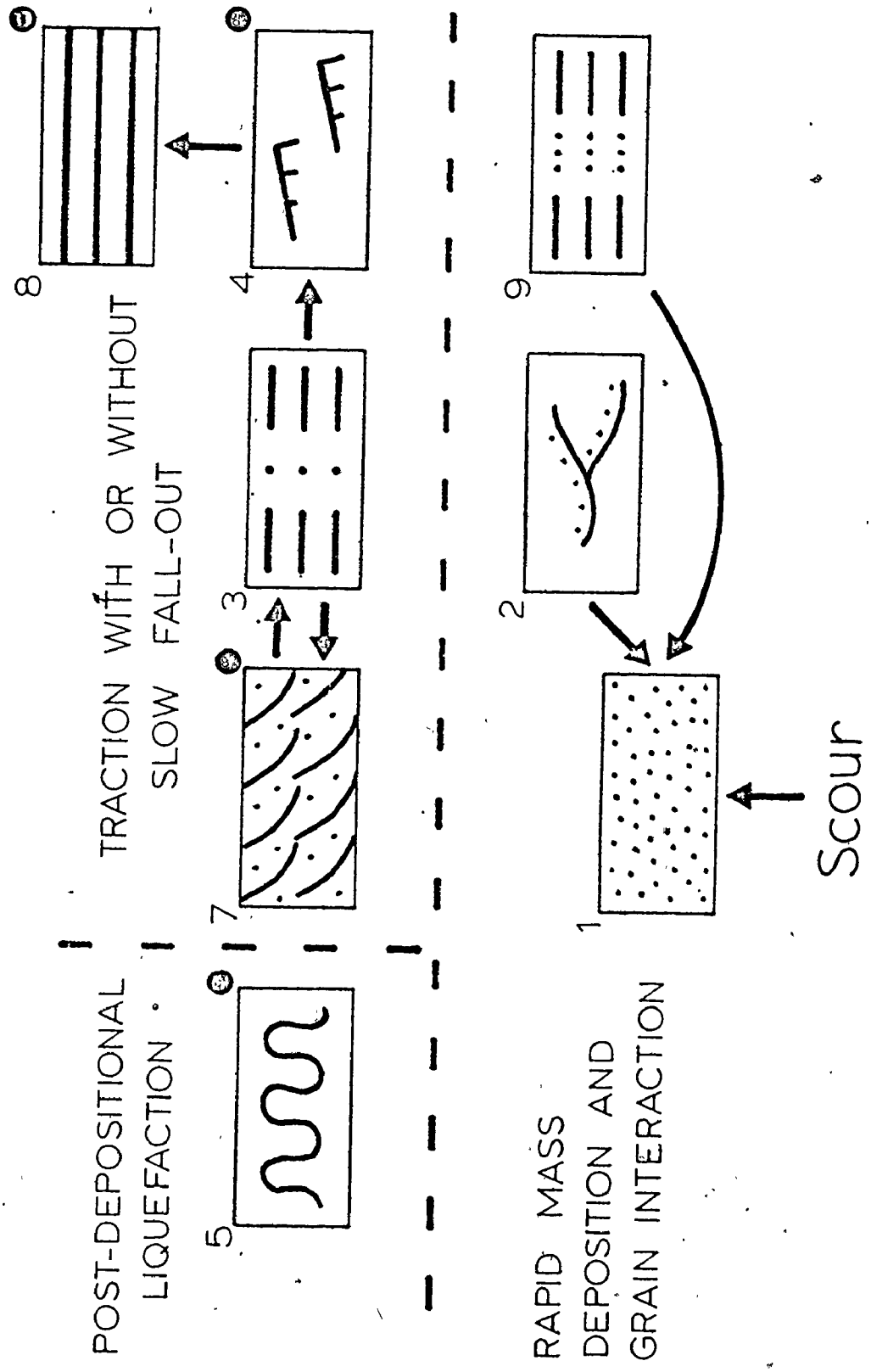
POST-DEPOSITIONAL
LIQUEFACTION
TRACTION WITH OR WITHOUT
SLOW FALL-OUT
RAPID MASS
DEPOSITION AND
GRAIN INTERACTION
Scour
F
F
F
1
2
3
4
5
6
7
8
9

below a scour surface and is not formed by deformation of ripples. It is therefore more reasonable to attribute convolution to post-depositional liquefaction and flowage caused by shearing and loading by a subsequent sediment gravity flow.

Tractional structures 3 and 4 are attributed to slow deposition from turbulent suspension accompanied by continuous bed-load transport. Most cross-stratification, however, occurs at the top of thick sandstones. Several layers containing cross-stratification are generally found in close stratigraphic proximity, suggesting (i) that cross-stratification may be the result of reworking of the tops of massive sandstones by strong currents after deposition, or (ii) that local variation in hydraulic parameters, such as slope, resulted in formation of dunes beneath several successive currents. In two thick sandstone (6) layers, cross-stratification is followed by upper flow regime horizontal stratification (3). In two other layers, this sequence is reversed. Under conditions of decreasing current velocity, we would expect plane bed to occur before dunes or sand waves (cross-stratification), with this sequence being followed by ripples and finally muddy lamination (Simons and others, 1965; Middleton and Southard, 1977). In addition to the occurrences in this study, cross-stratification was observed by Thomson and Thomasson (1969) to precede plane

lamination in deep-water sandstones. This unusual ordering of sedimentary structures will be discussed in a later section.

Depositional structures formed by traction are found at the top of thick sandstones (6). Structures 4, 5, 7 and 8 all have a high probability of being succeeded by shale or a scour surface.

Structures formed during rapid mass deposition

These structures make up the greatest proportion of thick sandstone (6) layers, and are succeeded upward by traction structures. Both massive sand, and massive sand with discontinuous internal scour surfaces, are interpreted to result from rapid deposition, either by fall-out without traction from a dense turbulent suspension, or by freezing of a sediment gravity flow previously supported by matrix strength, grain interaction and possibly turbulence (see interpretation section).

Coarse near-horizontal stratification is characterized by inversely graded stratification bands lying above scour surfaces. The only mechanism known to produce inverse grading during uni-directional flow is grain interaction, unless fine sediment can be deposited from a viscous sublayer at the base of the flow. Grain interaction might be expected near the bed during deposition from a swiftly-flowing, high-

concentration turbidity current. The coarse bands of stratified layers are very well graded from the base to the top of the layer, which suggests deposition from a turbidity current with longitudinal size sorting (Middleton and Hampton, 1976). Two possible mechanisms for the production of coarse stratification (9) will be discussed in a subsequent section.

Fluid-Escape Structures

Approximately 40% of all thick sandstones (6) contain dewatering structures. There is no evidence (such as truncation of pillars by lamination) that these fluid-escape channels formed during deposition. Some fluid-escape pillars extend through more than one layer, requiring post-depositional pore-fluid escape in the lowest layer.

Of what significance are fluid-escape structures? These features are uncommon or absent in classical turbidites and most sands which were emplaced by slow traction in fluvial and shallow-marine environments. (For a summary of some occurrences, see Rautman and Dott, 1977.) Rapid mass deposition of deep-water sands would trap pore fluid and require expulsion by (i) general upward percolation, forming dish structure, or (ii) localized escape through preferred channels, producing pillars and sheet structure. The second mechanism is probably favoured by abundant primary matrix,

which prevents effective general percolation. Pillars and sheet structure were responsible for all fluid-escape in the Tourelle Formation. In Chapter VI, evidence is presented which suggests a primary detrital matrix content of 10 to 15% for coarse Tourelle sandstones.

The hypothesis of rapid deposition suggests a second possible scenario for pore-fluid expulsion, which agrees well with field observations on timing of fluid escape. Grains deposited slowly by fall-out and traction achieve a stable tight-packed structure, whereas rapidly emplaced sediment may have excess pore space as a result of unstable packing (Andresen and Bjerrum, 1967). If this sediment is then disturbed, perhaps as a result of earth tremors or shearing and loading under the weight of later currents, liquefaction may occur. This liquefaction would result in pore-fluid expulsion, compaction, and perhaps some disturbance of depositional structures or fabric. Spectacular loading at the interface between some massive sandstones supports this hypothesis. In the case of localized escape in preferred conduits, fabric disturbance is probably confined solely to the elutriation channels. It is unlikely that spontaneous liquefaction would have occurred after deposition, as 45 to 50% porosity appears to be required for this process (Andresen and Bjerrum, 1967). Evidence presented in a later section and in Chapter VI, however, suggests that Tourelle

massive sandstones had a low initial porosity, because of poor sorting, and because pore spaces were filled with primary detrital matrix.

The presence of fluid-escape structures in thick sandstones (6) is interpreted as an indication of rapid deposition, either from suspension, or by "freezing" of dense flows. Pore fluid was expelled either during the last stages of deposition, or as a result of post-depositional *in situ* liquefaction. It is believed that these structures do not indicate transport by liquefied flow, for the following reasons.

(i) Liquefied flows would quickly become turbulent and change into dense turbidity currents (Middleton and Hampton, 1973; Lowe, 1976b).

(ii) At flow densities characteristic of liquefied flow, 10 to 15% mud matrix (Chapter VI) would make matrix strength and buoyancy much more important grain-support mechanisms than excess pore-fluid pressure.

(iii) Many layers which contain fluid-escape features are well graded and have scour marks on their bases. Both of these features are most easily explained by turbidity current flow, and not by liquefied flow.

(iv) There is no clear evidence, such as truncation of pillars or sheets by lamination, that pore-fluid escape occurred during deposition. For liquefied flows, syn-depositional fluid escape would be expected.

Fabric Review and Analysis

Review

Thick sandstones (6) can generally be classified as (i) stratified and well graded, or (ii) massive and poorly graded, although examination of Figure 2.21 (p. 66) indicates that both massive and stratified divisions may be present in the same layer. Stratified layers have strong and consistent (both vertically and areally) preferred grain fabric with a-axis parallel to flow and upcurrent imbrication commonly in excess of 20°. In some layers, a-axis orientation is also consistently rotated from sole markings. Vector magnitude has a minimum immediately above the base and again decreases at the top of layers. Within individual stratification bands, vector magnitude is strongest in fine subdivisions.

Massive layers have strongest grain orientations at the base and at the top. Basal samples may be bimodal. The middle portions of these layers are characterized by isotropic or bimodal fabrics. Grain orientation in each layer is generally highly variable, both vertically and areally. Imbrication also shows pronounced variability, and may be variously upcurrent or downcurrent, with downcurrent imbrications being associated with low vector magnitudes.

Bimodality and isotropic fabrics in both stratified

and massive layers can be linked to the presence of micro-domains of common a-axis orientation (see Chapter IV). In bimodal samples, micro-domains are present with a-axis fabric both parallel and transverse to flow. Similar clustering of sand grains in flume experiments has been noted by Schwarzacher (1951).

Theory

Parkash and Middleton (1970) reviewed theoretical arguments concerning production of appositional grain fabric. They concluded that strong unimodal orientations with a-axis parallel to flow can be produced by several mechanisms: (i) grain interaction during deposition from grain flow (Rees, 1968) or debris flow, (ii) slow deposition from suspension (Schwarzacher, 1951), and (iii) deposition from traction in the upper flow regime (Allen, 1964). Flow-parallel, flow-normal, and isotropic fabrics can be expected (i) in debris flow deposits, particularly within the rigid plug, and (ii) in sands deposited rapidly from suspension and quickly buried (Schwarzacher, 1951; Rukavina, 1965).

Imbrication angle for upper flow regime plane bed is generally less than 15° (Allen, 1964; Martini, 1965; Taira, 1976a). Steeper imbrications are associated with rapid deposition from suspension (Schwarzacher, 1951) and high flow

velocities (Johansson, 1976), and are common in massive deep-water sandstones (Parkash, 1969; Taira, 1976b).

Taira (1976a) determined fabric of sand deposited by a variety of mechanisms, using anisotropy of magnetic susceptibility (Rees, 1965; von Rad, 1970). He found that depositional mechanisms could be separated in terms of fabric by plotting imbrication angle (abscissa) against q (ordinate), where q is the intensity of magnetic lineation in the magnetic foliation plane, divided by the intensity of the foliation (originally defined by Rees, 1966). Figure 5.5 shows Taira's data and compilations. Notice that grain flow deposits have high imbrication angles (20° to 35°) and q-values higher than upper flow regime plane bed deposits.

In order to present a similar plot for visual fabric studies, a new parameter, Q (analogous to q), has been defined. Q equals the vector magnitude of the a-axis fabric divided by the vector magnitude of the imbrication.

Analysis

Figure 5.6 plots Q against upcurrent imbrication angle for Tourelle thick sandstones (6). Data points are superimposed on fields for upper flow regime plane bed and classical turbidites (massive division). These fields are derived from other studies which employed visual methods of fabric determination.

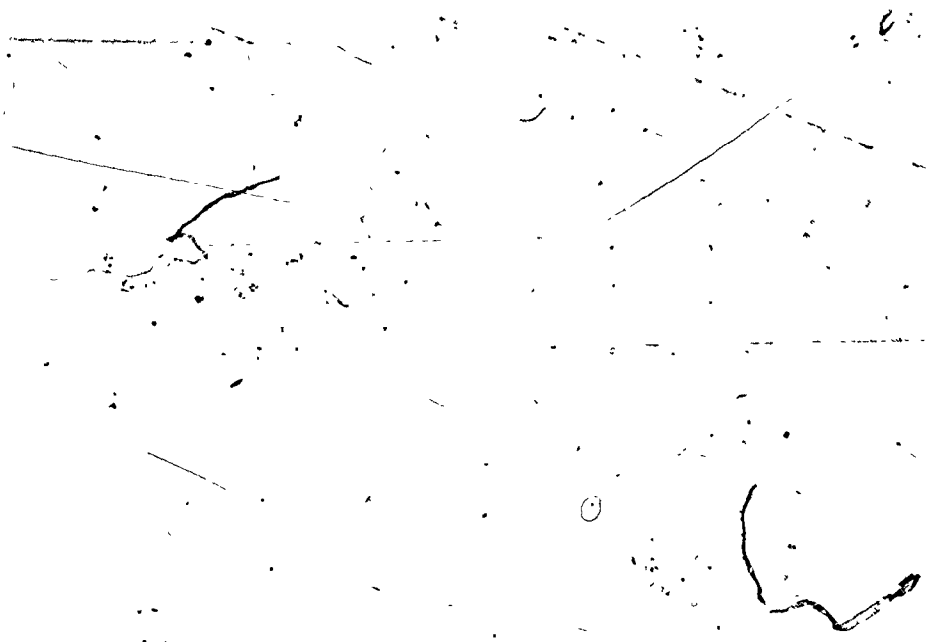

Fig. 5.5. Plot of q against imbrication angle for experimental grain flow deposits, and plane bed from flume experiments (stippled) and from rivers. Modified from Taira (1976a).

Fig. 5.6. Plot of Q against upcurrent imbrication angle for Tourelle thick sandstones (6). (▲- stratified layers, o - massive layers). The plot is superimposed on fields for (I) upper flow regime plane bed (Allen, 1964; Martini, 1965) and (II) massive division of classical turbidites (Parkash, 1969; de Grijs, 1971).

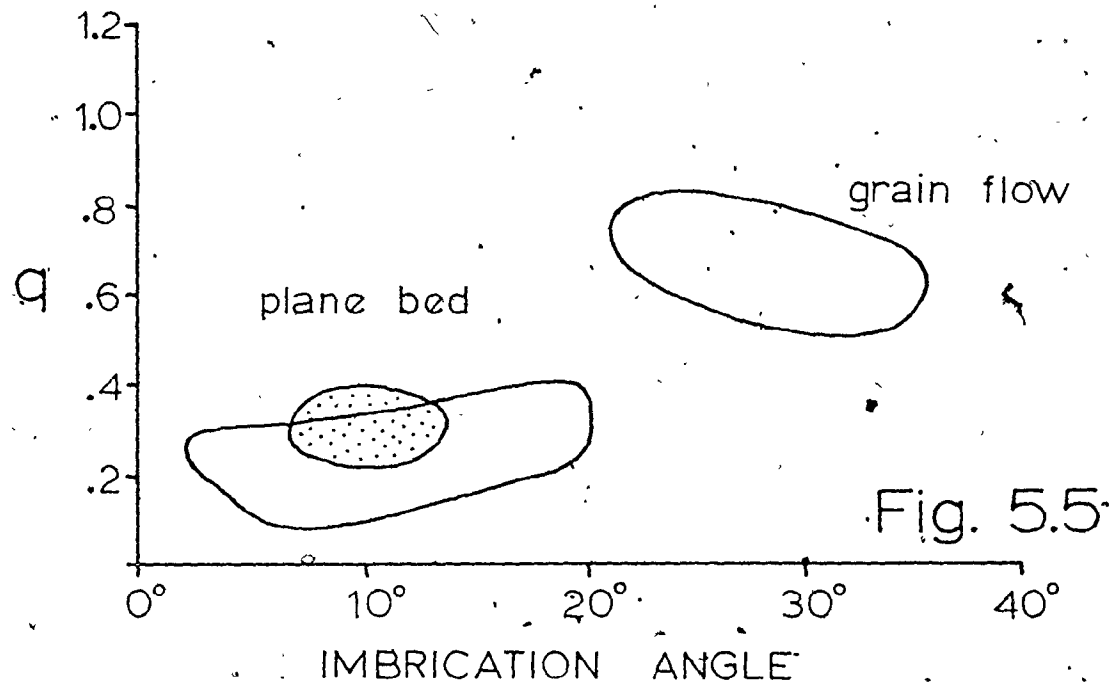
1.2
1.0
.8
.6
.4
.2
q
grain flow
plane bed
0°
10°
20°
30°
40°
IMBRICATION ANGLE

Fig. 5.5

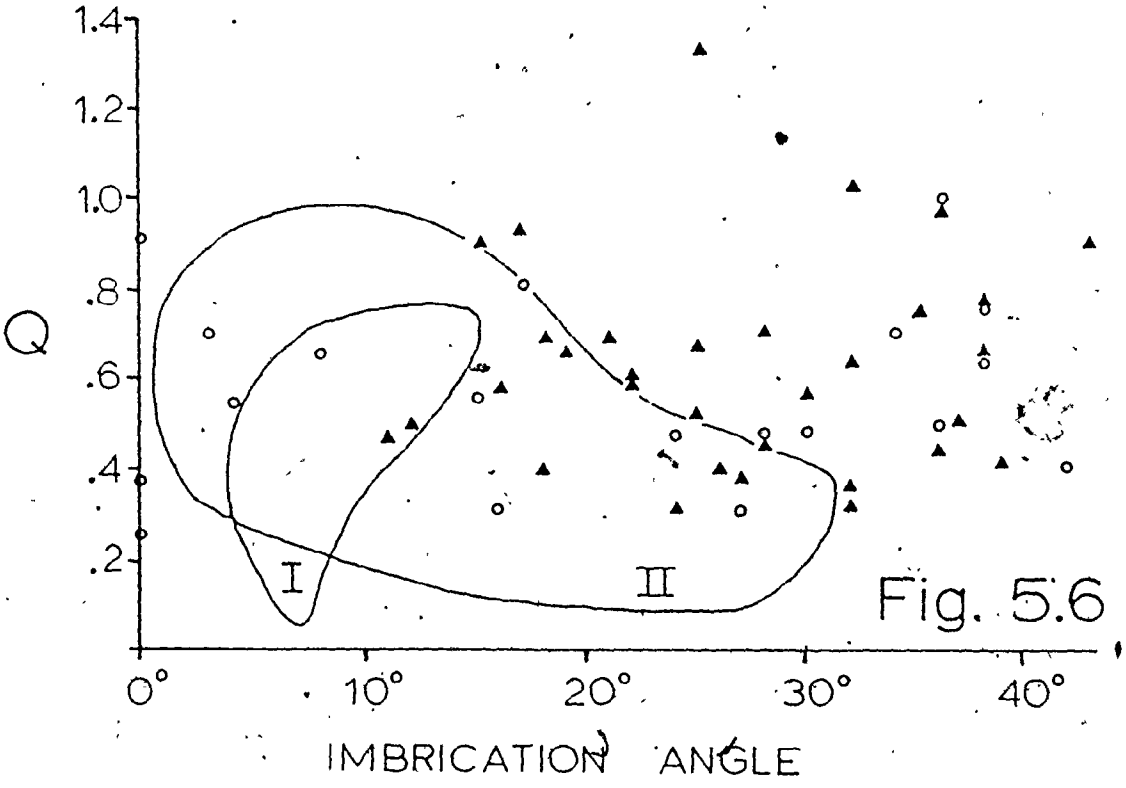
1.4
1.2
1.0
.8
.6
.4
.2
Q
I
II
0°
10°
20°
30°
40°
IMBRICATION ANGLE

Fig. 5.6

A few Tourelle data points with Q in excess of 1.6 and imbrication in excess of 45° have not been included.

Massive thick sandstones (6) have extremely variable upcurrent imbrication angles from 0° to 42°. Massive layers with high imbrication angles overlap the field for stratified, well-graded layers. These stratified layers are characterized by steep upcurrent imbrication (11° to greater than 45°) and moderate Q values. Analogy with Figure 5.5 strongly suggests that grain interaction is responsible for the depositional fabric of stratified layers (or divisions) and has contributed to the development of fabric in some samples from massive layers. Inverse grading in stratification bands and at the base of some massive layers also suggests grain interaction (dispersive pressure).

Bimodal and isotropic fabrics with variable imbrications in the middle of massive layers can be explained by rapid deposition from suspension, or deposition from a viscous (debris) flow. A choice between these two mechanisms can only be attempted after considering evidence presented in subsequent sections. Pore-fluid escape is always confined to pillars or sheets in massive sandstones, so that fabric disruption probably did not occur elsewhere.

It has been tacitly assumed in all discussions that the vector mean of a-axis fabric can be identified with local current direction, and in fact detailed studies by Parkash

and Middleton (1970) show this to be the case for classical turbidites. Figure 4.7 (p. 197) was used to display the consistency of a-axis orientation in stratified thick sandstones (6). With only one exception, however, vector means are rotated anticlockwise from flutes on the sole of the layer, with the greatest deviations being associated with basal samples. This is opposite to observations made by Parkash and Middleton (1970). Because a-axis means at the top of this layer are in good agreement with sole markings, there is no reason to assume that flutes were cut by a different current than that which deposited the sand. It is apparent, nevertheless, that flows which deposited stratified layers were most variable in the earliest stages of deposition, suggesting, perhaps, that deposition began below or just behind the head of the current where flow is divergent (Allen, 1971).

Micro-domains

As reported in Chapter IV, grains tend to cluster into micro-domains of parallel a-axis orientation. This clustering is the result of forces applied to the individual grains immediately prior to cessation of movement. Evidence presented above and in subsequent sections suggests that deposition occurred either from dense dispersions above a sediment bed,

or by "freezing" of part or all of a sediment gravity flow. For this reason, micro-domains cannot be attributed to spot disturbances on a sediment bed as a result of eddies penetrating the viscous sub-layer of a turbulent flow. It is most likely that these grain clusters are the result of jostling of several elongate grains into parallelism within a dense dispersion under shear. The a-axis orientations within micro-domains might be dispersed about the sample mean to produce an overall unimodal fabric. Both flow-parallel and flow-normal micro-domains would contribute to overall bimodality. The presence of flow-normal clusters would depend on the abundance of grains with transverse orientations within the depositing flow. Transverse orientation is possible in viscous flows (Jeffreys, 1922; Taylor, 1923), and, arguing on the basis of symmetry, should be second in importance to flow-parallel orientation in all flows.

Flow-normal orientation in gravels is attributed to rolling of clasts on the bed. In bimodal fabric sample 6a3, the non-imbricate mode (transverse?) is also the coarsest mode. This is insufficient evidence, however, to suggest rolling of these grains in a transverse position, particularly because sand-sized particles in all but the weakest fluid flows pivot into a flow-parallel orientation when brought to rest on the bed (Johansson, 1976).

Hydraulic and Dynamic Considerations

In this section, several problems will be considered which bear on the transportation mechanisms of thick sandstones (6). Symbols used in this section are defined in Appendix VI.

Turbulent suspension of coarsest size fraction

This analysis will assume that sediment grains were suspended only by the vertical component of fluid turbulence. In general this is not true for dense dispersions in which dispersive pressure (Bagnold, 1956), cohesive strength, and enhanced density and viscosity of the matrix may all contribute to suspension.

In general, the coarsest grains present in Tourelle sandstones are 3 mm diameter quartz or angular chert grains. This excludes large chert and shale blocks which may have had a low initial density. Settling velocity for single 3 mm quartz grains in a still fluid (w_o) is 37 cm s^{-1} (Blatt and others, 1972). If we assume reasonable values for current density, von Kármán "constant", and flow depth for the body of the turbidity current (see Middleton, 1966b), we can calculate an approximate mean current velocity required to suspend 3 mm diameter quartz grains (density 2.7 g cm^{-3}).

A useful criterion for turbulent suspension is given by

$u_* = w$ (Middleton and Southard, 1977). In a concentrated dispersion, however, hindered settling occurs. At high Reynolds number, true settling velocity is related to the settling velocity of a single grain and to the concentration, C, by the following expression (Richardson and Zaki, 1954).

$$w/w_o = (1-C)^{2.4} \quad \ldots\ldots 1$$

High grain concentration and presence of an interstitial fluid denser than water will increase effective viscosity and decrease the von Kármán constant, κ, below the value of 0.4 characteristic of clear flows. Let us assume (i) a von Kármán constant of 0.25, and (ii) rough turbulent flow with sand grains being the largest roughness elements. According to Roscoe (1953), effective viscosity increases with concentration:

$$\nu_e = \frac{(\nu\rho)_{water}}{\rho} (1 - 1.35\ C)^{-2.5} \quad \ldots\ldots 2$$

where $\nu_{water} = 0.015$ poise at 5°C.

Mean velocity, $\bar{u}$, is related to shear velocity by the following expression, for $\kappa = 0.25$ (Yalin, 1977).

$$\frac{\bar{u}}{u_*} = 5.76 \log \left[3.08 \frac{d}{k_s} \right] \quad \ldots\ldots 3$$

Flow depth, d, must be specified in order to use equation (3). Because of friction between the turbidity current and the overlying ambient fluid, the point of maximum velocity must be situated within the upper part of the flow. It is only below this point that the velocity distribution is logarithmic (Middleton and Southard, 1977). Total bank-full flow depth can be estimated on the basis of the thickness of thinning-upward sequences, which are interpreted to represent the depths of fan channels (see Chapter III). Reasonable estimates of depth below the point of maximum velocity in the body of bank-full flows range from 10 to 20 m.

Equation (1) can be combined with the suspension criterion, for different flow densities, to calculate values of u_* necessary to support 3 mm grains. These values can then be substituted into equation (3), for various flow depths, to allow estimates of mean velocity to be made. Table 5.3 shows the results of these calculations, which are also presented graphically in Figure 5.7.

Clearly $\bar{u}$ necessary to suspend the coarsest fraction is not a strong function of effective flow depth, but does depend strongly on flow density. Mean velocity estimates range from 2 to 8 m s^{-1}, which are of the same order of magnitude as velocities of approximately 10 m s^{-1} calculated by Heezen and Ewing (1952) for the Grand Banks turbidity current.

Table 5.3

Conditions for suspension of 3 mm quartz grains

ρ (g cm^{-3})	C	u_* (cm s^{-1})	d (cm)	$\bar{u}$ (cm s^{-1})	$\frac{u_* k_s}{\nu_e}$
1.1	0.059	32.0[a]	1000	739[b]	582
			1500	772	
			2000	795	
1.3	0.176	23.3	1000	538	311
			1500	562	
			2000	579	
1.5	0.294	16.0	1000	370	133
			1500	386	
			2000	397	
1.7	0.412	10.3	1000	238	46
			1500	248	
			2000	256	

(a) $u_* = 37.0\ (1-C)^{2.4}$

(b) $\bar{u} = u_* \left[5.76 \log \left(3.08 \frac{d}{k_s}\right)\right]$

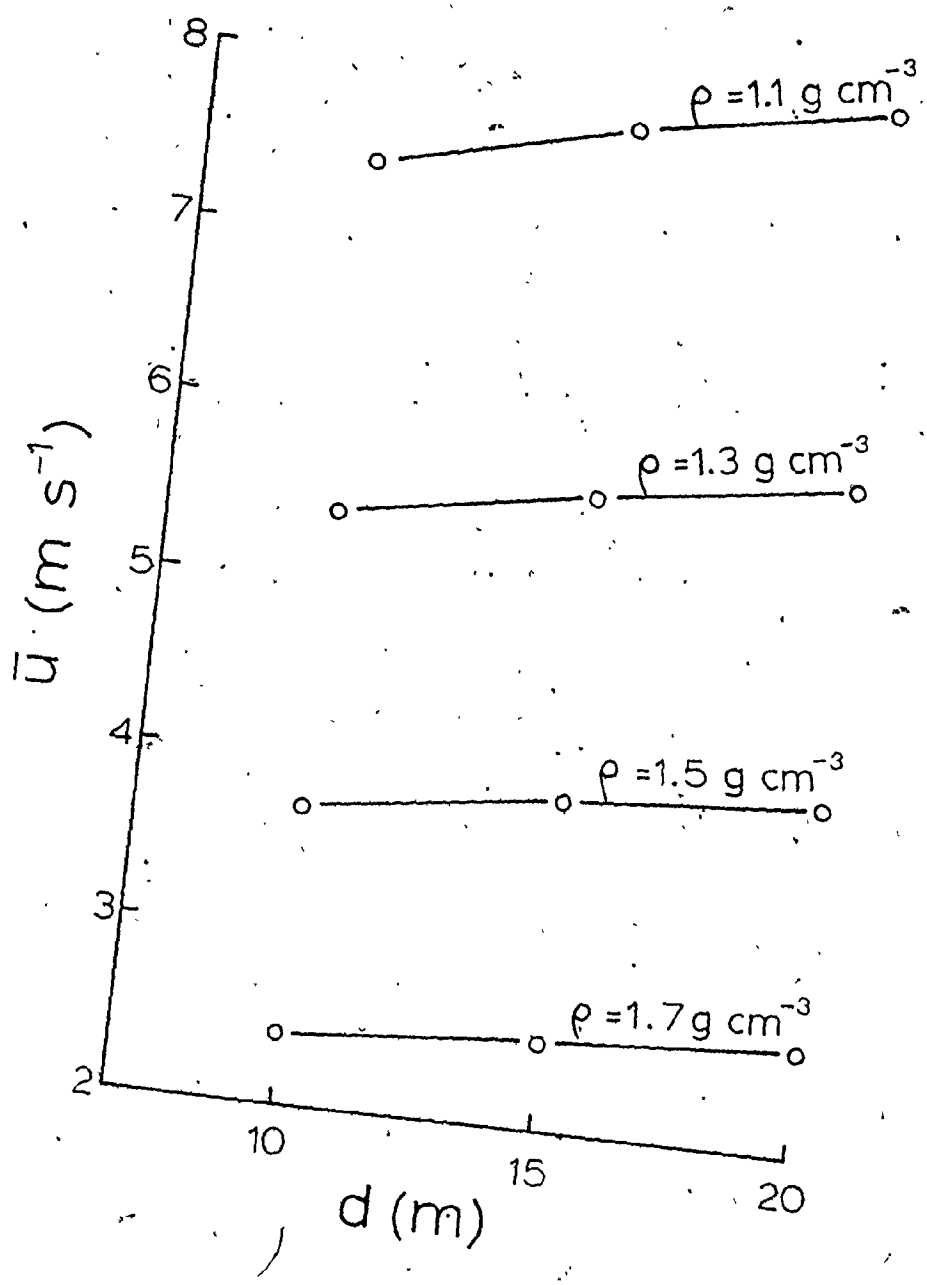

Fig. 5.7. Plot of mean velocity, $\bar{u}$, against flow depth, d, for turbulent flows of various densities which would be competent to carry 3 mm quartz grains in turbulent suspension. See text for details.

Equation (3) applies only for rough turbulent flow. According to Yalin (1977), flow is smooth if $(u_* k_s)/\nu_e$ is approximately less than 5, and rough if the grain boundary Reynolds number is greater than 70: $(u_* k_s)/\nu_e$ is tabulated in Table 5.3 for k_s = 0.3 cm. Because the dimensionless product is greater than 70 for $\rho < 1.5$ g cm^{-3}, the assumption of rough turbulent flow is not unreasonable.

Results summarized in Figure 5.7 are only approximate. Some reasons for this lack of rigour are presented below.

(i) For dense dispersions with primary matrix (see Chapter VI), dispersive pressure (Bagnold, 1956), matrix strength, and enhanced fluid density (causing buoyancy) and viscosity would help suspend grains.

(ii) Suspended sediment is known to dampen the amplitude of turbulent fluctuations (Yalin, 1977, p. 186), so that higher shear velocity would be required to produce the same turbulent fluctuations necessary to suspend the coarsest fraction.

(iii) The value of the von Kármán "constant", κ, may have been quite different from 0.25.

(iv) Current velocity may have been much higher than that required to suspend the coarsest grains present, if (a) coarser material was absent in the source area, and (b) deposition from suspension was a result of a decrease in current capacity rather than competence. The concentration

of suspended load at various levels in a flow can be calculated using the theory developed by Rouse (1937). Figure 5.8 is a graph of Rouse's theoretical relationship for $\kappa = 0.25$. C_o is the concentration of a particular grain size at an arbitrary level, a, above the bed, where $a = 0.05\ d$. If C_o remains approximately constant, it is clear that the total concentration of a certain size fraction in the flow must decrease when w/u_* increases (i.e. when u_* decreases), even if w/u_* for the particular grain size is much less than one, which is the criterion used for general suspension. Stated another way, grains of a particular size will be deposited as u_* decreases, due to decreased current capacity, even if the flow is competent to carry the grains according to the suspension criterion. According to this model, turbidity current deposits are poorly sorted because all grain sizes are affected by a decrease in capacity.

If capacity considerations outweigh competence considerations, then the velocity estimates in Table 5.3 must be viewed as minima. Let us assume for the moment, however, that the velocity estimates are reasonable approximations. What other hydraulic parameters can be estimated?

(a) Densiometric Froude number, Fr, is given by

$$Fr = \frac{\bar{u}}{\sqrt{\frac{\Delta\rho}{\rho} g\ d}} \qquad \ldots\ 4$$

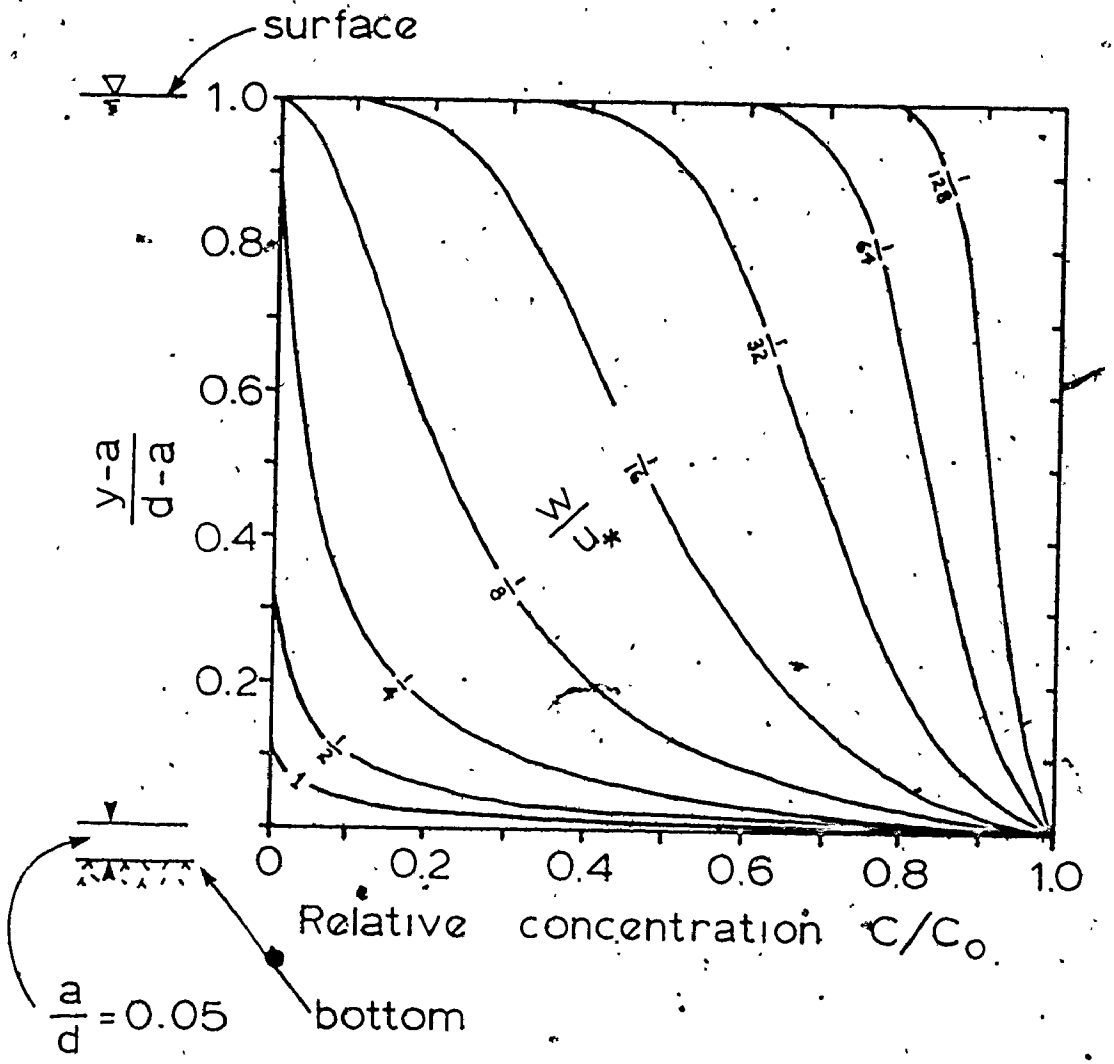

Fig. 5.8. Distribution of relative concentration of suspended sediment with relative depth above the datum y = 0.05 d (modified from American Society of Civil Engineers, 1963). Each curve is constructed for a different value of w/u_*, under the assumption that $\kappa = 0.25$. See text for discussion.

Table 5.4 presents values of Fr calculated for various combinations of $\bar{u}$, d, and ρ. If we assume the overlying fluid to be stagnant, flow is defined as subcritical if Fr is less than one, and supercritical if greater than one. Kennedy (1963) found that antidunes, or in-phase sediment waves, formed if Fr exceeded 0.84. There is evidence that antidunes begin to form at smaller Froude numbers in larger-scale flows (Nordin and Culbertson, 1963, their Fig. 6). If turbulent suspension was indeed the major grain-support mechanism for currents which deposited Tourelle thick sandstones (6), then it is reasonable to suggest that antidunes were the stable bed phase during deposition, particularly at the top of channel fills, where bank-full flow depth would have been shallowest. According to Hand (1974), antidunes under density currents must have wavelengths approximately 13 times the effective flow depth. Antidune stratification would therefore appear horizontal, even on large outcrops, for effective depths exceeding several metres.

(b) for the body of turbidity currents,

$$\bar{u}^2 = \frac{8 \cdot g}{f} \frac{\Delta\rho}{\rho} R S \quad \ldots 5$$

where R can be replaced by d for wide flows. Also,

$$\bar{u} = u_* \sqrt{8/f} \quad \ldots 6$$

Table 5.4

Froude number and slope estimates

ρ ($g\ cm^{-3}$)	d (cm)	$\bar{u}$ ($cm\ s^{-1}$)	Fr	S
1.1	1000	739	2.48	0.0115
	2000	795	1.88	0.0057*
1.3	1000	538	1.13	0.0024*
	2000	579	0.86	0.0012
1.5	1000	370	0.65	0.0008
	2000	397	0.49	0.0004

*see text for discussion

Combining (4) and (5) gives the following equation for slope.

$$S = \frac{u_*^2}{g\ d} \quad \frac{\rho}{\Delta\rho} \qquad \ldots . 7$$

Estimates of slope derived from this equation also appear in Table 5.4 and range from about 0.004 to 0.01. Nelson and others (1970) give average fan gradients on the Astoria Fan of 0.008 (inner fan valley), 0.003 (mid-fan), and 0.002

(outer fan). It was concluded in Chapter III that the Tourelle Formation was probably deposited in a mid-fan setting. If each fan was of similar size to the Astoria Fan, then only those slopes marked with an asterix in Table 5.4 are consistent with predicted gradients. Slopes may in fact have been steeper if Tourelle fans were smaller than the Astoria Fan (see Chapter VIII). Both steeper slopes and higher flow velocities would be allowed if deposition from suspension occurred as a result of decrease in capacity rather than decrease in competence.

Even though the mean velocity estimates may be minima, densiometric Froude number exceeds one for all slopes in excess of 0.002. For these Froude numbers, the velocity of the turbidity current head would have been less than that of the body (Middleton, 1966a), and longitudinal size sorting in the flow would have occurred. As Froude numbers exceed one, interfacial friction at the boundary between the flow and the ambient fluid quickly increases (Middleton, 1966b). This additional friction would inhibit further increases in mean velocity (equation 5), even on fairly steep slopes.

Concretion conglomerate

At areas E and G, compact bands or broad lenses of imbricate arenaceous clasts occur at the base of coarse to granular sandstone layers. These clasts have nominal diameters approaching 10 cm. Interstitial material is also coarse sand identical to that found in the bulk of the layer above. The bimodality of clast size in these layers and imbrication of the arenaceous pebbles and cobbles suggests that prior to deposition, the exhumed concretions were moving as bed-load at the base of the current. Davies and Walker (1974) came to a similar conclusion about quartz granule stratification in sandstones of the Cap Enragé Formation.

For fully turbulent flow, Shield's beta for initiation of movement (see Blatt and others, 1972) is 0.06, and

$$\tau_c = 0.06\ (\rho_s - \rho)\ g\ D \qquad \ldots\ 8$$

Table 5.5 presents a summary of various hydraulic conditions which would initiate rolling of 10 cm diameter sand spheres of density 2.7 g cm^{-3}. $\bar{u}$ is calculated using equation (3), under the assumption that $\kappa = 0.25$ and that concretion bands or lenses only occupied small areas of the bed, allowing $\bar{u}$ to be governed by sand roughness. The dense concentration of sand at the base of the current would also have diminished the effect of larger clasts protruding into

Table 5.5

Conditions to initiate rolling of 10 cm concretions

ρ (g cm^{-3})	τ_c (g cm^{-1} s^{-1})	u_* (cm s^{-1})	d (cm)	$\bar{u}$ (cm s^{-1})
1.1	941	29.2	1000	675[a]
			2000	725
1.3	823	25.2	1000	582
			2000	626
1.5	706	21.7	1000	501
			2000	539

(a) $\bar{u} = u_* \left[5.76 \log \left(3.08 \frac{d}{0.3 \text{ cm}}\right)\right]$

the flow.

Comparison with Table 5.3 indicates excellent agreement between u_* necessary to suspend 3 mm sand and u_* required to roll 10 cm concretion clasts. Only for the higher density flows is u_* for suspension insufficient to transport the larger cobbles as bed-load.

Cross-stratification

Cross-stratification is most commonly found at the top of thick sandstones (6), either as the fill of deep scours, or as the deposit of migrating bed forms. These bed forms may show construction analogous to climbing-ripple lamination (Figure 2.12), suggesting rapid sediment supply. Figure 5.9 is a sketch of a form set of cross-stratification preserved at area C. This particular set is not characterized by deep scour pits, and in this regard resembles bars or sand waves described by Costello (1974). It is believed, however, that cross-stratification in thick sandstones (6) is the result of migration of dunes and not sand waves, for the following reasons.

(i) Most cross-stratification is of the trough variety characteristic of dunes.

(ii) Lack of deep scour pits in the troughs of some bed forms may be the result of abundant sediment in suspension dampening turbulence, and rapid deposition.

(iii) All cross-stratification has asymptotic contacts with the underlying bed. This is a feature characteristic of dunes with abundant suspended load (Jopling, 1965).

(iv) In large natural flows, sand waves are usually much larger than dunes, with length to height ratios of 15 to greater than 90 (Costello, 1974). Bed forms in Figure 5.9

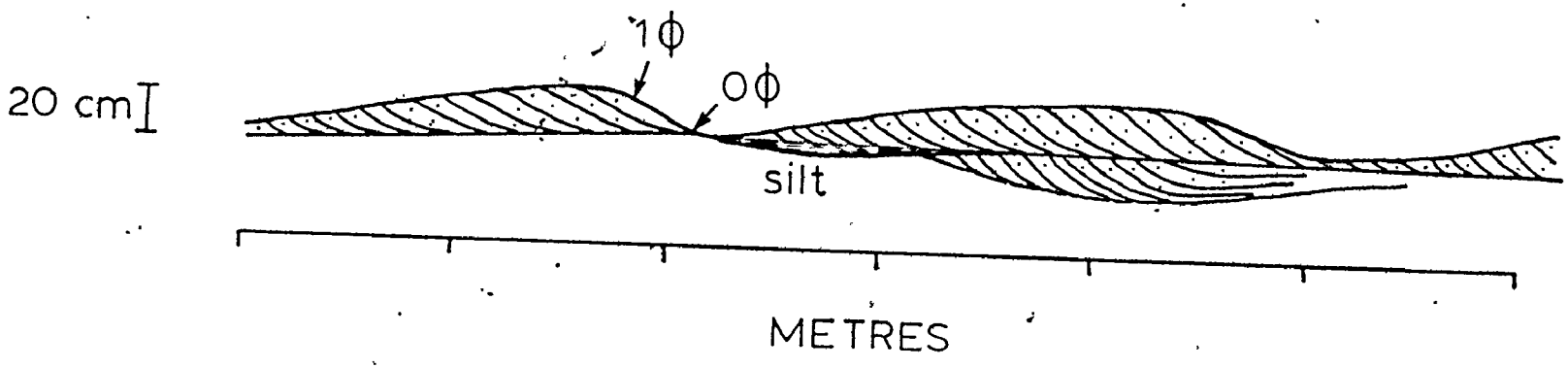

Fig. 5.9. Field sketch of locally preserved bed forms on top of a truncated sandstone (5) at area C. Sets are asymptotic at their base. Note silt lens over lowest cross-stratified scour fill. This silt may have been deposited in the lee of a migrating dune (Boersma, 1967, his Figure 2).

appear to have a regular spacing, with a form ratio of 14, in good agreement with length to height ratios of about 20 for dunes.

(v) Slope estimates derived in a later section are too high to allow formation of sand waves except in very shallow flows, which would be supercritical. Figure 5.10 shows stability fields for lower flow regime bed forms as a function of mean grain size and shear velocity. Megaripples (dunes) and megarippled sand waves would both deposit trough cross-stratification. Distinct sand waves without scour pits would only be preserved in the field of rippled sand waves. Costello's (1974) data indicate that this is also true for small-scale flows. Mean grain size for cross-stratification in Tourelle sandstones is about 1.5 ϕ. Rippled sand waves of this mean grain size are only stable up to a shear velocity of 4.7 cm s^{-1}. If we assume a dilute flow of density 1.05 g cm^{-3}, equation (7) gives slope, $S = 0.473/d$. $\bar{u}$ is given by equation (6), with friction factor, f, equal to 0.05 for sand waves (Pratt and Smith, 1972). The depth at which flow would become supercritical can then be calculated using equation (4). Specifically, flow would be supercritical for d less than 69 cm, which corresponds to a maximum slope of 0.007 for flow over sand waves. Slopes calculated in a later section on debris flow are several times greater, and would be too steep for sand waves to form.

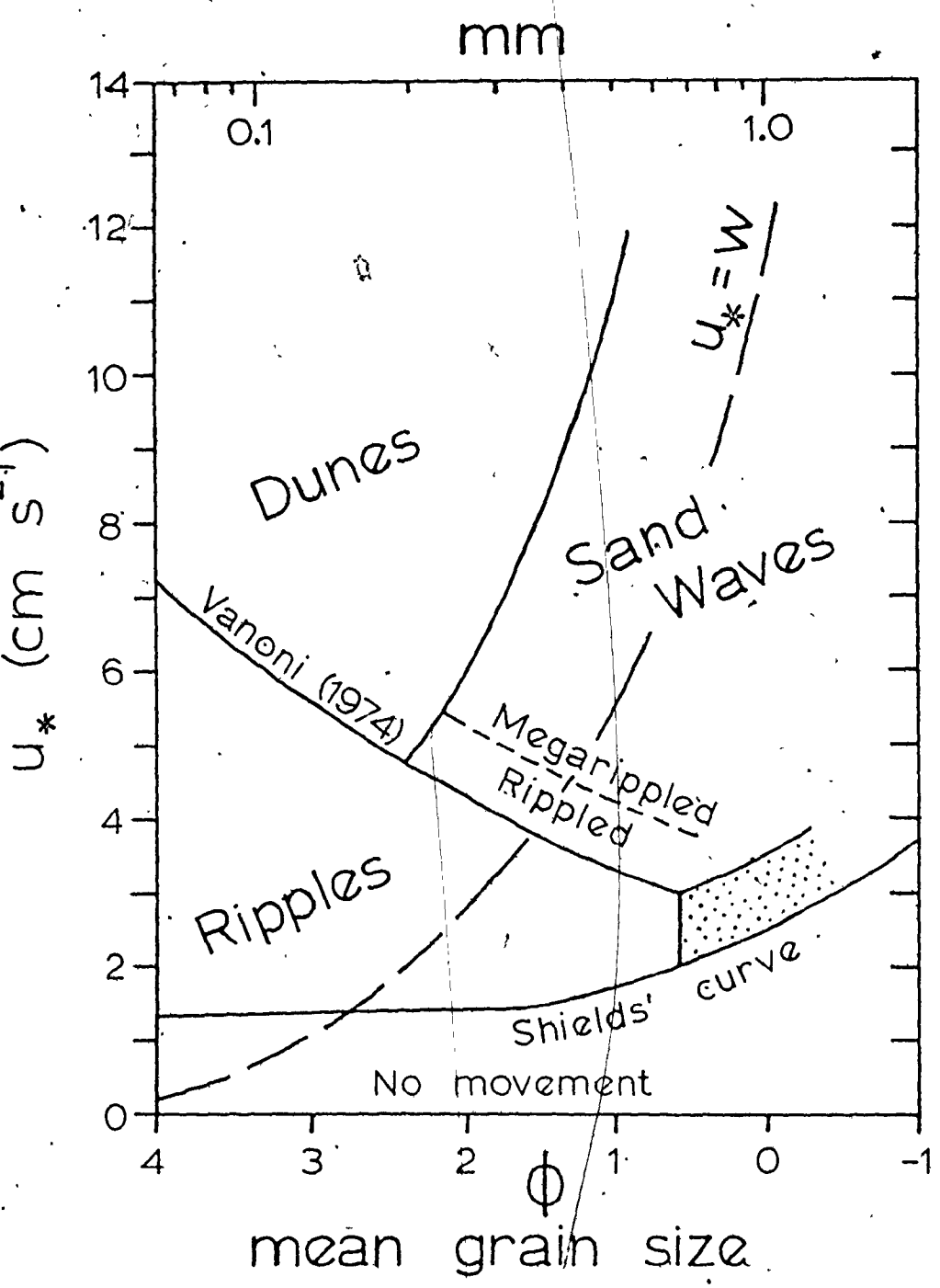

Fig. 5.10 Stability fields of lower flow regime bed forms as a function of shear velocity and mean grain size. The boundary between ripples and dunes is taken from Vanoni (1974). Sand waves are separated from dunes on the basis of hydraulic and bed form data from a macro-tidal environment presented by Dalrymple (1977, p. 223). Stippled area is for lower flow regime plane bed.

Figure 5.11 presents grain-size distributions for two separate divisions of cross-stratification at area K. Distribution parameters are summarized in Table 5.6, using symbols introduced in the earlier section on grain size. Because the size distribution was inherited from the underlying bed material, which was probably carried in turbulent suspension, there is no traction population (Visher, 1969), and therefore no coarse break with which to estimate shear velocity (Middleton, 1976). There is a fine break at 2 ϕ, however, for both curves. Lambiase (1977) found that this upper grain size break, corresponding to a change from intermittent suspension to full suspension, occurred at approximately $u_* = 5$ w for tidal currents with abundant suspended load. For 2 ϕ sand, this relationship gives $u_* = 14$ cm s^{-1}. This corresponds to $\bar{u} = 140$ cm s^{-1}, using equation (6) and a value of 0.08 for friction factor over a dune bed. At this mean velocity, dunes are indeed the stable lower regime bed form (Figure 5.13). Supercritical flow occurs when

$$\frac{8}{f}\,\frac{\rho}{\Delta\rho}\,\frac{u_*^2}{g\,d} < 1 \qquad \ldots\ldots 9$$

For $u_* = 14$ cm s^{-1}, $\rho = 1.05$ g cm^{-3}, and $f = 0.08$ for dunes (Pratt and Smith, 1972), flow is supercritical for d less than 420 cm, corresponding to slopes steeper than 0.010 (equation 7).

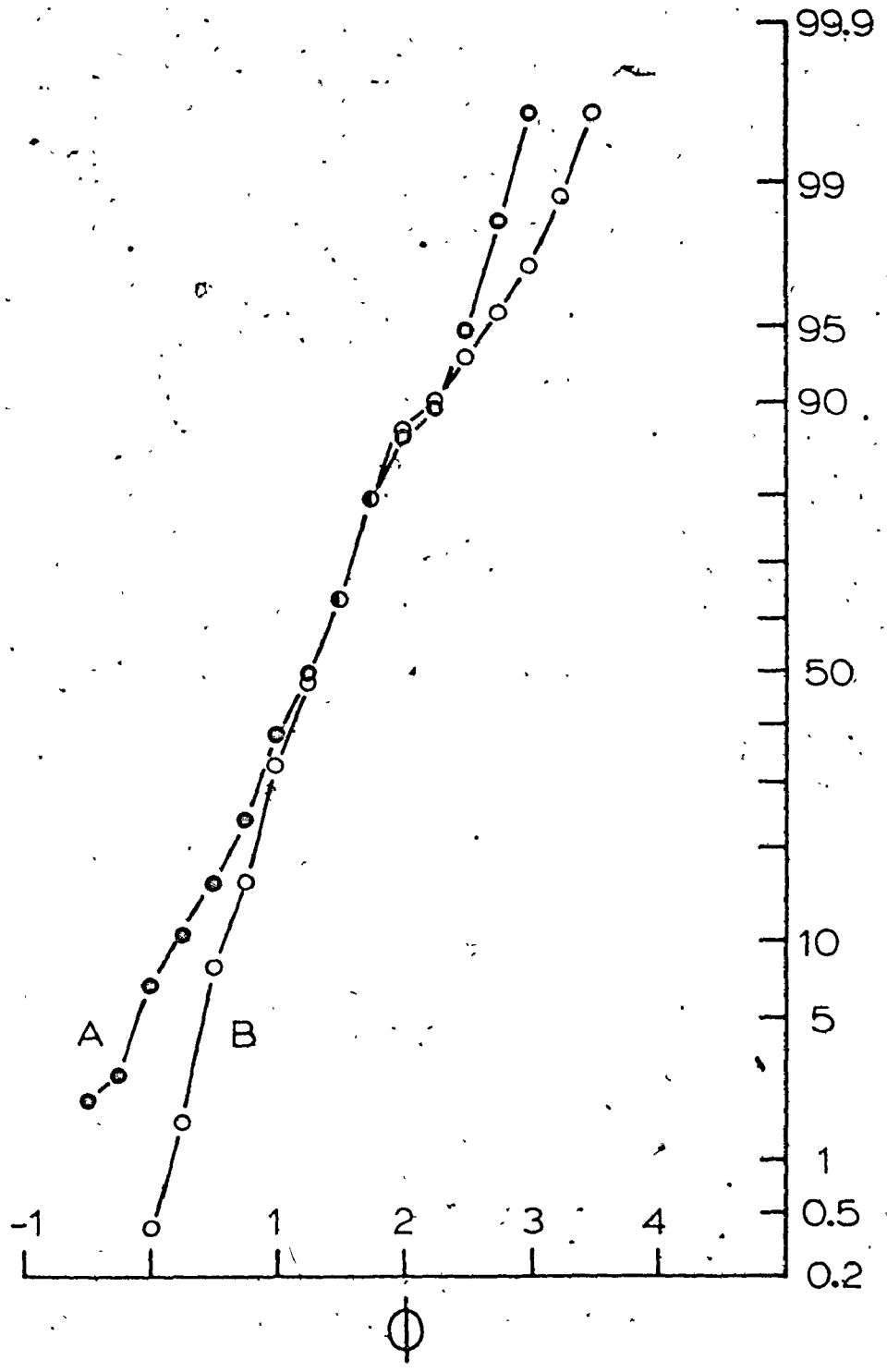

Fig. 5.11. Cumulative grain-size curves for quartz and feldspar grains in two cross-stratified divisions at area K. Curves are based on 250 points counted in thin section (Glagolev procedure). Note "break" in both curves at 2 ϕ.

Table 5.6

Grain size statistics for cross-stratified divisions (250 pts.)

Sample	mean (ϕ)	m_2	g_1^2	g_2	x_3	x_4
A	1.22	0.57	0.014	-0.023	-0.059	-0.046
B	1.36	0.44	0.681*	0.983*	0.410	0.940

If the population distribution is normal, 95% confidence limits for g_1^2 and g_2 are 0±0.0911 and 0±0.601. * indicates values of g_1^2 and g_2 that fall outside these limits.

Assuming that sufficient time was available for tractional structures to form, dunes would develop in flows thicker than 420 cm on slopes less than 0.010.

Dune to plane bed transitions

In the section on sedimentary structures, it was noted that (i) massive sand may pass upward into cross-stratification without an intervening plane-bed phase, and (ii) cross-stratification may pass upward into upper flow regime plane bed, contrary to what one would expect for deposition from a waning turbulent flow.

Evidence has been presented to suggest that some massive sandstones may have been deposited by fall-out from suspension beneath supercritical turbulent flows, perhaps as a result of decrease in current capacity. In order for dunes to form, such a current must generally go through a hydraulic jump and increase in thickness. For each set of flow parameters, it is possible to calculate conjugate depths of flow which correspond to subcritical (largest depth) and supercritical (smallest depth) conditions. Both the specific force, M_o, and the unit discharge, q, must remain constant through such a transition, although in turbidity currents, q may actually increase somewhat after the jump as ambient fluid is mixed into the flow. This effect will be neglected in the following analysis.

The two equations which must be satisfied through a hydraulic jump are given below.

$$q = \bar{u}\, d \qquad \ldots\ 10$$

$$M_o = \frac{q^2 \rho}{g\, \Delta\rho\, d} + \frac{d^2}{2} \qquad \ldots\ 11$$

In the previous section, it was shown that for a flow of density 1.05 g cm^{-3}, the minimum depth possible for dunes is 420 cm on a slope of 0.010. These conditions correspond to a mean velocity of 140 cm s^{-1} and a unit discharge of

5.88×10^4 cm^3 s^{-1}. Figure 5.12 is a specific force diagram based on these estimates. If flow changes from supercritical to subcritical along path 1, for example, depth will increase from 190 cm to 800 cm and mean velocity will decrease from 309 cm s^{-1} to 74 cm s^{-1}. If the transition does not occur until Fr = 1.0, there will be no sudden change in either depth or velocity. The point at which the transition from supercritical to subcritical flow occurs may depend on such factors as (i) a sudden decrease in bottom slope, or (ii) a sudden lateral constriction of the current in a submarine channel, causing oblique reflection of the head of the current and migration of a hydraulic jump into the centre of the flow.

Figure 5.13 is an extension to large depths of flume data for stability fields of bed configurations in medium sand. The boundaries between fields are taken from Harms and others (1975, p. 19), with the addition of a dividing line between subcritical and supercritical flow defined by densiometric Froude number equal to 1.0. Conjugate depths corresponding to hydraulic jumps 1, 2, 3 and 4 (Figure 5.12) are plotted on this diagram. For conditions specified above, there is no stable plane-bed phase between the field of supercritical flow and the field of dunes. In addition, supercritical flows less than about 190 cm deep cannot form sand waves or dunes after a hydraulic jump, because the corresponding subcritical flow would be in the ripple field.

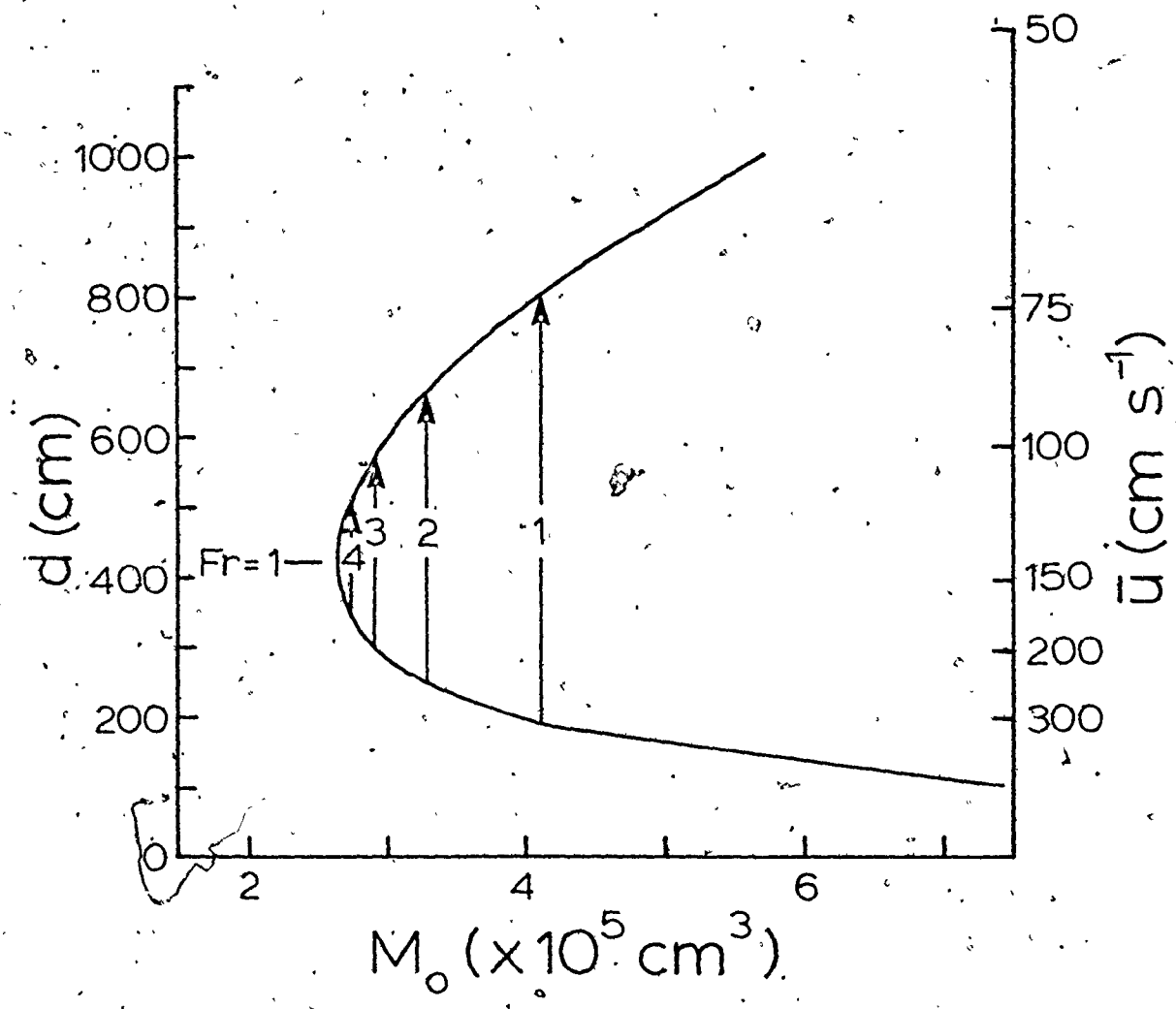

Fig. 5.12. Specific force diagram for turbidity current with $\rho = 1.05$ g cm^{-3} and $q = 5.88 \times 10^4$ cm^3 s^{-1}. Pathways 1 to 4 indicate possible hydraulic jumps. See text for discussion.

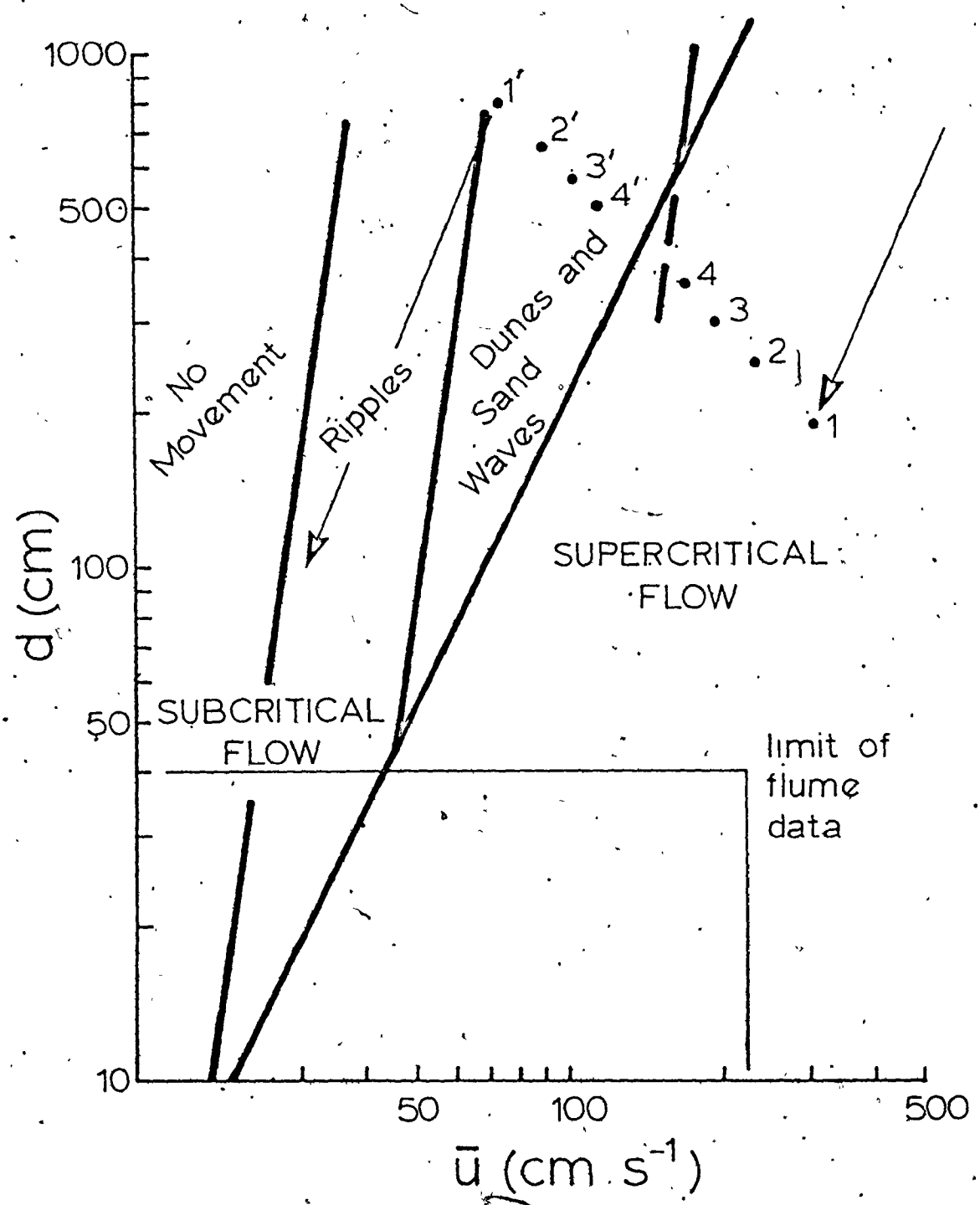

Fig. 5.13. Fields of stability for lower flow regime bed phases extrapolated from flume data (Harms and others, 1975, p. 19). Possible hydraulic jumps 1 to 4 (Figure 5.12) are plotted. See text for discussion.

For deeper flows on more gentle slopes, the plane-bed phase (Figure 5.13) could also be easily bypassed by a hydraulic jump, again resulting in transitions between massive sandstone and cross-stratification.

Field studies indicate that cross-stratification on the top of thick sandstones (6) is restricted to short stratigraphic intervals. Examples can be found at areas C and K (Appendix I). This stratigraphic restriction probably reflects local hydraulic conditions which favoured formation of dunes. The most important variables governing entry into the dune stability field are unit discharge, effective flow depth in the body of the current, and slope. Large, thick, supercritical flows with high discharge might remain thick enough to allow later formation of dunes, rather than passing directly into the ripple field. The easiest way to initiate dunes, however, is to decrease slope at constant discharge. This would cause the flow to decelerate, thicken, and perhaps undergo a hydraulic jump. It is believed that the restriction of cross-stratification to particular stratigraphic intervals resulted from irregularities and breaks in slope on the fan surface. In general, slope was too steep to allow dunes to form.

Upper flow regime plane lamination was twice observed to overlie cross-stratification. In both cases, grain size decreased from medium to fine or very fine sand on entering

the division of plane lamination. Flume experiments have shown that a decrease in grain size at constant or slowly decreasing velocity is sufficient to produce a transition from dunes to upper regime plane bed. This grain-size effect was probably responsible for similar transitions in some thick sandstones (6).

Large slabs and matrix strength

In previous sections, the assumption was made that suspension of clasts could be attributed solely to fluid turbulence. The presence of large slabs of chert and dolomitic siltstone within or at the top of some thick sandstones (6) of the massive variety draws this assumption into question, as they were probably too heavy to have been supported only by turbulence, and too large to have been "rolled" on the bed. Only in the region of divergent flow in the head of a turbidity current is the upward component of fluid force potentially large enough to carry large slabs off the bed. Large rafts of shale present less of a problem because they were probably much less dense at the time of deposition and could be buoyed up in a high concentration turbidity current. Fist-sized angular blocks of chert which may have been rolling along the sand bed during flow are found above the base of some layers. According to

Fahnestock and Haushild (1962), rolling of pebbles and cobbles on a sand bed only occurs in the upper flow regime over plane or antidune beds. In the lower regime, scour pits form upstream of large clasts and they move upstream and down into the bed.

The presence of large, apparently indurated, slabs of bedded chert and dolomitic siltstone (see Chapter II) is most easily explained by debris flow, with a dense matrix providing both cohesive strength and bouyancy for the support of large blocks (Rodine and Johnson, 1976). It is believed that fluid lift and drag forces would not have been sufficient to carry these slabs.

Debris flow has already been suggested as the mechanism of emplacement of slurry sandstones (3), which contain abundant matrix, disoriented cobbles of calcisiltite, and large rafts of indurated siltstone (see Chapter II). Is it reasonable to propose debris flow for emplacement of some thick massive sandstones in the Tourelle Formation? In order to answer this question, we must know (i) whether deposits similar in description to subaerial debris flows exist in the Tourelle Formation, and (ii) whether thick massive sandstones originally contained sufficient cohesive matrix to allow them to move as debris flows.

The presence of large indurated blocks suspended within sedimentary units is a feature shared by subaerial debris

flows (Johnson, 1970), as is the disorganized (or bimodal) fabric of massive layers. Hampton (1975) predicted inverse grading at the base of sandy debris flows undergoing plug flow, although some turbulent flows (Enos, 1977; Middleton and Southard, 1977, p. 8.16) might be normally graded or ungraded. Basal inverse grading and lack of grading are indeed present in some thick sandstones (6) (see Figure 2.22). Grooves (tool marks) strongly dominate over scour marks, as is predicted for viscous flows (Middleton and Hampton, 1976).

The lowest thick sandstone at area CVIII (Appendix I) is ungraded and contains abundant, disoriented, large shale and calcisiltite blocks which concentrate to form a rubbly uneven top to the unit. This layer is the most convincing candidate for debris flow.

Rodine and Johnson (1976) present a graphical procedure to calculate the volume of void space which must be exceeded and filled with cohesive matrix before grain interlocking ceases and debris flow can begin. During flow, the entire mass behaves as a dense viscous fluid. The graphical procedure requires plotting of cumulative grain size on Rosin's Law probability paper (Kittleman, 1964), and determining slope of the curve for each sample. Figure 5.14 shows Rosin's Law plots for eight thick sandstones (6) (7 massive, 1 stratified), and one slurry sandstone (3). Data were first corrected for the thin section effect using the

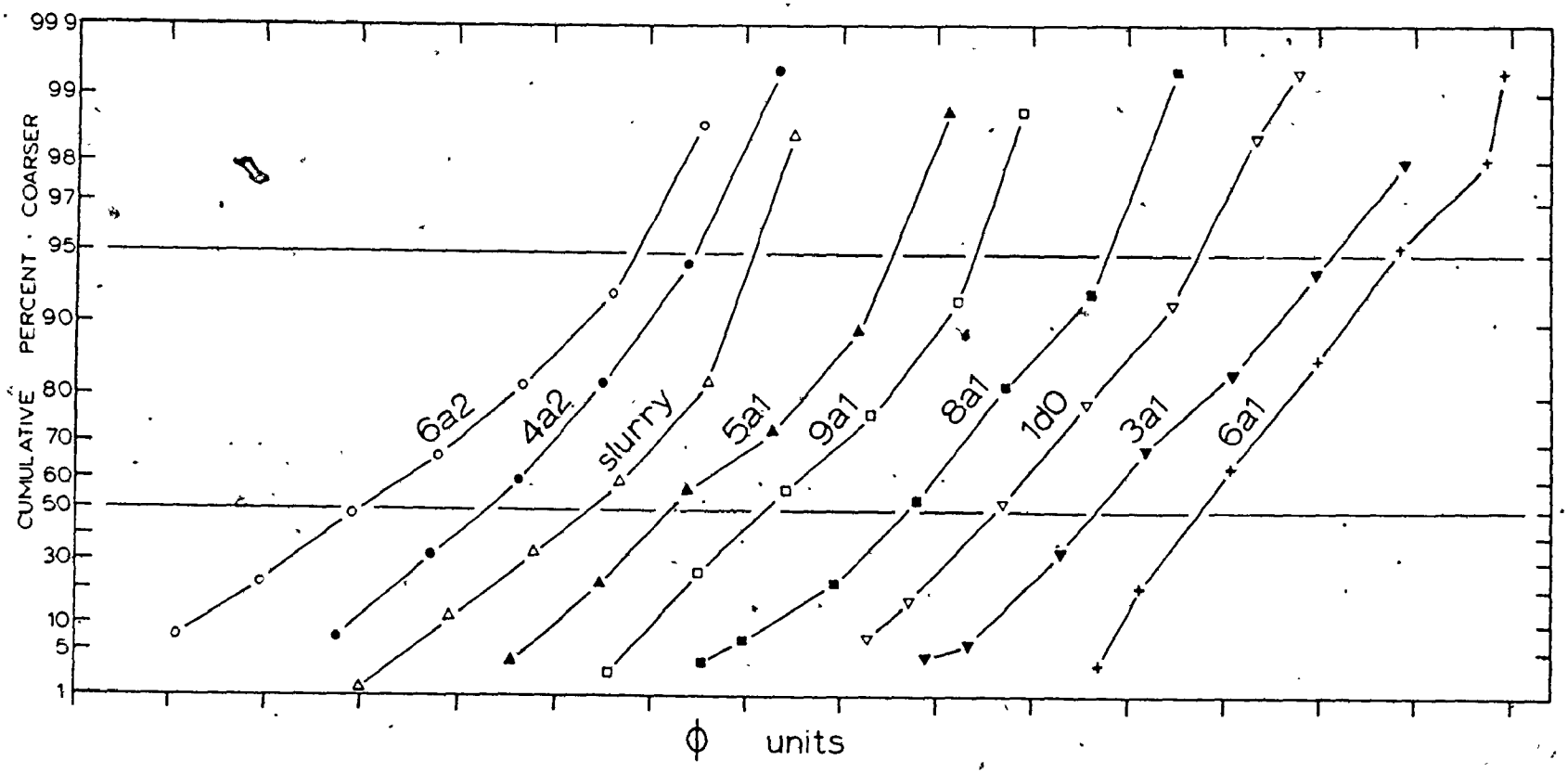

Fig. 5.14. Rosin's Law plots of grain-size distribution curves for various fabric substations, and one slurry sandstone (3) layer. All samples are from massive layers except 1d0, which comes from a stratified layer. Slopes of these curves are presented in Table 5.7.

empirical curve of Friedman (1958). Because only the slope of each line is important, no numerical ϕ scale is presented. ϕ_{50} for each sample is given in Table 5.7, which also indicates slope of each curve, and porosity before grain interlocking (see Figure 11 of Rodine and Johnson, 1976). Only 8 to 16 volume percent cohesive matrix (clay + water) would have been necessary for these Tourelle sands to have been capable of flow. According to Hampton (1975), common clays with as much as 65 weight percent water would be competent enough to carry granular sand. Therefore, only 4 to 7 volume percent of solid matrix material is required. All samples except 6a1 have sufficient matrix to have moved as debris flows. If some chloritic matrix is not "primary", then a few other samples would have to be eliminated as possible debris flow candidates.

While this analysis does not prove that some massive Tourelle sandstones were transported by debris flow, it does show that sufficient matrix was present in some layers for this mechanism to be viable, particularly in the later stages of deposition. Those layers containing large rafts of bedded chert and siltstone most certainly required a contribution from matrix strength, and may have travelled entirely as debris flows. The included blocks would then have been supported by matrix strength and buoyancy. Buoyancy would have been particularly important if the blocks were

Table 5.7

Porosity required to prevent grain interlocking using technique of Rodine and Johnson (1976)

Sample	ϕ_{50}	graph slope	critical porosity (%)	percent matrix (100 pts)	percent calcite "cement" (100 pts)
6a2	1.1	-0.75	8.5	7	1
4a2	1.7	-0.90	11.0	16	2
slurry	2.7	-0.78	9.0	33	4
5a1	1.8	-0.90	11.0	19	2
9a1	1.7	-0.97	12.0	16	7
8a1	1.9	-0.97	12.0	13	1
1d0	0.9	-1.07	13.0	12	10
3a1	1.4	-1.07	13.0	12	5
6a1	0.7	-1.28	16.0	3	4

not completely indurated and therefore less dense than solids in the rest of the flow. Modern siliceous ooze only has a density of 1.5 g cm^{-3} (Maxwell and others, 1970; Peterson and others, 1970), with density increasing slowly during a maturation process which terminates with the production of chert (Mizutani, 1971; von Rad and Rösch, 1974).

Johnson (1970, p. 486-7) gives details on how to calculate the approximate strength of a debris flow from the dimensions of large blocks carried in the flow. Specifically,

$$k = \frac{h}{4}\left(\rho_s - \frac{\rho}{n}\right) g \qquad \ldots\ 12$$

where k is the strength in dyne cm^{-2}, ρ_s and h are the density and thickness of the block, ρ is the overall density of the flow, and n depends on the depth of penetration of the block into the top of the flow. If 1/4 of the block is submerged, n = 4.

Case 1: The bedded chert block at area K (Figure 2.26) is 230 cm thick and appears to have settled into the top of a 420 cm thick layer of sandstone after deposition, causing deformation of overlying beds. The next current deposited its coarsest grains in the lee of this exposed block. If it is assumed that 7/8 of this block was submerged, we can plot k against ρ_s for debris flows of density 2.0 and 2.3 g cm^{-3} (Figure 5.15). This particular bedded chert block appears to

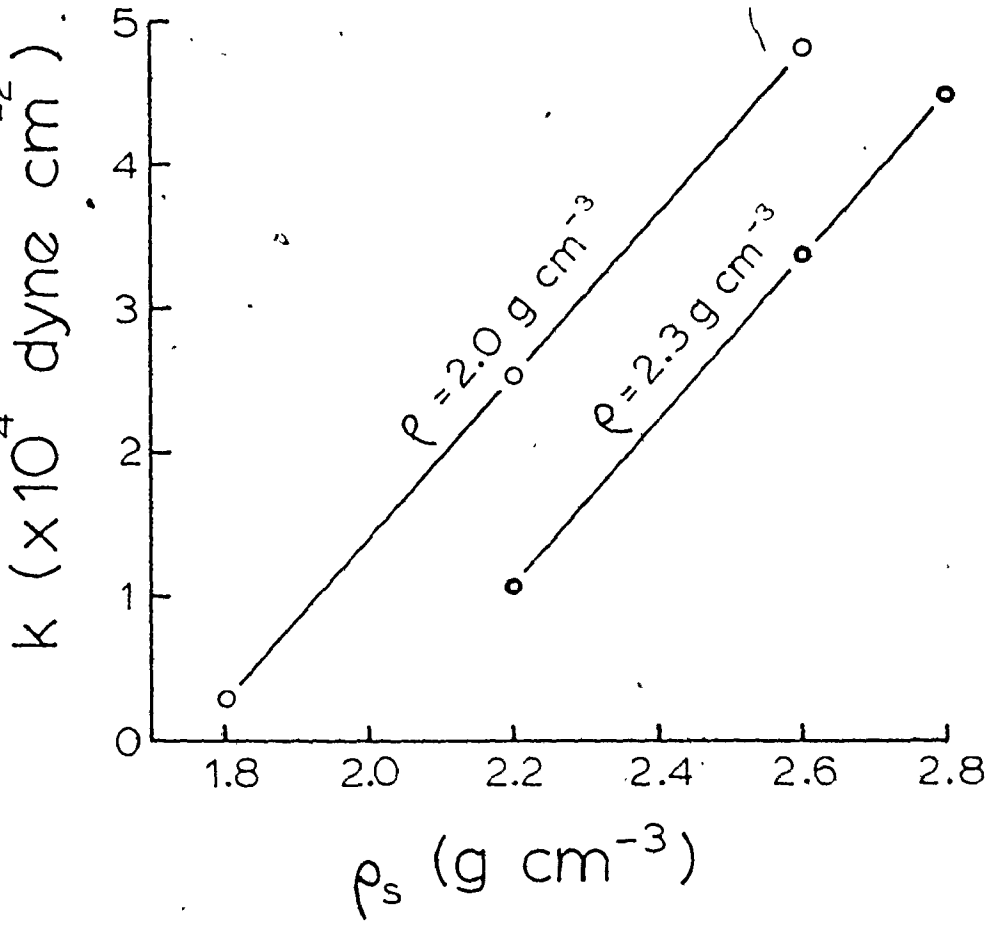

Fig. 5.15. Plot of strength, k, against block density, ρ_s, for debris flows of densities 2.0 g cm^{-3} and 2.3 g cm^{-3}. This plot is specific to case 1, discussed on the previous page.

have been quite indurated, suggesting an initial density of about 2.2 to 2.4 g cm^{-3}, and therefore a strength of about 1×10^4 to 3×10^4 dyne cm^{-2}. When flow ceased, the basal shear stress, τ_o, must have been equal to the strength. The angle of slope for sub-aqueous flows is then given by

$$\sin \alpha = \frac{k}{\Delta\rho \; g \; T_c} \qquad \ldots . \; 13$$

where T_c is the thickness of the flow and α is the angle of slope. For the sandstone containing this chert block, T_c = 420 cm, and α ranges from 1.1° to 5.2°. Slope, therefore, ranges from 0.019 to 0.090.

Case 2: At area L, there is a 100 cm diameter, round block of indurated siliceous siltstone within a 200 cm thick sandstone layer that appears to change laterally into a slurry sandstone (3). If we assume a block density of 2.4 g cm^{-3}, and flows with densities 2.0 and 2.3 g cm^{-3}, then strength, k, varies from 0.245×10^4 to 0.980×10^4 dyne cm^{-2}. Slope (equation 13) varies from 0.010 to 0.050.

Case 3: A second thick sandstone (6) layer at area K is 400 cm thick and encloses a block of dolomitic siltstone 230 cm thick. If we assume a density of 2.5 g cm^{-3} for the block, and flow densities of 2.0 and 2.3 g cm^{-3}, then strength varies from 1.13×10^4 to 2.80×10^4 dyne cm^{-2} and slope varies from 0.022 to 0.071.

Table 5.8 assembles strength and slope estimates from the three examples discussed above. Strengths are in the same range as strengths calculated by Johnson (1970, p. 486-90) for the subaerial Surprise Canyon debris-flow deposit. If we assume that the depositional slope for Tourelle flows was approximately the same in all cases, then slope must have been in the range 0.02 to 0.05. These slopes are approximately 2 to 5 times greater than slopes deduced from shear velocities required to produce dunes on the tops of some thick sandstones (6).

According to Middleton and Southard (1977, p. 8.17), debris flows will become turbulent when $k/(\rho\ \bar{u}^2)$ is less than 0.001. Values of $\bar{u}_c$ are listed in Table 5.8. The equation given by Enos (1977) gives slightly greater values for $\bar{u}_c$. These mean velocities are extremely high, ranging from about 10 to 40 m s^{-1}. It is unlikely, therefore, that debris flows with characteristics listed in Table 5.8 would have been turbulent.

Table 5.8

Strength and slope estimates for debris-flow model

Example	block thickness (cm)	n	flow thickness (cm)	ρ (g cm^{-3})	k (10^4 dyne cm^{-2})	S	$\bar{u}_c$ for turbulence (cm s^{-1})
1	230	$\frac{8}{7}$	420	2.3	1.0	0.019	2085[a]
				2.0	3.0	0.090	3873
2	100	.1	200	2.3	0.25	0.010	1043
				2.0	0.98	0.050	2214
3	230	1	400	2.3	1.13	0.022	2217
				2.0	2.80	0.071	3742

(a) $\bar{u}_c^2 = 10^3\ k/\rho$

Interpretation

Stratified layers

Evidence which must contribute to an assessment of depositional mechanics for stratified layers is summarized below.

(i) If fine sub-divisions are neglected, overall size grading is strongly developed, and conforms to the requirements of distribution grading.

(ii) Stratification bands are inverse graded with a difference of about 1 ϕ unit between coarse and fine sub-divisions. Each band is based by a near-horizontal scour surface. This stratification is associated with massive divisions, which may occur either above stratification, below, or in both positions. Within individual layers, coarse stratification is always found below tractional structures such as upper flow regime plane lamination, ripples, or cross-stratification.

(iii) a-axis fabric is strongly developed, with long axis parallel to flow and imbricate upcurrent. Imbrication angle is generally greater than 20°, which is a characteristic of grain interaction (Taira, 1976a) or deposition from high velocity currents (Johansson, 1976). Fabric is vertically consistent throughout entire stratified layers, and may show best lateral consistency at the tops of layers, rather

than at the base.

(iv) The highest vector magnitudes are found in fine sub-divisions of stratification bands.

(v) Competence considerations for a turbidity current carrying 3 mm sand require shear velocities of 15 to 32 cm s^{-1}, or mean velocities of 4 to 8 m s^{-1} in flows from 10 to 20 m thick. These estimates may be minima, as the poor size sorting in these sandstones is best explained by deposition as a result of decreasing current capacity rather than competence. Even these estimates, however, signify currents with high Froude numbers, and therefore suggest antidunes as the stable bed phase. Continued high velocities during deposition are suggested by the vertical consistency of fabric, and the fact that coarse stratification, which is interpreted as a deposit from supercritical flows, persists upward into medium sandstone. Recall that competence calculations were undertaken only for 3 mm sand grains, which are coarser than all grains in many stratified layers. If deposition was the result of decreased competence, then flows carrying medium sand (1 ϕ to 2 ϕ) would certainly not be supercritical, as they are believed to have been.

(vi) Although grooves are more common, large, abundant flutes may be present on the soles of stratified layers.

The presence of well-developed size grading of the entire size distribution can only be explained by turbidity

current transport, with the resulting implication of super-critical flow conditions. Middleton (1967) observed coarse-tail grading in deposits of experimental high-concentration turbidity currents. This style of grading is not characteristic of stratified layers, suggesting currents of lower density, perhaps 1.1 g cm^{-3}. Scour marks also support the hypothesis of turbulent suspension.

The coarse stratification must have formed at velocities greater than those required to produce normal tractional structures. High imbrication and inverse grading also indicate that grain interaction was important during deposition of stratification bands, perhaps as a result of high grain concentrations at the bed. Bagnold (1956) would attribute the inverse grading to dispersive pressure within a shearing layer of grains at the base of the flow. It is possible that the concentration of fine grains at the base of the flow, along with presence of a matrix of higher viscosity than water, could have resulted in formation of a thick pseudo-viscous sublayer which would aid in the trapping of fine particles. Coarser grains would be maintained in suspension by dispersive pressure; finer grains would not. Viscous sublayer thickness is given by

$$\delta = \frac{11.6\ \nu}{u_*} \qquad \ldots\ 14$$

This equation is normally only applicable to smooth turbulent flows ($u_* k_s/\nu < 5$). With abundant suspended material immediately above the bed, however, effective viscosity would be very high, perhaps 100 times the viscosity of water. With $\nu = (100)(0.015) = 1.5$ poise, and $u_* = 25$ cm s^{-1}, $\delta = 0.7$ cm, which may have been sufficient to help trap fine particles at the base of stratification bands. This fine layer at the base of the flow was certainly under intense shear, as both vector magnitudes of a-axis orientation and imbrication angles are high.

It is believed that the formation of discrete stratification bands was the result of one of two processes.

(i) Individual bands may represent stratification produced by migration and aggradation of long-wavelength antidunes. According to Hand (1974), the wavelength of antidunes in flows of about 10 m depth would be about 130 m. Scour on the downstream faces of these low features would produce the erosion surface at the base of a stratification band. Inverse grading would be produced by intense shearing of a basal layer of grains over the bed, which would then be buried by periodic rapid fall-out of grains from suspension into the zone of basal shearing. The thickness of bands would then depend on the intensity of deposition from suspension. Lulls in deposition, perhaps resulting from location on the migrating antidunes, would allow a basal scour surface and flowing grain layer to be re-established.

(ii) Stratification bands may have resulted from progressive "freezing" of the base of the current and upward migration of the sediment bed, as suggested by Carter (1975, p. 159). As competence and capacity decreased, grains would settle to the base of the flow and be driven along by shear transmitted from the overlying turbidity current, producing a flowing grain layer (Sanders, 1965). Inverse grading in this layer would be produced as described previously. At some critical thickness, it is possible that the entire flowing carpet of grains would collapse and be deposited by "freezing". The entire process would then start again. Each stratification band would preserve the fabric which had developed during shearing above the bed. The thickness of stratification bands has been observed to diminish as mean grain size decreases from the base to the top of stratified layers. This is interpreted to indicate decreasing current velocity throughout deposition, with the thickness of the flowing grain carpet being a function of flow strength.

At any time during the deposition of coarse stratification, prolonged rapid fall-out from suspension would produce a thick massive division. As current velocity and density decreased, tractional structures would begin to form.

Massive layers

The following observations must be satisfied by a model for deposition of thick massive sandstones.

(i) Layers may be well graded, inverse-to-normally graded, ungraded, or may show complex grading. The middle parts of layers generally are the most poorly sorted. Grading appears to be of the coarse-tail variety.

(ii) Some massive layers have discontinuous internal scour surfaces (Figures 2.11, 5.16) which occur below normal tractional sedimentary structures.

(iii) Sole markings are generally grooves, but irregular wavy bases have been observed. These basal waves may be quite regular in spacing. On one layer at section CIII, the wavelength of basal waves was 5 m, with a height of 20 cm.

(iv) a-axis grain orientation is most strongly developed at the base and tops of layers. The middle parts of single units may have bimodal or isotropic fabrics, with both upcurrent and downcurrent imbrications.

(v) If these layers were transported by turbidity currents, then flow velocities deduced from competence requirements would have been about the same as for stratified layers. Flow would also have been supercritical. These velocities are almost identical to those required to roll concretions along a sediment bed.

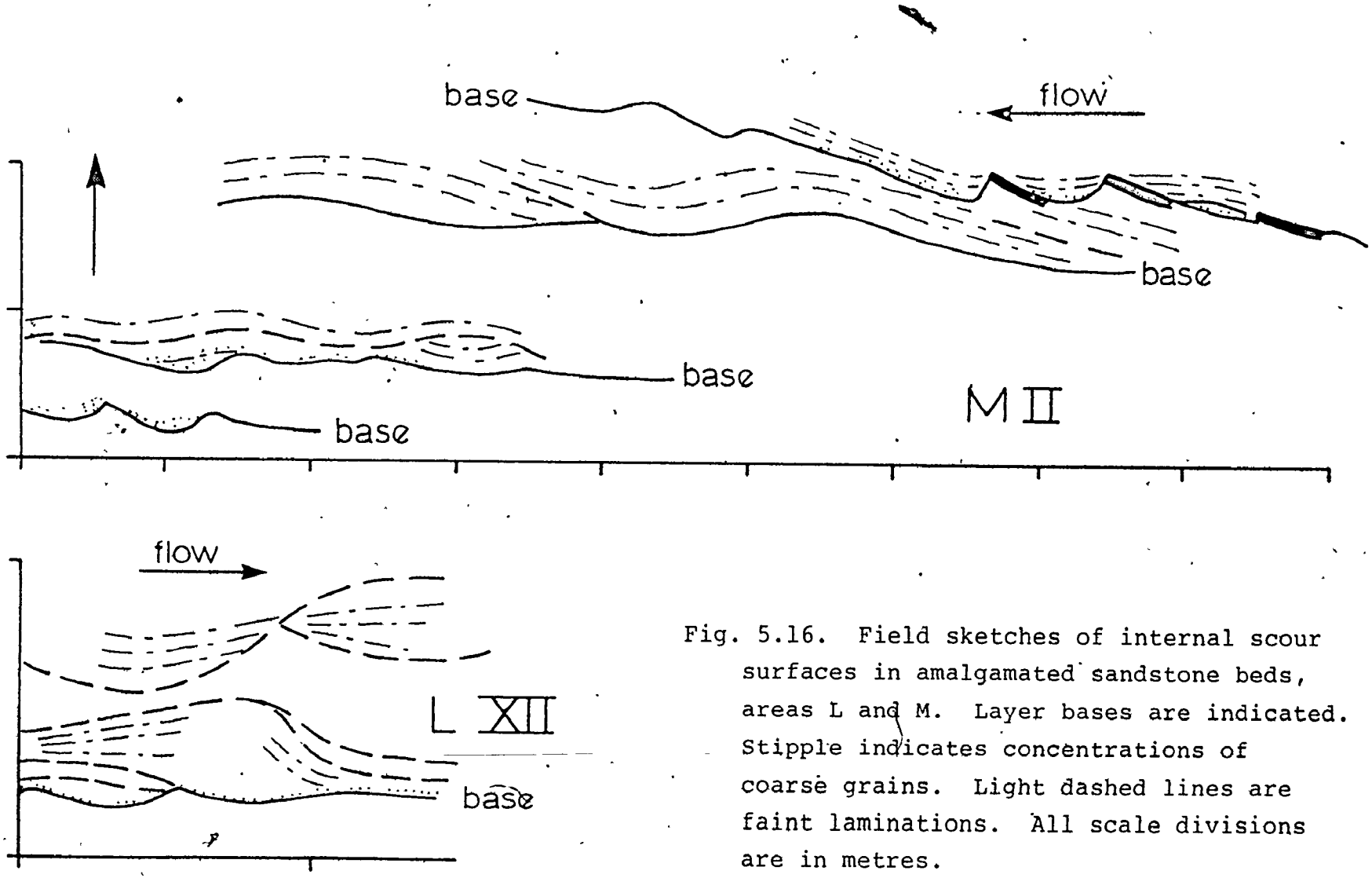

Fig. 5.16. Field sketches of internal scour surfaces in amalgamated sandstone beds, areas L and M. Layer bases are indicated. Stipple indicates concentrations of coarse grains. Light dashed lines are faint laminations. All scale divisions are in metres.

(vii) Some thick sandstones (6) have large blocks of dolomitic siltstone or bedded chert suspended above their soles. This observation suggests emplacement by debris flow. Most Tourelle sandstones actually have enough primary matrix to have moved as debris flows on slopes of 0.02 to 0.05 (1.2° to 2.9°). These flows would have been laminar, with yield strengths of 0.3×10^4 to 3.0×10^4 dyne cm^{-2}.

(viii) Some massive sandstones contain abundant fluid-escape pillars.

It is believed that most massive sandstones, and massive divisions in stratified layers, were deposited from dense supercritical turbulent suspensions. Middleton (1967) reported inverse grading at the base of beds deposited from experimental high-concentration turbidity currents, as well as coarse-tail grading at higher levels in the bed. During the final stages of deposition, a "quick" bed was formed. Shearing and churning of such a "quick" sand unit would produce a massive layer. Rapid fall-out of grains from suspension and instantaneous burial can also produce isotropic or bimodal fabrics, and a scattering of imbrication angles. This rapid deposition would favour later in situ liquefaction and pore-fluid escape.

Internal scour surfaces and periodic sediment waves on the base of layers are interpreted to be the result of supercritical flow involving, perhaps, irregular chutes and pools.

Deposition probably resulted from a decrease in current capacity at velocities greater than those predicted on the basis of competence. Concretion clasts and isolated cobbles of chert were probably moving as bed-load beneath such currents.

Those thick sandstones which contain enormous slabs or blocks of indurated Cap des Rosiers lithologies must have travelled as debris flows, unless block densities have been grossly overestimated. Fabric in the middle of these layers is poor or isotropic because of movement as a rigid plug. Shearing and grain interaction were concentrated at the base, resulting in improved a-axis grain orientation and possible inverse grading. Debris flow is only favoured for a small number of thick sandstones (6), particularly those which are extremely thick and essentially ungraded (subfacies 6c). Almost half of these layers have flat bases, and groove marks are the most common sole features.

There was probably a gradation between debris flows, and dense turbulent suspensions with additional support from grain interaction, matrix strength and density, and excess pore-fluid pressure. This continuum produced a log-normal layer thickness distribution for all sandstone facies.

In order for some thick sandstones (6) to have moved as debris flows, slopes within channels must have been on the order of 0.02 to 0.05. On these slopes, turbidity currents transporting coarse sand would certainly have been supercritical.

Deposition must, therefore, have resulted from a decrease in current capacity as slope decreased. The finer tails of these currents would have continued down the submarine fan, particularly as they must have become somewhat diluted by intense interfacial mixing with ambient fluid when the Froude number was greater than one (Middleton, 1966b).

Cross-stratification

It is believed that most cross-stratification was formed by migration of dunes during the late stages of flow. The examples studied suggest $u_* = 14$ cm s^{-1}, depth greater than 420 cm, and slope less than 0.01. This slope does not agree with slopes inferred from subaqueous debris flows, which are 2 to 5 times steeper. It is believed that dunes only formed locally on unusually gentle slopes, which explains the occurrence, in close stratigraphic proximity, of several layers with cross-stratified divisions at areas C and K. It is quite possible that turbidity currents went through a hydraulic jump at the break in slope, causing them to enter the dune field.

Summary

An examination of (i) grading and grain-size distributions, (ii) layer thickness distribution, (iii) sequences and associations of depositional structures, (iv) appositional grain fabric, and (v) various problems in sediment dynamics, has led to the following conclusions about depositional mechanics of Tourelle thick sandstones (6).

(i) Stratified layers were deposited from supercritical turbulent suspensions with densities of about 1.1 g cm^{-3}. Coarse, near-horizontal stratification was produced by grain interaction in a flowing grain layer sheared along the base of such a flow. Periodic "freezing" of the grain carpet during deposition resulted in preservation of inversely graded stratification bands. Each layer, however, shows strongly-developed normal grading. It is also possible that stratification bands were formed on the aggrading faces of long-wavelength antidunes.

(ii) Most massive layers, or divisions, were deposited from dense, supercritical turbulent suspensions. Deposition may have involved a "quick" sediment bed prior to consolidation. Unusually thick, and ungraded or poorly graded layers containing enormous blocks of bedded chert and dolomitic siltstone were more probably transported by laminar debris flow. This mechanism required slopes on the order of 0.02 to 0.05. On these slopes, deposition from associated turbidity currents would have been the result of a decrease in capacity rather

than a decrease in competence.

(iii) Tractional structures, including cross-stratification, are found above both massive and coarsely-stratified divisions. These structures formed after a transition from supercritical to subcritical flow, in the later stages of deposition. This transition may have involved a hydraulic jump. Dune cross-stratification is only found in restricted stratigraphic intervals, and formed only where local channel slope was less than about 0.01.

(iv) Imbricate bands of concretion conglomerate moved as bed-load at the base of thick turbidity currents. The conglomerate matrix (and overlying sediment) was carried in turbulent suspension above this sediment bed.

CHAPTER VI

MINERALOGY AND PETROGRAPHY OF TOURELLE SANDSTONES

> "In examining each particular deposit two different questions present themselves. It is necessary, in the first instance, to identify as accurately as possible the mineral nature of the various large and smaller particles, and in the second place to determine as far as possible the true nature of the rock from which they were originally derived." - Henry Clifton Sorby (1877)

The mineralogical composition of clastic rocks of the Tourelle Formation was investigated for exactly those reasons outlined by Sorby. R.K. Stevens (unpubl. manuscript, 1969) suggested that Tourelle sandstones, by analogy with sandstones of the Blow-me-Down Brook Formation (Stevens, 1970), were derived from uplifts situated to the southeast, in the interior of the Taconic orogenic belt. Previous Lower Ordovician detritus was derived from the stable craton to the northwest (Lajoie and others, 1974), consisting of gneissic Grenville basement, intrusive rocks, and a thin unconformable cover of Lower Paleozoic quartz sandstones and shelf carbonates. The

foremost objectives of this petrographic study are to discover whether evidence exists for a southeastern provenance, and to use mineralogical criteria to deduce the composition of this source area. This chapter will be concerned primarily with petrographic description of medium to coarse Tourelle sandstones. Interpretation of provenance will be the subject matter of Chapter VII.

Petrographic Methods

Detrital composition was determined by point counting (Glagolev procedure) using a hierarchical classification scheme as suggested by Griffiths (1960).

First count (200 points)

Seven variables were recognized at this level: (1) quartz, (2) feldspar and non-volcanic igneous rock fragments, (3) rock fragments, including siliceous mudstone and chert, (4) matrix, (5) sparry calcite cement or replacement, (6) mica flakes larger than 0.5 mm in size, and (7) others. Matrix includes all detritus less than 30 microns (0.03 mm) in size, fine mica, and pasty, authigenic, interstitial chlorite.

Four traverses of 50 points each were made on each thin

section. Results of these traverses were recorded separately as a check on internal consistency.

Five thin sections were point counted at three separate times, with at least two weeks between replications. Table 6.1 presents results of quartz counts for each 50 point traverse. Griffiths and Rosenfeld (1954) also used quartz percentage in an exhaustive evaluation of operator variation. They found significant differences among operators, and between traverses within individual thin sections, as well as interaction between operators and thin sections. Table 6.2 is an ANOVA on data from Table 6.1. There was no interaction between thin sections and measurements, allowing residual errors to be combined into one term. The ANOVA indicates that no significant difference exists between replicate measurements of the five thin sections. If, nevertheless, we utilise the fact that mean squares are estimates of variance components, we can estimate the variance associated with replicate measurements. This estimate provides a standard deviation for quartz percentages of 2.9%.

Table 6.1

Data for operator variation study of quartz content

Measurements[1]	Thin sections				
	6	7	18	23	29
1	16	17	24	24	25
	11	22	27	23	25
	9	19	26	26	24
	17	18	17	28	24
2	10	19	32	33	30
	16	16	27	26	22
	18	16	30	26	30
	12	17	22	30	20
3	14	23	28	27	34
	19	16	31	23	29
	18	19	25	27	28
	15	22	23	32	24

[1]Each measurement consists of four 50-point traverses.

Table 6.2

ANOVA table for operator variation study - quartz content

Source of variation	SS	df	MS	F_{obs}	$F_{.95}$	variance estimate[1]
Among measurements	68.2	2	34.1	2.99	3.17 NS	$\sigma^2 + k m \sigma_r^2$
Among thin sections	1476	4	369	32.34	2.54 **	
Residual error	604.8	53	11.41			$\hat{\sigma}^2$
Total	2149	59				

[1] k is number of columns, m is number of replications.

Second count

Basu and others (1975) have shown that the proportions of different quartz varieties can be successfully used in provenance interpretation (for a survey of previous debate, see Blatt and Christie, 1963; Conolly, 1965; Blatt, 1967; Folk, 1968). When practical, fifty or 100 quartz grains in the size interval from 0.25 to 0.50 mm (1 to 2 ϕ) were point counted using the following categories:

(i) monocrystalline quartz with less than 5° undulosity[1],

(ii) monocrystalline quartz with greater than 5° undulosity,

(iii) polycrystalline quartz with 2 or 3 crystals per grain,

(iv) polycrystalline quartz with more than 3 crystals per grain.

---

[1]A quartz crystal with non-parallel orientation of its crystallographic axis from one margin to the other will extinguish (darken) in a regular but non-uniform manner as the microscope stage is rotated in cross-polarized light. The angle of undulosity is a measure of the angular rotation of the stage necessary to cause all parts of a crystal to extinguish successively.

Third count

If rock fragments were abundant enough to warrant further study, as many points as practical were counted and categorized as (1) argillaceous fragments with aligned mica flakes (low-grade phyllite), (2) dark brown shale with flattened chert lenses, (3) siliceous mudstone and chert, (4) sandstone or siltstone clasts, (5) carbonate rock fragments, or (6) volcanic rock fragments and detrital chlorite. The most common fragments are described in a subsequent section.

General Petrography and Classification

Tables 6.3, 6.4 and 6.5 present the results of all three point counts. Data are grouped on the basis of estimated "modal" grain size. Comparison of some samples with their corresponding grain-size distribution curves indicates that these visual estimates (including field estimates) correspond to the coarsest quartile of the size distribution. Parameters used in triangular petrographic plots have also been tabulated. In order to standardize descriptions, discussion will focus on medium to coarse samples (0.3 to 0.8 mm). An average composition of medium to coarse Tourelle sandstones is given in Table 6.6.

Table 6.3

Major Component Percentages

Modal Size	0.1 to 0.3 mm												
Sample Number	1	2	3	4	5	6	7	8	9	10	11	12	13
Quartz	39.0	38.5	34.5	28.0	26.5	26.5	38.0	37.0	34.5	34.5	44.5	48.5	40.5
Feldspar	2.5	10.5	3.5	1.0	3.5	2.0	6.0	9.5	8.5	13.5	7.5	10.5	12.5
Rock Frag.	2.0	9.5	6.5	3.0	3.0	5.0	8.5	13.5	7.0	8.0	6.0	7.5	12.5
Matrix	18.5	32.5	46.5	37.0	36.5	48.5	42.0	23.5	26.0	26.5	35.5	13.0	16.5
Calcite Cement	35.5	6.5	3.5	20.0	14.5	14.5	2.0	14.5	22.5	13.5	5.0	19.5	15.5
Large Mica	--	0.5	1.5	9.0	13.5	2.5	2.5	1.5	1.5	2.5	0.5	0.5	2.0
Others	2.5	--	4.0	0.5	2.5	1.0	1.0	0.5	--	1.5	0.5	0.5	0.5
Q	90	66	78	88	80	79	72	62	69	62	77	73	62
F	6	18	7	3	11	6	12	15	17	24	13	16	19
R	4	16	15	9	9	15	16	23	14	14	10	11	19
Comment										←same layer→			

Table 6.3 continued

Modal Size	0.3 to 0.5 mm												
Sample Number	14	15	16	17	18	19	20	21	22	23	24	25	26
Quartz	47.5	46.0	27.5	41.5	47.0	47.0	43.5	48.5	47.0	50.5	47.5	42.5	43.5
Feldspar	8.0	8.5	9.0	7.5	9.5	8.5	10.5	7.5	6.0	9.0	10.0	3.5	11.5
Rock Frag.	12.0	11.5	13.0	17.0	15.0	6.0	9.5	4.0	12.0	14.5	13.0	18.0	16.5
Matrix	26.0	24.0	13.0	8.0	7.0	35.0	11.5	35.0	27.0	18.0	11.0	9.0	7.5
Calcite Cement	5.5	9.0	37.0	26.0	19.5	3.0	23.0	2.5	6.5	7.5	18.0	26.5	20.5
Large Mica	1.0	1.0	--	--	1.0	0.5	0.5	2.0	0.5	--	--	--	--
Others	---	--	--	--	1.0	--	1.5	0.5	1.0	0.5	0.5	--	0.5
Q	70	70	56	63	66	76	69	81	72	68	67	66	61
F	12	13	18	11	13	14	17	13	10	12	15	6	16
R	18	17	26	26	21	10	14	6	18	20	18	28	23
Comment		⊙											

Table 6.3 continued

Modal Size	0.5 to 0.8 mm					greater than 1 mm			
Sample Number	27	28	29	30	31	32	33	34	35
Quartz	46.5	55.0	49.0	51.0	45.0	41.5	22.0	56.0	44.5
Feldspar	6.0	8.5	6.0	7.5	6.5	8.5	4.0	2.0	16.5
Rock Frag.	26.0	7.5	17.0	13.0	16.0	17.5	56.5	25.5	12.5
Matrix	21.0	10.0	7.0	24.5	4.5	29.0	16.0	6.0	7.0
Calcite Cement	0.5	19.0	20.5	3.0	27.5	1.5	1.5	10.5	19.0
Large Mica	--	--	--	0.5	--	2.0	--	--	0.5
Others	--	--	--	0.5	0.5	--	--	--	--
Q	59	77	68	71	67	61	27	67	61
F	8	12	8	11	10	13	5	2	22
R	33	11	24	18	23	26	68	31	17
Comment	X	X	← same layer →			fresh			matrix of conglom.

X - Cross-stratification

Table 6.4

Quartz varieties

Modal size		.1 - .3 mm			.3 - .5 mm								.5 - .8 mm			
Sample number		2	8	11	14	15	16	17	18	20	21	22	23	24	25	26	27
monocryst'n	< 5° undul.	64	60	56	68	60	62	53	72	58	56	58	62	59	65	56	58
	> 5° undul.	24	26	36	25	32	27	29	29	30	34	26	28	29	28	34	24
polycryst'n	2-3 units	4	2	6	4	4	4	16	5	6	8	10	8	4	4	7	16
	> 3 units	8	12	2	3	4	7	2	4	6	2	6	2	8	3	3	2

Table 6.4 continued

Modal size		.5 - .8 mm			> 1 mm		
Sample number		28	29	31	32	34	35
monocryst'n	< 5° undul.	37	46	64	58	51	62
	> 5° undul.	51	37	18	36	35	28
polycryst'n	2-3 units	5	9	16	4	7	7
	> 3 units	7	8	2	2	7	3

Tourelle sandstone samples generally show poor sorting (Chapter V) and a high proportion of matrix (Figure 6.1). Evidence presented in a later section suggests that most sparry calcite "cement" was introduced by replacement of primary matrix and unstable lithic fragments, with the result that the sum of "matrix" and "calcite cement" is approximately constant at 25 to 35% (Table 6.3).

When data from Table 6.3 are plotted on a standard QFR classification diagram, Tourelle sands are seen to be quartz rich (50 to 90% Q) with rock fragments somewhat more abundant than feldspar grains (Figure 6.2). Wacke sandstones (greater than 15% matrix) are more common than arenites.

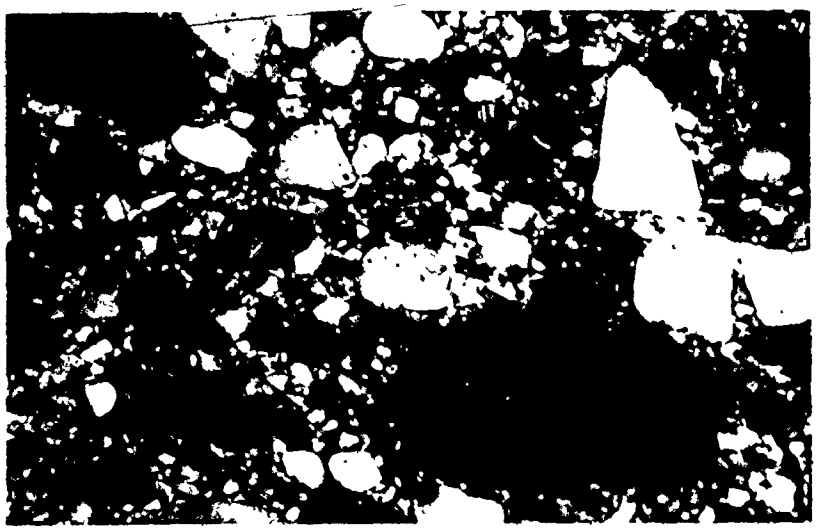

Fig. 6.1. Poorly sorted coarse Tourelle sandstone. Crossed nicols, 45x.

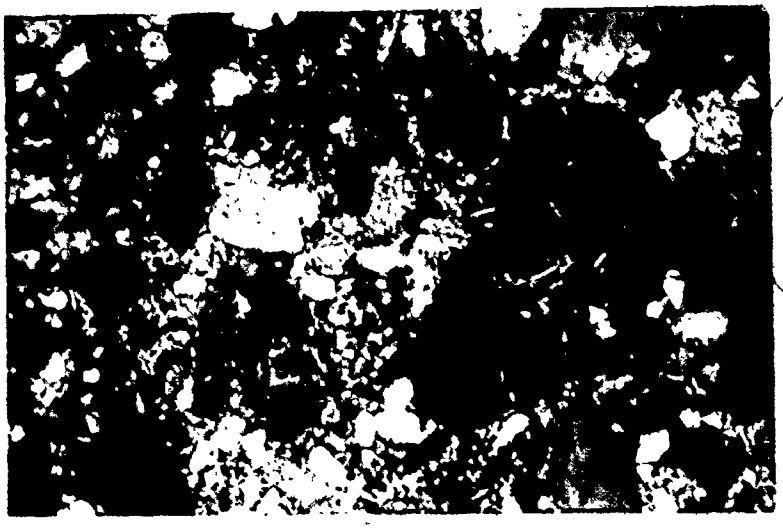

Poorly sorted coarse sandstone. Note large volcanic rock fragment on the right side of the photomicrograph. Other rock fragments are chert and micrite. Crossed nicols, 30x.

Table 6.5

Rock fragment varieties

Modal size	0.1 to 0.3 mm					0.3 to 0.5 mm					
Sample No.	2	5	8	9	11	14	16	17	18	20	23
Shale and low-grade phyllite	32	20	24	35	36	36	18	--	14	10	10
Dark shale	20	60	22	10	18	10	7	5	16	6	20
Chert	32	13	26	50	38	30	50	44	42	34	24
Sandstone and siltst.	8	--	10	--	--	8	4	5	6	12	2
Carbonate grains	--	--	4	5	--	2	3	15	2	8	12
Volcanic grains	8	7	4	--	8	14	18	31	20	30	32
100% Q_p	32.7	--	27.7	--	37.2	21.7	18.9	30.3	22.0	35.5	25.8
100% L_v	5.4	--	2.9	--	4.8	11.0	14.6	21.5	15.6	19.4	23.8
100% L_s	61.9	--	69.4	--	58.0	67.3	66.5	48.2	62.4	45.1	50.4

Table 6.5 continued

Modal size	0.5 to 0.8 mm							>1 mm			
Sample No.	24	25	26	27	28	29	31	32	33	34	35
Shale and low-grade phyllite	38	13	8	9	19	7	10	15	1	5	5
Dark shale	8	14	7	9	23	11	30	15	--	5	1
Chert	24	35	40	61	19	46	28	52	13	49	47
Sandstone and siltst.	8	17	4	6	2	5	10	4	8	10	10
Carbonate grains	2	10	14	7	10	5	6	2	22	4	--
Volcanic grains	20	11	27	8	27	26	16	12	56	27	37
100% Q_p	30.5	14.2	20.9	24.4	46.8	32.9	33.6	16.0	--	23.5	26.3
100% L_v	13.9	9.5	19.8	6.0	14.4	17.4	10.6	10.0	--	20.7	27.3
100% L_s	55.6	76.3	59.3	69.6	38.8	49.7	55.8	74.0	--	55.8	46.4

Table 6.6

Average composition of medium to coarse sands
(0.3 to 0.8 mm)

Component	mean	std. deviation
Quartz	45.6	5.6
Feldspar (+ IRF)	8.2	2.1
Rock fragments	13.4	4.9
Matrix	16.6	9.6
Calcite "cement"	15.3	10.5
Large micas	0.5	0.7
Others	0.4	0.4

Rock fragments can be further subdivided as (i) volcanic fragments, (ii) chert, or (iii) all other sedimentary fragments plus low-grade phyllite.

If we exclude samples that have undergone extensive diagenetic replacement of matrix and rock fragments by calcite (these are discussed in a later section), then all Tourelle samples conform with definitions of greywacke proposed by Geike (1882) and Pettijohn (1954).

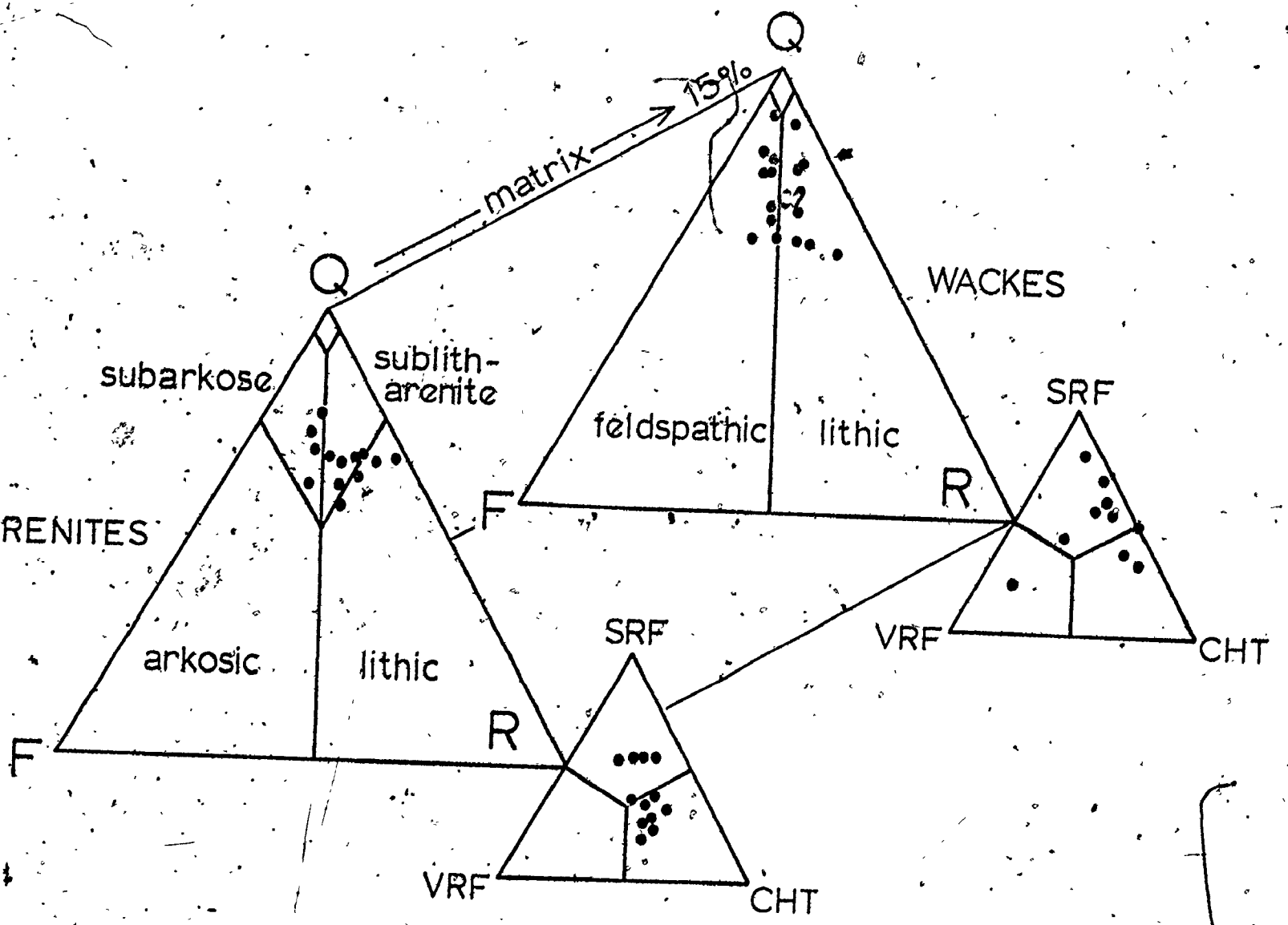

Fig. 6.2. QFR diagram for Tourelle sandstones. Q, quartz; F, feldspar and coarse-grained felsic igneous fragments; R, rock fragments including chert; SRF, sedimentary fragments other than chert; VRF, volcanic rock fragments; CHT, chert and siliceous mudstone.

Quartz

Quartz grains may be angular to very well rounded (see Chapter VII), and are generally monocrystalline with less than 5° of undulosity (Table 6.4). Although most grains are clear and transparent, a few show the presence of fine rutile needles or bubble trains. Abraded quartz overgrowths are extremely rare (Figure 6.3). Three polished thin sections of rounded quartz-grain separates (0 to 1 ϕ), which were studied using cathodo-luminescence petrography (Sipple, 1968), showed no overgrowths. In some coarse-grained samples, quartz grains which are in mutual contact show signs of pressure solution (long and concavo-convex contacts - see section on diagenesis). Quartz grains in calcite-cemented sandstones may be corroded or partially replaced. Silica released by these mechanisms has precipitated as a minor cement component between quartz grains. This cement is in optical continuity with the host quartz grains, but contains bubbles and inclusions which allow it to be recognized. Because authigenic quartz is very minor, it was grouped for point-counting purposes with clastic quartz.

Quartz grains which are distinctive indicators of their original provenance are (i) strongly sutured, polycrystalline grains (metamorphic origin) and (ii) clear β-quartz pseudomorphs (volcanic origin) with or without embayed margins (Figure 6.4). Both varieties are very rare.

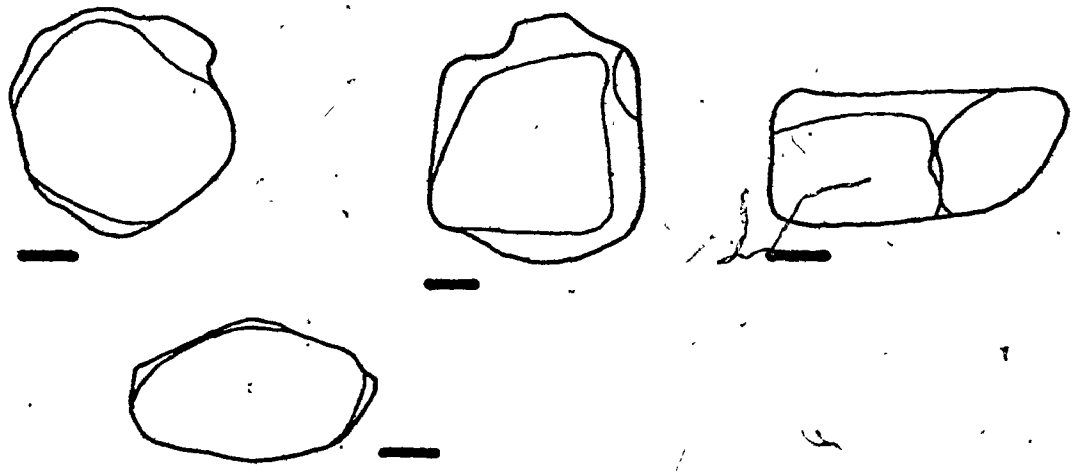

Fig. 6.3. Sketches of quartz grains with abraded quartz overgrowths. Bar scale equals 0.1 mm.

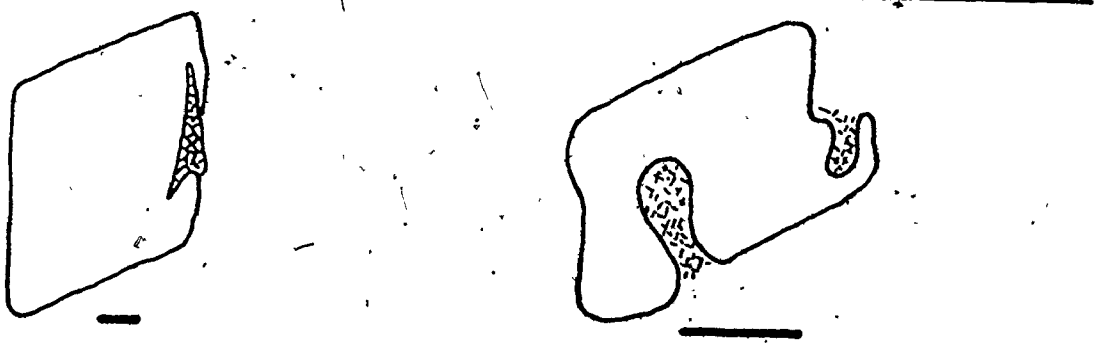

Fig. 6.4. Sketches of volcanic β-quartz pseudomorphs with embayed margins. Bar scale is 0.1 mm.

A plot of quartz varieties (Figure 6.5) on the diagram proposed by Basu and others (1975) indicates that the majority of the quartz (and by inference the Tourelle quartz population) appears to have been initially derived from a middle- and upper-rank metamorphic source area.

Feldspar

Feldspar composition was determined for samples 14, 18, 29 and 34, following staining with sodium cobaltinitrite. Data are tabulated in Table 6.7.

Most perthite has microcline as its K-feldspar component. If this perthite is grouped with other K-feldspar constituents, the ratio of K-feldspar to plagioclase is approximately 2:1.

The following varieties of mono-mineralic feldspar grains were recognized.

(i) Angular fragments of microcline. Grains are generally larger than the mean, and show coarse twinning with individual twin lamellae from 0.05 to 0.10 mm across. (Unless care is taken, therefore, small grains in unstained sections may be falsely identified as twinned plagioclase.) This microcline is very fresh, with little sign of alteration.

(ii) Untwinned orthoclase. These grains have a dusty brownish appearance in plane light, some of which may be due to minute bubbles. Grains are less angular than microcline.

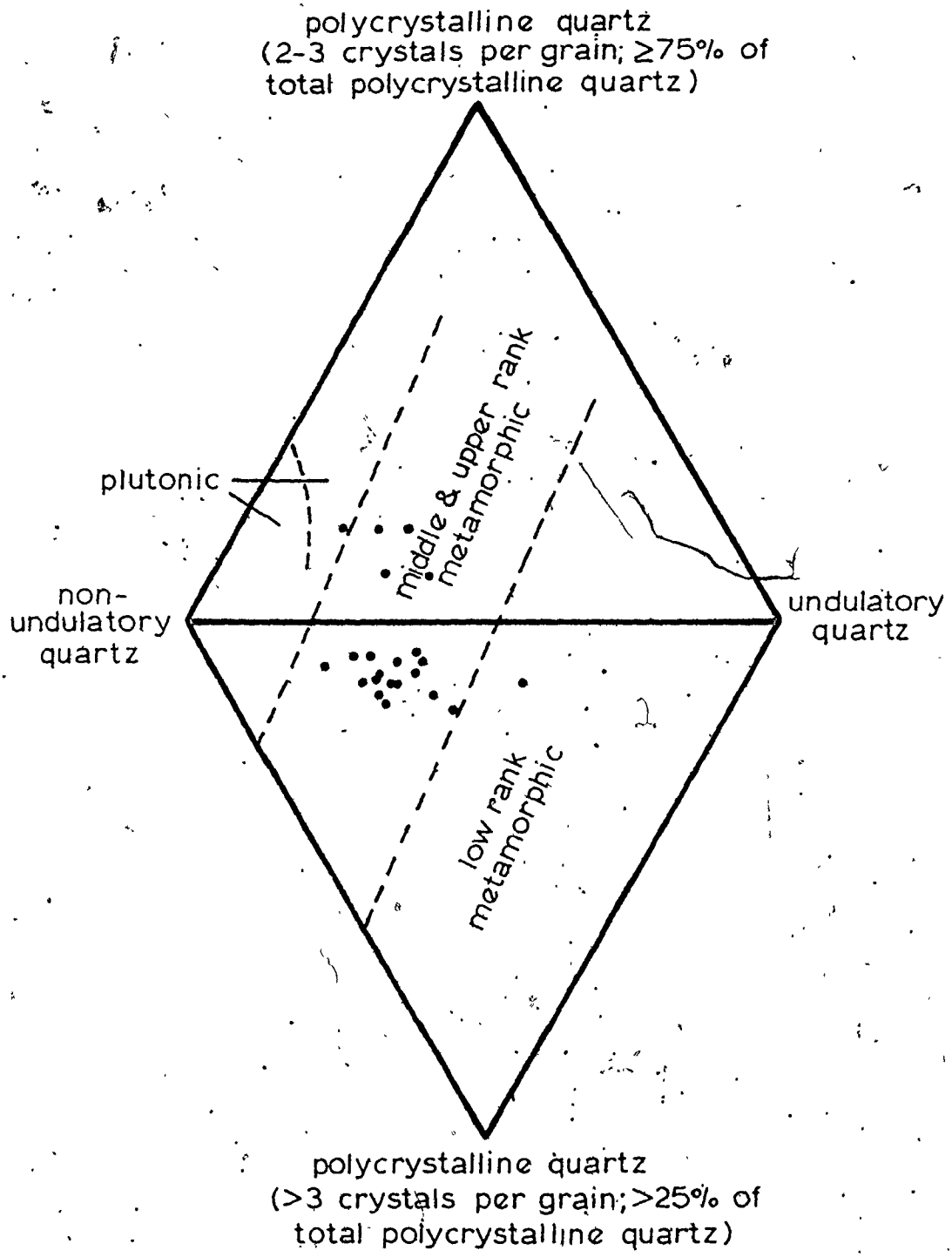

Fig. 6.5. Plot of Tourelle quartz varieties on the diagram proposed by Basu and others (1975). Each point corresponds to a different sample. Primary provenance appears to have been a middle to upper rank metamorphic terrain.

Table 6.7

Composition of Tourelle Formation feldspar fraction (100 pts.)

Sample no.	plagioclase	orthoclase	microcline	perthite
14	41	36	18	5
18	41	29	16	14
29	29	27	25	19
34	37	23	14	26
mean	37.0	28.8	18.3	16.0
std. dev.	5.7	5.4	4.8	8.8

(iii) Calcitized and dusty plagioclase. This plagioclase mode consists of the largest grains (greater than 0.5 mm), which are commonly untwinned and subrounded to rounded.

(iv) Angular twinned plagioclase. Grains are generally from 0.2 to 0.4 mm in diameter and show little if any alteration. Composition of several grains in sample 8, as determined by the Fouque method (Heinrich, 1965), is albite to sodic oligoclase.

Sedimentary Rock Fragments and Low-grade Phyllite

Grains described as low-grade phyllite consist of slightly metamorphosed shale in which muscovite plates (less than 20 microns across) have grown with a parallel to sub-parallel fabric (Figure 6.6a). The more common non-metamorphosed sedimentary rock fragments are described below.

Dark shale clasts (Figure 6.6b)

These angular, commonly tabular grains of coarse sand to granule size (0 to -2 ϕ), are composed of very dark brown (hematitic) mud containing flattened lenses of brownish chert.

Siliceous mudstone and chert (Figures 6.6c,d,e,f)

Only a few observed chert grains were composed of a mosaic of microcrystalline quartz crystals. Instead, fragments are very fine-grained and homogeneous, as are samples from large, bedded-chert blocks enclosed in some sandstone layers (Figures 2.26, 6.6c).

Chert clasts are generally dark brown or dark green in colour. One creamy-white, laminated pebble was observed. Granule- to pebble-sized chert fragments may show fine lamination (Figure 6.6d), and may contain silt-sized quartz

Fig. 6.6. Sedimentary rock fragments (photomicrograph magnifications approximate). See text for descriptions.

(A) Low-grade phyllite with aligned plates of mica. This fragment has been bent around resistant quartz grains. Crossed nicols, x 200.

(B) Dark shale with flattened lenses of chert. Crossed nicols, x 75.

(C) Fine-grained, homogeneous chert fragment. Crossed nicols, x 75.

(D) Laminated chert. Crossed nicols, x 75.

(E) Chert with scattered quartz silt grains. Crossed nicols, x 75.

(F) Chert fragment with quartz-infilled radiolarian tests. Plane light, x 30.

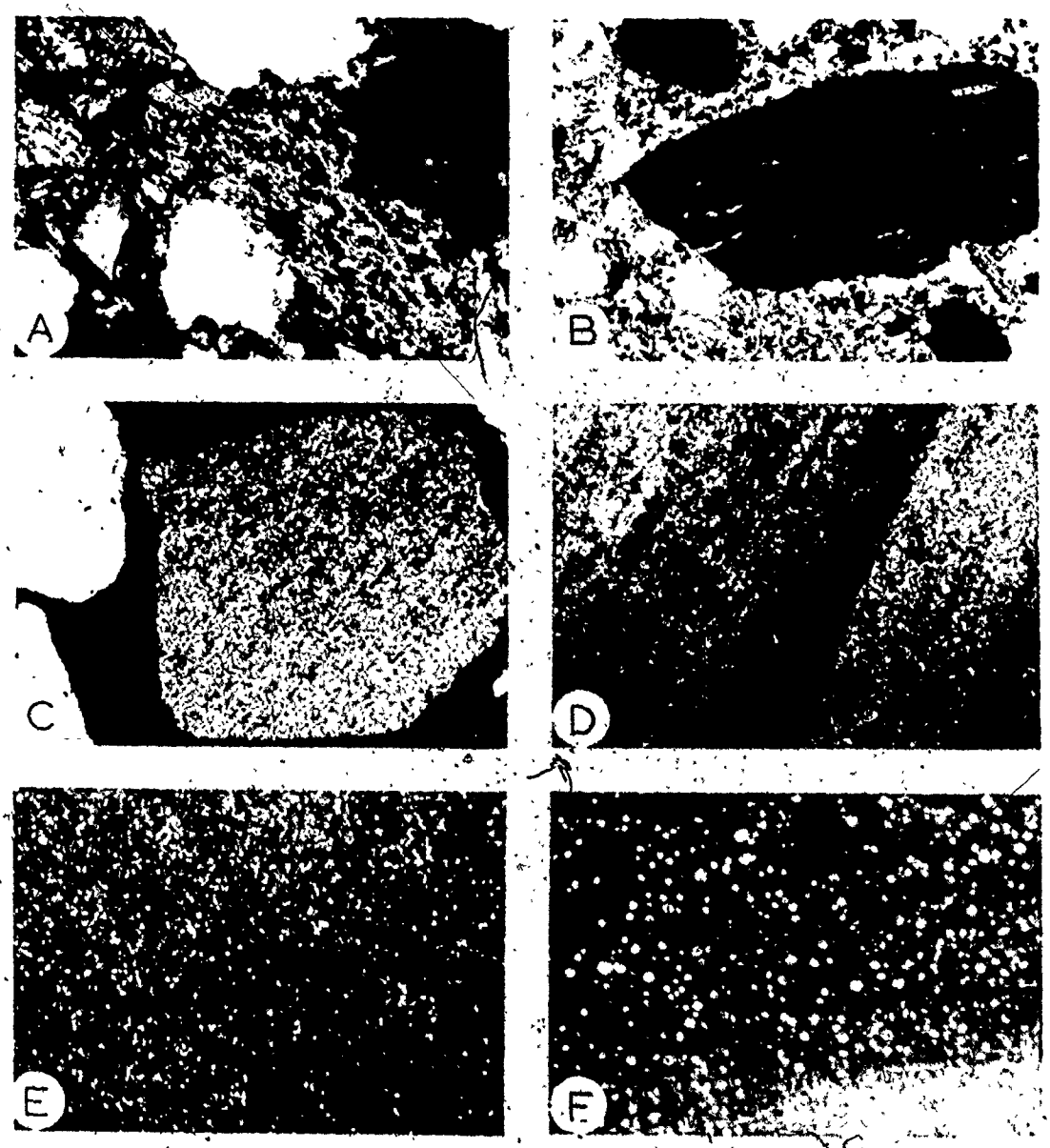

FIG. 6.6

grains (Figure 6.6e) or scattered quartz spheres which have resulted from diagenetic silica infilling of radiolarian tests (Figure 6.6f).

All sand- or granule-sized chert clasts, as well as most pebbles, are very angular. Some dark brown pebbles are rounded.

Carbonate rock fragments

Most carbonate clasts of fine-sand size consist of micrite, and may represent rip-up clasts from fine calcisiltite layers. Many larger fragments, particularly in coarse and granular sandstones, were derived from a contemporaneous carbonate bank margin (Chapter II). These consist of bioclastic debris or elliptical pellets in a micrite matrix (Figure 6.7).

Volcanic Rock Fragments

This detrital component is extremely important in provenance interpretation, because volcanic clasts are not observed in pre-upper Arenig, Ordovician sediments (Lajoie and others, 1974), and because distinctive volcanic associations are characteristic of different tectonic and plate tectonic settings (Carmichael and others, 1974).

Fig. 6.7. Carbonate rock fragments (photomicrograph magnifications approximate).

(A) Bioclastic and pelletal grain with a sparry cement. Crossed nicols, 75x.

(B) Bioclastic and pelletal grain with a micrite matrix. Plane light, 75x.

(C) Pelletal grain. Crossed nicols, 75x.

(D) Homogeneous micrite. Crossed nicols, 200x.

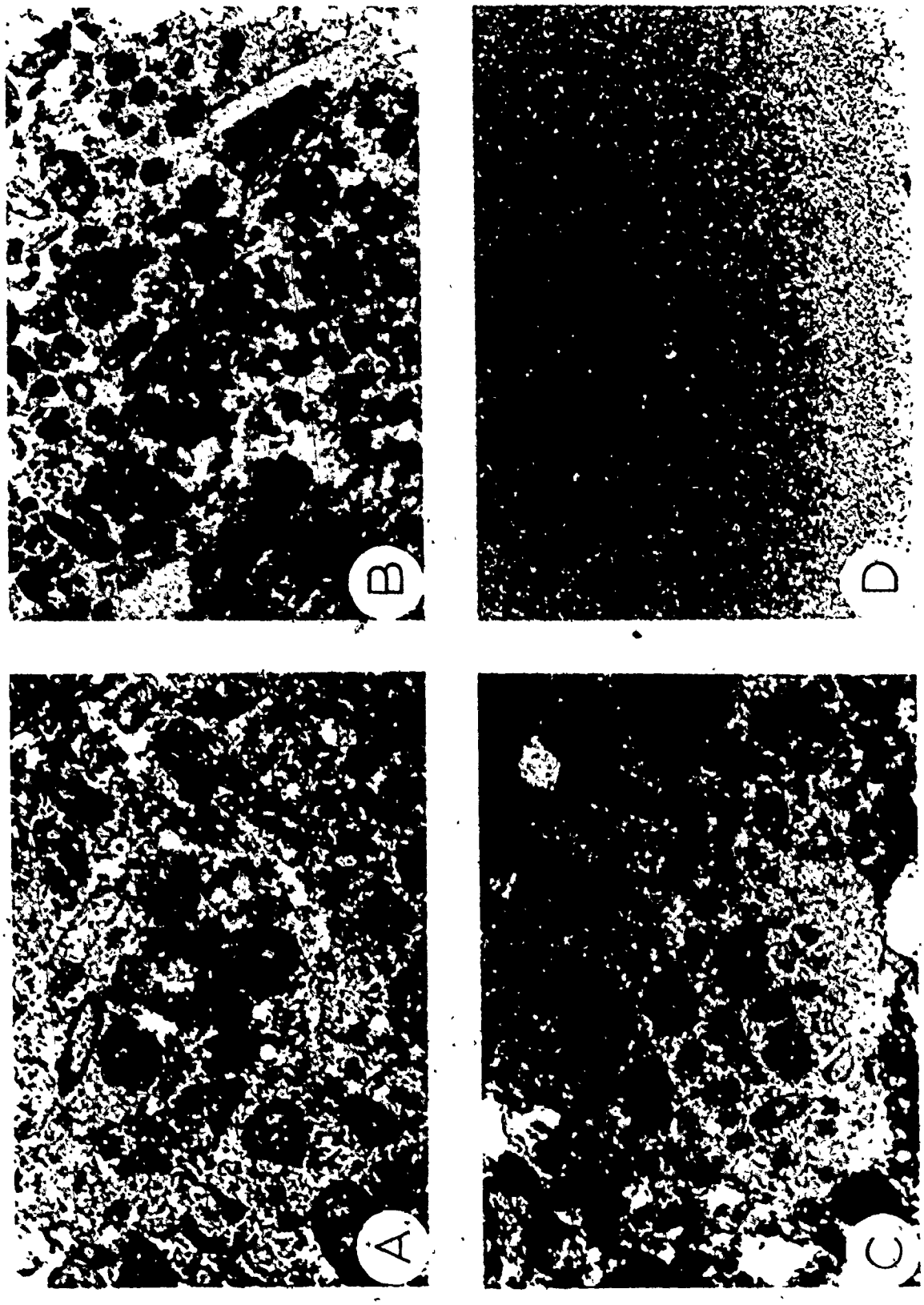

FIG. 6.7

Several friable, granular sandstones from area L were disaggregated (see heavy mineral section) and sieved into various size fractions. Grains of granule size (2 to 4 mm) were hand picked to eliminate composite sandstone particles, mounted in casting resin, and then thin sectioned to allow study of various rock fragments. Grains were counted using the ribbon method (Van der Plas, 1962), which yields number frequencies.

Volcanic fragments comprise 31% of all granule grains, and consist of the following volcanic lithologies.

(i) Spherulitic lavas (Figure 6.8a). Spherules are composed almost entirely of quartz. They are interpreted to result from devitrification of felsic, glassy flows (Smith, 1974).

(ii) Quartz porphyritic flows (Figure 6.8b). The felsic groundmass of some of these fragments strongly resembles microcrystalline quartz (chert).

(iii) Devitrified glass (Figure 6.8c). These clasts are composed of feathery, radiating, brown chlorite sheaves, and may almost be opaque.

(iv) Plagioclase porphyritic flows (Figure 6.8d).

(v) Lathwork grains (Figure 6.8e), which contain plagioclase laths in intergranular and intersertal textures (Dickinson, 1970).

(vi) Microlitic flows (Figure 6.8f).

Fig. 6.8. Volcanic rock fragments (photomicrograph magnifications approximate).

(A) Spherulitic lava formed of quartz and interstitial chlorite. Crossed nicols, x 200.

(B) Quartz porphyritic flow. Embayed β-quartz pseudomorph is set in a groundmass of plagioclase, quartz (?) and chlorite. Crossed nicols, x 200.

(C) Devitrified glass consisting of sheaves of feathery, radiating brown chlorite. Crossed nicols, x 200.

(D) Plagioclase porphyritic flow. Euhedral plagioclase phenocryst in a microcrystalline groundmass of quartz, feldspar, and chlorite. Crossed nicols, x 200.

(E) Lathwork grain with intersertal texture. Disoriented plagioclase laths are set in a groundmass of chlorite and pumpellyite. Crossed nicols, x 200.

(F) Microlitic flow. Crossed nicols, x 200.

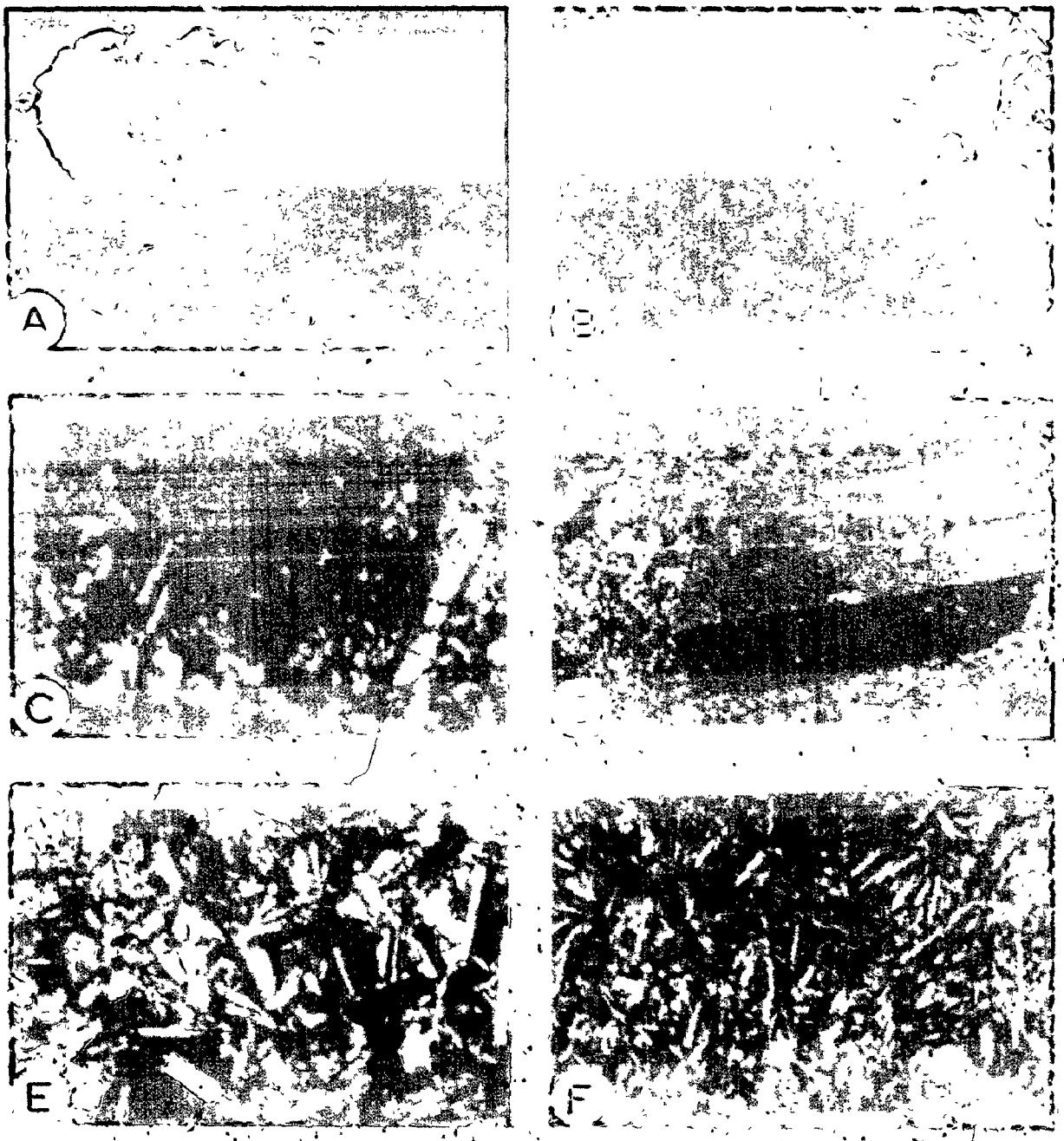

FIG. 6.8

(vii) Pyroclastic (fragmental) grains. Only one tuff fragment was observed to contain relict shard texture. The others were characterized by poor sorting and angular plagioclase crystals.

Table 6.8 shows the results of the grain count of volcanic rock fragments (277 grains), accompanied by an interpretation of the composition of each grain type. These compositions were established on the basis of mineralogy, phenocryst types and abundances, and texture.

The primary mineralogy of some, if not all, volcanic detritus was modified by prehnite-pumpellyite grade metamorphism before the grains were eroded from the source terrain. This conclusion is based on a lack of evidence for burial metamorphism of the Tourelle sandstones. Heavy minerals are observed which are unstable at this grade of metamorphism (see next section). The mineral phases now present in volcanic rock fragments are albite, chlorite, quartz, biotite, sphene, opaques (magnetite?), pumpellyite, calcite, and prehnite. This order is approximately that of decreasing abundance. Chlorite occurs as a groundmass replacement, and as alteration rims around primary biotite flakes and interstitial granular pumpellyite. Pumpellyite occurs in some microlitic or lathwork grains as an interstitial groundmass replacement, or as pseudomorphs after olivine or pyroxene (Figure 6.9). The pumpellyite grains are very iron rich, with brown interiors and dark green margins. Prehnite

Fig. 6.9. Occurrences of pumpellyite (photomicrograph magnifications approximate).

(A) Pumpellyite replacement of primary olivine or pyroxene phenocrysts in a microlitic grain. Bright parts of crystals are brownish; dark parts are chrome green. Crossed nicols, x 500.

(B) Same as (A), but in plane light. Note abundant opaque particles. These are probably magnetite or ilmenite.

(C) Interstitial pumpellyite (dark) in a lathwork grain. Feldspar is the light mineral. Plane light, x 200.

(D) Close-up of (C). Plane light, x 500.

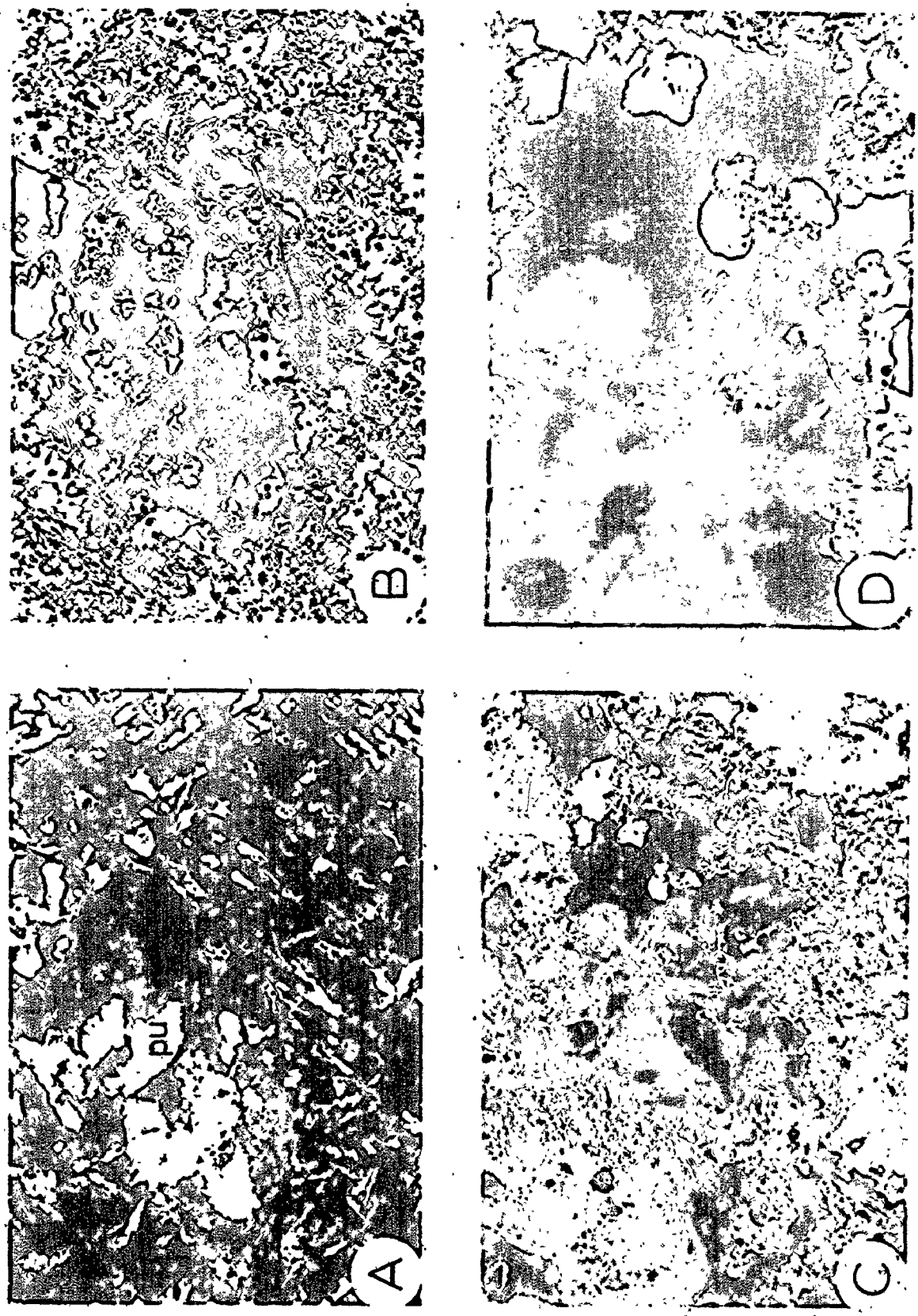

FIG. 6.9

Table 6.8

Volcanic detritus and lithologic interpretation

Description	percent	interpretation
(1) Spherulitic grains	6.1	rhyolite
(2) Quartz porphyritic grains	29.2	dacite/andesite
(3) Devitrified glass	10.8	andesite/basalt
(4) Plagioclase porphyritic grains	15.5	andesite/basalt
(5) Lathwork grains	26.7	basalt
(6) Microlitic grains	10.5	basalt
(7) Pyroclastic grains	1.1	
(a) Rhyolite and dacite	21.1	
(b) Andesite	28.0	
(c) Basalt	50.9	

is not common, but was observed as minute crystal aggregates around the outer rims of quartz spherules (identification by W.T. Jolly, Brock University, St. Catharines, Ontario).

Figure 6.10 is a pressure-temperature diagram showing inferred stability fields of low-grade metamorphic minerals (modified from Seki, 1969; Jolly, 1972, and discussions with W.T. Jolly, 1976). Both p_{H_2O} and p_{CO_2} are assumed constant, since metamorphic reactions are also functions of these variables at constant pressure and temperature (Coombs and others, 1970). The coexistence of iron-rich pumpellyite and prehnite without epidote or actinolite defines a range of burial depths from 1 to 5 km and metamorphic temperatures from 175 to 250°C. Depth of burial may even have been shallower than 1 km, because iron-rich pumpellyite has been found from drill holes in the thermal area of Iceland, in mafic lavas, at a depth of only 100 to 200 m (Sigvaldason, 1962, Figure 200.1). Because all mafic volcanic fragments do not show development of pumpellyite, these depths are maximum estimates.

Detrital Chlorite and Serpentine

These minerals are so minor that they are not considered as separate detrital components. Only a few grains of serpentine have been identified, compared with up to 8% serpentine in some Cloridorme greywackes (Enos, 1969a). Detrital chlorite grains are pale green to blue-green with anomalous interference colours (Berlin blue), and may be well rounded. Opaque

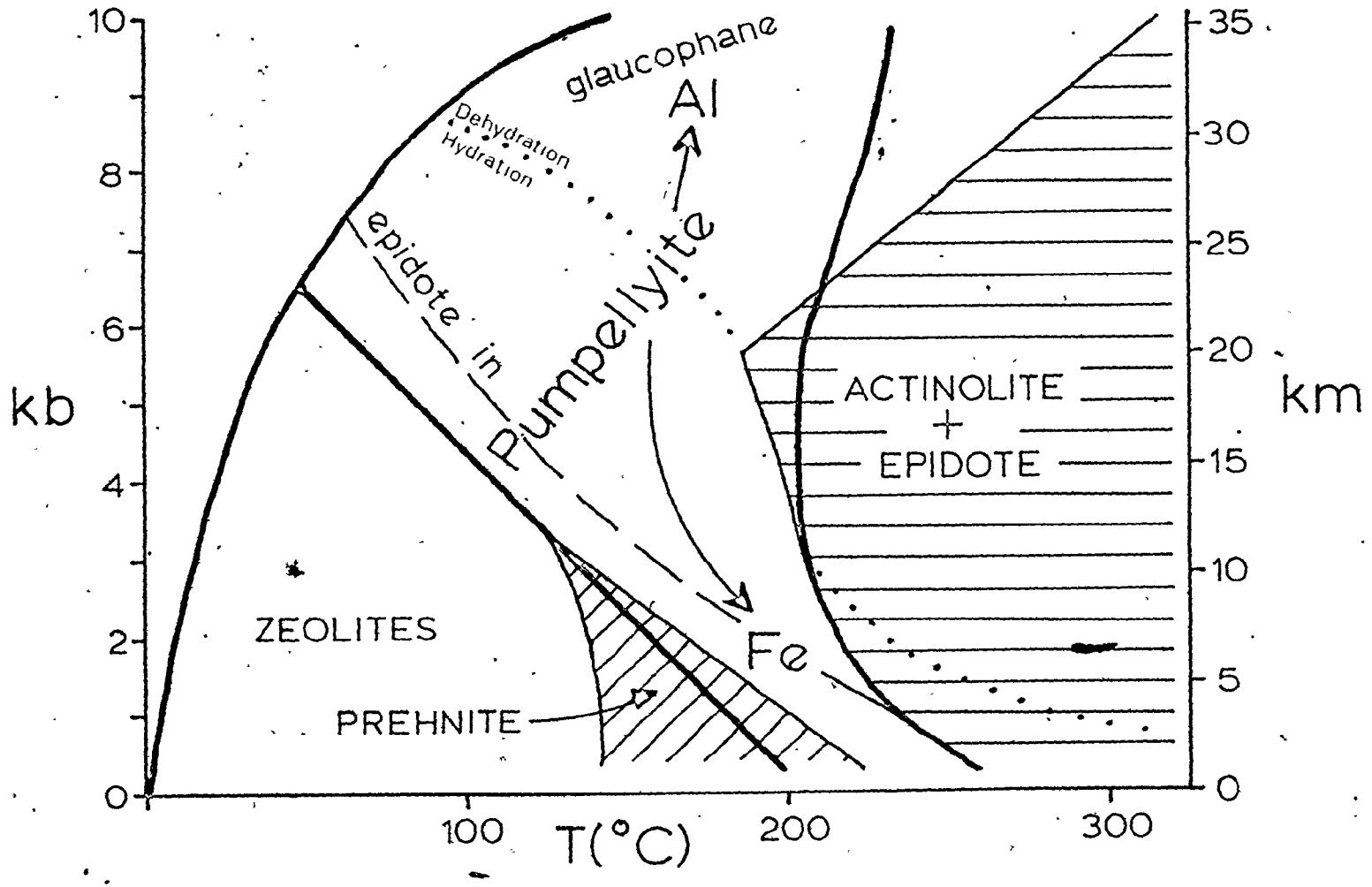

Fig. 6.10. Pressure-temperature stability diagram for low-grade metamorphic minerals, modified from Seki (1969), Jolly (1972), and discussions with W.T. Jolly, 1976.

inclusions are common in some larger grains. Transluscent chromite inclusions, however, were never observed. Chlorite grains were probably derived from amygdules in basaltic rock fragments (chlorite-filled amygdules have been observed), and are therefore grouped with volcanic rock fragments. Rare large grains identified as chlorite may in fact be serpentine, as they strongly resemble serpentine fragments in Cloridorme thin sections.

Heavy Minerals

The study of heavy minerals (SG greater than 2.97) is a well established petrographic technique (for reviews see Sindowski, 1949; Pettijohn and others, 1972; Füchtbauer, 1974). These accessory minerals commonly form less than 1% of a sandstone sample, but are very diagnostic of particular source terrains (Milner, 1926; Krumbein and Pettijohn, 1938, p. 463; Feo-Codecido, 1956). Even in mature quartz arenites that contain no distinctive major components for provenance evaluation, heavy mineral studies can yield valuable information on primary source area (Hubert, 1962).

Eleven coarse to granular Tourelle sandstones[1] were

[1]Sample distribution is: area A - 1, area D - 2, area G - 1, area K - 1, area L - 6.

disaggregated using 10% HCl and gentle crushing with a porcelain mortar and pestle. Disaggregation was not complete due to tenacious matrix binding. These samples were sieved to separate the 2 to 3 ϕ (0.250 to 0.125 mm) size fraction. The heavy mineral species were then separated by settling in a separatory funnel containing tetrabromoethane (density 2.97 gm/cm^3). A strong permanent magnet was used to separate magnetic grains (magnetite and ilmenite) before further processing. Table 6.9 presents data on the abundance of heavy minerals in each 2 to 3 ϕ fraction (note that sample numbers are not the same as those used for thin sections). Samples 1 to 3 come from carbonate concretions. Sample 4 comes from a well-sorted, calcite-cemented, cross-stratified unit.

Heavy mineral separates were mounted with cover slips in Canada Balsam (refractive index 1.54) on standard petrographic microscope slides. Rigorous splitting techniques were not employed, since the relative abundances of different mineral species, rather than their absolute proportions, are of foremost interest. Grains were counted using the ribbon method (Van der Plas, 1962). The non-micaceous mineral species are described below, within the stability framework proposed by Pettijohn and others (1972).

Table 6.9

Heavy mineral abundances in 2 ϕ to 3 ϕ size fractions

Sample	percent heavies	percent non-magnetic heavies
1	1.114	1.107
2	0.319	0.316
3	1.029	1.021
4	0.411	0.402
5	0.890	0.881
6	0.855	0.818
7	0.368	0.365
8	1.033	0.988
9	2.266	2.135
10	1.095	1.074
11	0.989	0.954

Ultrastable group

(i) Rutile: orange-yellow to yellow-red pleochroism, "metallic" surface, closely spaced polysynthetic twins, very high relief, subrounded (Figure 6.11a).

(ii) Zircon (ZIRC): prismatic to spherical, rounded grains, slight orange to bluish tinge, may be quite dark and strongly zoned, high relief (Figure 6.11b,c).

(iii) Tourmaline (TOUR): pleochroic from pale yellow (10YR 7/4) to black or very dark brown, negative elongation, may have closely spaced striations, very well rounded (Figure 6.11d).

Moderately stable group

(iv) Epidote group (EPID): includes both epidote and zoisite. Epidote (Figure 6.11e) shows characteristic pale olive green colour (pleochroic from light 10Y 5/4 to 10Y 6/6, or from light brown to pale green), pebbly surface due to high relief, high order interference colours or anomalous Berlin-blue interference. Zoisite (Figure 6.11f) occurs in platy grains showing cleavage and high first-order to low second-order interference colours. These may be rounded or have ragged edges, and commonly contain inclusions. Zoisite is biaxial positive (2V approximately 40°). Epidote group minerals may be highly altered, tattered, and corroded.

(v) Rounded garnet (PGNT): isotropic, well rounded (a few grains have ragged or broken edges), pale pink (pale 10R 6/6), high relief, contains bubble inclusions (Figure 6.11g).

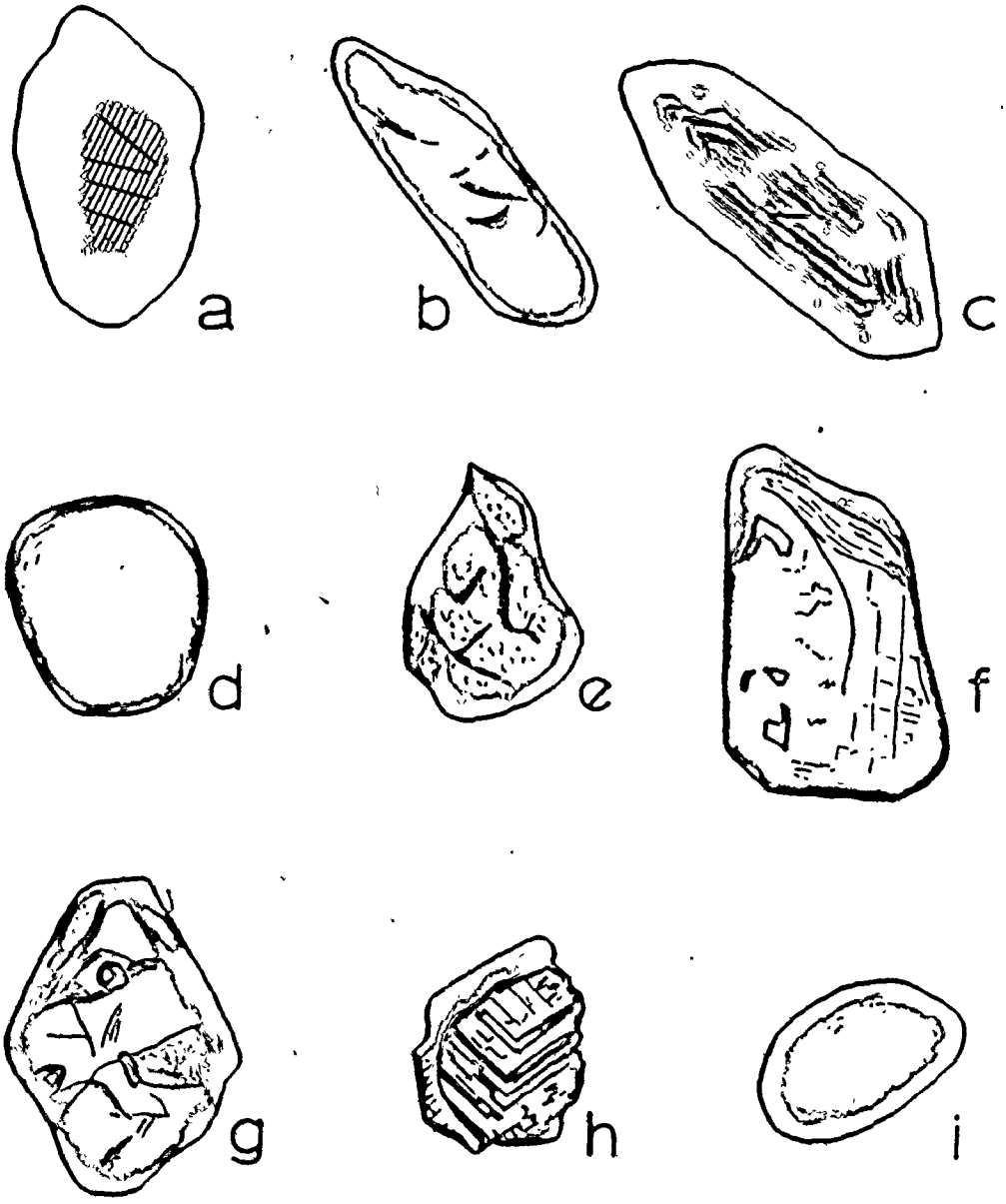

Fig. 6.11. Sketches of representative heavy mineral grains from Tourelle 2ϕ to 3ϕ size fractions. a, rutile; b, rounded zircon; c, rare dark zoned zircon; d, tourmaline; e, epidote; f, zoisite; g, rounded garnet (PGNT); h, etched and overgrown garnet (OGNT); i, honey-coloured sphene.

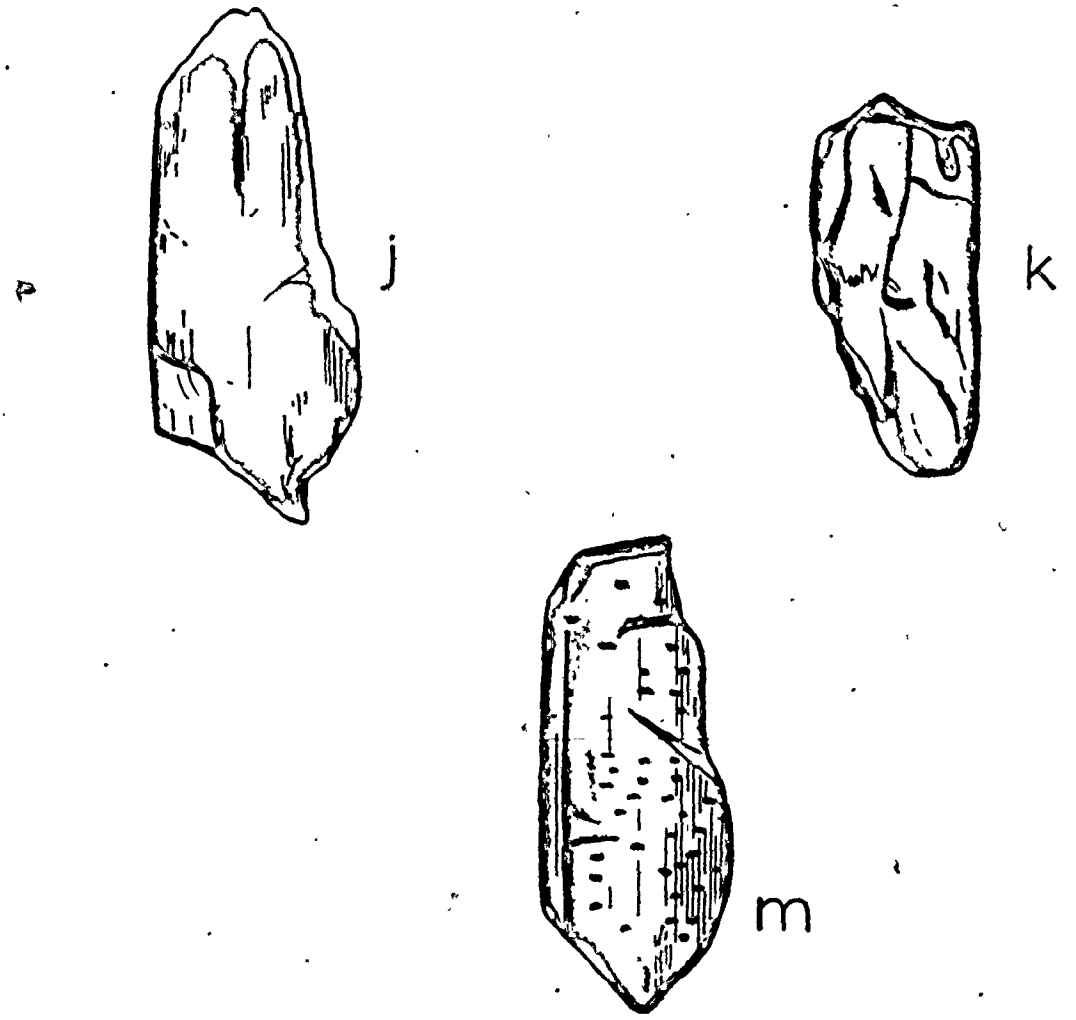

Fig. 6.11 continued. j, hornblende; k, clinopyroxene (augite); m, hypersthene (bronzite).

(vi) Overgrown and etched garnets (OGNT): very pale pink with sharply defined isometric crystal overgrowths which are interpreted as authigenic (Simpson, 1976), may have irregular etched surfaces, isotropic (Figure 6.11h).

(vii) Sphene: very high relief, may be very dark with masked interference colours, or honey-coloured with extremely high orders, very well rounded, particularly honey-coloured variety (Figure 6.11i).

Unstable group

(viii) Hornblende (HBLD): prismatic crystals with minor rounding, strongly pleochroic in greens (10GY 5/2 to 10GY 4/4) and bluish-green, may show cleavage, z against c = 20 to 28°. These grains may be strongly altered, particularly to chlorite (Figure 6.11j):

(ix) Basaltic (brown) hornblende (BHLD): prismatic crystals as above (both may occur as stubby fragments), pleochroic from brown-green (5Y 4/4) to green (10GY 4/4), z against c = 5 to 6°.

(x) Clinopyroxene (CPRX): commonly augite, prismatic green crystals (10GY 4/4), z against c = 35° (Figure 6.11k).

(xi) Hypersthene (HYPN): distinctive reddish-pink (10R 4/6) to green (10GY 4/4) pleochroism, prismatic form, positive elongation, parallel extinction, regularly

arranged platy inclusions characteristic of the variety bronzite (Figure 6.11m).

(xii) Enstatite (ENST): as hypersthene, but colourless and containing no inclusions.

A heavy mineral species of great importance is chromite, which occurs both as opaque grains and as dark cherry-red (5R 3/4), angular, translucent particles. In polished section, these grains are metallic with moderate reflectivity. Translucent chromites possess a Vickers microhardness of 1132 ± 101 (one standard deviation, 10 grains), whereas opaque grains with the same reflectivity have a microhardness of 1170 ± 107 (7 grains). McLeod and Chamberlain (1969) report Vickers microhardness of chromite as 1036 to 1600, in excellent agreement with these results.

Electron microprobe analyses of cherry-red and opaque grains identical to those described above indicate that they are indeed chromite (Table 6.10). Totals are less than 100% because all iron is expressed as FeO.

Heavy mineral data

Table 6.11 presents the results of grain counts for heavy mineral samples 1 to 11. Rutile is not included because only a few grains were observed. Micas, limonitic debris (isotropic) and unknowns (less than 2.0%) are also omitted.

Table 6.10

Electron microprobe analysis[1] of chromite grains in polished thin section

Grain descriptions	cherry-red, translucent	very deep red	near-opaque with reddish rim	opaque
No. of grains	3	2	1	1
SiO_2	0.1	tr	tr	tr
TiO_2	0.1	tr	0.1	tr
Al_2O_3	7.7	14.2	10.0	22.3
Cr_2O_3	60.2	52.2	54.3	45.1
FeO (Fe_T)	19.3	20.4	22.4	16.1
MnO	0.3	0.2	0.3	tr
MgO	9.9	10.4	9.9	13.2
CaO	0.0	0.0	tr	tr
Total	97.6	97.4	97.0	96.7

[1]Analyst: A. Thompson, Memorial Univ., St. John's, Newfoundland, Canada.

Table 6.11

Non-opaque heavy mineral percentages

Sample number	1*	2*	3*	4*	5	6	7	8	9	10	11
No. of grains	291	241	243	282	344	267	257	397	452	314	630
ZIRC	6.2	6.4	6.7	11.1	10.1	18.4	9.2	4.0	3.1	5.2	4.5
TOUR	1.0	5.1	tr	3.2	1.2	2.6	3.1	tr	tr	2.6	tr
EPID	49.3	20.0	42.1	18.6	35.6	40.1	42.7	31.0	26.3	46.5	37.6
PGNT	1.0	6.4	1.3	1.4	6.1	4.7	2.7	18.6	17.9	6.8	8.7
OGNT	29.3	23.7	32.5	44.3	28.4	24.7	27.7	7.8	1.3	11.1	17.7
SPHENE	1.7	1.7	tr	2.5	3.5	2.6	2.7	1.5	2.2	1.6	1.1
HBLD	2.8	20.8	5.9	8.6	6.7	3.0	4.9	12.6	21.4	14.9	14.2
BHLD	1.4	4.7	1.7	2.9	1.2	---	tr	12.6	14.8	2.9	6.4
CPRX	---	tr	tr	---	tr	tr	tr	5.0	1.8	tr	1.8
HYPN	---	---	tr	---	tr	---	tr	3.5	5.1	1.9	2.9
ENST	---	---	tr	---	---	---	tr	tr	---	---	1.3
CHROMITE	7.2	11.0	5.8	7.9	6.4	4.1	5.0	2.5	1.5	6.5	2.9
% heavies[1]	0.25	0.24	0.27	0.11	0.40	0.15	0.12	0.52	1.13	0.32	0.45
unstable group	4.2	26.0	10.3	11.5	8.9	4.0	6.9	34.0	43.1	20.0	26.6
OGNT/PGNT	28.3	3.7	26.0	31.0	4.7	6.6	10.3	0.42	0.07	1.6	2.0
% opaques (100 pts)	68	55	63	60	49	76	51	43	42	62	51

* concretions or calcite cemented.

[1] This is the approximate weight percent of the 2ϕ to 3ϕ size fraction represented by the heavy mineral species in this table.

The following trends can be observed from low to high sample numbers:

(i) a decrease in ZIRC,

(ii) an increase in unstable group components, particularly pyroxenes,

(iii) a decrease in the ratio of overgrown (and etched) to rounded garnets (OGNT/PGNT).

In a heavy mineral suite that is being depleted in unstable minerals by chemical breakdown, we would expect zircon (ultrastable) to remain constant as a percentage of the total rock sample, but to increase in relative abundance in the heavy mineral suite. Figure 6.12 is a plot of ZIRC (mineral percent in the heavy fraction) against the weight percent of heavies in each sample (see footnote, Table 6.11). It is also possible, if we assume grain percentages approximately equal to weight percentages, to convert ZIRC to the weight percent zircon in each 2 to 3 ϕ fraction, and to plot this variable against the weight percent heavies (Figure 6.13).

It is apparent that ZIRC increases as weight percent heavies decreases, in agreement with the model for chemical removal of unstable species proposed above. If this were the result of intrastratal solution (Pettijohn, 1941), we would expect weight percent zircon to remain approximately constant (assuming similar sediment source and depositional mechanism) regardless of the abundance of heavy minerals in

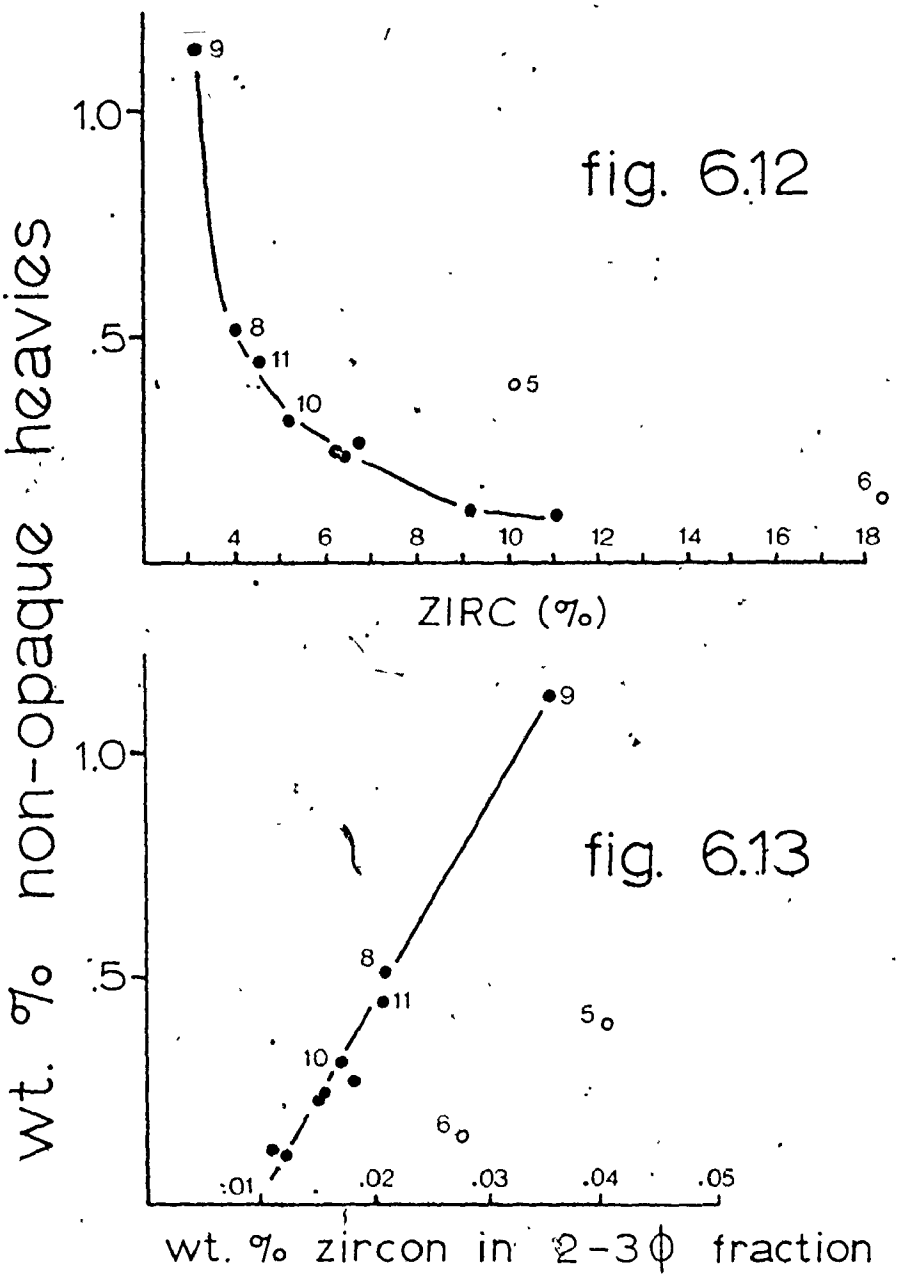

Fig. 6.12. Plot of ZIRC against weight percent heavies.

Fig. 6.13. Plot of weight percent zircon against weight percent heavies.

Samples 5 and 6 have anomalously high zircon contents. The least altered samples (8 to 11) are also numbered. Best-fit curves are based on black dots only.

the sandstone. This is not the case (Figure 6.13). Samples with a higher weight percent heavies also have a higher weight percent zircon. Because etching or corrosion of zircons was never observed, it is concluded that (i) no zircon was removed with unstable heavy species, and (ii) the increase in ZIRC in samples depleted in unstable heavies is a source area effect. Therefore post-depositional intrastratal solution was not the major mechanism for removal of unstable mineral species.

As ZIRC increases, the percentage of unstable heavies decreases (Figure 6.14), indicating that these are the minerals which were removed from the heavy fraction.

Garnets are particularly useful as indicators of chemical attack. The coexistence of both etched and overgrown grains with rounded fresh garnets in separates from the same sample constitutes evidence for chemical alteration before deposition of the Tourelle sandstones. As expected, the ratio OGNT/PGNT increases with progressive depletion of unstable species (Figure 6.15). Samples from concretions and a calcite-cemented, cross-stratified sample deviate from this trend, suggesting that in situ etching of garnets did occur in conjunction with local calcite cementation.

The data presented above lead to the following conclusions.

(i) Depletion of unstable components has not been a result of intrastratal solution.

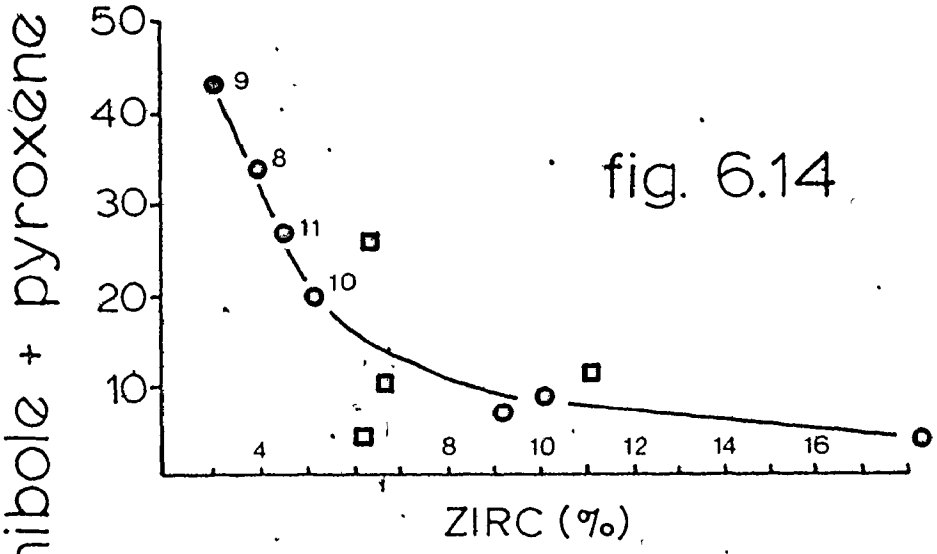

fig. 6.14

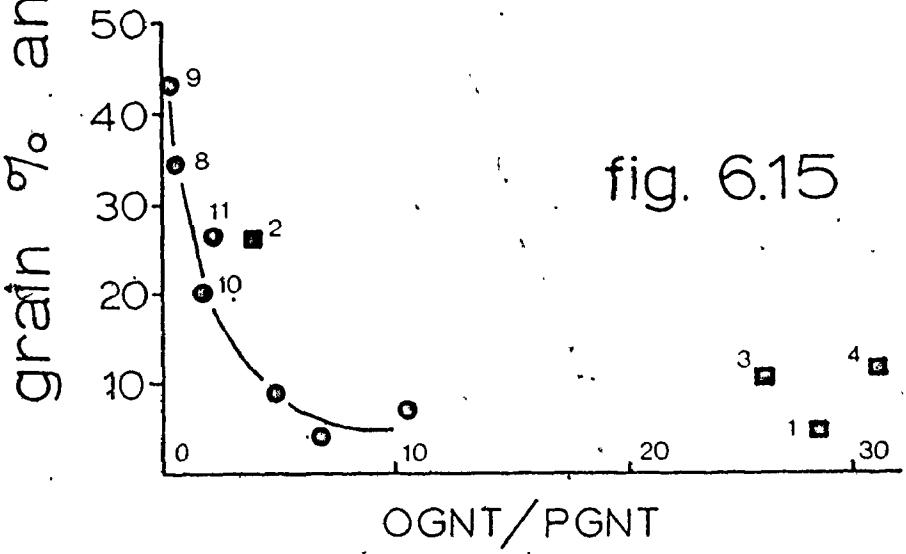

fig. 6.15

Fig. 6.14. Plot of ZIRC against percent amphibole and pyroxene grains.

Fig. 6.15. Plot of OGNT/PGNT against percent amphibole and pyroxene grains.

Best-fit curves are based on solid dots only. Solid squares correspond to calcite-cemented samples, including concretions.

(ii) Etching of garnets and elimination of some unstable minerals has taken place during carbonate cementation. For this reason, carbonate concretions are not the most suitable samples for heavy mineral studies. This conclusion differs from results of Bramlette (1941), Weyl and Werner (1951) and Ojakangas (1968), who found heavy minerals best preserved in samples which underwent early carbonate cementation.

(iii) The heavy mineral assemblages present in Tourelle sandstones are the result of mixing of two populations, one being depleted in unstable minerals and possessing etched and overgrown garnets, and the other containing an abundance of unstable mineral species, particularly amphiboles and pyroxenes. The fact that these end-members contain the same mineral species suggests that the two populations were derived from the same (or a similar) source terrain, with one population undergoing much more severe chemical weathering than the other.

(iv) Provenance interpretations should be based only on the least altered heavy mineral assemblage (samples 8, 9, 10 and 11). The mean percentages of mineral species in these samples are given in Table 6.12.

Table 6.12

Mean percentages for least-altered heavy mineral samples

Ultrastable group	
ZIRC	4.2
TOUR	0.7
Moderately stable group	
EPID	35.4
GRNT[1]	22.5
SPHENE	1.6
Unstable group	
HBLD	15.8
BHLD	9.2
CPRX	2.2
HYPN	3.4
ENST	0.3
Oxides	
CHROMITE	3.4

[1]Total garnet

Sandstone Diagenesis

Diagenetic changes in Tourelle sands have been limited to four processes:

(i) precipitation of calcite, both as pore-filling cement and as a replacement of detrital components,

(ii) compression of lithic fragments to form a pseudomatrix, particularly in fine-grained samples,

(iii) pressure solution of quartz grains and formation of syntaxial quartz overgrowths in optical continuity with primary particles,

(iv) replacement of primary matrix and unstable grains by pasty authigenic chlorite.

Calcite cementation

The post-depositional introduction of carbonate cement occurred very early. Calcite cementation is most important in (i) well-sorted cross-stratified units, (ii) fluid-escape pillars, and (iii) elliptical concretions and cementation bands. Individual concretions may be scoured into by subsequent currents (Figure 6.16), indicating that they formed just below the sediment-water interface. Concretions may

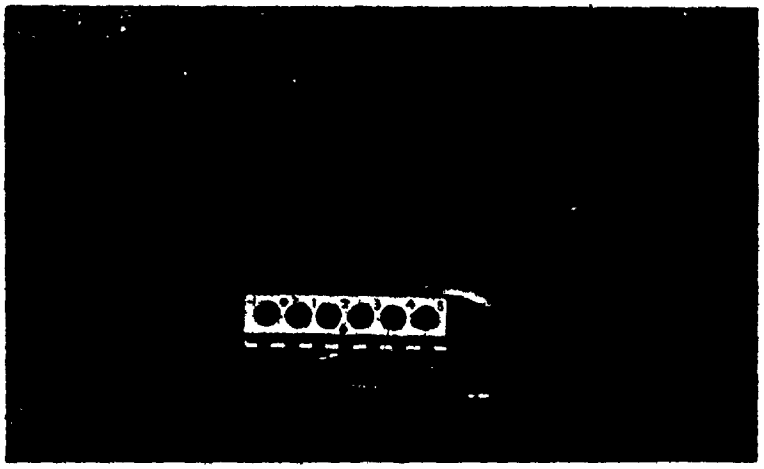

Fig. 6.16. Partially scoured cannonball concretion, area L. Scale 15 cm.

Fig. 6.17. Concretion conglomerate with granular sand matrix, area G. The conglomerate lies above an amalgamation surface. Scale 15 cm.

also form a gravel division at the base of thick sandstones (6) (areas E, G), suggesting that they had already formed in otherwise unconsolidated sand prior to being exhumed and resedimented (Figure 6.17). These basal gravels may have been winnowed from channel sands by later currents, producing a lag gravel, or deposited along with sand derived from a higher level in the submarine fan system. The latter mechanism was suggested by Osborne (1953) for similar concretion conglomerates in the Cambrian Charny Formation at Quebec City. Osborne proposed resedimentation of concretions due to lack of a local source (interbedded sandstones did not contain concretions). The presence of clast imbrication and a sand matrix identical in grain size to the overlying sandstone layer also suggest resedimentation of the Tourelle concretions. The sizes of the arenaceous clasts in the concretion conglomerates are substantially smaller than the sizes of in situ concretions, which may be the result of size sorting (competence - see Chapter V), abrasion, or incomplete concretion growth at the time of gravel emplacement.

In the case of both well-sorted, cross-stratified units and fluid-escape pillars, it is believed that calcite was precipitated as a void-filling cement, because there is reason to believe that original porosity was high. This assumption cannot be made for concretion samples. In all three occurrences of carbonate cementation, however, calcite

is seen to have vigorously replaced chert, volcanic rock fragments and untwinned feldspar. Less commonly, partially replaced quartz grains are observed. Unstable heavy minerals are generally depleted in concretions, and garnets have etched surfaces. In some calcite-cemented samples, the cement is noticeably dirty and chloritic, suggesting that it may have replaced primary matrix. This conclusion is in agreement with analytical evidence for carbonate replacement of primary matrix in concretions compiled by Chevalier and others (1975), and Chevalier (1976) for similar deep-water sandstones in the Cap Enragé Formation at St-Fabien, Quebec.

There appear to be two possible sources for carbonate cement. The sandstones contain a minor carbonate rock fragment component. Some of these fragments may have dissolved to allow local precipitation of calcite. This mechanism, however, would seem to be inadequate to account for the observed amount of cement.

The most likely source of carbonate is the calcareous silty shale which is interbedded with Tourelle sandstones. Even in amalgamated sandstone packets, each layer would have originally been covered by a blanket of this material. Cementation was nucleated in coarse sandstones either by a dark shale rip-up clast, or by fine sub-divisions in horizontal stratification (producing cementation bands). Both of these sites were likely enriched in organic matter.

Formation of pseudomatrix

Pseudomatrix (Dickinson, 1970) is produced during compaction of sandstones containing easily-deformed lithic fragments. These grains are compressed and squeezed into pore space between adjacent resistant clasts. The squashed rock fragments can commonly be recognized, however, because they retain their primary colouration and internal homogeneity.

Examination of Tourelle sandstones shows that compression of fine lithic fragments was an important means of pore-space reduction in some fine-grained samples. These fragments can still be recognized in plane light. Large rock fragments appear to be undeformed.

Pressure solution and quartz overgrowths

As noted in an earlier section, quartz grains in contact with one another may exhibit concavo-convex, and/or long grain contacts (Taylor, 1950). This texture is commonly interpreted to be the result of pressure solution (Weyl, 1959; Siever, 1962), although Sibley and Blatt (1976) showed that long and sutured grain boundaries in the Tuscarora orthoquartzite are commonly the result of quartz overgrowths (visible only with luminoscope), and not pressure solution. In Tourelle samples, minor amounts of authigenic quartz,

containing inclusions and bubbles, have precipitated between quartz grains, thus cementing them together. This authigenic quartz is in optical continuity with detrital quartz, and may also rim chert grains. Calcite cement or replacement, where present, must have formed after quartz overgrowths. Early calcite cementation within carbonate concretions has already been demonstrated. The above observations, however, require growth of calcite in non-concretion samples at a later time, after burial to depths necessary to induce pressure solution of quartz (2500 to 5000 m, Pettijohn and others, 1972). This requirement is removed, however, if an additional source of authigenic silica can be found. Perhaps silica liberated during concretion formation and detrital grain replacement was precipitated in adjacent sands not subjected to intense carbonate cementation. This mechanism would provide a temporal link between concretion formation and production of authigenic syntaxial quartz overgrowths in some coarse-grained sandstones.

Formation of authigenic chlorite and the matrix problem

All phyllosilicate matrix is composed of pasty authigenic chlorite with anomalous interference colours. Similar chloritic matter in turbidite sands has been variously interpreted as a recrystallization product of primary clay matrix

(e.g. Chevalier, 1976), or as the product of diagenetic breakdown of unstable feldspars and lithic fragments (Cummins, 1962). A common argument used by proponents of diagenetic matrix is derived from the observation that modern deep-sea sands have little matrix and are remarkably well sorted (Cummins, 1962; Hollister and Heezen, 1964). If these modern sands are analogous to ancient greywackes, then the greywacke matrix must be diagenetic. Also, Kuenen (1966) determined experimentally that only 10% lutite matrix can be expected in coarse turbidite sands. These arguments are undermined, however, by the discovery of up to 20% primary detrital matrix (mostly clay) in medium to coarse massive sands from Deep Sea Drilling Project sites 240 and 248 (Moore, 1974). It will be argued below that petrographic evidence from Tourelle sandstones is consistent with an initial matrix content of 10 to 15%, which has since recrystallized to chlorite. The remaining authigenic chlorite (about 10%) may be a product of breakdown of unstable feldspars and lithic grains.

In order to chose between the two alternatives of (i) primary detrital matrix, and (ii) diagenetic matrix (Cummins, 1962), we must examine the implications of both models.

If matrix was primary, and if all void space not filled originally with matrix was then filled with calcite cement, we would expect (i) a negative correlation between cement

and matrix, (ii) strong calcite cementation in sands which had high initial porosity, (iii) some replacement of matrix and detrital grains by calcite in concretions, and (iv) an identical framework composition in all samples of similar grain size (assuming a well-mixed source of framework grains), regardless of matrix content.

If, however, all sands were initially quite well sorted, and contained unstable framework grains (volcanic rock fragments, feldspar) which were diagenetically altered to form matrix, we would expect (i) a negative correlation between cement and matrix, because the presence of an early void-filling cement would inhibit solution of unstable components and growth of a diagenetic matrix, (ii) widespread (though not necessarily abundant) calcite cementation in sands other than those which were most porous, (iii) outward growth of concretions, not by replacement, but by filling of available porosity, and (iv) depletion of unstable fragments in sands which are now rich in matrix.

Both models require a negative correlation between percent matrix and percent cement. Such a relationship exists (Figure 6.18), particularly for sandstones with estimated modal size less than 0.3 mm. Finer samples lie above the regression line because of the arbitrary assignment of all grains smaller than 0.03 mm in size to "matrix". The slope of the regression line is not -1.0, as would be

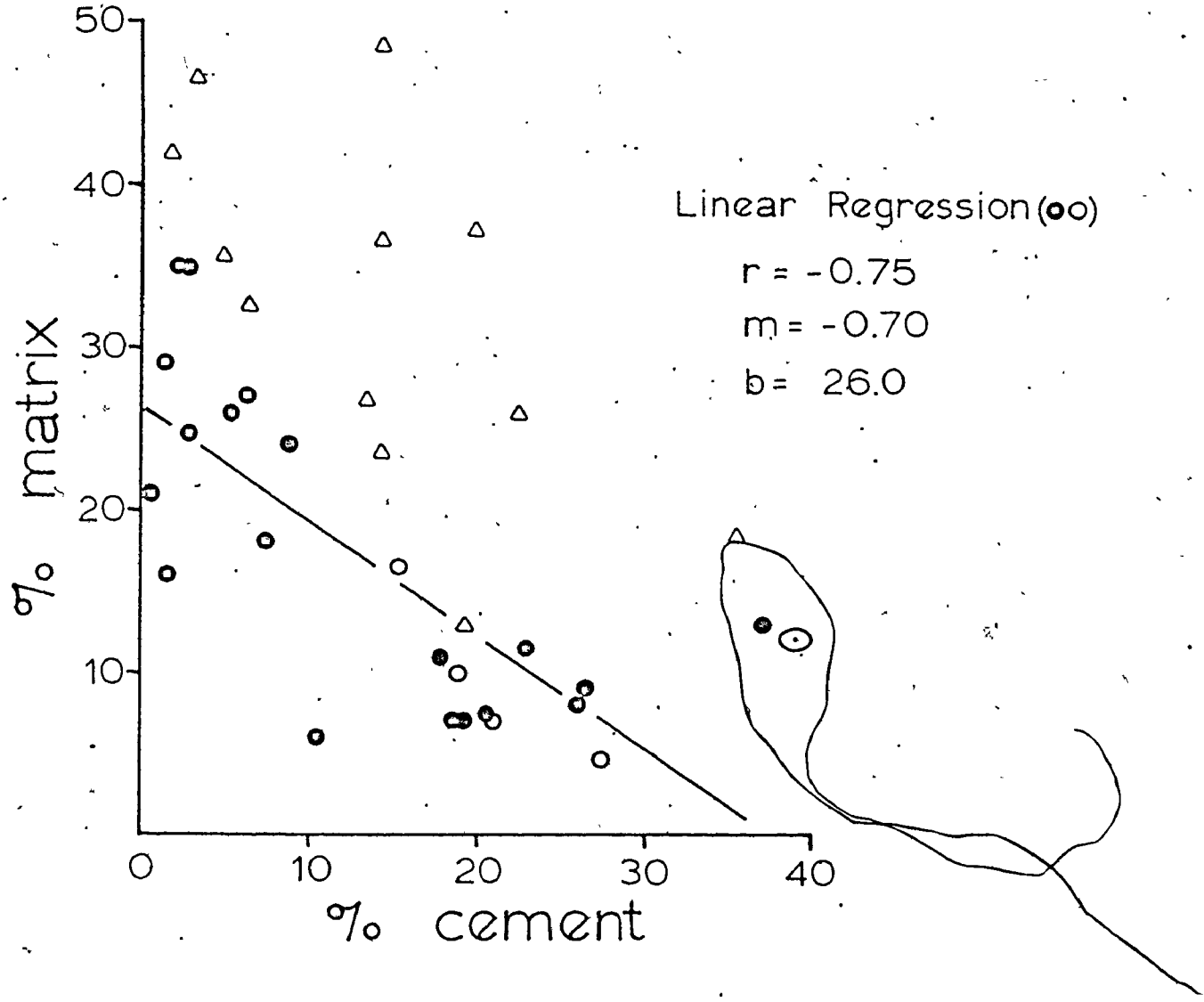

Fig. 6.18. Plot of percent matrix against percent cement for Tourelle samples. ● , sandstones with estimated mode greater than 0.3 mm; ○ , cross-stratified sands or samples from fluid-escape pillars, all with estimated modal size greater than 0.3 mm; △ , sandstones with mode from 0.1 to 0.3 mm. Regression line is calculated on the basis of circular points only.

expected for framework-supported sands, due to greater compaction of matrix-bound samples. This differential compaction is shown by the fact that obvious pressure solution effects are restricted to samples with only minor calcite cementation.

Strong calcite cementation is restricted to (i) cross-stratified sandstones, (ii) fluid-escape pillars and sheet structure, and (iii) carbonate concretions. The first two occurrences are in sands which had high initial porosities due to hydraulic sorting or to post-depositional elutriation of fine particles. Cross-stratified sands now have less than 10% matrix. This removal of fines was evidently sufficient to permit unhindered migration of pore fluids and calcite cementation. Because cementation appears to have gone to completion, which requires fluid migration through small pore spaces, all other sands which were not cemented in this fashion must have had very low initial porosities and permeabilities. Massive sandstone within millimetres of fluid-escape pillars is not calcite cemented, suggesting an abrupt change in permeability. It is believed that this abrupt change resulted from the fact that the pore space in massive sandstones was filled with a primary mud matrix.

Carbonate concretions were able to grow within massive sandstones. As mentioned in an earlier section, there is

evidence that framework grains were replaced by calcite during concretion growth. Primary matrix may also have been replaced within concretions, as suggested by Lajoie (1968) for other Paleozoic deep-water sandstones.

The most critical test of the two hypotheses depends on whether or not there is a significant negative correlation between percent unstable grains and percent matrix. Variables used in this analysis will be (i) the sum, in percent, of volcanic fragments and feldspar (sedimentary fragments should have been stable under diagenetic conditions), and (ii) percent matrix. Because both variables are functions of grain size (Figures 6.19 and 6.20), only samples with estimated "modal" size between 0.3 and 0.8 mm will be considered.

The maximum variability in the total of volcanic fragments and feldspar is only 7%, regardless of matrix content (Figure 6.21). Even if we include all rock fragments (Figure 6.22), 30% matrix must have been produced from 11% rock fragments and feldspar if Cummins' (1962) model is correct. This is clearly impossible, unless there was free movement of fluids during formation of diagenetic matrix, allowing all sands to contribute. This is not considered as a serious possibility, because we already know that pore fluids were unable to penetrate most sandstones to precipitate calcite cement (assuming that there was initial porosity for this cement to grow in).

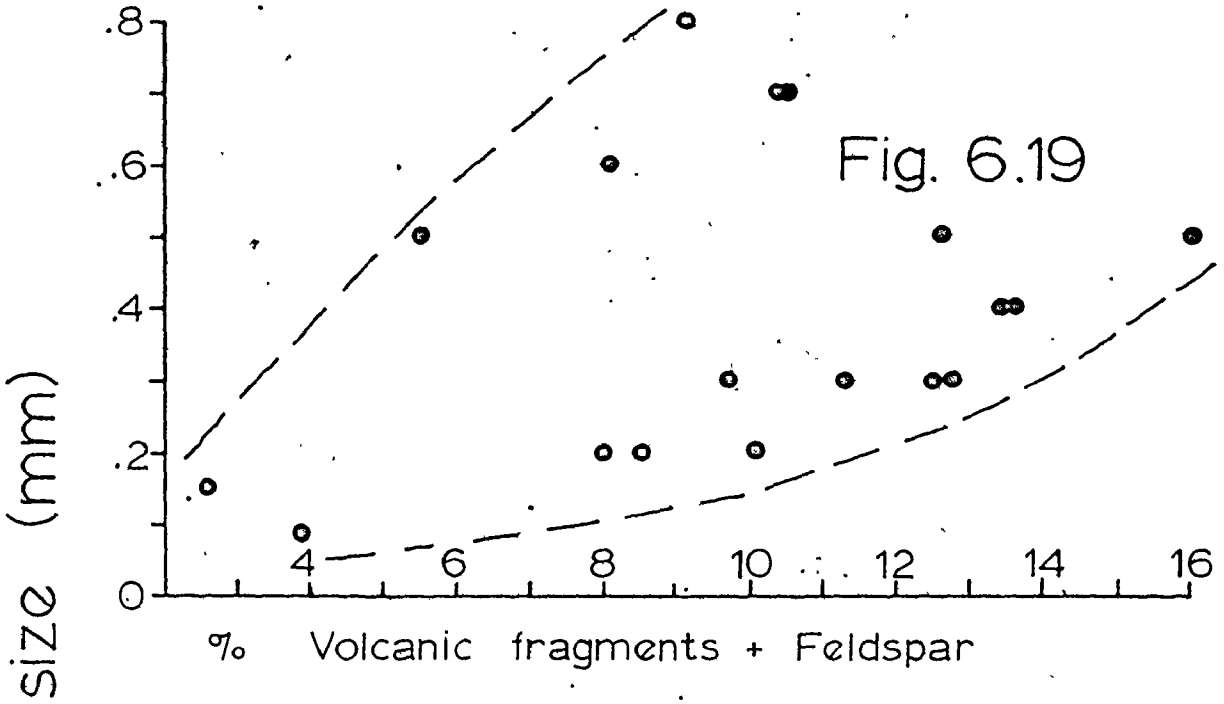

Fig. 6.19

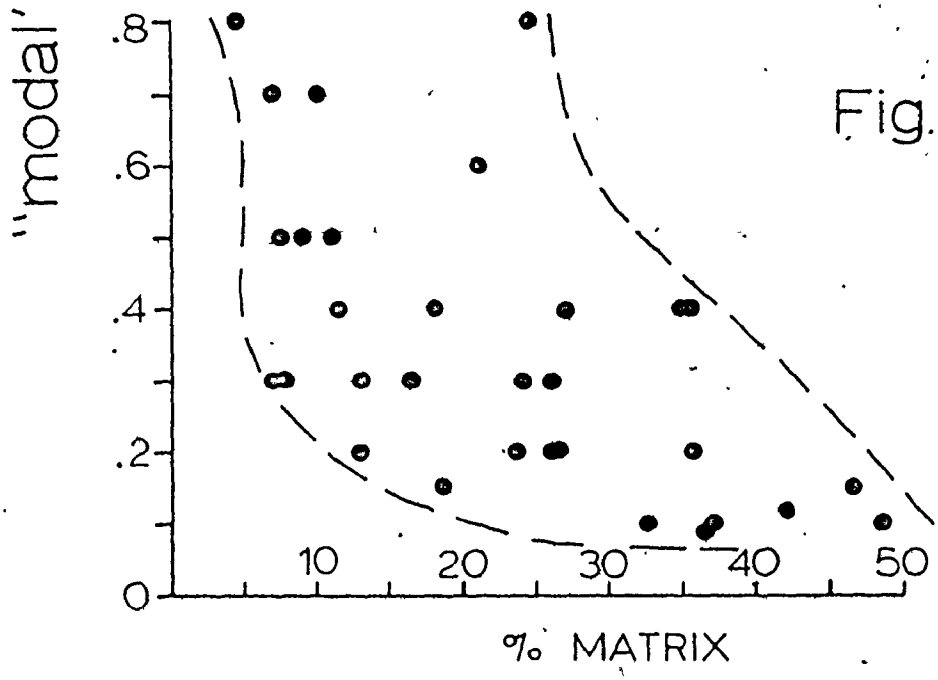

Fig. 6.20

Fig. 6.19. Plot of percent matrix against "modal" size in millimetres, for samples with "modal" size less than 1 mm.

Fig. 6.20. Plot of percent volcanic rock fragments and feldspar against "modal" size in millimetres, for samples with "modal" size less than 1 mm.

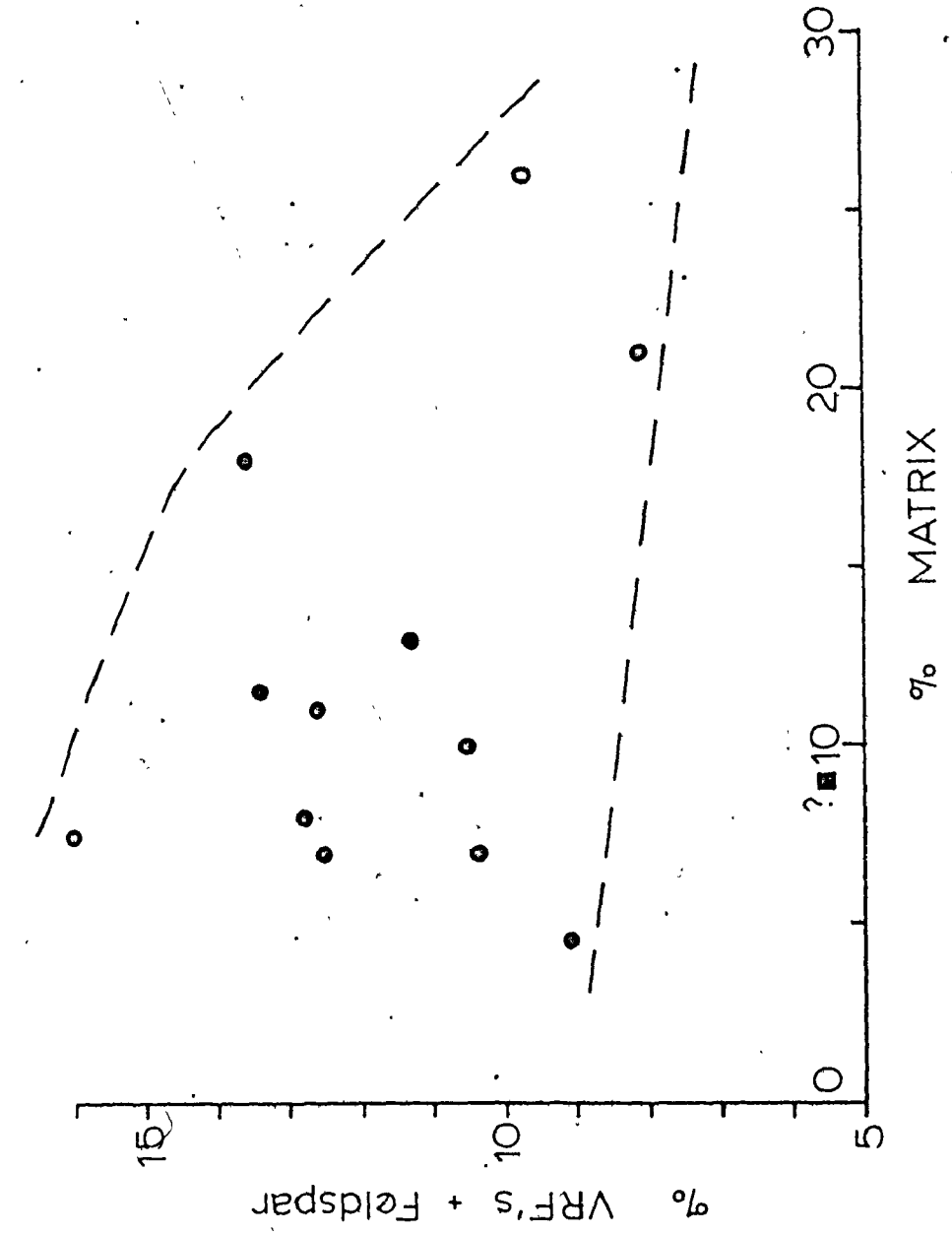

Fig. 6.21. Plot of percent volcanic rock fragments and feldspar against percent matrix for samples with "modal" size between 0.3 mm and 0.8 mm.

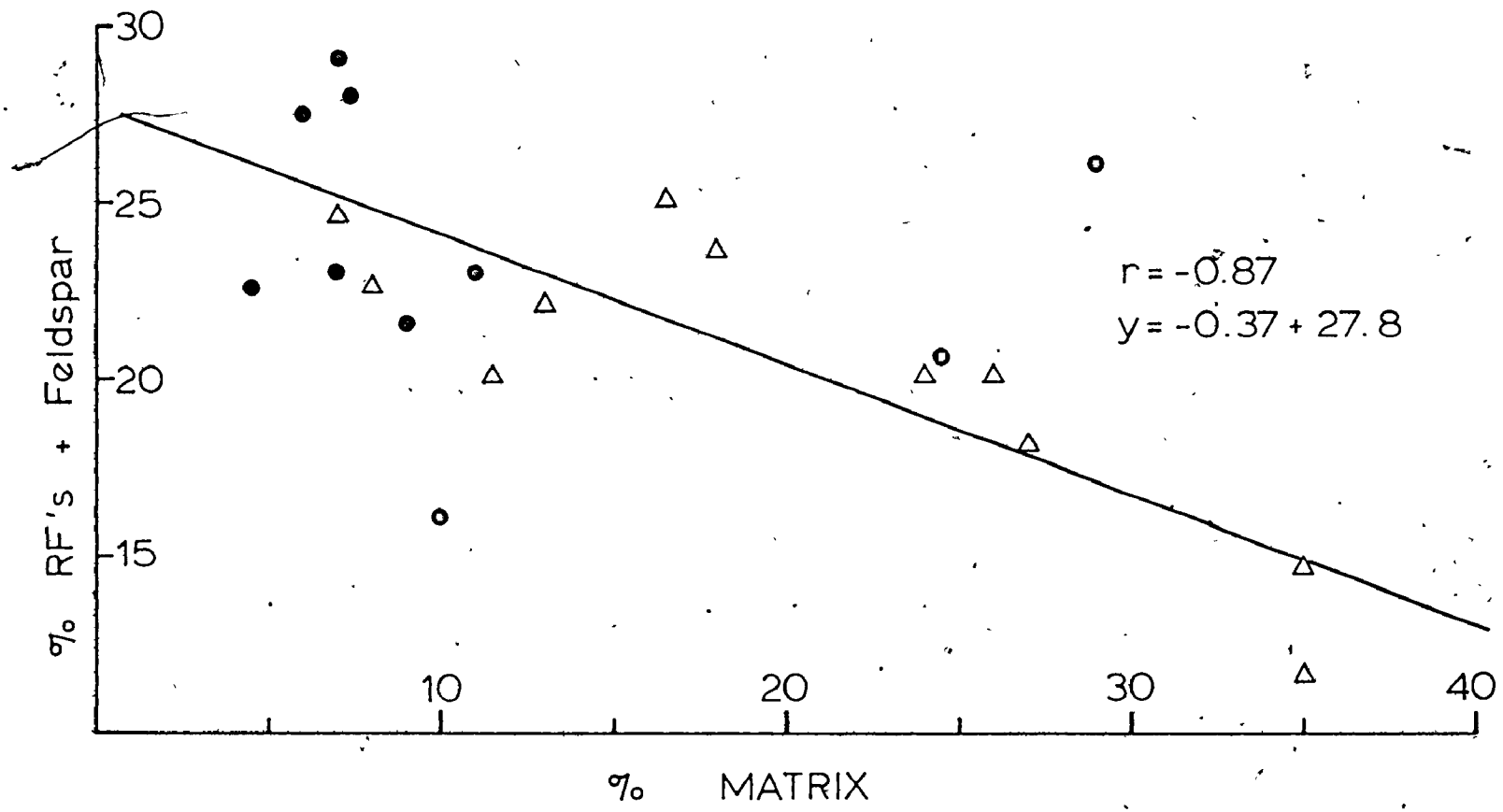

Fig. 6.22. Plot of percent rock fragments and feldspar against percent matrix. △ , "modal" size 0.3 to 0.5 mm; ● , "modal" size 0.5 to 0.8 mm. Regression line is calculated on the basis of all data points.

Even more damning evidence against Cummins' hypothesis that matrix is diagenetic comes from a comparison of samples 30 and 31 (Table 6.3), which both come from the same layer. Sample 31, however, was point counted inside a fluid-escape pillar. Both samples have approximately the same total percent of rock fragments plus feldspar, but sample 30 contains 20% more matrix than sample 31. If this additional matrix is the product of breakdown of rock fragments and feldspars, why are these components not depleted in sample 30? This paradox can only be avoided by assuming that the matrix in the bulk of the sandstone layer was primary, and not solely diagenetic.

Because (i) cross-stratified units contain less than 10% matrix, and (ii) breakdown of unstable components can only account for a maximum of 10% of the total matrix in poorly-sorted samples, it is unlikely that diagenetic growth of matrix at the expense of unstable grains is responsible for more than 10% matrix in any sample. All other matrix is either primary, or pseudomatrix. In some samples, particularly concretions, some detrital matrix has been replaced by calcite.

Summary of diagenetic history

The following sequence of events has modified Tourelle sandstones since deposition. Original sands contained up to 10-15% primary detrital matrix (compare Moore, 1974), except cross-stratified units and fluid-escape pillars, which were washed clean of most fines.

(i) Precipitation of carbonate pore-filling cement in clean sands and growth of carbonate concretions by replacement of primary matrix and unstable rock fragments. Silica released by this replacement may have contributed to the formation of authigenic quartz overgrowths in some adjacent coarse sands.

(ii) Compaction under lithostatic load, causing formation of pseudomatrix and pressure solution of contacting quartz grains.

(iii) Breakdown of unstable grains and formation of a diagenetic matrix component (less than 10%), accompanied by recrystallization of primary matrix to pasty chlorite.

(iv) Patchy replacement of chloritic matrix and unstable grains by sparry calcite.

This sequence is similar to that proposed by Chevalier (1976) for ancient sandstones, and by Galloway (1974) for core samples from modern northeast-Pacific arc-related basins.

Summary

The average composition of Tourelle sandstones is 45.6% quartz, 8.2% feldspar, 13.4% rock fragments, 16.6% chloritic matrix, and 15.3% calcite "cement". Most samples can be classified as lithic wackes or sublitharenites. Quartz grains are generally non-undulose, and may be well rounded. Potassium feldspar grains comprise two thirds of all feldspar detritus.

The most distinctive rock fragments are (i) chert and siliceous mudstone, and (ii) mafic to felsic volcanic detritus of prehnite-pumpellyite metamorphic grade. Chert fragments appear to have been derived from bedded chert units, and may contain infilled radiolarian tests.

The heavy mineral suite contains rounded ultrastable grains of zircon and tourmaline, abundant epidote group minerals and garnet, unstable prismatic grains of hornblende and pyroxene, and transluscent cherry-red chromite. This suite suggests both a multiple and complex source area.

Diagenetic history involved (i) precipitation of carbonate pore-filling cement in clean sands, and growth of carbonate concretions elsewhere by replacement of primary matrix and unstable rock fragments, (ii) minor pressure solution, (iii) minor breakdown of unstable grains to form a maximum of 10% "diagenetic matrix", and (iv) patchy replacement of unstable grains and chloritic matrix by sparry calcite.

Original sands contained up to 10 to 15% primary detrital matrix which has since recrystallized to chlorite.

Mineralogy of Tourelle sandstones will contribute to an evaluation of provenance in the next chapter.

CHAPTER VII

PROVENANCE OF THE TOURELLE FORMATION

Mineralogy

Comparison with other allochthonous Cambrian and Ordovician sandstones, Quebec Appalachians

Cambrian and Lower Ordovician allochthonous sandstones in Quebec range in composition from arkose to quartz arenite (Ollerenshaw, 1967; Hubert, 1973; Lajoie and others, 1974). Quartz and feldspar are the dominant framework constituents (Figure 7.1). Rock fragments, if present, are generally carbonate intraclasts, and not unstable lithic fragments. Quartz grains are well rounded, particularly in the Kamouraska Formation and similar quartz arenite units (Hubert, 1973). Feldspar composition varies from (i) mostly albite with rare microcline (Middle Cambrian), to (ii) microcline, albite, and rare oligoclase (Upper Cambrian), to (iii) oligoclase, microcline, and albite (Tremadocian), to (iv) microcline, oligoclase, and andesine (Lajoie and others, 1974). Common accessory minerals are zircon, rutile, tourmaline, apatite, pink garnet, hematite, ilmenite, pyrite, and sphalerite (Hubert, 1973; Lajoie and others, 1974). These heavy minerals are commonly

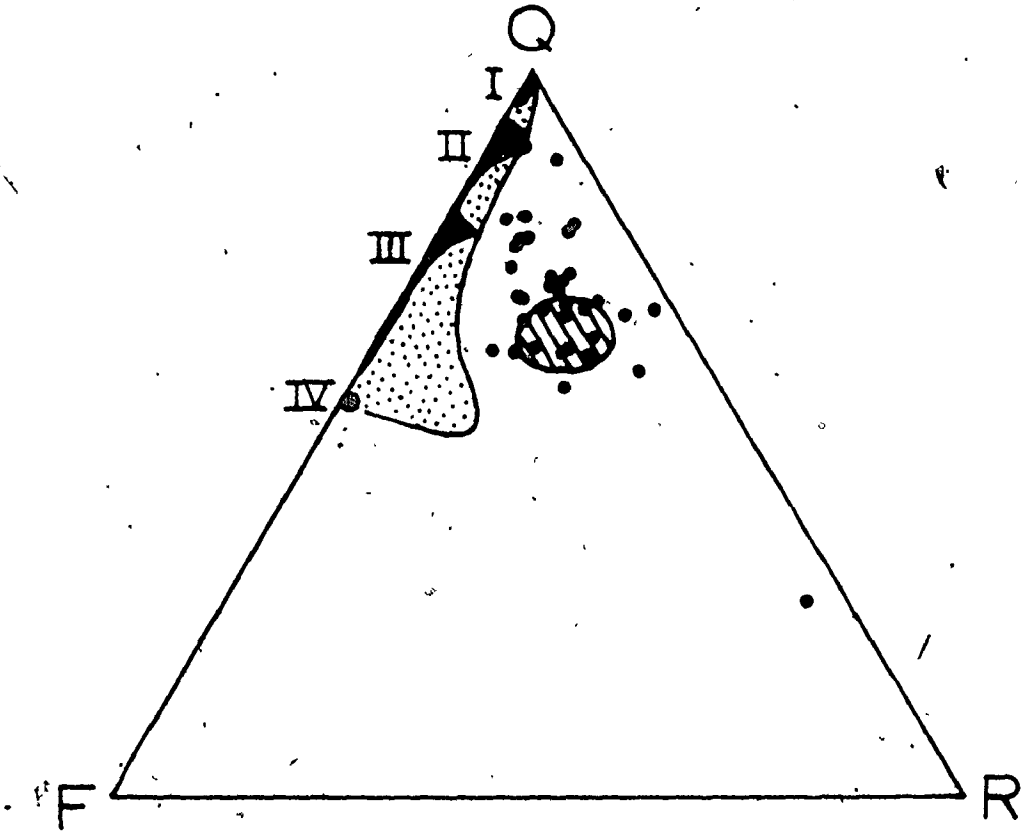

Fig. 7.1. Comparison of major-component composition of Tourelle Formation with published data from the Quebec Appalachians. Sources:
(1) Hubert (1973) - I - orthoquartzites (Rosaire Gp., Armagh Gp, Kamouraska Fm, Rivière Ouelle Fm)
- II - subarkose (Rosaire Gp, Armagh Gp, St. Roch Fm, Rivière Ouelle Fm)
- III - arkose (Armagh Gp, St. Roch Fm, Rivière Ouelle Fm).
(2) Ollerenshaw (1967) - IV - Shickshock Gp arkose (average).
(3) Lajoie and others (1974) - stippled pattern - Cambrian sandstones at Bic and Trois Pistoles (Cap Enragé Fm).
(4) Enos (1969a) - ruled pattern - Cloridorme Fm greywackes (averages).

well rounded (Hubert, 1973).

Lajoie and others (1974) attribute these Cambrian and Lower Ordovician sandstones to erosion of gneisses, plutons, and mature sedimentary rocks from the Grenville shield northwest of the Appalachian belt. A similar interpretation of feldspathic Cambrian clastics has been proposed for Newfoundland equivalents (Stevens, 1970). Ollerenshaw (1967) and Hubert (1973) do not agree with this hypothesis, and instead suggest a source terrain of basement (gneissic) rocks located to the southeast of the depositional basin during the Cambrian. This interpretation is based upon paleocurrent data, downcurrent variation in clast size (Ollerenshaw, 1967), and petrographic differences between arkoses and quartz arenites. Hubert (1973) believes that quartz arenites and limestone breccias were derived from a sedimentary apron around the Grenville shield, but that arkoses were derived from a southeastern provenance.

Enos (1969a) presents compositional data for greywackes of the Middle Ordovician Cloridorme Formation (Figure 1.7) which show strong similarity to Tourelle sandstone compositions (Figure 7.1). Whereas Cambrian and Lower Ordovician clastics contain essentially no unstable lithic grains, 22 greywackes from the Cloridorme Formation contain an average of 9.2% volcanic detritus (andesite to rhyolite), 2.0% low-grade schist fragments, and 4.3% serpentine grains. These sandstones average 24.3% argillaceous matrix. Accessory minerals consist

of abundant zircon, some tourmaline, traces of apatite, garnet, hornblende and magnetite, and locally abundant cherry-red, transluscent chromite. All feldspar is plagioclase, apparently of oligoclase composition (Enos, 1969a). Quartz grains may be well rounded.

Except for feldspar composition and the presence of significant serpentine, Cloridorme greywackes are very similar to Tourelle sandstones. Neither of these resemble pre-Arenig arenites described by Hubert (1973) and Lajoie and others (1974). This observation suggests that the provenance area of the Tourelle and Cloridorme Formations (and equivalents) was dissimilar to that postulated for Cambrian and Lower Ordovician detritus.

Comparison with orogenic sandstones

Recent studies of mineralogical composition of ancient immature sandstones, deposited in known tectonic settings, are reported by Dickinson (1970, 1971a, 1971b) and Graham and others (1976). These studies are particularly relevant to Tourelle Formation petrography, since detritus was probably derived from an Ordovician, continental margin orogenic belt (Williams and Stevens, 1974). Figure 7.2 shows QFR

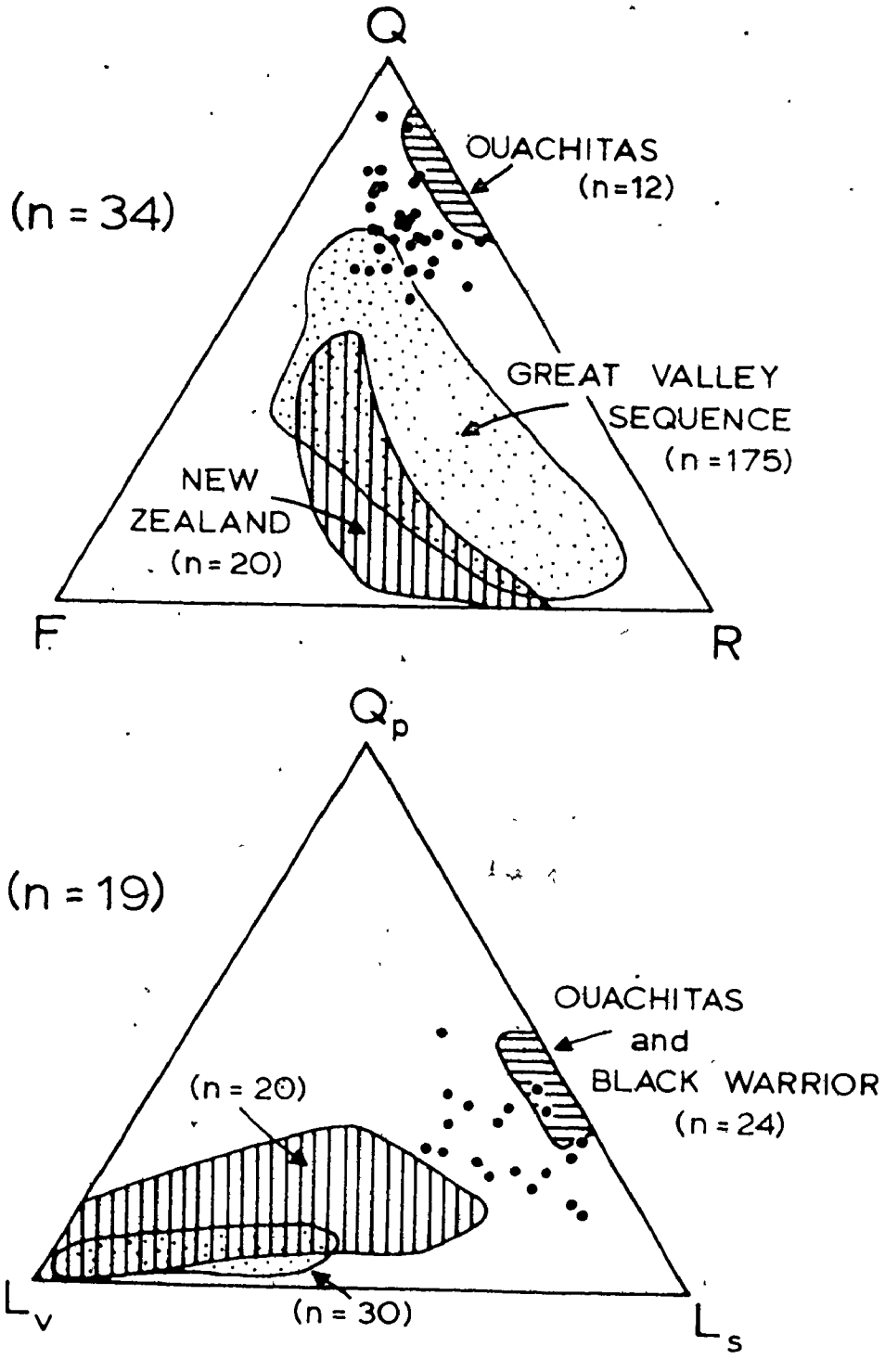

Fig. 7.2. QFR and $Q_pL_vL_s$ plots comparing Tourelle sandstones with orogenic sandstones. Fields for New Zealand greywackes, Great Valley Sequence, and Ouachita and Black Warrior Basin flysch are taken from Graham and others (1976). See text for expanation of variables.

and $Q_pL_vL_s$ plots[1] of Tourelle data, superimposed on fields for greywackes from New Zealand, the Great Valley Sequence (California), and the Ouachita Mountains and Black Warrior Basin (Carboniferous flysch, southeastern U.S.A.). Data are taken from Graham and others (1976).

New Zealand and Great Valley sequence rocks were derived from magmatic arcs on Andean-type continental margins. Hence the source area comprised volcanic rocks, plutonic rocks, low-grade metamorphic rocks, and sedimentary rocks. Other than quartz, volcanic rock fragments and feldspar are the most important major components. In New Zealand (Dickinson, 1971b), the ratio of plagioclase to total feldspar decreased from 1.0 to 0.5 with time, as a result of progressive unroofing of igneous plutons.

Ouachita and Black Warrior Basin sands were derived from a cratonic suture zone formed as a result of closing of the Proto-Atlantic Ocean (Graham and others, 1975), and therefore contain almost no volcanic detritus. These sands are quartzose and contain almost no feldspar, indicating a cratonic provenance of mature sedimentary rocks and a low-grade metamorphic terrain.

---

[1]The components of the second diagram are (1) Q_p - polycrystalline quartz grains, (2) L_v - volcanic rock fragments, and (3) L_s - sedimentary rock fragments (data in Table 6.5). Percentage data must be recalculated so that $Q_p + L_v + L_s = 100\%$.

Tourelle samples contain appreciably lower percentages of feldspar and rock fragments than New Zealand and Great Valley Sequence rocks. In particular, volcanic rock fragments account for less than 25% of polycrystalline grains ($Q_pL_vL_s$ plot), and the ratio of plagioclase to total feldspar is less than 0.5. The cluster of Tourelle points is much closer to Ouachita and Black Warrior Basin samples, indicating a strong cratonic and sedimentary provenance component. The only anomaly in the major detrital fraction is the persistent presence of volcanic rock fragments.

Mineralogical data for sands associated with modern plate-tectonic settings are generally not available. Deep-sea drilling site 181, situated on the slope above the Aleutian trench (Kulm, von Huene and others, 1973), provided sandstone samples which were probably deposited on oceanic crust off the coast of British Columbia (Andean-type margin). The ratio Q:F:R for these sands is 45:45:10. Volcanic grains constitute one third of all rock fragments, with the remainder consisting of biotite and ferromagnesian mineral grains. Epidote and garnet account for 2.7 and 0.3 percent of all framework grains. 88% of feldspar grains are plagioclase. These sands, which are much less quartz rich than sandstones of the Tourelle Formation, plot in the field of Great Valley Sequence rocks on a QFR plot (Figure 7.2).

Volcanic Rock Fragments

The age of the volcanic terrain which contributed detritus to the Tourelle Formation is unknown, but a Lower Ordovician age (Tremadoc or Arenig) is not unreasonable. Phillips and others (1976) suggested that closing of the Iapetus Ocean (Harland and Gayer, 1972) began in early Arenig time. Formation of subduction zones and volcanic arcs would be a product of this closing. There is, admittedly, no evidence for active volcanism during Tourelle deposition, and clast mineralogy indicates that the volcanic source had undergone prehnite-pumpellyite grade metamorphism prior to erosion. This latter observation does not necessarily require a long erosional hiatus, however, because pumpellyite has been found at depths of only 100 to 200 m in the thermal area of Iceland (Sigvaldason, 1962). In addition, not all mafic volcanic fragments show development of pumpellyite.

Table 7.1 compares the percentages of inferred volcanic rock types represented by detritus in the Tourelle Formation (Table 6.8) with calculated abundances for modern oceanic and continental volcanic arcs. A volcanic arc most easily explains the variety of lava compositions deduced from detrital fragments.

Tourelle sandstones can only be compared with modern arcs if volcanic detritus accurately represents the relative abundances of rock types in the source area. Is this a valid

Table 7.1

Volcanic rock fragment percentages compared with modern volcanic arcs

Occurrence	suite	basalt	andesite	dacite and rhyolite
Tourelle detritus		50.9	28.0	21.1
Average oceanic arc[1]	tholeiitic	42.5	29.7	12.7
	calc-alkaline	1.6	7.0	4.0
	shoshonitic	1.3	1.0	0.2
		45	38	17
Lesser Antilles[2]		24	68	8
South Sandwich Is.[2]		68	27	5
Central Washington[3]		33	61	6
Central Oregon[3]		88	14	3
Northern California[3]		68	30	2

Oceanic arcs (1) Jakes and White (1971)
(2) Baker (1968)
Continental arc (3) McBirney (1976) - Cascades

assumption, or are the observed proportions of volcanic lithologies the result of selective abrasion of basaltic fragments during fluvial transport? Cameron and Blatt (1971) reported negligible abrasion of "felsitic silicic" volcanic rock fragments in 160 km (100 miles) of fluvial transport, but little is known about abrasion rates for mafic detritus. Modern Columbia River sands contain 24 to 47% volcanic lithic grains (Whetten, 1966) as well as 8 to 10% hypersthene, augite, hornblende, and biotite. Whetten and others (1969) reported that most volcanic detritus in the downstream portion of the Columbia River is andesite in composition, even though much of the drainage basin is underlain by basalt. They attribute the observed volcanic detrital composition to lofty andesite volcanoes near the crest of the Cascade Range, and to reworking of Pleistocene flood deposits. Dickinson (1971b) reported a dominance of microlitic (basaltic - see Dickinson, 1970) volcanic detritus at the base of a Permian to Jurassic arc-trench gap sequence in New Zealand, with felsic volcanic fragments increasing in abundance through time as the arc matured. Ojakangas (1968) found that basalt and andesite detritus were alternately dominant during accumulation of the Great Valley Sequence in California. Dott (1966) reported mainly andesite and rhyolite detritus in the deltaic Eocene Coaledo Formation, Oregon, even though contemporaneous Eocene basalts are exposed nearby. Rogers (1966), however, found

mainly basalt and pyroxene-andesite fragments in Tertiary greywackes in western Oregon and Washington.

In the Tourelle Formation, volcanic rock fragments are concentrated in the coarse sand to granule size fractions, suggesting relative resistance to comminution. In finer size fractions typical of most sandstones, microlitic grains appear to be most common, although this may simply be the result of inability to correctly identify small fragments of felsic and porphyritic grains (Boggs, 1968). Because previous studies discussed above have not documented preferential abrasion of mafic volcanic fragments, there is no reason to believe that observed lithologic proportions misrepresent the availability to erosion of different volcanic rock types. It is possible, however, that high-relief andesite volcanoes contributed more detritus than expected, as is the case for modern Columbia River sands.

Data evaluation

Comparison of data presented in Table 7.1 suggests that the Ordovician arc contained a somewhat higher proportion of dacite and rhyolite than modern oceanic arcs. This is not unexpected, because the upper subaerial part of an oceanic arc is enriched, relative to the arc average, in calc-alkaline rocks containing an average of 32% dacite and rhyolite (Jakeš

and White, 1971). Calc-alkaline andesites, dacites, and rhyolites only become important, however, in mature oceanic arcs (Kuno, 1966). Even in continental arcs, represented in Table 7.1 by averages for the Cascade province (McBirney, 1976), dacite and rhyolite may be uncommon. In contrast, sheets of rhyolite tuff covering 70,000 km^2 have been produced by the most recent eruptive cycle in the Chilean and Peruvian Andes (Carmichael and others, 1974, p. 531).

Felsic members of the calc-alkaline suite are commonly represented by ash-flow or ash-fall tuffs. The Tourelle sandstones, however, only contain about 1% pyroclastic fragments. It is possible that vitric rhyolite tuffs and ignimbrites (ash-flow tuffs) may have suffered devitrification and growth of spherules to produce the "rhyolite" fragments in Tourelle sands (Ross and Smith, 1961). Unconsolidated ash-fall tuffs would be susceptible to rapid disintegration during transport.

Because of the great variation in lithologic proportions exhibited by both oceanic and continental arcs, it is not possible to assign the Ordovician arc to either category on the basis of bulk composition. The suite of mafic accessory minerals, however, affords an additional criterion. McBirney (1976) presents evidence that hornblende and biotite only occur in andesites erupted on thick continental crust such as that found in the Andes. Andesitic and dacitic fragments in

Tourelle sandstones contain primary biotite, and prismatic hornblende is an important constituent of the heavy mineral suite. These observations are inconsistent with the mineral composition of oceanic-arc andesites and dacites. There is no concrete evidence in the northern Appalachians that the North American continental margin was of Andean type in the Lower Ordovician. Neither volcanic centres, plutonic equivalents, nor ash-fall tuffs of this age have been documented. It is not impossible, however, that the remnants of a continental arc have not been recognized due to sedimentary cover (Gaspé Synclinorium), erosion, metamorphism, or uncertain age relationships. Phillips and others (1976) present evidence for northwestward subduction of oceanic crust under continental crust in South Mayo, northwestern Ireland, during the Arenig, which they interpret as an equivalent to tectono-stratigraphic zone D in Newfoundland (Williams and others, 1972). The mafic and felsic lavas described by Phillips and others (1976) in Ireland may in fact be equivalent to the Roberts Arm Group in Notre Dame Bay, Newfoundland (Strong, 1973) which also comprises basaltic and dacitic lavas.

Conclusions

The volcanic terrain which supplied detritus to the Tourelle Formation was a Lower Ordovician volcanic arc associated with closing of the Iapetus Ocean. This volcanic arc was either situated on the continental margin (Andean configuration) or offshore beyond a marginal ocean basin, on a fragment of continental basement. Continental basement is required to help account for (i) the high proportion of dacite and rhyolite, and (ii) the presence of primary biotite in volcanic fragments, and prismatic hornblende in the heavy mineral suite.

Bedded Chert Fragments

Chert grains below pebble size are very angular. Pebbles and cobbles may be angular to rounded (brown varieties are generally most rounded). These fragments are petrographically identical to bedded chert and siliceous mudstone samples from the Cap des Rosiers Group and from large isolated slabs in thick sandstone (6) layers. In sand- and granule-sized grains, infilled and replaced radiolarian tests are only rarely observed. It is believed that chert grains were derived locally by erosion of bedded chert horizons similar to those in the upper part of the Cap des Rosiers Group, although it is

possible that some chert may have been eroded from sediments overlying obducted ophiolite sheets (Garrison, 1974). Evidence presented in Chapter VIII suggests that Cap des Rosiers cherts are not indicative of abyssal depths. Modern siliceous oozes are restricted to abyssal depths because biogenic siliceous debris is masked by deposition of abundant calcareous oozes above the calcite compensation depth (4.6 km in modern oceans, Berger and Winterer, 1974). An exception is the Gulf of California (Calvert, 1966) where siliceous diatom skeletons may constitute 50% of the total sediment. Prior to the Jurassic, however, carbonate-secreting nannoplankton did not exist, and siliceous oozes were free to occur at all depths.

Low-grade Phyllite

These mildly metamorphosed shale fragments are the only metamorphosed rock fragments present in Tourelle sands. Some polycrystalline quartz grains are composed of sutured and stretched crystallites, suggesting a metamorphic history (Folk, 1968; Blatt, 1967). The source of this quartz, however, was likely not supracrustal.

Cameron and Blatt (1971) demonstrated that schist rock fragments disintegrate rapidly during fluvial transport. For this reason, a nearby source for low-grade phyllite fragments must be sought.

Heavy Minerals

Silicates

Figure 7.3 summarizes heavy mineral data for the four least altered Tourelle separates, and compares these abundances with the mean composition of heavy mineral suites in Pleistocene tills derived from the Grenville Province of the Canadian shield (Gwyn, 1971). The following features of the Tourelle heavy mineral suite are important for provenance evaluation.

(i) Ultrastable group minerals (zircon, tourmaline) are generally well rounded. Tourmaline also has high sphericity (Figure 6.11, p. 323). These characteristics are diagnostic of derivation from reworked sediments. Hence the ultrastable group (including traces of rutile) is multicycle. Honey-coloured sphene is also well rounded, suggesting recycling. The most probable original source for these minerals is the Grenville shield, composed of plutonic rocks and high grade gneisses. Hubert (1973), and Lajoie and others (1974) report the presence of rounded grains of zircon, rutile, and tourmaline in Cambrian and Lower Ordovician sandstones of the Quebec Complex. It is believed that recycling of similar sediments contributed ultrastable grains to the Tourelle heavy mineral suite.

(ii) Garnets (moderately stable) are somewhat more

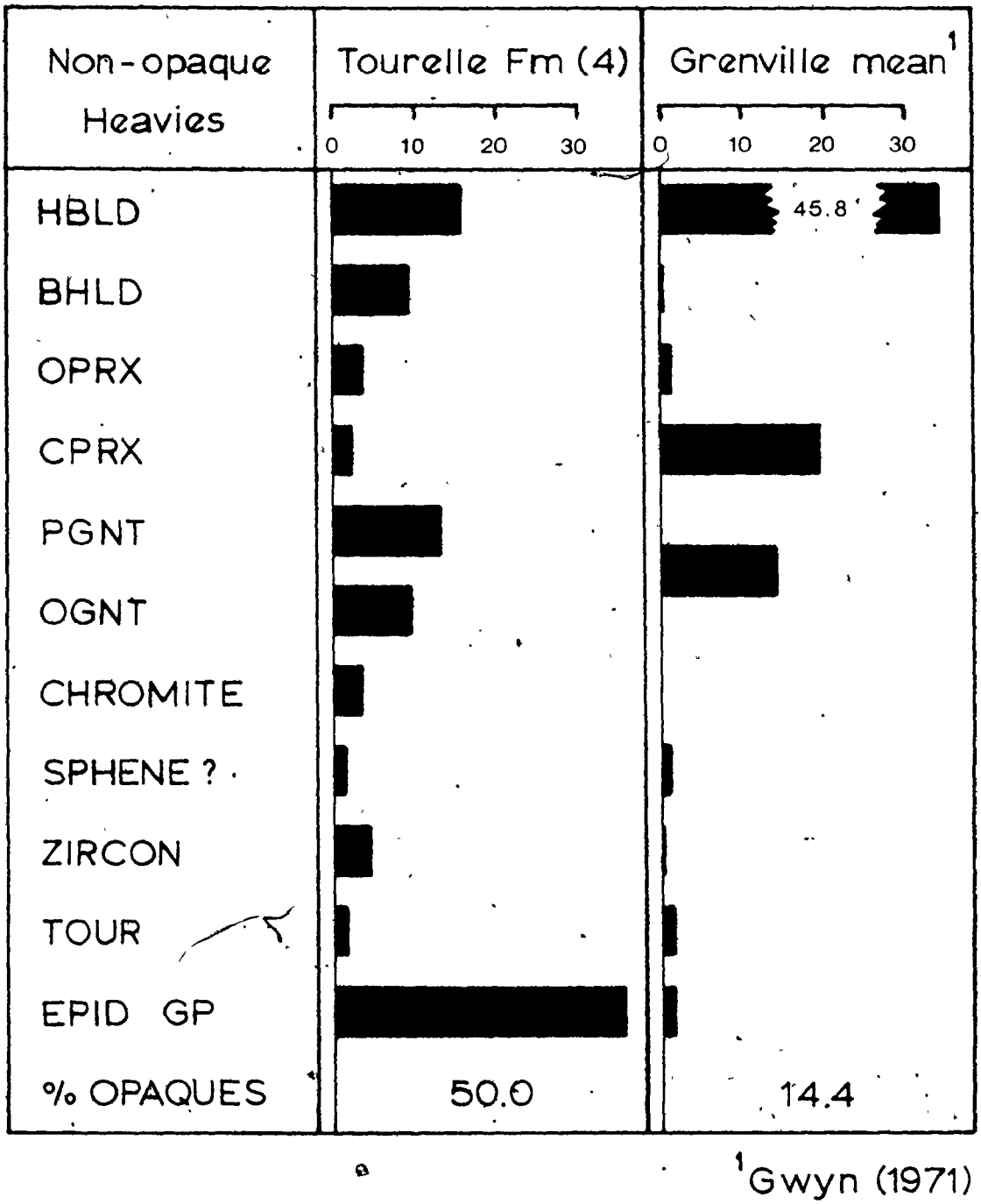

Fig. 7.3. Comparison of heavy mineral means from the Tourelle Formation and the Grenville Province of the Canadian Shield. Abbreviations are explained in Chapter VI. These data are for 2ϕ to 3ϕ heavy minerals.

abundant than in Grenville heavies, with one population being well rounded, suggesting recycling, and the other being characterized by chemical etching and authigenic overgrowths (Simpson, 1976). Both types of garnet may be found in one sample, indicating that etched surfaces and overgrowths in samples other than concretions (see Chapter VI) were formed prior to deposition. Samples with a high proportion of overgrown garnets (high OGNT/PGNT) are also depleted in amphiboles and pyroxenes, and enriched in zircon. Since all samples contain the same mineral species, it is believed that depletion and corrosion of the heavy mineral suite in some sandstone samples is a result of longer residence time in the weathering environment prior to mixing with fresh detritus and resedimentation into deeper water. The fresh detritus was likely transported directly by high gradient streams, whereas sand containing a depleted heavy mineral suite was trapped for some time in soil horizons or shallow marine environments. It is believed that the majority of garnets are recycled grains from an original Grenville provenance. Lajoie and others (1974) report common pink garnets in Cambrian sandstones at Bic and Trois Pistoles. Similar garnets are very common in the Charny Formation at Quebec City (G.V. Middleton, personal communication). Garnets may also have been contributed from metamorphic aureoles beneath obducted ophiolite sheets (Williams and Smyth, 1973).

(iii) Amphiboles and pyroxenes (unstable group) are generally restricted to Cenozoic deposits (Pettijohn, 1941), but are well preserved in some Tourelle sandstones. These minerals are prismatic and show only a slight degree of rounding. Thiel (1940) conducted abrasion experiments on various minerals in a water-filled rotating drum. In a 40 day period, he simulated 2800 km (1800 miles) of transport and then compared Wadell sphericity[1] with the characteristics of freshly crushed minerals. For 0.5 to 1.0 mm quartz, Wadell sphericity before and after 100 days was 0.70 and 0.71, for garnet 0.76 and 0.77, for tourmaline 0.75 and 0.77, and for hornblende 0.63 and 0.76. 57% (by weight) of all hornblende originally present was no longer retained by the 0.5 mm sieve, as compared with 22% for quartz. Clearly, hornblende (and by inference other amphiboles and pyroxenes) is much more easily worn than garnet or tourmaline, which suggests that the prismatic nature of amphiboles and pyroxenes in the Tourelle heavy mineral suite is a textural anomaly. These minerals have certainly not undergone the same degree of abrasion and rounding as zircon, tourmaline, rutile, sphene, and garnet. It is therefore necessary to conclude that the amphibole and pyroxene grains do not have the same provenance

---

[1]Wadell sphericity equals the diameter of a circle equal in area to the area of the grain in its stable rest position, divided by the diameter of the smallest circumscribed circle.

as multicycle zircon, tourmaline, rutile, and garnet. Pyroxenes are characteristic minerals of basic igneous rocks (Feo-Codecido, 1956). Hornblende, basaltic hornblende, and hypersthene occur in continental arc lavas and intrusives (McBirney, 1976). Williams and Smyth (1973) also report the presence of brown and green hornblende, augite, and diopside from metamorphic aureoles beneath ophiolites in western Newfoundland.

(iv) Epidote group minerals (epidote, zoisite) are extremely abundant in the Tourelle heavy mineral suite when compared to Grenville-derived heavies. These minerals are common products of low-grade metamorphism of volcanic rocks (Winkler, 1967), but are not present in prehnite-pumpellyite grade volcanic rock fragments in the Tourelle Formation. It is not unusual, however, for low-grade metamorphic phases to exist as vein fillings within volcanic rocks of a somewhat different metamorphic grade (Jolly and Smith, 1972). Hence, epidote group minerals are interpreted as vein fillings in lavas with a regional prehnite-pumpellyite grade of metamorphism. Epidote may also be derived from altered ultramafic rocks (R.K. Stevens, personal communication).

Chromite

A conspicuous minor constituent in heavy mineral separates and thin sections of Tourelle sandstones is chromite

(see Chapter VI, Table 6.10). Since grains in heavy mineral mounts are much thicker than standard thin sections, only chromite grains with cherry-red transluscent margins were counted. All other chromite grains would have been regarded as opaques. The only source for abundant chromite detritus is ultramafic rocks (Berry and Mason, 1959), particularly the cumulate zones of layered ultramafic intrusions and ophiolite masses. Ophiolite complexes (Church, 1972), which are interpreted as obducted slices of oceanic crust and upper mantle (Coleman, 1971), are well described from the Quebec Appalachians, Newfoundland and the British Caledonides (Church and Stevens, 1971; Dewey and Bird, 1971; Upadhyay and others, 1971; Williams, 1971; Church and Gayer, 1973; Laurent, 1975; Williams and others, 1977). Transluscent red and brown chromite in Tourelle thin sections is very similar to chromite detritus in the Middle Ordovician Cloridorme Formation and to chromite in peridotites from Mont Albert, immediately to the south of the study area (MacGreggor and Smith, 1963). In order to determine accurately the amount of chromite in the Tourelle heavy mineral suite, a composite 2 to 3 ϕ heavy mineral sample was analysed spectrophotometrically for chromium (see Appendix V). The percentage Cr was determined to be 6.8 ± 0.2%. Table 6.10 indicates that Tourelle chromites contain approximately 55% Cr_2O_3, or 38% Cr. Therefore the Tourelle heavy fraction contains

approximately 18% chromite. Grain counts only yielded an average of 3.4% chromite. The other 14.6% was therefore counted as opaque grains. It should be noted that heavy minerals were only separated from very coarse to granular sandstones. Examination of finer sandstones, however, indicates that chromite is a common minor constituent regardless of grain size. It is therefore believed that samples used for heavy mineral analysis were not unusually enriched in chromite.

In order to make an estimate of the total amount of chromite in Tourelle sandstones, the following information is needed:

(i) the weight percent of chromite in one size fraction (in this case, the 2 to 3 ϕ fraction);

(ii) the abundance of 2 to 3 ϕ material in coarse sandstones;

(iii) the grain size distribution of chromite.

If we assume that thin section size classes are approximately equal to sieve size classes, then 22% (by volume) of coarse-sandstone framework grains (as deduced from quartz grain-size distributions in Chapter V) are between 2 and 3 ϕ in size. If we allow for a maximum of 30% matrix and calcite cement, this estimate decreases to 15% of the entire sandstone. The weight percent of chromite in heavy minerals of this size fraction is 18.0%. The

eleven samples used for heavy mineral analysis averaged 0.915% heavies in their 2 to 3 ϕ fractions. Therefore, the proportion of 2 to 3 ϕ chromite in coarse sandstones can be estimated as

$$(15\%)(0.00915)(0.180) = 0.0247\%$$

In order to determine the grain-size distribution of chromite, the longest dimension of 150 grains was measured in four thin sections of granular sandstone. All chromite grains were measured in each section. This area sample is weighted by the length of grains, and not by their volume. In order to convert the data to volume percent, the number of grains measured in each 1/4 ϕ interval was multiplied by the area of a circle with diameter equal to the midpoint of the size interval (in mm). Cumulative curves of chromite grain size are plotted in Figure 7.4, for both the area sample, and for converted data (volume percent).

The graphic mean size (Folk, 1968) computed for the volume-percent curve is 1.43 ϕ. No chromite grains larger than 0 ϕ were observed, even though quartz grains in several thin sections had diameters approaching -2 ϕ. Rittenhouse (1944) suggests a hydraulic size of 0.8 ϕ for magnetite (SG 5.2) and ilmenite (SG 4.7). Hydraulic size is defined as the difference in size between a given heavy-mineral species and the size of a quartz sphere with the same settling velocity in water (Rubey, 1933). The specific gravity of

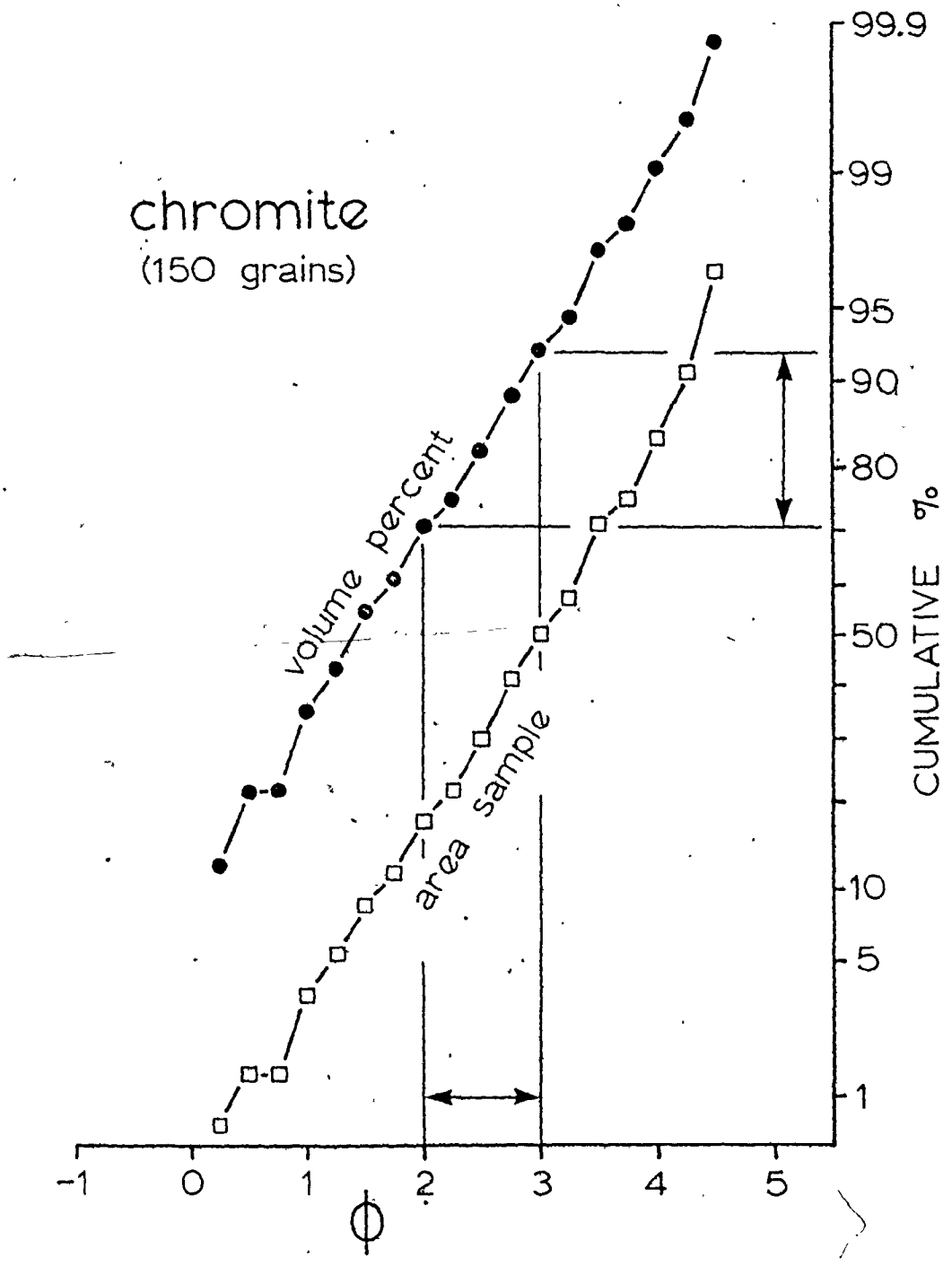

Fig. 7.4. Cumulative grain-size curves for chromite fragments. 22% of all chromite is found in the 2ϕ to 3ϕ size interval. □ , area sample; ● , data converted to volume percent.

chromite is approximately 4.5, requiring a hydraulic size similar to that of magnetite and ilmenite. Therefore, -1 ϕ chromite grains should be present if the sizes of quartz and chromite are hydraulically equivalent. Chromite grains of this size have not been observed, perhaps because chromite crystals in ultramafic source rocks were smaller than 0 ϕ in size, or because of insufficient sample size.

Figure 7.4 indicates that 22% of the chromite population (by weight) occurs in the 2 to 3 ϕ size fraction of coarse to granular sandstones. The 1 to 2 ϕ fraction is richest in chromite (36%). On the basis of these results, the Tourelle sandstones contain

$$(0.0247)(100)/(22)\% = 0.113\% \text{ chromite (by weight)}$$
$$= 0.0462\% \text{ Cr}$$
$$= 0.462 \text{ g Cr/kg sandstone.}$$

If we assume a sandstone density of 2.7 g/cm^3, concentrations become 3.04×10^{-3} g chromite/cm^3 sandstone, or 1.25×10^{-3} g Cr/cm^3 sandstone.

These figures can be compared with Normanskill greywackes (Weber and Middleton, 1961) which average 3.83×10^{-4} g Cr/cm^3 sandstone. This is a typical value for sandstones (Rankama and Sahama, 1950). Most chromium in Normanskill greywackes is in the matrix fraction. A heavy mineral separate only contained 0.09% Cr, compared with 6.8% for Tourelle heavies.

Goldschmidt (1937) and Rankama and Sahama (1950) reported a concentration of 3.75 g Cr per kg peridotite or dunite. Upper mantle density is approximately 3.30 g/cm^3. Hence chromium concentration in peridotite is 1.24×10^{-2} g/cm^3. Therefore, each volume of peridotite eroded contributed enough chromite for 10.0 volumes of sandstone. If we assume that (1) the Tourelle Formation is 500 m thick, (2) Tourelle equivalents were originally deposited along 1000 km of the Ordovician continental margin (Chapter I), (3) the width of the Tourelle Formation was originally 40 km, and (4) coarse sandstones which contain chromite comprise 40% of the formation, we can calculate the volume of peridotite which must have been eroded. This volume is 800 km^3. The Cloridorme Formation also contains abundant chromite, as do the autochthonous St. Irénée and Beaupré Formations on the north shore of the St. Lawrence River (E.S. Belt, personal communication), suggesting that this figure is an underestimate of total eroded peridotite. For this reason, a volume of 2000 km^3 will be assumed. Coleman and Irwin (1974) presented a map, and thickness data, which allow an estimate of the volume of peridotite in the Papuan ophiolite. This volume is 1.12×10^5 km^3, or 56 times the estimated amount of peridotite required to explain the amount of chromite in the Tourelle Formation, its equivalents, and the Cloridorme, St. Irénée and Beaupré Formations. The Papuan ophiolite has a 7 km thickness of peridotite, whereas Williams and Stevens (1974) indicated approximately 3 km for the Bay of Islands Complex in

western Newfoundland. If we apply this difference as a correction factor, the areal extent of the eroded portion of the Ordovician ophiolite rises to 4.2% of the area of the Papuan ophiolite. This erosion all took place in the span of approximately 50 m.y. As a comparison, the Papuan ophiolite was emplaced approximately 60 m.y. ago (Coleman and Irwin, 1974), and retains much of its original peridotite. It therefore seems reasonable to suggest that the ophiolite slab obducted onto the Ordovician continental margin had dimensions similar to its Papuan analogue.

Summary

Provenance requirements resulting from study of the Tourelle heavy mineral suite are:

(a) a sedimentary source containing rounded ultrastable heavies,

(b) a volcanic source with epidote vein fillings, intruded by coarse-grained equivalents,

(c) an ophiolite source with chromite cumulates and pyroxene-rich peridotites.

Quartz Characteristics

A plot of quartz types in the previous chapter (Figure 6.5) suggests a middle- to upper-rank metamorphic source area for Tourelle quartz (Basu and others, 1975), which is consistent with derivation from amphibolite- and granulite-grade gneisses of the Grenville province (Douglas, 1970, p. 121-131). This method, however, is only designed for first cycle detritus, and therefore only indicates original provenance. In very mature quartz arenites, even polycrystalline quartz and grains with undulose extinction are selectively removed (Blatt and Christie, 1963).

Many quartz grains, particularly those in the coarse sand and granule sizes, are well rounded (Figure 7.5). These grains reach roundness values of 0.8 on the chart of Krumbein (1941)[1]. Quartz grains were not point counted for roundness because many samples have ragged grain margins due to reaction with calcite, and because operator variation in visual estimation of roundness is large (Griffiths and Rosenfeld, 1954; Blatt and others, 1972).

Abrasion studies of quartz grains indicate that extremely long distances of transport are necessary to achieve significant rounding (Thiel, 1940; Kuenen, 1959). For this reason, rounded quartz grains are frequently interpreted as

---

[1] On Krumbein's chart, roundness varies from 0.1 (angular) to 0.9 (very well rounded).

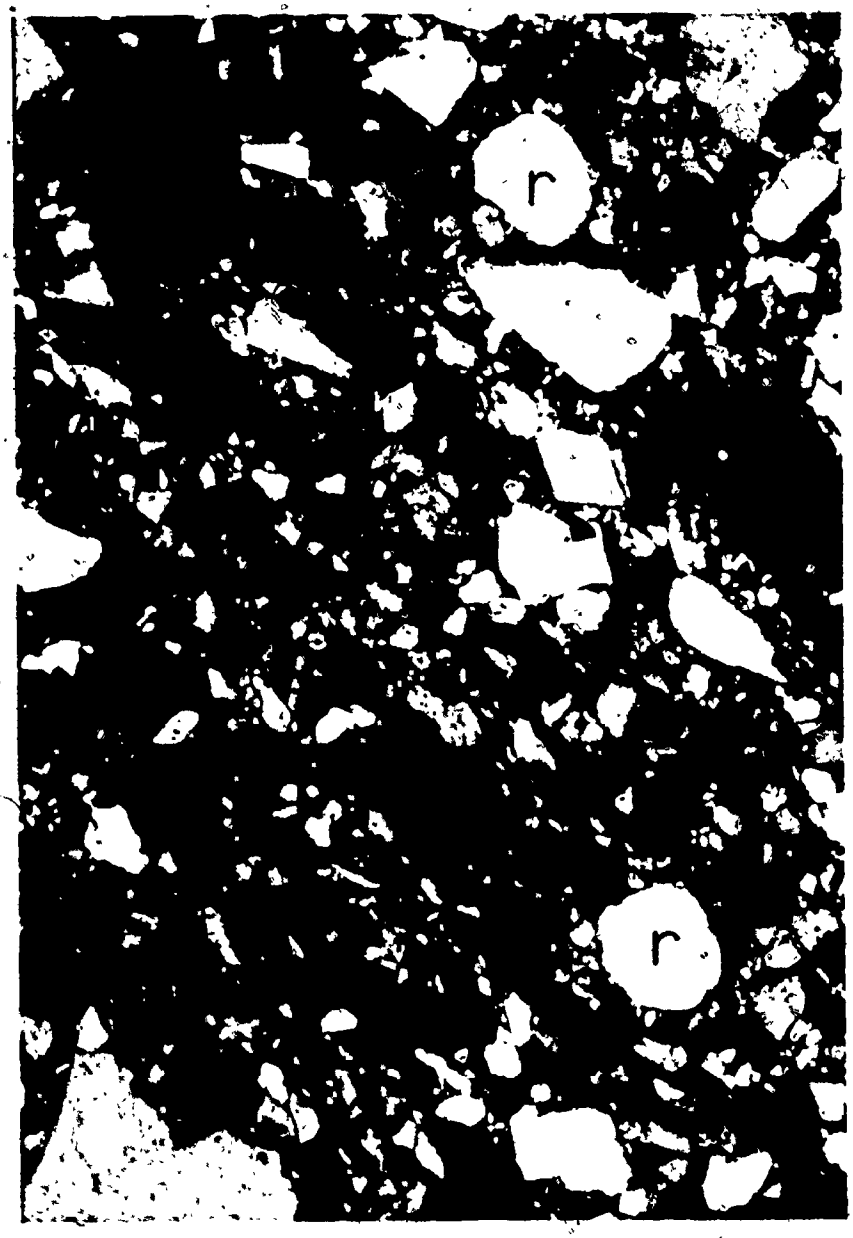

Fig. 7.5. Coarse Tourelle sandstone with large well-rounded quartz grains (r). Note very poor sorting. Crossed nicols, 120 x.

the product of more than one sedimentary cycle (Pettijohn and others, 1972). The fact that no basement pebbles were observed in the Tourelle Formation, in spite of competence of currents to carry pebbles and cobbles, lends support to this interpretation.

Regional Paleocurrents and Sediment Input

Equal-area current rose diagrams for all areas (A through M) are presented in Figure 1.5 (p. 10). In order to remove the effect of gentle folding about north-south axes, the bedding strikes for all paleocurrent data were normalized to an average value of 070°. In all areas except AII and M, paleocurrent measurements were rotated to a horizontal position about the strike direction, due to gentle (less than 20°) fold plunges. At AII, rotation by faulting was first removed, and at area M, the measured fold plunge of 23°E was first rotated to a horizontal position.

Parea (1968) demonstrated that paleocurrent measurements from allochthonous rocks in the northern Apennines were consistent with data from autochthonous formations of the same age. He stated that "the translation of allochthonous slabs parallel to themselves is a rule and the rotation of slabs, although possible, lacks any field evidence". On the basis of this observation, current directions in the transported

Tourelle Formation are assumed to have undergone no post-depositional rotation.

Figure 7.6 presents a compilation of all paleocurrent data from the Tourelle Formation. As indicated in Chapter III, all but a few of these measurements are consistent with scour and tool marks on coarse channel sandstones. The compilation shows that, in general, current flow was from east to west (oblique to the strike direction) with a large dispersion. Areas K and L contribute a minor mode indicating flow to the east. It was concluded in Chapter III that this mode represents sediment contribution from either an eastward-flowing mid-fan channel cutting obliquely down the surface of an asymmetric fan, or from a feeder channel to the west. This would suggest deposition in the area of overlap between two submarine fans. Mutti (1974, Figure 3) indicates equally divergent paleocurrent data associated with multiple feeder channels in mid-fan deposits of the Oligocene to Lower Miocene Messanagros Sandstone, Greece.

If we identify the regional strike direction with the original trend of the Lower Ordovician continental margin, Figure 7.6 indicates a mean paleoflow component toward the North American craton, which is consistent with a southeastern provenance.

It is likely that the Tourelle Formation and equivalents between Mont Joli and Marsoui were fed by several feeder channels. Unusually coarse, thick, channelized facies occur

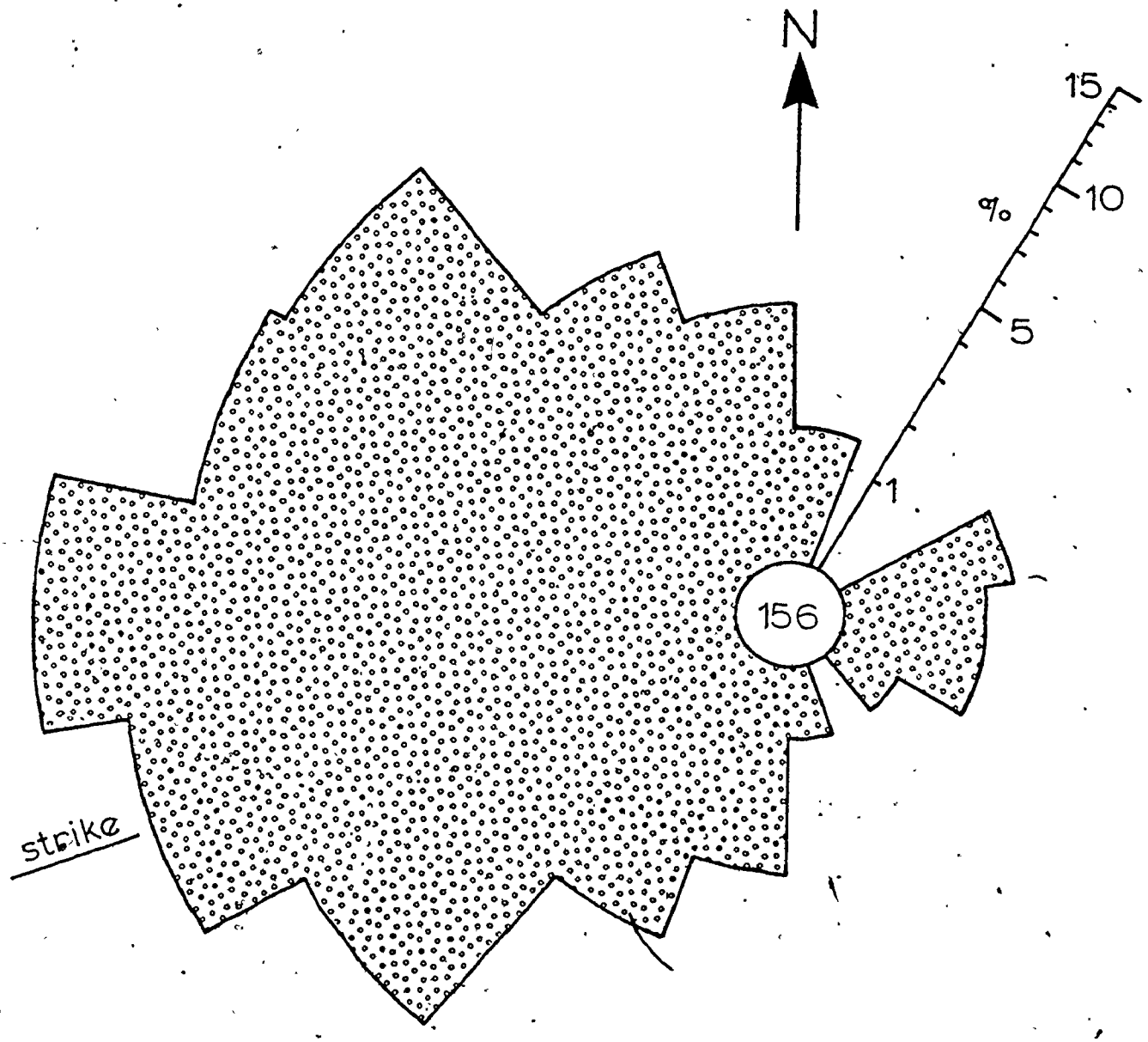

Fig. 7.6. Compilation of paleocurrent data from the Tourelle Formation. Each measurement corresponds to the average of sole markings on one layer. These data are only for layers whose current sense is known.

(i) in the Ste-Marthe channel, (ii) at area M, (iii) in the Cap Chat channel, and (iv) 5 km east of Ste-Félicité, where thick amalgamated sandstones contain boulders of green chert up to several metres long. The distances between these localities are 14 km, 28 km, and 43 km, respectively. It is interesting that paleoflow just west of Ste-Félicité is toward the east, suggesting the presence of yet another feeder channel. The short distances between these feeder channels suggests that the Tourelle Formation and equivalents consisted of a series of coalescing fans similar to the configuration of some modern alluvial fans, and to the San Lucas submarine fan, which is fed by four submarine canyons in 60 km (Normark, 1970).

Slump Folds

Paleoslope dips inferred from slump fold axes at area A are plotted in Figure 7.7. Data are not abundant enough to warrant a stereographic plot to determine slip-line (Hanson, 1967, 1971). Data which do not possess a sense of overturning are from slide blocks of dolomitic siltstone immediately below the Tourelle sandstones. The mode of paleoslope dips is approximately NW, and deviates by 50° from the regional strike.

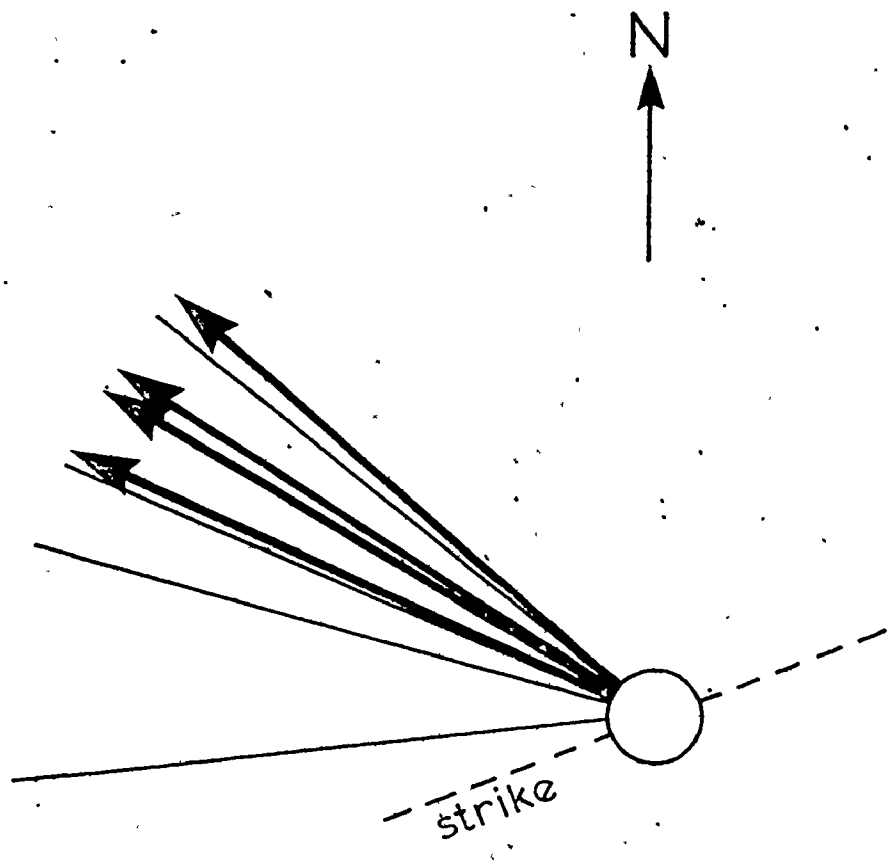

Fig. 7.7. Paleoslope dips deduced from slump fold geometry at area A. Bold arrows represent data from the sandstone slump on the east side of Cap des Méchins (Figure 2.31), where overturning of folds is conspicuous. Linear trends are from a slumped horizon of dolomitic siltstone on the west side of Cap des Méchins. Consistent overturning of folds is not evident at this locality.

Carbonate Conglomerate

Clasts from limestone breccia at area M contain shallow-water fauna and pelletal grains (Chapter II). Conodonts separated from these clasts belong to the North Atlantic province, and are of probable late Arenig age. Since graptolite fauna from the Tourelle Formation are of identical age, deposition of shelf carbonates shoreward of the Tourelle deep-water environment must be accommodated in any basin reconstruction.

Summary

The analysis of various provenance criteria has resulted in the following source area requirements.

(i) The original source area for most quartz and feldspar detritus was the Grenville province of the Canadian shield (mineralogy, quartz varieties, ultrastable heavy minerals), or a similar block of continental crust marginal to the craton. This material is believed to have passed through at least one previous sedimentary cycle prior to deposition in the Tourelle Formation (quartz and ultrastable heavy mineral roundness, lack of basement pebbles).

(ii) During Tourelle deposition, an inactive continental arc, or offshore volcanic arc on continental crust, was being

actively eroded (volcanic rock fragment composition, prismatic hornblende and pyroxenes). These volcanic rocks had been regionally metamorphosed at shallow depths to prehnite-pumpellyite grade, and were cut by veins containing epidote group minerals. Associated with these lavas were mildly metamorphosed, low-grade phyllites.

(iii) Bedded chert fragments were derived by erosion of cherts similar to those present in the underlying Cap des Rosiers Group (Chapter VIII).

(iv) The sand population of the Tourelle Formation was derived by mixing of river-derived sand (low OGNT/PGNT, fresh unstable heavy minerals, no shallow-water fauna) and sand which spent a longer time in the weathering environment, perhaps in a soil mantle (depleted heavy mineral suite) or in shallow marine environments. Because no sands contain resedimented shell debris, the former alternative is favoured.

(v) Ultramafic rocks, presumably obducted ophiolites, were being eroded, and contributed chromite grains and prismatic pyroxene to the heavy mineral suite. Hence, ophiolite obduction must have taken place at least as early as upper Arenig time (ca. 475 m.y. ago). This age is in reasonable agreement with radiometric dates of ophiolite obduction in Newfoundland (Dallmeyer and Williams, 1975 ; Mattinson, 1975; Archibald and Farrar, 1976; Dallmeyer, 1977). The ophiolite sheet is estimated to have been of comparable

size to the Papuan ophiolite (Davies, 1968). It is disturbing, however, that more ophiolitic detritus is not present. Several hundred metres of pillow lava (basalt), and kilometres of sheeted dikes, gabbros and peridotites (Williams and Stevens, 1974) are not represented in the detrital fraction of the Tourelle Formation. Only in the Middle Ordovician Cloridorme Formation does serpentine detritus become important. Perhaps unstable ophiolite fragments were selectively abraded and otherwise decomposed before reaching the site of Tourelle deposition. Certainly the mechanism of ophiolite emplacement is still poorly understood (Brookfield, 1977). Dismemberment of oceanic crust by faulting may have resulted in exposure of only peridotite. In Papua, ultramafics are preferentially exposed on the landward side of the continental margin (Davies, 1968).

(vi) Paleocurrents within the study area generally indicate flow from east to west with a component toward the continental interior. This evidence is corroborated by palcoslope dip directions inferred from slump folds. A minor paleocurrent mode from west to east may be the result of channel switching on the mid-fan, or overlap of adjacent fan systems.

(vii) Feeder channels (submarine canyons) are separated by distances ranging from 10 to 40 km, presenting the possibility of lateral coalescence of several small fan systems.

(viii) A shallow-water carbonate bank of unknown dimensions existed during Tourelle deposition.

The provenance requirements summarized above will be used in Chapter IX to reconstruct late Arenig paleogeography and paleotectonic regime.

CHAPTER VIII

FIELD DESCRIPTION: PRE-TOURELLE SEDIMENTS

General Description of Facies

Pre-Tourelle sediments are assigned to the Cap des Rosiers Group of Upper Cambrian to Lower Ordovician age, and are exposed both along the coast and inland in the Rivière Ste-Anne Nappe (Biron, 1972). The lithologies that were examined in coastal outcrops are discussed below.

Mudstones

Units of mudstone may be up to tens of metres thick with red, green or grey colouration. When fissility is well developed, the rock is called shale. Mudstones may show banding between green and dark grey varieties on a scale of centimetres to tens of centimetres. Some green bands are characterized by sharp flat bases followed by an upper transition into more fissile grey mudstone (Figure 8.1). This may indicate that green bands were actually deposited by density currents carrying only clay-sized material (or

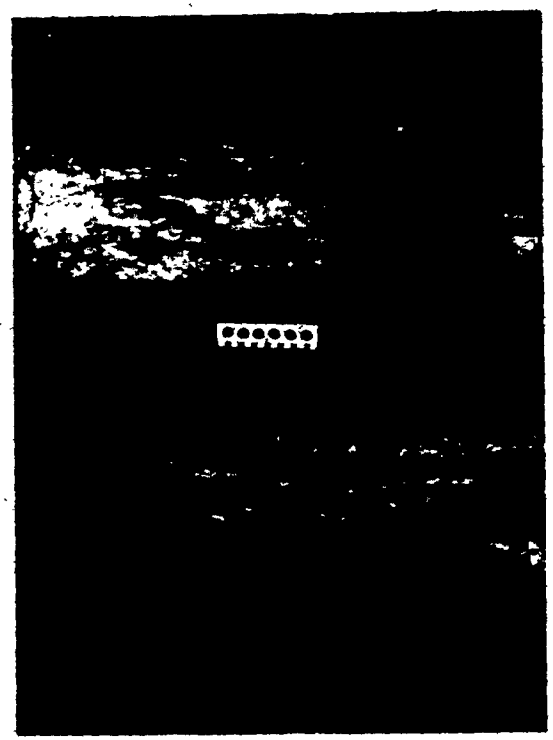

Fig. 8.1. Banded green and grey mudstone at Pointe Ste-Anne. Note upward gradation between green (light) and grey (dark). Scale 15 cm.

Fig. 8.2. Dolomitic siltstone facies at Petit Cap Percé. Two-lane highway gives scale.

flocs). A similar mechanism for deposition of Recent muds in the western Mediterranean Sea has been proposed by Rupke (1975).

Bioturbation of all mudstones is minor.

Dolomitic siltstones

This lithology is identical to facies 2b of the Tourelle Formation, and generally occurs interbedded with grey or green shale (Figure 8.2). The following charactertistics of these siltstones are essential to an interpretation of depositional mechanism.

(a) Inorganic sole markings are very rare (Figure 8.3).

(b) Soles may exhibit infilled vertical and horizontal deposit- or filter-feeder tubes. These do not continue into the siltstone above (see the section on fossil traces for one exception).

(c) Bases are sharp, with layer tops being somewhat more gradational but still abrupt.

(d) Internal sedimentary structures are confined almost entirely to ripples, climbing ripples, and convoluted ripples (Figure 8.4). Convolution, where present, only occurs above ripples. Ripples may be separated by mud drapes (Figure 2.5, Figure 8.4), producing flaser bedding or wavy bedding (Reineck and Singh, 1975). In general, ripple lamination is formed by an alternation of dolomitic silt and silty mud.

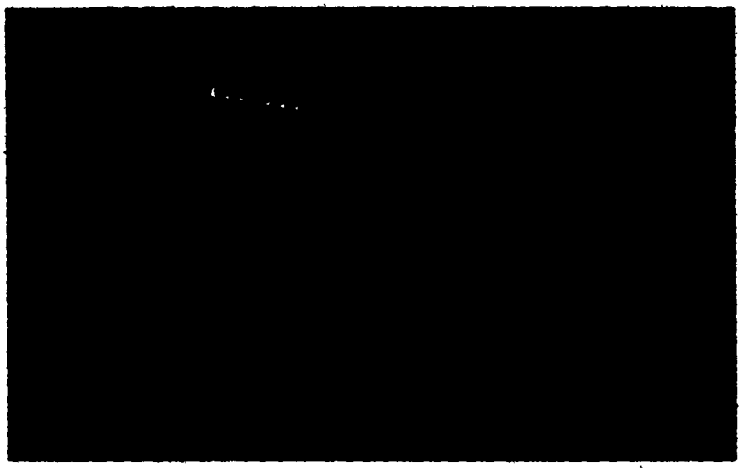

Fig. 8.3. Flutes on base of dolomitic siltstone layer west of Petit Cap Percé. Scale 15 cm.

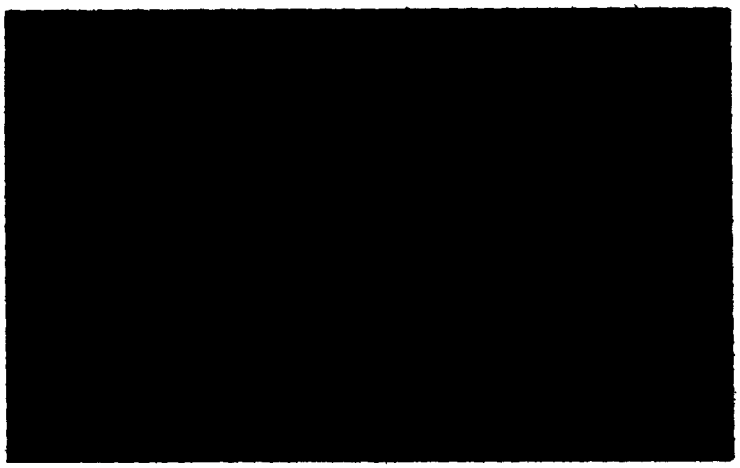

Narrow, small flutes on a dolomitic siltstone layer west of Petit Cap Percé. Scale 15 cm.

Fig. 8.4. Internal structures of dolomitic siltstone layers, Tourelle Formation and Cap des Rosiers Group. All scales are in centimetres. Slabs were etched in hydrochloric acid before being photographed.

(A) Mud-draped ripples producing "wavy bedding" (Reineck and Singh, 1975). This sample comes from a single layer.

(B) & (C) Ripples and deformed ripples.

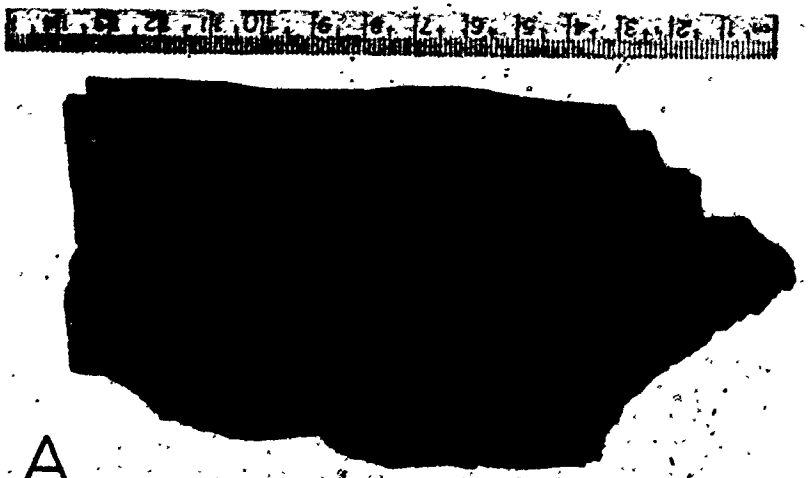

A

FIG. 8.4

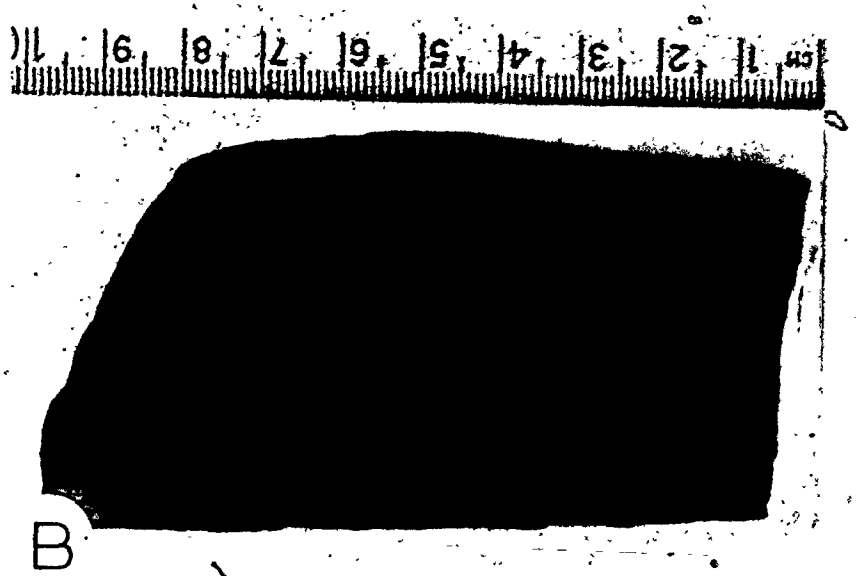

B

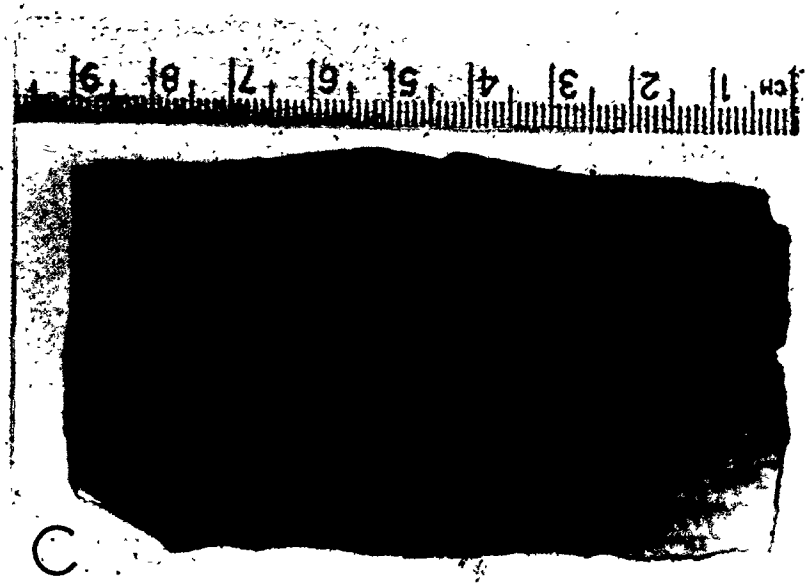

C

(e) Siltstones are generally less than 20 cm thick, but form well over 50% of facies 2b units.

(f) Individual layers are parallel sided and continuous across outcrop areas.

According to criteria tabulated by Nelson and others (1975) and Mutti (1977), these dolomitic siltstones are best classified as proximal overbank turbidites. Mud drapes may be due to fluctuating overbank spill, transport of clays as flocculated particles, or reworking of detritus by bottom currents.

In thin section, these siltstones are composed of densely packed dolomite crystals (90 to 95%) with scattered quartz silt grains. It is believed that all grains are primary, because quartz and dolomite particles are of similar size (approximately 0.02 mm), and because some dolomite crystals seem to have rounded corners.

Two lenticular fine pebble conglomerate layers are found interbedded with dolomitic siltstone layers. These are less than 50 cm thick, and are essentially chert, carbonate, and phosphatic pebble conglomerates. In addition, a few dolomitic siltstone layers possess a lower division of fine pebble conglomerate with the following component clasts:

(i) micritic carbonate with stylolite seams and scattered dolomite rhombs;

(ii) dolomitized bioclastic limestones with only vague outlines of fossil fragments;

(iii) very well sorted pelletal limestone clasts with sparry calcite cement and scattered dolomite rhombs (Figure 8.5). Many pellets are completely replaced by micro-crystalline quartz;

(iv) very finely crystalline chert, which is true micro-crystalline quartz and not cherty mudstone (compare with bedded chert rock fragments in Tourelle Formation, Chapter VI). Many of these grains are replacements of bioclastic or pelletal carbonate rocks, with shell debris remaining unreplaced (Figure 8.6);

(v) nodular to massive, isotropic phosphorite (Figure 8.7);

(vi) dolomitic siltstone;

Pyrite nodules are also present.

The conglomerate layers record a complex diagenetic history (Figure 8.8) starting with replacement of the margins of carbonate clasts by chert, and precipitation of a rim of fibrous chalcedony around grain boundaries. The remaining pore space was then filled with sparry carbonate cement (dolomite?), followed by growth (by replacement) of euhedral dolomite rhombs.

Figs 8.5 to 8.8. Clast varieties and diagenesis in conglomerates found in the dolomitic siltstone facies, Cap des Rosiers Group west of Pointe Bourdage (photomicrograph magnifications approximate).

Fig. 8.5. Pelletal grain with sparry cement. Crossed nicols, 75x.

Fig. 8.6. Chert clast containing unreplaced carbonate fossil fragments. Crossed nicols, 75x.

Fig. 8.7. Nodular phosphorite under strong illumination. Plane light, 75x.

Fig. 8.8. Diagenesis of conglomerate layers. The margin of this pelletal carbonate grain (left) was replaced by chert (Ch), followed by growth of a rim of fibrous chalcedony. The remaining pore space (upper right) was filled with sparry carbonate cement (dolomite?). Crossed nicols, 200x.

FIG. 8.6

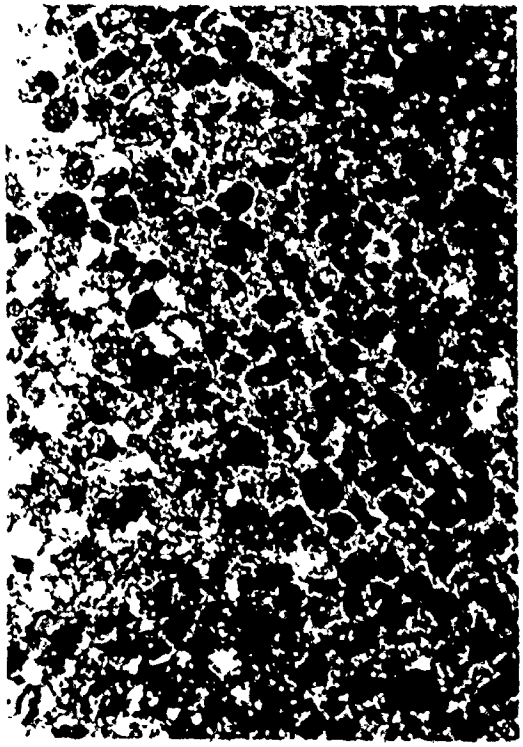

FIG. 8.5

FIG. 8.8

FIG. 8.7

Calcisiltites and calcarenites

These limestone layers are composed almost entirely of carbonate grains in a sparry calcite cement. In calcarenite layers, micritic grains are most common, with minor bioclastic fragments, quartz grains, and rare ooids (Figure 8.9). This facies contains graded, laminated or rippled calcarenites, generally less than 20 cm thick, and thin ribbon limestones (Figure 8.10), each only a few cm thick and bounded by shale partings. In ribbon limestone units, individual layers commonly appear massive and have sharp bases and tops. Some ribbon limestones are nodular (Figure 8.11). Similar calcisiltites with thin or absent shale partings are rippled throughout (Figure 8.12). These thin-bedded facies are similar to deposits classified by Wilson (1975, p. 356) as deep shelf margin facies, deposited at the toe of a carbonate-bank slope.

At Pointe Ste-Anne (Figure 8.19, 245 m in section), thin lenticular beds composed of ripples and starved ripples occur in a background of shale (Figure 8.13). Nelson and others (1975) indicate that starved ripples are common in overbank deposits. Nevertheless, these lenticular ripple trains may have been produced by the winnowing action of bottom currents.

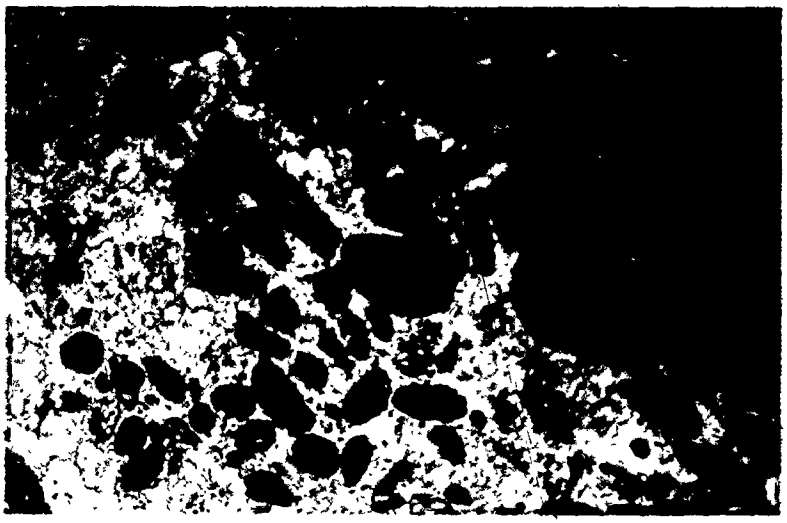

Fig. 8.9. Photomicrograph of calcarenite sample from Pointe Ste-Anne. Plane light, 30x.

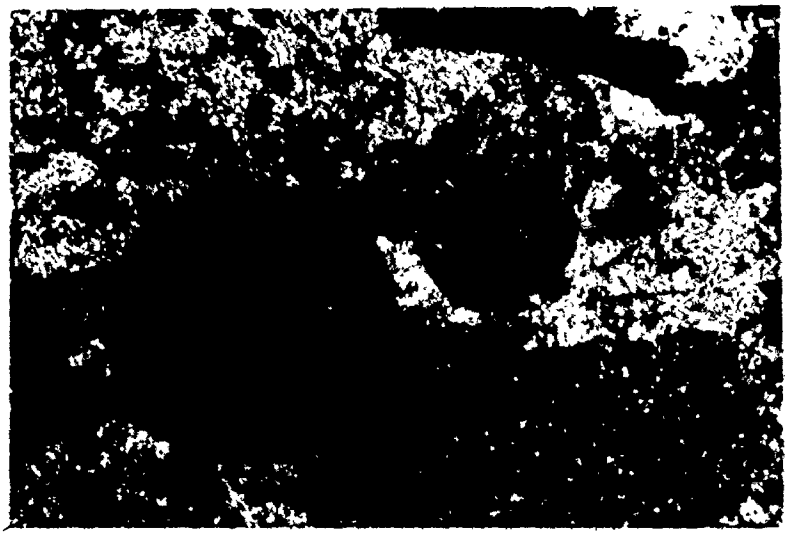

Ooid in coarse calcarenite, Pointe Ste-Anne. Cement is sparry calcite. Crossed nicols, 200x.

Fig. 8.10. Calcisiltites and calcarenites.

(A) Fine calcarenites and calcisiltites west of Pointe Ste-Anne. Scale 1 m. Top is to the right. Paired burrows are common.

(B) Fine calcarenites at Anse à Perré, west of Ste-Anne des Monts. Hammer for scale. Top is to the left.

(C) Ribbon limestones at Pointe Ste-Anne. These appear massive and may have paired burrows on their soles. Scale 1 m. Top is to the right.

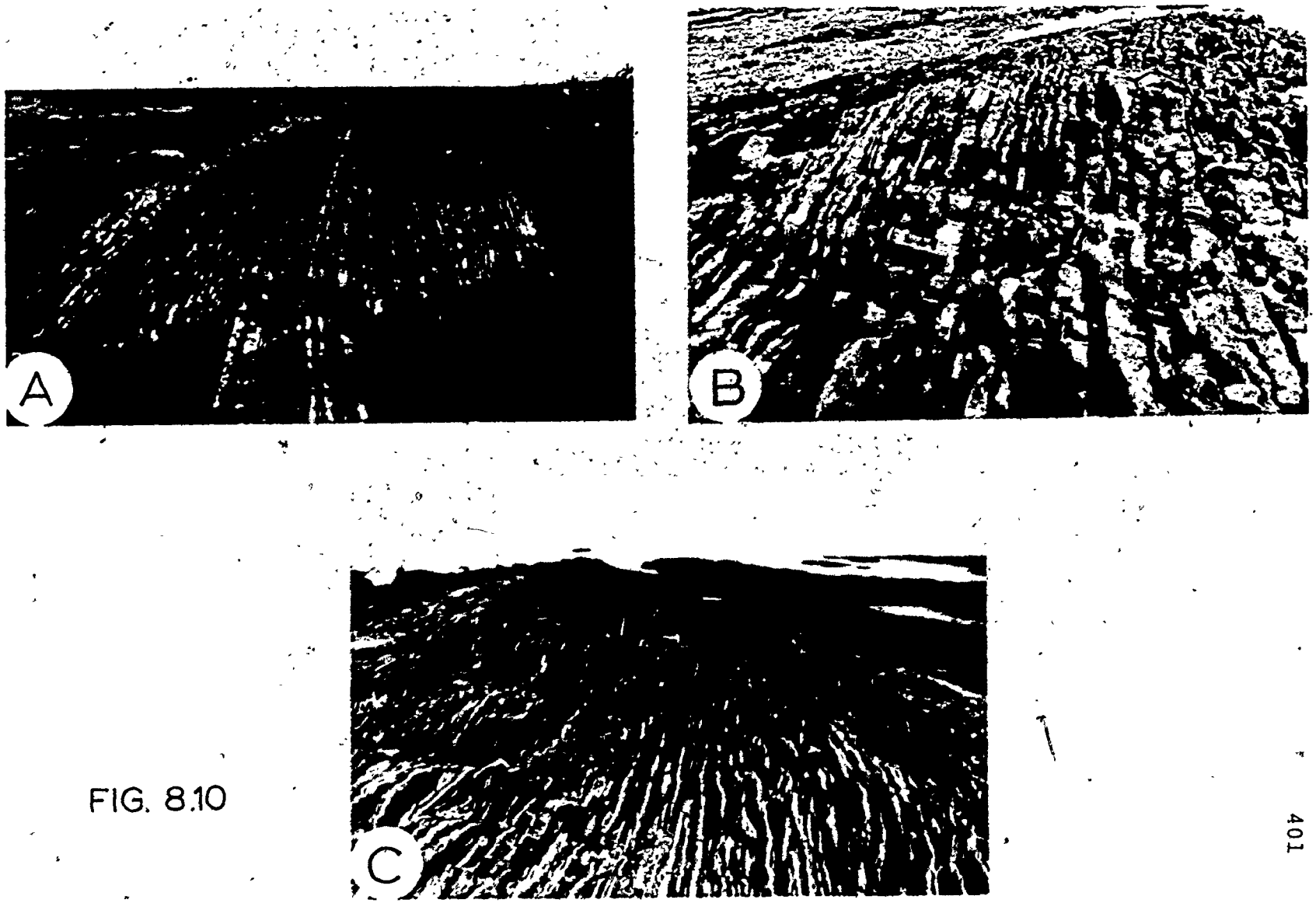

FIG. 8.10

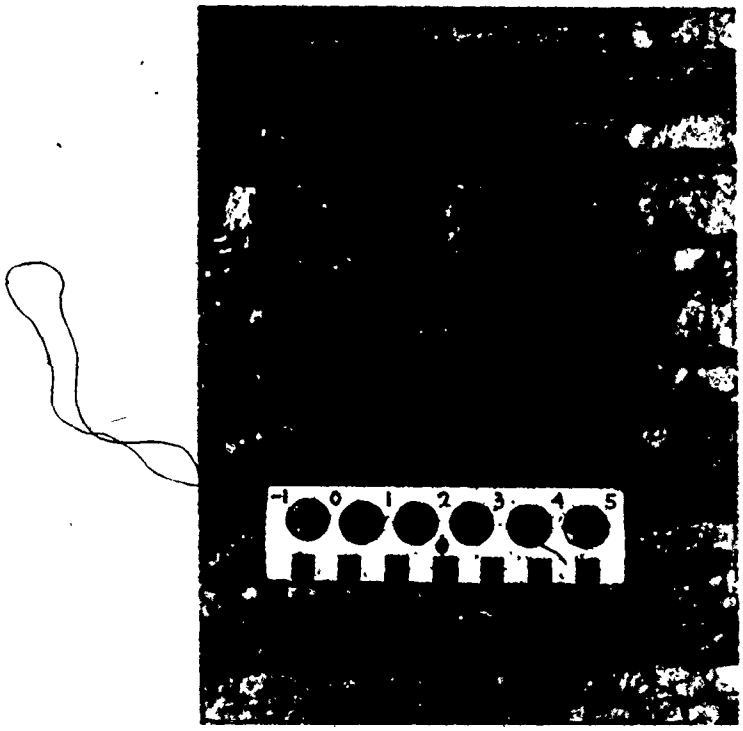

Fig. 8.11. Nodular limestones below area A, Cap des Méchins. Scale 15 cm.

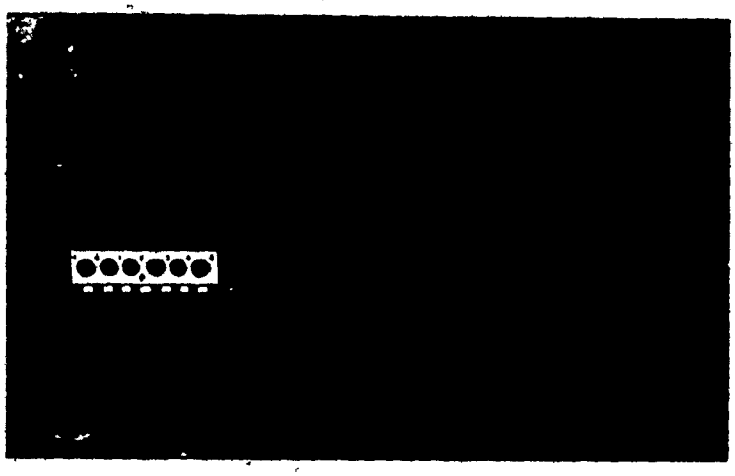

Fig. 8.12. Rippled calcisiltite with rare shale partings east of Ste-Marthe. Scale 15 cm.

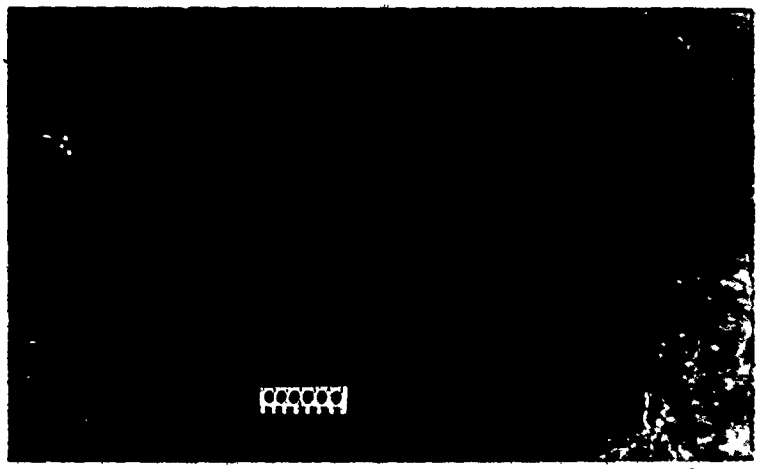

Fig. 8.13. Thin rippled calcisiltites with starved ripples at Point Ste-Anne. Scale 15 cm.

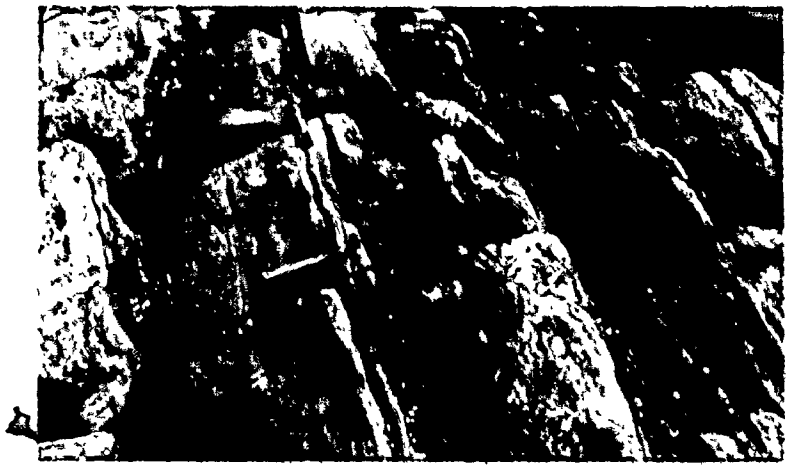

Fig. 8.14. Stratified and cross-stratified calcarenites above conglomerate packet, Pointe Ste-Anne. Hammer for scale. Top is to the right.

Calcarenites associated with limestone breccia beds commonly display stratification or cross-stratification (Figure 8.14). At Pointe Ste-Anne, one 130 cm thick calcarenite contains abundant dish structure.

Quartz siltstones and arenites

Quartz siltstones are almost identical in outcrop appearance to dolomitic siltstones. Quartz arenites occur in layers to 5 m thick at Pointe Ste-Anne. These are massive layers of fine to medium sandstone with abundant fluid-escape structures (Figure 8.15) and possible dish structure. Quartz is the dominant detrital component, with feldspar, mica, and carbonate rock fragments being of minor importance. Quartz cement has grown in optical continuity with original grains, resulting in an interlocking fabric and long grain contacts. Original grain boundaries are commonly partially outlined by minute bubbles or mica flakes.

Quartz arenites, unlike Tourelle sandstones, are well sorted. This may explain the presence of dish structure.

Fig. 8.15. Fluid-escape structures in thick quartz arenites, Pointe Ste-Anne.

(A) Sinuous pillars. Scale 15 cm.

(B) Upper surface of a layer showing sheet structure. Hammer for scale.

(C) Large pillars causing deformation of lamination along their margins. These laminations resemble large dish structure. Scale 15 cm.

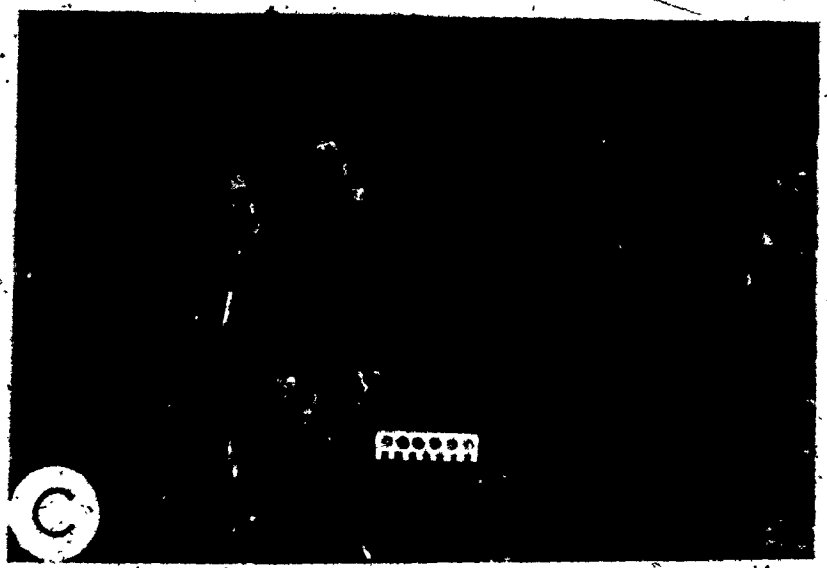

FIG. 8.15

Breccias

With but one exception at Pointe Ste-Anne (next section), breccia beds consist of densely packed fine calcarenite and ribbon limestone clasts (Figure 8.16), some of which have rounded margins. These beds are graded and may be capped by stratified to cross-stratified coarse calcarenite. Clasts are large thin plates (less than 10 cm thick) derived from clastic carbonate layers which have failed, slumped, and broken up in a manner similar to the behavior of ribbon limestones at Green Point in western Newfoundland (Figure 8.17). This process requires both the deposition of thin calcisiltites and calcarenites on a submarine slope, and early submarine cementation.

Bedded chert (and siliceous mudstone)

Bedded cherts may be dark brown or green in colour and occur both as thin beds interstratified with fissile shale (Figure 8.18a), or as thick laminated units (Figure 8.18b). These cherts may be internally burrowed. Some chert beds contain quartz-infilled radiolarian tests (Figure 6.6f).

West of Marsoui, bedded chert occurs above the Ste-Marthe channel, which is filled with coarse sandstones of the

Fig. 8.16. Limestone breccia at Pointe Ste-Anne, containing densely packed fine calcarenite and ribbon limestone clasts. Scale 15 cm.

Fig. 8.17. Green Point (Newfoundland) model for formation of limestone breccias by slumping of thin limestone layers on a submarine slope. The layer closest to the observer contains tight slump folds. The layer on the right had broken up into irregular polygons following (i) submarine cementation, and (ii) movement on the slope. Failure of this layer would have produced a limestone breccia layer similar to that in figure 8.16. Breccias of this type are also found at Green Point. This photo shows the bases of the layers.

Fig. 8.18. Bedded chert of the Cap des Rosiers Group.

(a) Alternation of thin chert beds and fissile shale. These cherts are associated with a dolomitic siltstone unit west of Pointe Bourdage. Scale 15 cm.

(b) Massive, laminated bedded chert west of Pointe Bourdage. These cherts contain rare burrows and are pale green in colour. Scale 15 cm. Top is to the left.

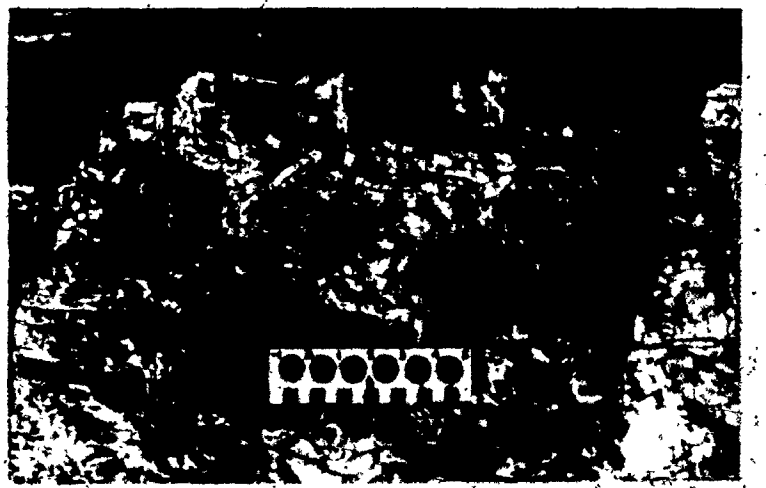

FIG. 8.16

FIG. 8.17

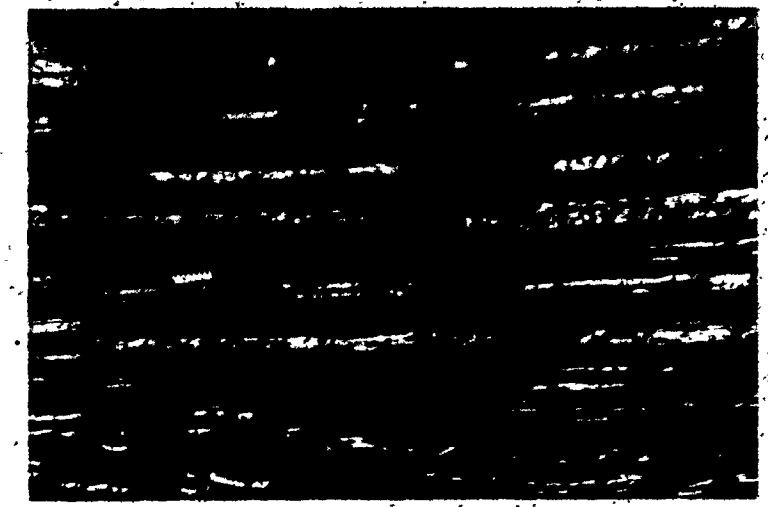

FIG. 8.18a

FIG. 8.18b

Tourelle Formation. This channel is interpreted as a submarine canyon cut into the top of the Cap des Rosiers Group (Chapter III), which would suggest that bedded chert may have been deposited on a depressed shelf margin or directly on the upper part of a submarine slope.

Point Ste-Anne Section

Point Ste-Anne is located 4 km west of Ste-Anne des Monts (see Figure 1.5). A 385 m section was measured through the Cap des Rosiers Group at this locality to illustrate the pattern of sedimentation prior to Tourelle deposition (Figure 8.19). This section overlies a thick unit of red shale. The following features are noteworthy.

(i) The lower breccia layers (30 to 34 m) contain cobbles and boulders of rippled quartz arenite and limestone in a matrix of coarse quartz sand (Figure 8.20). The lowest thick breccia (3 m thick) is inverse-to-normally graded.

(ii) Fine quartz arenites at the base of the section are thick (to 5 m), poorly graded, and contain abundant fluid-escape structures, including dish structure.

(iii) All clastic layers below 170 m in the section contain quartz detritus, whereas layers above this level (starting at 230 m) contain only limestone clasts. Sixty metres of shale intervenes between deposits of these two

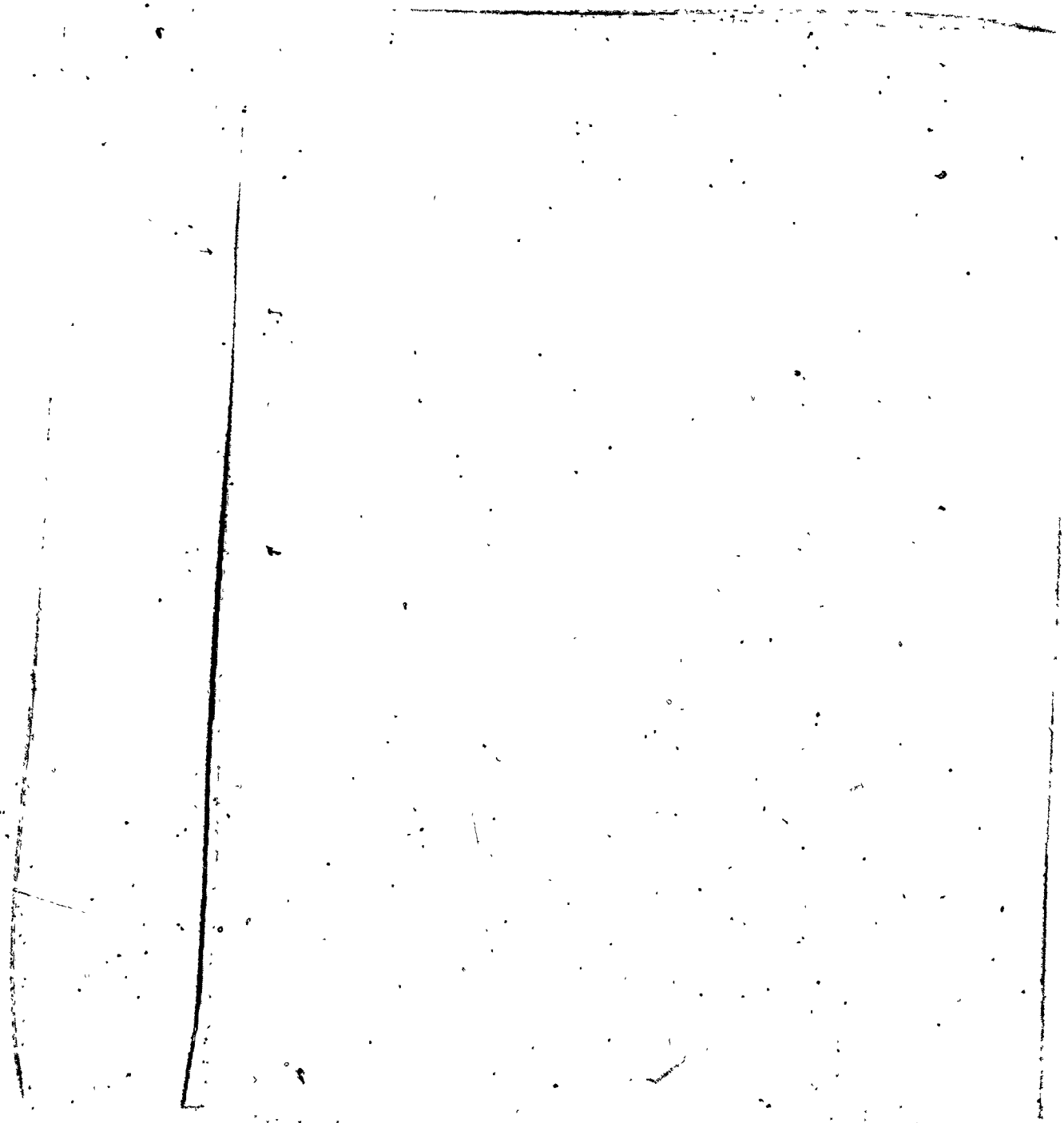

Fig. 8.19. Stratigraphic section through the upper part of the Cap des Rosiers Group, Pointe Ste-Anne. Symbols are explained along the margin of the section. Scale is in metres. See text for discussion.

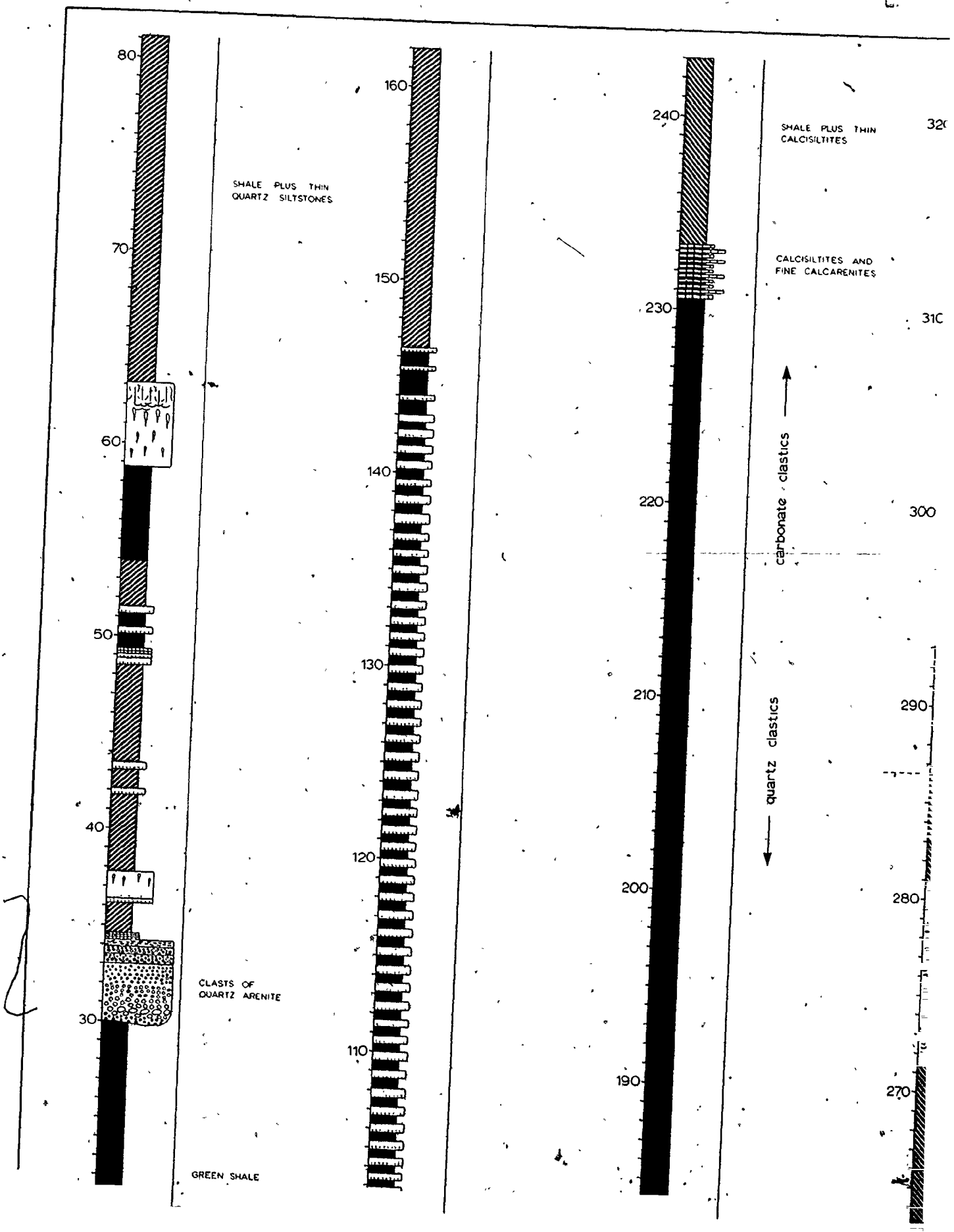
80
70
60
50
40
30
SHALE PLUS THIN QUARTZ SILTSTONES
CLASTS OF QUARTZ ARENITE
GREEN SHALE
160
150
140
130
120
110
240
230
220
210
200
190
SHALE PLUS THIN CALCISILTITES
CALCISILTITES AND FINE CALCARENITES
carbonate - clastics
quartz clastics
320
310
300
290
280
270

3 of

POINTE STE-ANNE

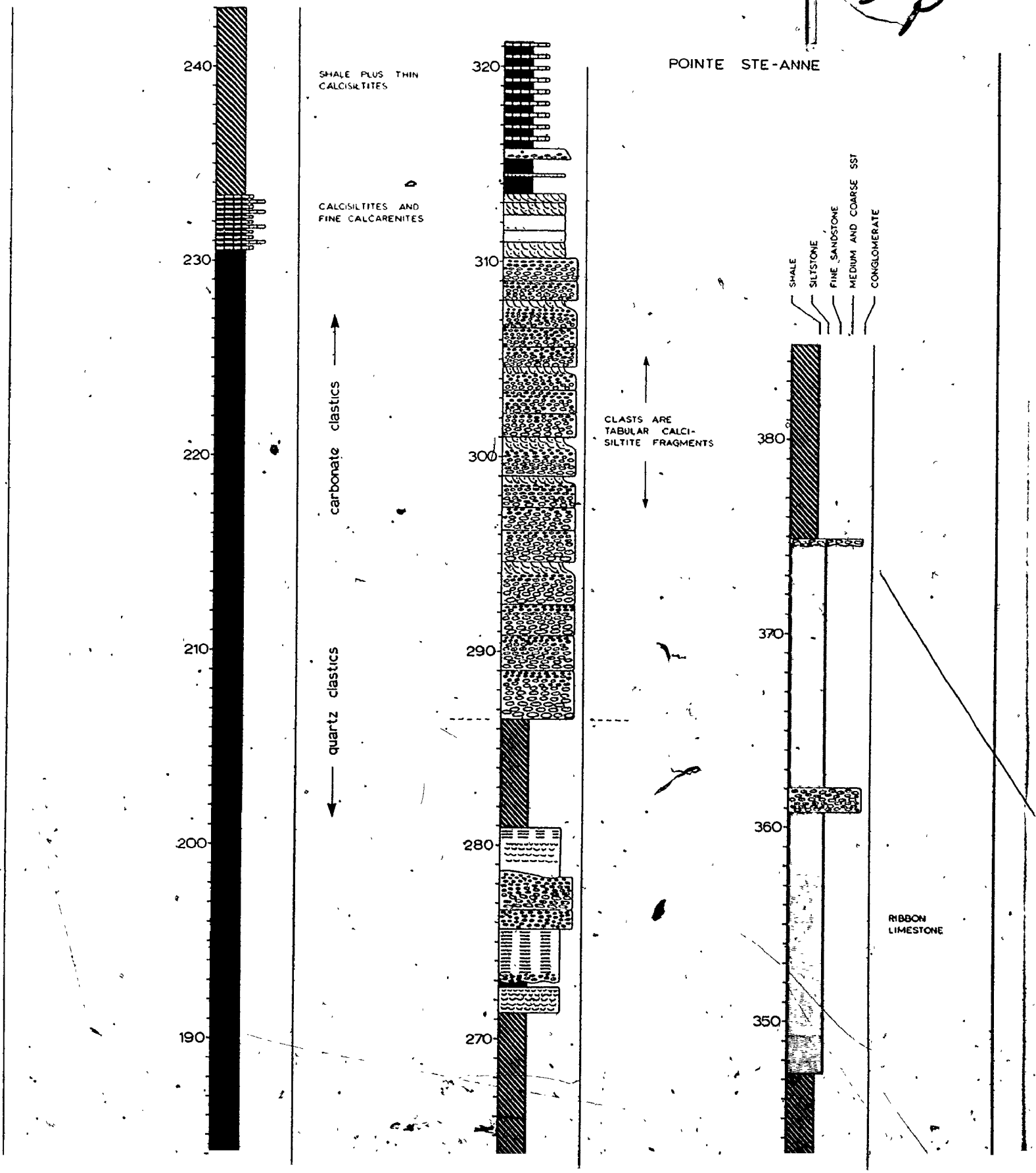

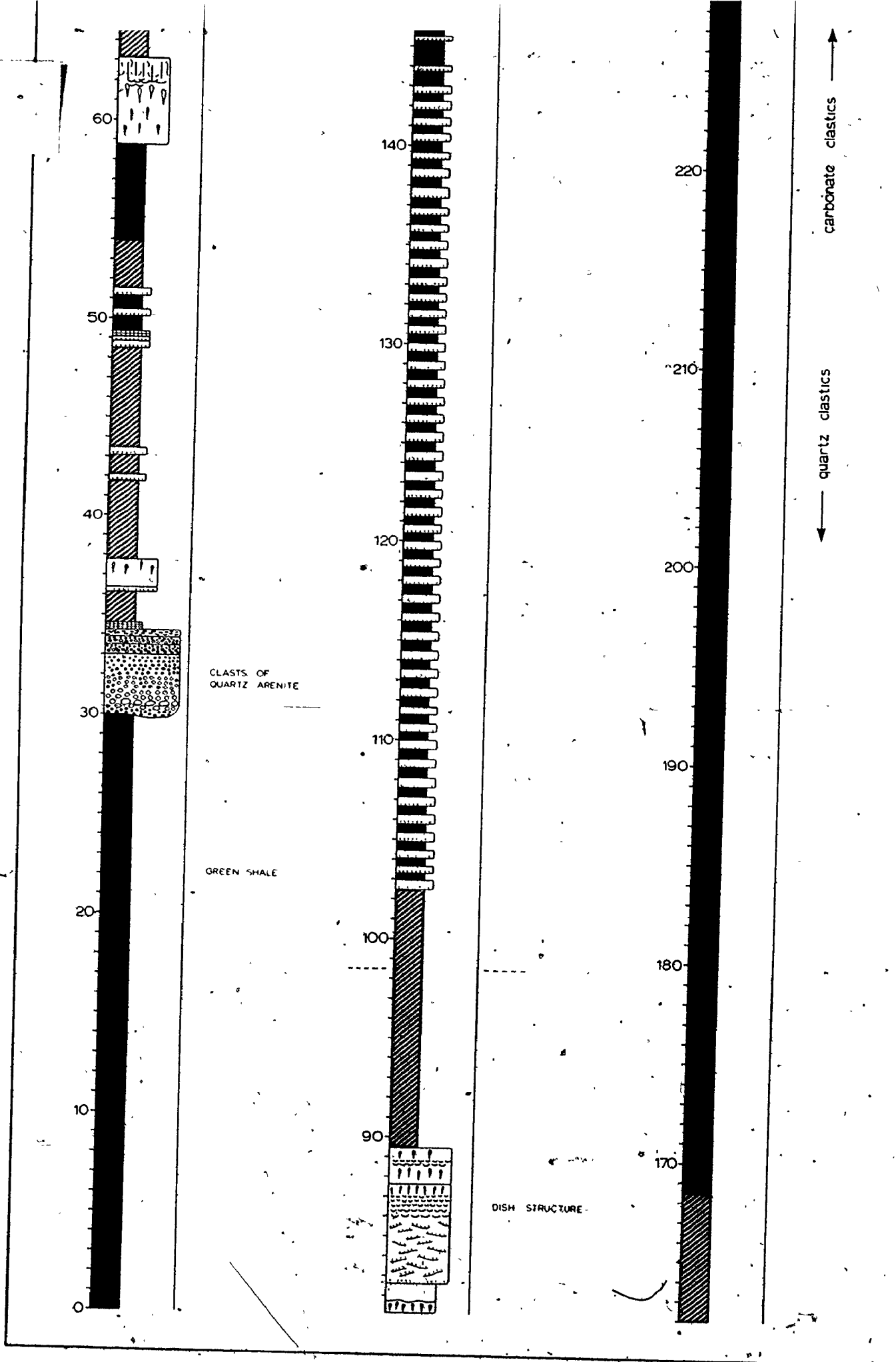
carbonate clastics
quartz clastics
CLASTS OF QUARTZ ARENITE
GREEN SHALE
DISH STRUCTURE
0
10
20
30
40
50
60
90
100
110
120
130
140
170
180
190
200
210
220

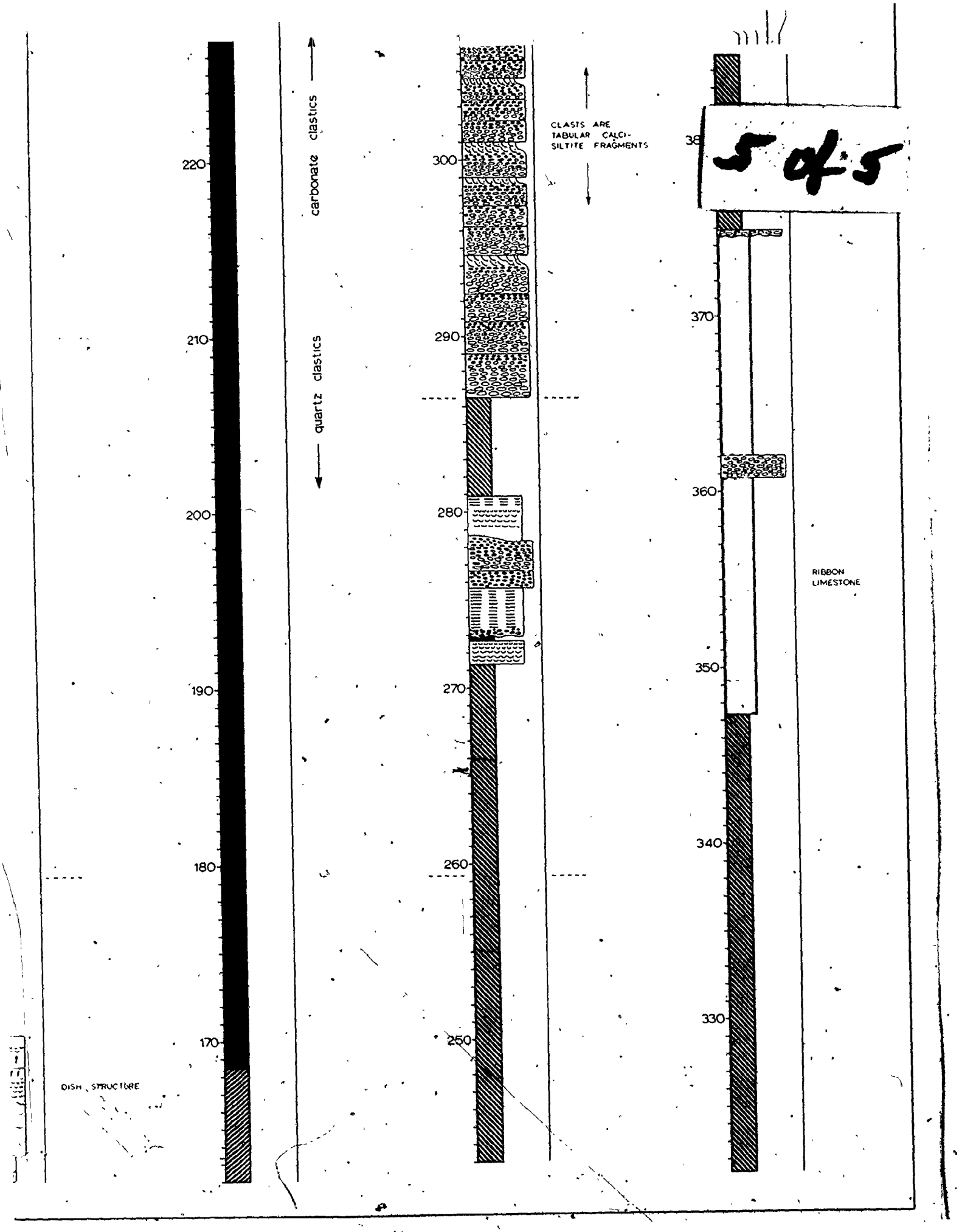
carbonate clastics
quartz clastics
CLASTS ARE TABULAR CALCI-SILTITE FRAGMENTS
5 of 5
RIBBON LIMESTONE
DISH STRUCTURE
220
210
200
190
180
170
300
290
280
270
260
250
380
370
360
350
340
330

different mineralogical compositions. The upper half of this is black shale. This shale implies a significant period of isolation from sources of coarse detritus, perhaps on a submarine slope or in a deep basin.

(iv) The lowest carbonate clastics are fine calcarenites and calcisiltites (230 to 271 m). These are followed by two packages of coarse calcarenites and limestone breccia (Figure 8.21). Calcarenites above breccia beds commonly form cross-bed sets. In the packet from 287 to 313 m, graded breccia layers decrease in thickness from several metres at the base of the packet to less than 1 m at the top. Hence these breccias form a fining and thinning upward sequence (positive cycle) suggesting deposition in a submarine channel (Ricci Lucchi, 1975).

(v) Limestone breccias are overlain by thin calcisiltites and ribbon limestones, which may represent deep shelf margin deposits (Wilson, 1975). Similar beds must certainly have been deposited on or at the top of a submarine slope, because they provided clasts for intercalated limestone breccia layers.

In the deformed Cap des Rosiers Group west of Marsoui, it again appears that quartz clastics (in this case siltstones) occupy the base of the observed stratigraphy and are overlain as one proceeds westward by mudstones, siliceous mudstones, dolomitic siltstones, fine calcarenites, and thin calcisiltites

Fig. 8.20. Lowermost breccia layer at Pointe Ste-Anne. Boulders of quartz arenite and limestone are set in a matrix of coarse quartz sand. This layer is inverse-to-normally graded. Hammer for scale. Top is to the right.

Fig. 8.21. Limestone breccia near the top of the Pointe Ste-Anne section.

(A) General view of the 27 m thick breccia unit. Layers thin upward. Top is to the right.

(B) Close-up of a breccia layer. Clasts are fragments of slumped and broken calcisiltite and calcarenite layers, and were derived in a similar fashion to platy clasts in limestone breccias at Green Point, western Newfoundland. Scale 1 m. Top is to the right.

FIG. 8.21a

FIG. 8.21b

FIG. 8.20

(including ribbon limestone). This stratigraphy is then cut into by feeder channels for Tourelle fans and is capped by bedded chert.

Fossil Traces

The trace fossil assemblage of the Cap des Rosiers Group achieves higher densities and is more widespread than the trace fossil assemblage of the Tourelle Formation. Siliceous mudstones and bedded cherts are frequently burrow mottled and may have horizontal grazing traces or suspension-feeder tubes preserved on bedding surfaces. Burrowing is very minor, however, so that primary lamination is preserved.

The greatest densities of fossil traces are found on the bases of dolomitic siltstone layers (Figure 8.22a,b). The assemblage is that of Planolites, and vertical suspension-feeder tubes. It is not always apparent whether these tubes are paired (Arenicolites or Diplocraterion), or single (Skolithos). Examination of slabbed siltstone beds indicates that these tubes were present in subjacent muds and were infilled by deposition of silt. Only in one dolomitic siltstone interval did vertical tubes pass up into the siltstone layers (Figure 8.22c). These siltstones were quite muddy and may have been deposited slowly, allowing bottom dwellers to survive sedimentation.

Fig. 8.22. Fossil traces on the soles of dolomitic siltstone layers. Trace fossils are named on the basis of similarity with published illustrations.

(A) Dense population of Planolites and vertical tubes on a dolomitic siltstone layer west of Petit Cap Percé. Note flutes on overlying layers. Scale 15 cm.

(B) Close-up of (A). Scale in centimetres.

(C) Vertical tubes which pass up into overlying dolomitic siltstone layer west of Pointe Ste-Anne. Scale in centimetres.

(D) Paired vertical burrows on the base of a dolomitic siltstone layer in the large slide block, area A. Scale in centimetres.

(E) Abundant suspension-feeder tubes, area J. Scale in centimetres.

(F) Same as (D). Short horizontal traces represent segments of burrows which were not themselves consistently horizontal. Scale in centimetres.

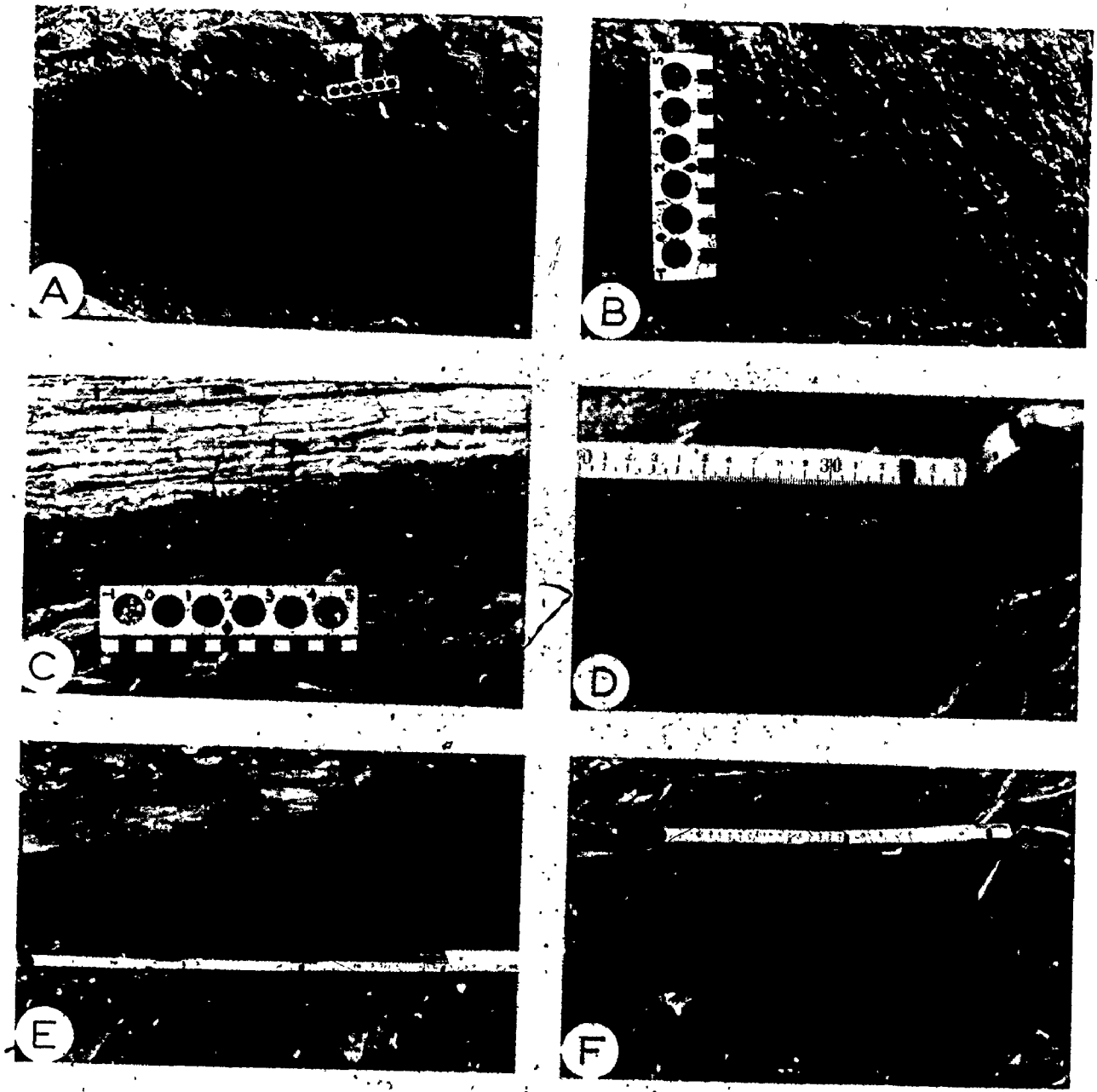

Fig. 8.22

Some suspension-feeder tubes strongly suggest a paired configuration (Figure 8.22d,e), whereas denser populations preclude such an evaluation (Figure 8.22f). Small vertical tubes on one ribbon limestone at Pointe Ste-Anne are clearly paired.

Environmental Interpretation

There are several lines of evidence which suggest that carbonate clastics were deposited on a submarine slope, perhaps in front of an active carbonate bank.

(i) Some dolomitic siltstones possess mud-draped ripples which may be the result of slow reworking of silt by bottom currents. In modern oceans, clear-water currents capable of transporting sediment below storm wave-base are restricted to the continental slope (Bouma and Hollister, 1973).

(ii) Thin calcisiltites resemble facies deposited at the toe of a carbonate-bank slope. The abrupt tops of many of these layers cause them to resemble strongly the Lower Niesenflysch, Switzerland, which is interpreted by Bouma and Hollister (1973) as a contourite deposit.[1]

---

[1] Contourites are clastic layers deposited by "relatively slow moving (less than 0.5 m/sec), relatively clear (sediment concentrations less than 100 to 200 micrograms/litre), contour-following ocean-bottom circulation" (Bouma and Hollister, 1973, p.92).

(iii) Carbonate breccias are formed of tabular fragments of slumped and brecciated calcisiltite and fine calcarenite layers. This requires deposition of the fine clastic limestones on a submarine slope. This same facies, however, occurs interbedded with derived breccias, both at Pointe Ste-Anne, and at Green Point in western Newfoundland, suggesting that the breccias themselves may have been deposited in aggrading slope channels.

(iv) The local high densities of suspension-feeder burrows and their dominance of the Cap des Rosiers Group ichnocoenose suggests deposition at outer shelf or upper slope depths (Dörjes and Hertwick, 1975).

These carbonate clastics also underlie the Tourelle Formation (particularly abundant dolomitic siltstones), and are of Lévis zone B and C age (J. Riva, personal communication, 1975), which is just slightly older than sandstones of the Tourelle Formation (Lévis zone D). If these facies are indeed slope deposits, then it is probably the same slope over which the Tourelle sands were transported. This requires the same directional source for both carbonate clastics and the mineralogically immature detritus of the Tourelle Formation. Paleocurrent measurements obtained from dolomitic siltstones within the deformed Cap des Rosiers Group west of Marsoui indicate longitudinal transport from east to west. Measurements on quartz siltstones are variable and probably can not be trusted.

Quartz clastics are identical mineralogically to quartz arenites of Kamouraska type (Hubert, 1973), and therefore are interpreted to have been derived from a northern cratonic provenance (Lajoie and others, 1974). The coarser facies were presumably deposited in submarine channels. This interpretation requires that quartz clastics and carbonate clastics have a different source area (see preceding paragraph). At Pointe Ste-Anne, the time period representing the transition from a northern to a southern provenance is recorded by 60 m of mudstone (Figure 8.19).

Sub-Tourelle Deformation

Terminology

The following definitions will be required for this discussion.

(i) Mélange: a mappable body of deformed rocks characterized by the inclusion of native and exotic blocks in a pervasively sheared, commonly pelitic matrix (Hsu, 1968).

(ii) Broken formation: a body of pervasively sheared strata that contains no exotic elements and that functions as a rock-stratigraphic unit (Hsu, 1968).

(iii) Olistostrome: a sedimentary deposit occurring within a normal geologic sequence that is characterized by

lithologically heterogeneous material, more or less intimately admixed, and that was accumulated as a semifluid body (Flores, 1955).

(iv) Wildflysch: includes both mélange and olistostrome (Hsu, 1974).

(v) Sedimentary mélange: a deformed olistostrome with tectonically admixed exotic blocks (Hsu, 1974).

Field observations

The Cap des Rosiers Group between Marsoui and Cap des Méchins is moderately to intensely deformed, and has been referred to as the Cap Chat mélange (Biron, 1974; St. Julien and Hubert, 1975). It has even been suggested that the Tourelle Formation outcrops may be large blocks or olistoliths in this mélange or wildflysch (Biron, 1974). Liard (1973) described a similar zone of mélange beneath the Métis Formation (Chapter I) south of Matane.

In order to reconstruct tectonic events associated with Tourelle deposition, it is necessary to discover the significance of this deformed zone. Was the Tourelle Formation deposited on top of a pre-existing wildflysch? Did deformation take place during tectonic emplacement of the allochthon?

The best exposure of the deformed zone of the Cap des Rosiers Group occurs between Pointe Bourdage (just west of

Marsoui), and 2 km west of Cap à la Marte (town of Ste-Marthe). The total length of this shore zone is 8 km. Low-tide aerial photographs were enlarged to a scale of 1 cm = 10 m. The 8 km of coastline was then mapped directly on these photo enlargements. Strike and dip of bedding, cleavage, and fault traces; and orientation of fold axes and axial planes were measured. Paleocurrent measurements (from sole markings) were also recorded at various stations. These were classified from 1 (reliable) to 3 (unreliable) on the basis of proximity to a fold axis of known plunge which could be used for restoration of bedding to a horizontal position.

Two maps are provided in the rear pocket of the thesis, one from Pointe Bourdage to Pointe Noire (eastern portion), and the other from Cap à la Marte westward (western portion). These are called the Pointe Bourdage and Ste-Marthe sheets, respectively. Maps must be read from upper right to lower left. The legend and symbols for these maps are presented in Figure 8.23. The following features are particularly important.

(i) The eastern part of the Pointe Bourdage map sheet exposes enormous fragments of folded Cap des Rosiers lithologies enclosed in an uncleaved matrix consisting of dark grey shale and abundant small blocks of more resistant grey mudstone (Figure 8.24a). Other clasts include angular blocks of siltstone (Figure 8.24b,c), two 20 m long slabs of bedded chert (Figure 8.24d), large deformed masses of siltstone (see map

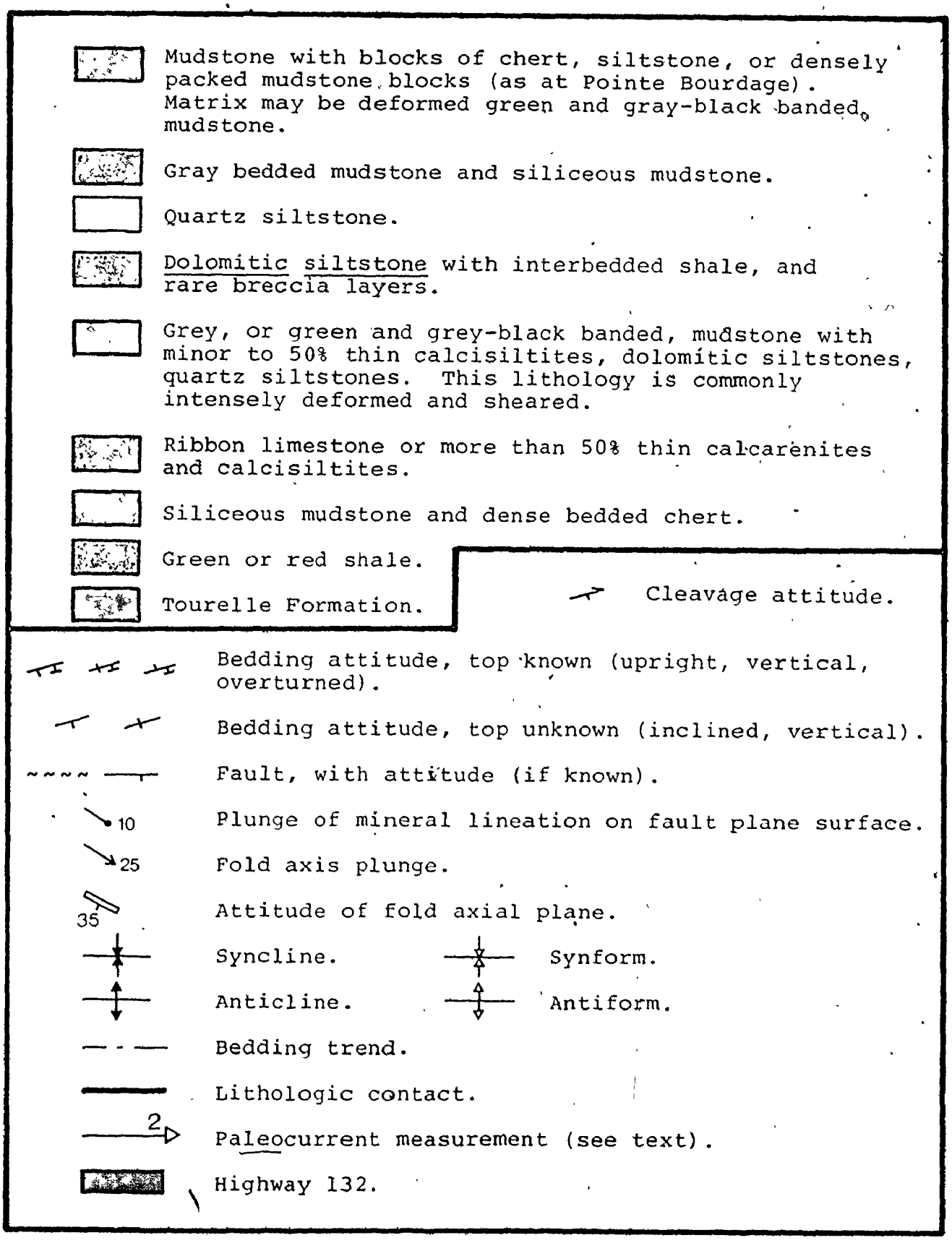

Fig. 8.23. Legend for Pointe Bourdage and Ste-Marthe map sheets.

Fig. 8.24. "Argile-à-blocs" at Pointe Bourdage and in nearby cliff exposures.

(A) Irregular blocks of resistant dark grey mudstone in a softer and lighter-coloured shaly matrix on Pointe Bourdage. Scale 15 cm.

(B) Dispersed siltstone blocks in shale matrix in the cliff behind Pointe Bourdage. Hammer for scale.

(C) As (A), with scattered, angular, light-coloured siltstone fragments. Scale 15 cm.

(D) Large block of bedded chert at Pointe Bourdage. This is enclosed in the matrix shown in (A) and (C).

(E) Enormous siltstone block (olistolith) exposed in the cliffs west of Pointe Bourdage. The cliff is about 60 m high.

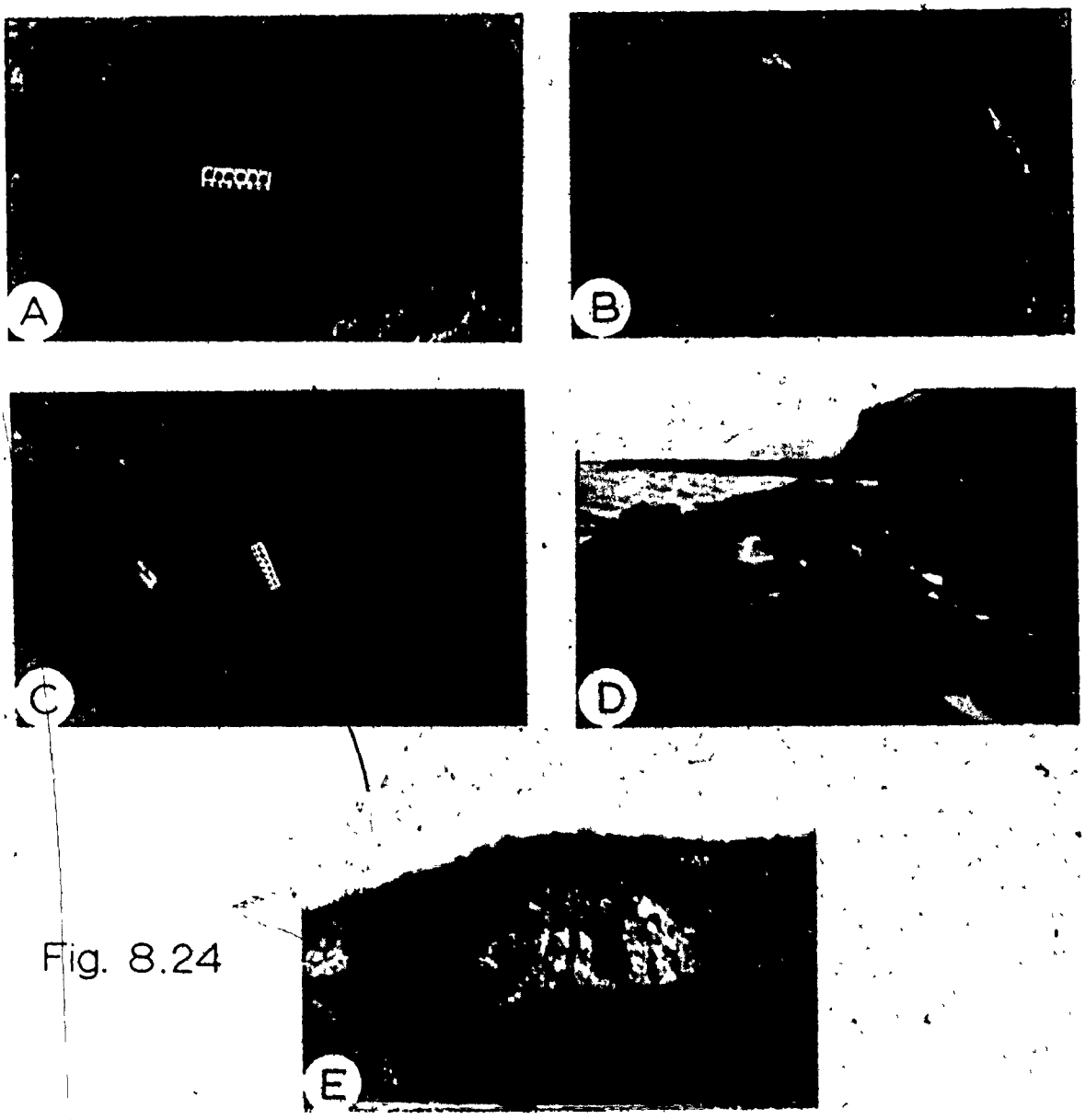

Fig. 8.24

west of Petit Pisseux brook), and at least one enormous block (about 45 by 35 m) exposed in cliffs south of the highway (Figure 8.24e). All large, truncated outcrops of Cap des Rosiers Group lithologies east of Grand Pisseux brook are also interpreted as enormous fragments. This "argile-à-blocs" (St. Julien, 1968) is interpreted as a gravity-induced accumulation of debris at the front of the thrust sheets, and may therefore be as young as Caradocian (St. Julien and Hubert, 1975). Logan's Line, which marks the boundary between the nappe zone and the autochthon, intersects the coast just east of Pointe Bourdage at Marsoui. Nappe movement ceased before the "argile-à-blocs" (or olistostrome) was overridden. It is believed that the folding within Cap des Rosiers olistoliths occurred during nappe movements long before the formation of "argile-à-blocs" at the front of the thrust sheets.

(11) Deformation west of Petit Cap Percé can be attributed almost solely to tight folding, which has resulted in intense breakage and deformation in shaly units, particularly in the cores of folds (Figure 8.25). In ribbon limestones at Cap à la Marte, folding was locally so intense that broken layers may resemble limestone breccia (Figure 8.25d).

Fig. 8.25. Deformation of incompetent units.

(A) Tightly folded ribbon limestones at Anse à Perré, west of Ste-Anne des Mont. Hammer for scale.

(B) Intensely folded ribbon limestones at Pointe Noire. Scale 15 cm.

(C) Broadly folded calcisiltites, Cap à la Marte. Hammer for scale.

(D) Brecciated calcisiltites at Cap à la Marte. This brecciation is due to intense folding. Scale 15 cm.

FIG. 8.25

(iii) In general, folds plunge in a westerly direction, resulting in the exposure of higher stratigraphic levels from east to west. As at Pointe Ste-Anne, quartz clastics are overlain by carbonate clastics. The Ste-Marthe channel cuts into the top of this succession and is filled with coarse Tourelle sandstones. This channel is overlain by massive bedded cherts.

(iv) Paleocurrent measurements from carbonate clastics generally indicate current directions from 180° to 360°. It is believed that in a true mélange, current directions measured on many different blocks would form a random distribution.

(v) The Tourelle Formation equivalents west of Ste-Marthe underwent the same deformation as underlying strata. Folds are much larger due to greater competence of these thick sandstones. Fragments of Tourelle sandstone layers have become detached from the major units and dispersed as isolated "knockers" in adjacent shaly horizons. Isolated beds of Tourelle lithology can also be seen interbedded with lithologies of the Cap des Rosiers Group. Large blocks of Cap des Rosiers lithology found within sandstone layers in the Tourelle Formation may have undergone some soft-sediment bending, but are never deformed. This observation reinforces the belief that the Cap des Rosiers Group was not deformed prior to Tourelle deposition. No disconformity between these rock units has been observed or previously documented.

Deformation features and structural considerations

The intensity of folding in these rocks is not a result of deep burial (high pressure and temperature), because metamorphism and regional cleavage are absent. Deformed rocks pass northward at Logan's Line into an undeformed "argile-à-block" unit which indicates that nappe emplacement occurred at high crustal levels. Coarse sandstones within the deformed unit commonly show evidence that mud from adjacent pelitic layers has been squeezed into the interstices between sand grains. R.K. Stevens (unpubl. manuscript, 1969) attributes this to fluid behavior of muds under high hydrostatic pressure during deformation. This hypothesis would account for extremely ductile behavior and tight folding of shaly units in fold cores. Interbedded clastic and shale units may form folds with very tight noses but little brittle fracture. This suggests either deformation of unconsolidated beds, or low strain rates. Deformation at a low rate of strain is favoured, because it has already been demonstrated that calcisiltites underwent early submarine cementation, and because fluidization of sandy layers to form clastic dikes did not occur, as would be expected during deformation of unconsolidated sand beds enclosed in mud. Slow deformation would allow ductile behavior of thin carbonate clastic layers by pressure solution, and fragmentation of more competent beds to form isolated "knockers" (Figure 8.26). Hsu (1974)

Fig. 8.26. Large lozenge-shaped knocker of Tourelle sandstone in deformed Cap des Rosiers Group west of Cap au Renard. Hammer for scale.

Large knocker of interbedded dolomitic siltstone and limestone, eastern Ste-Anne des Monts. This forms part of a linear trend of smaller blocks. Hammer for scale.

attributes fragmentation to brittle extension followed by compressional shear failure. Both of these mechanisms can be seen in the deformed Cap des Rosiers Group. Minor fragmentation produces a broken formation; major fragmentation produces a mélange. Observations west of Marsoui show conclusively that the Cap des Rosiers Group in this lowest structural slice is a broken formation and not a mélange (Figure 8.27).

Figure 8.28 is a lower hemisphere, equal-area projection of fold axes from the deformed Cap des Rosiers Group, and is styled after plots used to deduce slip-line orientation for flexural folds and sediment slumps (Hansen, 1971; Stone, 1976). The fold axes appear to cluster about a great circle girdle which is called the slip plane, following the analytical methods of Hansen (1967, 1971). Folds are consistently overturned toward the north, with the rotation couple being clockwise on the left of the diagram and anticlockwise on the right. This configuration is consistent with tectonic transport from south to north in the direction of the slip line. The constant overturning of folds to the north suggests a structured process. It is believed that this process was the slow gravity-slide emplacement of nappes terminating in Caradocian time (McKerrow and Ziegler, 1971; St. Julien and Hubert, 1975) rather than rapid emplacement of a large slide mass similar to that described by Moore and others (1976) from the northeast Indian Ocean.

Fig. 8.27. Deformed Cap des Rosiers Group in a cliff exposure, east end of Ste-Anne des Monts. In spite of locally intense breakage, stratigraphy is preserved. This is therefore classified as a "broken formation".

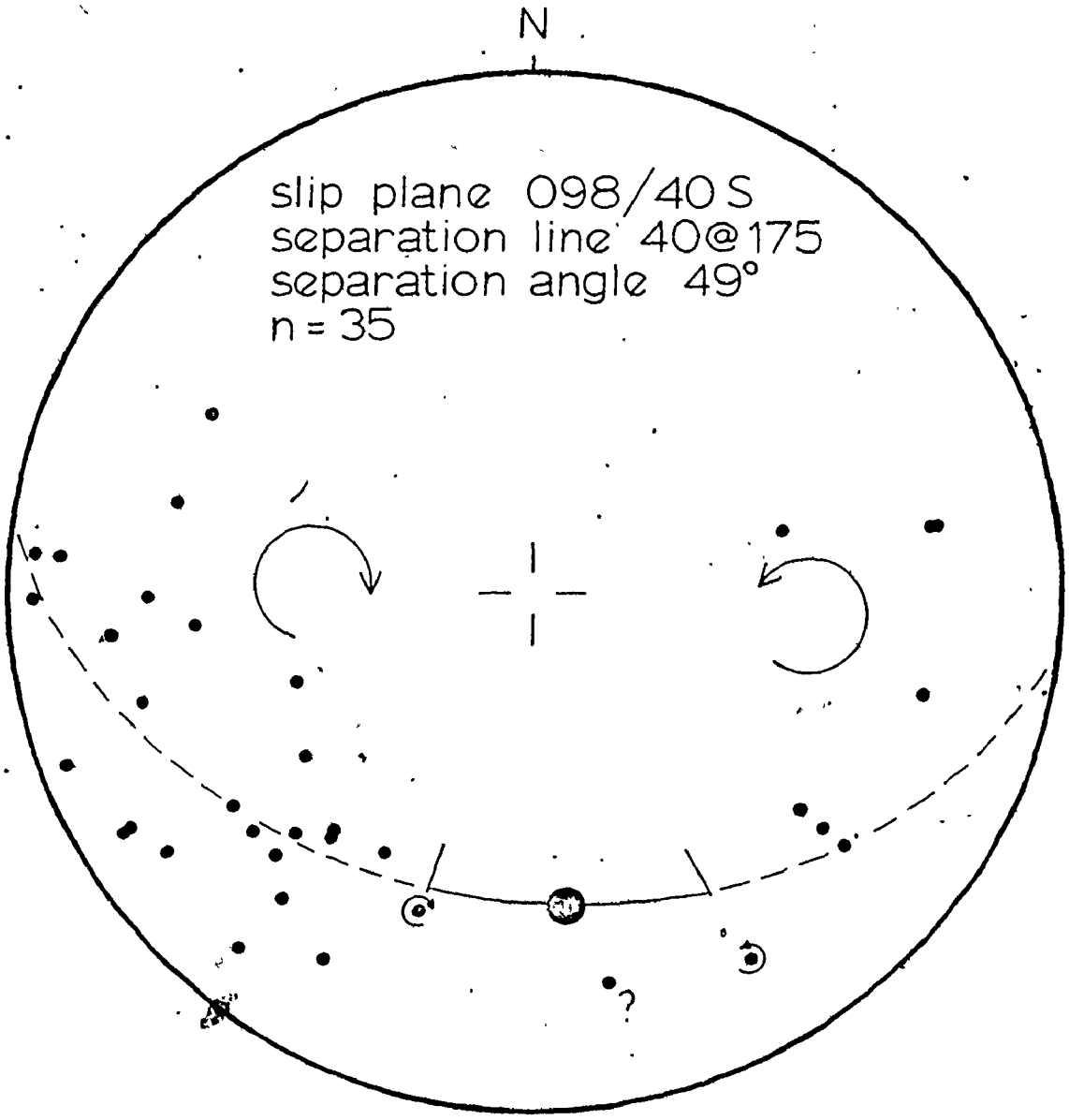

Fig. 8.28. Equal-area, lower hemisphere stereographic plot of axes of asymmetric folds in the deformed Cap des Rosiers Group, following the analytical method of Hansen (1967, 1971). Large black dot represents the head of an arrow pointing up the slip plane to the north and coincident with the direction of tectonic transport.

Structural interpretation

The Cap des Rosiers Group and the Tourelle Formation occur in the lowest exposed structural slice, and were deformed simultaneously during gravity-slide emplacement of nappes associated with the Taconic orogeny. High hydrostatic pressures, alternation of competent and incompetent units, and relatively low strain rates combined to produce intense folding and local dismemberment of clastic units. The product of this deformation is a "broken formation". During nappe advance, large and small blocks became detached from the nose of the allochthon and slid with overlying muds into the adjacent Middle Ordovician shale basin, producing an "argile-à-blocs". This olistostrome was likely continuously overridden during nappe advance, but is preserved adjacent to Logan's Line at Marsoui.

Summary

Pre-Tourelle sediments, which are assigned to the Lower Ordovician Cap des Rosiers Group, consist of the following facies:

(i) mudstones;

(ii) rippled or convoluted dolomitic siltstones with rare fine-pebble conglomerate layers. Pebbles are chert, bioclastic or pelletal limestone, dolomitic siltstone, and phosphorite;

(iii) thin calcisiltites, fine to coarse calcarenites, and limestone breccia. The calcarenites are from 10 cm to several metres thick, and may be cross-stratified when associated with conglomerate horizons. Breccia layers are graded, and composed of disc-shaped fragments of calcisiltite and calcarenite beds;

(iv) thin quartz siltstones, and quartz sandstones which may be several metres thick. The thick sandstones are graded, and contain abundant fluid-escape structures;

(v) siliceous mudstone and bedded chert. These cherts occur in beds from several centimetres to several metres thick, and are commonly laminated. Some bedded cherts contain infilled radiolarian tests. Because bedded chert lies above a large feeder channel filled with coarse Tourelle sands at Ste-Marthe, it is believed that these cherts were deposited on a submarine slope, rather than at abyssal depths.

The coarser clastic facies can be divided into two groups. Quartz clastics are found at the base of the section and are interpreted to have been derived from the Canadian shield and deposited within or adjacent to deep-sea channels. Carbonate clastics comprise limestone breccias, calcarenites, and thin calcisiltites. The conglomerates were deposited in slope channels below a carbonate bank, as a result of slumping and brecciation of thinner calcarenites and calcisiltites. The thin siltstones, or "ribbon limestones" were deposited

on the distal margin of the carbonate-bank slope. Both these calcisiltites, and dolomitic siltstones, may be overbank deposits from submarine channels, or may have been deposited by bottom currents. Carbonate clastics and bedded cherts immediately below the Tourelle Formation display a trace fossil assemblage containing paired tubes of suspension-feeding organisms. This assemblage suggests deposition at depths no greater than the upper parts of modern continental slopes.

In between the lower quartz clastics and the upper carbonate clastics at Pointe Ste-Anne is a 60 m thick unit of shale, which is interpreted to represent the period of transition between a northern source (quartz clastics) and a southern source (carbonate clastics and Tourelle Formation).

After Tourelle deposition, the entire Lower Ordovician assemblage was uplifted, and slid as gravity nappes into a Middle Ordovician shale basin. Deformation within the Cap des Rosiers Group took place at this time. The Tourelle Formation, which is dominated by thick, coarse sandstone beds, was more resistant to intense deformation, and instead developed large folds overturned to the northwest. These thrust sheets, or nappes, stopped moving in Caradocian time. To the north of Logan's Line, allochthonous rocks pass into an "argile-à-blocs" unit containing large and small blocks and debris shed from the advancing thrust sheets. This

olistostrome, or wildflysch, formed well after Tourelle deposition, and therefore has no bearing on paleotectonic reconstructions before or during the period of sandstone deposition.

CHAPTER IX

PALEOGEOGRAPHIC AND PALEOTECTONIC RECONSTRUCTION

Paleotectonic Reconstruction

Previous ideas

It is not intended in this section to review all published paleotectonic interpretations of Canadian Appalachian development encompassing the time of Tourelle deposition. Instead, only the most recent contributions will be examined.

There is little dispute that the initiation of the Taconic/Caledonian orogeny was related to interaction of crustal plates along the ancient continental margin of North America (Bird and Dewey, 1970; Williams and Stevens, 1974; Kennedy, 1975a; Laurent, 1975; St. Julien and Hubert, 1975). It is also generally accepted that orogeny was initiated by collision of a volcanic arc with the continental margin, either as a result of an aborted attempt to subduct the continental margin along a southeastward-dipping subduction zone (Chapple, 1973; Williams and Stevens, 1974; Laurent, 1975; McBride, 1976; Swinden and Strong, 1976), or as a result of closing of a

marginal ocean basin landward of a northwestward-dipping subduction zone (Dewey and Bird, 1971; Dewey, 1974; Kennedy, 1975; Williams, 1975, 1977; Williams and others, 1977). St. Julien and Hubert (1975) and Phillips and others (1976) favoured northwestward subduction without a marginal sea; Lambert and McKerrow (1976) proposed collision of a subduction zone and a ridge-transform system in the Arenigian.

Because there is no convincing evidence for calc-alkaline volcanism on the continental margin in the late Early Ordovician, any volcanic arc was probably (i) ensimatic, or (ii) situated on a micro-continent marginal to the Grenville craton. It is unreasonable to assume that subduction was too short-lived to produce calc-alkaline magmas. Phillips and others (1976) argue that the Arenigian Iapetus Ocean was 600 to 800 km wide in Ireland. Subduction of this amount of oceanic crust would certainly produce a volcanic arc.

The continental margin - island arc collision resulted in obduction of a large ophiolite sheet onto the continental margin (Stevens, 1970; Dewey and Bird, 1971; Laurent, 1975; St. Julien and Hubert, 1975; Williams, 1975, 1977). This ultramafic slab then slid off the tectonically elevated margin toward the continental interior, perhaps for a distance of 100 km (Williams, 1975). Sedimentary slices were successively detached, along decollement surfaces, and assembled beneath the ophiolite slab, so that the entire allochthon slid <u>en masse</u>

into the shale basin produced by foundering of the former carbonate platform fringing the craton (Stevens, 1970; Williams and Stevens, 1974). According to this model, immature sandstones containing ophiolite detritus, of which the Tourelle Formation is an example, were derived by subaerial erosion of the sliding allochthon (Stevens, 1970).

St. Julien and Hubert (1975) presented a comprehensive analysis of Quebec Appalachian tectonic development consistent with plate tectonic theory (Le Pichon and others, 1973). Their model is based mainly on relationships in the Quebec City area. In the Arenigian, they proposed (i) an ensimatic northwestward-dipping subduction zone marginal to the continent, and (ii) a calc-alkaline volcanic arc (Ascot-Weedon Formations) situated above this subduction zone, also on oceanic crust. Unfortunately, however, this model does not provide a source area for Tourelle sandstones and equivalents from Mont Joli to western Newfoundland. According to St. Julien and Hubert (1975), neither older sedimentary strata nor obducted ophiolites were exposed subaerially until the Late Ordovician. It is clear that this tectonic reconstruction is inadequate for much of Quebec and for western Newfoundland.

Critical requirements produced by this study

Examination of sandstone mineralogy, paleocurrent patterns, and slump fold axes in the Tourelle Formation, and stratigraphy of the upper part of the Cap des Rosiers Group (Chapter VIII), has produced several observations that must be explained by any paleotectonic reconstruction. These are listed below.

(i) The upper part of the Cap des Rosiers Group is dominated by carbonate clastics ranging in grain size and layer thickness from thin ribbon limestones (calcisiltites) to thick limestone breccia beds. The clasts in carbonate breccias are restricted to fragments of calcisiltite and calcarenite beds which were deposited on a submarine slope. Dolomitic siltstones are also present in this facies assemblage, and are particularly abundant at the base of the Tourelle Formation. These carbonate clastics are underlain by a thick shale horizon, which overlies quartz siltstones and sandstones of Kamouraska type. It is reasonable to assume that the quartz clastics were derived from the Canadian Shield (Lajoie and others, 1974). The thick shale unit represents a long period of isolation from any coarse terrigenous source. It is believed that subsequent deposition of carbonate clastics resulted from elevation of a land mass to the southeast, in the interior of the orogenic belt. Continued uplift eventually resulted in rapid subaerial erosion and derivation of Tourelle sands.

(ii) The bulk of Tourelle detritus was derived by erosion of pre-existing sedimentary rocks, containing rounded quartz grains and rounded ultrastable heavy minerals. There is no evidence that crystalline basement was exposed in the source area.

(iii) Although there is no evidence for active volcanism during Tourelle deposition, there is a significant amount of volcanic detritus in the sandstones, including angular plagioclase and prismatic grains of hornblende, basaltic hornblende, and pyroxenes. The composition of volcanic fragments, and the presence of hornblende and primary biotite, both indicate that the volcanic source was a calc-alkaline arc situated on continental crust. Some lavas had been metamorphosed to prehnite-pumpellyite grade and were associated with low-grade phyllites. The volcanic pile was cut by veins containing epidote group minerals.

(iv) Chert fragments are common in Tourelle sandstones, suggesting subaerial exposure of bedded cherts similar to those present in the underlying Cap des Rosiers Group.

(v) An ophiolite sheet of dimensions similar to the Papuan ophiolite had been obducted onto the continental margin at some distance from the site of Tourelle deposition. Only chromite, and perhaps prismatic pyroxene and rare serpentine grains were preserved during transport. Certainly the basal peridotite of this ophiolite slab must have been exposed to

subaerial erosion. Because serpentine increases in importance in Middle Ordovician flysch (e.g. Cloridorme Formation), it is reasonable to assume that the ophiolite mass was continuously moving toward the craton, perhaps as a result of gravity sliding.

(vi) Paleocurrents on sandstone layers are dominantly from east to west (Figure 7.6), producing a definite component of flow toward the craton and away from the interior of the orogenic belt. Slump folds also suggest a paleoslope dip to the northwest during Tourelle deposition.

(vii) Limestone clasts containing a shallow-water fauna and Arenigian or Llanvirnian conodonts have been observed in Tourelle deposits. The age deduced from conodonts is the same as the age deduced from graptolite fauna in Tourelle shales and sandstones. For this reason, an active, open-marine, shallow-water carbonate bank must have fringed the source area during Tourelle sedimentation.

Identification of source areas

It is believed that most Tourelle detritus was derived by subaerial erosion of poorly consolidated or unconsolidated Cambrian and Lower Ordovician quartz-rich sandstones similar to those presently found throughout the allochthonous belt.

These source rocks were originally derived by erosion of crystalline Grenville basement (Lajoie and others, 1974), either on the craton, or on marginal micro-continents. Uplift at the continental margin, associated with ophiolite obduction, was responsible for erosion of these sandstones.

Except for basaltic pillow lavas in the Shickshock Group, volcanic rocks are not exposed south of the study area in the Gaspé Peninsula. It is possible that an equivalent of the Ascot-Weedon calc-alkaline arc is covered by Silurian and Devonian rocks in the Gaspé Synclinorium. Because the Tourelle Formation is allochthonous, however, we may permit ourselves to look farther afield for a volcanic source area. According to McBride (1976), the Tetagouche volcanics in northern New Brunswick range in age from Late Cambrian to Middle Ordovician. In addition, they are inferred to be deposited on a micro-continental block of crystalline basement (Rast and Stringer, 1974; McBride, 1976; Poole, 1976). This calc-alkaline assemblage contains a significant proportion of rhyolite, and is associated with phyllites (Poole and Rodgers, 1972, Stop 9-1). It is therefore believed that the Tetagouche calc-alkaline volcanic arc may have been the source for volcanic detritus found in the Tourelle Formation.

Outliers of obducted ophiolite are present throughout the northern Appalachians (Laurent, 1975; Williams, 1975), and include ultramafic rocks on Mont Albert immediately south

of the study area. This ophiolite sheet was originally quite large and extensive (Williams and others, 1977), and was probably partly responsible for metamorphism of Fleur de Lys and Shickshock Group equivalents, and formation of ophiolitic mélange as it moved across the ancient continental slope and rise (Williams, 1977). Because allochthonous ophiolite occurs in the uppermost structural unit, most of the original sheet has been completely eroded. There is every reason to believe that this ophiolite sheet contributed all chromite and serpentine detritus found in the Tourelle, Métis, Blow-me-down Brook, Cloridorme, Beaupré, and St. Irénée Formations (see Chapter VII).

All detailed studies indicate that the root zone of the ophiolite sheet lies to the west or northwest of the volcanic arcs (Laurent, 1975; St. Julien and Hubert, 1975; Poole, 1976; Williams and others, 1977). If this is generally true, then the root zone in the Gaspé Peninsula may be covered by Silurian and Devonian strata of the Gaspé Synclinorium. It is interesting that St. Julien and Hubert (1975) interpret the Middle Ordovician Mictaw Group in the southern Gaspé Peninsula as flysch deposited on oceanic crust.

Plate tectonic model

Figure 9.1 presents a plate tectonic model consistent with provenance requirements for the Tourelle Formation. A southeastward-dipping subduction zone is assumed on the basis of arguments presented by other workers (Strong and others, 1974; Williams and Stevens, 1974; Laurent, 1975; Swinden and Strong, 1976). The model involves closing of a marginal ocean basin between the craton and an offshore micro-continent, and is very similar to a model proposed independently by McBride (1976).

Foundering of the carbonate bank (stage III) is well documented in western Newfoundland (Stevens, 1970). A similar situation occurred in the Miocene on the island of Timor, north of Australia. Timor was then situated on the northern margin of the Australian plate (Audley-Charles, 1973). An attempt to subduct continental crust along a northward-dipping subduction zone resulted in foundering of Timor to depths of at least 2 to 3 km. The Bobonaro Scaly Clay, an olistostrome deposit, was then deposited on top of the previous carbonate bank (Audley-Charles, 1965, 1974).

Timor also provides an excellent modern analogy to stage IV of Figure 9.1. Continental crust of the Australian plate has again become involved in subduction beneath the Banda Arc (Katili, 1975), and volcanism and plate convergence appear to have ground to a halt (Brouwer, 1942; Fitch, 1970).

Fig. 9.1. Plate tectonic model.

Stage I: Late Precambrian and Cambrian. A marginal microcontinent of Grenville basement had separated from North America, leaving an Atlantic-type continental margin. Sediments on this margin were feldspathic sandstones (e.g. Charny Formation) and carbonate breccias.

Stage II: Initiation of subduction beneath the marginal microcontinent and onset of volcanism (Tetagouche volcanics) in the Late Cambrian.

Stage III: Obduction of ophiolite in the late Early Ordovician, as the continental margin of North America began to enter the subduction zone and foundered to oceanic depths. Feldspathic sandstones and lavas of the Shickshock Group were metamorphosed beneath the overriding ophiolite sheet.

Stage IV: Continued plate convergence in the late Arenigian, resulting in strong uplift at the point of plate collision. A modern example of this process can be found in the vicinity of Timor. Volcanism ceased at this time. The uplifted collision zone formed the provenance of the Tourelle Formation. The allochthon then slid away from the elevated collision zone into the foredeep shale basin under the influence of gravity, detaching additional thrust sheets from the autochthon as it moved forward.

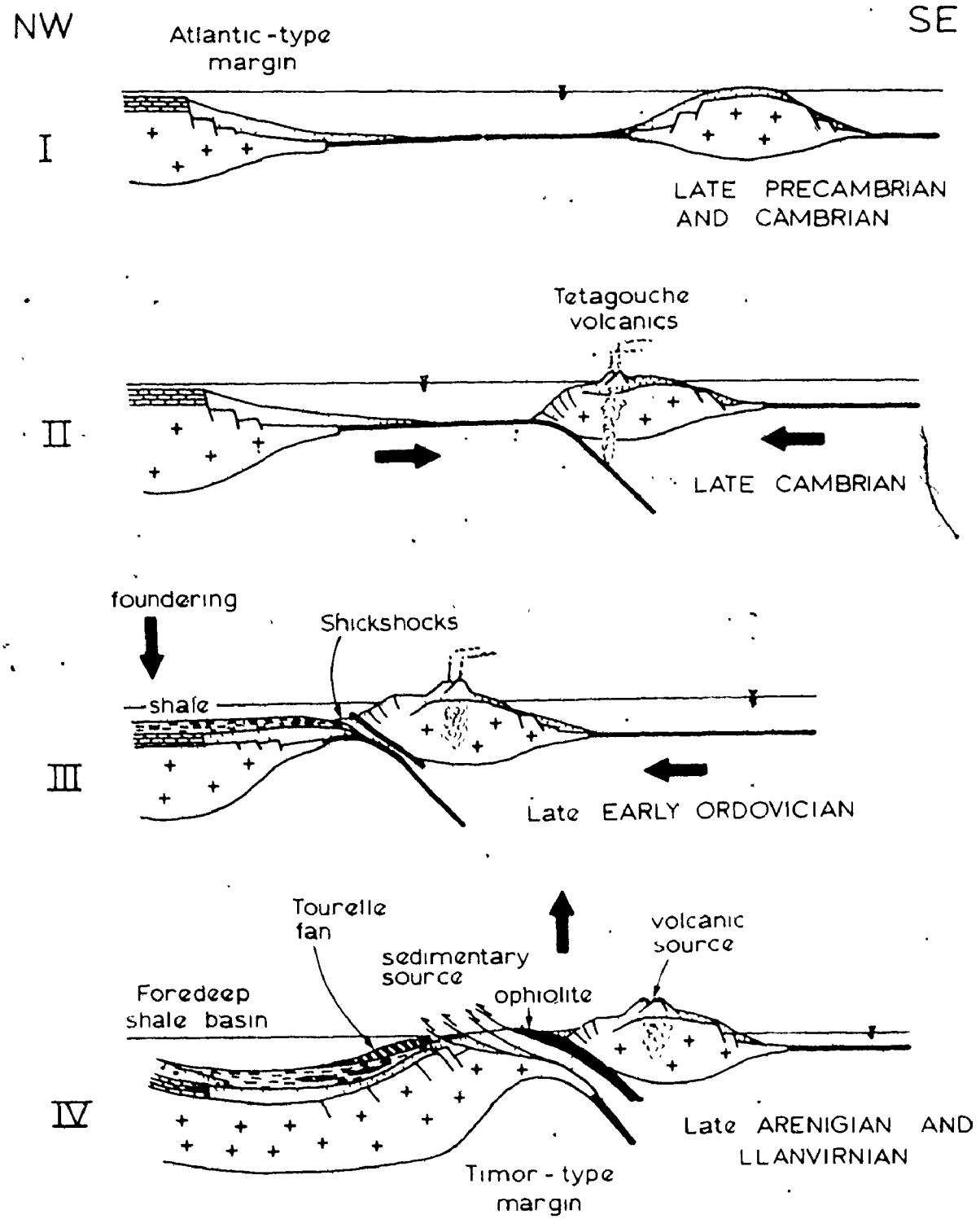
NW
SE
Atlantic-type margin
I
LATE PRECAMBRIAN AND CAMBRIAN
Tetagouche volcanics
II
LATE CAMBRIAN
foundering
Shickshocks
shale
III
Late EARLY ORDOVICIAN
Tourelle fan
sedimentary source
volcanic source
Foredeep shale basin
ophiolite
IV
Late ARENIGIAN AND LLANVIRNIAN
Timor-type margin

Instead, major uplift by thrust faulting and isostatic rebound is occurring both on Timor, and on volcanic islands north of Timor (Brouwer, 1942; Fitch, 1970; Audley-Charles, 1974). Pleistocene uplifts of 500 to 1000 m have been recorded. Similar uplift along the Arenigian continental margin of North America initiated erosion of sedimentary rocks, ophiolite, and volcanic rocks, leading to deposition of the Tourelle Formation.

Following stage IV (Figure 9.1), thrust slices of the incipient allochthon were further uplifted, and slid under the influence of gravity into the developing foredeep basin. Additional thrust sheets were added to the base of the allochthon as it moved forward. The lowest structural slice includes sandstones of the Tourelle Formation.

Carbonate clastics of the upper part of the Cap des Rosiers Group, and fragments of shallow-water limestone within the Tourelle Formation, were derived from carbonate banks fringing the slowly moving allochthon, as previously suggested by Stevens (1970).

Paleogeography

Critical requirements produced by this study

Several observations have been made concerning submarine fan geometry (Chapter III), depositional slope (Chapter V), spacing of feeder channels (Chapter VII), and the role played by rivers in transporting sand directly to submarine canyons (Chapter VII). The most important of these are listed below.

(i) The sand population of the Tourelle Formation was derived by mixing of fresh river sands, and sands which had been more deeply weathered, perhaps in a soil mantle. Because no transported shallow-water fauna or shell fragments are present in these sands, it is probable that the terrigenous material spent little if any time in shallow-marine environments. It is believed that a useful modern analogy in terms of river - canyon configuration is the Congo dispersal system, in which river sands are funnelled directly into the submarine canyon during peak discharge periods. The Tourelle Formation contains an enormous amount of sand deposited in a relatively short time period (Figure 1.7). For this reason, it is assumed that the rivers involved were swift flowing and carried large amounts of coarse sandy bed-load. The maximum size was coarse sand because of source area deficiencies.

(ii) Paleocurrents generally indicate flow from east to west, with a component toward the continental interior.

A minor paleocurrent mode from west to east may be the result of channel switching on the mid-fan, or overlap of adjacent coalescing fans. The second alternative is favoured, because it has been demonstrated that sediment input centres, or feeder channels, were separated by distances of only 15 to 40 km. A modern analogue is the San Lucas Fan (Normark, 1970).

(iii) Channel slopes were probably as steep as 0.02 to 0.05 (Chapter V). This result, in conjunction with the shallow inferred depths of mid-fan channels and the spacing of feeder channels, suggests that individual fans were quite small and steep. The La Jolla Fan (30 x 22 km) may be a reasonable modern analogue.

Dispersal system geometry

Figure 9.2 is a paleogeographic reconstruction of the Tourelle depositional environment consistent with the author's observations. Most sediment dispersal was deflected to the west (left, looking down-fan), perhaps because of constriction within a narrow elongate trough sloping gently to the west. There is evidence that collision of the continent and volcanic arc was diachronous, occurring earliest in the north-east and latest in the southwest (Phillips and others, 1976; Dallmeyer, 1977). For this reason, uplift would have been earliest in the east, creating a gentle slope to the west along

Fig. 9.2. Schematic block diagram of the Tourelle dispersal system. High-discharge rivers brought coarse sand to deltas above small Tourelle fans. These deltas built out over a pre-existing carbonate bank. River sand was then funnelled directly into submarine canyons and onto the submarine fans below. These fans were deflected to the west (left) because of constriction within a narrow elongate trough sloping gently to the west (toward the reader). Feeder channels for the coalescing Tourelle fans were from 15 to 40 km apart.

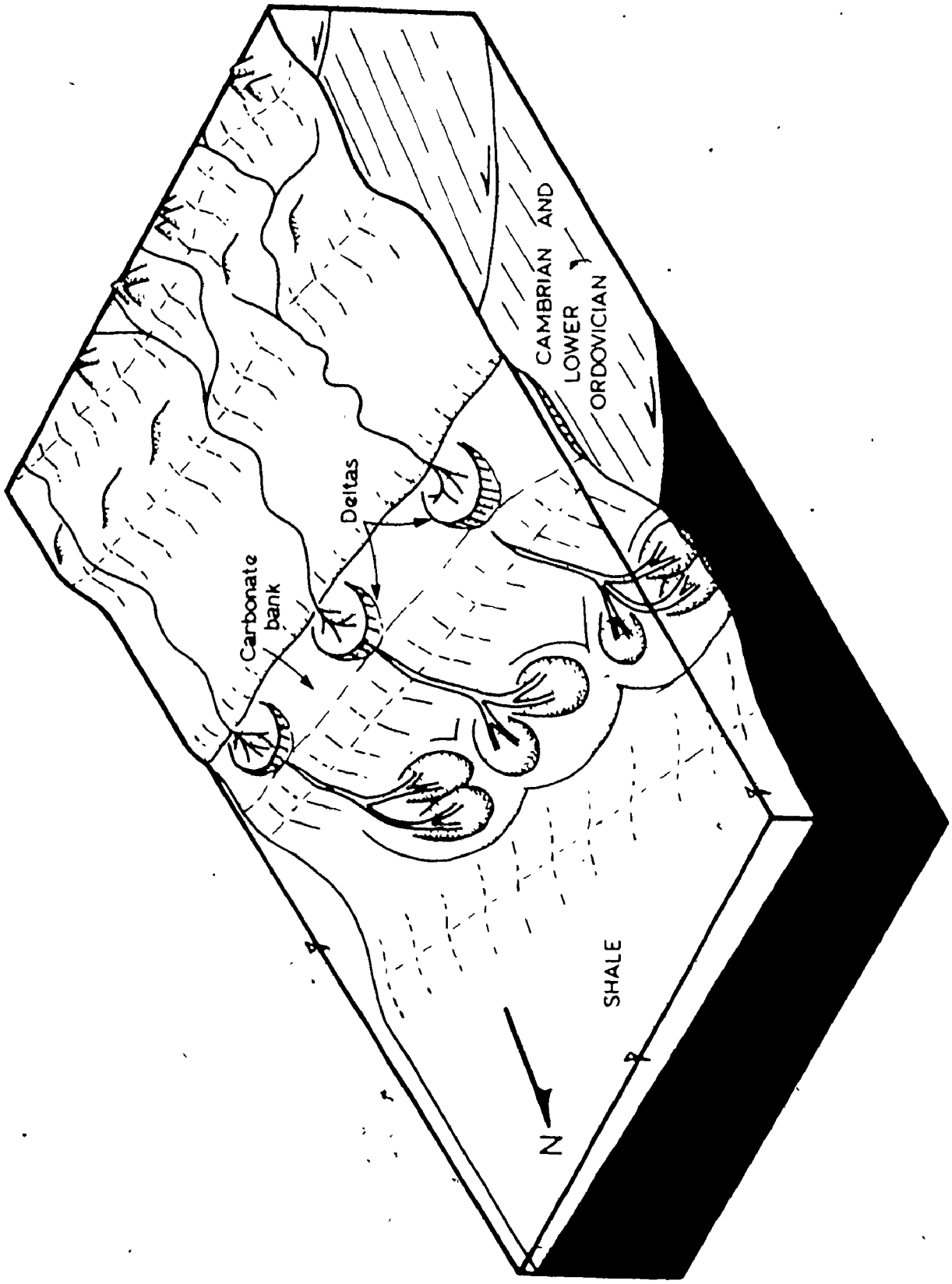
CAMBRIAN AND
LOWER
ORDOVICIAN
Deltas
Carbonate
bank
SHALE
N

the depositional trough.

As the allochthon moved forward, this foredeep trough migrated toward the continent, and eventually was situated above the old carbonate bank margin. It was at this time that the Cloridorme Formation was deposited.

Summary

On the basis of provenance criteria developed in Chapter VII, a plate tectonic model is presented which involves closing of a marginal ocean basin along a southeastward-dipping subduction zone, and collision of the ancient continental margin of North America with a volcanic arc situated on a micro-continent of crystalline Grenville basement. The volcanic arc is identified with the Tetagouche volcanic complex in northern New Brunswick.

During collision, a large sheet of ophiolite was obducted onto the continental margin and thrust over Cambrian and Lower Ordovician sediments. Sedimentary slices were successively detached and assembled beneath the ophiolite slab, and the entire allochthon then slid *en masse* into the shale basin produced by foundering of the former carbonate platform fringing the craton. Sands of the Tourelle Formation were eroded from this complex source area and deposited in front of the moving allochthon. At a later time, these

deposits were added to the base of the transported sequence.

The Tourelle dispersal system consisted of a series of small, closely-spaced and coalescing submarine fans fed directly by high-discharge river systems. Paleoflow on the submarine fans was deflected to the west because of (i) diachronous collision between the continent and the volcanic arc, and (ii) confinement within an elongate depositional trough.

SUMMARY

Depositional Environment and Facies Organization

The Tourelle Formation was deposited in deep water, and is best examined within the framework of the submarine fan facies model. Medium to coarse sandstone comprises 70% of the formation. Sandstone facies are dominated by thick sandstones (6), which may contain enormous blocks of dolomitic siltstone or bedded chert up to 16 m in length. Some of these layers display cross-stratification, coarse near-horizontal stratification, internal scour surfaces, and fluid-escape structures. All of these features are uncommon or absent in classical turbidites. Most thick layers, however, are massive, and range in thickness up to 22 m. They may be poorly graded, ungraded, or inverse-to-normally graded. Important associated facies are thick units of shale or interbedded shale and rippled siltstones, slurry sandstones, classical turbidites, slumps and isolated olistoliths, and clastic dikes and sills.

The following observations indicate that the bulk of the Tourelle Formation was deposited on the channelized mid-fan.

(i) Several major channels, with maximum depth in excess of 13 m, are located in the study area.

(ii) Most asymmetric megasequences thin upward, as

predicted by Italian workers for the fill of submarine fan channels. Examination of thinning upward cycles in the Tourelle Formation suggests a model for the filling of channels which involves (1) a period of open flow through the channel, (2) plugging of the channel by one or more thick layers, deposited by rapid fall-out from turbulent suspension or by "freezing" of a dense dispersion or debris flow, and (3) progressive abandonment. Slurry sandstones are most common at the top of thinning upward sequences.

(iii) At some outcrop areas, amalgamated packets of coarse sandstone alternate with thick shale (1) or siltstone (2) horizons up to 40 m thick. Thick shales (1) are interpreted as mud blankets deposited over abandoned mid-fan lobes, and siltstones (2) as overbank deposits adjacent to distributary channels. Paleoflow reversals between sandstone packets suggest deposition in the area of overlap between two coalescing submarine fan systems. Each sandstone packet represents a complete mid-fan distributary complex.

The present submarine fan model does not predict the observed high degree of randomness in lithologic transitions. Well-defined thinning or thickening upward trends are not common, although thinning upward cycles dominate sequence (Markov) analysis. This lack of apparent order may be the result of (i) irregular erosion by fan channels, or (ii) complex progradation and aggradation in these channels.

Deposition of Thick Sandstones (6)

The two end members of the thick sandstone (6) facies, in terms of internal depositional structures, are stratified layers, and massive layers.

Stratified layers

Coarse, near-horizontal stratification consist of inversely graded stratification bands from several to about 10 cm thick. Each band is based by a near-horizontal scour surface. This stratification occurs below normal tractional structures, such as upper flow regime plane lamination or ripple lamination. It may be sandwiched between divisions of massive sandstone.

If only the coarse parts of stratification bands are sampled, stratified layers are well graded (distribution grading). a-axis fabric is strongly developed, with long axis parallel to flow and imbricate upcurrent. The highest vector magnitudes are found in fine sub-divisions of stratification bands. Imbrication angle is generally greater than 20°, which is a characteristic of grain interaction.

Stratified layers (or divisions) are believed to have been deposited beneath supercritical turbidity currents with densities on the order of 1.1 g cm^{-3}. Stratification bands resulted from progressive "freezing" of a flowing grain layer at the base of the current. Shearing within this grain carpet

produced inverse grading and strong a-axis fabric with steep upcurrent imbrications.

Massive layers

Massive layers may be well graded, poorly graded, inverse-to-normally graded, ungraded, or may show complex grading. Grading appears to be of the coarse-tail variety. The middle parts of layers generally are the most poorly sorted. a-axis grain orientation is most strongly developed at the base and top of layers. The middle parts of single units may have bimodal or isotropic fabrics, with both upcurrent and downcurrent imbrications. Sole markings are generally grooves. Many layers contain fluid-escape structures.

If these layers were transported by turbidity currents, then flow velocities deduced from competence requirements would have been about 4 to 8 m s^{-1}, in flows from 10 to 20 m thick. Similar velocities would have been required to roll exhumed concretions along a sediment bed. These estimates may be minima, as the poor size sorting in these sandstones is best explained by deposition as a result of decreasing current capacity rather than competence. Even these estimates, however, signify currents with high Froude numbers, and therefore suggest antidunes as the stable bed phase.

Some thick sandstones (6) have large blocks of dolomitic siltstone or bedded chert suspended above their soles, suggesting

emplacement by debris flow. Most Tourelle sandstones actually had enough primary matrix to have moved as debris flows on slopes of 0.02 to 0.05 (1.2° to 2.9°). These flows would have been laminar, with yield strengths of 0.3×10^4 to 3.0×10^4 dyne cm^{-2}.

It is believed that most massive layers, or divisions, were deposited rapidly from dense, supercritical turbulent suspensions as a result of decreasing current capacity. Deposition may have involved a "quick" sediment bed prior to consolidation. Unusually thick, and ungraded or poorly graded layers containing enormous blocks of bedded chert and dolomitic siltstone were more probably transported by laminar debris flow.

Tractional structures, including cross-stratification, are found above both massive and coarsely-stratified divisions. These structures formed after a transition from supercritical to subcritical flow, perhaps involving a hydraulic jump. Dune cross-stratification is only found in restricted stratigraphic intervals, and only formed under thick flows on slopes less than 0.01. In general, steeper slopes precluded dune stability.

Mineralogy and Provenance

The average composition of Tourelle sandstones is 45.6% quartz, 8.2% feldspar, 13.4% rock fragments, 16.6% chloritic matrix, and 15.3% calcite "cement". Most samples can be

classified as lithic wackes or sublitharenites. Quartz grains are generally non-undulose, and may be well rounded. Potassium feldspar grains comprise two thirds of all feldspar detritus.

The most distinctive rock fragments are (i) chert and siliceous mudstone, and (ii) mafic to felsic volcanic detritus of prehnite-pumpellyite metamorphic grade. Chert fragments appear to have been derived from bedded chert units, and may contain infilled radiolarian tests.

The heavy mineral suite contains rounded ultrastable grains of zircon and tourmaline, abundant epidote group minerals and garnet, unstable prismatic grains of hornblende and pyroxene, and transluscent cherry-red chromite. This suite suggests both a multiple and complex source area.

The original source area for most quartz and feldspar detritus was the Grenville province of the Canadian Shield. This material is believed to have passed through at least one previous sedimentary cycle prior to deposition in the Tourelle Formation. This conclusion is based on roundness of quartz and ultrastable heavy mineral grains, and lack of basement pebbles.

Volcanic fragments were derived from an inactive offshore volcanic arc on continental crust. These volcanic rocks had been regionally metamorphosed at shallow depths to prehnite-pumpellyite grade, and were cut by veins containing epidote group minerals.

Ultramafic rocks, presumably obducted ophiolites, were being eroded, and contributed chromite grains and prismatic pyroxene to the heavy mineral suite. Hence, ophiolite obduction must have taken place at least as early as upper Arenig time (ca. 475 m.y. ago). The ophiolite sheet is estimated to have been of comparable size to the Papuan ophiolite.

The complex and immature provenance of the Tourelle Formation is interpreted to be the result of erosion of rising cordillera in the interior of the nascent Taconic orogenic belt. Both regional Tourelle paleocurrents and paleoslope dip directions inferred from slump folds indicate a component of sediment transport toward the continental interior. The Tourelle Formation represents the first influx of immature detritus from a southeastern source. Previous Cambrian and Lower Ordovician sediments were eroded directly from the Grenville craton to the northwest. The Tourelle Formation and equivalents, such as the Blow-me-down Brook and Métis Formations, are therefore sensitive indicators of the timing of orogenic developments.

Paleotectonic and Paleogeographic Reconstruction

Provenance criteria are best explained by a plate tectonic model involving closing of a marginal ocean basin along a southeastward-dipping subduction zone, and collision of the ancient continental margin of North America with a volcanic arc situated on a micro-continent of crystalline Grenville

basement. During collision, a large sheet of ophiolite was obducted onto the continental margin and thrust over Cambrian and Lower Ordovician sediments. The volcanic arc is identified with the Tetagouche volcanic complex in northern New Brunswick. Previously published plate tectonic models do not provide a source area for the Tourelle Formation, and must therefore be considered inadequate.

Sedimentary slices were successively detached and assembled beneath the ophiolite slab, and the entire allochthon then slid en masse into the shale basin produced by foundering of the former carbonate platform fringing the craton. Sands of the Tourelle Formation were eroded from this complex source area and deposited in front of the moving allochthon.

The Tourelle dispersal system consisted of a series of small, closely-spaced and coalescing submarine fans fed directly by high-discharge river systems. Paleoflow on the submarine fans was deflected to the west because of (i) diachronous collision between the continent and the volcanic arc, and (ii) confinement within an elongate depositional trough.

BIBLIOGRAPHY

Allen, J. R. L., 1964, Primary current lineation in the Lower Old Red Sandstone (Devonian), Anglo-Welsh Basin: Sedimentology, v. 3, p. 89-108.

_____, 1970, The sequence of sedimentary structures in turbidites, with special reference to dunes: Scot. J. Geol., v. 6, p. 146-161.

_____, 1971, Mixing at turbidity current heads, and its geological implications: J. Sediment. Petrology, v. 41, p. 97-113.

American Society of Civil Engineers, Task Committee on Preparation of Sedimentation Manual, 1963, Suspension of Sediment: Amer. Soc. Civil Engineers Proc., v. 89, No. HY5, p. 45-76.

Andresen, A., and Bjerrum, L., 1967, Slides in subaqueous slopes in loose sand and silt: in, Richards, A. F., ed., Marine Geotechnique, Univ. Ill. Press, Urbana, Chicago, p. 221-239.

Archibald, D. A., and Farrar, E., 1976, K-Ar ages of amphiboles from the Bay of Islands ophiolite and the Little Port Complex, western Newfoundland, and their geological implications: Can. J. Earth Sci., v. 13, p. 520-529.

Audley-Charles, M. G., 1965, A Miocene gravity slide deposit from eastern Timor: Geol. Mag., v. 102, p. 267-276.

_____, 1973, Paleoenvironmental significance of chert in the Franciscan Formation of western California: discussion concerning the signifance of chert in Timor: Geol. Soc. Amer., Bull., v. 84, p. 363-368.

_____, 1974, Banda Arcs: in, Mesozoic-Cenozoic Orogenic Belts, The Geol. Soc. (Lond.), Spec. Publ. 4, p. 349-363.

Bagnold, R. A., 1956, The flow of cohesionless grains in fluids: Roy. Soc. London, Phil. Trans., Ser. A, v. 249, p. 235-297.

Baker, P. E., 1968, Comparative volcanology and petrology of the Atlantic island-arcs: Bull. Volcanol., v. 32, p. 189-206.

Barnes, C. R., and Fåhraeus, L. E., 1975, Provinces, communities, and the proposed nektobenthic habit of Ordovician conodontophorids: Lethaia, v. 8, p. 133-149.

Basu, A., Young, S. W., Suttner, L. J., James, W. C., and Mack, G. H., 1975, Re-evaluation of the use of undulatory extinction and polycrystallinity in detrital quartz for provenance interpretation: J. Sediment. Petrology, v. 45, p. 873-882.

Béland, J., 1957, Ste-Félicité - Grosses Roches area: Quebec Dept. Mines, Prelim. Rept. 339, 8 p.

Berger, W. H., and Winterer, E. L., 1974, Plate stratigraphy and the fluctuating carbonate line: Spec. Publs int. Ass. Sediment., 1, p. 11-48.

Berry, L. G., and Mason, B., 1959, Mineralogy, W. H. Freeman and Co., San Francisco, 630 p.

Berry, W. B. N., 1960, Graptolite faunas of the Marathon region, west Texas: Texas Univ. Publ. 6005, 179 p.

Billingsley, P., 1961, Statistical methods in Markov chains: Ann. Math. Statist., v. 32, p. 12-40.

Bird, J. M., and Dewey, J. F., 1970, Lithosphere plate - continental margin tectonics and the evolution of the Appalachian orogen: Geol. Soc. Amer., Bull., v. 81, p. 1031-1060.

Biron, S., 1972, Géologie de la région de Ste-Anne des Monts: Quebec Dept. Nat. Resources, Prelim. Rept. (+ map), open file.

_____, 1973, Géologie de la région de Marsoui: Quebec Dept. Nat. Resources, Prelim. Rept. (+ map), open file.

_____, 1974, Géologie de la région des Méchins: Quebec Dept. Nat. Resources, Prelim. Rept. (+ map), open file, 12 p.

Blatt, H., 1967, Original characteristics of clastic quartz: J. Sediment. Petrology, v. 37, p. 401-424.

_____, and Christie, J. M., 1963, Undulatory extinction in quartz of igneous and metamorphic rocks and its significance in provenance studies of sedimentary rocks: J. Sediment. Petrology, v. 33, p. 559-579.

Blatt, H., Middleton, G. V., and Murray, R., 1972, Origin of Sedimentary Rocks: Prentice-Hall, Inc., 634 p.

Boersma, J. R., 1967, Remarkable types of mega cross-stratification in the fluviatile sequence of a subrecent distributary of the Rhine, Amerongen, the Netherlands: Geol. Mijnbouw, v. 46, p. 217-235.

Boggs, S., Jr., 1968, Experimental study of rock fragments: J. Sediment. Petrology, v. 38, p. 1326-1339.

Bouma, A. H., 1962, Sedimentology of some Flysch Deposits; a graphic approach to facies interpretation: Elsevier, Amsterdam, 168 p.

_____, and Hollister, C. D., 1973, Deep ocean basin sedimentation: in, Middleton, G. V., and Bouma, A. H., eds, Turbidites and Deep-water Sedimentation, Pacific Section, Soc. Econ. Paleontol. Mineral., Short Course, Anaheim, p. 79-118.

Bramlette, M. N., 1941, The stability of minerals in sandstone: J. Sediment. Petrology, v. 11, p. 32-36.

Brookfield, M. E., 1977, The emplacement of giant ophiolite nappes I. Mesozoic - Cenozoic examples: Tectonophysics, v. 37, p. 247-303.

Brouwer, H. A., 1942, Summary of the geological results, Geol. Exp. to the Lesser Sunda Islands, v. 4, p. 345-401.

Calvert, S. E., 1966, Accumulation of diatomaceous silica in the sediments of the Gulf of California: Geol. Soc. Amer., Bull., v. 77, p. 569-596.

Cameron, K. L., and Blatt, H., 1971, Durabilities of sand size schist and "volcanic" rock fragments during fluvial transport, Elks Creek, Black Hills, South Dakota: J. Sediment. Petrology, v. 41, p. 565-576.

Carmichael, I. S. E., Turner, F. J., and Verhoogen, J., 1974, Igneous Petrology: McGraw-Hill, New York, 739 p.

Carter, R. M., 1975, A discussion and classification of subaqueous mass-transport with particular application to grain-flow, slurry-flow, and fluxoturbidites: Earth-Sci. Rev., v. 11, p. 145-177.

Chapple, W. M., 1973, Taconic orogeny: abortive subduction of the North American continental plate? Geol. Soc. Amer., Abs. with Programs (Ann. Mtg), v. 5, No. 7, p. 573.

Chevalier, J., 1976, Diagenèse de grès Cambro-Ordovicien, St-Fabien, Québec: M.Sc. Thesis, Univ. of Montreal, 93 p.

_____, Lajoie, J., and Coulomb, J.-J., 1975, Matrix of turbidites: replacement of primary matrix in Cambrian flysch sandstones, Canadian Appalachians, Quebec: IX Internat. Congr. Sedimentology, Theme VII, p. 127-134.

Chough, S., and Hesse, R., 1976, Submarine meandering thalweg and turbidity currents flowing for 4000 km in the northwest Atlantic Mid-Ocean channel, Labrador Sea: Geology, v. 4, p. 529-534.

Church, W. R., 1972, Ophiolite: its definition, origin as oceanic crust, and mode of emplacement in orogenic belts, with special reference to the Appalachians: in, Irving, E., ed., The Ancient Oceanic Lithosphere, Dept. Energy, Mines and Resources, Ottawa, Canada, p. 71-85.

_____, and Gayer, R. A., 1973, The Ballantrae ophiolite: Geol. Mag., v. 110, p. 497-510.

_____, and Stevens, R. K., 1971, Early Paleozoic ophiolite complex of the Newfoundland Appalachians as mantle/oceanic crust sequences: J. Geophys. Res., v. 76, p. 1460-1466.

Colburn, I. P., 1968, Grain fabrics in turbidite sandstone beds and their relationship to sole mark trends on the same beds: J. Sediment. Petrology, v. 38, p. 146-158.

Coleman, R. G., 1971, Plate tectonic emplacement of upper mantle peridotites along continental edges: J. Geophys. Res., v. 76, p. 1212-1222.

_____, and Irwin, W. P., 1974, Ophiolites and ancient continental margins: in, Burk, C. A., and Drake, C. L., eds, The Geology of Continental Margins, Springer-Verlag, New York, p. 921-932.

Conolly, J. R., 1965, The occurrence of polycrystallinity and undulatory extinction in quartz in sandstones: J. Sediment. Petrology, v. 35, p. 116-135.

Coombs, D. S., Horodyski, R. J., and Naylor, R. S., 1970, Occurrence of prehnite-pumpellyite facies metamorphism in northern Maine: Amer. J. Sci., v. 268, p. 142-156.

Corbett, K. D., 1972, Features of thick-bedded sandstones in a proximal flysch sequence, Upper Cambrian, southwest Tasmania: Sedimentology, v. 19, p. 99-114.

Costello, W. R., 1974, Development of bed configurations in coarse sands: Ph.D. Thesis, Mass. Inst. Technology, Rept 74-1, 120 p.

Cummins, W. A., 1962, The greywacke problem: Liverpool Manchester Geol. Jour., v. 3, p. 51-72.

Curray, J. R., 1956, Analysis of two dimensional orientation data: J. Geol., v. 64, p. 117-131.

_____, and Moore, D. G., 1974, Sedimentary and tectonic processes in the Bengal deep-sea fan and geosyncline: in, Burk, C. A., and Drake, C. L., The Geology of Continental Margins, Springer-Verlag, New York, p. 617-628.

Dallmeyer, R. D., 1977, Diachronous ophiolite obduction in western Newfoundland: evidence from $^{40}Ar/^{39}Ar$ ages of the Hare Bay metamorphic aureole: Amer J. Sci., v. 277, p. 61-72.

_____, and Williams, H., 1975, $^{40}Ar/^{39}Ar$ release spectra of hornblende from the Bay of Islands metamorphic aureole, western Newfoundland: their bearing on the timing of ophiolite obduction at the Ordovician continental margin: Can. J. Earth Sci., v. 12, p. 1685-1690.

Dalrymple, R. W., 1977, Sediment dynamics of macrotidal sand bars, Bay of Fundy: Ph.D. Thesis, McMaster Univ., Hamilton, Ont., 630 p.

Dapples, E. C., and Rominger, J. F., 1945, Orientation analysis of fine-grained clastic sediments: J. Geol., v. 53, p. 246-261.

Davies, H. L., 1968, Papuan ultramafic belt: XXIII Internat. Geol. Congr., Prague, v. 1, p. 209-220.

Davies, I. C., and Walker, R. G., 1974, Transport and deposition of resedimented conglomerates: the Cap Enragé Formation, Cambro-Ordovician, Gaspé, Quebec: J. Sediment. Petrology, v. 44, p. 1200-1216.

de Grijs, J. W., 1971, Dimensional grain orientation and preliminary radiographic studies of the sandstones from the Finger Lakes Stone Quarry: B.Sc. Thesis, McMaster Univ., Hamilton, Ont., 50 p.

Dewey, J. F., 1974, Continental margins and ophiolite obduction: Appalachian Caledonian system: in, Burk, C. A., and Drake, C. L., eds, The Geology of Continental Margins, Springer-Verlag, New York, p. 933-952.

_____, and Bird, J. M., 1971, Origin and emplacement of the ophiolite suite: Appalachian ophiolites in Newfoundland: J. Geophys. Res., v. 76, p. 3179-3206.

Dickinson, W. R., 1970, Interpreting detrital modes of graywacke and arkose: J. Sediment. Petrology, v. 40, p. 695-707.

_____, 1971a, Clastic sedimentary sequences deposited in shelf, slope, and trough setting between magmatic arcs and associated trenches: Pacific Geol., v. 3, p. 15-30.

_____, 1971b, Detrital modes of New Zealand greywackes: Sediment. Geol., v. 5, p. 37-56.

Dixon, W. J., and Massey, F. J., Jr., 1957, Introduction to Statistical Analysis (2nd edition): McGraw-Hill, New York, 488 p.

Dörjes, J., and Hertwick, G., 1975, Recent biocoenoses and ichnocoenoses in shallow-water marine environments: in, Frey, R. W., ed., The Study of Trace Fossils, Springer-Verlag, New York, p. 459-491.

Dott, R. H., Jr., 1963, Dynamics of subaqueous gravity depositional processes: Amer. Ass. Petrol. Geol., Bull., v. 47, p. 104-128.

_____, 1966, Eocene deltaic sedimentation at Coos Bay, Oregon: J. Geol., v. 74, p. 373-420.

Douglas, R. J. W., ed., 1970, Geology and Economic Minerals of Canada: Geol. Surv. Can., Econ. Geol. Rept. 1, 838 p.

Dzulynski, S., and Walton, E. K., 1965, Sedimentary Features of Flysch and Greywacke: Elsevier, New York, 274 p.

Eckis, R., 1928, Alluvial fans of the Cucamonga district, southern California: J. Geol., v. 36, p. 224-247.

Einstein, H. A., 1941, The viscosity of highly concentrated underflows and its influence on mixing: Amer. Geophys. Union, Trans., v. 22, p. 597-603.

Enos, P., 1969a, Cloridorme Formation, Middle Ordovician flysch, northern Gaspé Peninsula, Quebec: Geol. Soc. Amer., Spec. Pap. 117, 66 p.

_____, 1969b, Anatomy of a flysch: J. Sediment. Petrology, v. 39, p. 680-723.

_____, 1977, Flow regimes in debris flow: Sedimentology, v. 24, p. 133-142.

Fahnestock, R. K., and Haushild, W. L., 1962, Flume studies of the transport of pebbles and cobbles on a sand bed: Geol. Soc. Amer., Bull., v. 73, p. 1431-1436.

Feo-Codecido, G., 1956, Heavy-mineral techniques and their application to Venezuelan stratigraphy: Amer. Ass. Petrol. Geol., Bull., v. 40, p. 984-1000.

Fisher R. A., 1948, Statistical Methods for Research Workers, 10th edition: Oliver and Boyd, Edinburgh, 354 p.

Fitch, T. J., 1970, Earthquake mechanisms and island arc tectonics in the Indonesian - Phillippine region: Seismol. Soc. Amer., Bull., v. 60, p. 565-591.

Flores, G., 1955, Discussion: in, Beneo, E., Les résultats des études pour la recherche petrolifère en Sicilie (Italie), 4th World Petroleum Congr., Rome, Proc. Sect. 1, p. 121-122.

Folk, R. L., 1968, Petrology of Sedimentary Rocks: Hemphill's, Austin, Texas, 170 p.

Friedman, G. M., 1958, Determination of sieve-size distribution from thin section data for sedimentary petrological studies: J. Geol., v. 66, p. 394-416.

Füchtbauer, H., 1974, Sediments and Sedimentary Rocks 1 (Sedimentary Petrology, part II), John Wiley and Sons, Inc., New York, 464 p.

Galloway, W. E., 1974, Deposition and diagenetic alteration of sandstone in northeast Pacific arc-related basins: implications for graywacke genesis: Geol. Soc. Amer., Bull., v. 85, p. 379-390.

Garrison, R. E., 1974, Radiolarian cherts, pelagic limestones and igneous rocks in eugeosynclinal assemblages: Spec. Publs. int. Ass. Sediment., 1, p. 367-400.

Geike, A., 1882, Textbook of Geology: Macmillan, London, 971 p.

Gingerich, P. D., 1969, Markov analysis of cyclic alluvial sediments: J. Sediment. Petrology, v. 39, p. 330-332.

Goddard, E. N., Trask, P. D., de Ford, R. K., Rove, O. N., Singewald, J. T., Jr., Overbeck, R. M., 1970, Rock-color chart: distributed by Geol. Soc. Amer., Boulder, Colorado.

Goldschmidt, V. M., 1937, The principles of distribution of chemical elements in minerals and rocks: J. Chem. Soc. for 1937, p. 655-673.

Graham, S. A., Dickinson, W. R., and Ingersoll, R. V., 1975, Himalayan - Bengal model for flysch dispersal in the Appalachian - Ouachita system: Geol. Soc. Amer., Bull., v. 86, p. 273-286.

_____, Ingersoll, R. V., and Dickinson, W. R., 1976, Common provenance for lithic grains in Carboniferous sandstones from Ouachita Mountains and Black Warrior Basin: J. Sediment. Petrology, v. 46, p. 620-632.

Griffiths, J. C., 1960, Modal analysis of sediments: Rev. Géogr. Phys. Géol. Dyn., (2), v. III, fasc. 1, p. 29-48.

_____, and Rosenfeld, M. A., 1954, Operator variation in experimental research: J. Geol., v. 62, p. 74-91.

Gwyn, H., 1971, Heavy mineral assemblages in tills and their use in distinguishing glacial lobes in the Great Lakes Region: Ph.D. Thesis, Univ. of Western Ont., London, Ont., 192 p.

Hampton, M. A., 1972, The role of subaqueous debris flow in generating turbidity currents: J. Sediment. Petrology, v. 42, p. 775-793.

_____, 1975, Competence of fine-grained debris flows: J. Sediment. Petrology, v. 45, p. 834-844.

Hand, B. M., 1961, Grain orientation in turbidites: Compass, v. 28, p. 133-144.

_____, 1974, Supercritical flow in density currents: J. Sediment. Petrology, v. 44, p. 637-648.

Haner, B. E., 1971, Morphology and sediments of Redondo submarine fan, southern California: Geol. Soc. Amer., Bull., v. 82, p. 2413-2432.

Hansen, E., 1967, Methods of deducing slip line orientations from the geometry of folds: Yb. Carnegie Instn, Wash., v. 65, p. 387-405.

_____, 1971, Strain Facies: Springer-Verlag, New York, 207 p.

Harbaugh, J. W., and Bonham-Carter, G., 1970, Computer Simulation in Geology: Wiley-Interscience, New York, 575 p.

Harland, W. B., and Gayer, R. A., 1972, The Arctic Caledonides and earlier oceans: Geol. Mag., v. 109, p. 289-314.

Harms, J. C., and Fahnestock, R. K., 1965, Stratification, bed forms, and flow phenomena (with an example from the Rio Grande): Soc. Econ. Paleontol. Mineral., Spec. Publ. 12, p. 84-115.

_____, Southard, J. B., Spearing, D. R., and Walker, R. G., 1975, Depositional Environments as Interpreted from Primary Sedimentary Structures and Stratification Sequences: Soc. Econ. Paleontol. Mineral., Short Course No. 2, 161 p.

Harrison, P. W., 1957, New technique for three-dimensional fabric analysis of till and englacial debris containing particles from 3 to 40 millimetres in size: J. Geol., v. 65, p. 98-105.

Hattori, I., 1976, Entropy in Markov chains and discrimination of cyclic patterns in lithologic successions: Math. Geol., v. 8, p. 477-497.

Heezen, B. C., 1974, Atlantic-type continental margins: in, Burk, C. A., and Drake, C. L., eds, The Geology of Continental Margins, Springer-Verlag, New York, p. 13-24.

_____, and Ewing, M., 1952, Turbidity currents and submarine slumps, and the 1929 Grand Banks earthquake: Amer. J. Sci., v. 250, p. 849-873.

Heinrich, E. W., 1965, Microscopic Identification of Minerals: McGraw-Hill, New York, 414 p.

Hobday, D. K., and Mathew, D., 1975, Late Paleozoic fluviatile and deltaic deposits in the northeast Karroo Basin, South Africa: in, Broussard, M. L., ed., Deltas, Houston Geol. Soc., p. 457-470.

Hollister, C. D., and Heezen, B. C., 1964, Modern graywacke-type sands: Science (AAAS), v. 146, p. 1573-1574.

Horn, D. R., Ewing, M., Delach, M. N., and Horn, B. M., 1971, Turbidites of the Hatteras and Sohm Abyssal Plains, western North Atlantic: Marine Geol., v. 11, p. 287-323.

Hsu, K. J., 1968, Principles of mélanges and their bearing on the Franciscan - Knoxville paradox: Geol. Soc. Amer., Bull., v. 79, p. 1063-1074.

_____, 1974, Mélanges and their distinction from olistostromes: Soc. Econ. Paleontol. Mineral., Spec. Publ. 19, p. 321-333.

_____, 1977, Studies of Ventura Field, California, I; facies geometry and genesis of Lower Pliocene turbidites: Amer. Ass. Petrol. Geol., Bull., v. 61, p. 137-168.

Hubert, C., 1973, Kamouraska, la Pocatière, Saint-Jean-Port-Joli area: Quebec Dept. Nat. Resources, Geol. Rept. 151, 205 p.

Hubert, J. F., 1962, A zircon-tourmaline-rutile maturity index and the interdependence of the composition of heavy mineral assemblages with the gross composition and texture of sandstones: J. Sediment. Petrology, v. 32, p. 440-450.

Jakeš, P., and White, A. J. R., 1971, Composition of island arcs and continental growth: Earth Planet. Sci. Lett., v. 12, p. 224-230.

Jeffreys, G. B., 1922, The motion of ellipsoidal particles immersed in a viscous fluid: Roy. Soc. London, Proc., Ser. A, v. 102, p. 161-179.

Johansson, C. E., 1976, Structural studies of frictional sediments: Geogr. Ann., Ser. A, No. 4, p. 201-301.

Johnson, A. M., 1970, Physical Processes in Geology: Freeman, Cooper and Co., San Francisco, 577 p.

Jolly, W. T., 1972, Degradation (hydration) - aggradation (dehydration) and low-rank metamorphism of mafic volcanic sequences: XXIV Internat. Geol. Congr., Montreal, Sect. 2, p. 11-18.

_____, and Smith, R. E., 1972, Degradation and metamorphic differentiation of the Keweenawan tholeiitic lavas of northern Michigan, U.S.A.: J. Petrology, v. 13, p. 273-309.

Jones, I. W., 1934, Marsoui map area, Gaspé Peninsula: Quebec Bur. Mines Ann. Rept. for 1933, part D, p. 3-39.

Jopling, A. V., 1965, Hydraulic factors controlling the shape of laminae in laboratory deltas: J. Sediment. Petrology, v. 35, p. 777-791.

_____, and Walker, R. G., 1968, Morphology and origin of ripple-drift cross-lamination, with examples from the Pleistocene of Massachusetts: J. Sediment. Petrology, v. 38, p. 971-984.

Katili, J. A., 1975, Volcanism and plate tectonics in the Indonesian island arcs: Tectonophysics, v. 26, p. 165-188.

Kennedy, J. F., 1963, The mechanics of dunes and antidunes in erodible-bed channels: J. Fluid Mech., v. 16, p. 521-544.

Kennedy, M. J., 1975a, Repetitive orogeny in the northeastern Appalachians - new plate models based upon Newfoundland examples: Tectonophysics, v. 28, p. 39-87.

_____, 1975b, The Fleur de Lys Supergroup: a stratigraphic comparison of Moine and Dalradian equivalents in Newfoundland with the British Caledonides: Geol. Soc. London, Jour., v. 131, p. 305-310.

Kittleman, L. R., 1964, Application of Rosin's distribution in size frequency analysis of clastic rocks: J. Sediment. Petrology, v. 34, p. 483-502.

Kruit, C., Brouwer, J., Knox, G., Schollnberger, W., van Vliet, A., 1975, Une excursion aux cones d'alluvions en eau profonde d'age tertiare près de San Sebastian (Province de Guipuzcoa, Espagne): IX Internat. Congr. Sedimentology, Nice, excursion guidebook 23, 75 p.

Krumbein, W. C., 1941, Measurement and geological significance of shape and roundness of sedimentary particles: J. Sediment. Petrology, v. 11, p. 64-72.

_____, and Dacey, M. F., 1969, Markov chains and embedded Markov chains in geology: Math. Geol., v. 1, p. 79-96.

_____, and Pettijohn, F. J., 1938, Manual of Sedimentary Petrography: Appleton-Century, New York, 549 p.

Kuenen, Ph. H., 1959, Experimental abrasion of pebbles, 3. Fluviatile action on sand: Amer. J. Sci., v. 257, p. 172-190.

_____, 1966, Matrix of turbidities: experimental approach: Sedimentology, v. 7, p. 267-297.

Kulm, L. D., von Huene, R. E., and others, 1973, Initial Reports of the Deep Sea Drilling Project, Volume XVIII: Washington (U.S. Government Printing Office), 1077 p.

Kuno, H., 1966, Lateral variation in basalt magma type across continental margins and island arcs: Geol. Surv. Can., Pap. 66-15, p. 317-336.

Laird, M. G., 1970, Vertical sheet structures - a new indicator of sedimentary fabric: J. Sediment. Petrology, v. 40, p. 428-434.

Lajoie, J., 1968, Turbidites sans matrice: produits de diagenèse: Natur. Can., v. 95, p. 1243-1255.

_____, Héroux, Y., and Mathey, B., 1974, The Precambrian shield and the Lower Paleozoic shelf: the unstable provenance of the Lower Paleozoic flysch sandstones and conglomerates of the Appalachians between Beaumont and Bic, Quebec: Can. J. Earth Sci., v. 11, p. 951-963.

Lambert, R. St. J., and McKerrow, W. S., 1976, The Grampian Orogeny: Scot. J. Geol., v. 12, p. 271-292.

Lambiase, J. J., 1977, Sediment Dynamics in the Macrotidal Avon River Estuary, Nova Scotia: Ph.D Thesis, McMaster Univ., Hamilton, Ont., 415 p.

Laurent, R., 1975, Occurrences and origin of the ophiolites of southern Quebec, northern Appalachians: Can. J. Earth Sci., v. 12, p. 443-455.

LePichon, X., Francheteau, J., and Bonnin, J., 1973, Plate Tectonics: Elsevier, Amsterdam, 300 p.

Liard, P., 1973, Legend for map sheets of Mont Joli, Matane, Sayabec, Ste. Blandine E: Quebec Dept. Nat. Resources, DP 290.

Logan, W. E., 1846, On the geology of the Chat and Cascapédia Rivers, Gaspé, and part of Chaleur Bay: Geol. Surv. Can., Rept. Prog. for 1844, p. 5-66.

_____, 1863, Geology of Canada: Geol. Surv. Can., Rept. Prog., 1843 - 1863.

Lowe, D. R., 1975, Water escape structures in coarse-grained sediments: Sedimentology, v. 22, p. 157-204.

_____, 1976a, Grain flow and grain flow deposits: J. Sediment. Petrology, v. 46, p. 188-199.

_____, 1976b, Subaqueous liquefied and fluidized sediment flows and their deposits: Sedimentology, v. 23, p. 285-308.

_____, and LoPiccolo, R. D., 1974, The characteristics and origins of dish and pillar structures: J. Sediment. Petrology, v. 44, p. 484-501.

MacGregor, I. D., and Smith, C. H., 1963, The use of chrome spinels in petrographic studies of ultramafic intrusions: Can. Mineral., v. 7, p. 403-412.

Martini, I. P., 1965, The sedimentology of the Medina Formation outcropping along the Niagara escarpment (Ontario and New York State): Ph.D Thesis, McMaster Univ., Hamilton, Ont., 420 p.

Mattinson, C. R., 1964, Mount Logan area: Gaspé Peninsula: Quebec Dept. Nat. Resources, Geol. Rept. 118.

Mattinson, J. M., 1975, Early Paleozoic ophiolite complexes of Newfoundland: isotopic ages of zircons: Geology, v. 3, p. 181-200.

Maxwell, A. E., and others, 1970, Initial Reports of the Deep Sea Drilling Project, Volume III: Washington (U.S. Government Printing Office), 806 p.

McBirney, A. R., 1976, Some geologic constraints on models for magma generation in orogenic environments: Can. Mineral., v. 14, p. 245-254.

McBride, D. E., 1976, Tectonic setting of the Tetagouche Group, host to the New Brunswick polymetallic massive sulphide deposits: in, Strong, D. F., ed., Metallogeny and Plate Tectonics, Geol. Ass. Can., Spec. Pap. 14, p. 473-485.

McBride, E. F., and Kimberly, J. E., 1963, Sedimentology of Smithwick Shale (Pennsylvanian), eastern Llano region, Texas: Amer. Ass. Petrol. Geol., Bull., v. 47, p. 1840-1854.

McGerrigle, H. W., 1954, The Tourelle and Coucelette areas: Quebec Dept. Mines, Geol. Rept. 62, 63 p.

McKerrow, W. S., and Ziegler, A. M., 1971, The Lower Silurian paleogeography of New Brunswick and adjacent areas: J. Geol., v. 79, p. 635-646.

McLeod, C. R., and Chamberlain, J. A., 1969, Reflectivity and Vickers microhardness of ore minerals: Geol. Surv. Can., Pap. 68-64 (charts and tables).

Meckel, L. D., 1972, Anatomy of distributary channel-fill deposits in recent mud deltas (abst.): Amer. Ass. Petrol. Geol., Bull., v. 56, p. 639.

Middleton, G. V., 1962, Size and sphericity of quartz grains in two turbidite formations: J. Sediment. Petrology, v. 32, p. 725-742.

_____, 1965, The Tukey chi-squared test: J. Geol., v. 73, p. 547-549.

_____, 1966a, Experiments on density and turbidity currents: I. Motion of the head: Can. J. Earth Sci., v. 3, p. 523-546.

_____, 1966b, Experiments on density and turbidity currents: II. Uniform flow of density currents: Can. J. Earth Sci., v. 3, p. 627-637.

_____, 1967, Experiments on density and turbidity currents: III. Deposition of sediment: Can. J. Earth Sci., v. 4, p. 475-505.

_____, 1969, Grain flows and other mass movements down slopes: in, Stanley, D. J., ed., The New Concepts of Continental Margin Sedimentation, Amer. Geol. Inst. Short Course Lecture Notes, p. GM-B-1 to GM-B-14.

Middleton, G. V., 1970, Experimental studies related to the problems of flysch sedimentation: Geol. Ass. Can., Spec. Pap. 7, p. 253-272.

_____, 1976, Hydraulic interpretation of sand size distributions: J. Geol., v. 84, p. 405-426.

_____, and Hampton, M. A., 1973, Sediment gravity flows: mechanics of flow and deposition: in, Middleton, G. V., and Bouma, A. H., eds, Turbidites and Deep-water Sedimentation, Soc. Econ. Paleontol. Mineral., Short Course, Anaheim, p. 1-38.

_____, and _____, 1976, Subaqueous sediment transport and deposition by sediment gravity flows: in, Stanley, D. J., and Swift, D. J. P., eds, Marine Sediment Transport and Environmental Management, John Wiley and Sons, p. 197-218.

_____, and Southard, J. B., 1977, Mechanics of Sediment Movement: Soc. Econ. Paleontol. Mineral., Short Course No. 3, Binghampton, New York.

Milner, H. B., 1926, Supplement to Introduction to Sedimentary Petrography: Murby, London, 157 p.

Mizutani, S., 1971, Silica minerals in the early stages of diagenesis: Sedimentology, v. 15, p. 419-436.

Moore, C., 1974, Turbidites and terrigenous muds, DSDP Leg 25: Initial Reports of the Deep Sea Drilling Project Volume XXV, Washington (U.S. Government Printing Office), p. 441-479.

Moore, J. C., 1973, Cretaceous continental margin sedimentation, southwest Alaska: Geol. Soc. Amer., Bull., v. 84, p. 595-614.

Moore, D. G., Curry, J. R., and Emmel, F. J., 1976, Large submarine slide (olistostrome) associated with Sunda Arc subduction zone, northeast Indian Ocean: Marine Geol., v. 21, p. 211-226.

Morris, R. C., 1971, Classification and interpretation of disturbed bedding types in the Jackfork flysch rocks (Upper Mississippian), Ouachita Mountains, Arkansas: J. Sediment. Petrology, v. 41, p. 410-424.

Mutti, E., 1974, Examples of ancient deep-sea fan deposits from circum-Mediterranean geosynclines: Soc. Econ. Paleontol. Mineral., Spec. Publ. 19, p. 92-105.

Mutti, E., 1977, Distinctive thin-bedded turbidite facies and related depositional environments in the Eocene Hecho Group (south-central Pyrenees, Spain): Sedimentology, v. 24, p. 107-132.

_____, and Ghibaudo, G., 1972, Un esempio di torbiditi di conoide sottomarina esterna: le Arenarie di San Salvatore (Formazione di Bobbio, Miocene) nell'Appenino di Piacenza: Mem. Acc. Sci. Torino, Classe Sci. Fis. Mat., Nat., Serie 4, n. 16, 40 p.

_____, and Ricci Lucchi, F., 1972, Le torbidite dell'Appenino settentrionale: introduzione all'analisi di facies: Mem. Soc. Geol. Italiana, v. 11, p. 161-199.

Nelson, C. H., Carlson, P. R., Byrne, G. V., and Alpha, T. R., 1970, Development of the Astoria Canyon-fan physiography and comparison with similar systems: Marine Geol., v. 8, p. 259-291.

_____, and Kulm, V., 1973, Submarine fans and channels: in, Middleton, G. V., and Bouma, A. H., eds, Turbidites and Deep-water Sedimentation, Pacific Sect., Soc. Econ. Paleontol. Mineral., Short Course, Anaheim, p. 39-78.

_____, Mutti, E., and Ricci-Lucchi, F., 1975, Comparison of proximal and distal thin-bedded turbidites with current-winnowed deep-sea sands: IX Internat. Congr. Sedimentology, Nice, Theme 5, p. 317-324.

_____, and Nilsen, T. H., 1974, Depositional trends of modern and ancient deep-sea fans: Soc. Econ. Paleontol. Mineral., Spec. Publ. 19, p. 69-91.

Nordin, C. F., Jr., and Culbertson, J. K., 1963, Discussion of "Forms of bed roughness in alluvial channels" by D. B. Simons and E. V. Richardson: Amer. Soc. Civil Engineers, Trans., v. 128, pap. no. 3414, p. 303-308.

Normark, W. R., 1970, Growth patterns of deep-sea fans: Amer. Ass. Petrol Geol., Bull., v. 54, p. 2170-2195.

Ojakangas, R. W., 1968, Cretaceous sedimentation, Sacramento Valley, California: Geol. Soc. Amer., Bull., v. 79, p. 973-1008.

Ollerenshaw, N. C., 1967, Cuoq-Langis area: Matane and Matapedia Counties: Quebec Dept. Nat. Resources, Geol. Rept. 121, 192 p.

Onions, D., and Middleton, G. V., 1968, Dimensional grain orientation of Ordovician turbidite greywackes: J. Sediment. Petrology, v. 38, p. 164-174.

Osborne, F. F., 1953, Concretion conglomerate in the Charny Sandstone, Quebec: Roy. Soc. Can., Trans., v. 47, sec. 4, p. 55-60.

Palmer, H. D., 1976, Erosion of submarine outcrops, La Jolla submarine canyon: Geol. Soc. Amer., Bull., v. 87, p. 427-432.

Parea, G. C., 1968, The possibility of reconstruction of the pre-tectonic current trend in allochthonous turbidite formations: XXIII Internat. Geol. Congr., Praque, Sect. 3, p. 225-234.

Parkash, B., 1969, Depositional Mechanism of greywackes, Cloridorme Formation (Middle Ordovician), Gaspé, Quebec: Ph.D. Thesis, McMaster Univ., Hamilton, Ont., 238 p.

_____, and Middleton, G. V., 1970, Downcurrent textural changes in Ordovician turbidite greywackes: Sedimentology, v. 14, p. 259-293.

Peterson, M. N. A., and others, 1970, Initial Reports of the Deep Sea Drilling Project, Volume II: Washington (U.S. Government Printing Office), 491 p.

Pettijohn, F. J., 1941, Persistence of minerals and geologic age: J. Geol., v. 49, p. 610-625.

_____, 1954, Classification of sandstones: J. Geol., v. 62, p. 360-365.

_____, 1957, Sedimentary Rocks, 2nd edition: Harper and Row, New York, 718 p.

_____, Potter, P. E., and Siever, S., 1972, Sand and Sandstone: Springer-Verlag, New York, 618 p.

Phillips, W. E. A., Stillman, C. J., and Murphy, T., 1976, A Caledonian plate tectonic model: Geol. Soc. London, Jour., v. 132, p. 579-610.

Poole, W. H., 1976, Plate tectonic evolution of the Canadian Appalachian region: Geol Surv. Can., Pap. 76-1B, p. 113-126.

Poole, W. H., Kelley, D. G., and Neale, E. R. W., 1964, Age and correlation problems in the Appalachian region of Canada: in, Osborne, F. F., ed., Geochronology in Canada, Roy. Soc. Can., Spec. Publ. 8, p. 61-84.

_____, and Rodgers, J., 1972, Appalachian geotectonic elements of the Atlantic provinces and southern Quebec: XXIV Internat. Geol. Congr., Montreal, guidebook for excursion A63 and C63, 200 p.

Pratt, C. J., and Smith, K. V. H., 1972, Ripple and dune phases in a narrowly graded sand: Amer. Soc. Civil Engineers, Proc., v. 98, No. HY5, p. 859-874.

Ramsay, J. G., 1961, The effects of folding upon the orientation of sedimentation structures: J. Geol., v. 69, p. 84-100.

Rankama, K., and Sahama, Th. G., 1950, Geochemistry: Univ. of Chicago Press, 911 p.

Rasetti, F., 1946, Cambrian and Early Ordovician stratigraphy of the lower St. Lawrence valley: Geol. Soc. Amer., Bull., v. 57, p. 687-706.

Rast, N., and Stringer, P., 1974, Recent advances and the interpretation of geological structure of New Brunswick: Geosci. Can., v. 1, No. 4, p. 15-25.

Raup, O. B., and Miesch, A. T., 1957, A new method for obtaining significant average directional measurements in cross-stratification studies: J. Sediment. Petrology, v. 27, p. 313-321.

Rautman, C. A., and Dott, R. H., Jr., 1977, Dish structures formed by fluid escape in Jurassic shallow marine sandstones: J. Sediment. Petrology, v. 47, p. 101-106.

Raymond, P. E., 1914, The succesion of faunas at Lévis, P.Q.: Amer. J. Sci., Ser. 4, v. 38, p. 523-530.

Rees, A. I., 1965, The use of anisotropy of magnetic susceptibility in the estimation of sedimentary fabric: Sedimentology, v. 4, p. 257-271.

_____, 1966, The effect of depositional slopes on the anisotropy of magnetic susceptibility of laboratory deposited sands: J. Geol., v. 74, p. 856-867.

_____, 1968, The production of preferred orientation in a concentrated dispersion of elongated and flattened grains: J. Geol., v. 76, p. 457-465.

Reineck, H.-E., and Singh, I. B., 1975, Depositional Sedimentary Environments: Springer-Verlag, New York, 439 p.

Ricci Lucchi, F., 1969a, Channelized deposits in the Middle Miocene flysch of Romagna (Italy): Giorn. di Geologia, v. 36, p. 203-282.

_____, 1969b, Recherches stratonomiques et sedimentologiques sur le Flysch Miocene de la Romagne (Formation Marnoso-arenacea): Comm. Medit. Neog. Strat., Proc. IV Sess., Giorn. di Geologia, S2, v. 35, No. 4, p. 163-198.

_____, 1975a, Depositional cycles in two turbidite formations of northern Apennines (Italy): J. Sediment. Petrology, v. 45, p. 3-43.

_____, 1975b, Miocene paleogeography and basin analysis in the Periadriatic Apennines: in, Coy, S., ed., Geology of Italy, Tripoli, Petroleum Exploration Soc. of Libya, p. 5-111.

Richardson, J. F., and Zaki, W. N., 1954, Sedimentation and fluidization: Inst. Chem. Engineers (London), Trans., v. 32, p. 35-53.

Rittenhouse, G., 1944, Sources of modern sands in the Middle Rio Grande Valley, New Mexico: J. Geol., V. 52, p. 145-183.

Robertson, C. A., 1976, Grain orientation of massive sandstones: B.Sc Thesis, McMaster Univ., Hamilton, Ont., 41 p.

Rodgers, J., 1965, The Long Point and Clam Bank Formations, western Newfoundland: Geol. Ass. Can., Proc., v. 16, p. 83-94.

_____, 1968, The eastern edge of the North American continent during the Cambrian and Early Ordovician: in, Zen, E-an, and others, eds, Studies of Appalachian Geology: northern and maritime, Wiley Interscience, New York, p. 141-149.

_____, 1970, The Tectonics of the Appalachians: Wiley Interscience, New York, 271 p.

_____, and Neale, E. R. W., 1963, Possible "Taconic" klippen in western Newfoundland: Amer. J. Sci., v. 261, p. 713-730.

Rodine, J. D., and Johnson, A. M., 1976, The ability of debris, heavily freighted with coarse clastic materials, to flow, on gentle slopes: Sedimentology, v. 23, p. 213-234.

Rogers, J. J. W., 1966, Geochemical significance of source rocks of some graywackes from western Oregon and Washington: Texas J. Sci., v. 18, p. 5-20.

Roscoe, R., 1953, Suspensions: in, Hermans, J. J., ed., Flow Properties of Disperse Systems, Interscience Publ., Inc., New York, p. 1-38.

Ross, C. S., and Smith, R. L., 1961, Ash-flow tuffs - their origin, geologic relations and identification: U.S. Geol. Surv., Prof. Paper 366, 81 p.

Rouse, H., 1937, Modern conceptions of the mechanics of turbulence: Amer. Soc. Civil Engineers, Trans., v. 102, p. 436-505.

Rubey, W. W., 1933, Settling velocities of gravel, sand, and silt particles: Amer. J. Sci., Ser. 5, v. 25, p. 325-338.

Rukavina, N. A., 1965, Particle orientation in turbidites; theory and experiment: Ph.D. Thesis, Rochester Univ., Rochester, N.Y., 57 p.

Rupke, N. A., 1975, Deposition of fine-grained sediments in the abyssal environment of the Algéro-Balearic Basin, western Mediterranean Sea: Sedimentology, v. 22, p. 95-110.

Rusnak, G. A., 1957, The orientation of sand grains under conditions of unidirectional fluid flow: J. Geol., v. 65, p. 384-409.

Rust, B. R., 1972, Pebble orientation in fluvial sediments: J. Sediment. Petrology, v. 42, p. 384-388.

St. Julien, P., 1968, Les "argiles-à-blocs" du sud-ouest des Appalaches du Québec: Natur. Can., v. 95, p. 1345-1356.

_____, and Hubert, C., 1975, Evolution of the Taconic orogen in the Quebec Appalachians: Amer. J. Sci., v. 275-A, p. 337-362.

_____, _____, Skidmore, B., and Béland, J., 1972, Appalachian Structure and Stratigraphy, Quebec: XXIV Internat. Geol. Congr., Montreal, guidebook for excursion 56, 99 p.

Sanders, J. E., 1965, Primary sedimentary structures formed by turbidity currents and related resedimentation mechanisms: Soc. Econ. Paleontol. Mineral., Spec. Publ. 12, p. 192-219.

Schwarzacher, W., 1951, Grain orientation in sands and sandstones: J. Sediment. Petrology, v. 12, p. 162-172.

Scott, K. M., 1966, Sedimentology and dispersal pattern of a Cretaceous flysch sequence, Patagonian Andes, Southern Chile: Amer. Ass. Petrol. Geol., Bull., v. 50, p. 72-107.

Seilacher, A., 1964, Biogenic sedimentary structures: in, Imbrie, J., and Newell, N. D., eds, Approaches to Paleoecology, John Wiley and Sons, Inc., New York, p. 296-315.

Seki, Y., 1969, Facies series in Low-grade metamorphism: Geol. Soc. Japan, Jour., v. 75, p. 255-266.

Sestini, G., and Pranzini, G., 1965, Correlation of sedimentary fabric and sole marks as current indicators in turbidites: J. Sediment. Petrology, v. 35, p. 100-108.

Sharp, R. P., and Nobles, L. H., 1953, Mudflow of 1941 at Wrightwood, California: Geol. Soc. Amer., Bull., v. 64, p. 547-560.

Shepard, F. P., 1966, Meander in valley crossing a deep-ocean fan: Science (AAAS), v. 154, p. 385-386.

_____, and Dill, R. F., 1966, Submarine Canyons and Other Sea Valleys: Rand McNally and Co., Chicago, 381 p.

Sheridan, R. E., 1974, Atlantic continental margin of North America: in, Burk, C. A., and Drake, C. L., eds, The Geology of Continental Margins, Springer-Verlag, New York, p. 391-408.

Sibley, D. F., and Blatt, H., 1976, Intergranular pressure solution and cementation of the Tuscarora orthoquartzite: J. Sediment. Petrology, v. 46, p. 881-896.

Siever, R., 1962, Silica solubility, 0°-200°C, and the diagenesis of siliceous sediments: J. Geol., v. 70, p. 127-150.

Sigvaldason, G. E., 1962, Epidote and related minerals in two deep geothermal drill holes, Reykjavik and Hveragerdi, Iceland: U.S. Geol. Surv., Prof. Paper 450-E, E77-E79.

Simons, D. B., Richardson, E. V., and Nordin, C. F., Jr., 1965, Sedimentary structures generated by flow in alluvial channels: Soc. Econ. Paleontol. Mineral., Spec. Publ. 12, p. 34-52.

Simpson, G. S., 1976, Evidence of overgrowths on, and solution of, detrital garnets: J. Sediment. Petrology, v. 46, p. 689-693.

Sindowski, F. K. H., 1949, Results and problems of heavy mineral analysis in Germany; a review of sedimentary petrological papers, 1936-1948: J. Sediment. Petrology, v. 19, p. 3-25.

Sippel, R. F., 1968, Sandstone petrography, evidence from luminescence petrography: J. Sediment. Petrology, v. 38, p. 530-554.

Smith, J. V., 1974, Feldspar Minerals, 2. Chemical and Textural Properties: Springer-Verlag, New York, 690 p.

Smoor, P. S., 1960, Dimensional grain orientation studies of turbidite greywackes: M.Sc. Thesis, McMaster Univ. Hamilton, Ont., 97 p.

Sorby, H. C., 1859, On the structures produced by the currents present during deposition of stratified rocks: Geologist, vol. II, p. 137-147.

_____, 1877, The application of the microscope to geology: Mon. Micro. Jour., vol. XVII, p. 113-136.

Spotts, J. H., 1964, Grain orientation and imbrication on Miocene turbidity current sandstones, California: J. Sediment. Petrology, v. 34, p. 229-253.

Stanley, D. J., 1963, Vertical petrographic variability in Annot Sandstone turbidites: some preliminary observations and generalizations: J. Sediment. Petrology, v. 33, p. 783-788.

_____, 1967, Comparing patterns of sedimentation in some modern and ancient submarine canyons: Earth Planet. Sci. Lett., v. 3, p. 371-380.

_____, 1975, Submarine canyon and slope sedimentation (Grès d'Annot) in the French Maritime Alps: IX Internat. Congr. Sedimentology, Nice, guidebook, 129 p.

_____, and Bouma, A. H., 1964, Methodology and paleogeographic interpretation of flysch formations: a summary of studies in the Maritime Alps: in, Bouma, A. H., and Brouwer, A., eds, Turbidites, Developments in Sedimentology 3, Elsevier, p. 34-64.

Stevens, R. K., 1970, Cambro-Ordovician flysch sedimentation and tectonics in west Newfoundland and their possible bearing on a proto-Atlantic Ocean: Geol. Ass. Can., Spec. Pap. 7, p. 165-178.

Stone, B. D., 1976, Analysis of slump slip lines and deformation fabric in slumped Pleistocene lake beds: J. Sediment. Petrology, v. 46, p. 313-325.

Strong, D. F. , 1973, Lushs Bight and Roberts Arm Groups of central Newfoundland, possible juxtaposed oceanic and island-arc volcanic suites: Geol. Soc. Amer., Bull., v. 84, p. 3917-3928.

_____, Dickson, W. L., O'Driscoll, C. F., Kean, B. F., and Stevens, R. K., 1974, Geochemical evidence for eastward Appalachian subduction in Newfoundland: Nature, v. 248, p. 37-39.

Swinden, H. S., and Strong, D. S., 1976, A comparison of plate tectonic models of metallogenesis in the Appalachians, the North American Cordillera, and the east Australian Paleozoic: in, Strong, D. F., ed., Metallogeny and Plate Tectonics, Geol. Ass. Can., Spec. Pap. 14, p. 443-471.

Taira, A., 1976a, Grain orientation and depositional processes - fabric analyses of modern and laboratory flume deposits: Ph.D. Thesis, Univ. of Texas at Dallas, p. 234-309.

_____, 1976b, Settling velocity distributions, magnetic fabrics and sedimentary structures of the Pliocene Pico Formation, Ventura Basin, California: implications for the depositional processes of turbidites and associated deposits: Ph.D. Thesis, Univ. of Texas at Dallas, p. 310-365.

Taylor, G. L., 1923, The motion of ellipsoidal particles in a viscous fluid: Roy. Soc. London, Proc., Ser. A, v. 103, p. 58-61.

Taylor, J. M., 1950, Pore space reduction in sandstone: Amer. Ass. Petrol. Geol., Bull., v. 34, p. 701-716.

Terzaghi, K., 1956, Varieties of submarine slope failures: 8th Texas Conf. Soil Mech. Foundation Engineering, Proc., 41 p.

Thiel, G. A., 1940, The relative resistance to abrasion of mineral grains of sand size: J. Sediment. Petrology, v. 10, p. 103-124.

Thomson, A. F., and Thomasson, M. R., 1969, Shallow to deep water facies development in the Dimple Limestone (Lower Pennsylvanian), Marathon region, Texas: Soc. Econ. Paleontol. Mineral., Spec. Publ. 14, p. 57-78.

Upadhyay, H. D., Dewey, J. F., and Neale, E. R. W., 1971, The Betts Cove ophiolite complex; Newfoundland: Appalachian oceanic crust and mantle: Geol. Ass. Can., Proc., v. 24, p. 27-34.

Van der Knaap, W., and Eijpe, R., 1969, Some experiments on the genesis of turbidity currents: Sedimentology, v. 11, p. 115-124.

Van der Plas, L., 1962, Preliminary note on the granulometric analysis of sedimentary rocks: Sedimentology, v. 1, p. 145-157.

Vanoni, V. A., 1974, Factors determining bed forms of alluvial streams: Amer. Soc. Civil Engineers, Proc., v. 100, No. HY3, p. 363-377.

Visher, G. S., 1969, Grain size distributions and depositional processes: J. Sediment. Petrology, v. 39, p. 1074-1106.

Von Rad, U., 1970, Comparison between "magnetic" and sedimentary fabric in graded and cross-laminated sand layers, southern California: Geol. Rundsch., v. 60, p. 331-354.

_____, and Rösch, H., 1974, Petrography and diagenesis of deep-sea cherts from the central Atlantic: Spec. Publs int. Ass. Sediment., 1, p. 327-348.

Walker, R. G., 1965, The origin and significance of the internal sedimentary structures of turbidites: Yorkshire Geol. Soc., Proc., v. 35, p. 1-32.

_____, 1966, Shale Grit and Grindslow Shales: transition from turbidite to shallow water sediments in Upper Carboniferous of northern England: J. Sediment. Petrology, v. 36, p. 90-114.

_____, 1975a, Generalized facies models for resedimented conglomerates of turbidite association: Geol. Soc. Amer., Bull., v. 86, p. 737-748.

_____, 1975b, Nested submarine-fan channels in the Capistrano Formation, San Clemente, California: Geol. Soc. Amer., Bull., v. 86, p. 915-924.

_____, Facies models. 2, Turbidites and associated coarse clastic deposits: Geosci. Can., v. 3, p. 25-36.

Walker, R. G., 1977, Deposition of Upper Mesozoic resedimented conglomerates and associated turbidites in southwestern Oregon: Geol. Soc. Amer., Bull., v. 88, p. 273-285.

_____, in press, Deep-water sandstone facies and ancient submarine fans: models for exploration for stratigraphic traps: Amer. Ass. Petrol. Geol., Bull.

_____, and Mutti, E., 1973, Turbidite facies and facies associations: in, Middleton, G. V., and Bouma, A. H., eds, Turbidites and Deep-water Sedimentation, Pacific Section, Soc. Econ. Paleontol. Mineral., Short Course, Anaheim, p. 119-158.

Wanless, R. K., Stevens, R. D., Lachance, G. R., and Delabio, R. N., 1973, Age determinations and geological studies: K-Ar isotopic ages, Rept. 11: Geol. Surv. Can., Paper 73-2, 139 p.

Weber, J. N., and Middleton, G. V., 1961, Geochemistry of turbidities of the Normanskill and Charny Formations: Geochim. Cosmochim. Acta, v. 22, p. 200-288.

Wentworth, C. M., 1967, Dish structure, a primary sedimentary structure in turbidites (abst.): Amer. Ass. Petrol. Geol., Bull., v. 51, p. 485.

Weyl, P. K., 1959, Pressure solution and the force of crystallization - a phenomenological theory: J. Geophys. Res., v. 64, p. 2001-2025.

Weyl, R., and Werner, H., 1957, Schwermineraluntersuchungen im Jungtertiär und Altquartär Schleswig-Holsteins: III Internat. Congr. Sedimentology, Groningen-Wageningen, Proc., p. 293-303.

Whetten, J. T., 1966, Sediments from the lower Columbia River and the origin of graywacke: Science (AAAS), v. 152, p. 1057-1058.

_____, Kelley, J. C., and Hanson, L. G., 1969, Characteristics of Columbia River sediment and sediment transport: J. Sediment. Petrology, v. 39, p. 1149-1166.

Williams, H., 1971, Mafic-ultramafic complexes in western Newfoundland Appalachians and the evidence for their transportation: Geol. Ass. Can., Proc., v. 24, p. 9-25.

_____, 1975, Structural succession, nomenclature, and interpretation of transported rocks in western Newfoundland: Can. J. Earth Sci., v. 12, p. 1874-1894.

Williams, H., 1977, Ophiolitic mélange and its significance in the Fleur de Lys Supergroup, northern Appalachians: Can. J. Earth Sci., v. 14, p. 987-1003.

_____, Hibbard, J. P., and Bursnall, J. T., 1977, Geological setting of asbestos-bearing ultramafic rocks along the Baie Verte lineament, Newfoundland: Rept. of Activities, Geol. Surv. Can., Paper 77-1A, p. 351-360.

_____, Kennedy, M. J., and Neale, E. R. W., 1972, The Appalachian Structural Province: in, Price, R. A., and Douglas, R. J. W., eds, Variations in Tectonic Styles in Canada, Geol. Ass. Can., Spec. Pap. 11, p. 181-261.

_____, and Smyth, W. R., 1973, Metamorphic aureoles beneath ophiolite suites and Alpine peridotites: tectonic implications with west Newfoundland examples: Amer. J. Sci., v. 273, p. 594-621.

_____, and Stevens, R. K., 1974, The ancient continental margin of eastern North America: in, Burk, C. A., and Drake, C. L., eds, The Geology of Continental Margins, Springer-Verlag, New York, p. 781-796.

Wilson, J. L., 1975, Carbonate Facies in Geologic History: Springer-Verlag, New York, 471 p.

Winkler, H. G. F., 1967, Petrogenesis of Metamorphic Rocks, 2nd edition: Springer-Verlag, New York, 237 p.

Wood, A., and Smith, A. J., 1959, The sedimentation and sedimentary history of the Aberystwyth Grits (Upper Llandoverian): Geol. Soc. London, Quart. J., v. 114, p. 163-195.

Yalin, M. S., Mechanics of Sediment Transport, 2nd edition: Pergamon Press, Oxford, 298 p.

Zen, E-an, 1968, Nature of the Ordovician orogeny in the Taconic area: in, Zen, E-an, and others, eds, Studies of Appalachian Geology: northern and maritime, Wiley Interscience, New York, p. 129-140.

APPENDIX I

Area Composite Sections and Outcrop Maps

APPENDIX I

AREA COMPOSITE SECTIONS AND OUTCROP MAPS

Each area is represented by a composite section constructed as outlined in Table AI.1. The legend for section drawings is presented before the composite sections. Thinning upward (+) and thickening upward (-) megasequences are indicated alongside the section drawings. These asymmetric cycles are discussed in Chapter III.

Following the composite sections are outcrop maps for most areas. The legend for these maps appears on the map for area A.

Table AI.1

Key to composite section construction

Composite section	Individual section segments (references in metres)
A	AI
B	BI
C	CIII, CIV(46.0 to 49.8, CV, CVI(1.6 to 52.8), CVII/CVIII
D	DII(to 191.9), DIII(12.6 to top)/DI
E	EI(to 126.2), EII(14.7 to top)
F	FI(to 51.8), FIII(18.4 to top)/FIV
G	GI
H	HI
J	JI(58.1 to 205.3), JII(88.1 to 105.2), JIII(41.8 to top)
K	KVI, KV(to 30.6), KIV (to 30.0), KIII(33.3 to 106.9), KII(30.6 to top), KI(34.2 to top)
L	LIII(to 30.8), LVII(to 3.2), KVIII(to 3.8), LXI(38.8 to 60.5), LXII(15.1 to 25.7), LXIII(0.3 to top)
M	MII, MIb(21.0 to 29.1)/MIV(to 33.5), MV(26.7 to top)

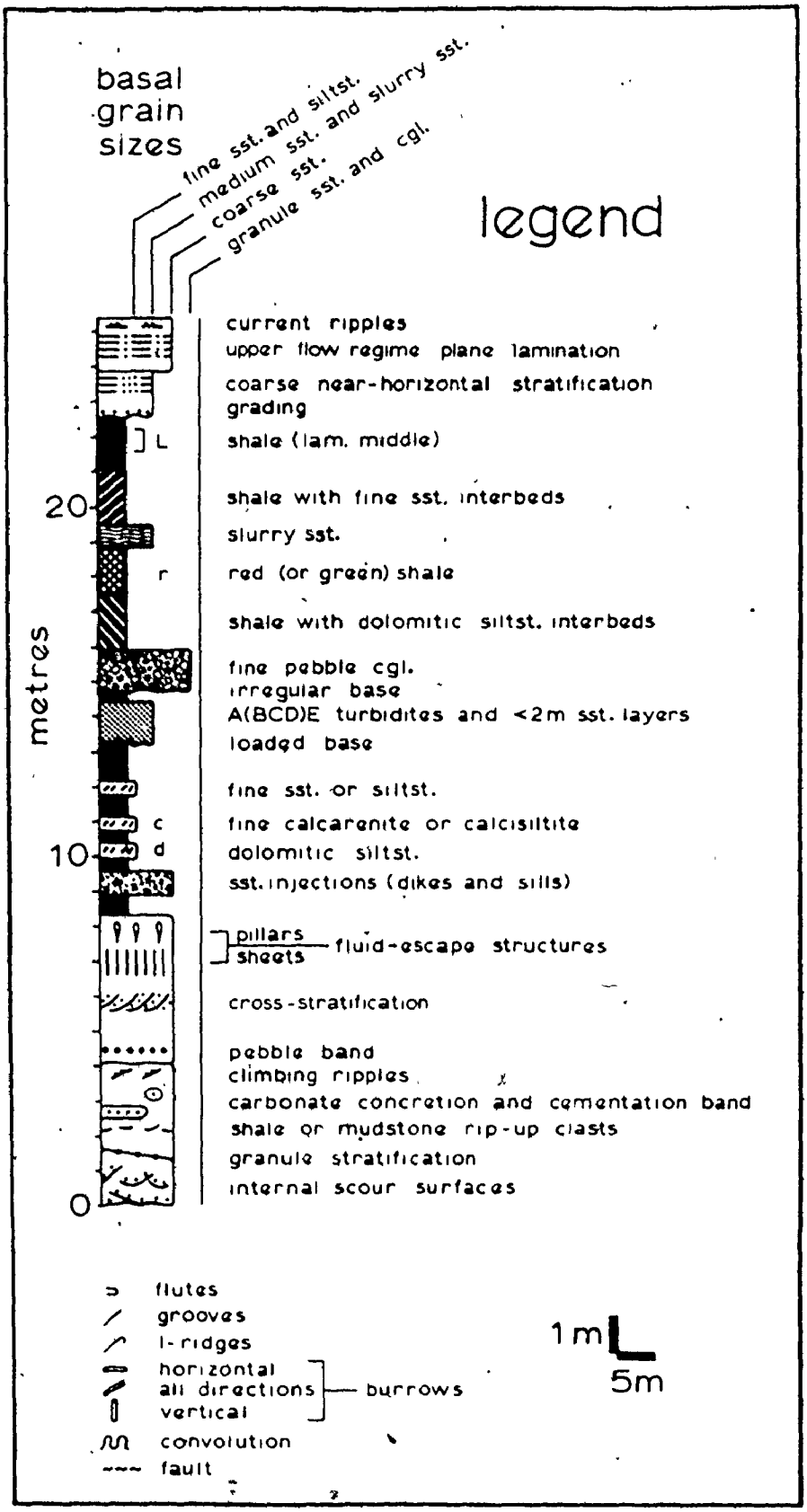
basal grain sizes
fine sst. and siltst.
medium sst. and slurry sst.
coarse sst.
granule sst. and cgl.
legend
current ripples
upper flow regime plane lamination
coarse near-horizontal stratification
grading
L
shale (lam. middle)
shale with fine sst. interbeds
slurry sst.
r
red (or green) shale
shale with dolomitic siltst. interbeds
fine pebble cgl.
irregular base
A(BCD)E turbidites and <2m sst. layers
loaded base
fine sst. or siltst.
c
fine calcarenite or calcisiltite
d
dolomitic siltst.
sst. injections (dikes and sills)
pillars
sheets
fluid-escape structures
cross-stratification
pebble band
climbing ripples
carbonate concretion and cementation band
shale or mudstone rip-up clasts
granule stratification
internal scour surfaces
metres
20
10
0
flutes
grooves
I-ridges
horizontal
all directions
vertical
burrows
convolution
fault
1m
5m

Area A

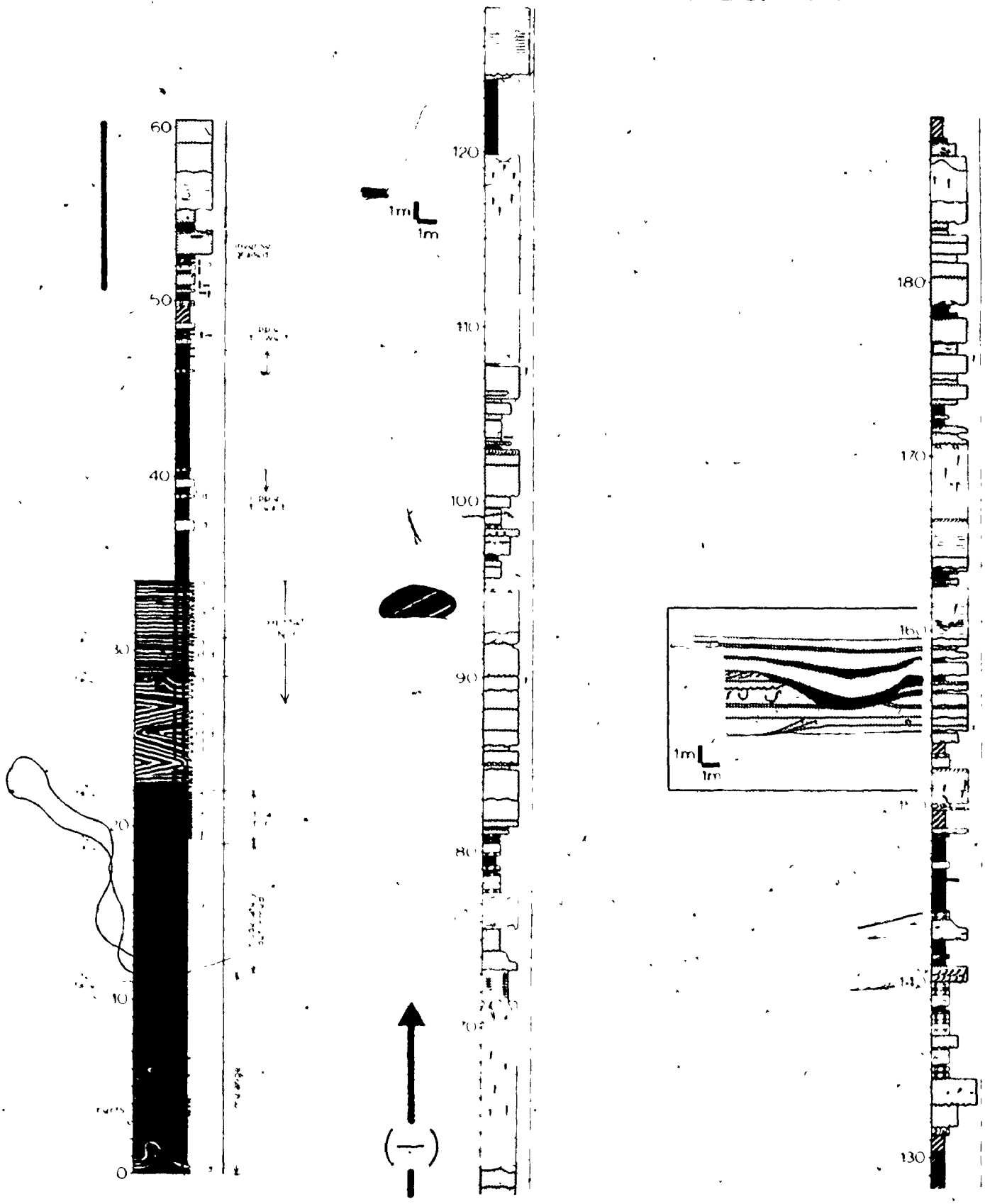
60
50
40
30
20
10
0
120
110
100
90
80
70
180
170
160
150
140
130
1m
1m
1m
1m

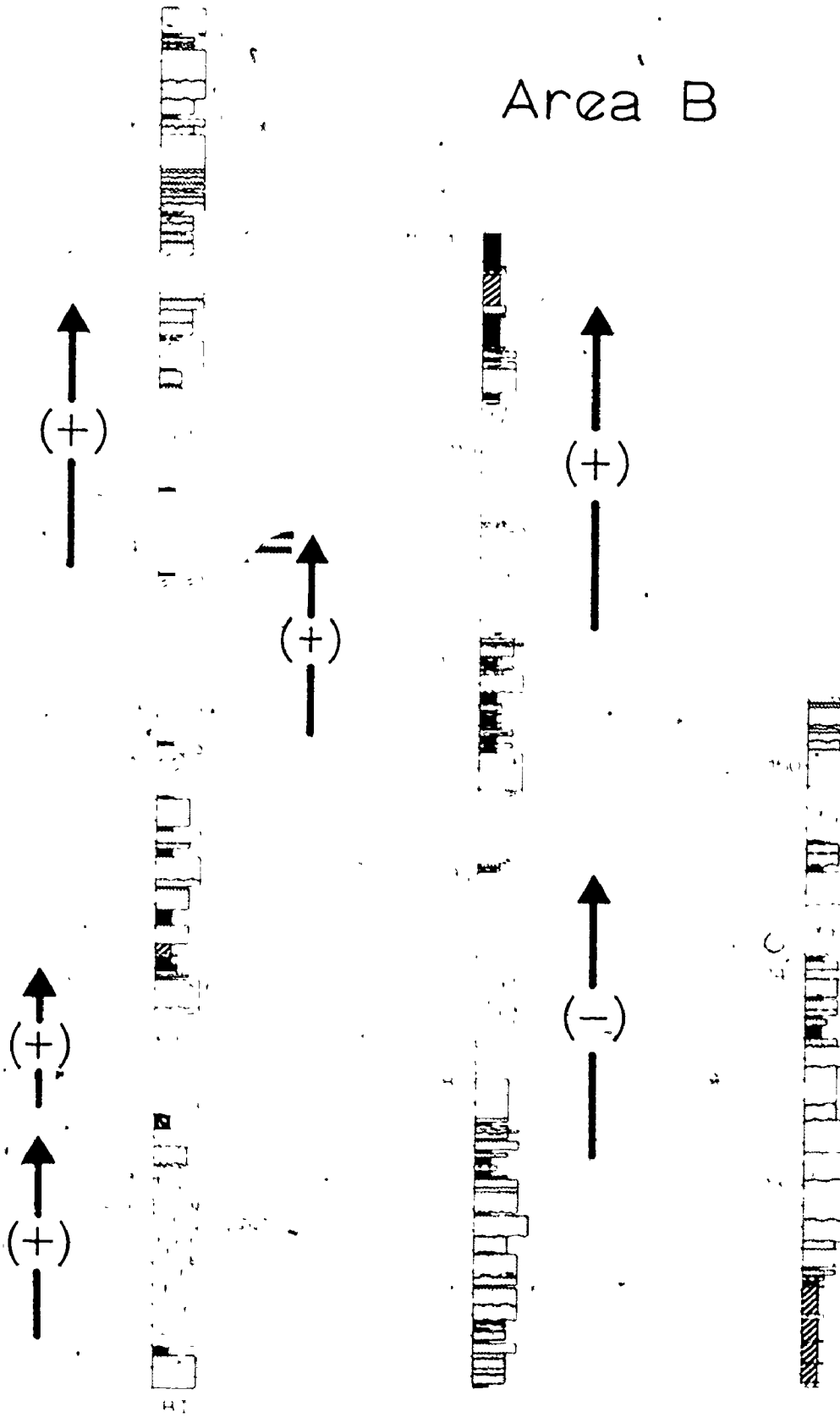
Area B
(+)
(+)
(+)
(+)
(+)
(−)

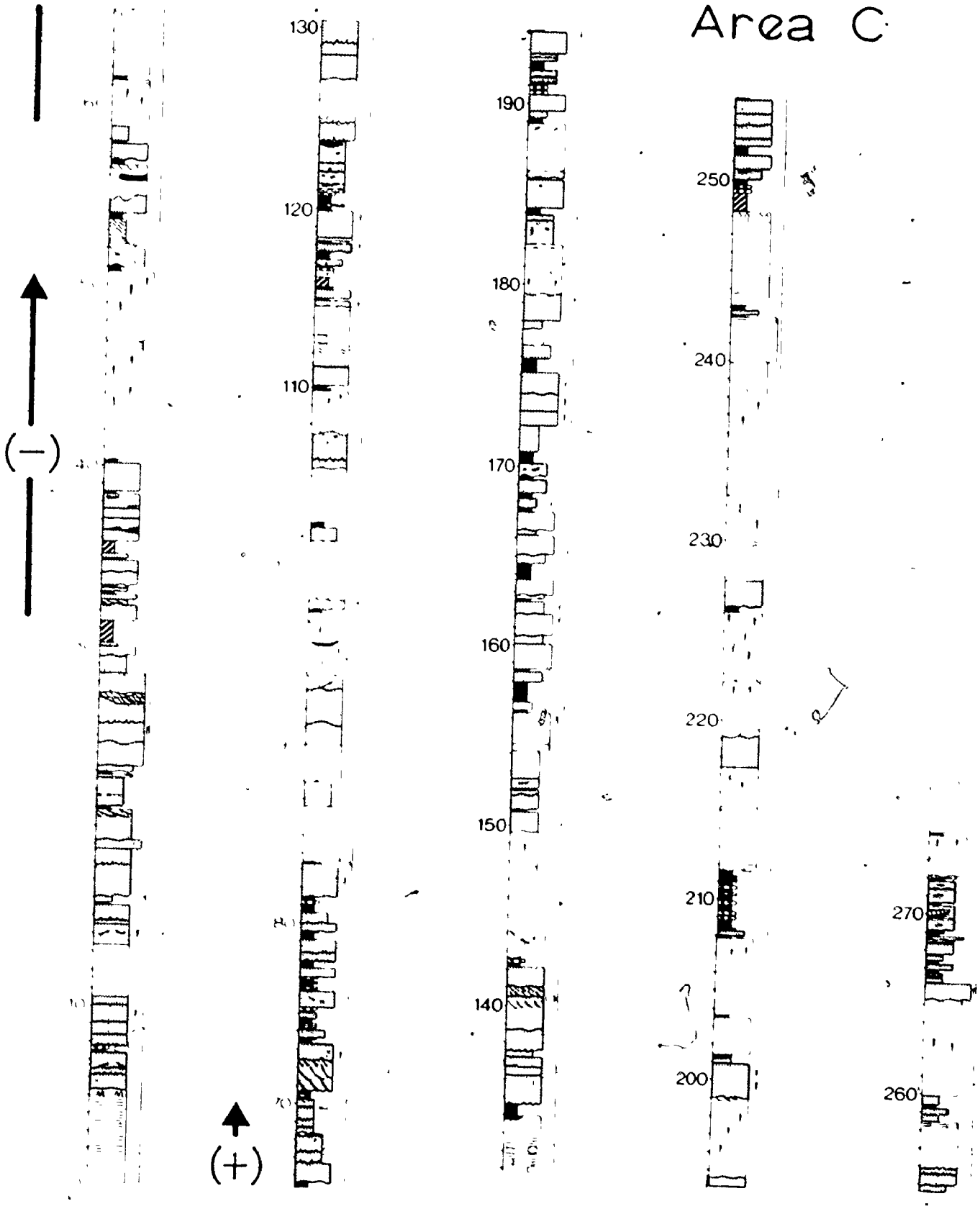
Area C
130
120
110
190
180
170
160
150
140
250
240
230
220
210
200
270
260
(−)
(+)

Area C(VIII)

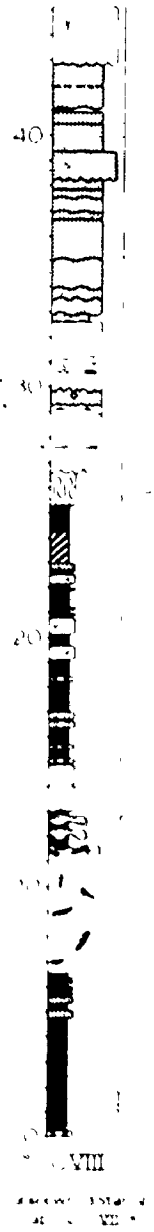

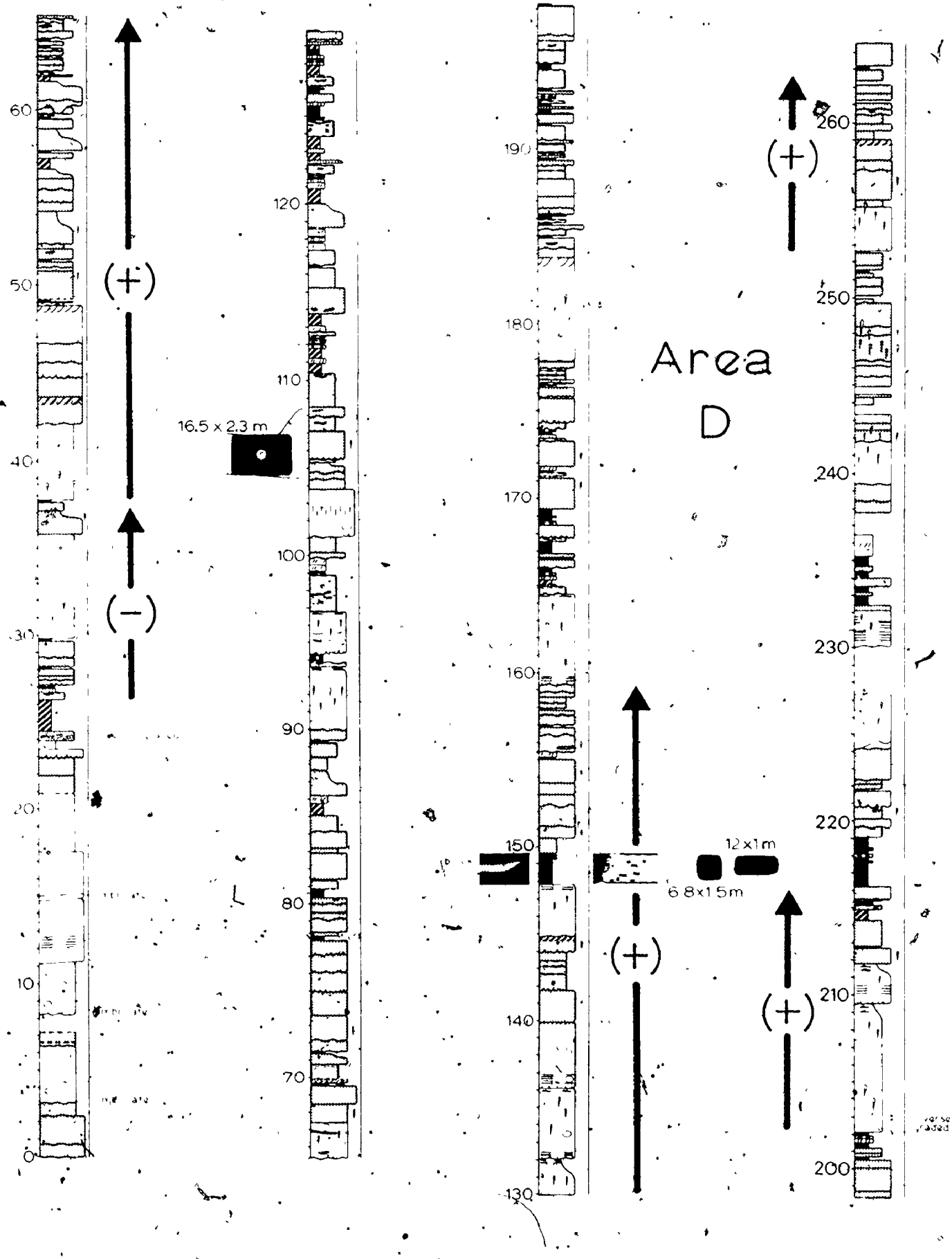
Area
D
16.5 x 2.3 m
12x1m
6.8x1.5m
(+)
(−)
0
10
20
30
40
50
60
70
80
90
100
110
120
130
140
150
160
170
180
190
200
210
220
230
240
250
260

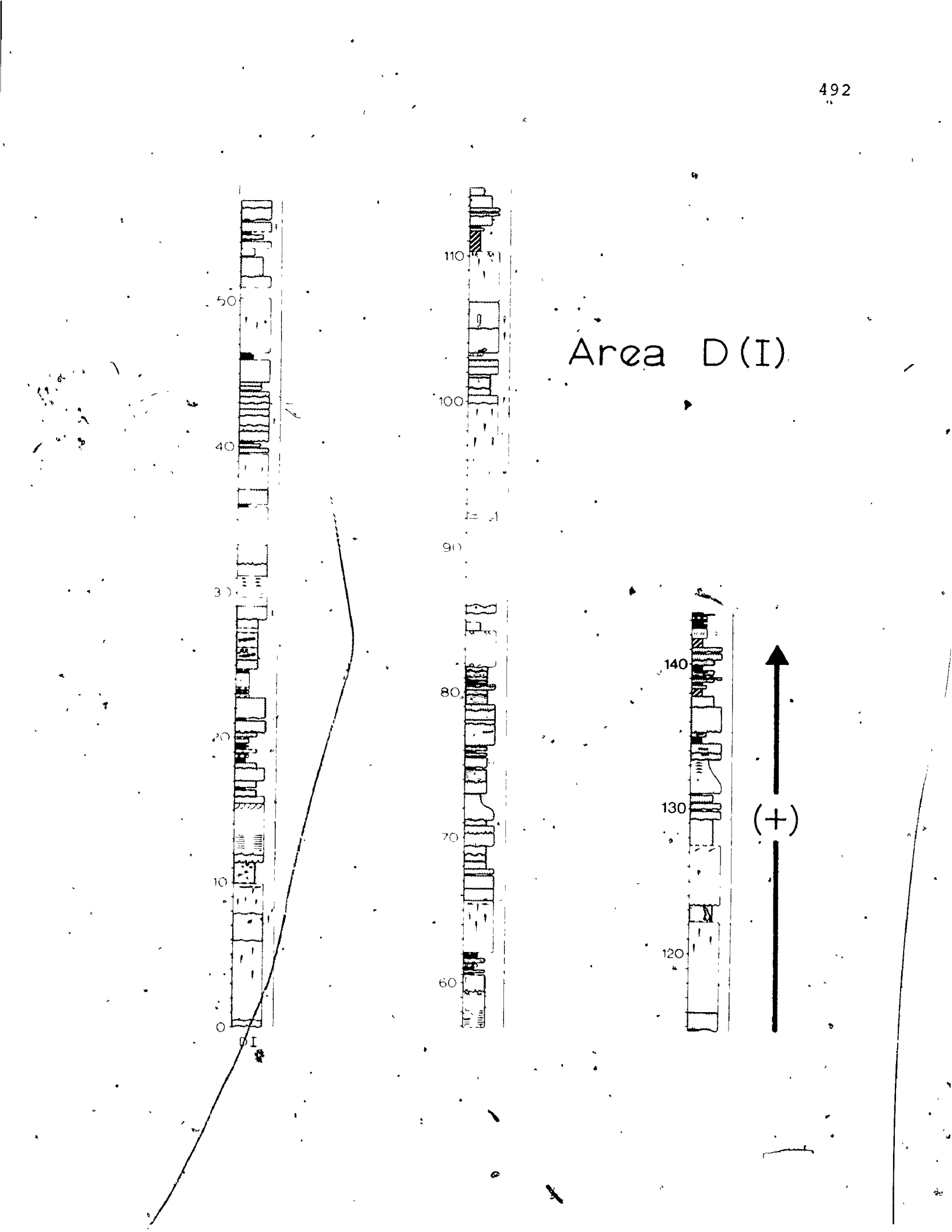
Area D(I)
0
10
20
30
40
50
60
70
80
90
100
110
120
130
140
(+)

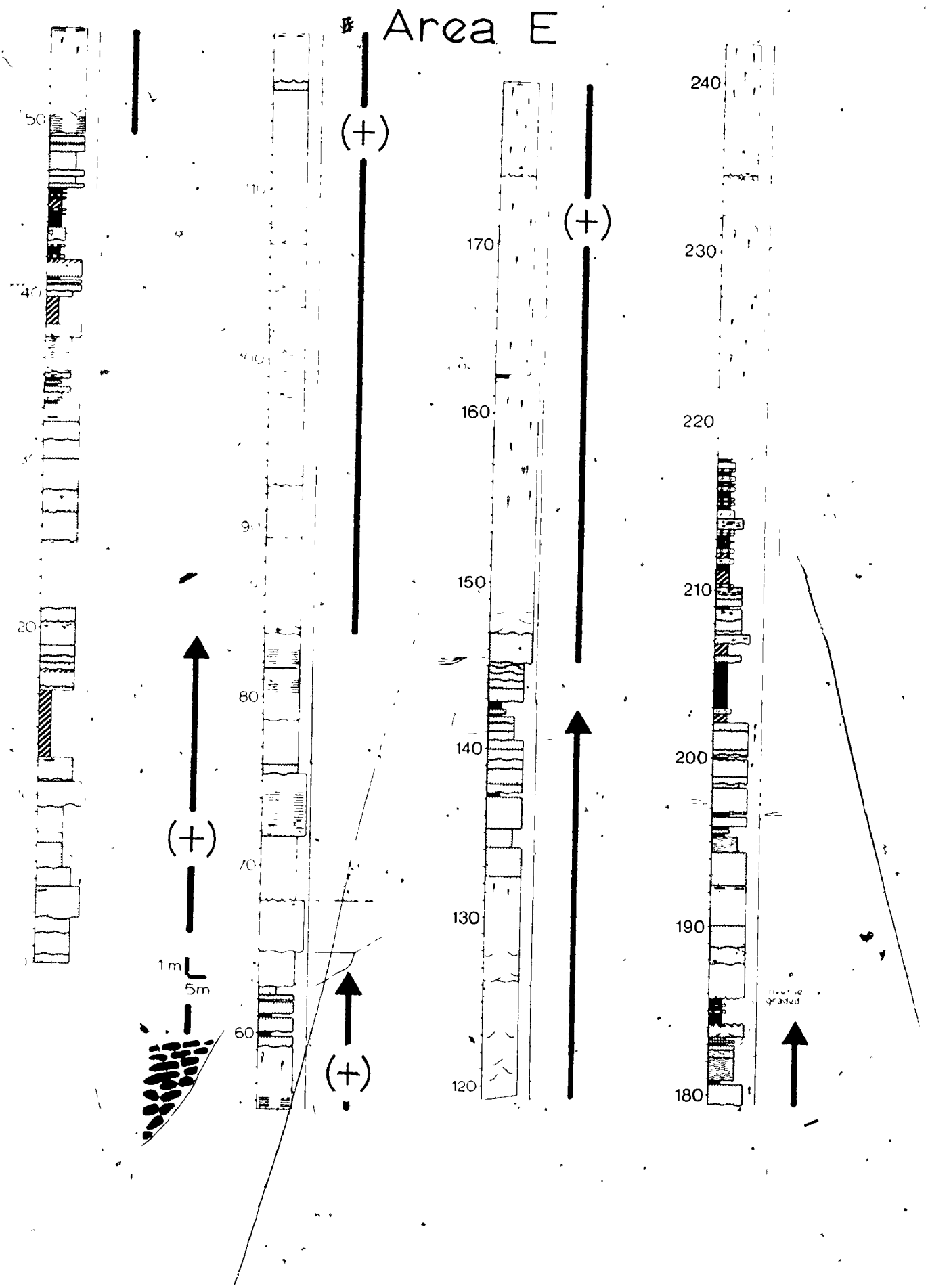
Area E
(+)
(+)
(+)
(+)
50
40
20
110
100
90
80
70
60
170
160
150
140
130
120
240
230
220
210
200
190
180
1m
5m

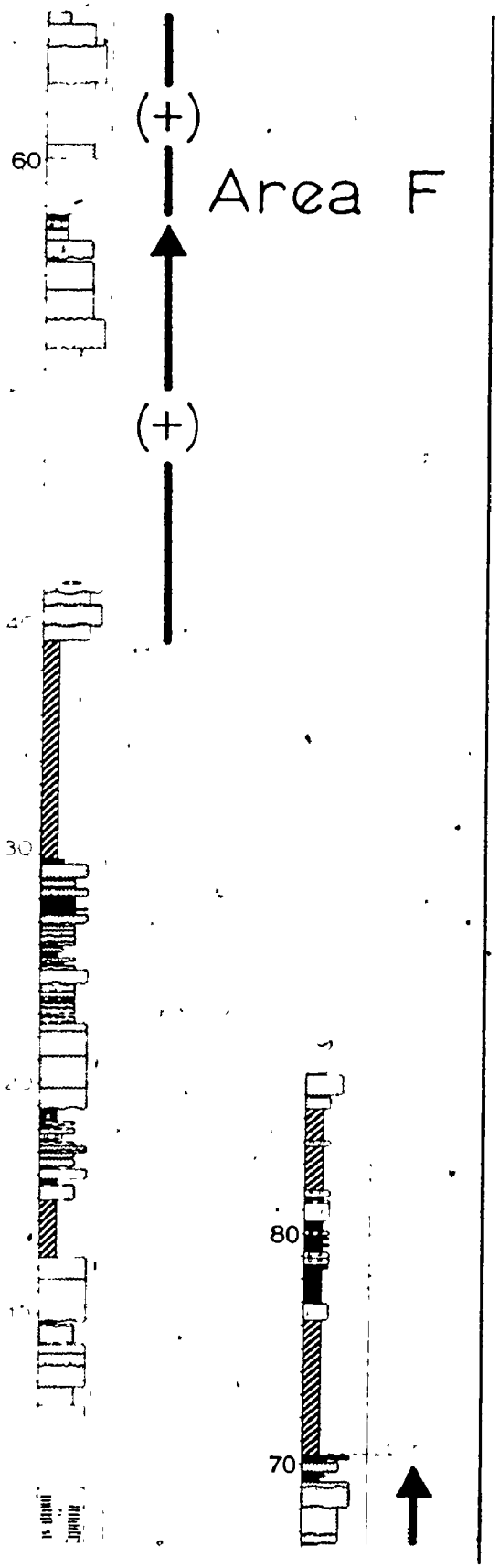
(+)
Area F
(+)
60
40
30
80
70

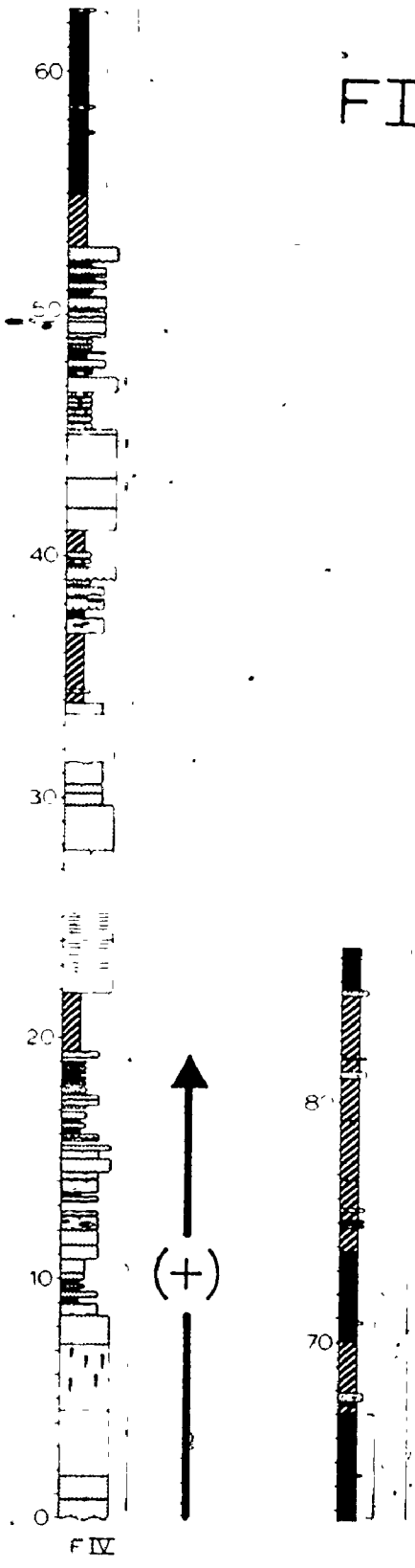
FIV
60
50
40
30
20
10
0
(+)
80
70
FIV

Area G

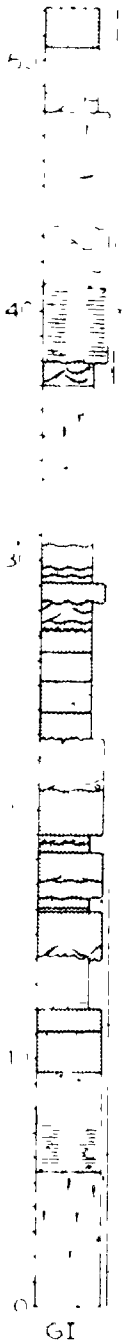

Area H

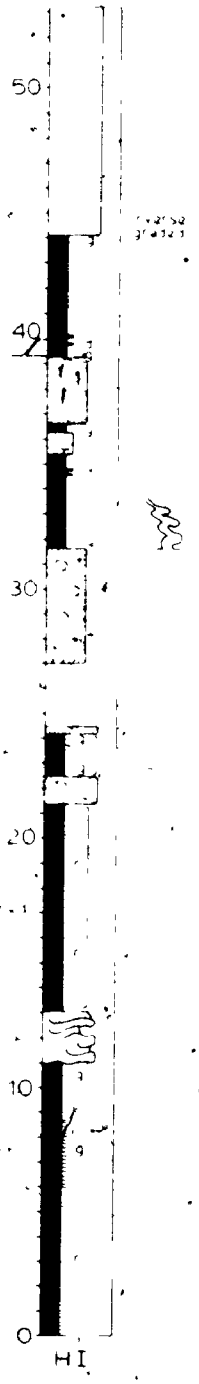

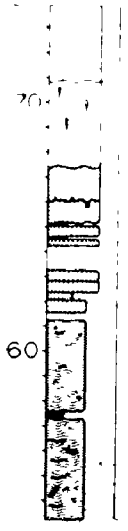

Area J

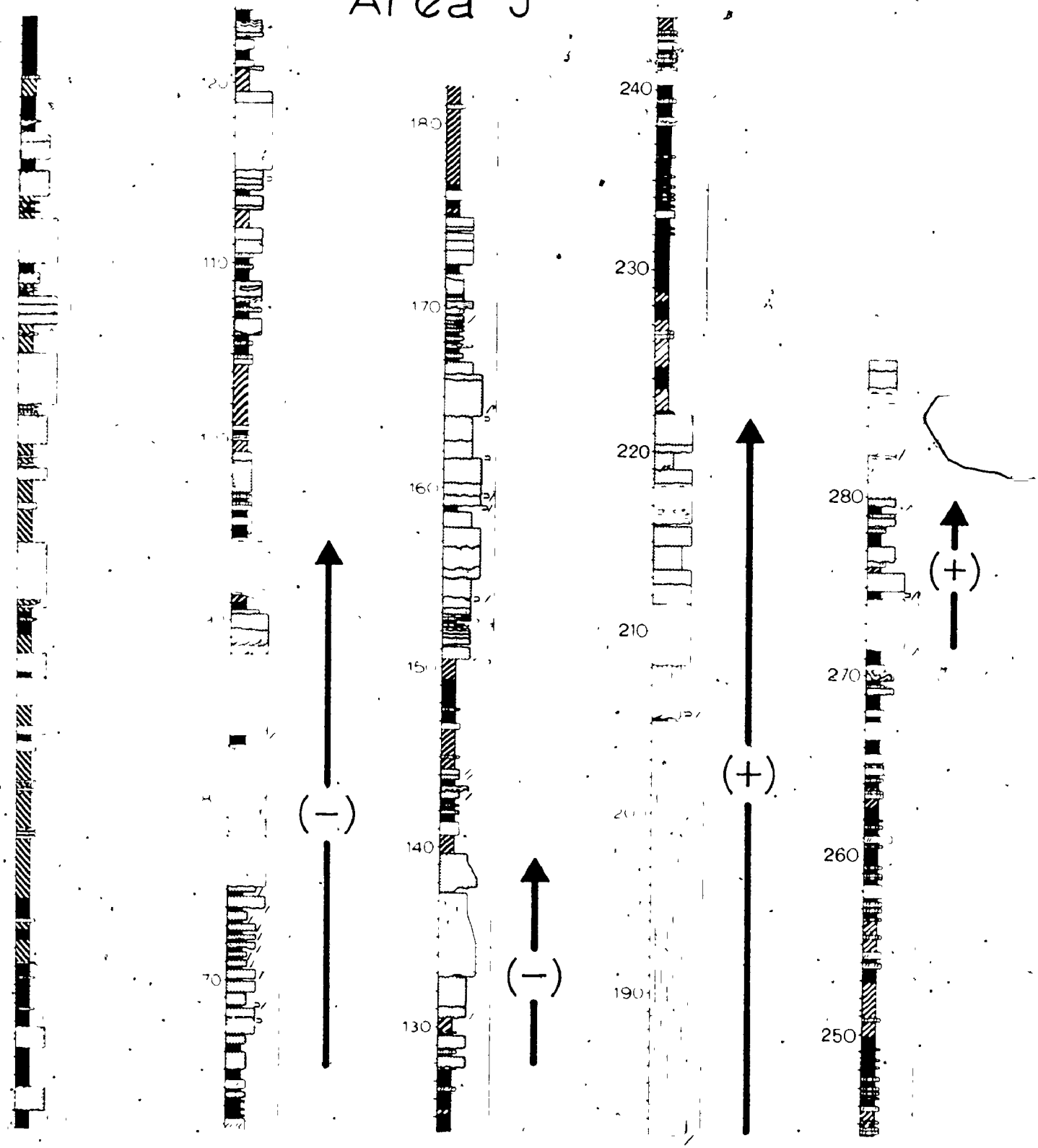
110
70
180
170
160
150
140
130
240
230
220
210
190
280
270
260
250
(−)
(−)
(+)
(+)

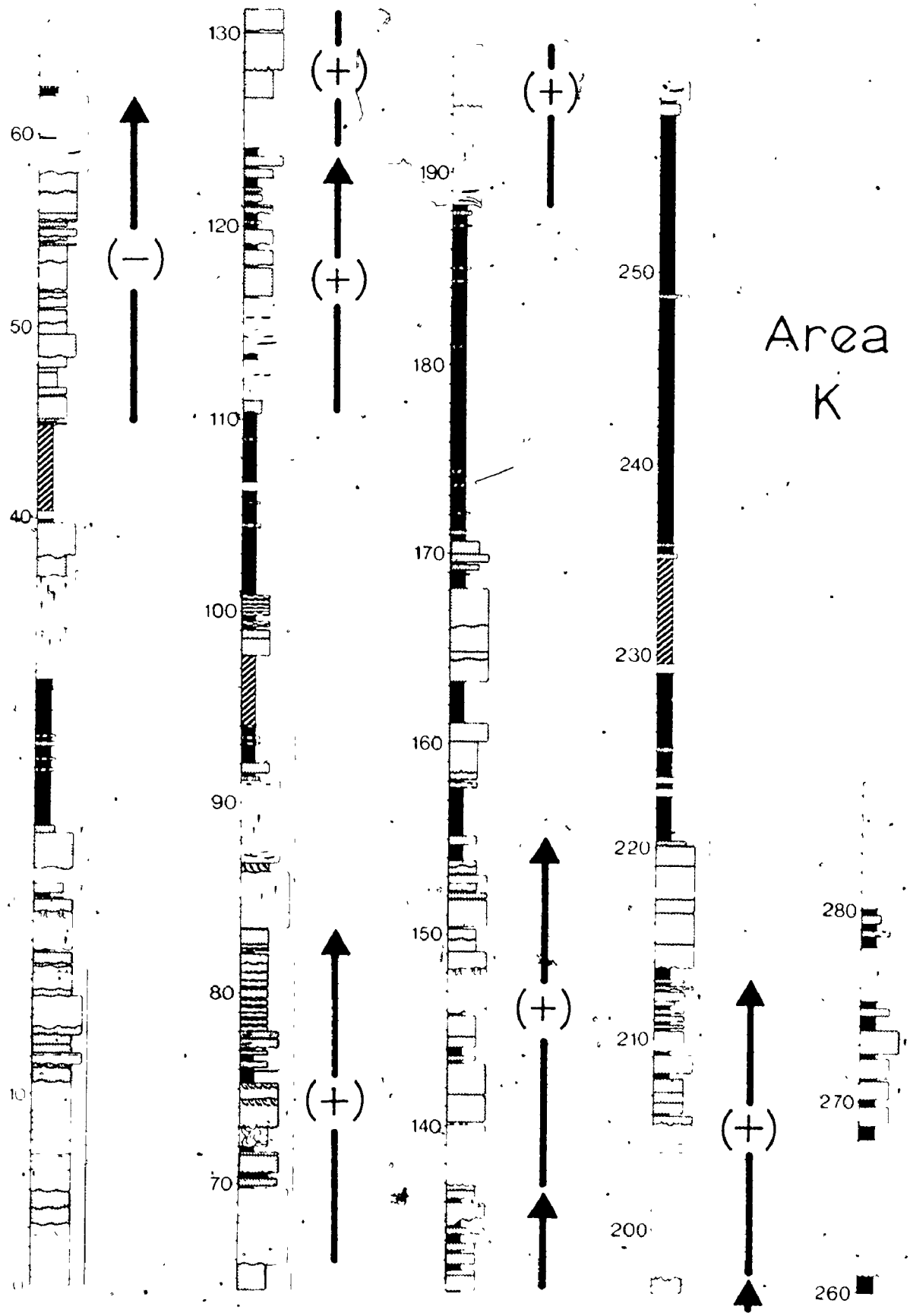
Area
K
(−)
(+)
(+)
(+)
(+)
(+)
(+)
60
50
40
10
130
120
110
100
90
80
70
190
180
170
160
150
140
250
240
230
220
210
200
280
270
260

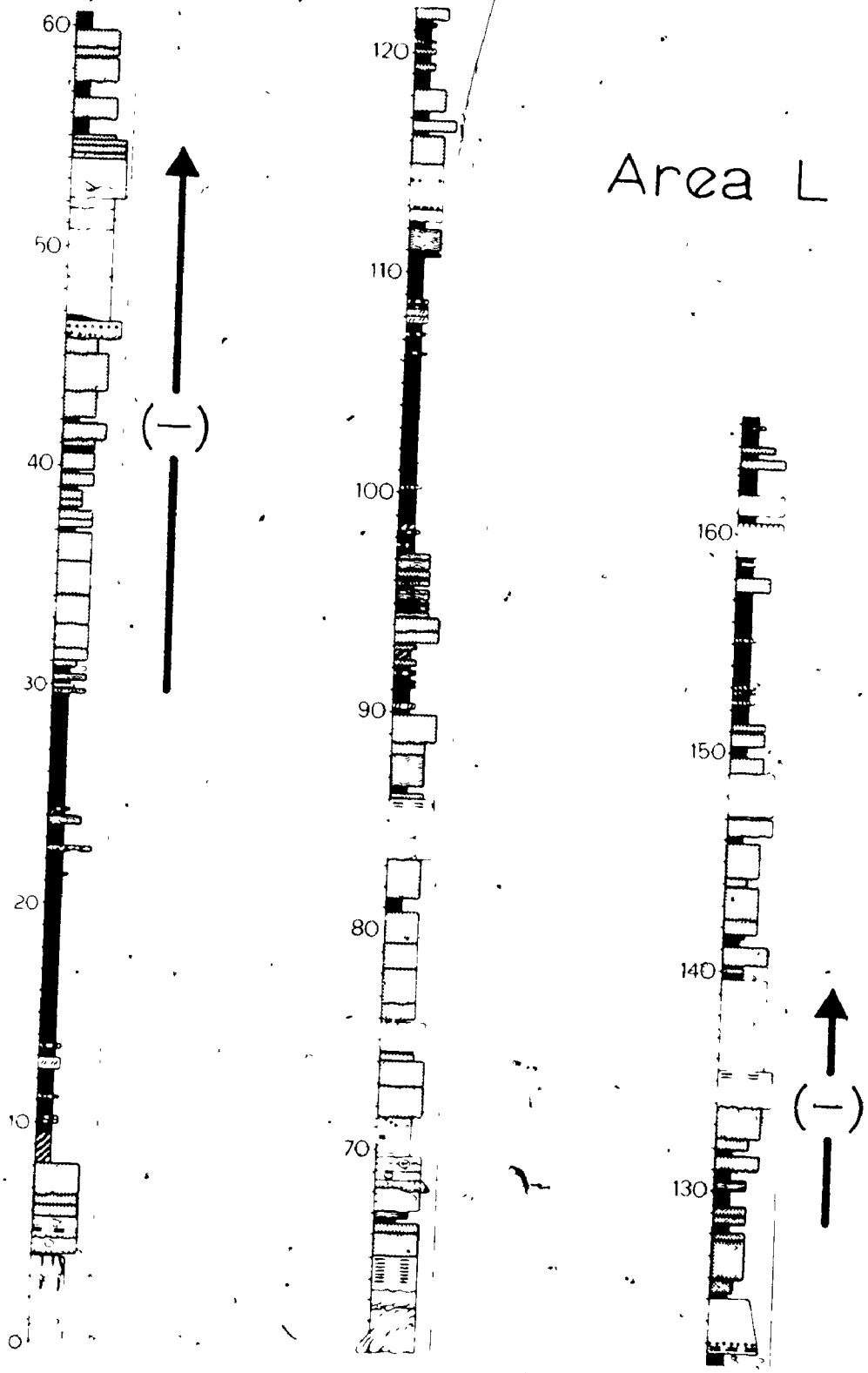
Area L
60
50
40
30
20
10
0
120
110
100
90
80
70
160
150
140
130
(—)
(—)

Area M (west)

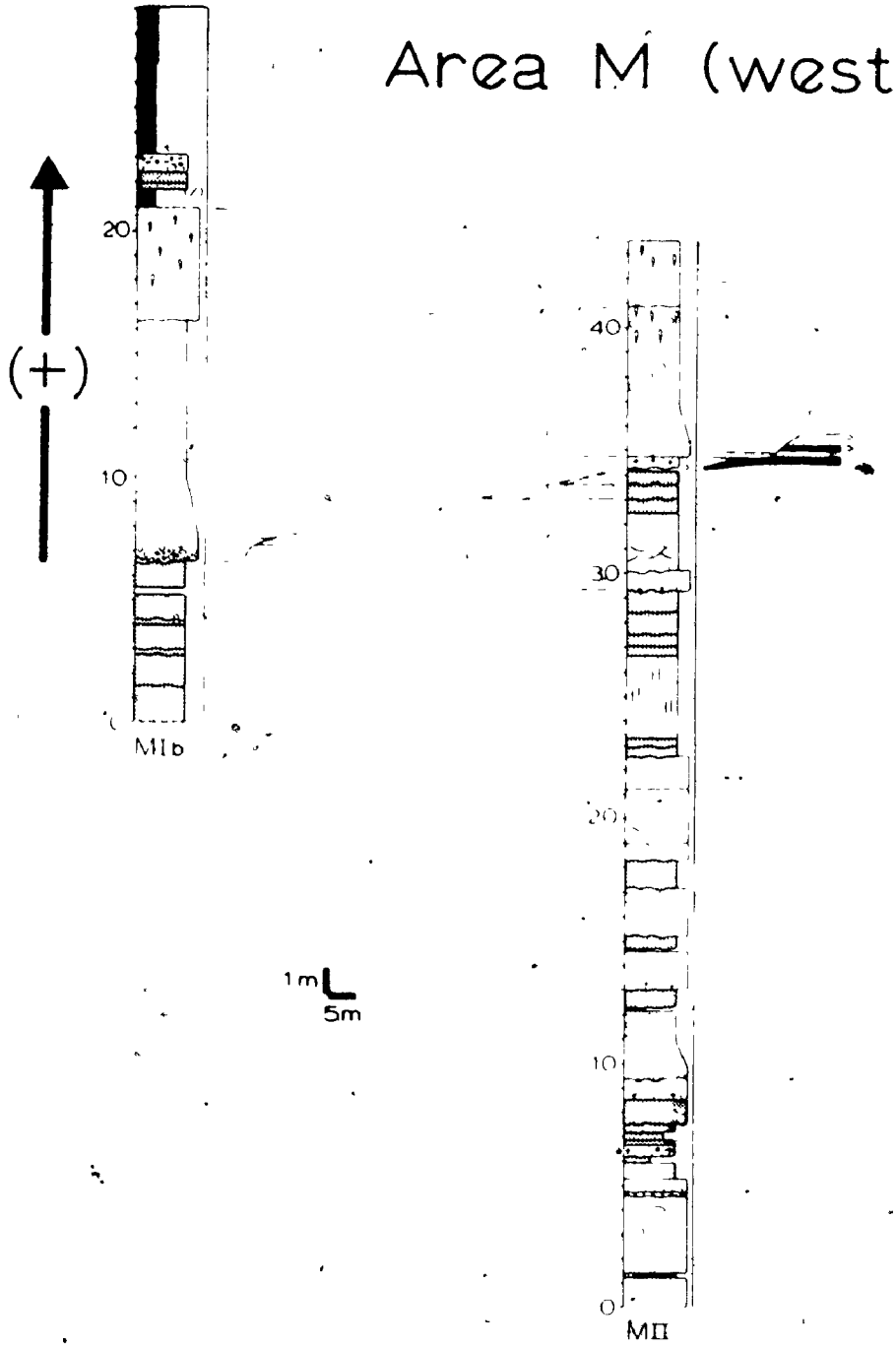

Area M (east)

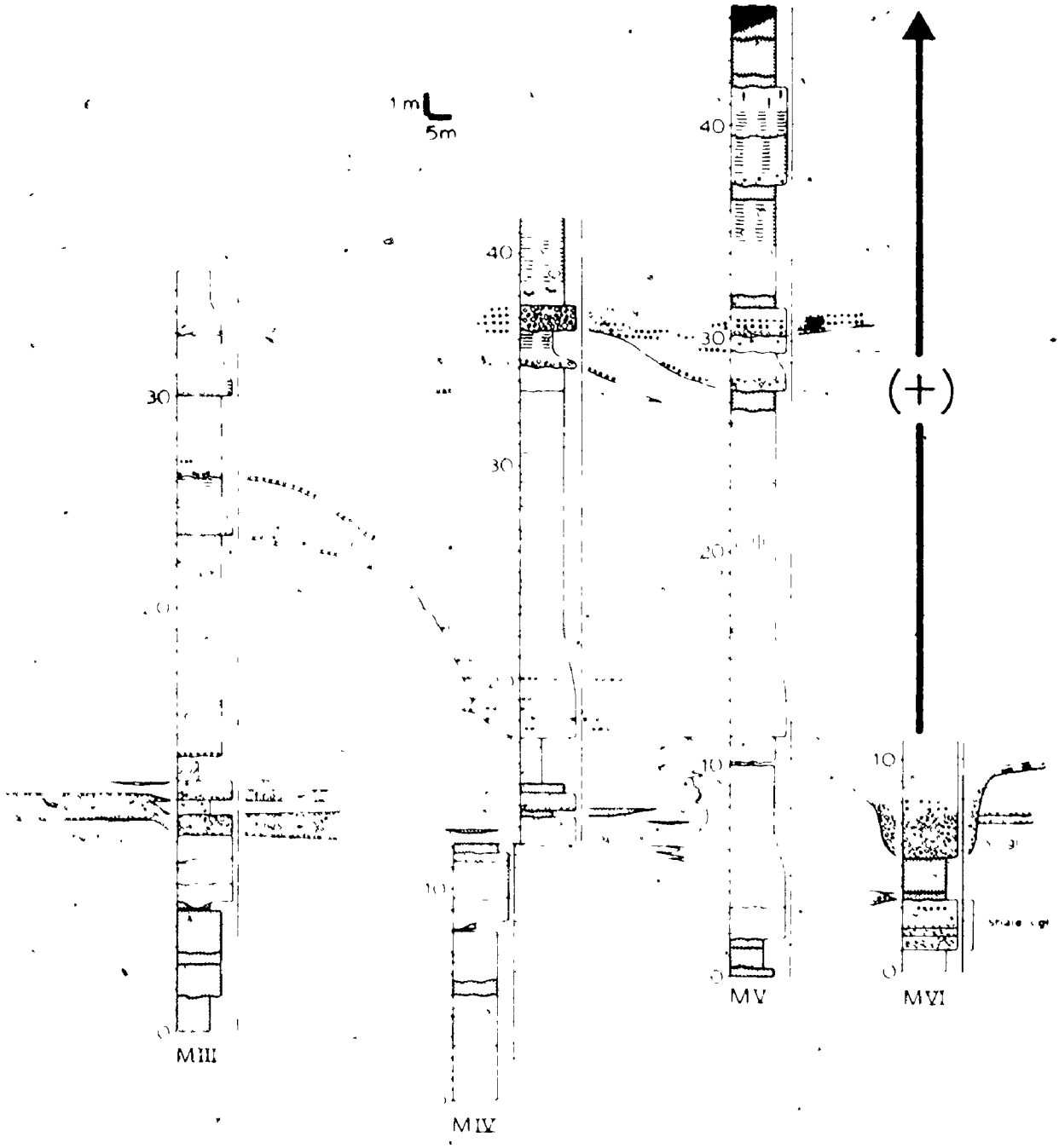

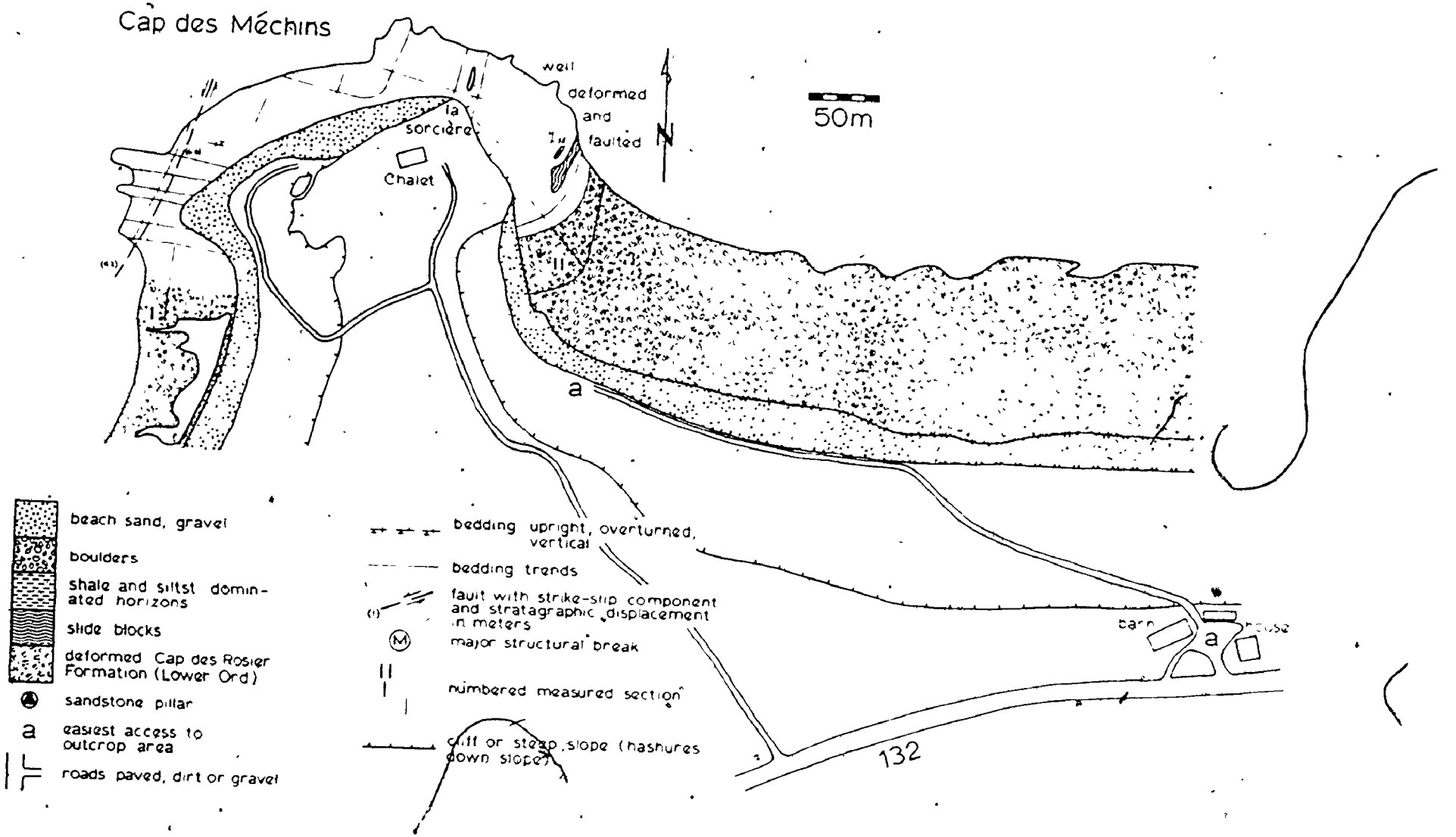
Cap des Méchins
well deformed and faulted
la sorcière
Chalet
50m
N
a
barn
house
132
beach sand, gravel
boulders
shale and siltst dominated horizons
slide blocks
deformed Cap des Rosier Formation (Lower Ord)
sandstone pillar
easiest access to outcrop area
roads paved, dirt or gravel
bedding upright, overturned, vertical
bedding trends
fault with strike-slip component and stratagraphic displacement in meters
major structural break
numbered measured section
cliff or steep slope (hashures down slope)

Area A

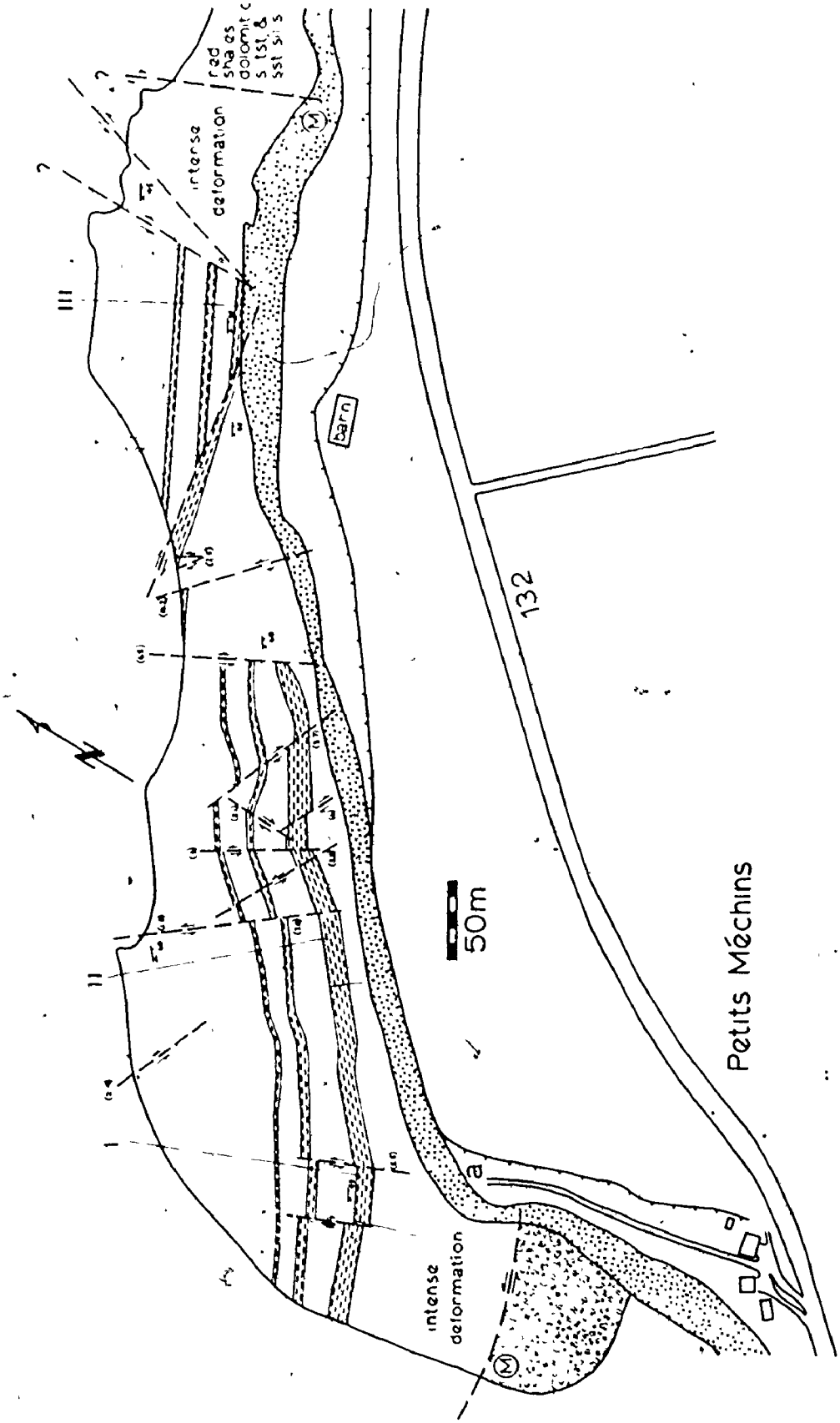
red shales dolomitic s tst & sst s/s
intense deformation
barn
132
50m
Petits Méchins
intense deformation

Area B

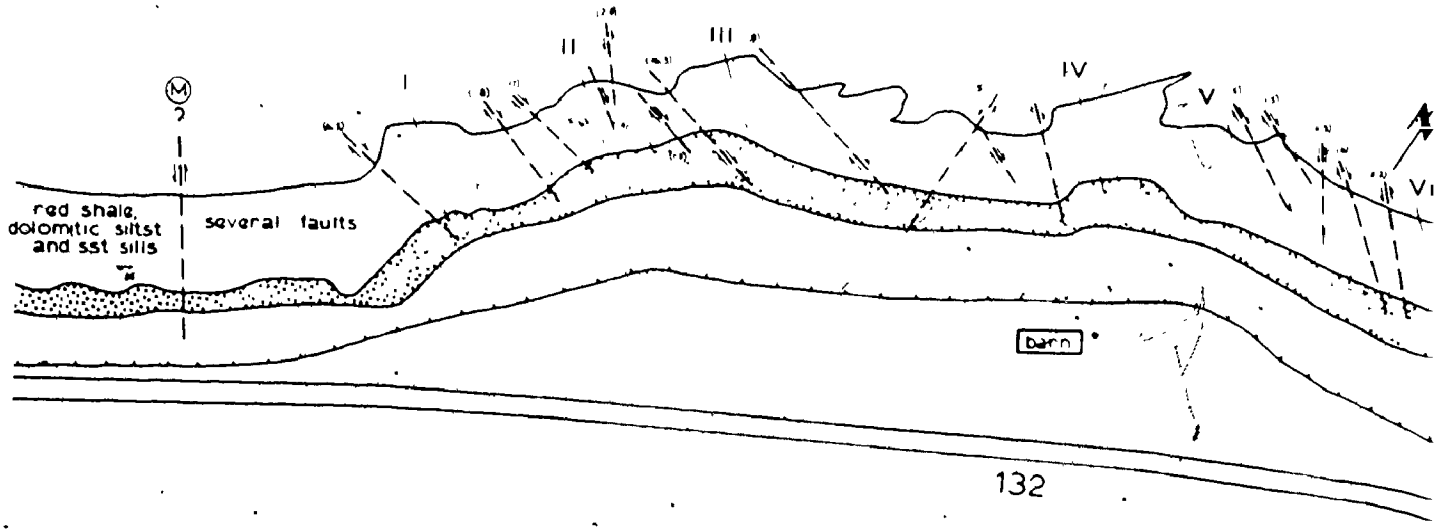
M
?
I
II
III
IV
V
VI
red shale, dolomitic siltst and sst sills
several faults
barn
132

Area C

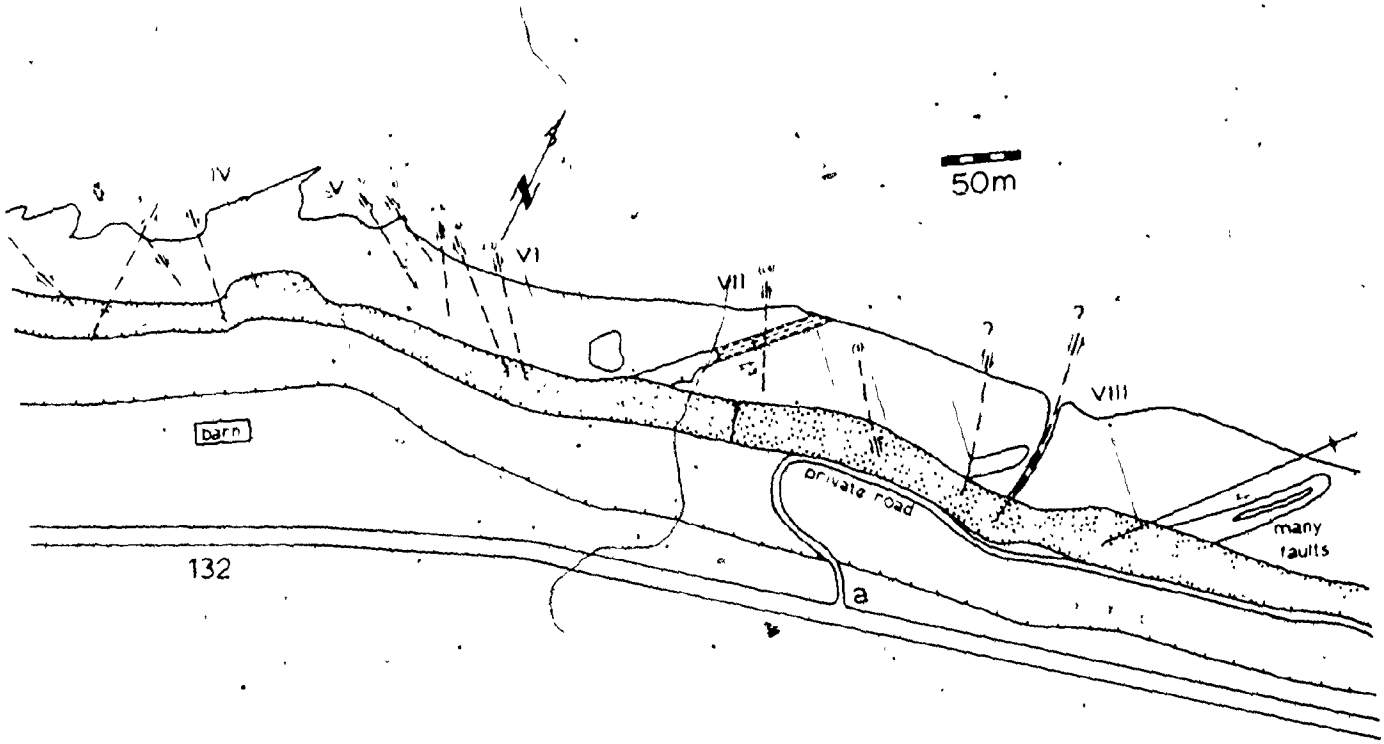
50m
IV
V
VI
VII
VIII
barn
private road
many faults
132
a

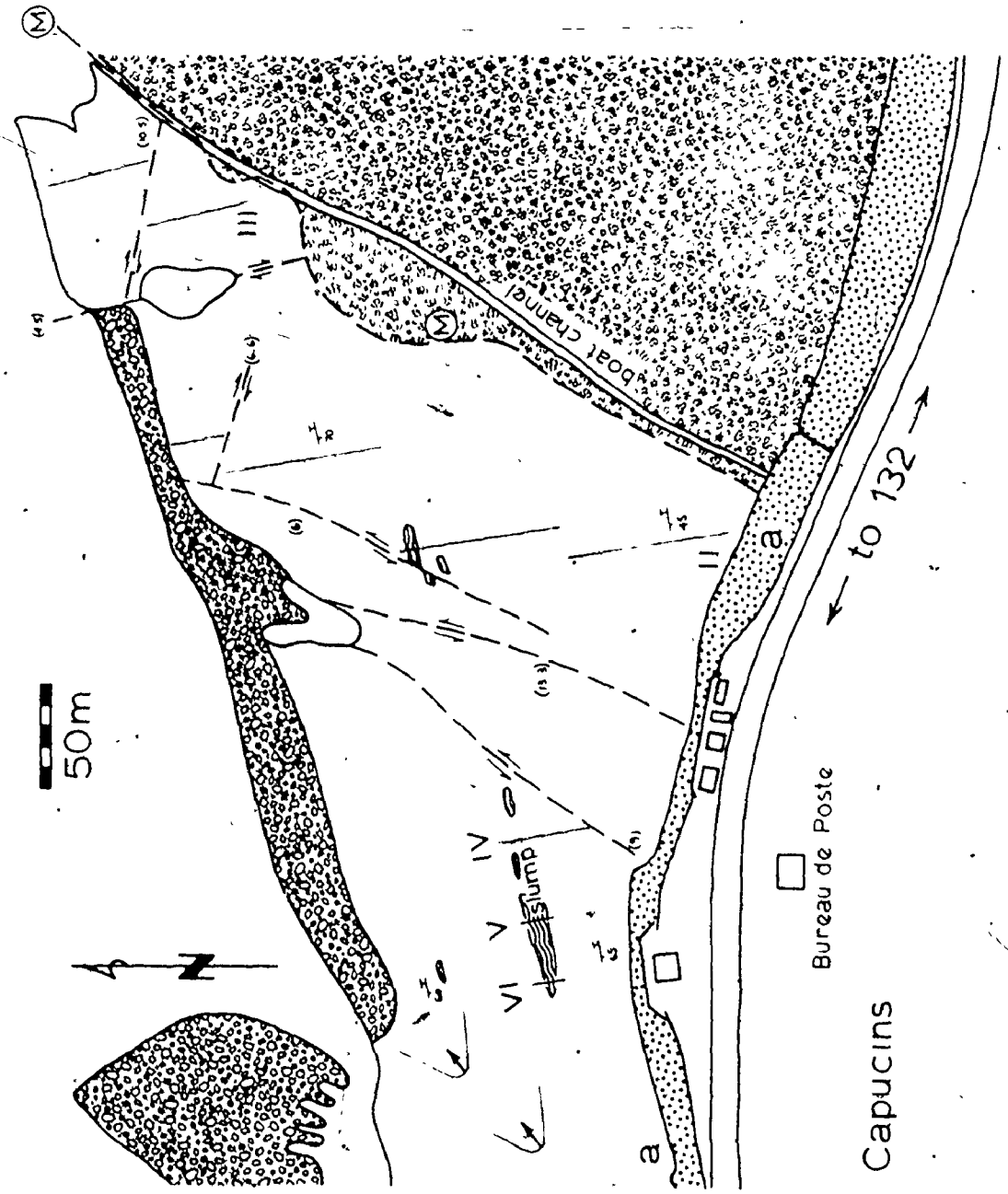
boat channel
50m
Slump
Bureau de Poste
Capucins
to 132
a
a
IV
V
VI

Area D

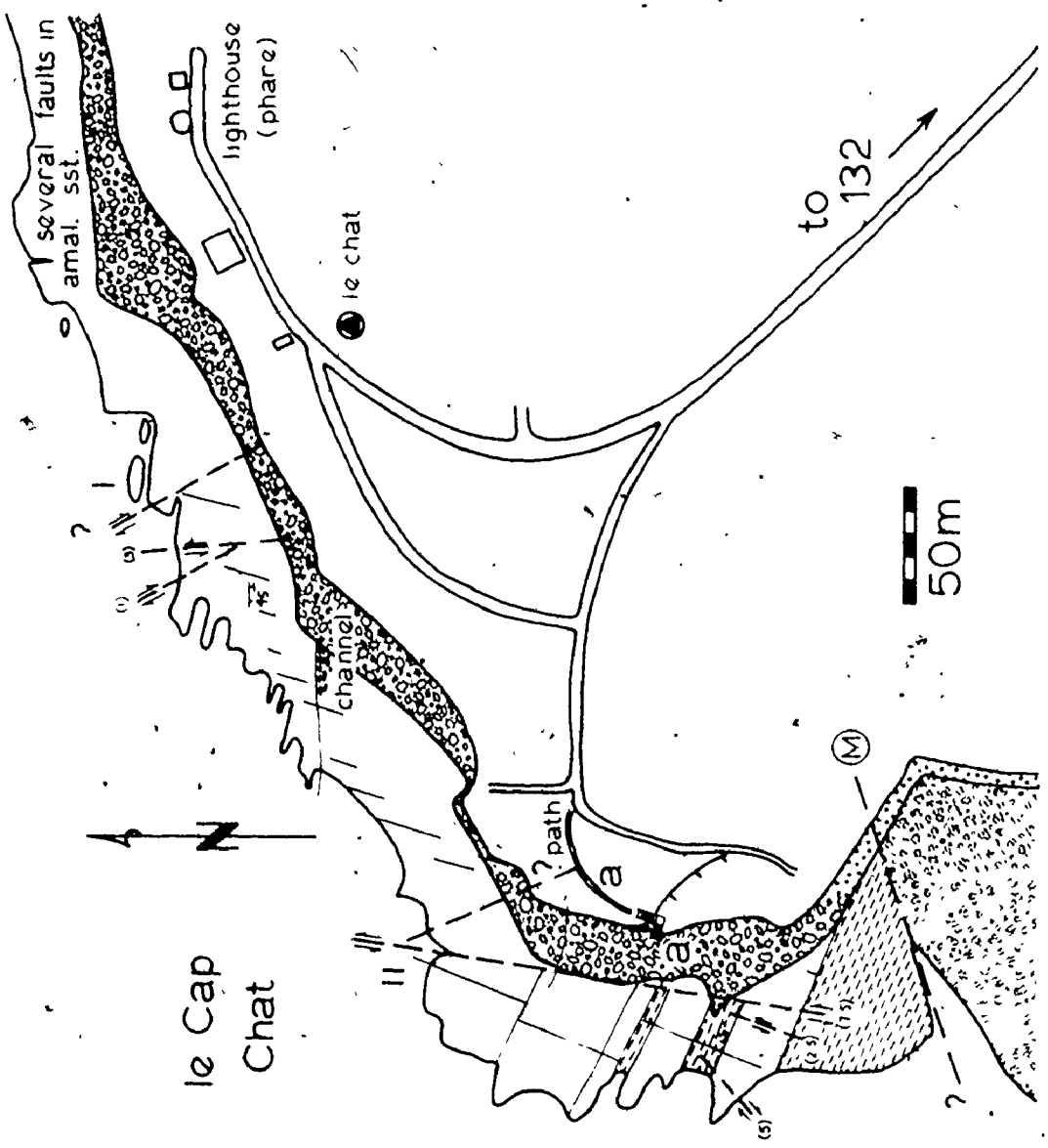
several faults in amal. sst.
lighthouse (phare)
le chat
to 132
channel
? path
a
a
M
50m
le Cap Chat

Area E

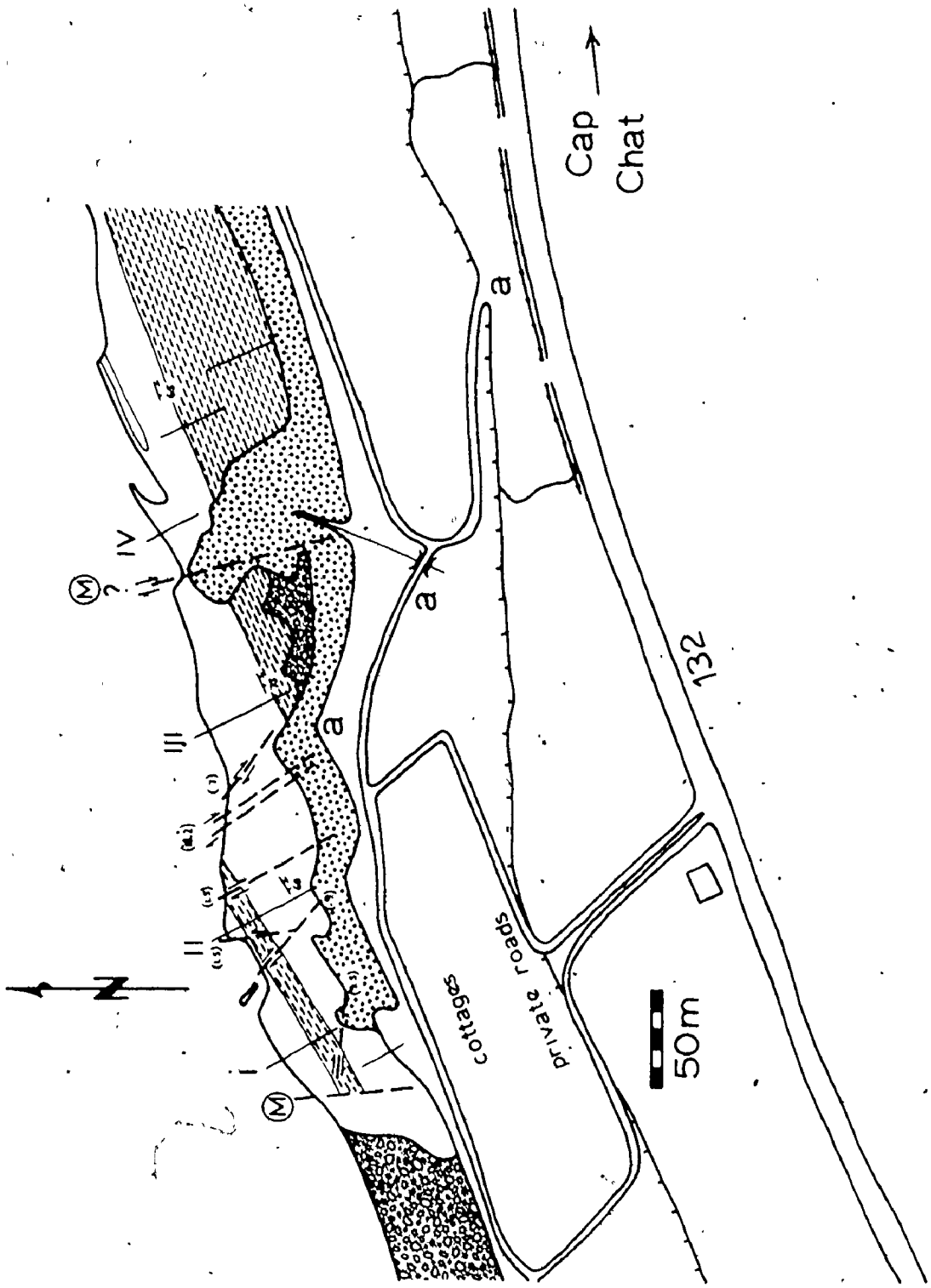

Area F

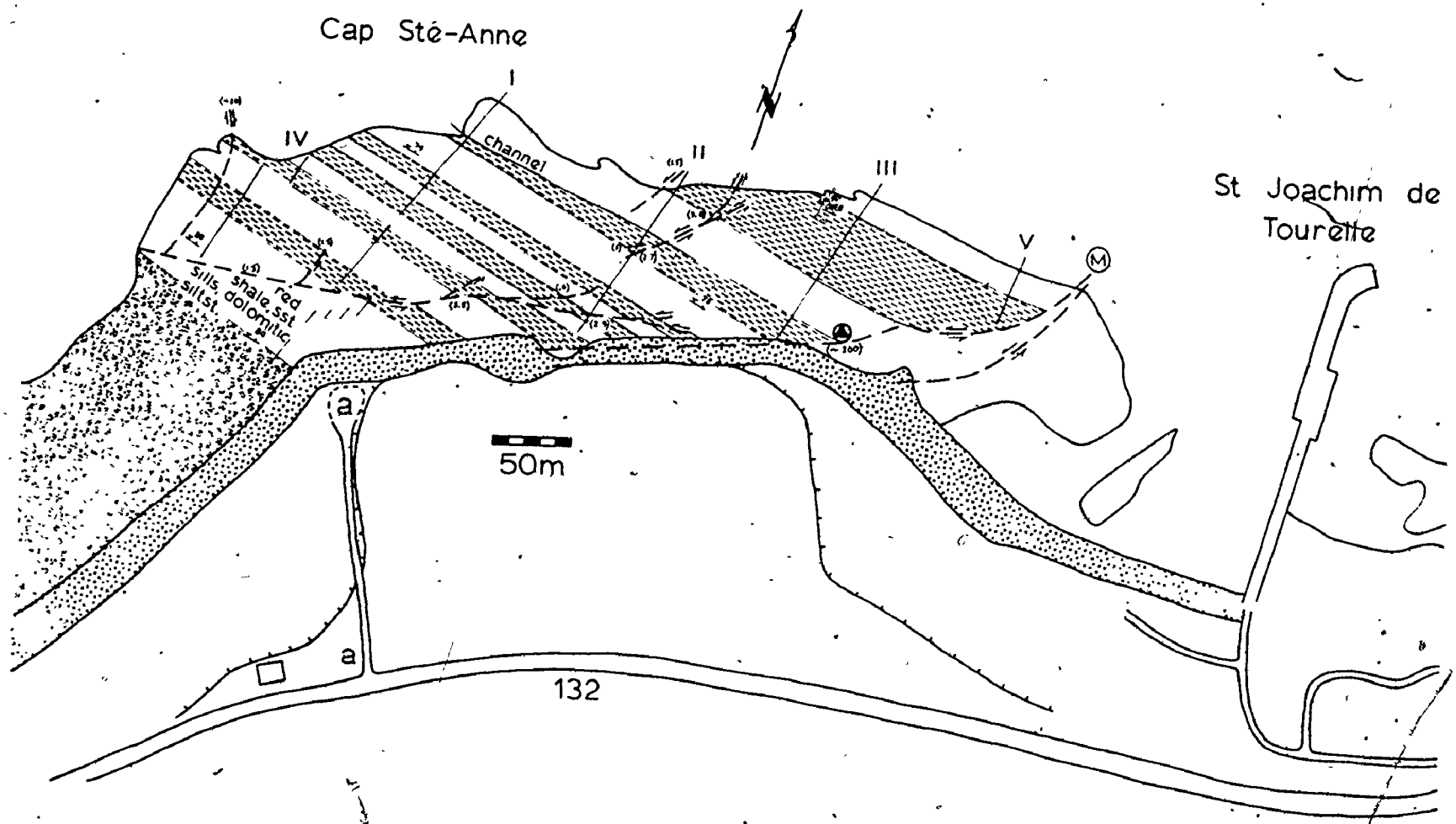
Cap Sté-Anne
I
II
III
IV
V
channel
St Joachim de Tourelle
red shale sst
silts dolomitic
50m
a
a
132

Area J

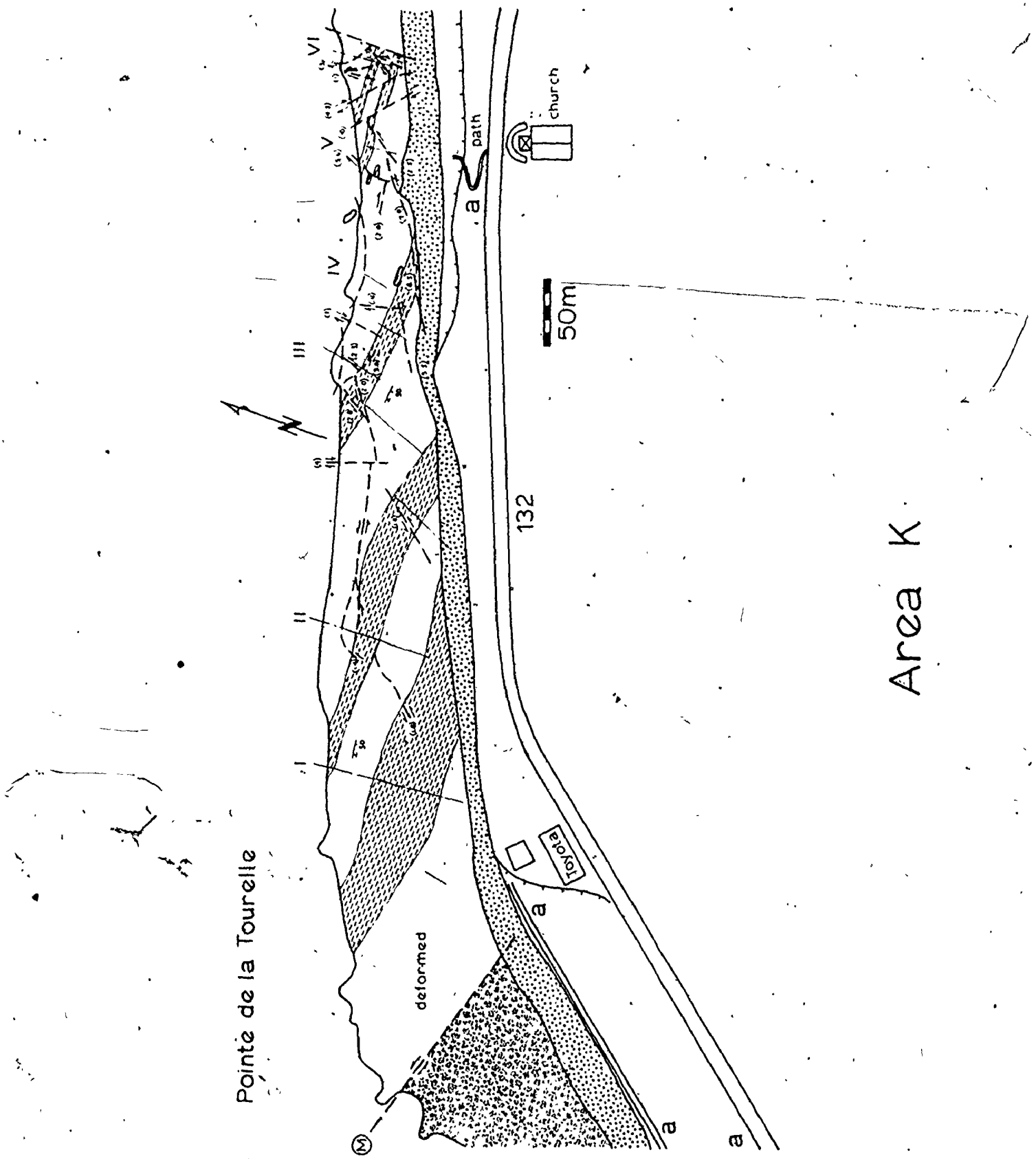
Area K
Pointe de la Tourelle
VI
V
IV
III
II
I
deformed
path
church
132
50m
Toyota
a
a
a
a
Σ

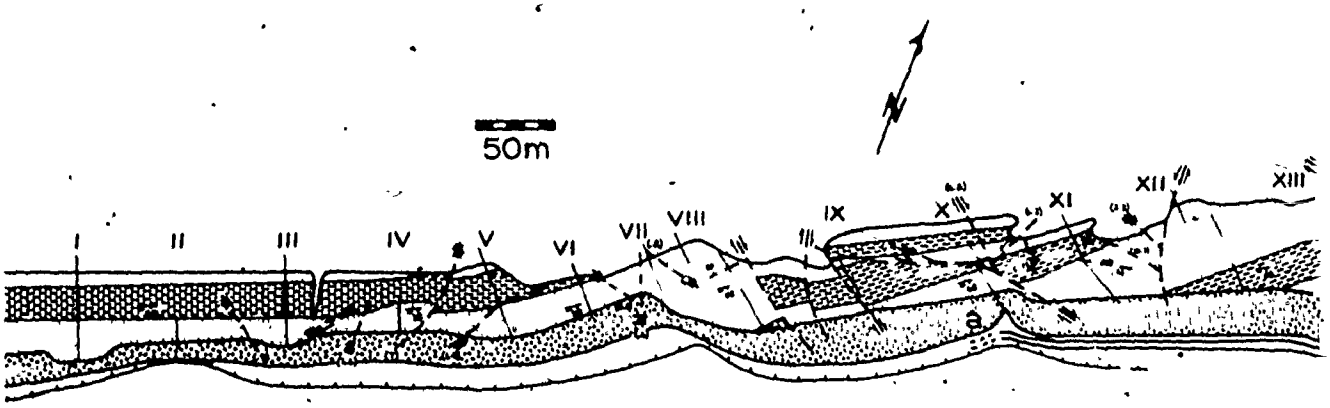

Area L

1 of 1

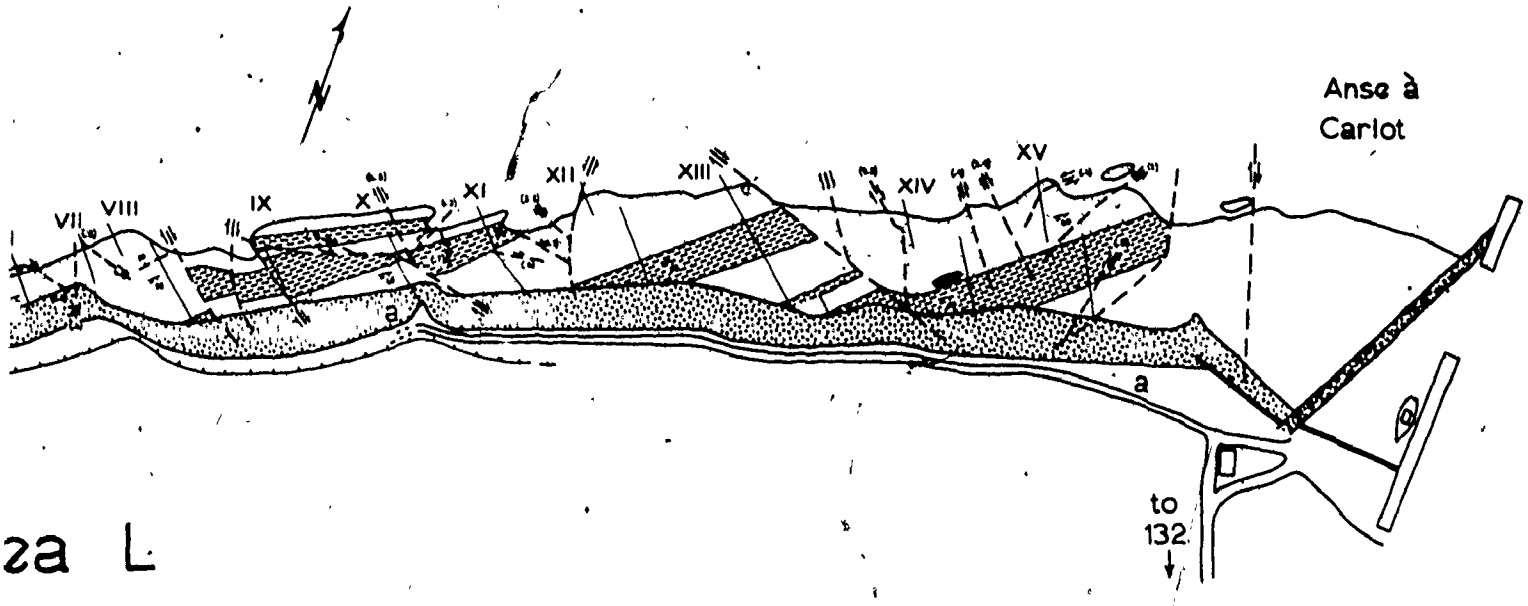

za L

1 2 of 2

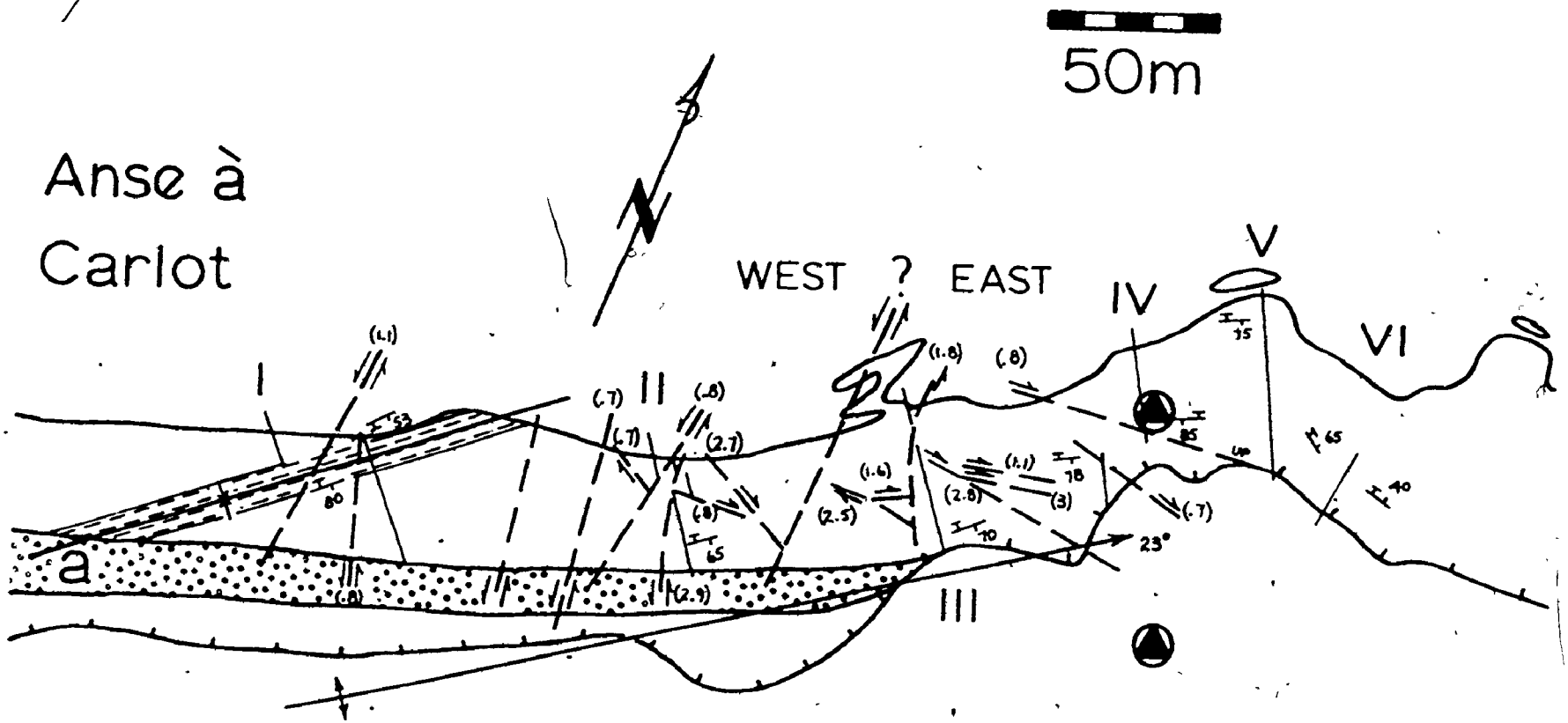
50m
Anse à
Carlot
WEST
?
EAST
I
II
III
IV
V
VI
a
(1.1)
(.7)
(.8)
(2.7)
(1.8)
(.8)
(1.4)
(2.5)
(1.1)
(2.8)
(3)
(.7)
(.8)
(2.9)
23°

Area M

APPENDIX II

Acetate Peel Preparation for Fabric Study

APPENDIX LI

ACETATE PEEL PREPARATION FOR FABRIC STUDY

(1) Specimens must be slabbed and properly marked to ensure that correct orientation is always known. Use a marker that is not soluble in water, or a lead pencil. Care should be taken in later steps, as most marker inks are soluble in acetone.

(2) Grind surface to be replicated on a rotating wheel with 100 mesh carborundum grit until all saw marks are removed. Then fine grind the surface with 600 mesh carborundum powder on a glass plate until the entire surface has an even polish. Clean carefully.

(3) Prepare two solutions: (i) 5% $BaCl_2$; (ii) 0.10 potassium rhodizonate ($C_6K_2O_6$) in 40 ml distilled water. This second reagent is available from Eastman Kodak Co., Rochester, N.Y. 14650, U.S.A. A fresh batch of solution (ii) should be used for each 10 to 15 samples.

(4) To etch, hold sample with tongs, and immerse for 1 minute in 50% hydrofluoric acid (HF). This must be done in a well ventilated fume hood, as HF is extremely caustic and volatile.

(5) Rinse sample in a basin of distilled water.

(6) Dip several times into a vessel containing 5% $BaCl_2$ solution.

(7) Set the etched surface in a shallow vessel containing K-rhodizonate solution. Be sure to prop up one side of the sample so that the etched surface does not lie directly on the bottom of the container. Leave the first samples in the solution for only 30 seconds. As the reagent becomes depleted, a longer period will be required.

(8) Rinse in water under a tap. The sandstone should be stained red, with most stain being concentrated on (i) calcite cement, and (ii) phyllosilicate matrix and rock fragments.

(9) Allow sample to dry. DO NOT RUB ETCHED SURFACE.

(10) If the stain is unsatisfactory or very uneven, return to step (2) using fine carborundum powder only.

(11) Support sample so that stained surface is approximately horizontal and flood the surface with acetone. Starting at the lowest corner, "roll" on a pre-cut sheet of thin, clear

acetate. Allow this peel to cure for at least 30 minutes.

(12) Ensure that orientation lines are transferred from the specimen to the peel, and remember which side of the peel represents the top of the bed. When this is done, the peel may be removed and mounted between two 51 x 75 mm microscope slides for viewing. Quartz and most feldspar grains will appear white; matrix and cement will be red.

APPENDIX III

Fabric Diagrams and Grading Chart

APPENDIX III

FABRIC DIAGRAMS AND GRADING CHART

This appendix contains all additional fabric diagrams for stations 1 and 7 which do not appear in the text. For an explanation of these diagrams, see the caption for Figure 4.5. Following these diagrams is a figure showing grading for all fabric localities (Figure AIII.1). Grain size was determined by averaging the largest dimensions of the 10 largest clasts visible at one time on the Shadowmaster screen, and is therefore an estimate of the coarsest percentile of each size distribution. The thickness of each layer is also indicated.

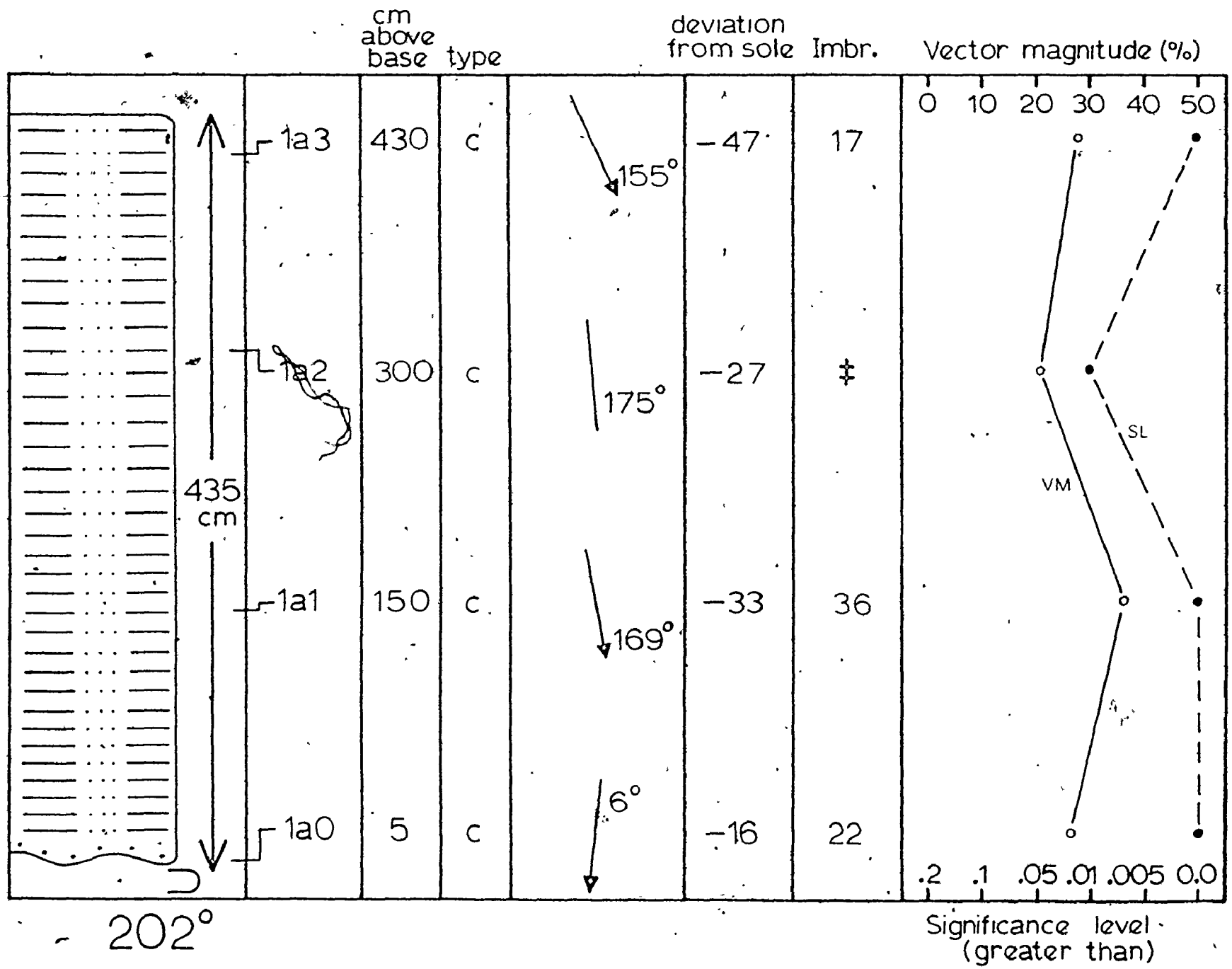
cm above base
type
deviation from sole
Imbr.
Vector magnitude (%)
0 10 20 30 40 50
1a3
430
c
155°
-47
17
1a2
300
c
175°
-27
‡
1a1
150
c
169°
-33
36
1a0
5
c
6°
-16
22
435 cm
SL
VM
.2 .1 .05 .01 .005 0.0
Significance level (greater than)
202°

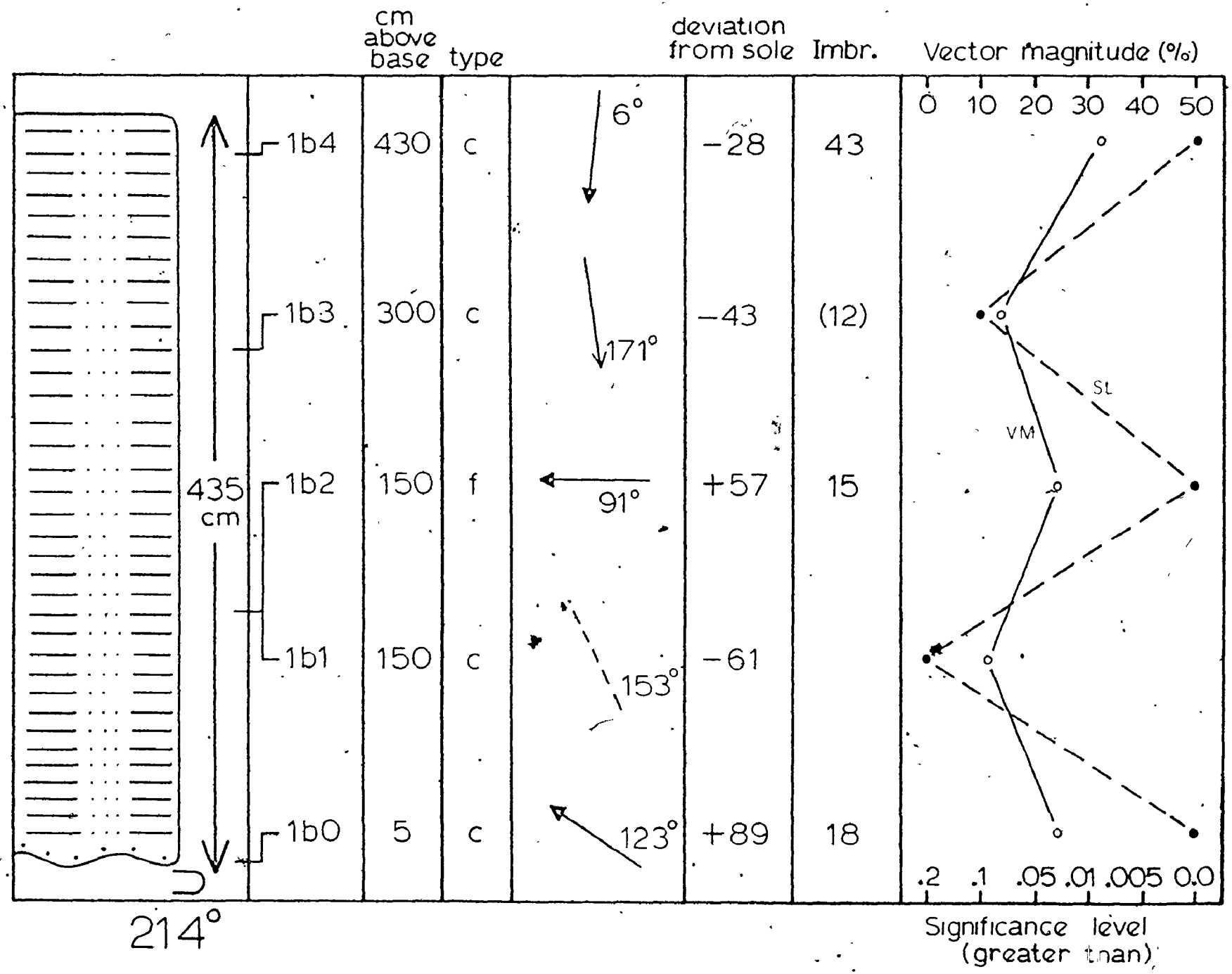
cm above base
type
deviation from sole
Imbr.
Vector magnitude (%)
0 10 20 30 40 50
1b4
430
c
6°
-28
43
1b3
300
c
171°
-43
(12)
1b2
150
f
91°
+57
15
1b1
150
c
153°
-61
1b0
5
c
123°
+89
18
435 cm
214°
SL
VM
.2 .1 .05 .01 .005 0.0
Significance level (greater than)

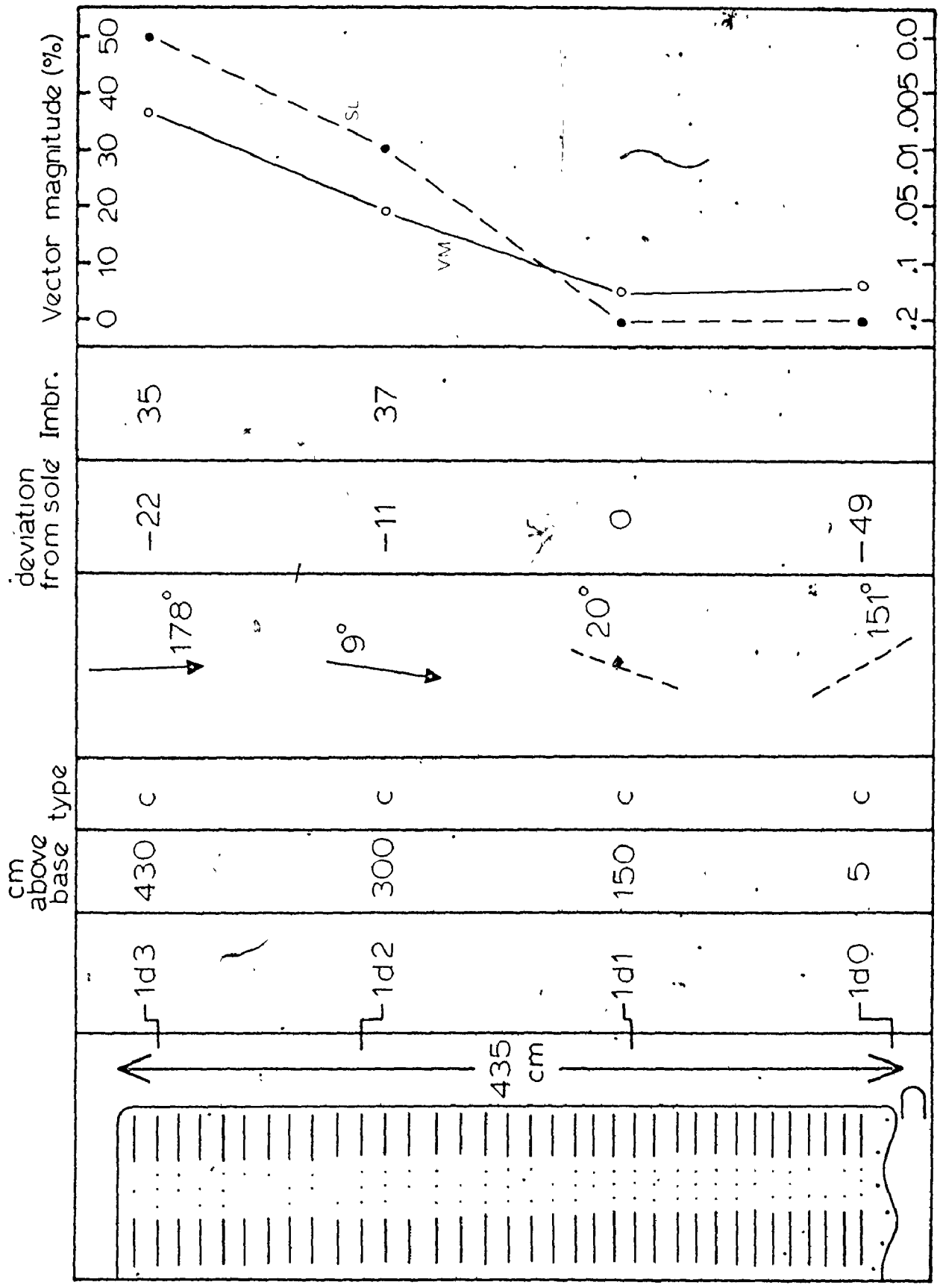
Vector magnitude (%)
0 10 20 30 40 50
SL
VM
Significance level (greater than)
.2 .1 .05 .01 .005 0.0
deviation from sole
Imbr.
35
37
-22
-11
0
-49
178°
9°
20°
151°
cm above base
type
430
300
150
5
c
c
c
c
1d3
1d2
1d1
1d0
435 cm
200°

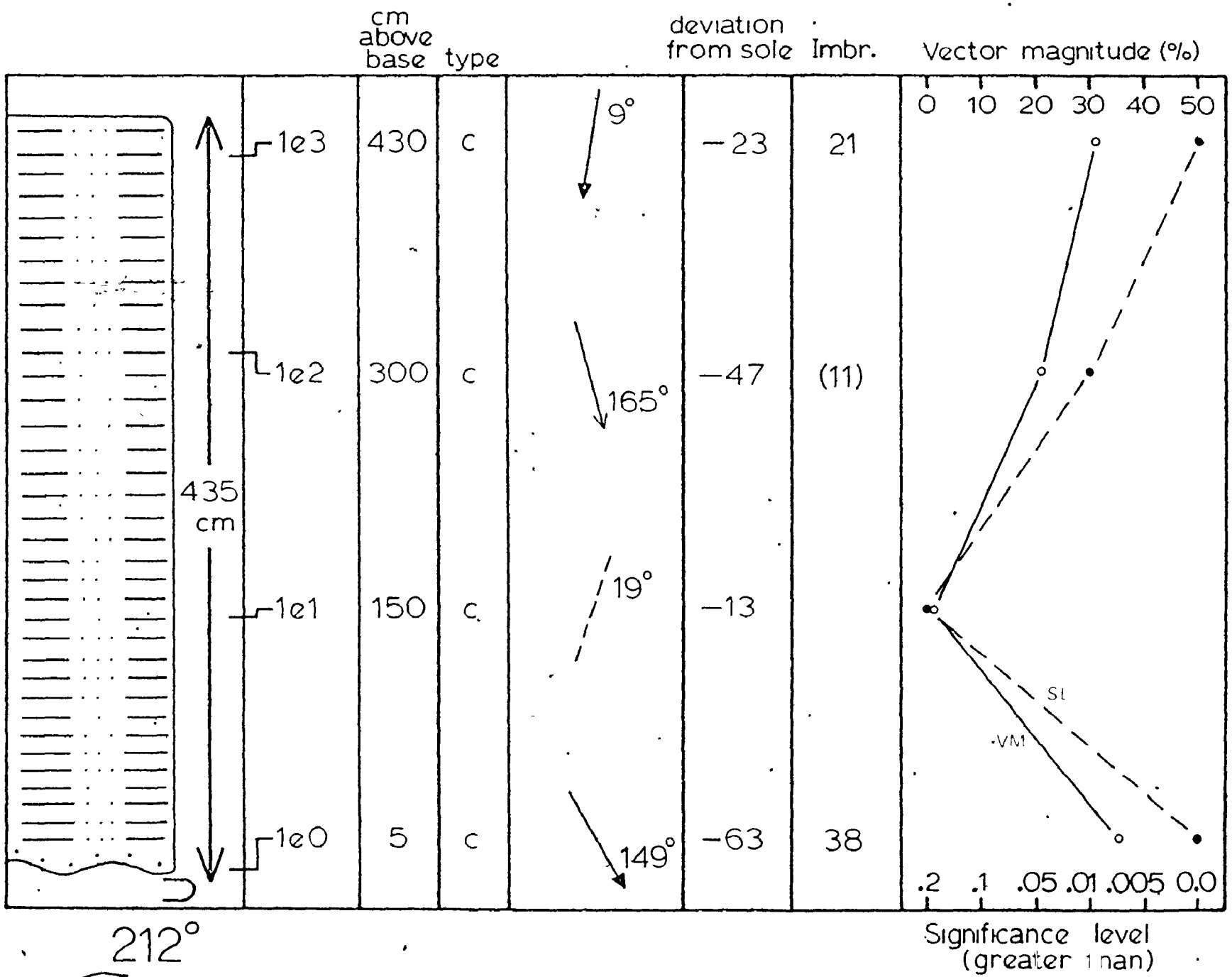
cm above base
type
deviation from sole
Imbr.
Vector magnitude (%)
0 10 20 30 40 50
1e3
430
c
9°
−23
21
1e2
300
c
165°
−47
(11)
435 cm
1e1
150
c
19°
−13
1e0
5
c
149°
−63
38
St
VM
.2 .1 .05 .01 .005 0.0
Significance level (greater than)
212°

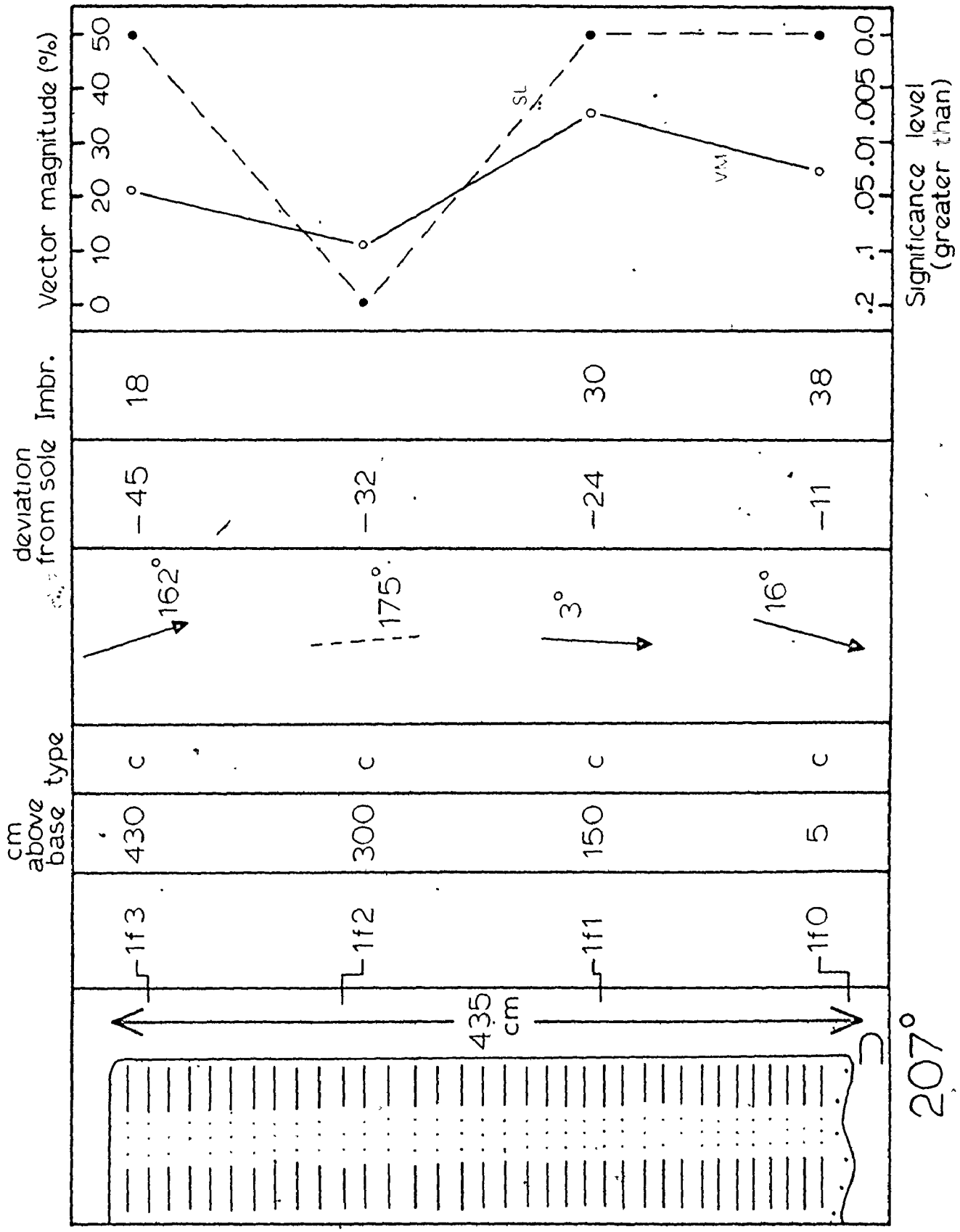
Vector magnitude (%)
0 10 20 30 40 50
.2 .1 .05 .01 .005 0.0
Significance level (greater than)
SL
VM
deviation from sole
Imbr.
18
30
38
−45
−32
−24
−11
162°
175°
3°
16°
cm above base
type
c
430
300
150
5
1f3
1f2
1f1
1f0
435 cm
207°

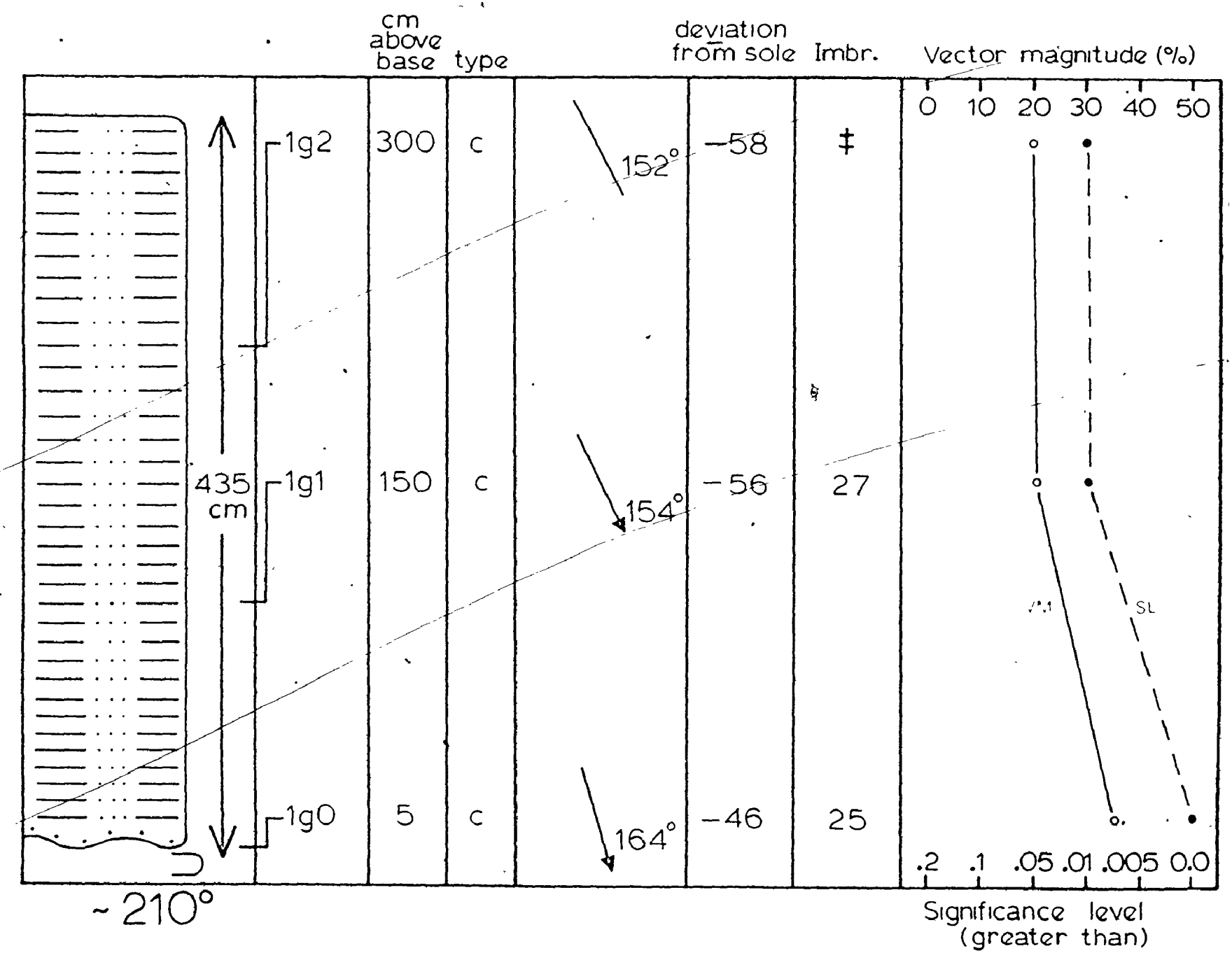
cm above base
type
deviation from sole
Imbr.
Vector magnitude (%)
0 10 20 30 40 50
1g2
300
c
152°
-58
‡
435 cm
1g1
150
c
154°
-56
27
1g0
5
c
164°
-46
25
VM
SL
.2 .1 .05 .01 .005 0.0
Significance level (greater than)
~210°

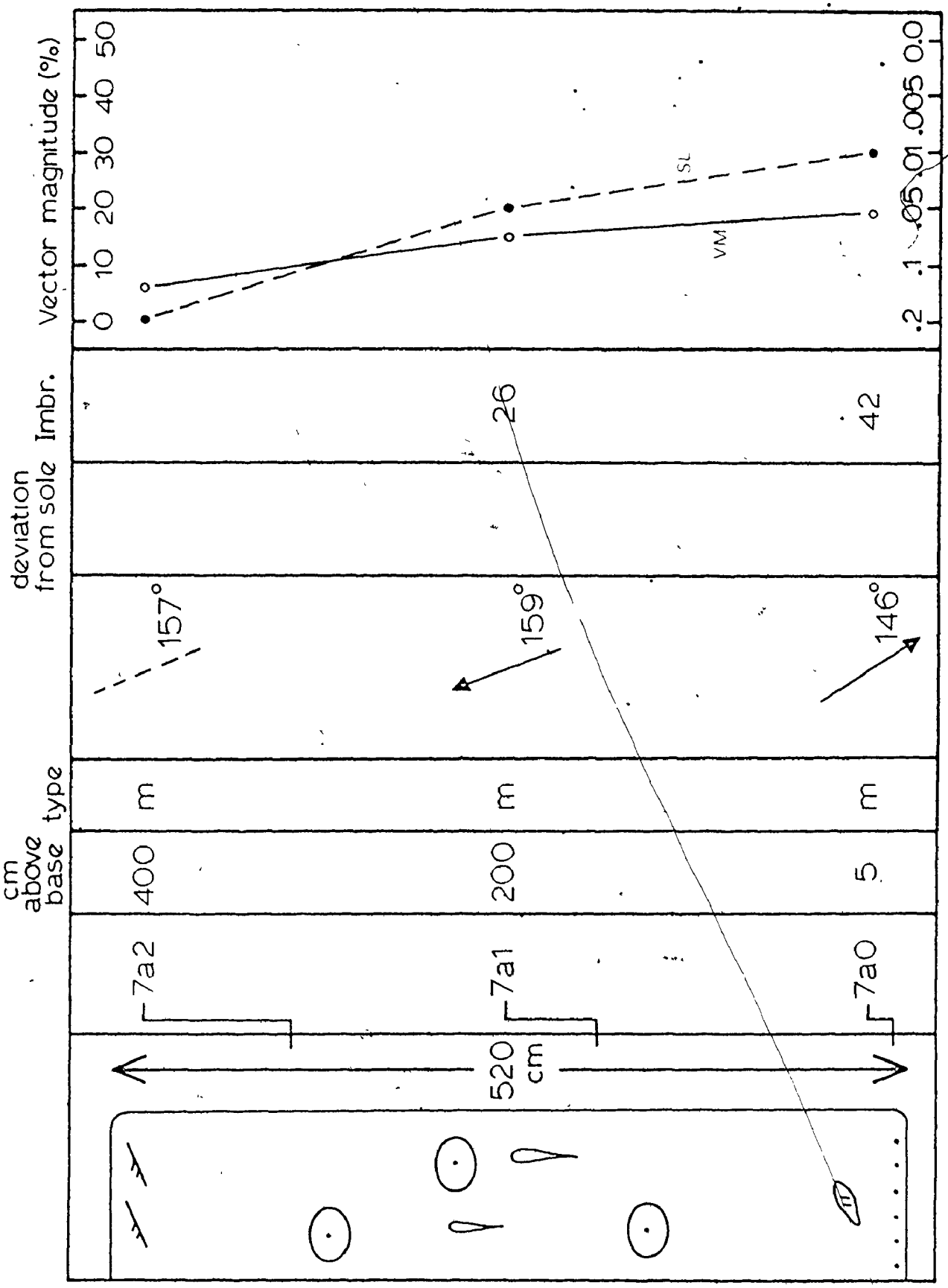
Vector magnitude (%)
0 10 20 30 40 50
SL
VM
.2 .1 .05 .01 .005 0.0
Significance level (greater than)
deviation from sole
Imbr.
26
42
157°
159°
146°
cm above base
type
m
m
m
400
200
5
7a2
7a1
7a0
520 cm

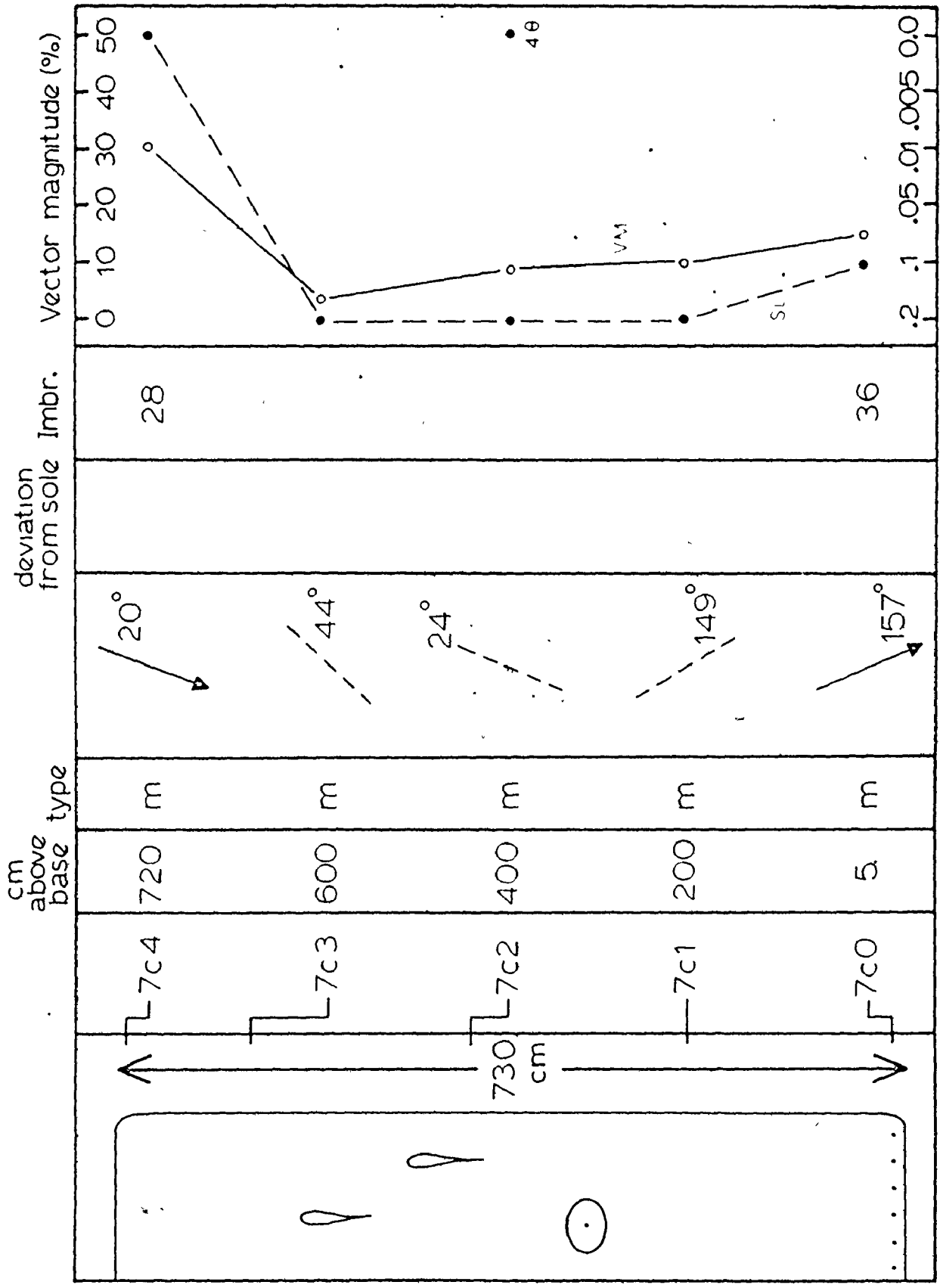
Vector magnitude (%)
0 10 20 30 40 50
Significance level (greater than)
.2 .1 .05 .01 .005 0.0
4θ
VM
SL
Imbr.
28
36
deviation from sole
20°
44°
24°
149°
157°
cm above base
type
720 m
600 m
400 m
200 m
5 m
7c4
7c3
7c2
7c1
7c0
730 cm

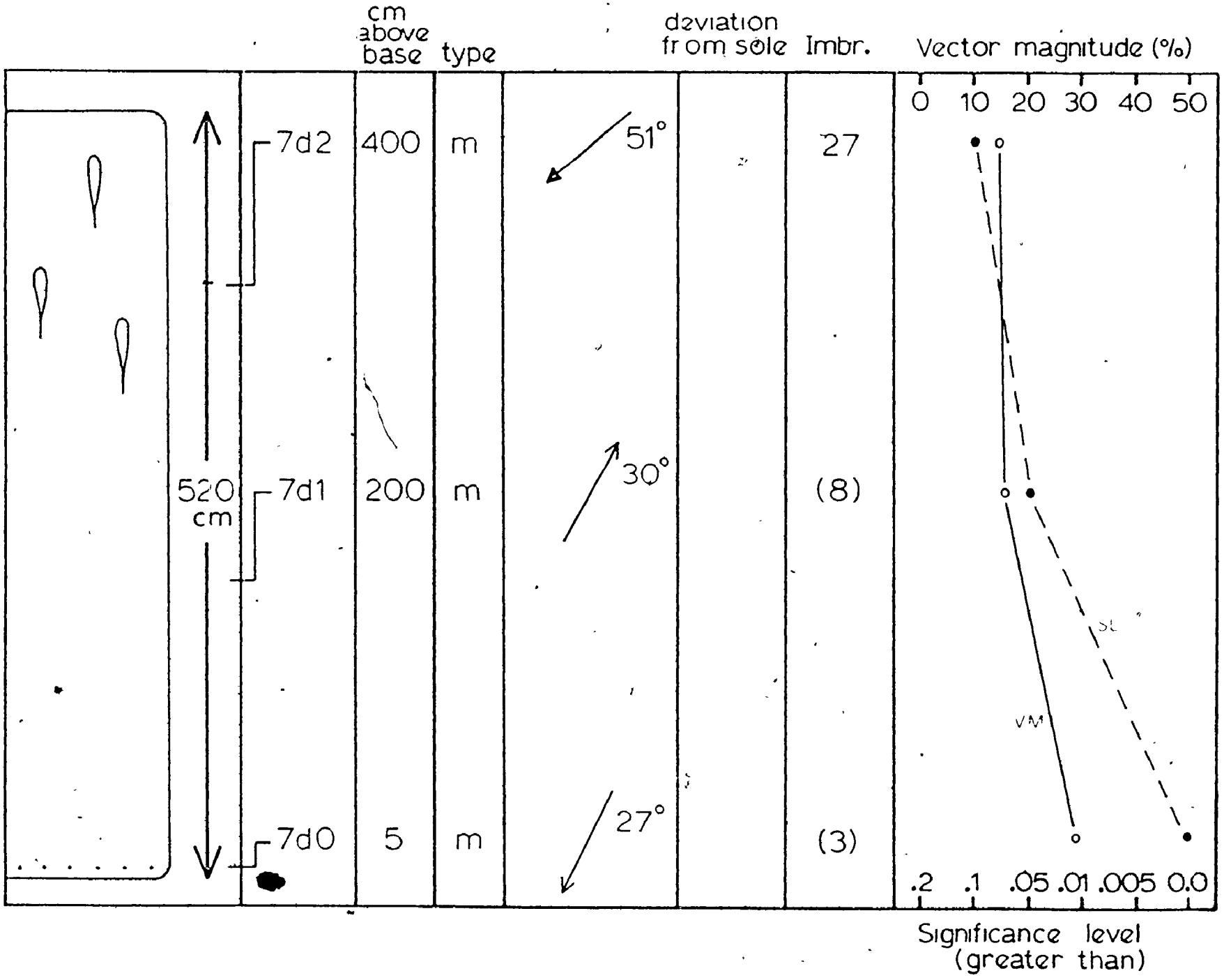
cm above base
type
deviation from sole
Imbr.
Vector magnitude (%)
0 10 20 30 40 50
7d2
400
m
51°
27
520 cm
7d1
200
m
30°
(8)
7d0
5
m
27°
(3)
VM
.2 .1 .05 .01 .005 0.0
Significance level (greater than)

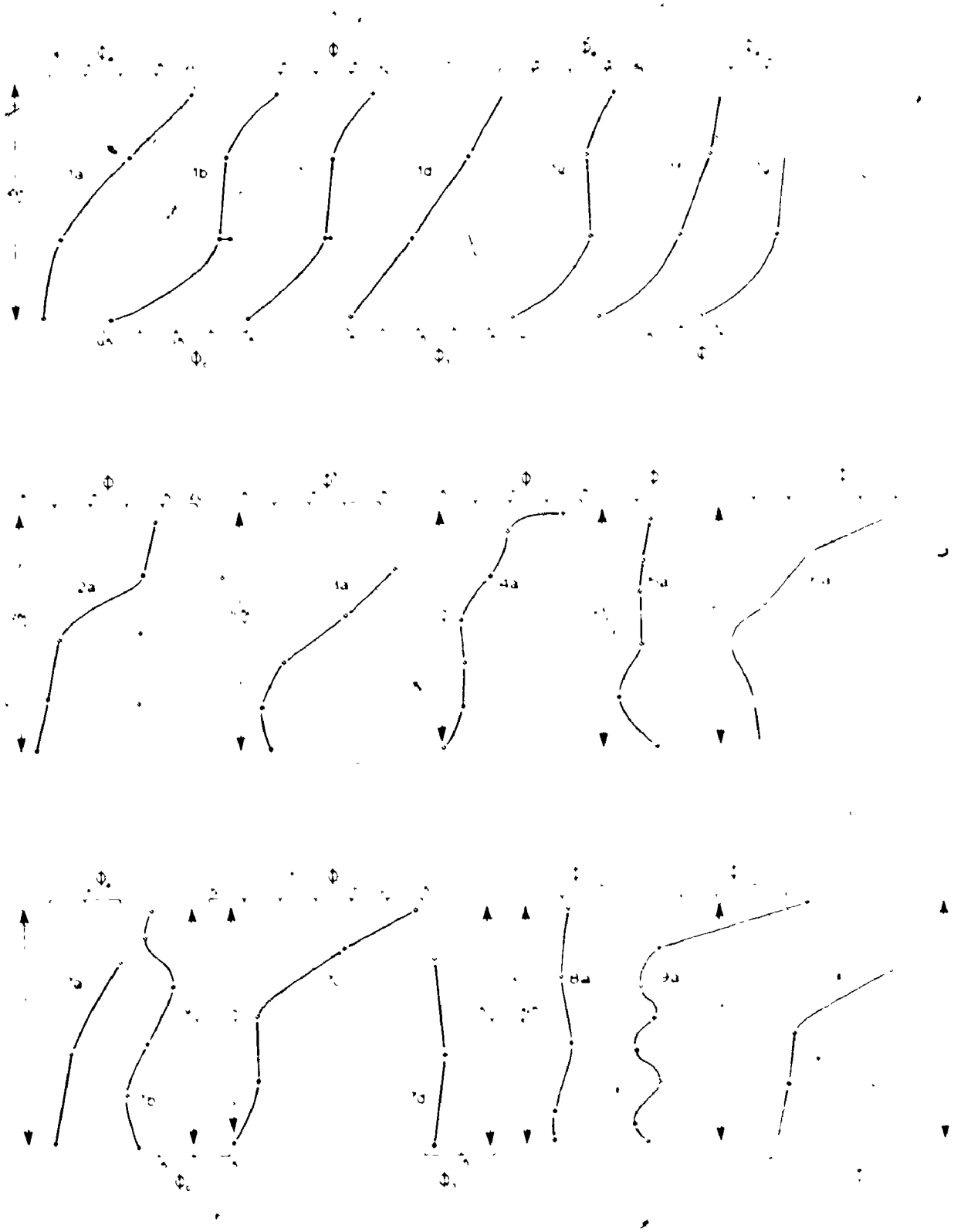

Fig. AIII.1. Grain-size variation for all fabric localities.

APPENDIX IV

Fabric Data and Statistics

APPENDIX IV

FABRIC DATA AND STATISTICS

The table that follows summarizes fabric results for all layers examined in Chapter IV. Orientations ($\bar{\theta}$) and imbrications (β) are marked with an asterix if significance level for the Tukey chi-squared test was greater than 0.20. q is defined in Chapter V.

All values represent 100 measured grains in each sample, except for those samples followed by (c). These determinations were made on only the coarsest and most elongate grains (see Chapter IV). The number of such grains appears in brackets after VM of the grain orientation.

Most data were analysed following 2 θ transformation (Harrison, 1957). When bimodality was suspected, however, a 4 θ transformation was also employed.

Fabric data and statistics

Sample	Orientation $\bar{\theta}$	Orientation VM(θ)	Imbrication β	Imbrication VM(β)	q
1a0	006	27.14	22 N	44.95	0.604
1a1	169	36.87	36 N	34.96	1.054
1a2	175	20.49	28 N	11.80*	1.736
1a3	155	28.46	17 N	29.63	0.961
1b0	123	24.25	18 E	34.00	0.713
1b1	153	11.91*			
1b2	091	23.76	15 E	23.04	1.031
1b3	171	13.47	12 N	29.96	0.450
1b4	006	32.00	43 N	34.76	0.921
1c0	005	20.31	32 N	62.43	0.325
1c1	163	10.18*			
1c2	009	21.72	26 N	54.11	0.401
1c3	007	30.66	25 N	23.00	1.333
1c4	172	30.61	25 N	57.06	0.536
1d0	151	7.37*			
1d1	020	5.56*			
1d2	009	18.67	37 N	38.31	0.487
1d3	178	37.05	35 N	48.15	0.769
1e0	149	35.34	38 N	44.32	0.797
1e1	019	7.56*			
1e2	165	21.24	11 N	44.39	0.478
1e3	009	31.05	21 N	44.45	0.699
1f0	016	23.02	38 N	36.88	0.624
1f1	003	35.84	30 N	56.92	0.630
1f2	175	11.46*			
1f3	162	32.05	18 N	51.96	0.617

Sample	Orientation $\bar{\theta}$	Orientation VM(%)	Imbrication β	Imbrication VM(%)	q
1g0	164	41.61	25 N	51.19	0.813
1g1	154	20.33	27 N	51.75	0.393
1g2	152	19.94	16 N	9.32*	2.139
2a0	032	26.01	39 N	59.18	0.440
2a1	021	17.12	28 N	34.75	0.493
2a2	012	33.77	21 N	48.77	0.692
2a3	168	12.24*			
2a4	011	44.51	32 N	43.14	1.032
2a5	001	18.90	32 N	42.32	0.447
2a6	009	31.53	36 N	47.68	0.661
2a7(2θ)	106	13.07			
(4θ)		25.17			
3a0	051	22.76	34 E	35.23	0.646
3a1	019	9.49*			
3a2	022	14.92	25 S	22.83	0.654
3a3	033	4.01*			
3a4	050	11.61*			
4a0	085	36.21	15 E	64.58	0.561
4a1	010	10.24*			
4a2	131	4.97*			
4a3	015	32.40	38 N	41.38	0.783
4a4	033	16.65	4 N	30.90	0.539
4a5(2θ)	051	8.70*			
(c)	036	15.26*(37)			
4a6	076	11.47*			

Sample	Orientation $\bar{\theta}$	Orientation VM(%)	Imbrication β	Imbrication VM(%)	q
5a0	173	45.08	17 N	55.83	0.807
5a1	159	17.90	36 N	17.76	1.008
5a2	003	19.21	5 S	20.78	0.924
5a3(2θ)	173	11.66*			
(c)	017	35.08(25)	4 S	43.28	0.811
5a4	014	12.59*			
5a5	006	26.75	30 N	55.24	0.484
6a0(2θ)	093	4.13*			
(4θ)		16.06			
(c)	093	19.50*(34)			
6a1	001	22.37	28 N	42.24	0.530
6a2	178	16.75	16 S	36.52	0.459
6a3(2θ)	133	10.88*			
(4θ)		22.63	(36 N)	39.48	0.573
(c)	138	41.08(44)	2 S	32.69	1.257
6a4	080	8.98*			
6a5	007	8.96*			
7a0	146	18.53	42 N	45.89	0.404
7a1(2θ)	159	15.27	26 S	22.51	0.678
(4θ)		10.05*			
7a2	157	5.67*			
7b0	167	28.41	38 N	43.16	0.658
7b1(2θ)	076	9.74*			
(c)	157	7.28*			
7b2(2θ)	126	14.63	24 W	27.31	0.536
(c)	109	28.13			
7b3	048	11.65*			

Sample	Orientation $\bar{\theta}$	VM(%)	Imbrication β	VM(%)	q
7b4	063	6.85*			
7b5	035	37.01	5 N	11.59*	3.193
7c0	157	14.50	36 N	30.28	0.479
7c1	149	9.55*			
7c2(2θ)	024	9.35*			
(4θ)		34.13			
(c)	169	25.76*(23)			
7c3	044	2.77*			
7c4	020	30.21	28 N	63.13	0.479
7d0(2θ)	032	29.34	3 N	42.34	0.693
(4θ)		21.35			
(c)	023	45.07			
7d1	030	16.35	8 S	38.97	0.420
7d2(2θ)	051	14.87	27 E	49.22	0.302
(c)	065	23.83*(20)			
8a0(2θ)	055	5.87*	10 E	27.25	0.215
(4θ)		26.20			
(c)	147	10.73*(44)	33 W	23.61	0.454
8a1	179	20.81	10 N	(bimodal)	
8a2(2θ)	172	25.61	32 N	64.61	0.396
(c)	168	27.24(55)			
8a3	022	9.64*			
8a4	124	31.72	16 E	54.87	0.578

Sample	Orientation $\bar{\theta}$	VM(%)	Imbrication β	VM1(%)	q
9a0	168	15.40	16 S	48.93	0.315
9a1	002	22.46	8 S	32.34	0.694
9a2(2θ)	174	0.95*			
(c)	121	2.13*(66)			
9a3	004	41.33	33 S	23.43	1.764
10a0	168	25.26	22 S	42.56	0.594
10a1	147	16.99	24 S	54.37	0.312
10a2	159	26.22	19 S	37.03	0.708
10a3	174	36.18	28 S	51.63	0.701
10a4	066	2.37*			
10a5(2θ)	050	12.60*			
(4θ)		20.44			

APPENDIX V

Chromium Analysis of Heavy Minerals

APPENDIX V

CHROMIUM ANALYSIS OF HEAVY MINERALS

Procedure

Solution preparation

(1) Thoroughly mix 0.2000 g of finely powdered sample and 1.00 g lithium metaborate in a 45 ml platinum crucible. Prepare a standard solution in identical fashion using 0.2000 g K_2CrO_4.

(2) Fuse for 15 minutes in a muffle furnace at 900°C.

(3) Place crucible quickly into a 100 ml beaker containing 25 ml of 4% nitric acid. When cool, add 50 ml more of the acid, submerging the crucible. Add a teflon-covered stirring bar and stir on low heat to complete solution.

(4) Transfer to a 250 ml flask and make up to volume. Mix thoroughly.

Determination of chromium

(1) Dilute the standard solution to 1:20, 1:40, and 1:100.

(2) Place 100 ml aliquots of each standard solution and the sample solution in separate 250 ml beakers.

(3) Add 5 ml 25% sulphuric acid (H_2SO_4).

(4) Add 2.5 ml of 3% hydrogen peroxide (H_2O_2).

(5) Add 15% NaOH drop by drop with a pipet (about 20 ml are needed) until R_2O_3 precipitates. Then continue addition and adjust pH to 8 or 9 (use pH paper). If pH is already too high, adjust with H_2SO_4 solution.

(6) Add 3 drops of 4% $KMnO_4$.

(7) Heat on steam overnight and evaporate to about 80 ml.

(8) Filter into a 100 ml flask and make up to volume. The solutions will be pale yellow in colour.

(9) Measure absorbance, in a 1 cm cell, of each standard solution at 365 mμ. Also measure a blank solution of 1.00 gm lithium metaborate dissolved in 75 ml 4% nitric acid and made up to 250 ml. Distilled water is used to zero the instrument, which in this case was a Beckman model B spectrophotometer.

(10) Dilute sample (if necessary, into the linear range defined by the standards, and measure absorbance.

Results

Sample weight was 0.2020 g, and standard weight was 0.2003 g. Table AV.1 presents absorbance and concentration for the various solutions. These data are plotted in Figure AV.1. Experimental error is estimated on the basis of the uncertainty in the line which is fit to the data points.

The heavy mineral sample solution (100 ml) had a concentration of $(10)(2.650 \times 10^{-4}\ M) = 2.650 \times 10^{-3}\ M$. The total amount of chromium was

$$(2.650 \times 10^{-3}\ \frac{\text{moles}}{\ell})(0.1\ \ell)(52.00\ \frac{g}{\text{mole}}) = 1.378 \times 10^{-2}\ g$$

Therefore, the percent of chromium in the original sample was

$$(\frac{1.378 \times 10^{-2}\ g}{0.2020\ g})(100\%) = 6.82\%$$

Error associated with the position of the line of best fit is ±0.2%. This does not include dilution errors associated with preparation of the sample solution. It is unlikely, however, that error in the sample is any larger than error in the standards.

Table AV.1

Absorbances and concentrations for chromium determination

Sample	dilution	concentration (10^{-4} M)	absorbance actual	absorbance corrected
Blank		0.000	0.008	0.000
Standard	1:20	5.157	0.848	0.840
	1:40	2.578	0.441	0.433
	1:100	1.031	0.167	0.159
Heavy minerals	1:10	2.650	0.445	0.437

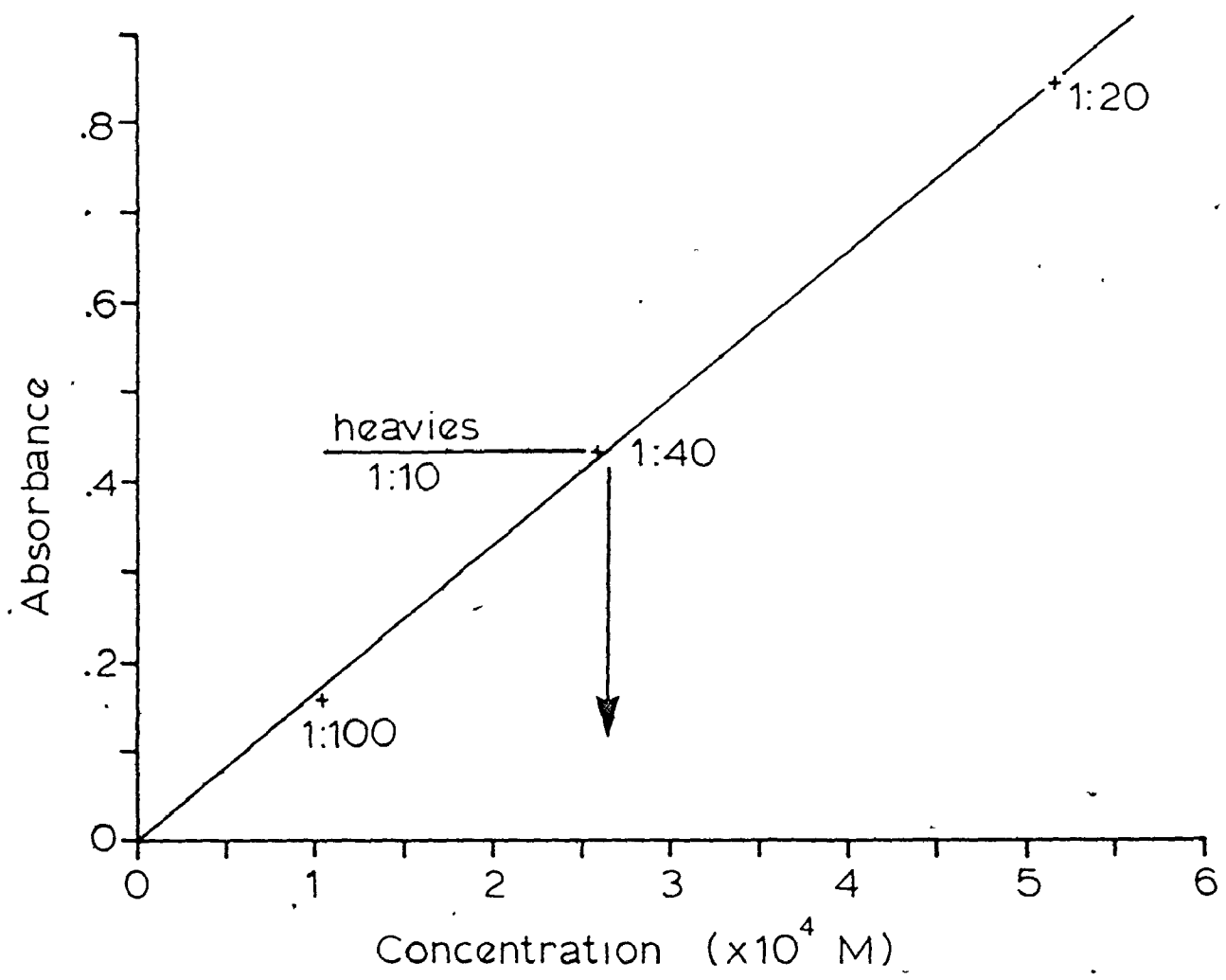

Fig. AV.1. Absorbance vs concentration for chromium standards and Tourelle heavy mineral sample.

APPENDIX VI

Explanation of Hydraulics Symbols

Symbol

- a - arbitrary datum ($a = 0.05\ d$) used to calculate relative concentrations of suspended sediment.
- C - fractional volume concentration of grains in a fluid.
- C_o - C at the reference level a.
- d - flow depth.
- D - grain diameter.
- f - friction factor.
- Fr - Froude number based on reduced gravity $g' = g(\Delta\rho/\rho)$.
- g - acceleration due to gravity (980 $cm\ s^{-1}$).
- h - thickness of a block in a debris flow.
- k - strength of a debris flow.
- k_s - equivalent sand roughness.
- M_o - specific force, applicable to conservation of momentum in a fluid.
- n - parameter specifying the depth of penetration of a block into the top of a debris flow. If 1/4 of the block is submerged, $n = 4$.
- q - unit discharge.
- R - hydraulic radius, which is approximated by d for wide flows.
- S - slope.
- T_c - critical thickness at which a debris flow stops moving.
- $\bar{u}$ - mean velocity.
- u_* - shear velocity.
- w - settling velocity of a grain in a dispersion.
- w_o - settling velocity of a single grain in a still fluid.
- γ - angle of slope.

Symbol

δ - viscous sublayer thickness.

κ - von Kármán constant.

ν - kinematic viscosity.

ν_e - effective kinematic viscosity.

ρ - flow density.

ρ_s - solid density.

$\Delta\rho$ - density difference between the flow and clear water (i.e. ρ-1).

τ_c - critical boundary shear stress for initiation of movement.

PTE BOURDAGE SHEET

Colour

1 of 1

SHEET

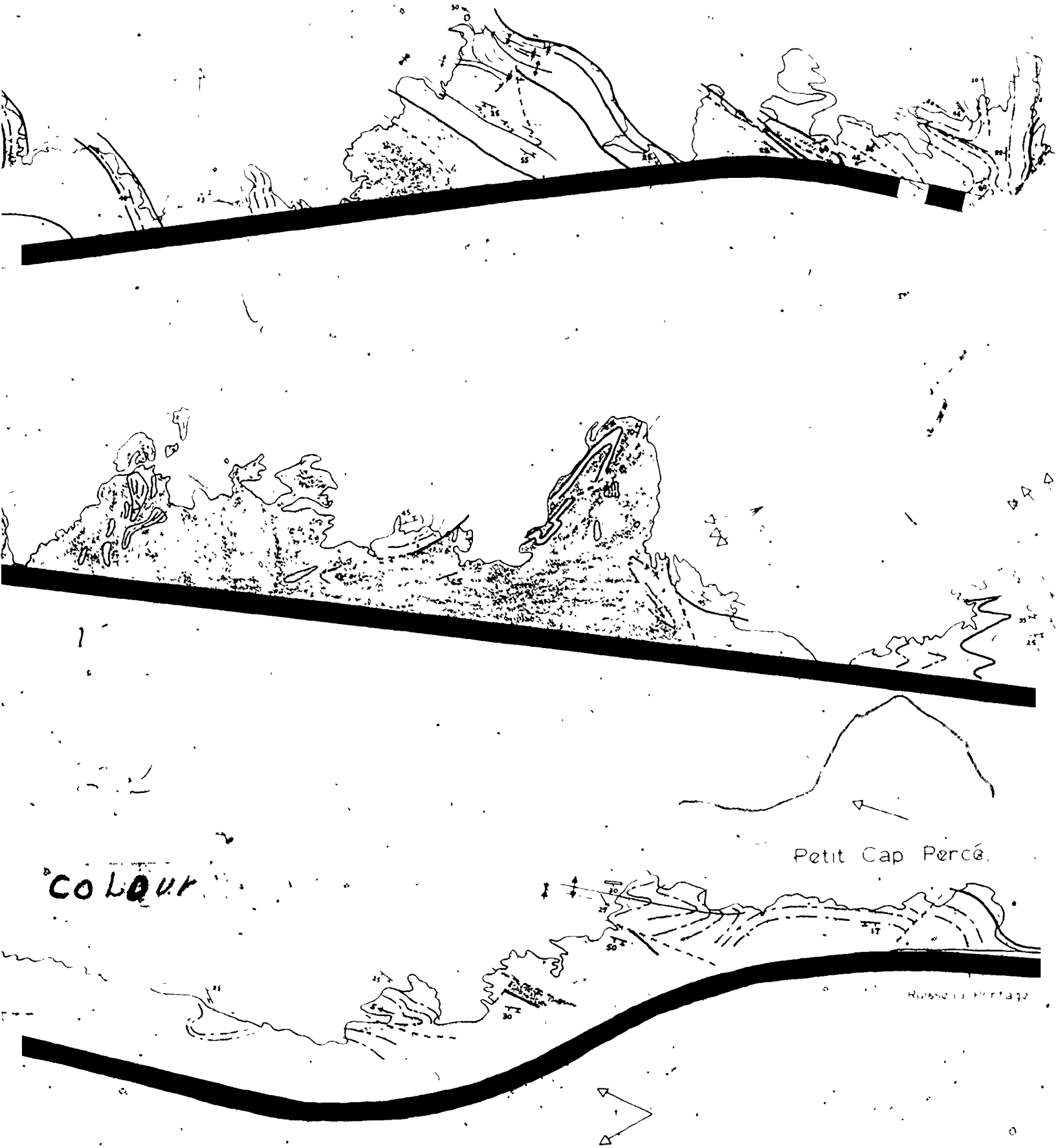


Pte Bourdage
t Cap Percé
COLOUX

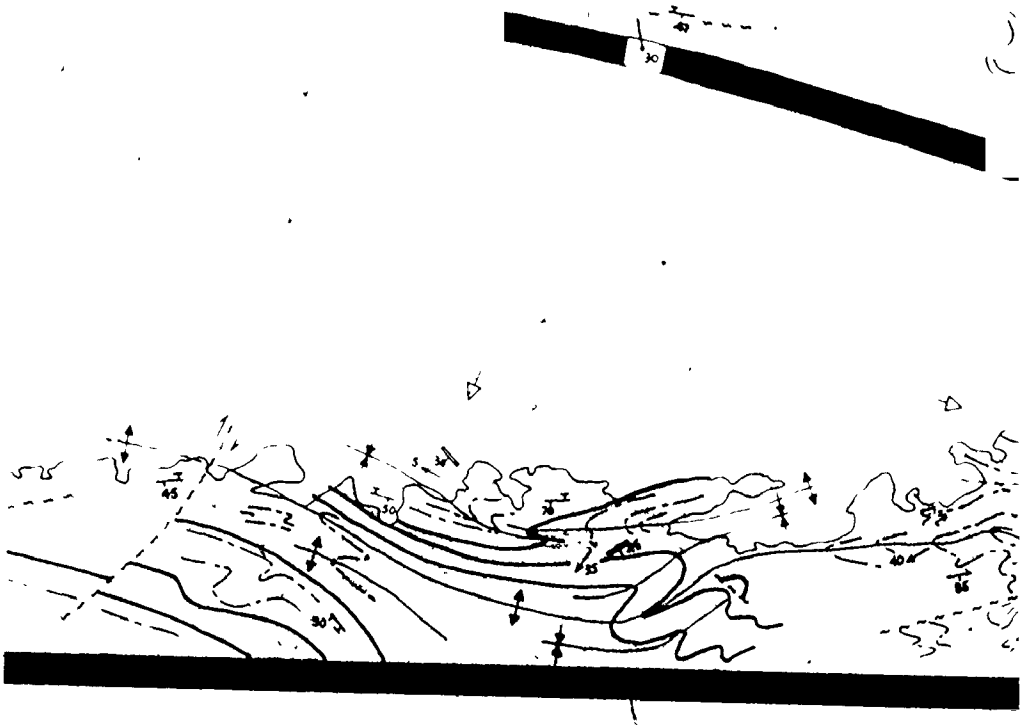

COLOUR

4 of

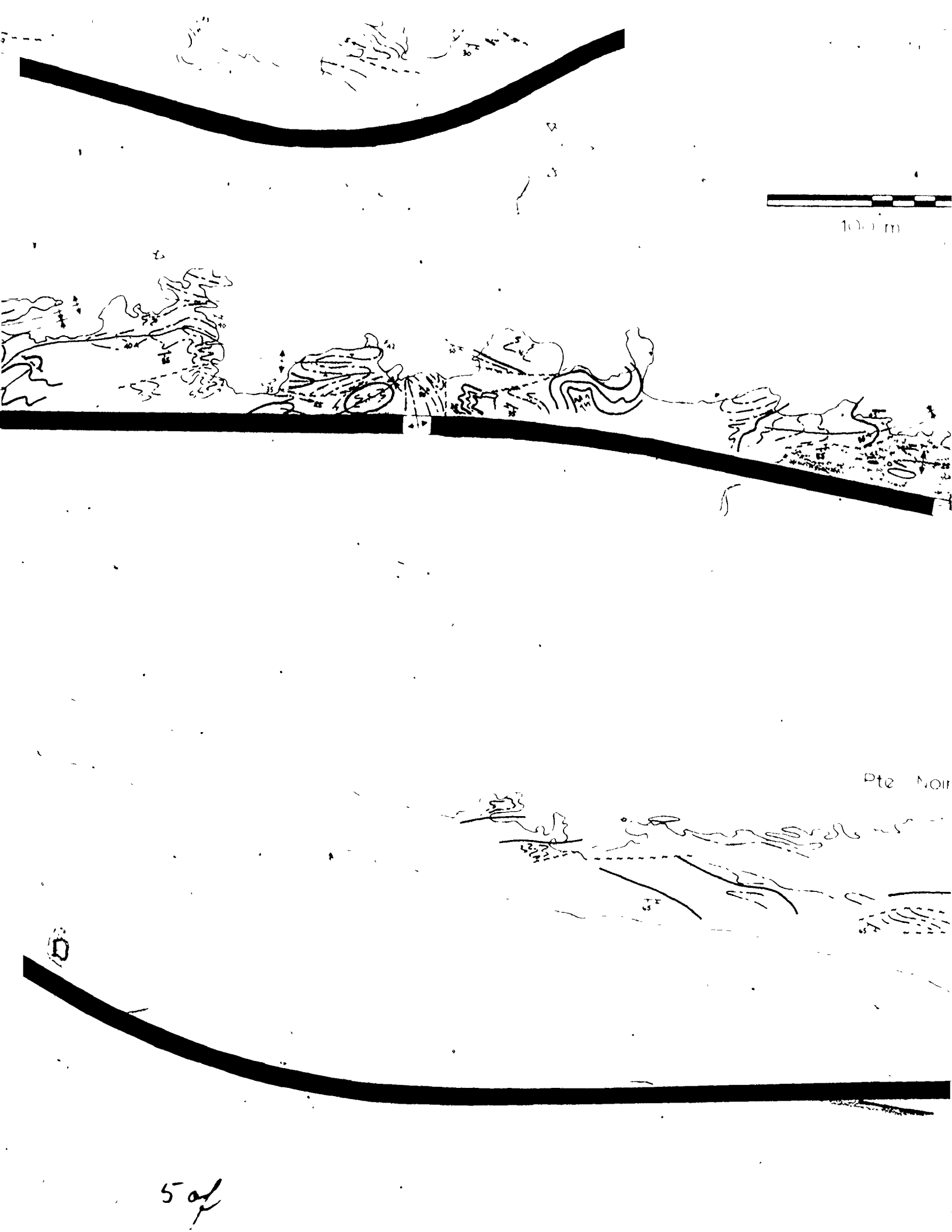
Pte

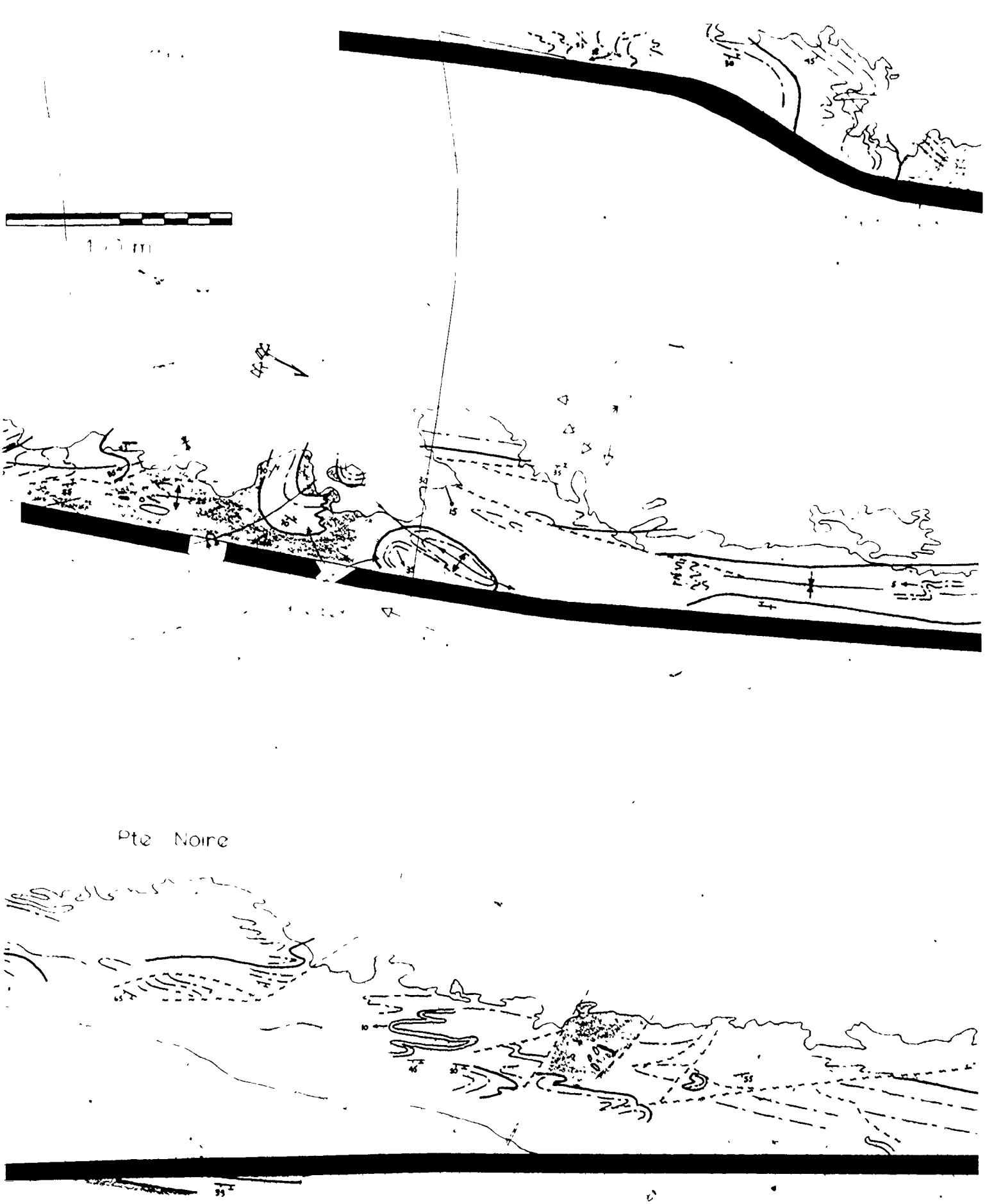
Pte Noire

STE-MARTHE SHEET

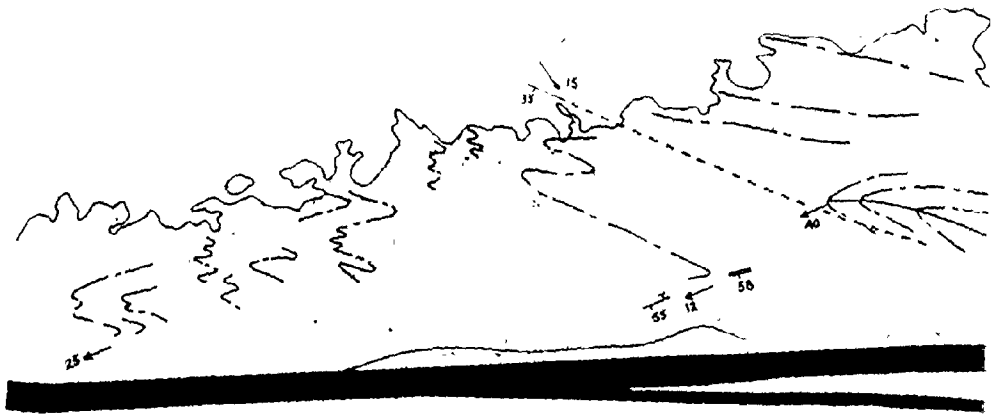

100 m

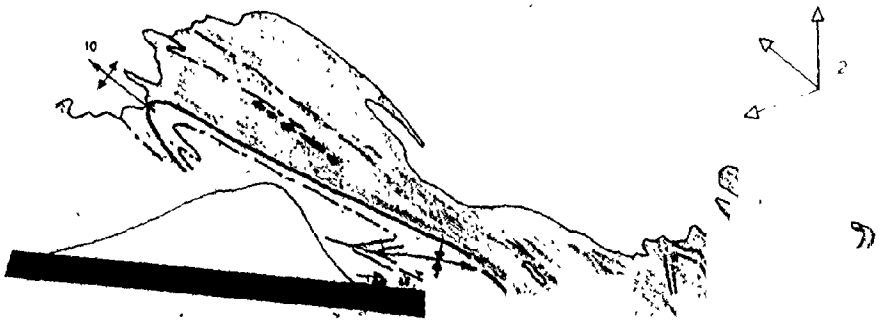

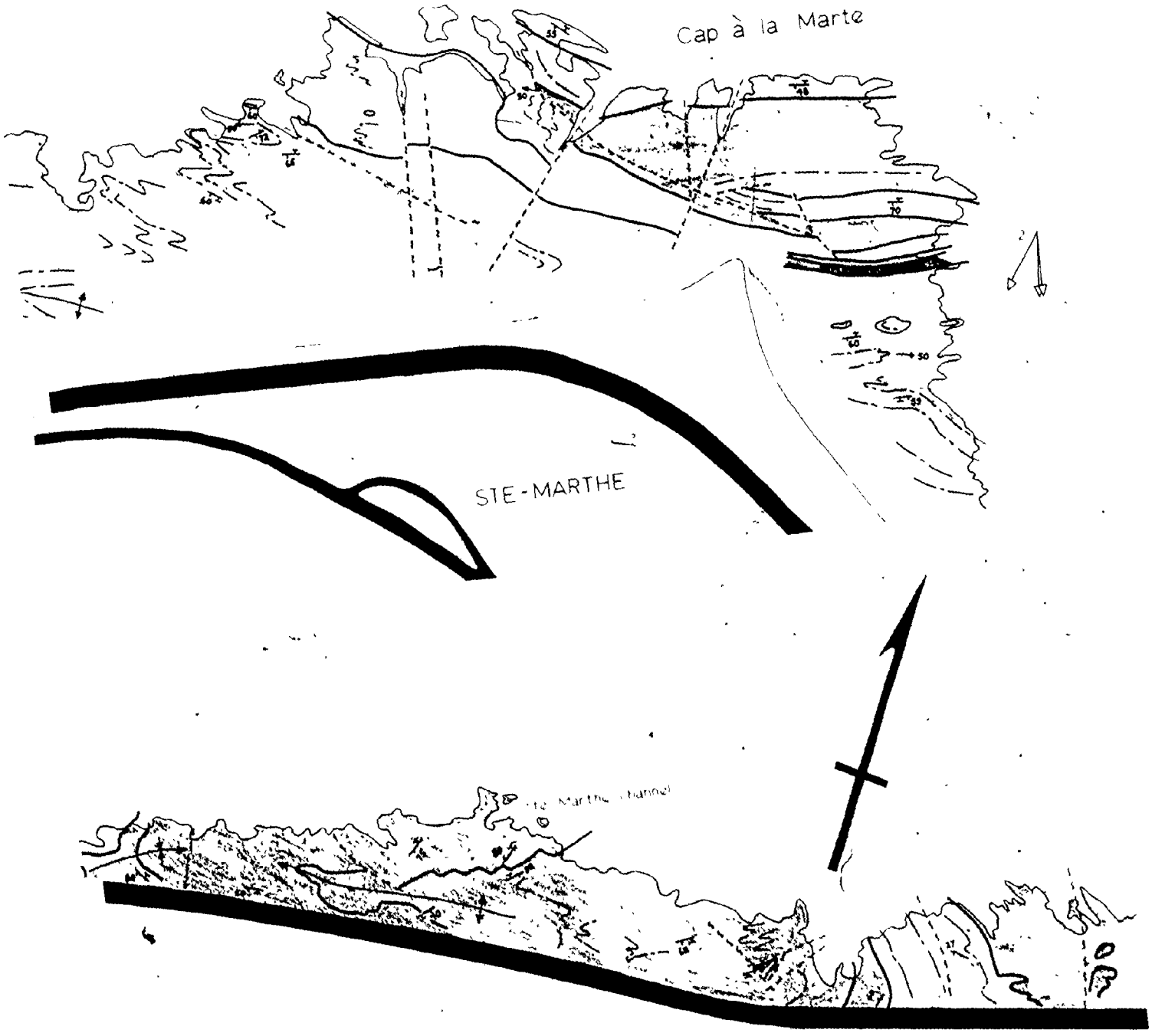

COLOUR

channel

3 of 2 | COLOUR

100 m

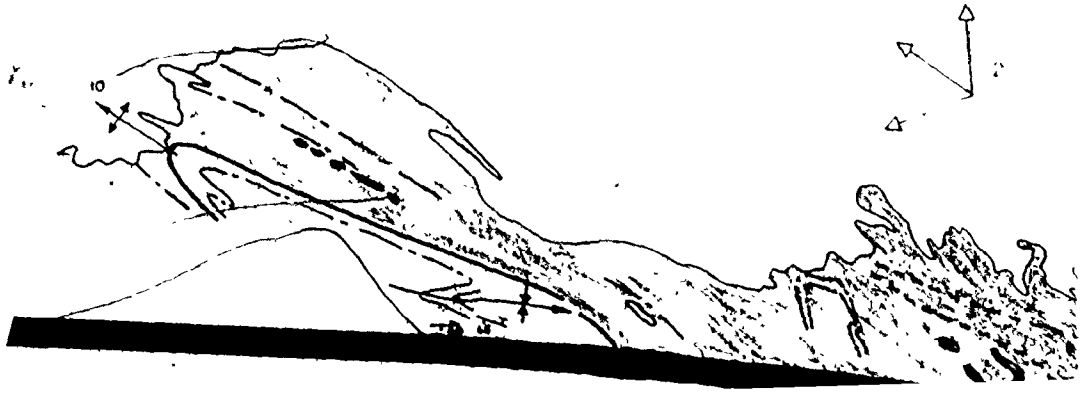

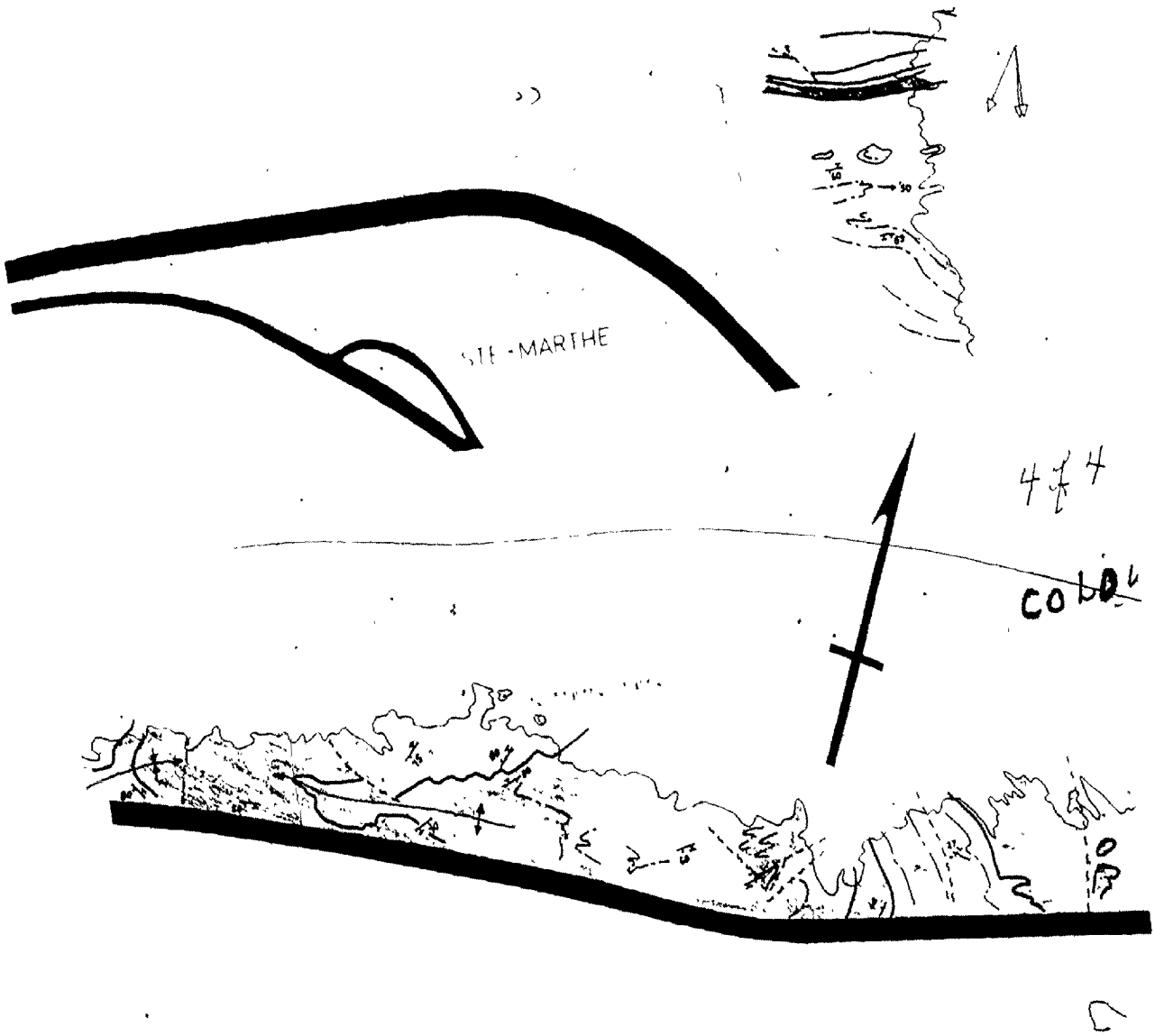
STE-MARTHE
COLD

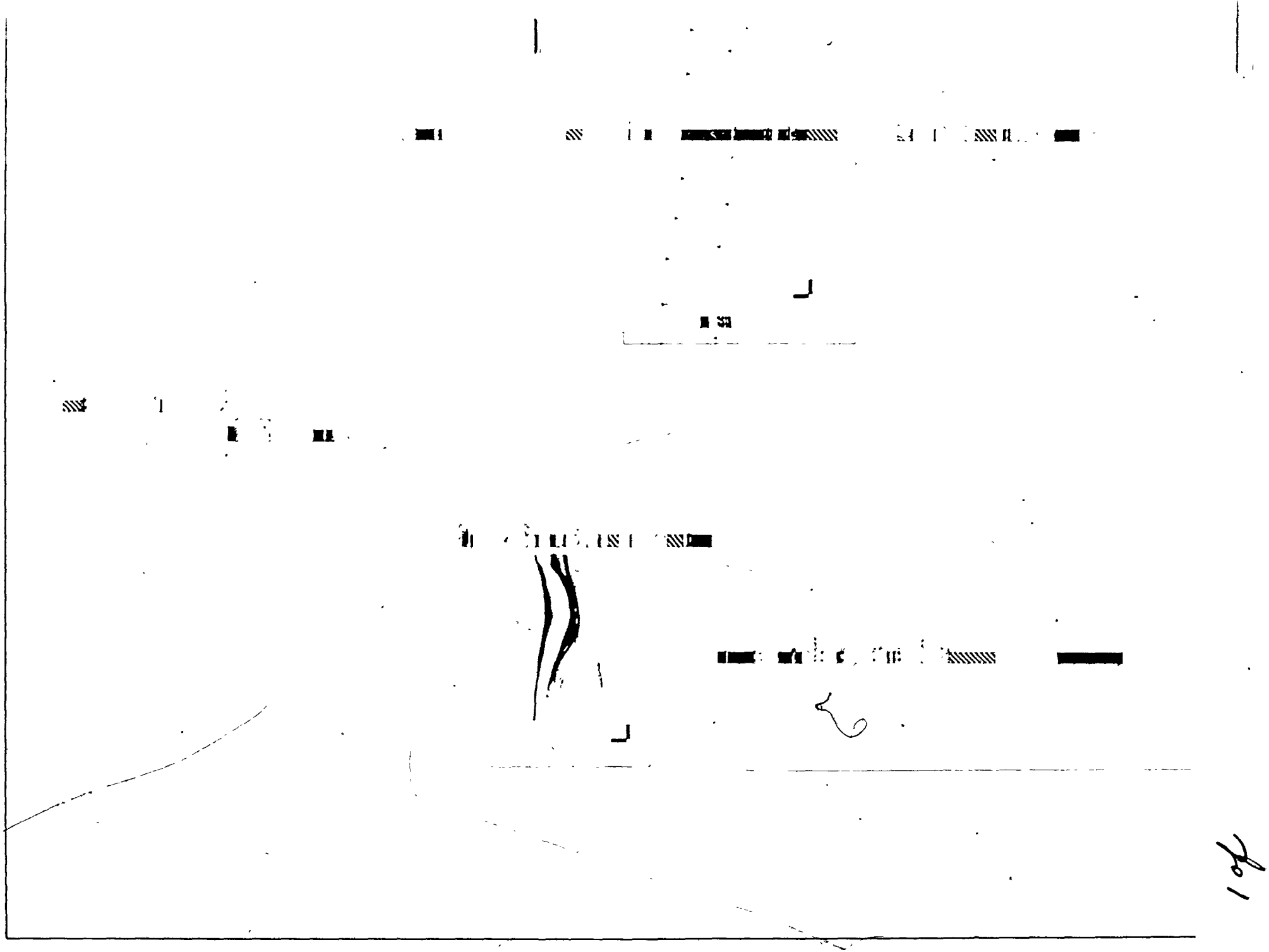

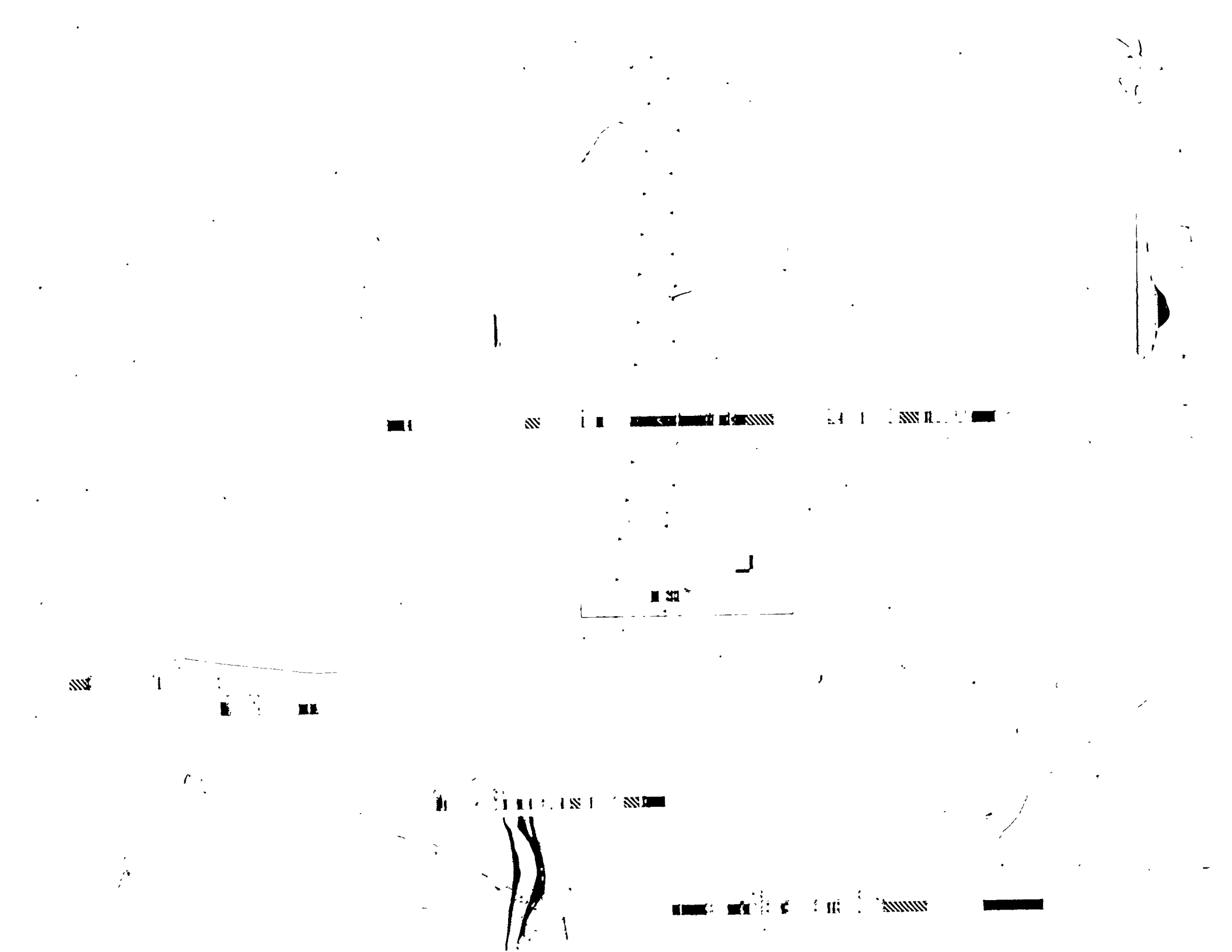

3 of

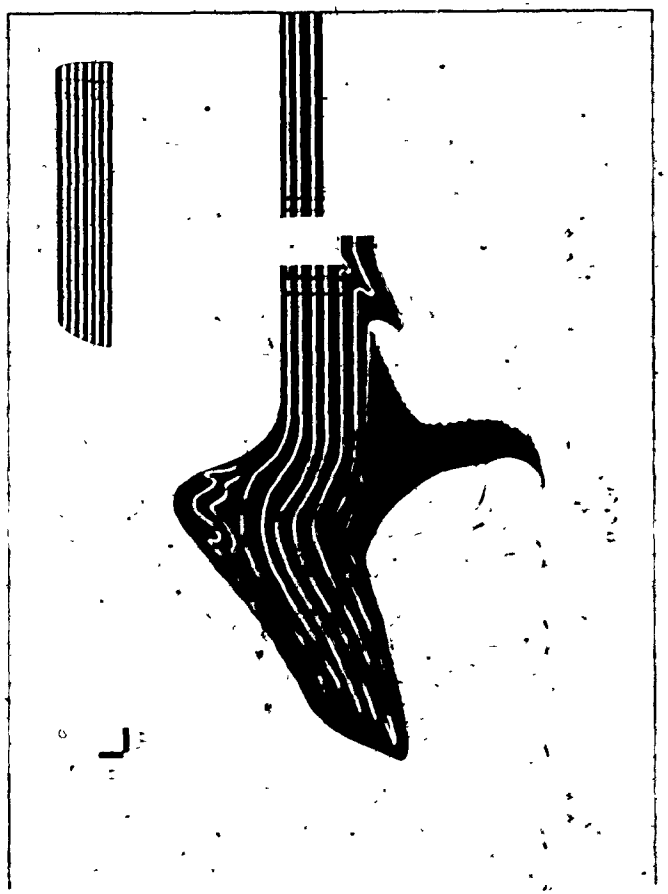

AI

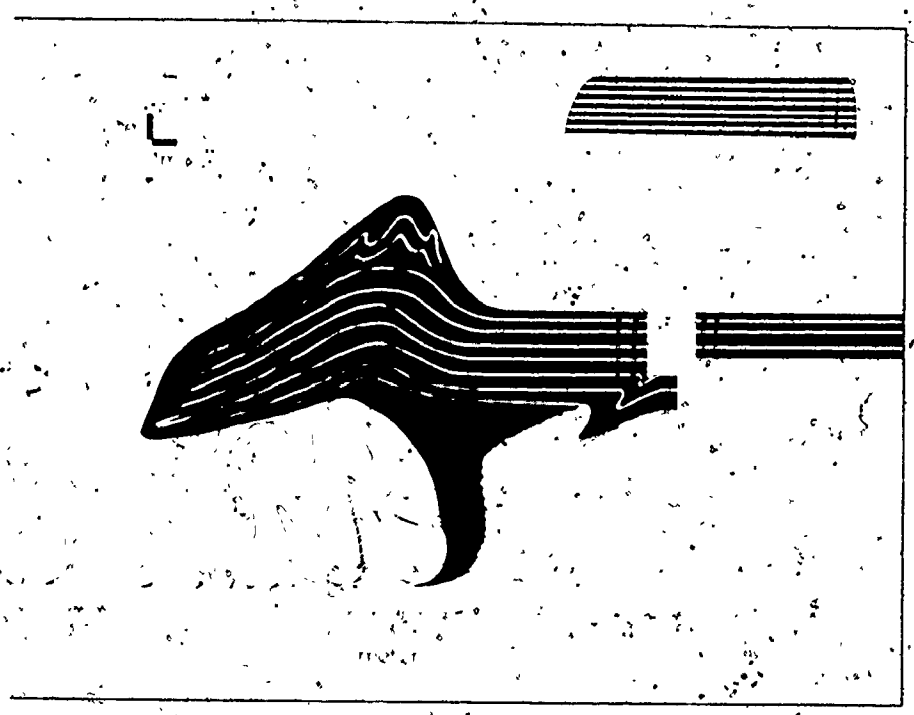

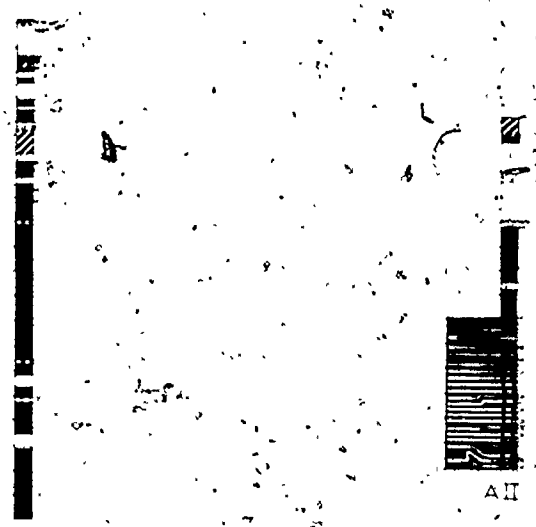
AII

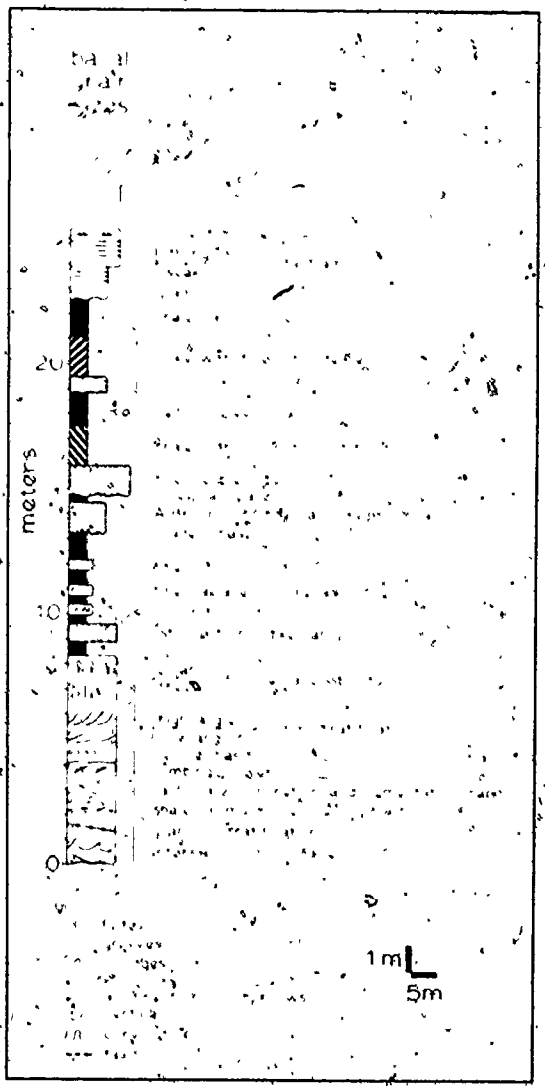
meters
20
10
0
1m
5m


AI

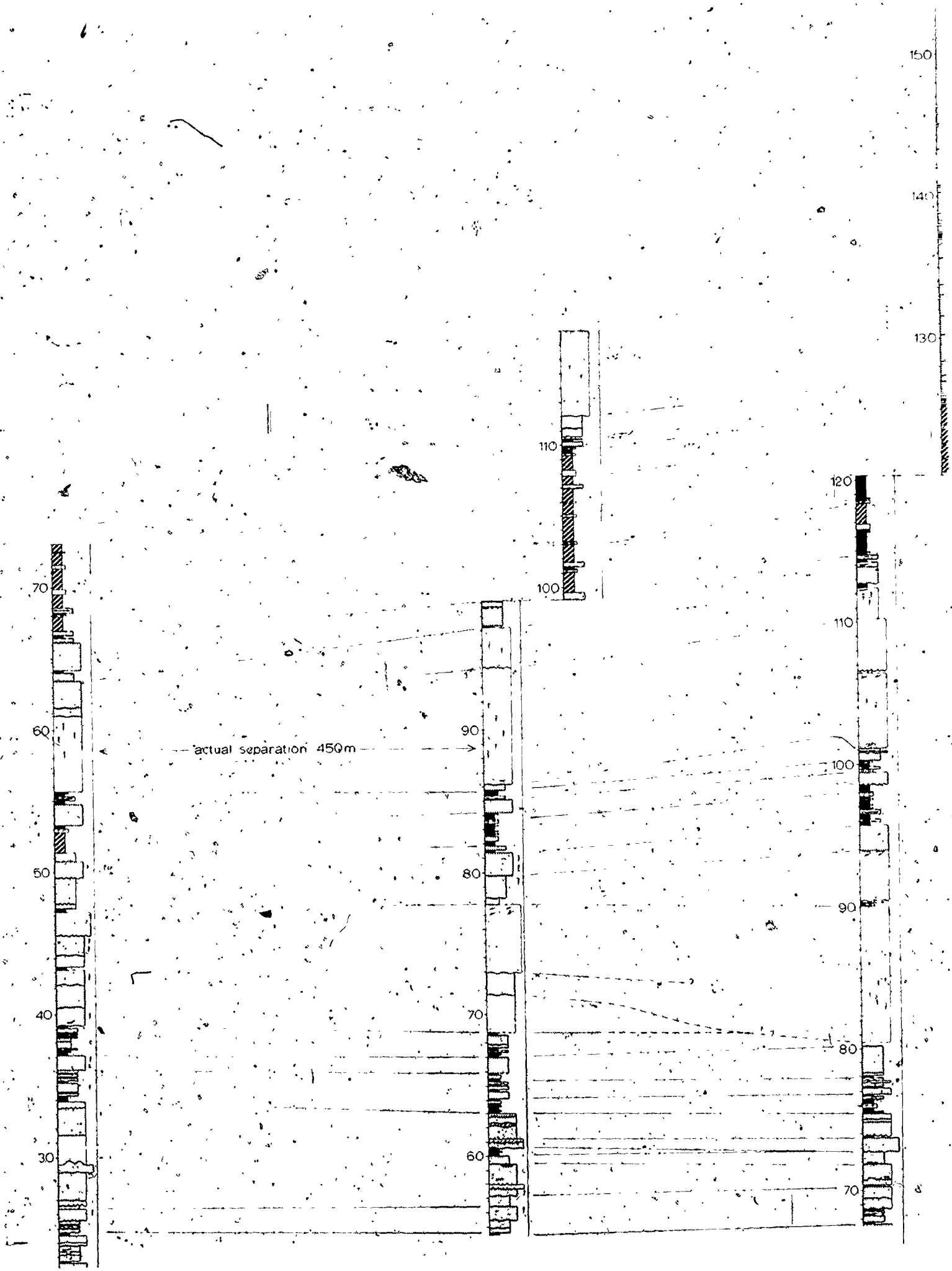
150
140
130
110
100
120
110
70
60
50
40
30
90
80
70
60
actual separation 450m
100
90
80
70

2 of 2

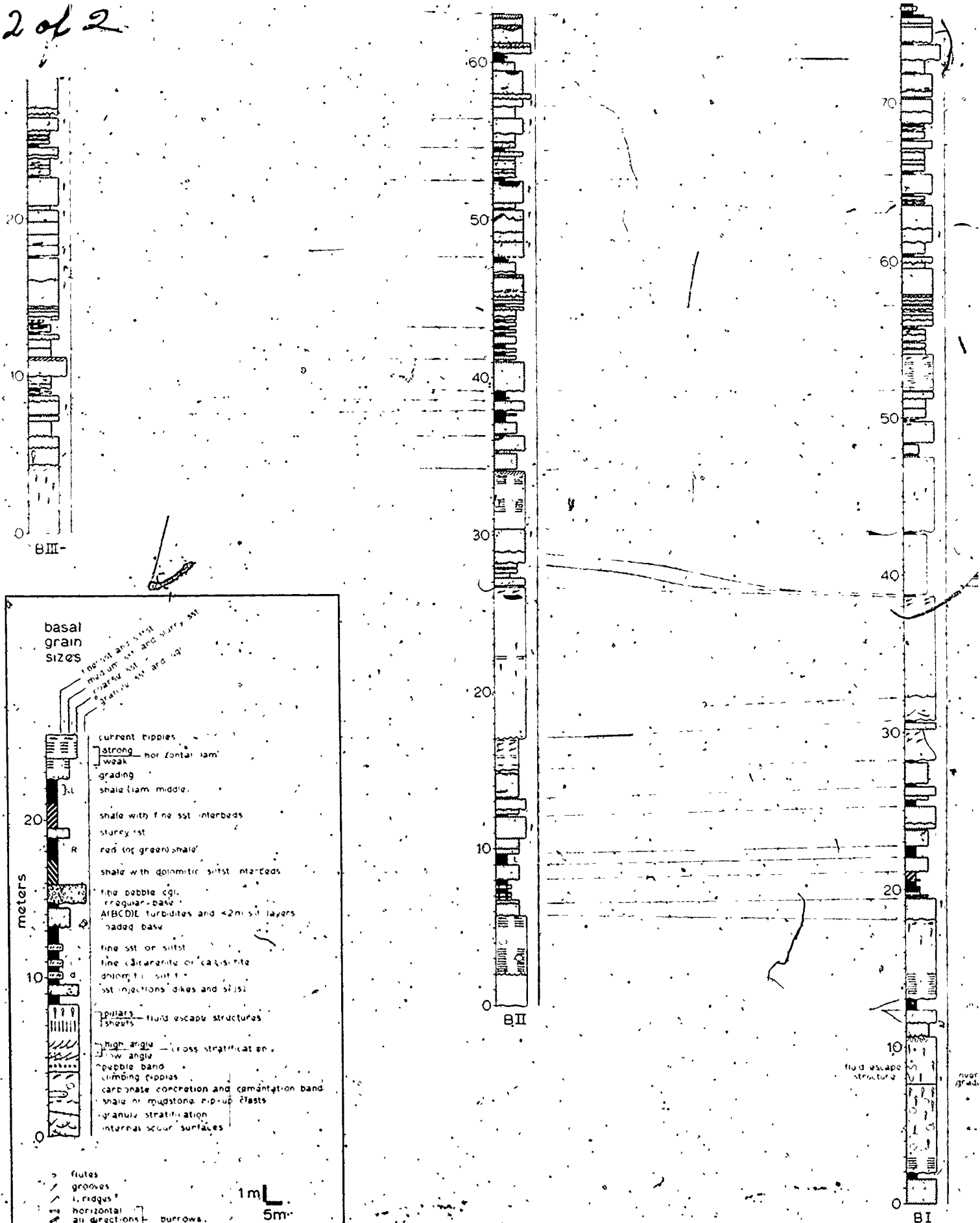
basal grain sizes
mudstone and siltst
mudstone sst and slurry sst
coarse sst
granule sst and cgl
current ripples
strong
weak
horizontal lam
grading
shale (lam. middle)
shale with fine sst interbeds
slurry sst
R
red (or green) shale
shale with dolomitic siltst interbeds
fine pebble cgl.
irregular base
ABCDE turbidites and <2m sst layers
loaded base
fine sst or siltst
fine calcarenite or calcisiltite
dolomitic siltst
sst injections, dikes and sills
pillars
sheets
fluid escape structures
high angle
low angle
cross stratification
pebble band
climbing ripples
carbonate concretion and cementation band
shale or mudstone rip-up clasts
granule stratification
internal scour surfaces
meters
flutes
grooves
ridges
horizontal
all directions
vertical
burrows
convolution
fault
1m
5m
BIII
BII
BI
fluid escape structure

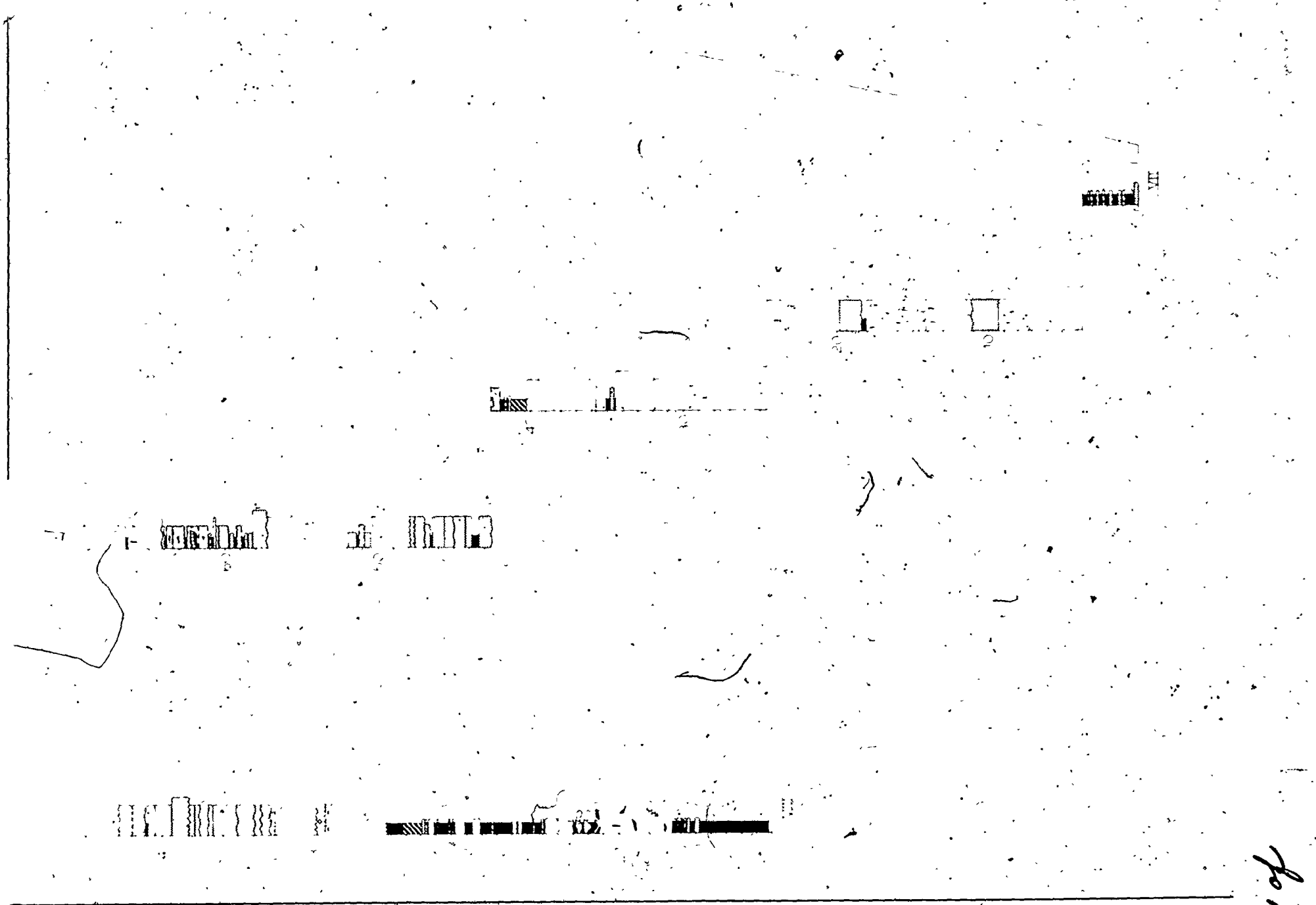

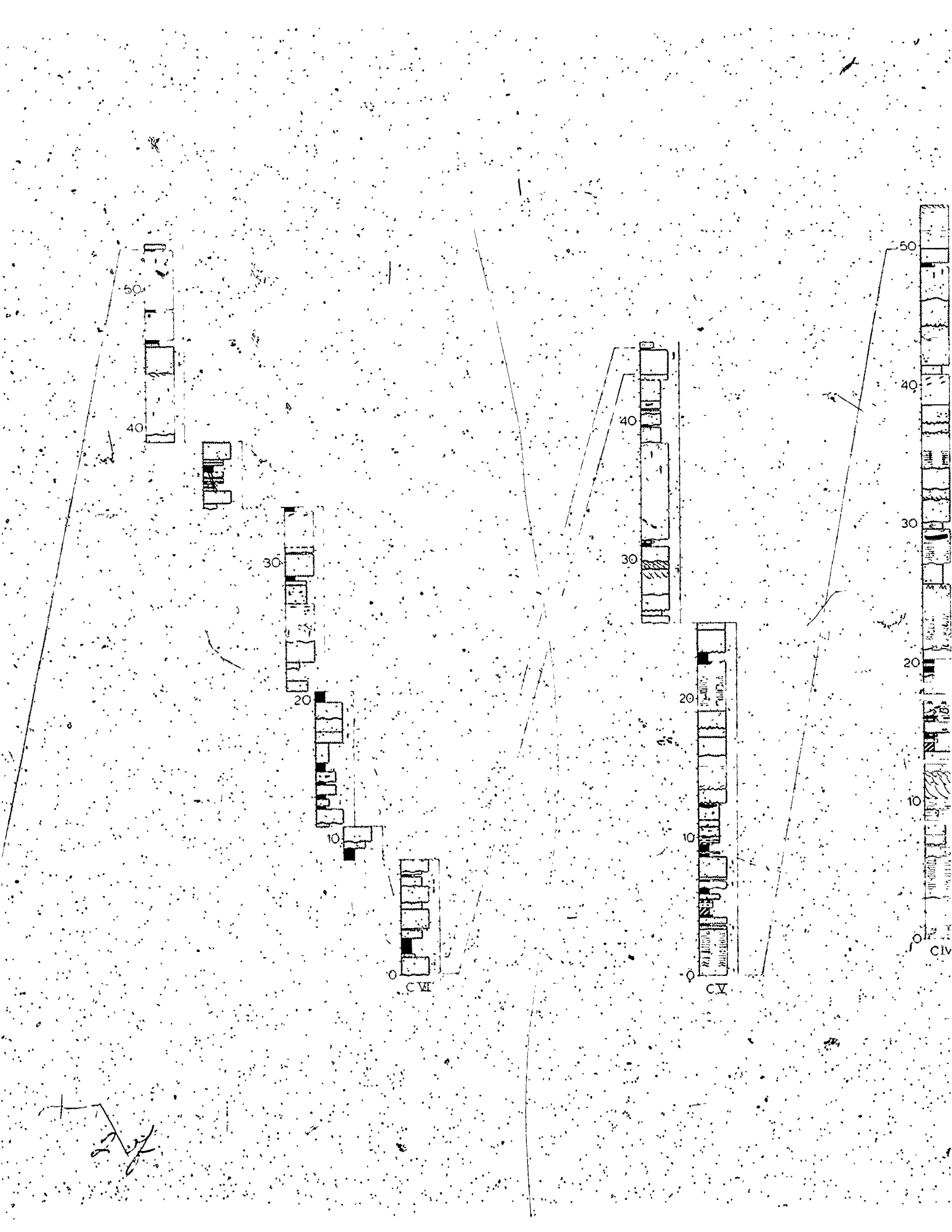
50
40
30
20
10
0
CVI
40
30
20
10
0
CV
50
40
30
20
10
0
CIV

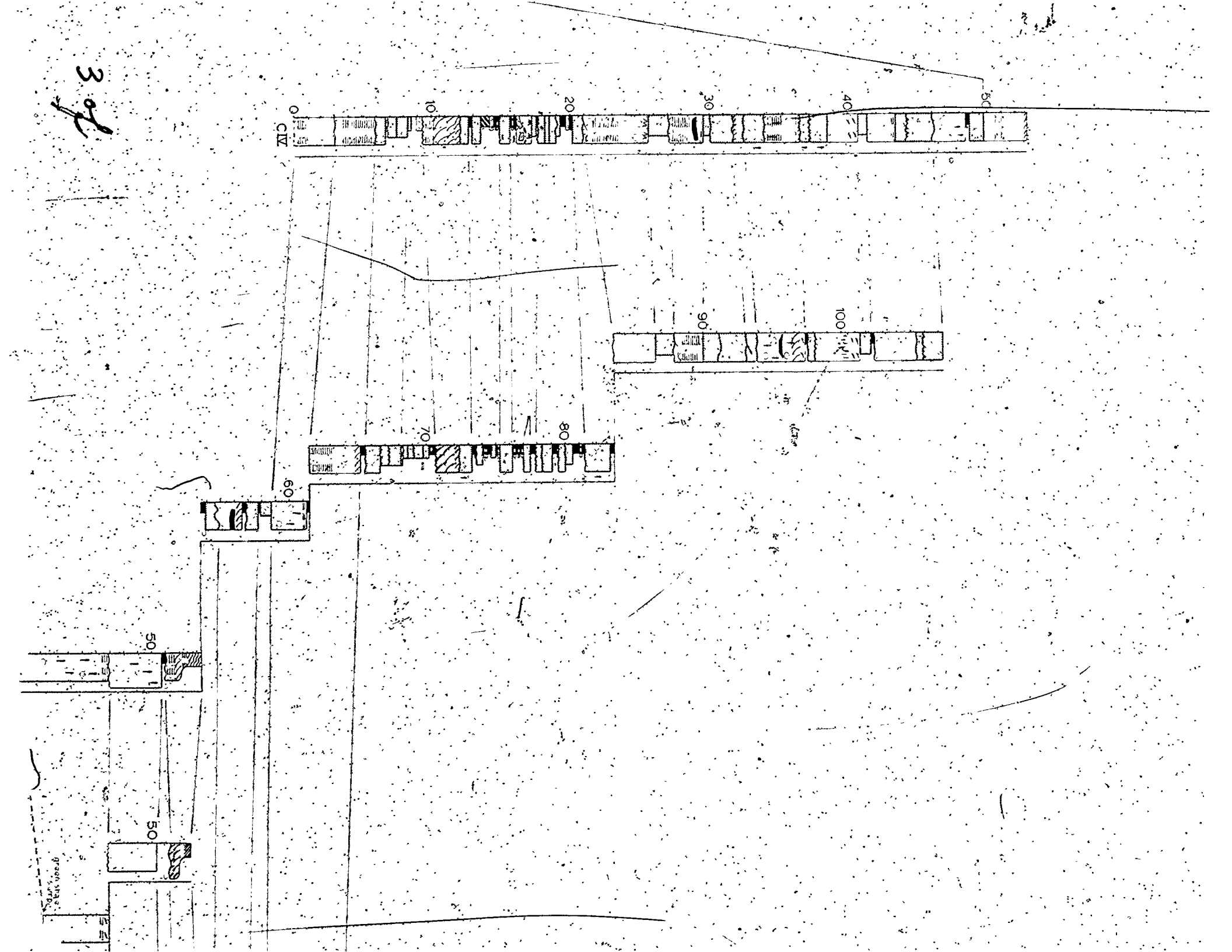
0
10
20
30
40
50
60
70
80
90
100
50
50

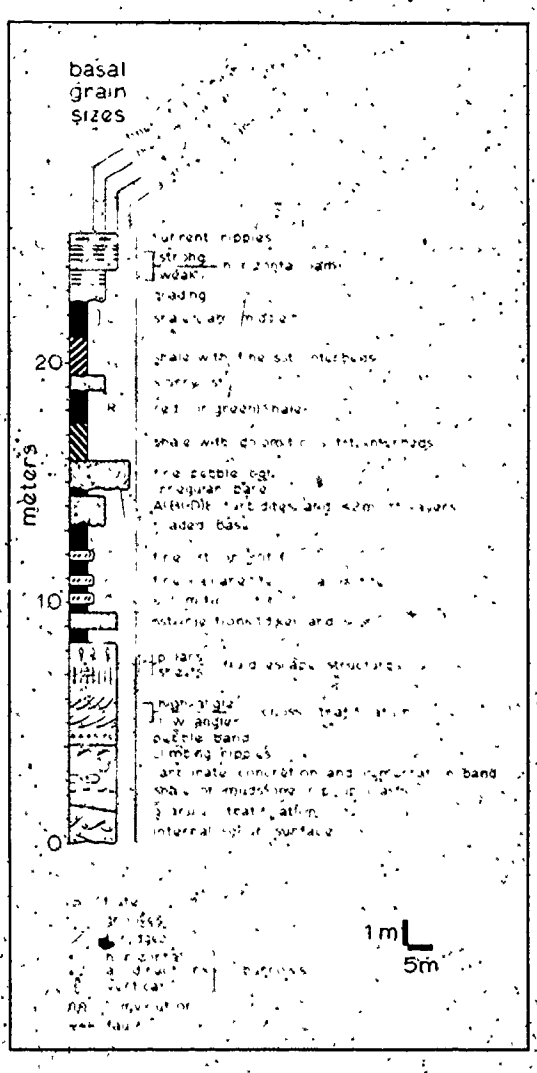
basal
grain
sizes
meters
20
10
0
current ripples
1m
5m

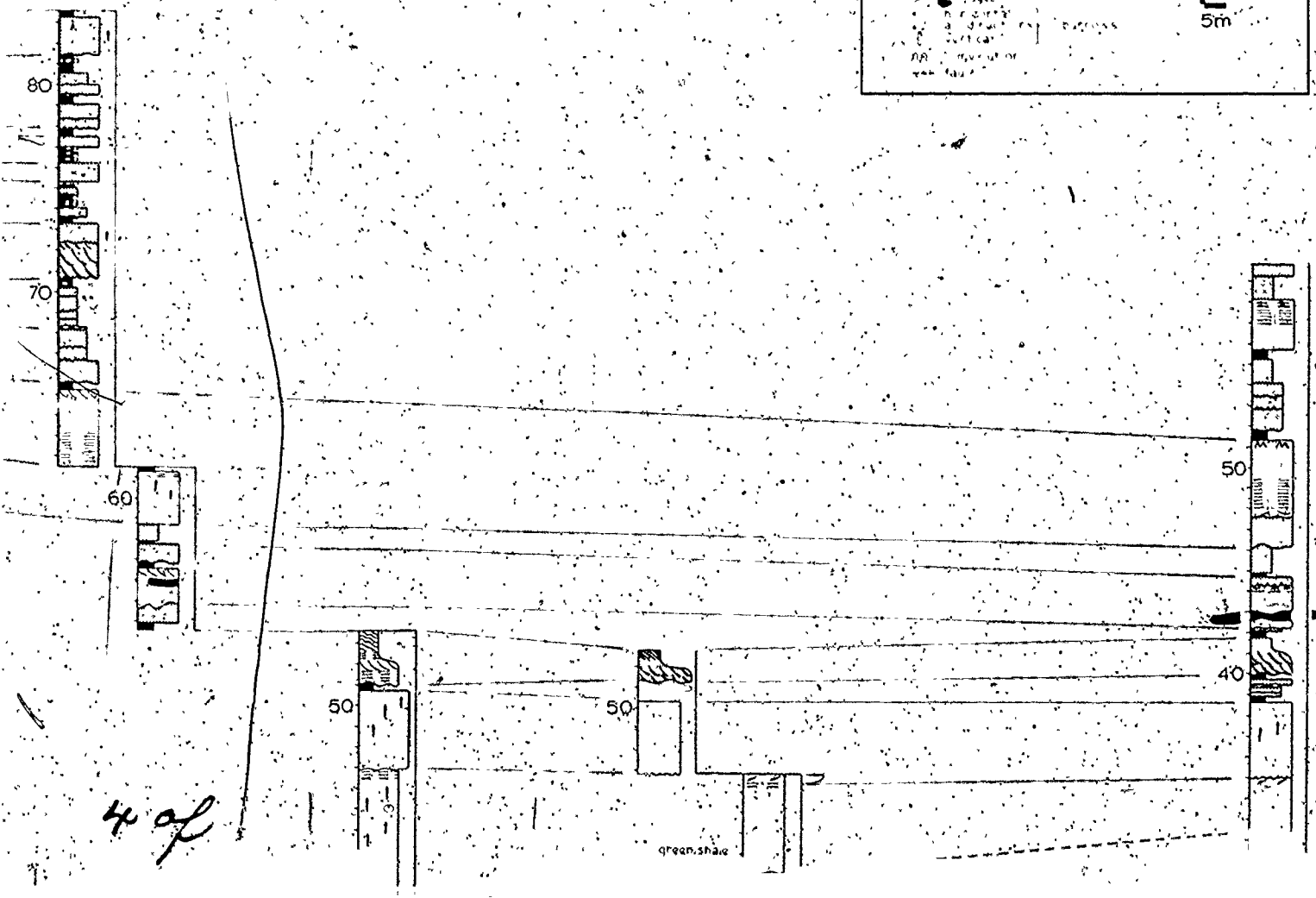
80
70
60
50
50
50
40
green shale

4 of

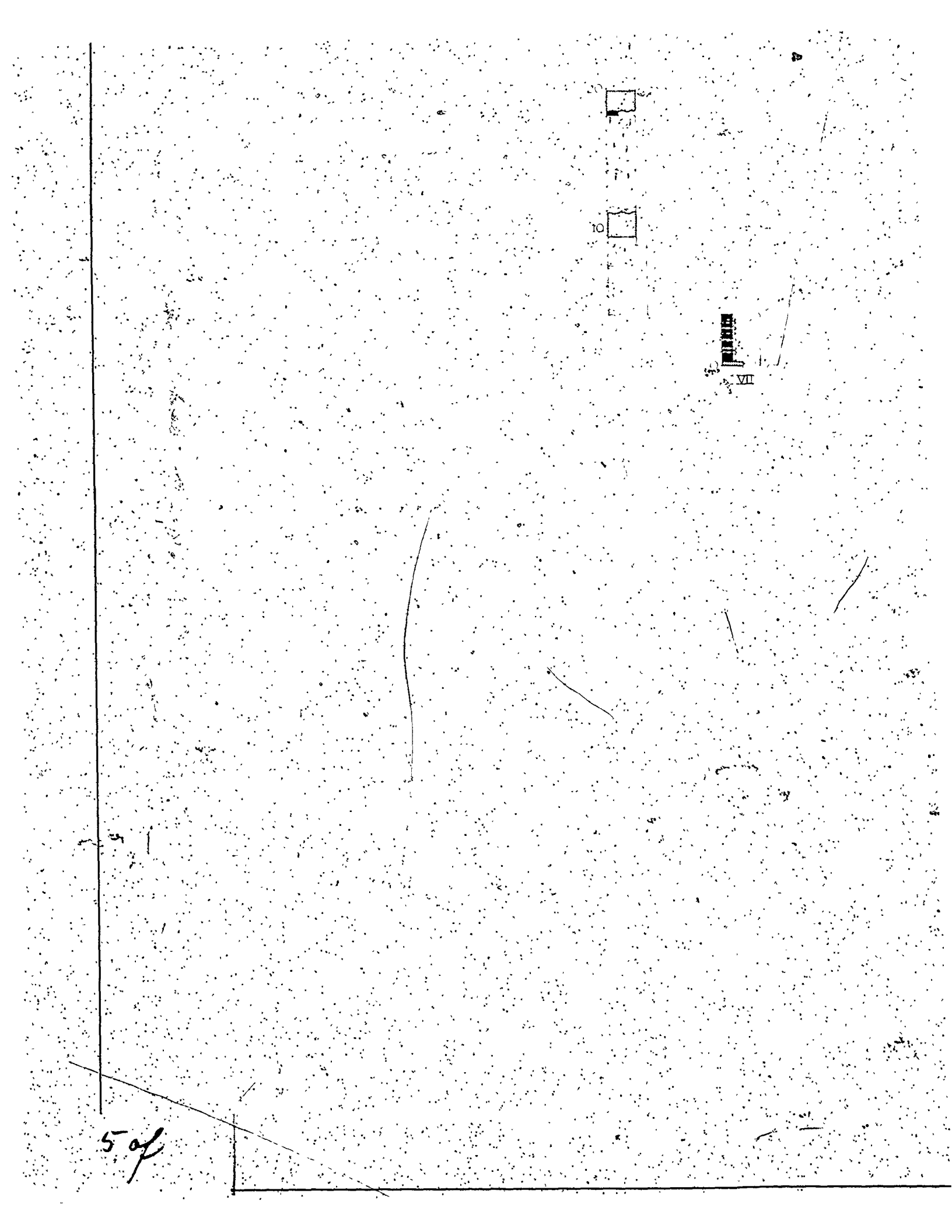

5 of

60

10
0
CIV
70
60
50
40
30
20
10
0
CIII
50

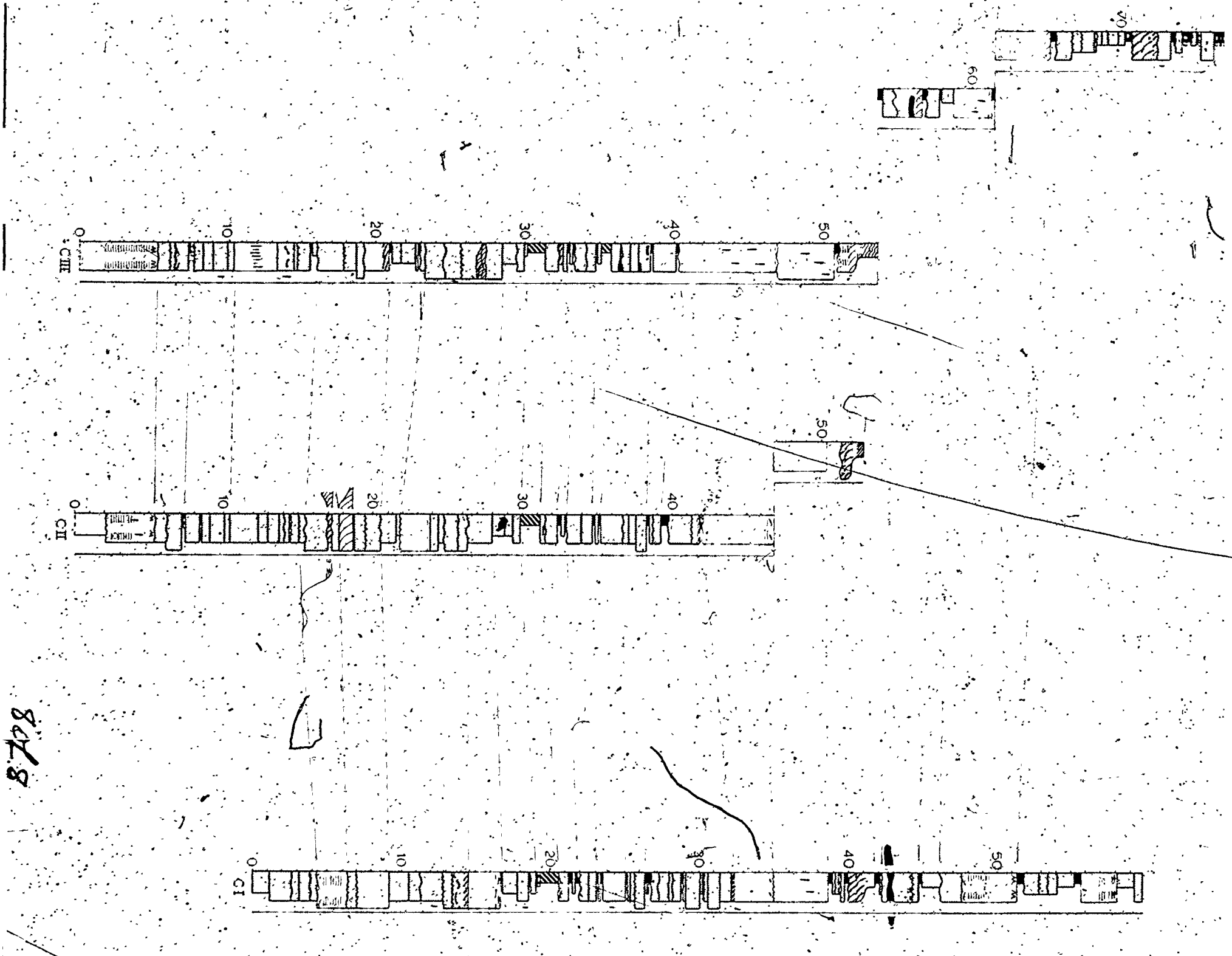

8798

1 of

BLANK

BLANK

3a

4 of 1

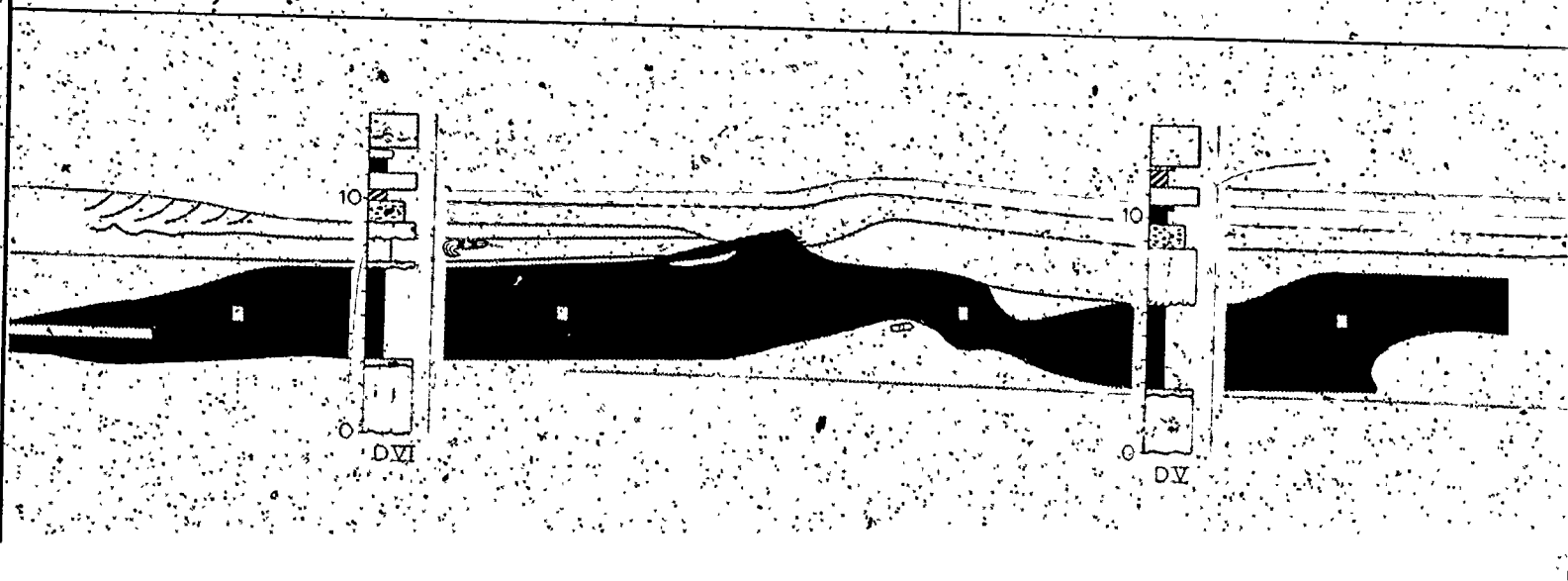

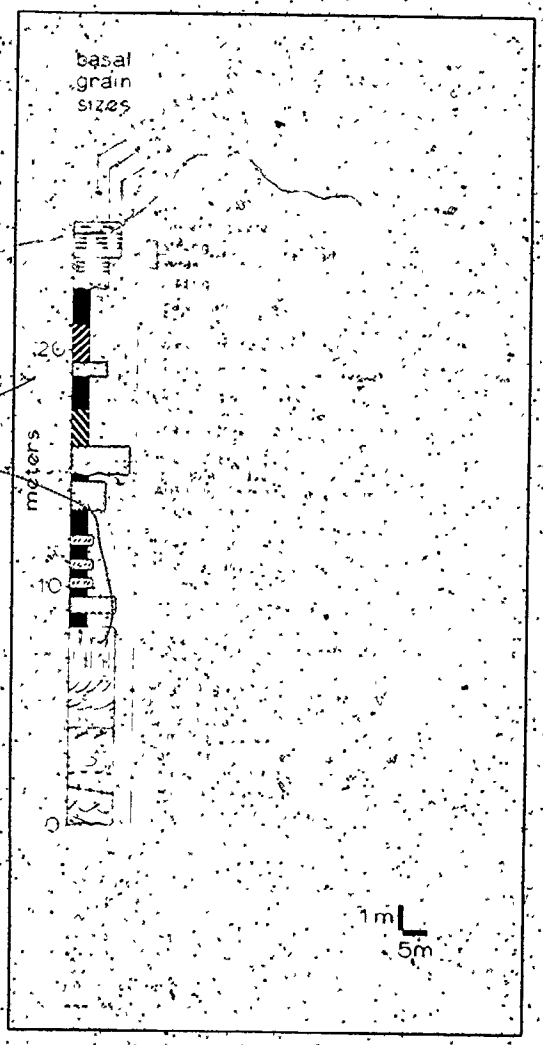
basal
grain
sizes
20
meters
10
0
1m
5m

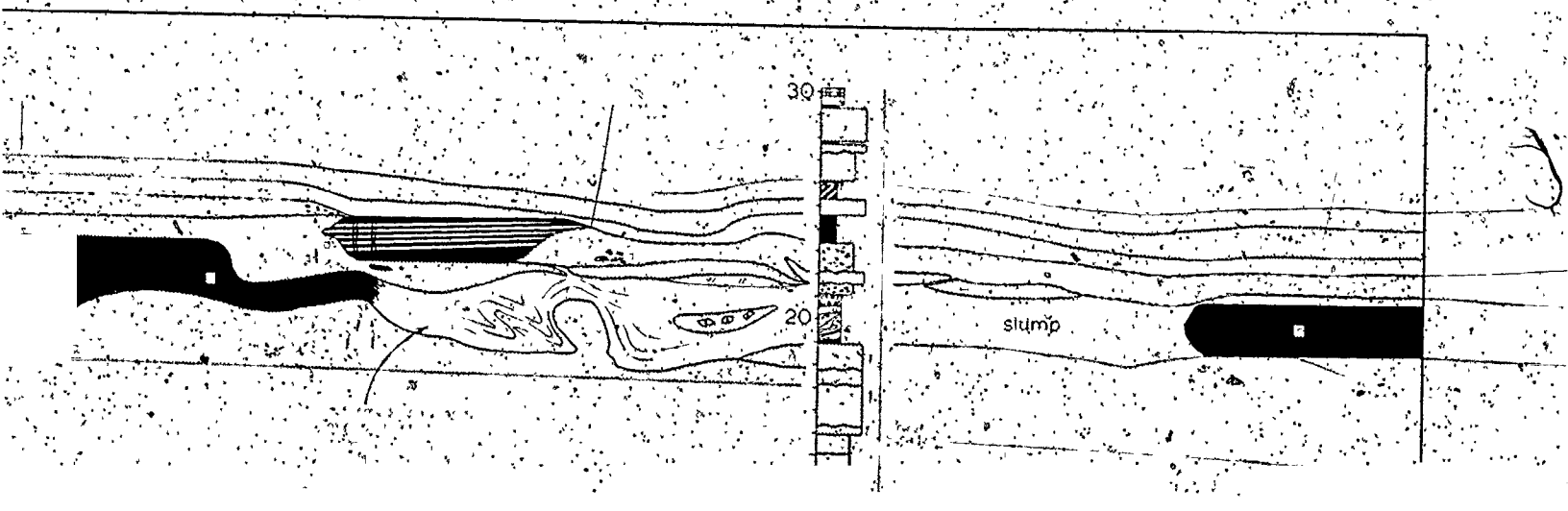
30
20
slump

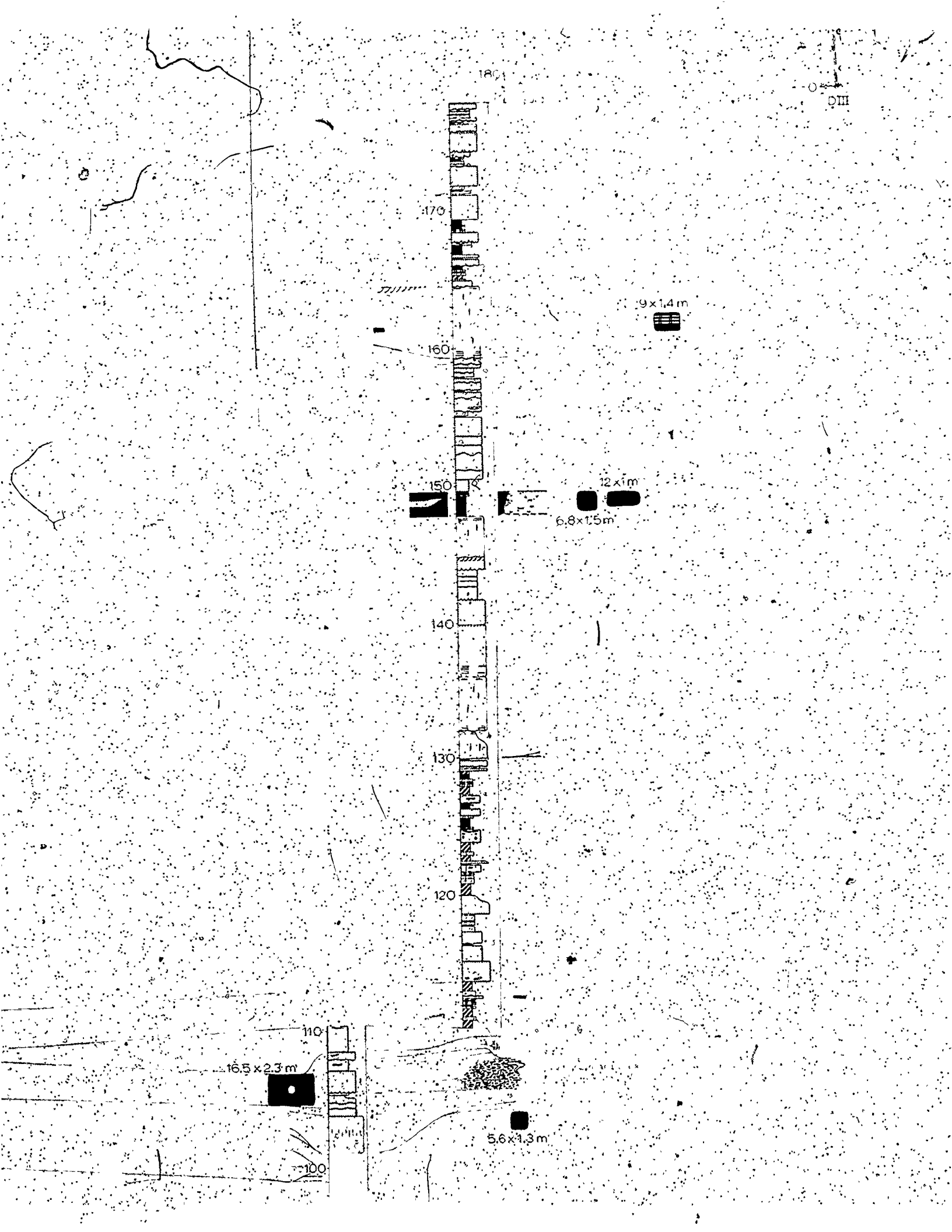
180
170
160
150
140
130
120
110
100
9x1.4 m
12x1m
6.8x1.5m
16.5x2.3 m
5.6x1.3 m
DIII

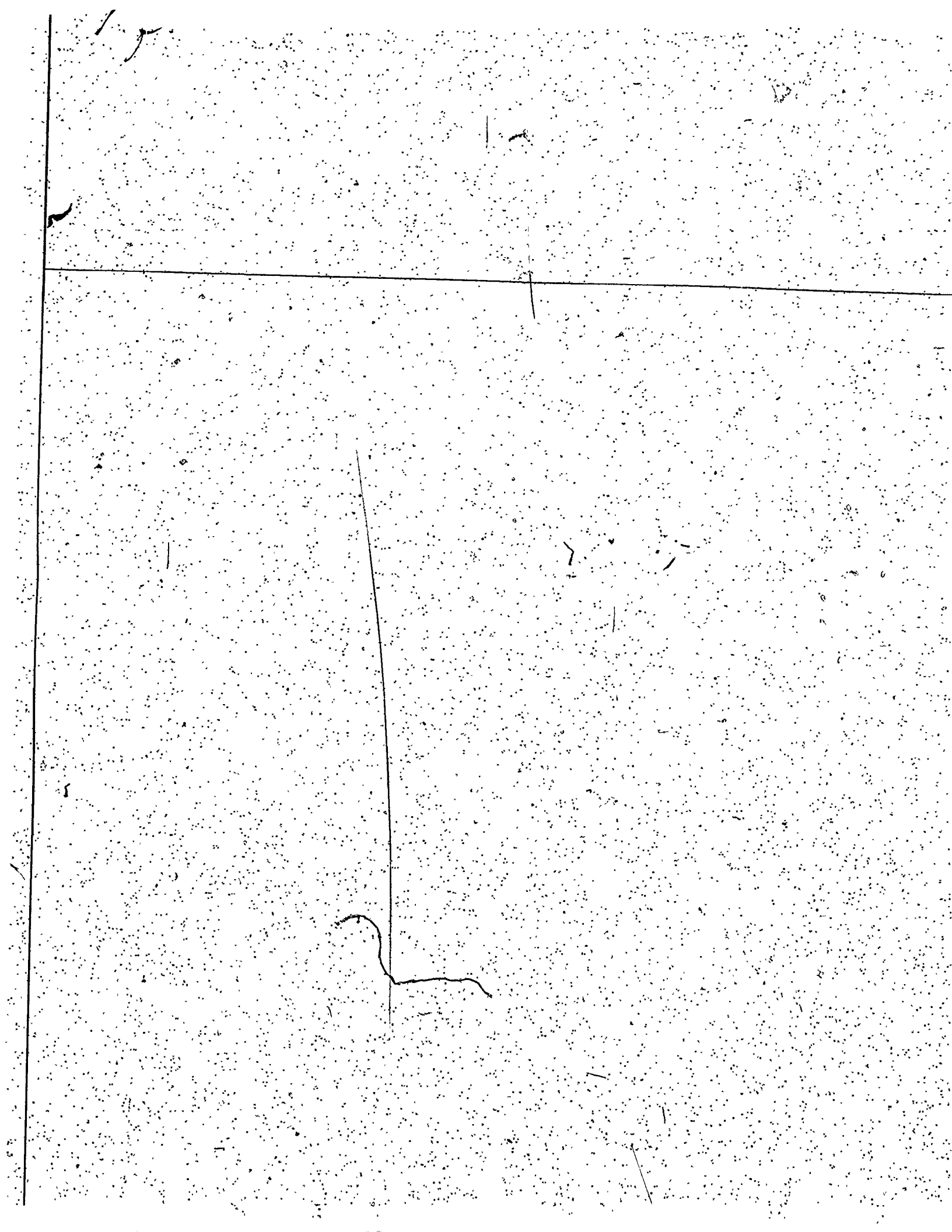

8 of

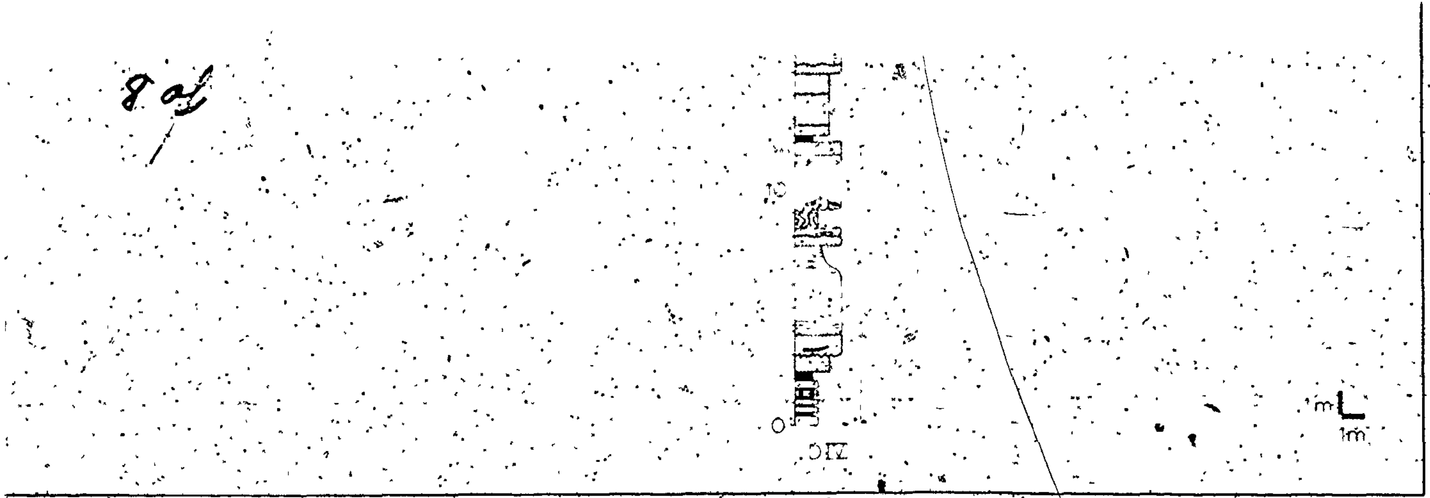

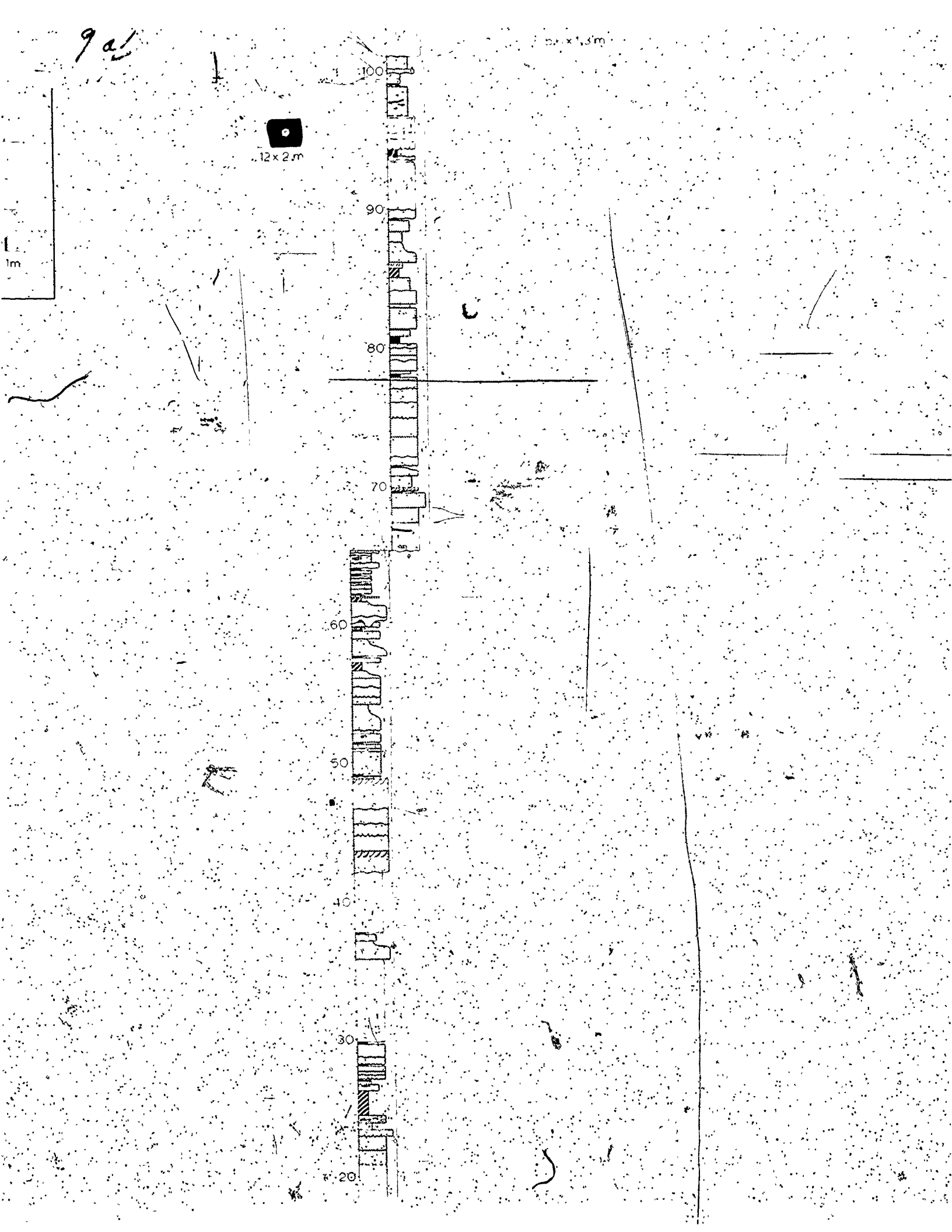
9a
12 x 2 m
100
90
80
70
60
50
40
30
20

BLANK

11 of BLANK

1-87 11

D II

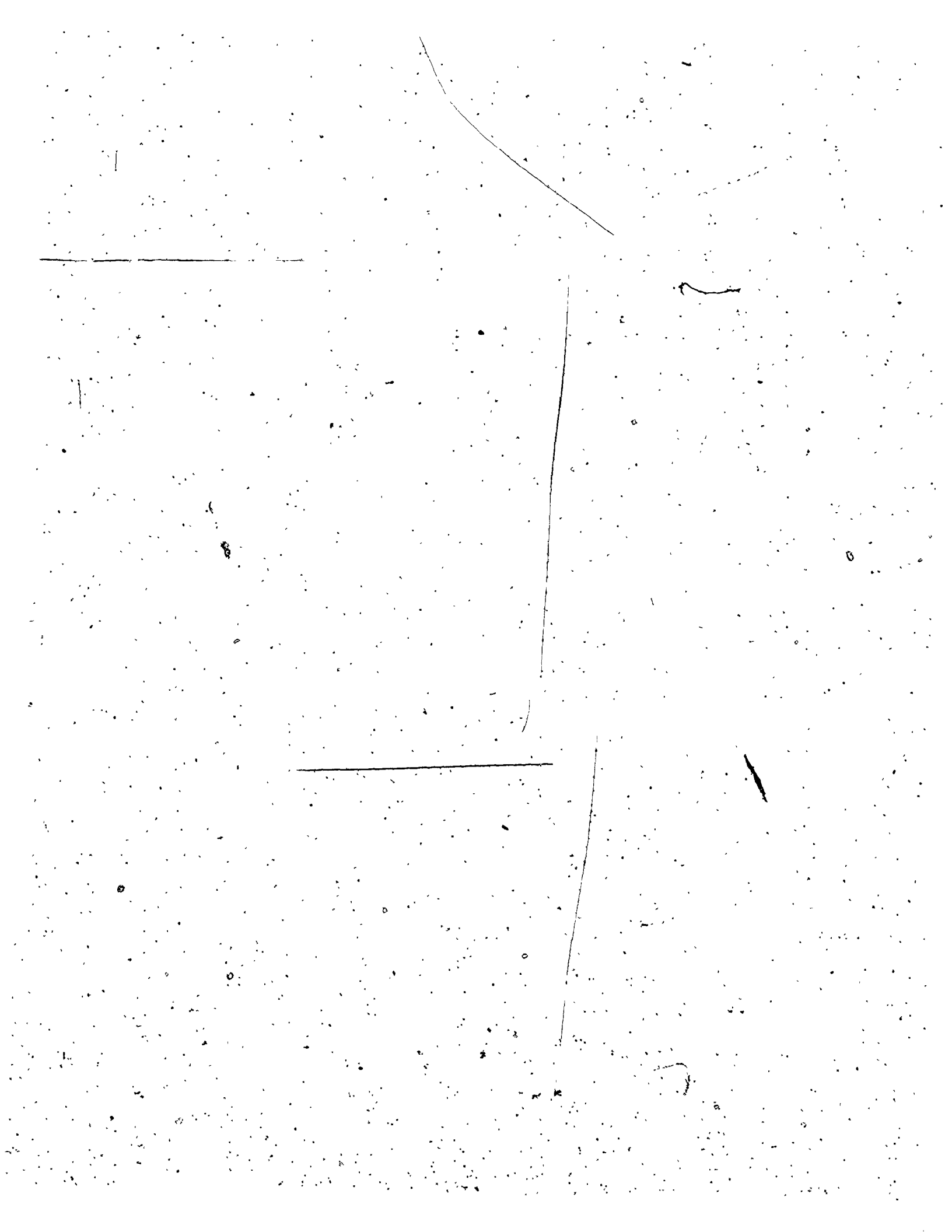

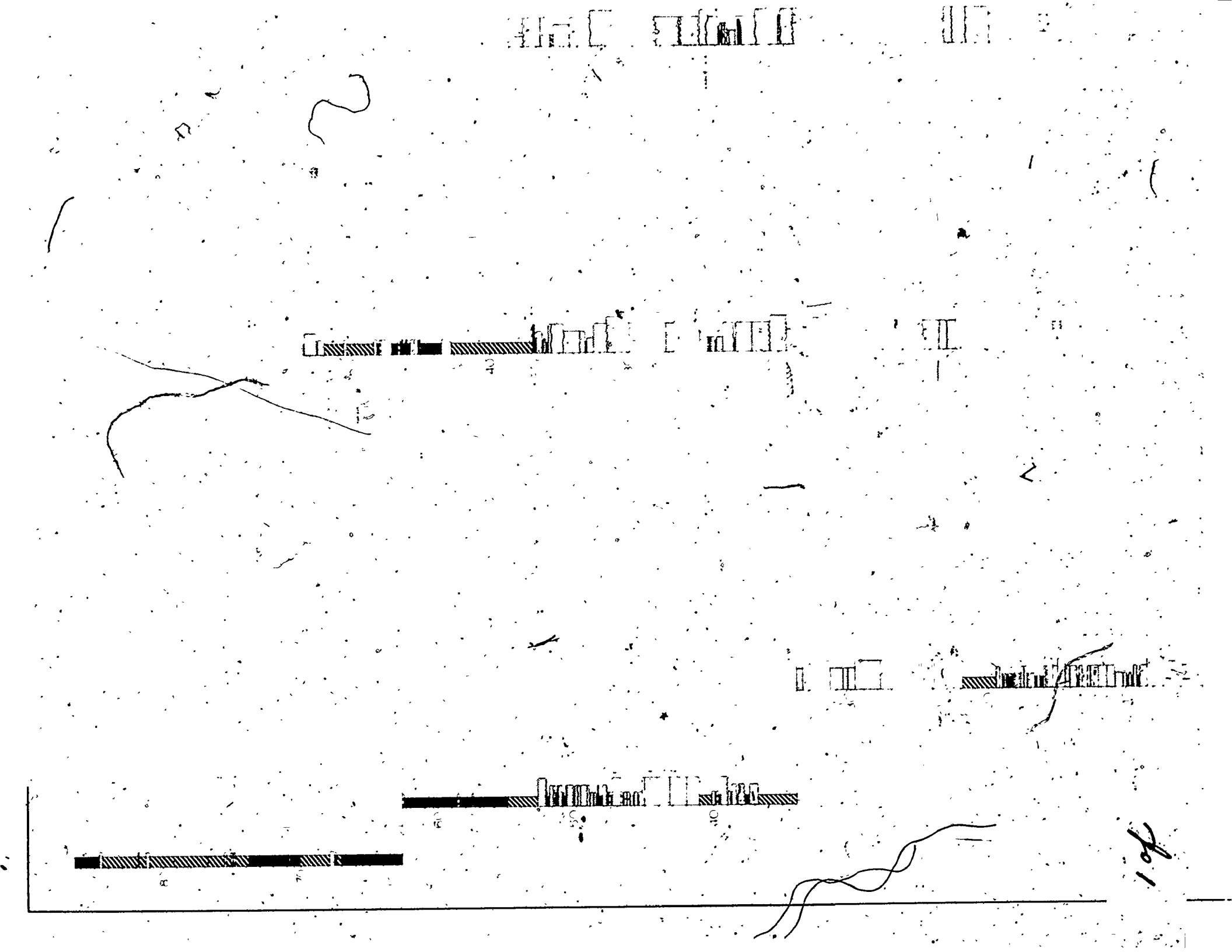

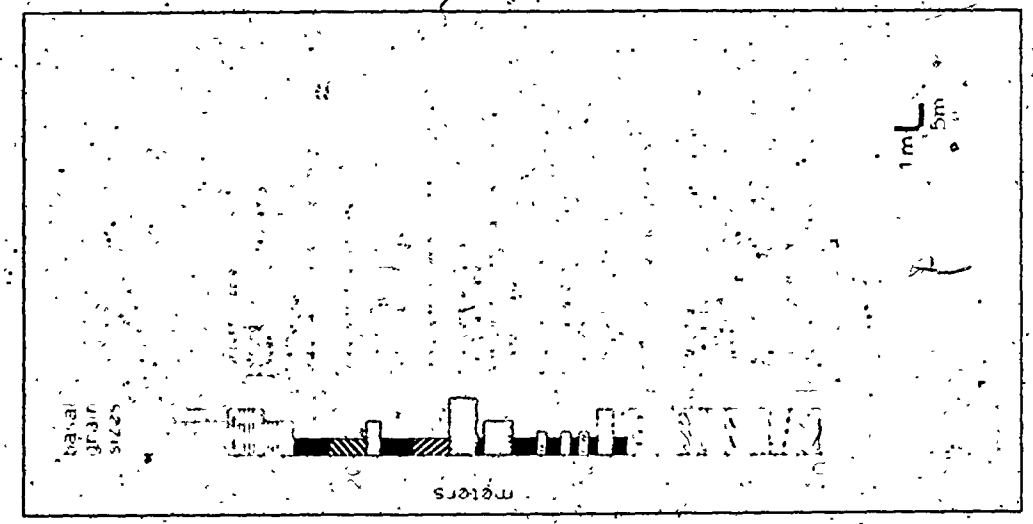
1m
5m
metres

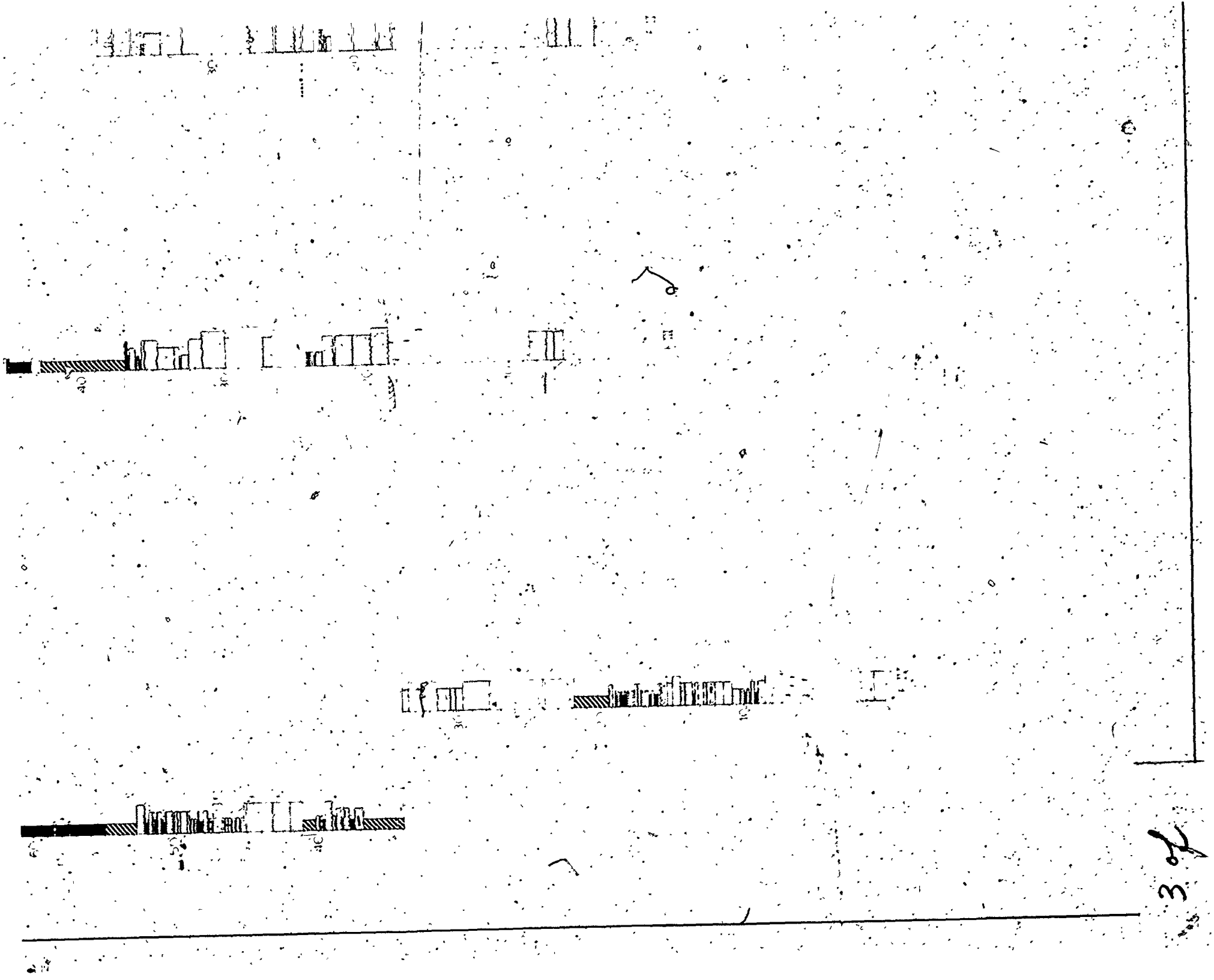

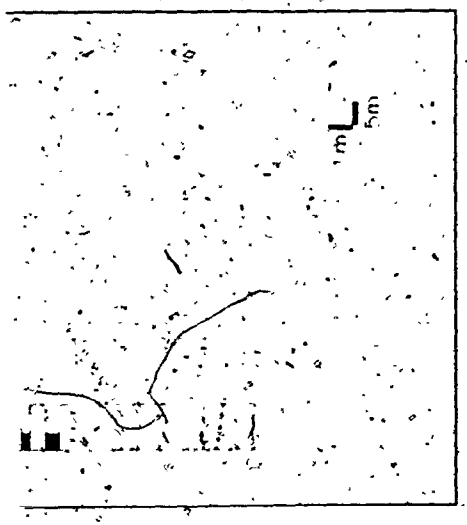
5m

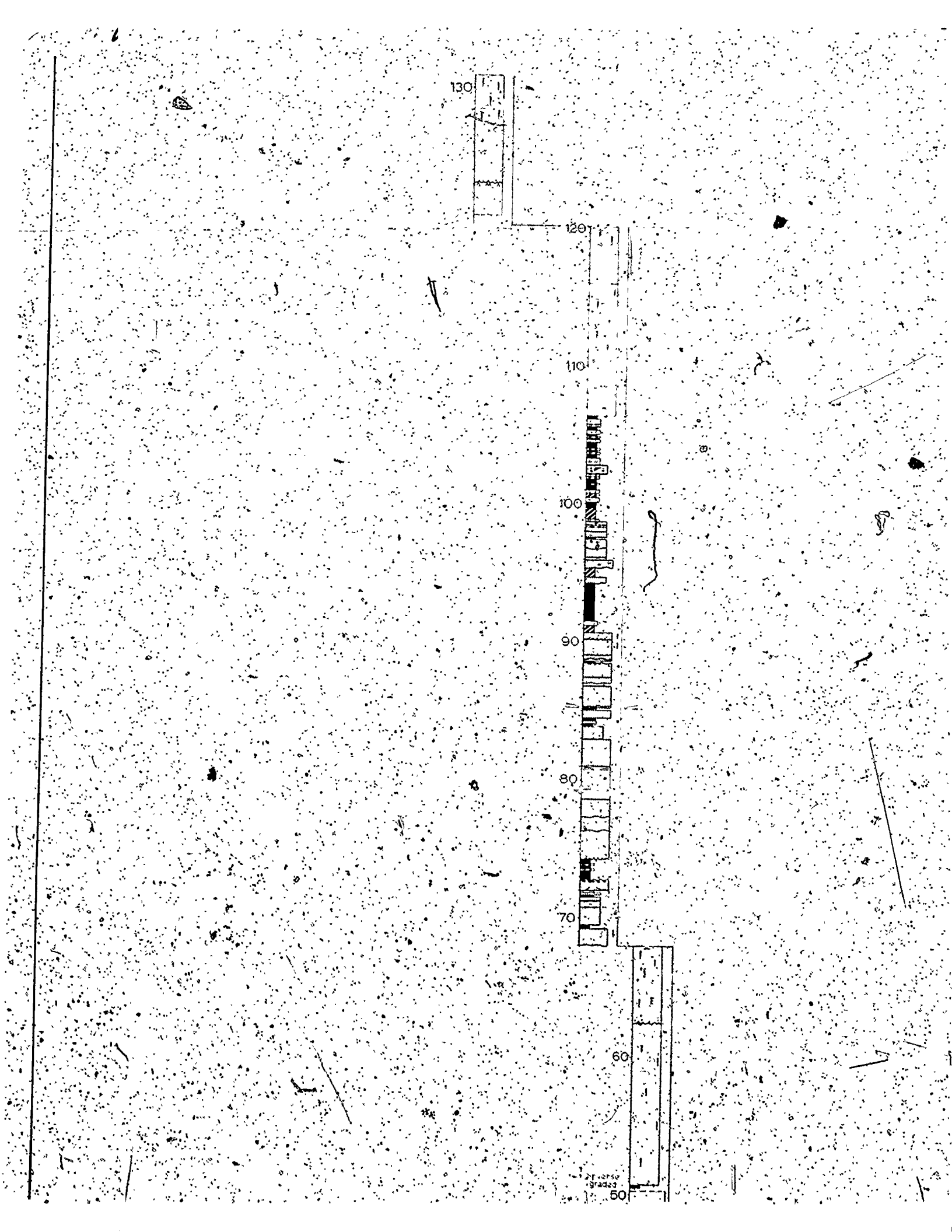
130
120
110
100
90
80
70
60
50

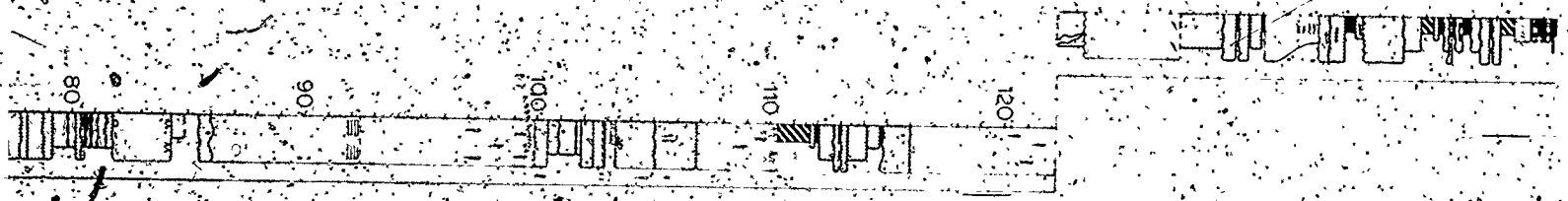
80
90
100
110
120

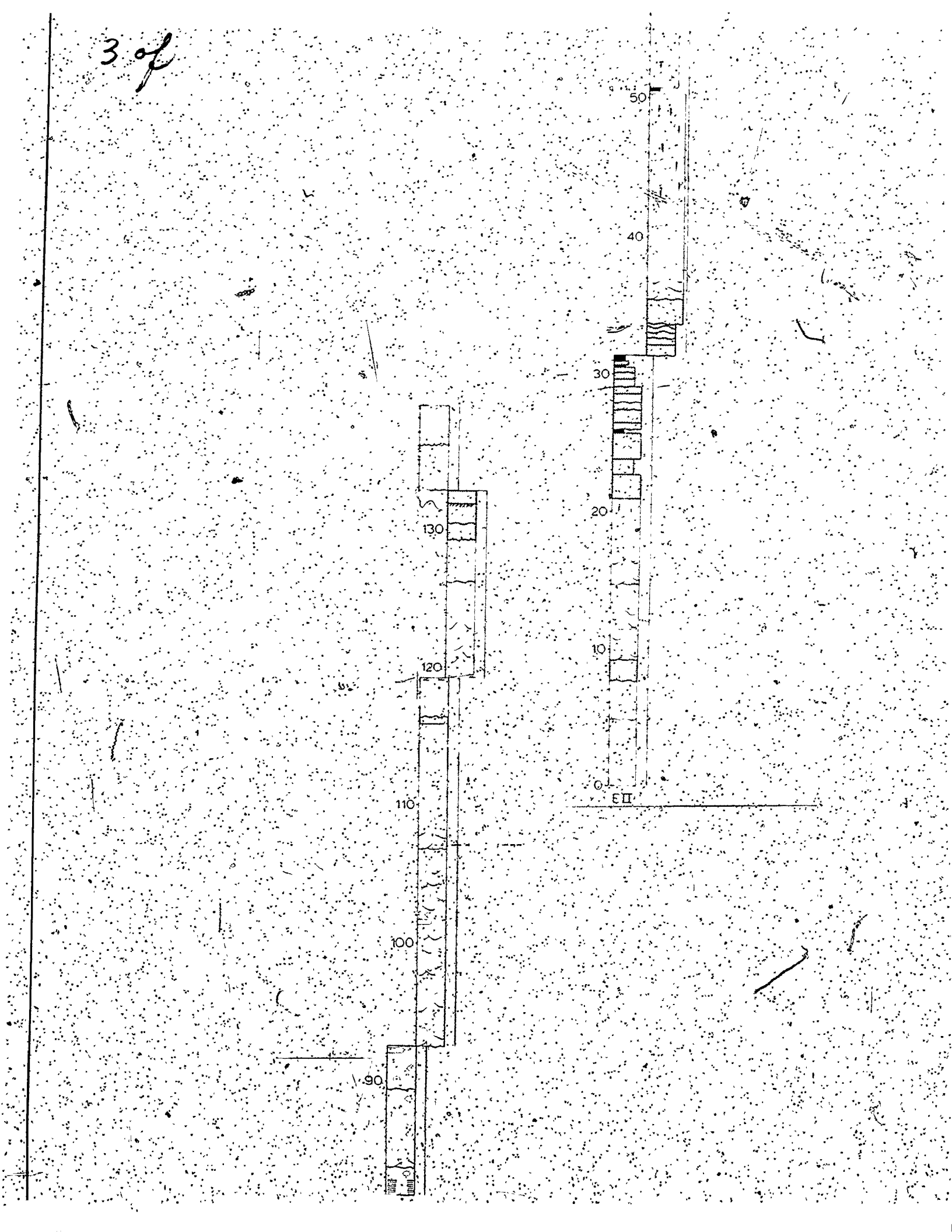
50
40
30
20
10
0
E II
130
120
110
100
90

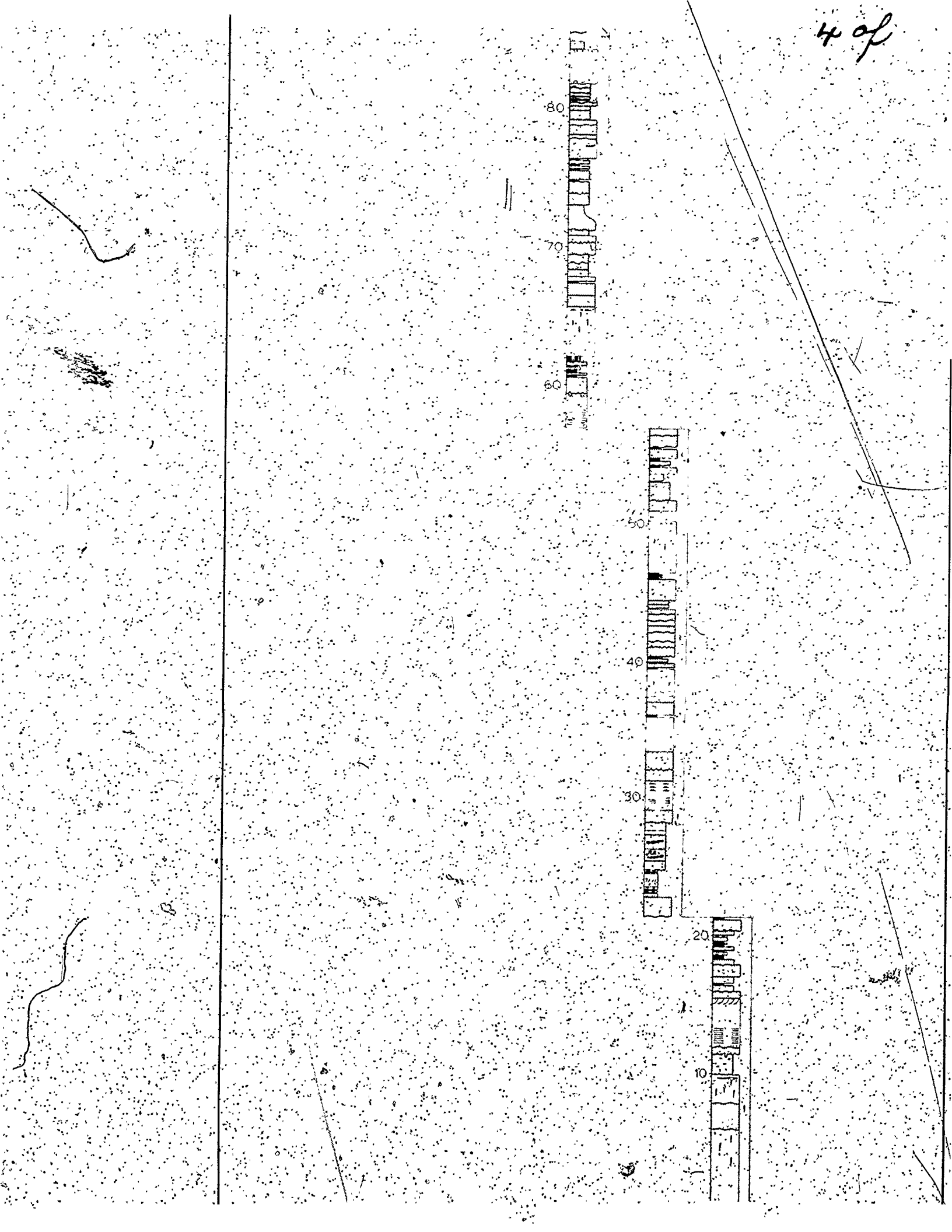
80
70
60
50
40
30
20
10

5 of

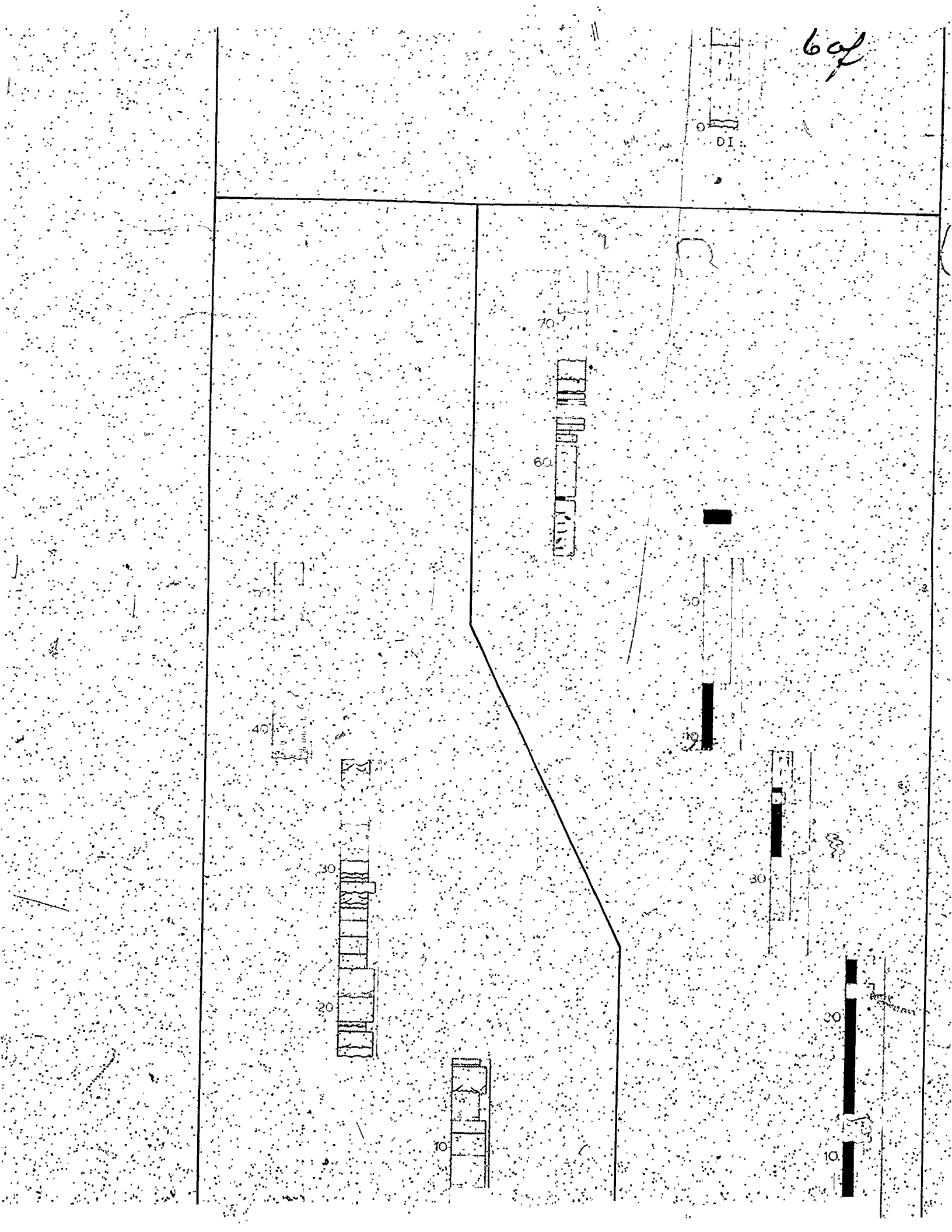
0
70
60
50
40
30
20
10

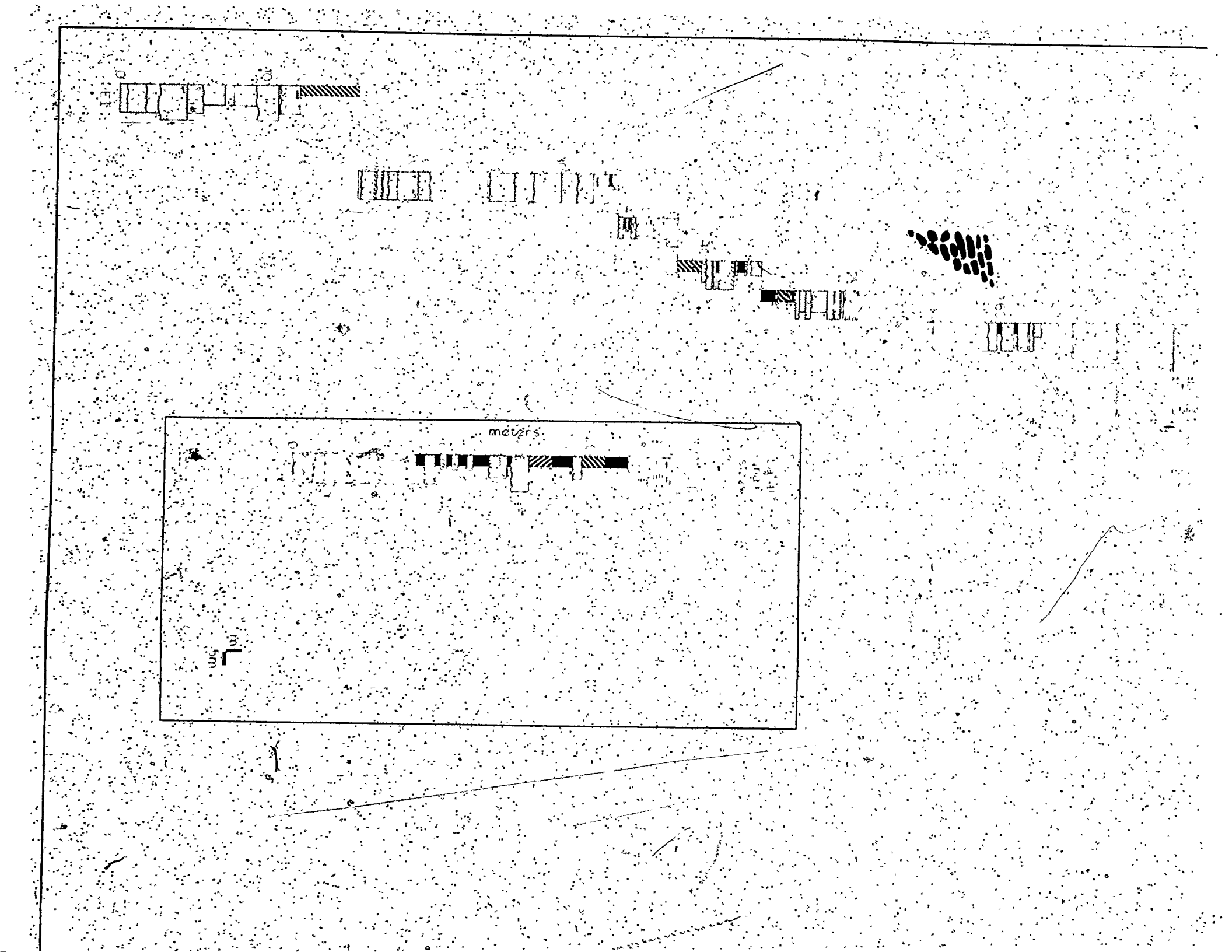
meters

8078.

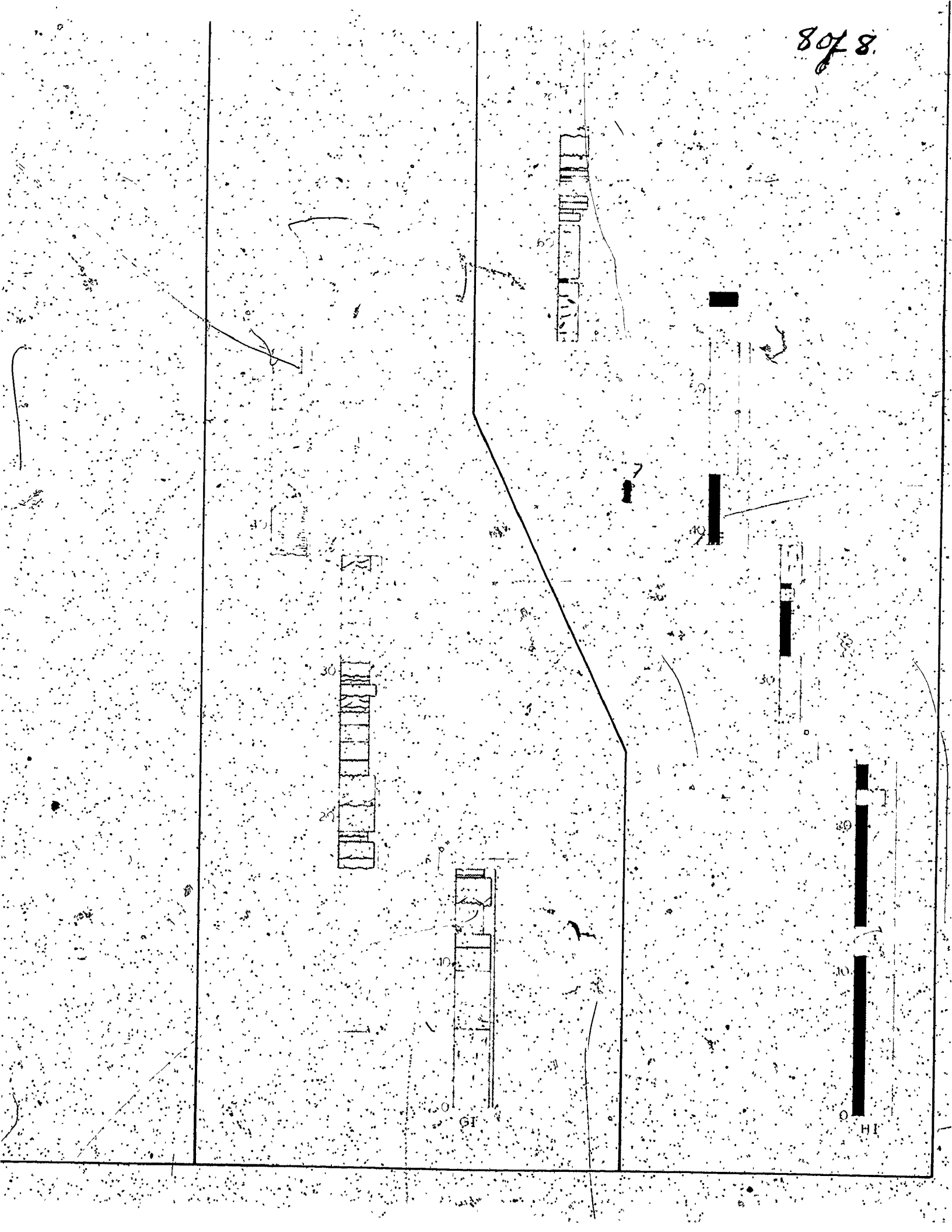

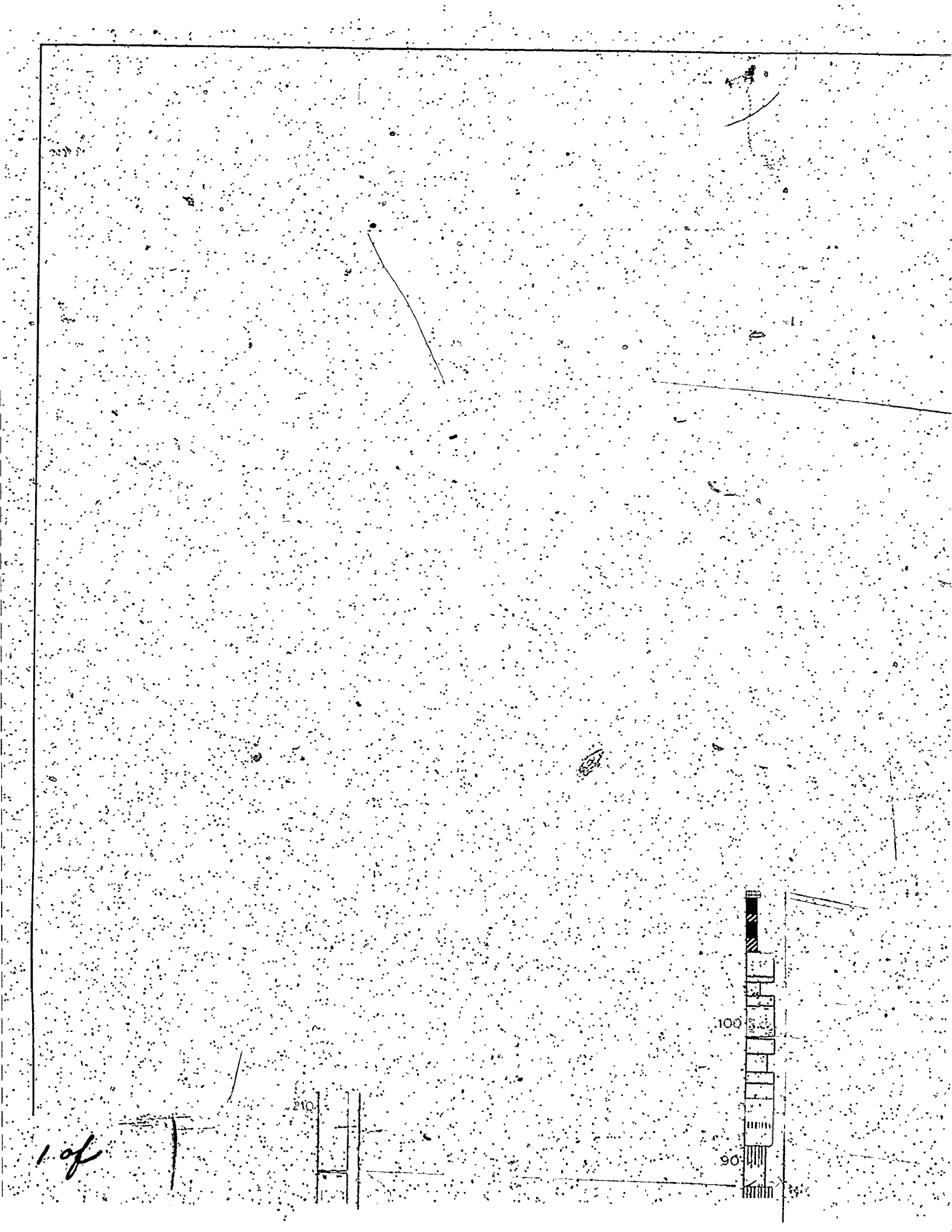
100
90
210

100
70
50
40
30
100
90

3 of

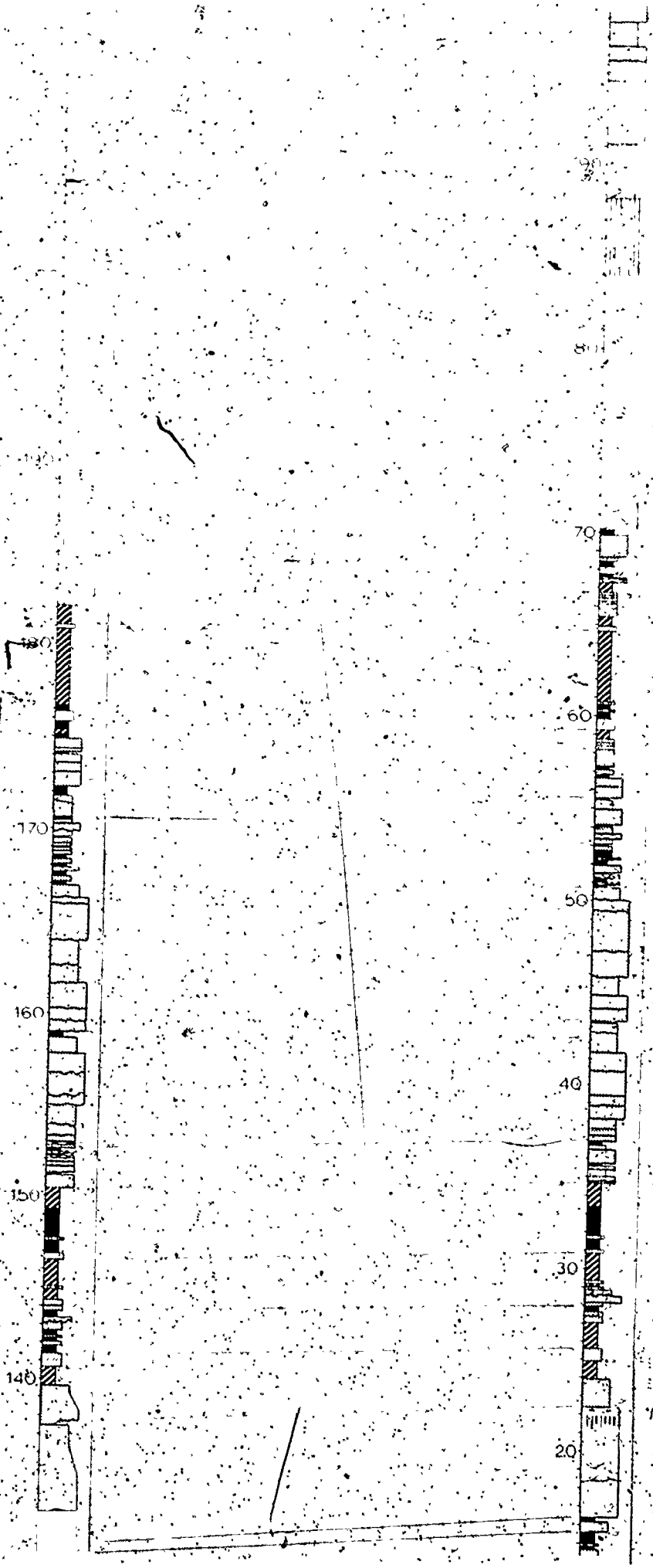

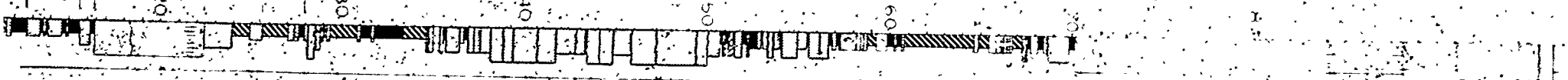
20
30
40
50
60

5 of

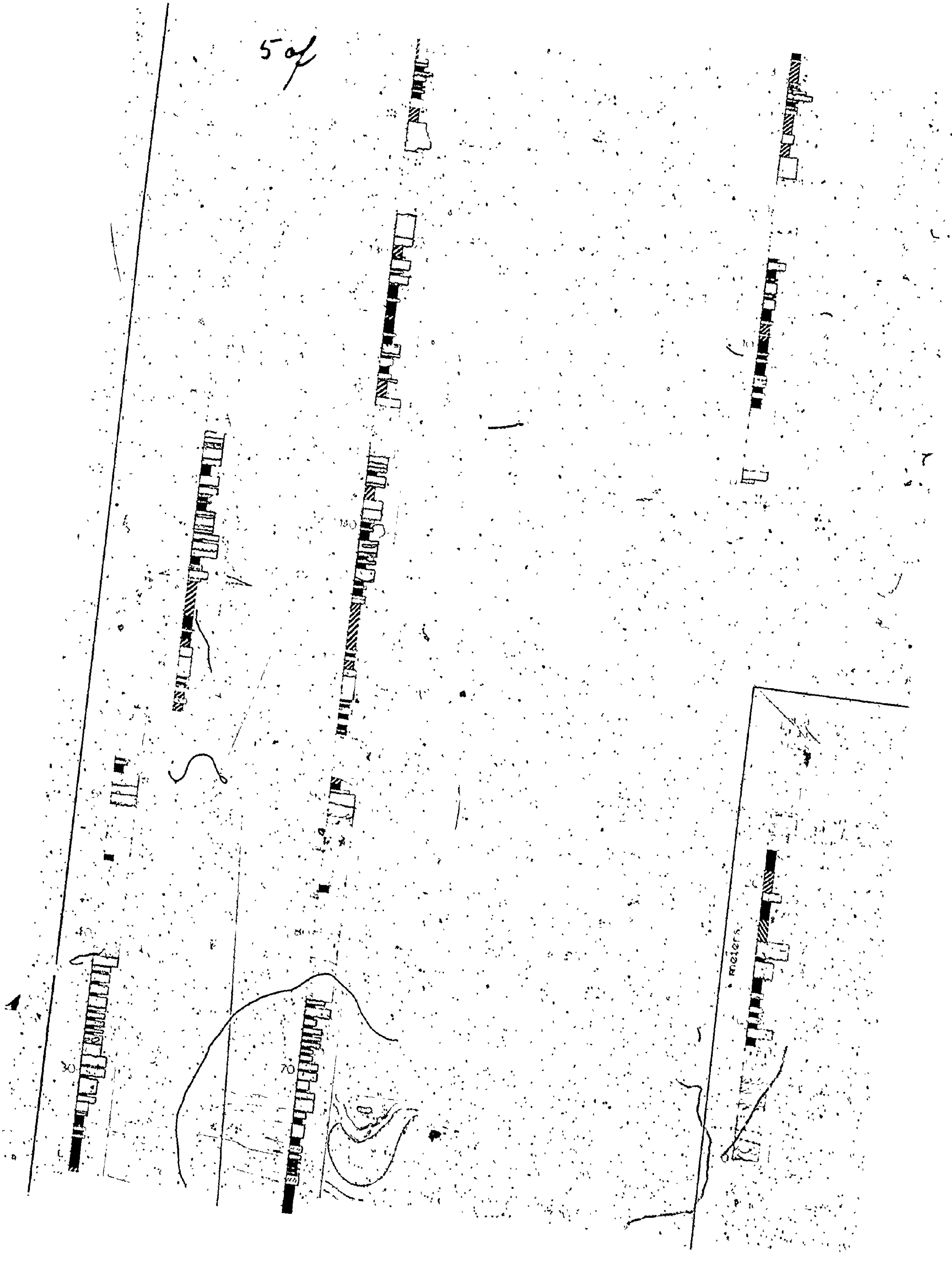

meters
1m
5m

Fig.

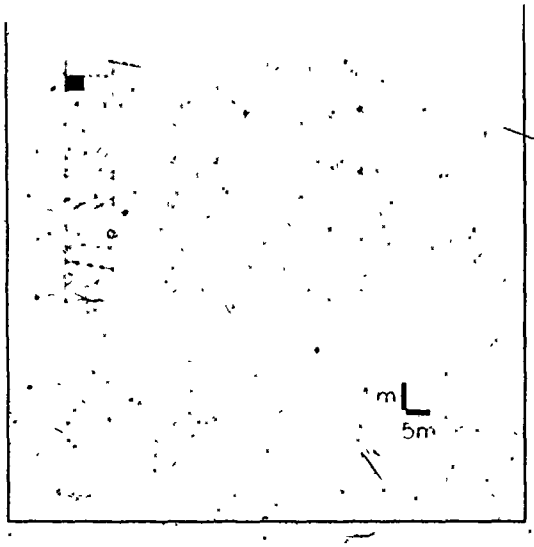
m
5m

1 of

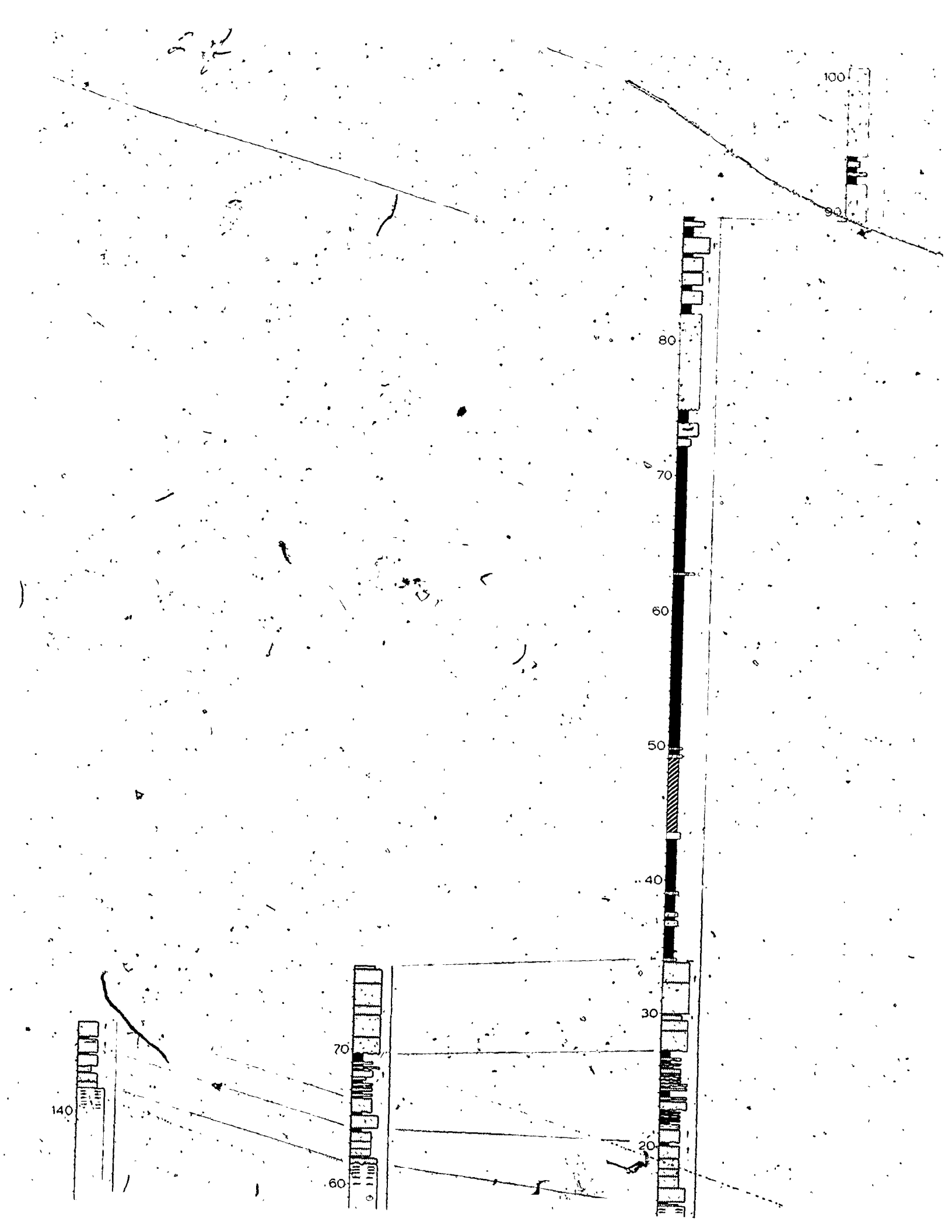
100
90
80
70
60
50
40
30
20
70
60
140

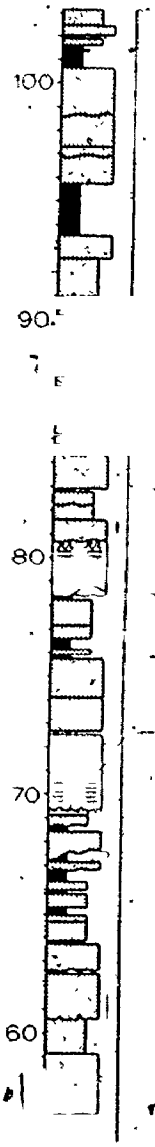
100
90
80
70
60

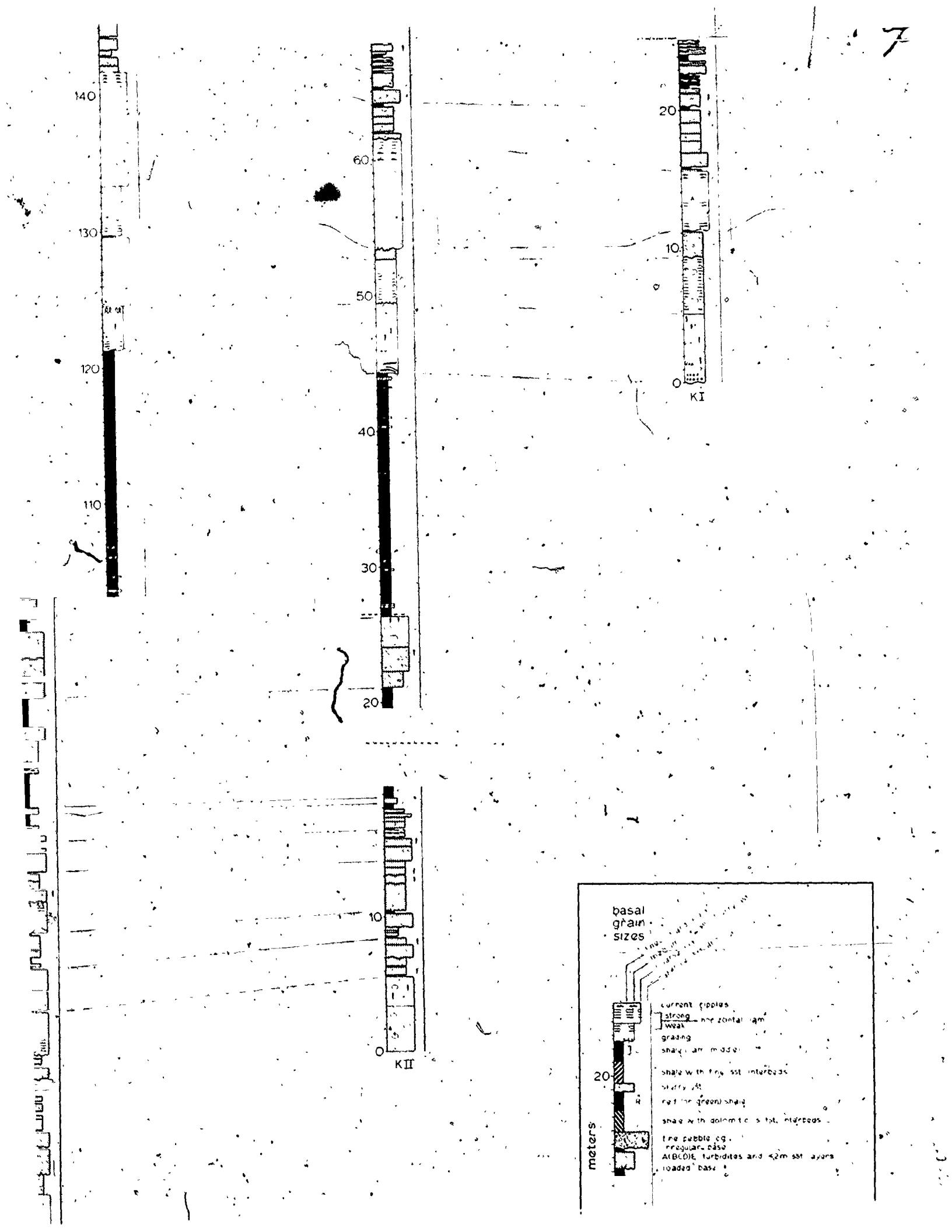
140
130
120
110
60
50
40
30
20
20
10
0
KI
10
0
KII
basal
grain
sizes
meters
20

5 of

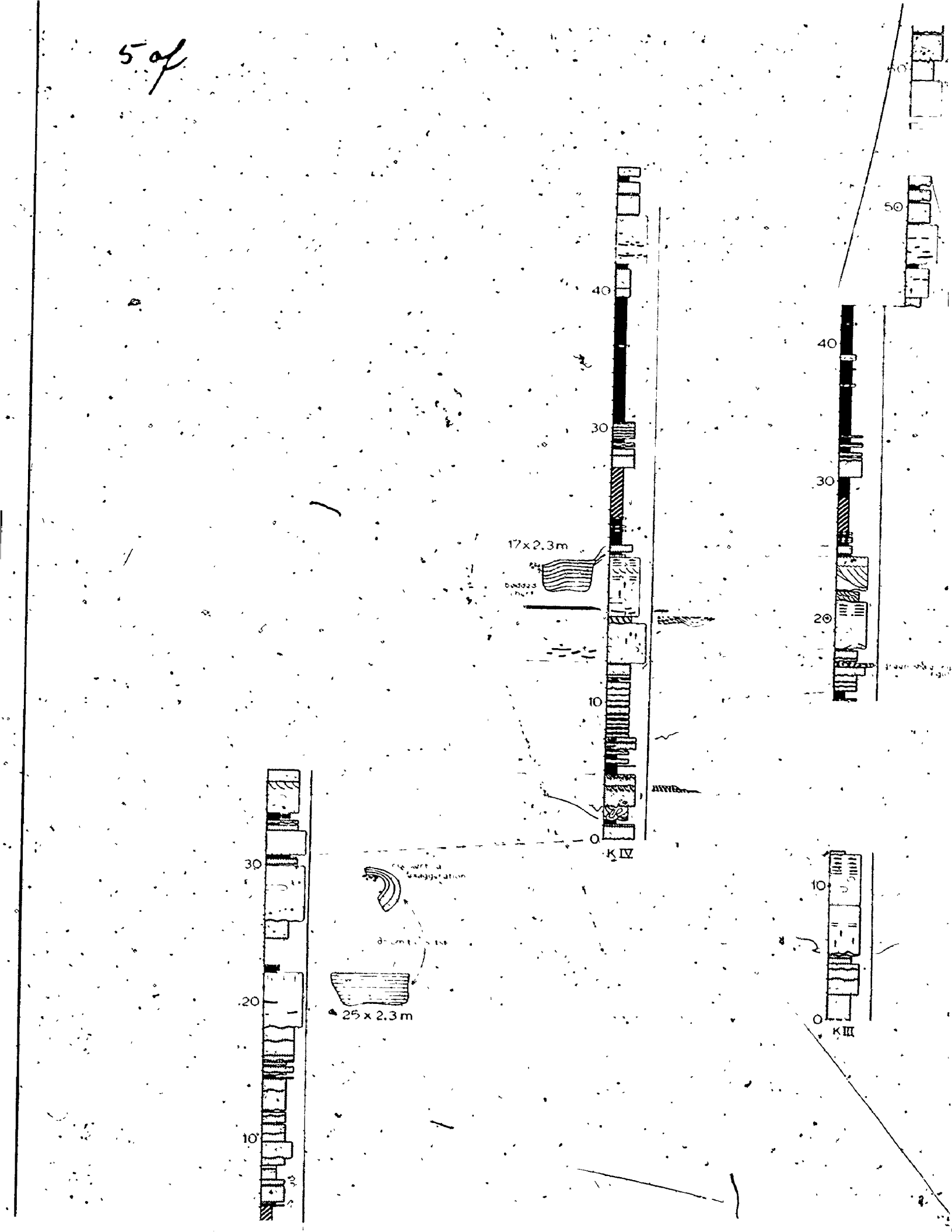

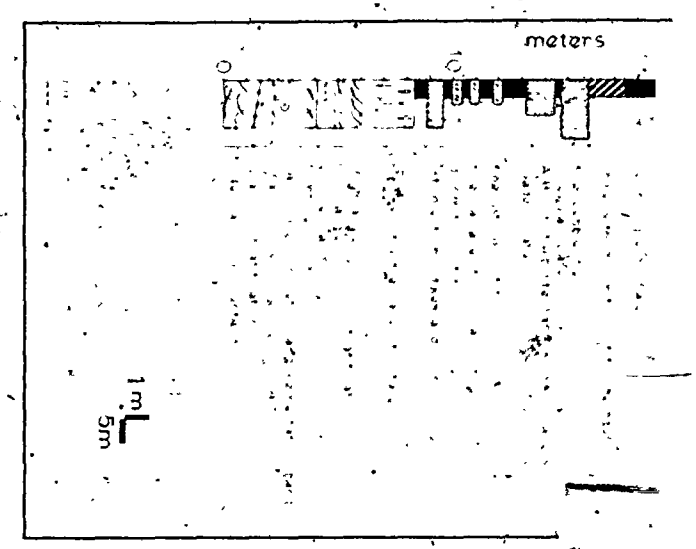
meters
0
5
1m
5m

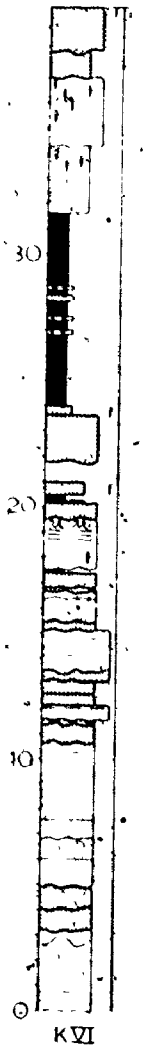
30
20
10
0
KVI

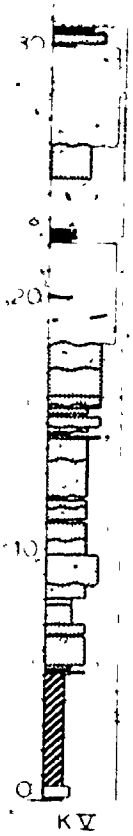
30
20
10
0
KV

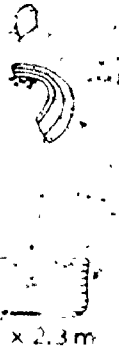
x 2.3 m

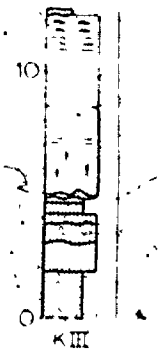
KIV
10
0
KIII

BLANK

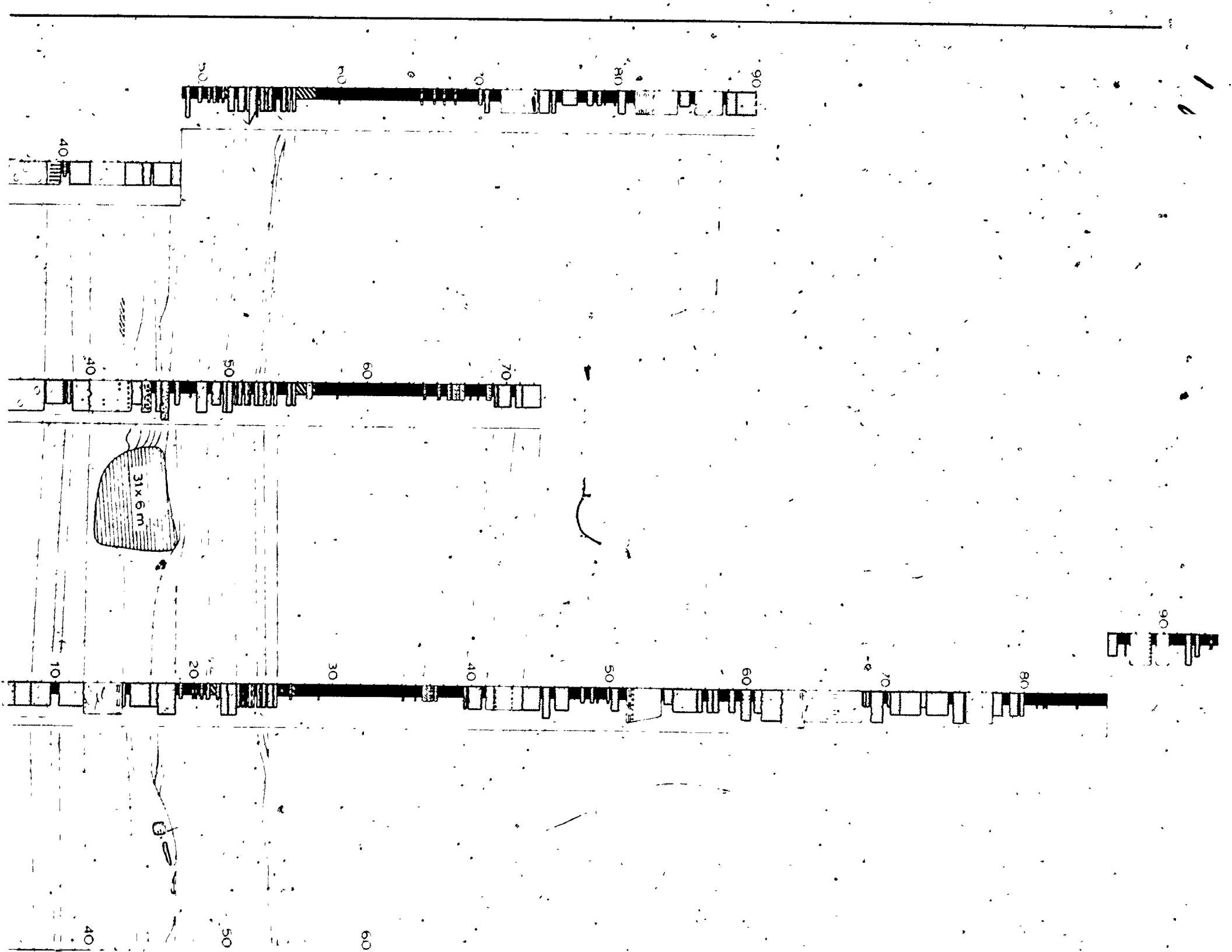
31 x 6 m


60
50
40

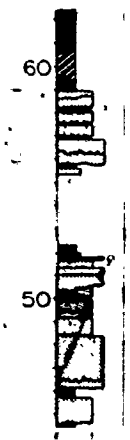
60
50

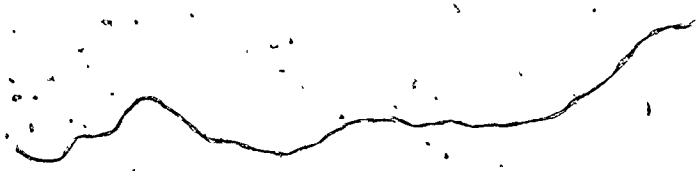

4 of 4 BLANK

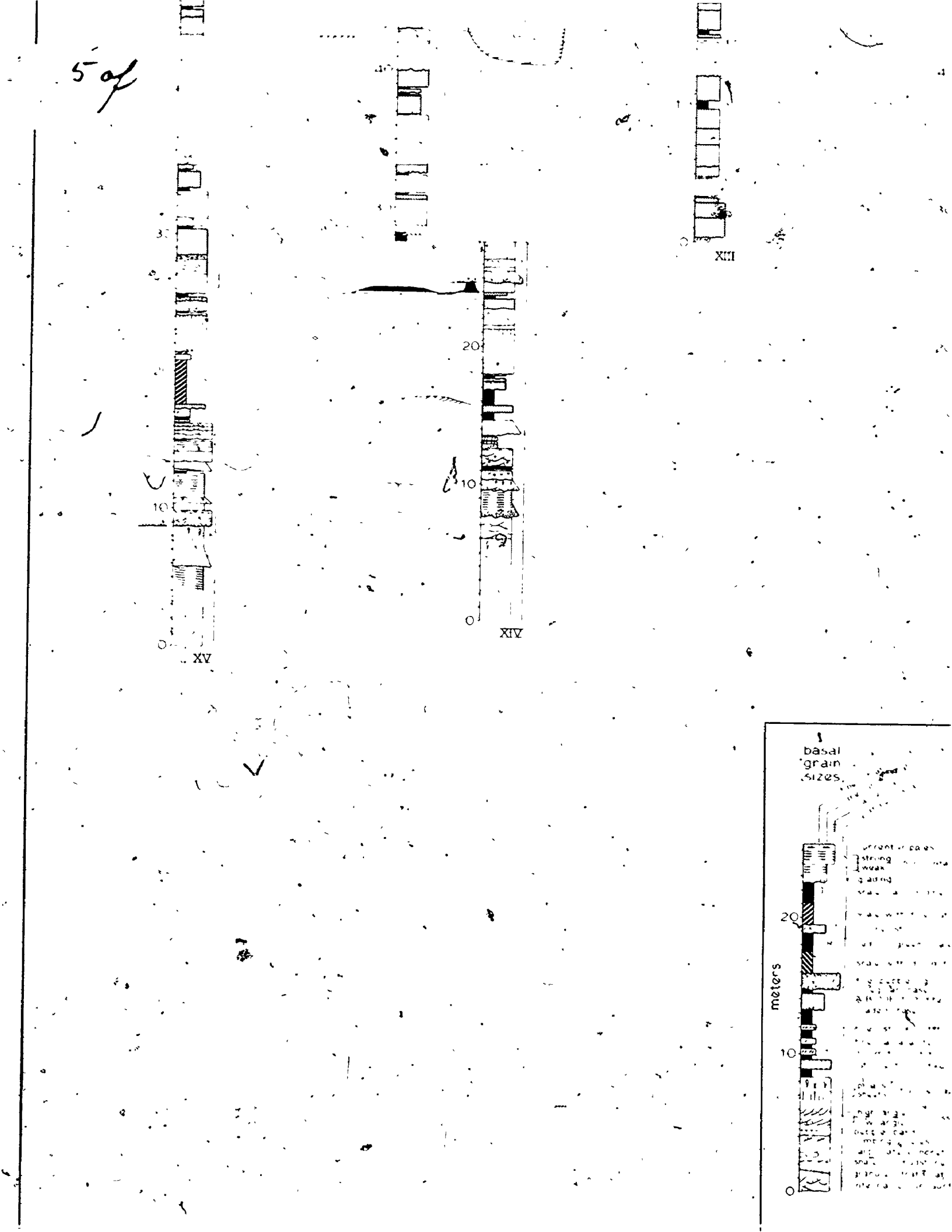
XII
XIV
XV
20
10
0
basal
grain
sizes
meters

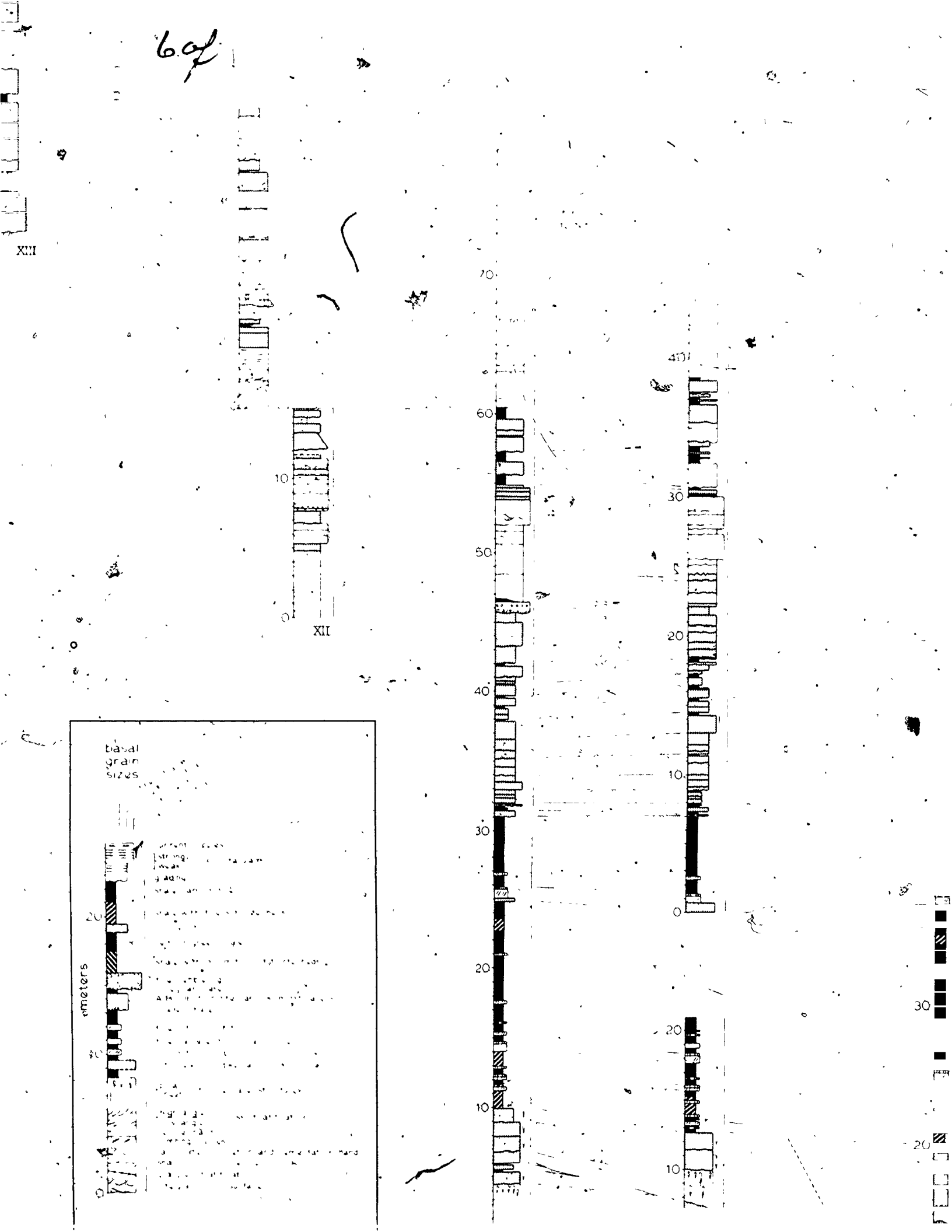
6.9
XIII
XII
70
60
50
40
30
20
10
0
40
30
20
10
0
20
10
basal
grain
sizes
meters
20
30
20
10

50
40
30
20
10
VIII
VII
VI

40
30
20
10
20
10
0
50
40
30
20
10

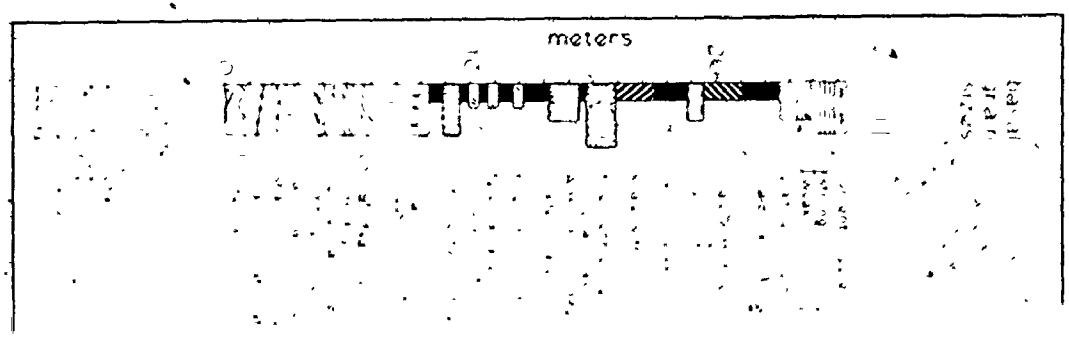
meters

10 of

XII

XI

X

IX

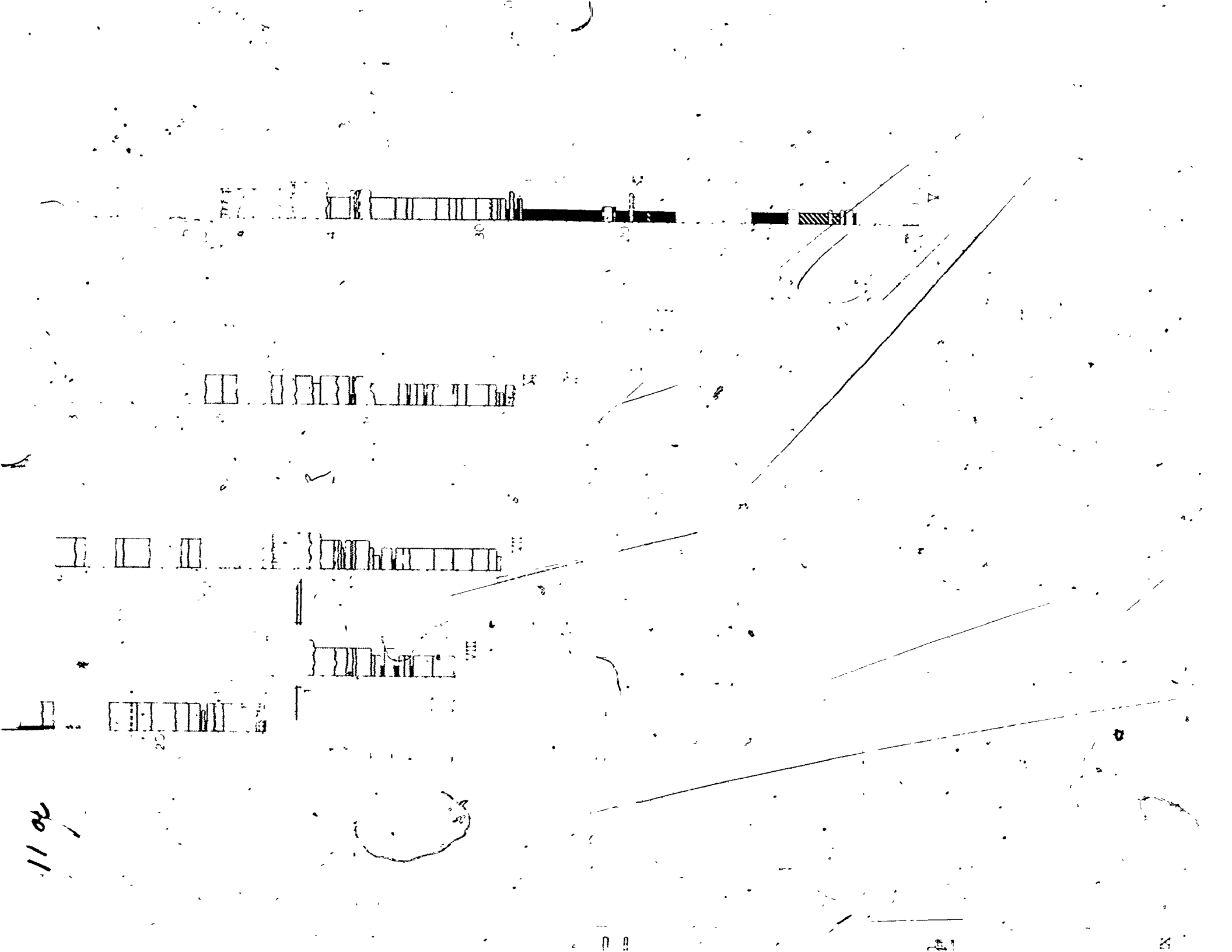

IV
III

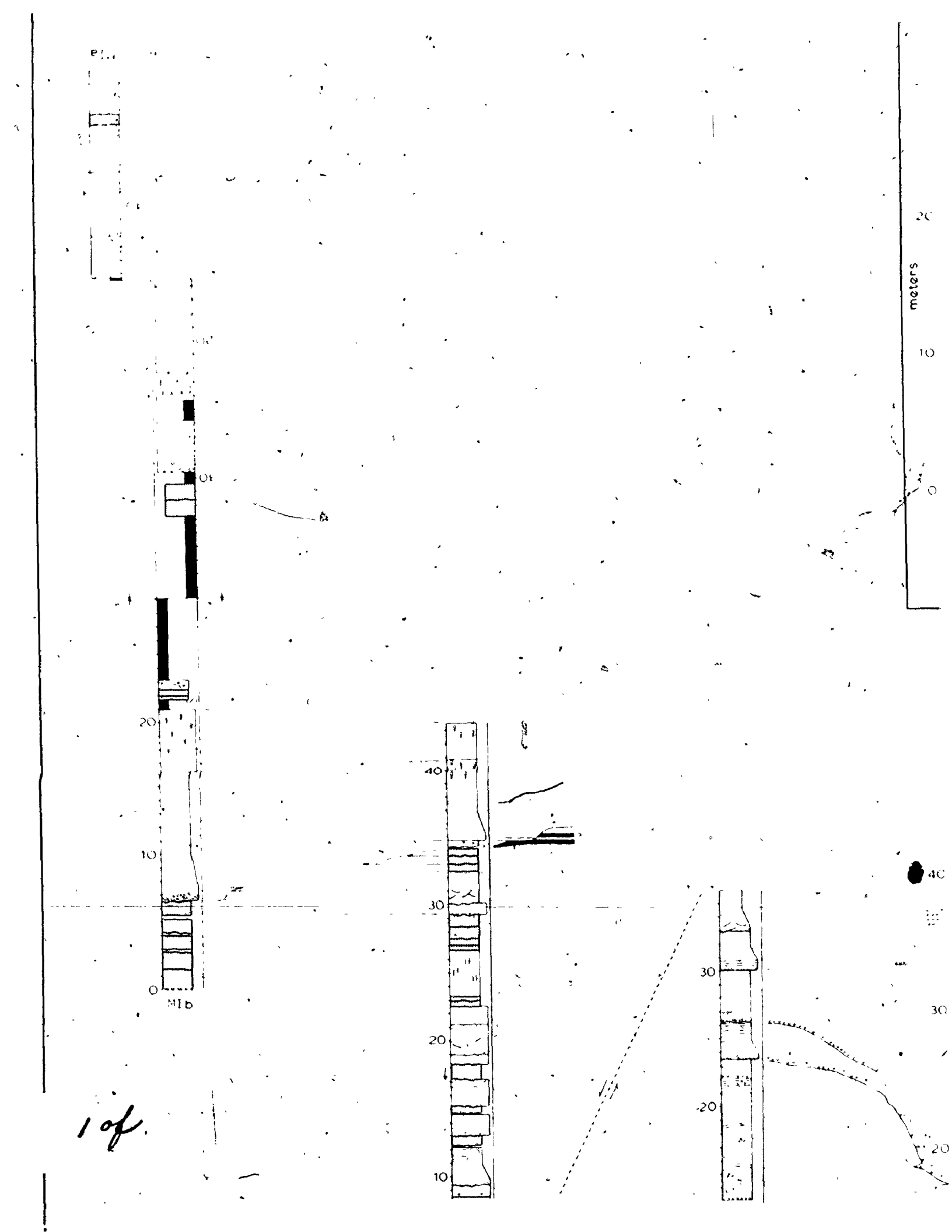

1 of

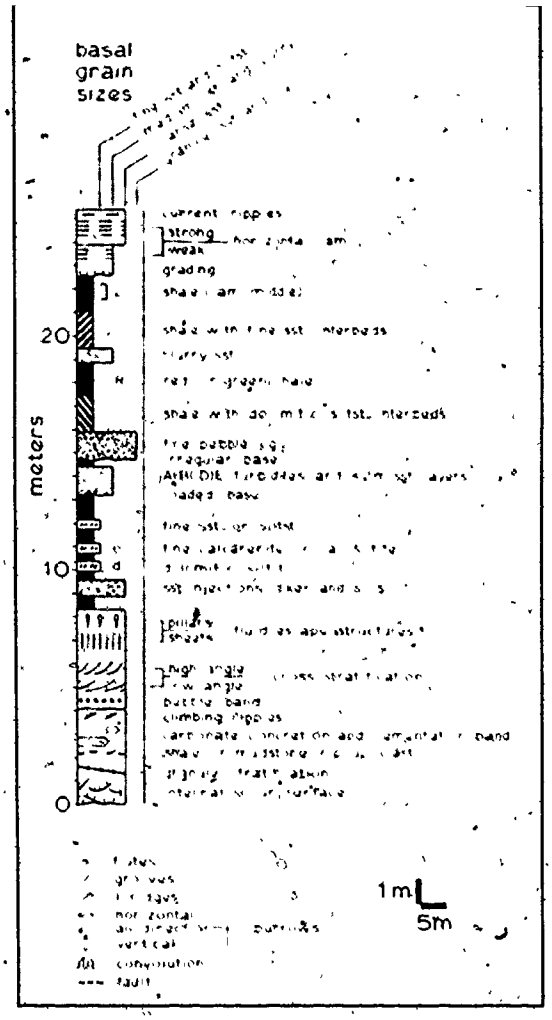
basal
grain
sizes
meters
20
10
0
1m
5m

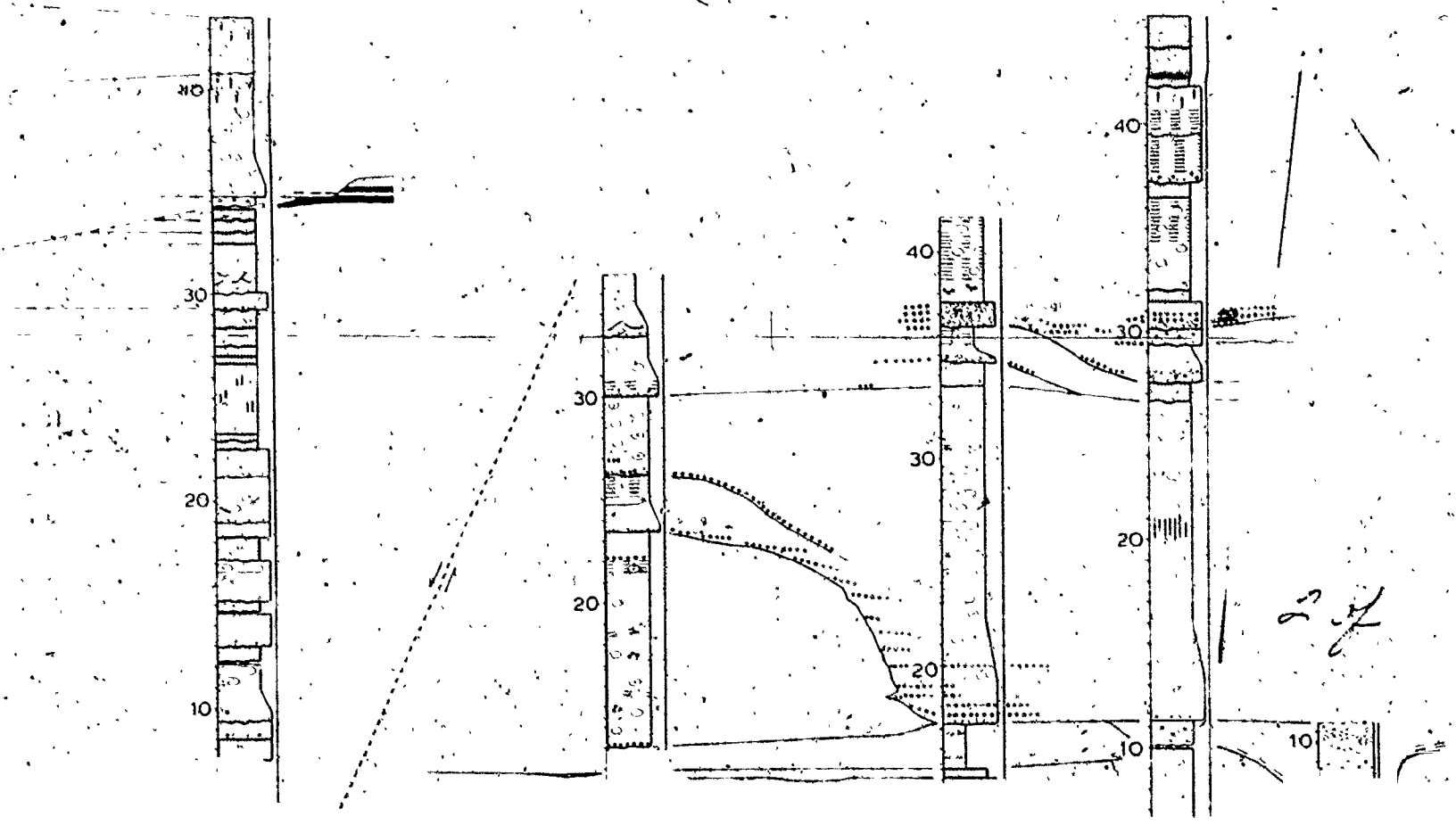
40
30
20
10
40
30
20
10
40
30
20
10


30
20
10
0
MIb
40
30
20
10
0
II
30
20
0
III

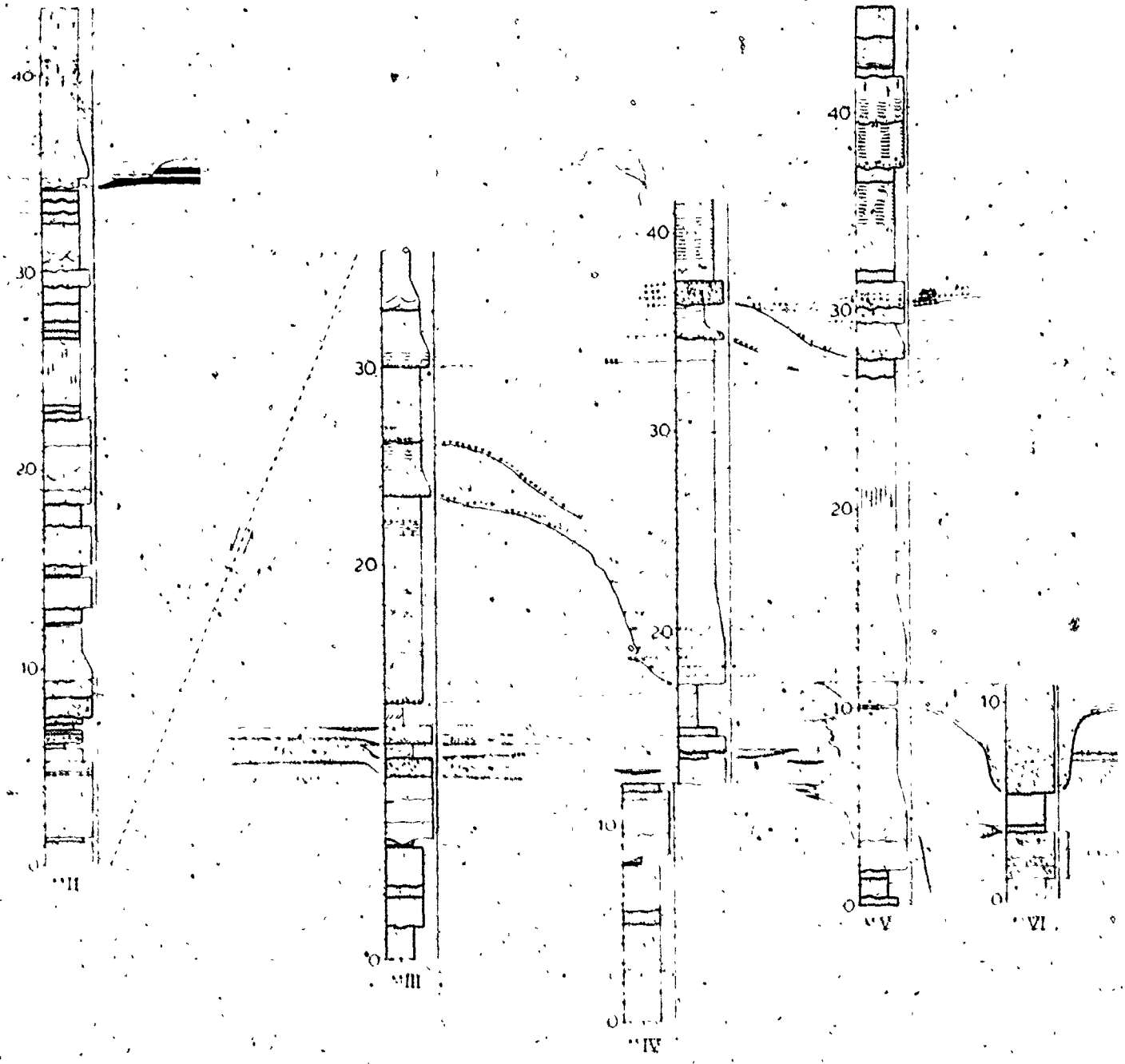
40
30
20
10
0
II
III
IV
V
VI